MOLLUSK BREEDING AND GENETIC IMPROVEMENT

EDITED BY: Yuehuan Zhang, Liqiang Zhao, Julian Ransangan, Zhongming Huo and Weiwei You

PUBLISHED IN: Frontiers in Marine Science

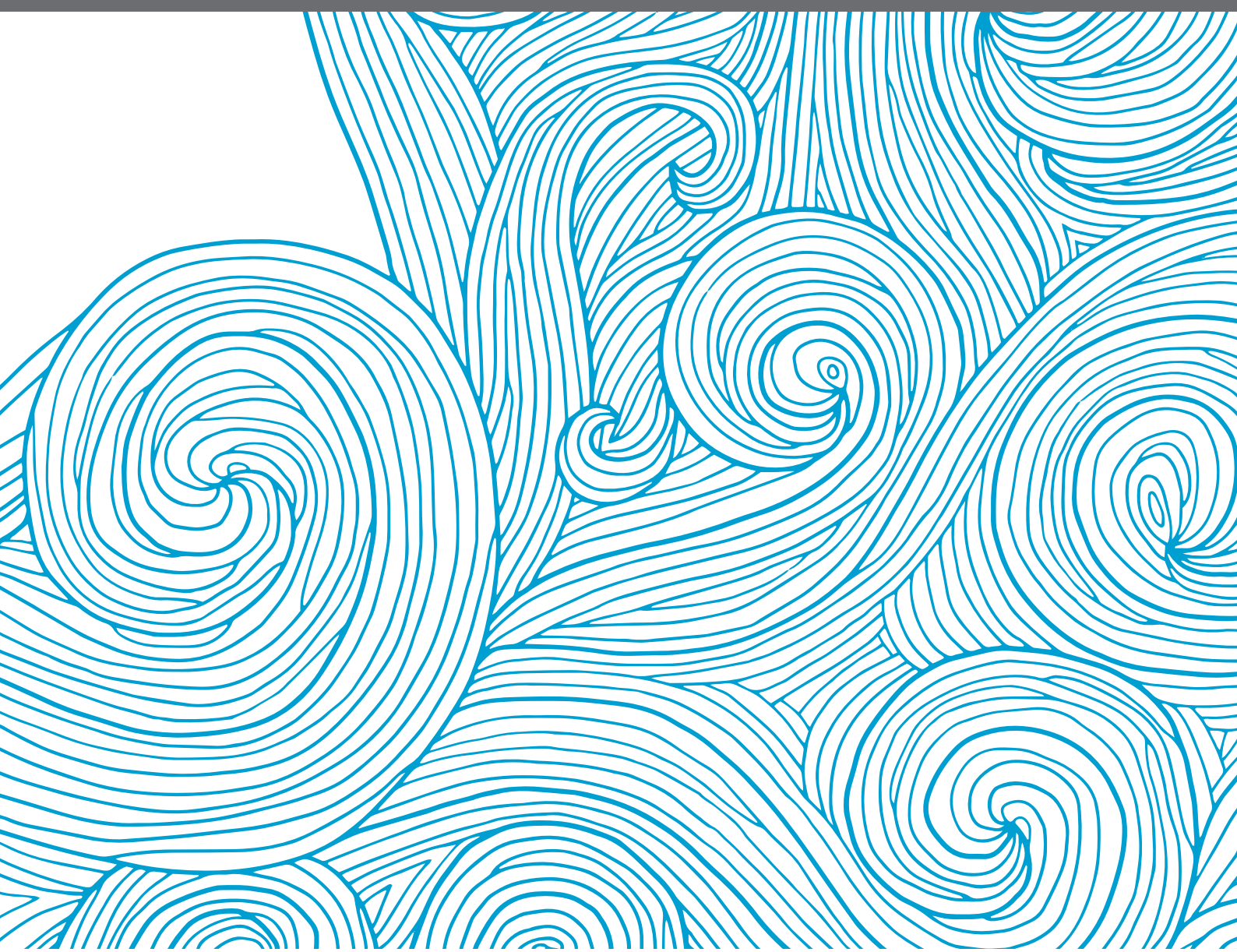

frontiers Research Topics

ISSN 1664-8714
ISBN 978-2-83250-153-5
DOI 10.3389/978-2-83250-153-5

About Frontiers

Frontiers is more than just an open-access publisher of scholarly articles: it is a pioneering approach to the world of academia, radically improving the way scholarly research is managed. The grand vision of Frontiers is a world where all people have an equal opportunity to seek, share and generate knowledge. Frontiers provides immediate and permanent online open access to all its publications, but this alone is not enough to realize our grand goals.

Frontiers Journal Series

The Frontiers Journal Series is a multi-tier and interdisciplinary set of open-access, online journals, promising a paradigm shift from the current review, selection and dissemination processes in academic publishing. All Frontiers journals are driven by researchers for researchers; therefore, they constitute a service to the scholarly community. At the same time, the Frontiers Journal Series operates on a revolutionary invention, the tiered publishing system, initially addressing specific communities of scholars, and gradually climbing up to broader public understanding, thus serving the interests of the lay society, too.

Dedication to Quality

Each Frontiers article is a landmark of the highest quality, thanks to genuinely collaborative interactions between authors and review editors, who include some of the world's best academicians. Research must be certified by peers before entering a stream of knowledge that may eventually reach the public - and shape society; therefore, Frontiers only applies the most rigorous and unbiased reviews.
Frontiers revolutionizes research publishing by freely delivering the most outstanding research, evaluated with no bias from both the academic and social point of view. By applying the most advanced information technologies, Frontiers is catapulting scholarly publishing into a new generation.

What are Frontiers Research Topics?

Frontiers Research Topics are very popular trademarks of the Frontiers Journals Series: they are collections of at least ten articles, all centered on a particular subject. With their unique mix of varied contributions from Original Research to Review Articles, Frontiers Research Topics unify the most influential researchers, the latest key findings and historical advances in a hot research area! Find out more on how to host your own Frontiers Research Topic or contribute to one as an author by contacting the Frontiers Editorial Office: frontiersin.org/about/contact

MOLLUSK BREEDING AND GENETIC IMPROVEMENT

Topic Editors:
Yuehuan Zhang, South China Sea Institute of Oceanology, Chinese Academy of Sciences (CAS), China
Liqiang Zhao, Guangdong Ocean University, China
Julian Ransangan, University Malaysia Sabah, Malaysia
Zhongming Huo, Dalian Ocean University, China
Weiwei You, Xiamen University, China

Citation: Zhang, Y., Zhao, L., Ransangan, J., Huo, Z., You, W., eds. (2022). Mollusk Breeding and Genetic Improvement. Lausanne: Frontiers Media SA. doi: 10.3389/978-2-83250-153-5

Table of Contents

frontiers in Marine Science

ORIGINAL RESEARCH
published: 17 August 2021
doi: 10.3389/fmars.2021.721292

A Significant Genetic Admixture in Farmed Populations of the Noble Scallop *Chlamys nobilis* Revealed by Microsatellite DNA Analysis in Southern China

Haitao Ma[1,2,3]†, Dongmei Yu[4]†, Shu Xiao[1,2,3], Yanping Qin[1,2,3], Yang Zhang[1,2,3], Jun Li[1,2,3], Yuehuan Zhang[1,2,3]* and Ziniu Yu[1,2,3]**

[1] Key Laboratory of Tropical Marine Bio-Resources and Ecology, Guangdong Provincial Key Laboratory of Applied Marine Biology, South China Sea Institute of Oceanology, Chinese Academy of Sciences, Guangzhou, China, [2] South China Sea Bio-Resource Exploitation and Utilization Collaborative Innovation Center, Guangzhou, China, [3] Innovation Academy of South China Sea Ecology and Environmental Engineering, Chinese Academy of Sciences, Guangzhou, China, [4] Guangdong Key Laboratory of Animal Conservation and Resource Utilization, Guangdong Public Laboratory of Wild Animal Conservation and Utilization, Institute of Zoology, Guangdong Academy of Sciences, Guangzhou, China

OPEN ACCESS

Edited by:
Jinghui Fang,
Yellow Sea Fisheries Research Institute, Chinese Academy of Fishery Sciences (CAFS), China

Reviewed by:
Yuewen Deng,
Guangdong Ocean University, China
Karsoon Tan,
Shantou University, China

***Correspondence:**
Haitao Ma
htma@scsio.ac.cn
Yuehuan Zhang
yhzhang@scsio.ac.cn
Ziniu Yu
carlzyu@scsio.ac.cn

† These authors have contributed equally to this work

Specialty section:
This article was submitted to Marine Fisheries, Aquaculture and Living Resources, a section of the journal Frontiers in Marine Science

Received: 06 June 2021
Accepted: 28 July 2021
Published: 17 August 2021

Citation:
Ma H, Yu D, Xiao S, Qin Y, Zhang Y, Li J, Zhang Y and Yu Z (2021) A Significant Genetic Admixture in Farmed Populations of the Noble Scallop Chlamys nobilis Revealed by Microsatellite DNA Analysis in Southern China. Front. Mar. Sci. 8:721292. doi: 10.3389/fmars.2021.721292

The noble scallop, *Chlamys nobilis,* is an important bivalve mollusk with high commercial value and is usually farmed in the waters of southern China. To date, very little is known about the genetic diversity and population structure of *C. nobilis*. In this study, 10 microsatellite loci of four farmed *C. nobilis* populations were compared with one another and compared wild population in southern China. A total of 83 alleles were found. Surprisingly, the level of genetic diversity of the farmed *C. nobilis* populations was higher than that of the wild population. Although the population genetic of wild population was completely in the Hardy–Weinberg equilibrium, due to heterozygote deficiency, significant deviations from the Hardy–Weinberg equilibrium were found in all farmed populations, suggesting a genetic admixture caused by the mixing of seeds from various hatcheries. The *Fst* and AMOVA values showed significant genetic differences between wild and farmed populations. The Bayesian assignment also confirmed that genetic admixture was significant and widespread in artificial breeding of *C. nobilis*. Furthermore, the UPGMA tree topology and PCA demonstrated that the genetic diversity of wild population can be clearly distinguished from farmed populations. In a nutshell, the findings of this study not only fill the knowledge gaps in genetic diversity of wild and farmed *C. nobilis* populations, but also serve as a guide for maintaining the genetic diversity of *C. nobilis* in both farmed and wild populations.

Keywords: *Chlamys nobilis*, cultivated population, genetic admixture, microsatellite, population structure, wild population

INTRODUCTION

Scallops are important animal protein source for humans (Liu et al., 2007; Tan et al., 2019). The global scallop landings have increased remarkably in the past decades (Food and Agriculture Organisation (FAO), 2020). The main reason for the dramatic increase in production is the development of scallop farming operations in Japan and China (Bourne, 2000;

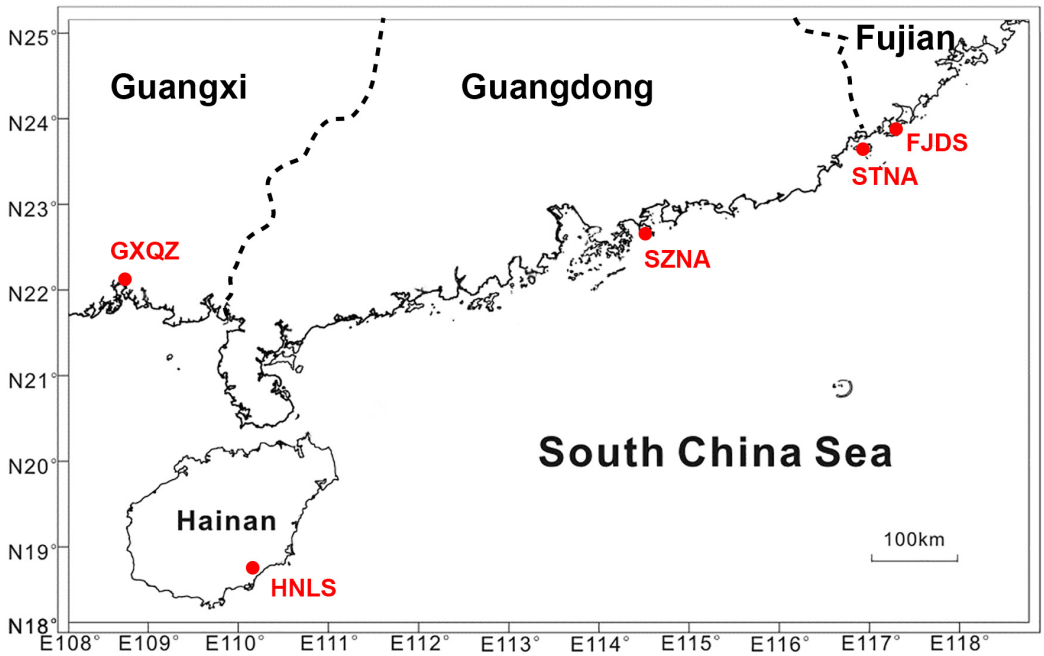

FIGURE 1 | Sampling locations of wild and cultured *Chlamys nobilis* populations in South China.

TABLE 1 | Characteristics of *Chlamys nobilis* microsatellite loci used in this study.

Locus	Primer	Size (bp)	Annealing temp. (°C)
*Cn*108	F:ACAAGGAGCAGAGTATAACG R:GAGAACACCCATGCAAAA	172–202	60
*Cn*113	F:CAGCCACAAACTGGGTAA R:GAGGATGATGAGGAGGAA	201–226	60
*Cn*115	F:CCATTTGGGTTAGTTCCT R:GTCCATCGTCGTCTTCAT	88–112	60
*Cn*206	F:TTCATTAGCGGAGGTTTTCG R:CTTTCCGGTGAATCCTTTGA	113–196	60
*Cn*207	F:TAGGGCATTTGCATACTTG R:CTTCGGATGAATGGGTCT	410–487	50
*Cn*208	F:AACGGGCGAGTACAAAGG R:GCACTGCCCAAACCACTA	328–477	64
*Cn*209	F:TATCCGTCCCACAAATCA R:GAACCGACATAAAACCTC	188–223	60
*Cn*222	F:TTTGGAGGGCACTGTATC R:TTGTCGTCTGAGTTTGGT	199–261	50
*Cn*223	F:AGGCTATCACTCCTTCAC R:GCTCCGCTTGACAATCTA	256–339	60
*Cn*224	F:GTCACCAAGGCTACTTTC R:GTCGGTTGTCACTCACTT	180–196	60

Tan et al., 2020b). The noble scallop, *Chlamys nobilis*, is an economically important bivalve species that naturally inhabits the coastal waters of southern China and Japan. In China, *C. nobilis* was initiated farmed in the Fujian province in the 1970s and later introduced to the Guangdong and Hainan provinces (Tan et al., 2020a).

With the expansion of the scale of *C. nobilis* aquaculture, the mass mortality rate of farmed *C. nobilis* has become more prominent since 2006. The production of *C. nobilis* seed in the hatchery is currently poorly managed due to the lack of necessary information about the origin of broodstock and seeds. In hatcheries, broodstock are usually selected from farmed stocks (Yuan et al., 2009). It is generally believed that the reproduction of animals in small or isolated populations will result in reduced heterozygosity and inbreeding depression, as well as reduced survival rates (Reed and Frankham, 2003). To avoid those potential problems, scallop farmers usually purchase scallop seeds from various sources or use seeds produced by mixing broodstocks obtained from various sources. As a result, there are significant variations in aquaculture traits among scallops in different farms, such as growth, survival rate, and disease resistance. It is worth noting that mixing population seeds from different sources may lead to a higher levels of genetic diversity and fewer heterozygotes in the populations (Ferguson, 1995; Thai et al., 2007), which might explain the high mortalities within scallop populations (Nagashima et al., 2005).

Molecular markers are an important tool for studying population genetic and can provide useful information about genetic diversity of populations (Williams and Benzie, 1998; Azuma et al., 2008; Janson et al., 2015; Phinchongsakuldit et al., 2015), as well as understand the connectivity among populations and its adaptive potential to adapt to different environments (Petersen et al., 2010). To date, genetics studies on

TABLE 2 | Genetic variability of 10 microsatellite loci in five populations for *Chlamys nobilis*.

Locus	Parameter	FJDS (*n* = 30)	SZNA (*n* = 30)	STNA (*n* = 32)	GXQZ (*n* = 30)	HNLS (*n* = 30)	Average across population
*Cn*108	*A*	8	9	10	10	6	10
	Ho	0.733	0.733	0.875	0.700	0.800	0.768
	He	0.831	0.839	0.877	0.692	0.747	0.848
	R	8.000	9.000	9.994	10.00	6.000	9.044
	PIC	0.792	0.802	0.849	0.659	0.692	0.759
	P_{HW}	n.s.	*	n.s.	n.s.	n.s.	
*Cn*113	*A*	5	4	6	4	3	6
	Ho	0.300	0.067	0.125	0.133	0.133	0.151
	He	0.662	0.431	0.505	0.466	0.188	0.615
	R	5.000	4.000	5.875	4.000	3.000	5.110
	PIC	0.603	0.358	0.468	0.407	0.175	0.402
	P_{HW}	**	**	**	**	n.s.	
*Cn*115	*A*	7	8	8	10	6	11
	Ho	0.633	0.733	0.656	0.633	0.567	0.645
	He	0.718	0.832	0.807	0.773	0.581	0.818
	R	7.000	8.000	7.935	10.00	6.000	9.437
	PIC	0.665	0.793	0.766	0.731	0.548	0.701
	P_{HW}	n.s.	n.s.	n.s.	n.s.	n.s.	
*Cn*206	*A*	5	5	6	9	7	11
	Ho	0.633	0.433	0.344	0.667	0.800	0.575
	He	0.640	0.742	0.447	0.736	0.802	0.736
	R	5.000	5.000	5.875	9.000	7.000	7.142
	PIC	0.559	0.681	0.417	0.691	0.757	0.621
	P_{HW}	n.s.	**	n.s.	n.s.	n.s.	
*Cn*207	*A*	4	5	6	6	5	7
	Ho	0.233	0.333	0.219	0.400	0.600	0.357
	He	0.584	0.725	0.730	0.670	0.741	0.776
	R	4.000	5.000	6.000	6.000	5.000	5.758
	PIC	0.491	0.662	0.680	0.605	0.682	0.624
	P_{HW}	**	**	**	*	n.s.	
*Cn*208	*A*	8	7	8	10	7	10
	Ho	1.000	0.733	0.781	0.833	0.667	0.803
	He	0.827	0.790	0.822	0.776	0.727	0.851
	R	8.000	7.000	7.934	10.00	7.000	8.922
	PIC	0.790	0.743	0.783	0.732	0.671	0.744
	P_{HW}	n.s.	n.s.	n.s.	n.s.	n.s.	
*Cn*209	*A*	5	6	7	7	5	10
	Ho	0.533	0.733	0.438	0.567	0.633	0.581
	He	0.710	0.761	0.631	0.764	0.681	0.774
	R	5.000	6.000	6.812	7.000	5.000	7.236
	PIC	0.653	0.716	0.564	0.710	0.620	0.653
	P_{HW}	n.s.	n.s.	n.s.	*	n.s.	
*Cn*222	*A*	5	5	5	4	3	6
	Ho	0.233	0.233	0.594	0.300	0.400	0.352
	He	0.638	0.657	0.740	0.627	0.386	0.709
	R	5.000	5.000	4.938	4.000	3.000	5.540
	PIC	0.592	0.604	0.680	0.546	0.342	0.553
	P_{HW}	**	**	**	**	n.s.	
*Cn*223	*A*	6	6	6	7	5	7
	Ho	0.767	0.633	1.000	0.767	0.800	0.793
	He	0.767	0.746	0.773	0.833	0.706	0.802
	R	6.000	6.000	5.937	7.000	5.000	6.980
	PIC	0.713	0.697	0.723	0.795	0.651	0.716

(Continued)

TABLE 2 | Continued

Locus	Parameter	FJDS (*n* = 30)	SZNA (*n* = 30)	STNA (*n* = 32)	GXQZ (*n* = 30)	HNLS (*n* = 30)	Average across population
	P_{HW}	n.s.	n.s.	n.s.	n.s.	n.s.	
*Cn*224	*A*	5	4	3	3	4	5
	Ho	0.333	0.433	0.438	0.167	0.433	0.361
	He	0.574	0.537	0.378	0.159	0.403	0.438
	R	5.000	4.000	2.997	3.000	4.000	4.168
	PIC	0.499	0.485	0.322	0.150	0.349	0.361
	P_{HW}	n.s.	n.s.	n.s.	n.s.	n.s.	
Mean (all loci)	*A*	5.800	5.900	6.500	7.000	5.100	
	Ho	0.540	0.507	0.547	0.517	0.583	
	He	0.695	0.706	0.671	0.650	0.596	
	R	5.800	5.900	6.430	7.000	5.100	
	PIC	0.636	0.654	0.625	0.603	0.526	
	P_{HW}	**	**	**	**	n.s.	

*A, total number of alleles; Ho, observed heterozygosity; He, expected heterozygosity; R, allelic richness; PIC, polymorphism information content; P_{HW}, Hardy–Weinberg probability test: *P < 0.05, **P < 0.01 following sequential Bonferroni correction; n.s., non-significant.*

bivalves has been very limited and mainly focusing on bivalve species with important commercial value (Benzie and Williams, 1997; Nagashima et al., 2005; Sato et al., 2005; Song et al., 2006; Gurney-Smith et al., 2017). For *C. nobilis*, only information on few microsatellites (Ma and Yu, 2009a,b) and mitochondrial DNA variation in farmed and wild stocks of *C. nobilis* in southern China (Yuan et al., 2009) are available. It is found that the genetic diversity of wild *C. nobilis* population is lower than that of farmed population from the same region in southern China, and the genetic composition of farmed *C. nobilis* is highly affected by hatchery operations (Yuan et al., 2009).

In order to verify the discovery of Yuan et al. (2009), in this study, we use 10 microsatellite markers to examine the genetic diversity of wild and farmed *C. nobilis* populations in coastal water of southern China. Microsatellites were chosen in this study because of their neutral, clear scoring of alleles, hypervariability, codominance, and abundance properties, making them the best choice for studying genetic variation of individuals and populations (Zhan et al., 2009). The aim of this study was to use microsatellites to explore the genetic variation of *C. nobilis* among hatcheries, and between hatchery and wild populations. Understanding the genetic diversity and differentiation among *C. nobilis* populations is essential for establishing appropriate guidelines for establishment and maintenance of farmed *C. nobilis* populations.

MATERIALS AND METHODS

Sample and DNA Extraction

A total of 152 adult *C. nobilis* were randomly collected from four *C. nobilis* farms [Dongshan (Fujian province, FJDS) (30 individuals), Nan'ao (Shenzhen city of Guangdong province, SZNA) (30 individuals), Nan'ao island (Shantou city of Guangdong province, STNA) (32 individuals), and Qinzhou (Guangxi province, GXQZ) (30 individuals)] and one wild population (Lingshui, Hainan province, HNLS) (30 individuals) along the southern coast of China (**Figure 1**).

The adductor muscle was extracted and stored in 70% ethanol. The genomic DNA was extracted individually using phenol-chloroform (Sambrook and Russell, 2000). Subsequently, 0.8% agarose gel electrophoresis was used to screen for the integrity of the extracted genomic DNA, and then ND-1000 UV-Vis spectrophotometer (NanoDrop, Wilmington, DE, United States) was used to determine the quality and quantity of extracted genomic DNA.

Data Collection

In order to avoid scoring errors, nine previously reported microsatellite loci (Ma and Yu, 2009a,b) and a newly developed microsatellite locus (*Cn*224) with a unique band size of were selected. The sequences of primers and microsatellite core, as well as the optimal annealing conditions are summarized in **Table 1**. Amplifications were conducted in 20-μL reactions (0.25–0.5 U Taq polymerase (Tiangen, Beijing, China), 80 ng of template DNA, 0.2 mM dNTPs, 1 × PCR buffer, 0.2–1 μM primers (each), and 1.0–2.0 mM $MgCl_2$). For PCR, the initial denaturation was set at 95°C for 5 min, and then at 94°C for 30 s for 30 cycles, followed by primer-specific annealing at 72°C for 1 min, and a final extension at 72°C for 10 min. The PCR products were then separated by electrophoresis on an 8% non-denaturing polyacrylamide gel, and then observed using silver staining. For allele size determination, each gel contains a control DNA sample and a 50-bp DNA ladder (Takara).

Data Analysis

In order to identify the scoring errors, invalid alleles, and large-allele drop out in microsatellite products, MICRO-CHECHER was used according to the manufacturing instructions (Oosterhout et al., 2004). For the analysis of microsatellite loci variation in the five populations, POPGENE 1.31 software was use to calculate the number of alleles, allele frequency, effective number of alleles, as well as expected and observed heterozygosities (Yeh et al., 1999). Locus polymorphism [polymorphism information content

(*PIC*)] and allelic richness (*R*) were estimated according to the formula described by Botstein et al. (1980) and was calculated (EIMousadik and Petit, 1996), respectively. An independent *T*-test was performed, followed by a Turkey multiple comparison test (Turkey HSD) to test for significant differences in genetic diversity between *C. nobilis* from hatchery and wild populations.

GENEPOP4.0 was used to evaluate the statistical significance of Hardy–Weinberg equilibrium (*HWE*) and linkage disequilibrium test (*LD*) (Raymond and Rousset, 1995). Chi-square tests were used to test for significant differences, while sequential Bonferroni correction was used to adjust the significance of *p* values for multiple tests (Rice, 1989).

Genetic variation among populations were evaluated using pairwise *Fst* values, and bootstrap analysis (1000 permutations) was used to test for their significant difference using FSTAT2.9.3. Analysis of molecular variance (AMOVA) was used to compare hierarchical genetic structure between and within populations using ARLEQUIN 3.0 (Excoffier et al., 2005).

In order to evaluate individual migrant events across ocean currents, GENECLASS 2.0 was used to estimate the probability of each individual being assigned to a particular population based on multilocus genotype data (Piry et al., 2004).

Principal component analysis (PCA) between populations was performed using NTSYS software (Rohlf, 2005). To evaluate the genetic relationships among populations, POPULATION was used to calculate A matrix of pairwise D_A distance (Nei, 1972), and then a UPGMA dendrogram was constructed using PHYLIP3.5c (Felsenstein, 1993).

RESULTS

Genetic Variation Within *C. nobilis* Population

All 10 microsatellite loci were polymorphic in all five *C. nobilis* populations. 83 different alleles were observed in these 10 loci, ranging in size from 66 to 464 bp. Microsatellites *Cn*206 and *Cn*115 have the highest polymorphisms (11 alleles), whereas locus *Cn*224 has the least polymorphism (five alleles). Moderate-to-high polymorphism information content (*PIC*) was detected at most microsatellite loci in each population (**Table 2**).

The intra-population allele frequencies of all 10 microsatellite loci revealed differences among the five populations (**Figure 2**). The mean number of alleles in all loci of the wild *C. nobilis* population (HNLS) (5.1) was significantly lower than that of the farmed *C. nobilis* populations (5.8–7.0). Since the number of alleles is sensitive to the sample size, allele richness was used for comparison. Consistent with the mean number of alleles, the allele richness of the wild *C. nobilis* population was also the lowest (5.1). Moreover, the average expected heterozygosity of the wild *C. nobilis* population (0.596) was significantly lower than that of the farmed *C. nobilis* populations (0.650–0.706). The polymorphism information content (*PIC*) also showed similar trends, in which the *PIC* of wild *C. nobilis* population (0.526) was significantly lower than that of farmed *C. nobilis* populations (0.603–0.654). However, observed heterozygosity showed the opposite trend. The observed heterozygosity of the wild *C. nobilis* population (0.583) was significantly higher than that of the farmed *C. nobilis* populations (0.507–0.547) (**Table 2**). Nevertheless, there was no statistical difference in genetic diversity between wild and farmed *C. nobilis* populations ($P > 0.05$).

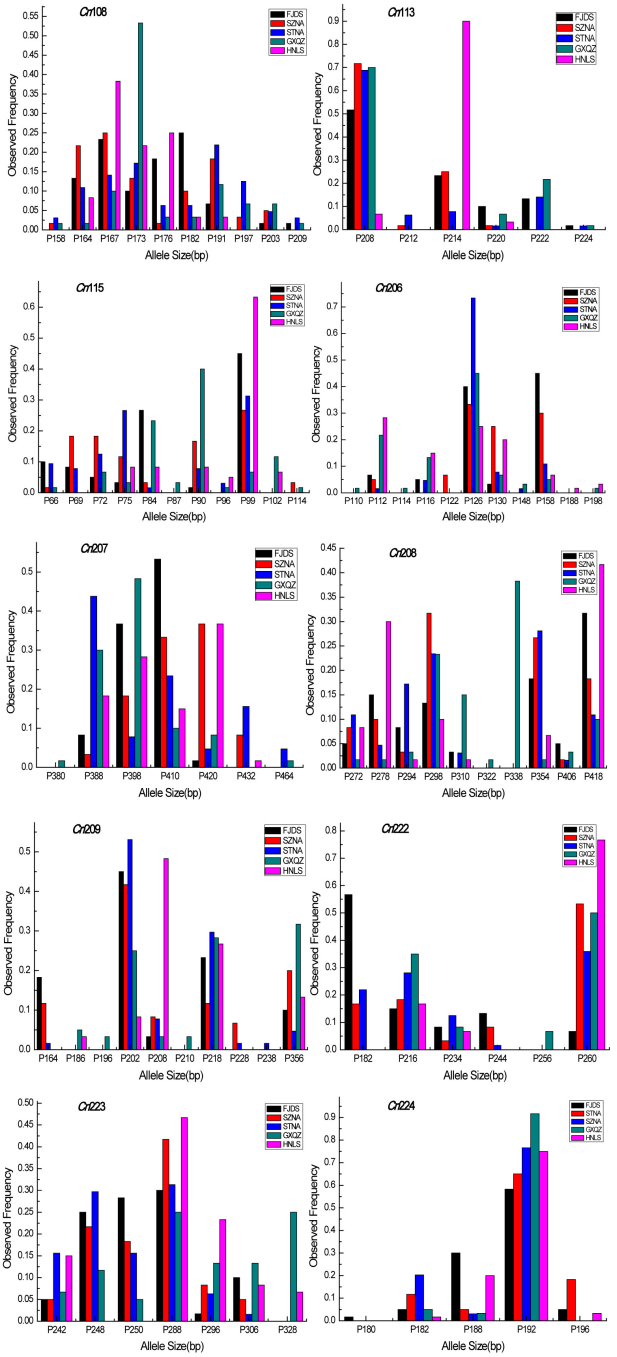

FIGURE 2 | Allele size frequency distributions of the 10 microsatellite loci in five *C. nobilis* populations in this study.

The results of MICRO-CHECKER revealed that there were no major allele dropout, scoring errors and null alleles in the wild *C. nobilis* population. However, there were null alleles at few microsatellite loci in every farmed *C. nobilis* populations. In farmed *C. nobilis* populations, significant deviations from Hardy–Weinberg equilibrium were observed in 10 of the 50 tests at the 5% level after sequential Bonferroni correction for multiple tests, indicating heterozygote deficiencies. However, for the wild *C. nobilis* population, all microsatellite loci were at the H-W equilibrium value. No linkage disequilibrium was detected among any loci in this study, indicating that these loci were genetically independent.

Genetic Differentiation and Relationships Among Populations

Pairwise *Fst* analyses revealed that the genetic differentiation between wild and farmed *C. nobilis* populations (0.129–0.186) was significantly higher than that among farmed *C. nobilis* populations (0.046–0.14) (**Table 3**). Similar results have been recorded from the Analysis of molecular variances (AMOVA) of microsatellites, in which the variations within individuals, among individuals within populations, and among populations were 71.40% ($P = 0.000$), 16.81% ($P = 0.000$), and 11.79% ($P = 0.000$), respectively, and there were significant genetic differentiation among the five populations (**Table 4**).

Bayesian assignment placed all wild individuals in their own population with a score of 100. However, farmed populations suffered a relatively high proportion of misclassifications (**Table 5**).

Genetic relationships between populations were graphically illustrated by a dendrogram (**Figure 3**) and PCA (**Figure 4**). The UPGMA dendrogram showed that four farmed *C. nobilis* populations were clustered together and the wild population (HNLS) formed another cluster. Similar findings were observed in the PCA scatter plots where two major groups can be seen (i.e., FJDS-GXQZ and HNLS).

TABLE 3 | Pairwise *Fst* values between five noble scallop populations based on 10 microsatellite loci.

	FJDS	SZNA	STNA	GXQZ	HNLS
FJDS	0.000				
SZNA	0.060**	0.000			
STNA	0.077**	0.046**	0.000		
GXQZ	0.140**	0.093**	0.087**	0.000	
HNLS	0.172**	0.129**	0.183**	0.186**	0.000

***$P < 0.01$ following sequential Bonferroni correction.*

TABLE 5 | Results of assignment tests based on the Bayesian method for 10 microsatellite loci of *C. nobilis* individuals.

Population	Assigned to				
	FJDS	SZNA	STNA	GXQZ	HNLS
FJDS	**27**	1	1	1	0
SZNA	1	**29**	0	0	0
STNA	2	1	**29**	0	0
GXQZ	0	1	0	**29**	0
HNLS	0	0	0	0	**30**

In bold, number of individuals that were correctly assigned.

DISCUSSION

Maintaining genetic diversity is important for both wild and farmed populations as it offers genotypes that respond adaptively to changing environments (Fisher, 1958); in particular, heterozygous individuals are often superior to homozygous individuals in many aquaculture traits, including growth, fertility, and disease resistance (Thai et al., 2007). In aquaculture, as a result of limited broodstock and inbreeding activities, many shellfish species have reduced genetic variability compared to their wild stocks (Hedgecock and Sly, 1990; Evans et al., 2004; Li et al., 2007). In this study, we found that a high level of genetic diversity was maintained in the wild *C. nobilis* population (HNLS). However, the most genetic parameters (except *Ho*) of farmed *C. nobilis* populations were significantly higher than wild *C. nobilis* population. In agreement with the findings of Yuan et al. (2009) that based on mitochondrial 16S rRNA and COI genes, the farmed population of *C. nobilis* has a higher genetic diversity index than the wild population. In addition, similar observations have also been documented in other marine organisms, such as *Salvelinus alpinus* (Primmer et al., 1999) and *Salmo salar* L. (Elliott and Reilly, 2003).

In farmed stocks, it is generally believe that genetic variation is positively associated with the number of broodstock used. However, we found that all hatchery populations showed significant heterozygosity deficiency. In hatchery populations, heterozygote deficiency is typically considered to result from inbreeding. Although there was significant heterozygosity deficiency in all hatchery populations, the diversity levels of hatchery populations were still higher than the wild population. Therefore, the possibility explanation for this phenomenon is that the possibility of inbreeding was very small, which maybe due to the mixing of broodstock during selection and propagation process (Pucher et al., 2013). The results of Bayesian assignment test confirmed that the genetic admixture of germplasms in

TABLE 4 | Analysis of molecular variance (AMOVA) of 10 microsatellite loci in five *C. nobilis* populations.

Source of variation	Degrees of freedom	Sum of squares	Variance components	Percentage of variation (%)	*P* value
Among populations within groups	4	124.044	0.44496	11.79	0.000
Among individuals within populations	147	582.463	0.63413	16.81	0.000
Within individuals	152	409.500	2.69408	71.40	0.000
Total	303	1116.007	3.77316		

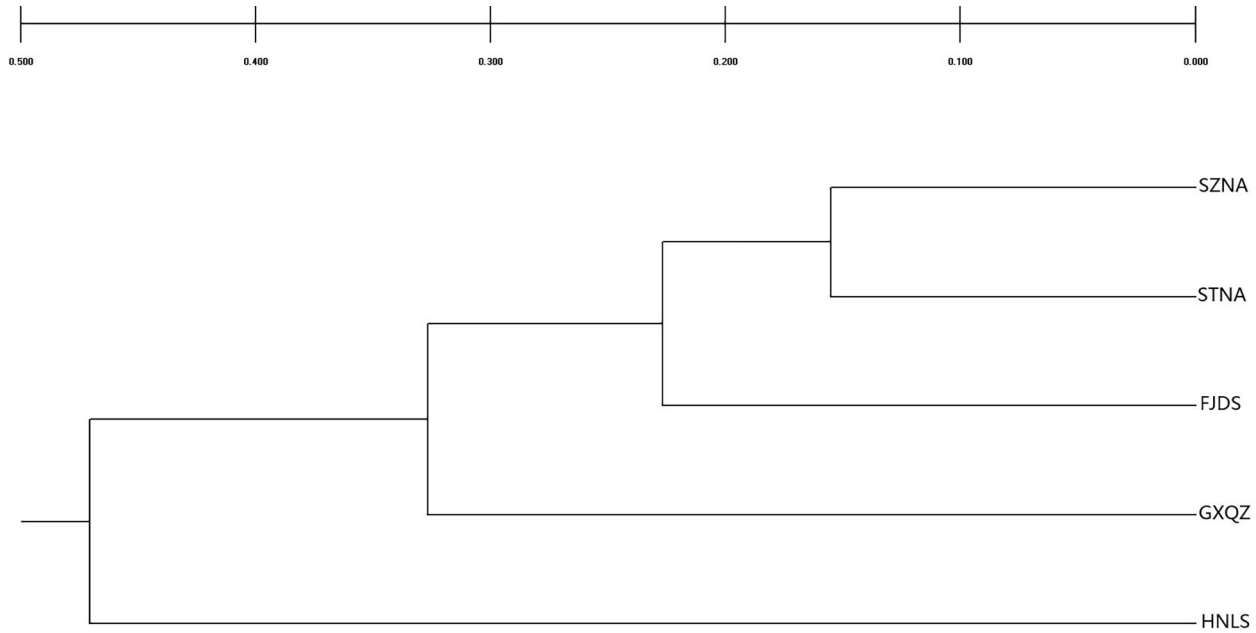

FIGURE 3 | UPGMA dendrogram showing the phylogenetic relationships among five samples of *C. nobilis*, based on a matrix of genetic distance (Nei, 1972). Bootstrap values are given for nodes at least 62% or more support.

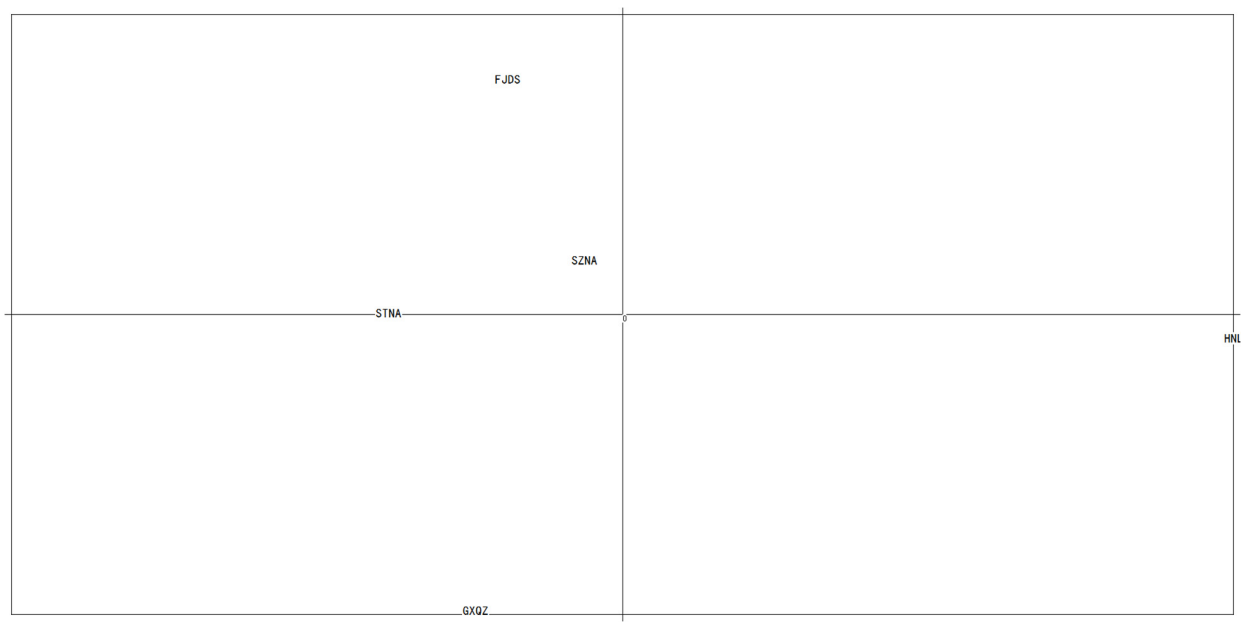

FIGURE 4 | Principal component analysis plotting the relationships of *C. nobilis* populations, based on a matrix of genetic distance (Nei, 1972).

the farmed *C. nobilis* populations is significant. Therefore, the effect of reduced genetic diversity caused by heterozygote deficiency was offset by the effect of increasing genetic diversity of broodstock from multiple wild populations. It is not unclear whether this high polymorphism caused by genetic admixture is beneficial to the survival of this species. In Vietnam, Thai et al. (2007) found that the levels of genetic diversity of carp in most hatchery was similar to that of wild carp populations, and the high genetic diversity of farmed carp was mainly contributed by hybridization with imported stocks.

The highest mean heterozygosity observed across all loci was in the wild population (HNLS) compared to all hatchery populations and was nearly identical to its mean expected heterozygosity because the wild population was in HWE.

However, all examined farmed populations showed significant deviations from Hardy–Weinberg equilibrium. These deviations were mainly caused by heterozygote deficiency. In farmed *C. nobilis* populations, heterozygote deficiency is typically considered to be caused by a limited number broodstock and/or, inbreeding (Kohlmann et al., 2005; An et al., 2011). In our case, the significant deviations from HWE in hatchery populations were caused by genetic admixture. Accordingly, others have also observed high proportions of deviation from HWE in previous studies of *C. nobilis* (Hui et al., 2006).

The genetic differentiation measured by the *Fst* values is generally described as negligible (0–0.05), moderate (0.05–0.15), great (0.15–0.25), and very great (above 0.25) (Wright, 1978; Hartl and Clark, 1997). In our study, negligible and moderate genetic differentiation was identified in four farmed *C. nobilis* populations. Great genetic differentiation was found between wild and hatchery *C. nobilis* populations, except for between wild and SZNA. The AMOVA further indicated that there was significant genetic differentiation among the five populations. The significant genetic differences among Chinese farmed populations and the population of Hainan were clearly differentiated from other populations, which Yuan et al. (2009) also found. However, they did not analyze the cause of this significant differentiation. The results from the Bayesian assignment test indicate that it may be caused by founder effects and admixture.

Bayesian assignment test showed that the genetic admixture was significant and widespread in artificial breeding of *C. nobilis*. In this study, individuals from the wild *C. nobilis* population form a single genetic group, which suggests that the wild population in Lingshui, Hainan province did not mixed with other populations. Therefore, more attention should be paid to its protection.

The UPGMA tree topology and PCA showed there is a clear division between wild and farmed *C. nobilis* populations. This genetic pattern showed that STNA and SZNA farmed populations are closely related, and that STNA and SZNA could have derived from similar broodstock.

Recently, the reduction of wild scallop resources has led to an increase in the transfer of seed and stock for aquaculture. Contradict with previous reports (Yuan et al., 2009), our data revealed that due to genetic admixture, the genetic diversity of farmed *C. nobilis* populations is higher than that of the wild population. Although the four farmed *C. nobilis* populations still have considerable genetic variation, heterozygote deficiency and significant genetic differentiation populations were detected. Therefore, in order to achieve sustainable development of *C. nobilis* aquaculture and hatchery seed production, it is important that hatcheries to maintain an effective population sizes and avoid the breeding of closely related broodstock.

CONCLUSION

In conclusion, both wild *C. nobilis* population (HNLS), and farmed *C. nobilis* populations recorded high levels of genetic diversity. Interestingly, the genetic diversity of farmed *C. nobilis* populations was significantly higher than that of wild *C. nobilis* population, but the farmed *C. nobilis* populations showed significant heterozygosity deficiency. Since genetic admixture occur in the artificial breeding of *C. nobilis*, the effect of reducing genetic diversity due to heterozygote deficiency was offset by the effect of increased genetic diversity in broodstock from multiple wild populations. These findings of this study not only fill the knowledge gaps in the genetic diversity of wild and farmed *C. nobilis*, but also serve as guidelines for maintaining the genetic diversity of *C. nobilis* in both farmed and wild populations.

DATA AVAILABILITY STATEMENT

The original contributions presented in the study are included in the article/supplementary material, further inquiries can be directed to the corresponding authors.

AUTHOR CONTRIBUTIONS

YHZ and ZY conceived the study. HM and DY carried out the field and laboratory work, participated in the data analysis, and drafted the manuscript. SX and YQ collected the noble scallop populations. YZ and JL contributed to the microsatellite analysis. All authors approved the manuscript for publication.

FUNDING

This work was supported by the National Natural Science Foundation of China (31702340, 31872566, and 32002387), National Marine Genetic Resource Center, Guangdong Academy of Sciences (GDAS) Special Project of Science and Technology Development (2018GDASCX-0107), the Chinese Ministry of Science and Technology through the National Key Research and Development Program of China (2018YFD0901400 and 2020YFD0901100), Key Special Project for Introduced Talents Team of Southern Marine Science and Engineering Guangdong Laboratory (Guangzhou) (GML2019ZD0404), the Network Service Local Plan STS of the Chinese Academy of Sciences (KFJ-STS-QYZD-158), the Strategic Priority Research Program of the Chinese Academy of Sciences (XDA13020202), the Innovation Academy of South China Sea Ecology and Environmental Engineering, Chinese Academy of Sciences (ISEE2018PY01 and ISEE2018ZD02), the Open Foundation of State Key Laboratory of Loess and Quaternary Geology (SKLLQG1813 and SKLLQG1918), the China Agriculture Research System of MOF and MARA, and the Science and Technology Planning Project of Guangdong Province, China (2017B030314052).

REFERENCES

An, H. S., Kim, E. M., Lee, J. H., Noh, J. K., An, C. M., Yoon, S. J., et al. (2011). Population genetic structure of wild and hatchery black rockfish *Sebastes inermis* in Korea, assessed using cross-species microsatellite markers. *Genet. Mol. Res.* 10, 2492–2504. doi: 10.4238/2011.october.13.6

Azuma, N., Kunihiro, Y., Sasaki, J., Mihara, E., Mihara, Y., Yasunaga, T., et al. (2008). Genetic variation and population structure of Hair Crab (*Erimacrusisenbeckii*) in Japan inferred from Mitochondrial DNA sequence analysis. *Mar. Biotechnol.* 10, 39–48. doi: 10.1007/s10126-007-9033-1

Benzie, J. A. H., and Williams, S. T. (1997). Genetic structure of Giant Clam (*Tridacna maxima*) populations in the West Pacific is not consistent with dispersal by present-day ocean currents. *Evolution* 51, 768–783. doi: 10.2307/2411153

Botstein, D., White, R. L., Skolnick, M., and Davis, R. W. (1980). Construction of a genetic linkage map in man using restriction fragment length polymorphisms. *Am. J. Hum. Genet.* 32, 314–331.

Bourne, N. F. (2000). The potential for scallop culture-the next millenium. *Aquac. Int.* 8, 113–122.

EIMousadik, A., and Petit, R. J. (1996). High level of genetic differentiation for allelic richness among populations of the argan tree [*Argania spinosa* (L.)Skeels] endemic to Morocco. *Theor. Appl. Genet.* 92, 832–839. doi: 10.1007/s001220050200

Elliott, N. G., and Reilly, A. (2003). Likelihood of a bottleneck even inthe history of the Australian population of Atlantic salmon (*Salmosalar* L.). *Aquaculture* 215, 31–44. doi: 10.1016/s0044-8486(02)00055-8

Evans, B., Bartlett, J., Sweijd, N., Cook, P., and Elliott, N. G. (2004). Loss of genetic variation at microsatellite loci in hatchery produced abalone in Australia (*Haliotis rubra*) and South Africa (*Haliotis midae*). *Aquaculture* 233, 109–127. doi: 10.1016/j.aquaculture.2003.09.037

Excoffier, L., Laval, G., and Schneider, S. (2005). Arlequin ver. 3.0: an integrated software package for population genetics data analysis. *Evol. Bioinform.* 1, 47–50.

Felsenstein, J. (1993). *PHYLIP (Phylogeny Inference Package) version 3.50*. Seattle: University of Washington.

Ferguson, M. M. (1995). "The role of molecular genetic markers in the management of cultured fishes," in *Molecular Genetics in Fisheries*, eds G. R. Carvalho and T. J. Pitcher (London: Chapman & Hall), 81–104. doi: 10.1007/978-94-011-1218-5_4

Fisher, R. A. (1958). *The Genetical Theory Of Natural Selection, 2nd Revised Edn*. New York: Dover Publication.

Food and Agriculture Organisation (FAO) (2020). *Fishery and aquaculture statistics. Global production by production source 1950-2018 (FishstatJ)*. Rome: FAO Fisheries and Aquaculture Department.

Gurney-Smith, H. J., Wade, A. J., and Abbott, C. L. (2017). Species composition and genetic diversity of farmed mussels in British Columbia. *Can. Aquac.* 466, 33–40. doi: 10.1016/j.aquaculture.2016.08.038

Hartl, D. L., and Clark, A. G. (1997). *Principles of population genetics, 3rd edn*. Sunderland: Sinauer Associates.

Hedgecock, D., and Sly, F. (1990). Genetic drift and effective population sizes of hatchery-propagated stocks of the Pacific oyster *Crassostrea gigas*. *Aquaculture* 88, 21–38. doi: 10.1016/0044-8486(90)90316-f

Hui, M., Bao, Z. M., Zhan, A. B., Hu, X., Lu, W., Chang, D., et al. (2006). Ten polymorphic dinucleotide microsatellite markers of the noble scallop *Chlamys nobilis*. *Mol. Ecol. Notes* 6, 1033–1035. doi: 10.1111/j.1471-8286.2006.01420.x

Janson, S., Wouters, J., Bonow, M., Svanberg, I., and Olsén, K. H. (2015). Population genetic structure of crucian carp (*Carassius carassius*) in man-made ponds and wild populations in Sweden. *Aquac. Int.* 23, 359–368. doi: 10.1007/s10499-014-9820-4

Kohlmann, K., Kersten, P., and Flajshans, M. (2005). Microsatellite-based genetic variability and differentiation of domesticated, wild and feral common carp (Cyprinus carpio L) populations. *Aquaculture* 247, 253–266. doi: 10.1016/j.aquaculture.2005.02.024

Li, Q., Xu, K. F., and Yu, R. H. (2007). Genetic variation in Chinese hatchery populations of the Japanese scallop (*Patinopecten yessoensis*) inferred from microsatellite data. *Aquaculture* 269, 211–219. doi: 10.1016/j.aquaculture.2007.04.017

Liu, B. Z., Dong, B., Xiang, J. H., and Zaizhao, W. (2007). The phylogeny of native and exotic scallops cultured in China based on 16S rDNA sequences. *Chin. J. Oceanol. Limnol.* 25, 85–90. doi: 10.1007/s00343-007-0085-x

Ma, H. T., and Yu, Z. N. (2009a). Development of twenty-two polymorphic microsatellite loci in the noble scallop, *Chlamys nobilis*. *Conserv. Genet.* 10, 1587–1590. doi: 10.1007/s10592-008-9800-1

Ma, H. T., and Yu, Z. N. (2009b). Isolation and characterization of twenty-three microsatellite loci in the noble scallop, *Chlamys nobilis*. *Conserv. Genet. Resour.* 1, 131–134. doi: 10.1007/s12686-009-9032-9

Nagashima, K., Sato, M., Kawamata, K., Nakamura, A., and Ohta, T. (2005). Genetic structure of Japanese scallop population in Hokkaido, analyzed by mitochondrial haplotype distribution. *Mar. Biotechnol.* 7, 1–10. doi: 10.1007/s10126-004-3046-9

Nei, M. (1972). Genetic distance between populations. *Am. Nat.* 106, 283–292.

Oosterhout, C. V., Hutchinson, W. F., Wills, D. P. M., and Shipley, P. (2004). MICRO-CHECKER: software for identifying and correcting genotyping errors in microsatellite data. *Mol. Ecol. Notes* 4, 535–538. doi: 10.1111/j.1471-8286.2004.00684.x

Petersen, J. L., Ibarra, A. M., and May, B. (2010). Nuclear and mtDNA lineage diversity in wild and cultured Pacific lion-paw scallop, *Nodipectensubnodosus* (Baja California Peninsula, Mexico). *Mar. Biotechnol.* 157, 2751–2767. doi: 10.1007/s00227-010-1534-1

Phinchongsakuldit, J., Chaipakdee, P., Collins, J. F., Jaroensutasinee, M., and Brookfield, J. F. Y. (2015). Population genetics of cobia (*Rachycentron canadum*) in the Gulf of Thailand and Andaman Sea: fisheries management implications. *Aquac. Int.* 21, 197–217. doi: 10.1007/s10499-012-9545-1

Piry, S., Alapetite, A., Cornuet, M. J., Paetkau, D., Baudouin, L., and Estoup, A. (2004). GENECLASS2: a software for genetic assignment and first-generation migrant detection. *J. Hered.* 95, 536–539. doi: 10.1093/jhered/esh074

Primmer, C. R., Aho, T., Piironen, J., Estoup, A., Cornuet, J. M., and Ranta, E. (1999). Microsatellite analysis of hatchery stocks and naturalpopulations of Arctic charr, *Salvelinus alpinus*, from the Nordicregion: implications for conservation. *Hereditas* 130, 277–289. doi: 10.1111/j.1601-5223.1999.00277.x

Pucher, J., Steinbronn, S., Mayrhofer, R., Schad, I., El-Matbouli, M., and Focken, U. (2013). "Improved sustainable aquaculture systems for small-scale farmers in northern Vietnam," in *Sustainable land use and rural development in southeast Asia: Innovations and policies for mountainous areas*, eds H. L. Fröhlich, P. Schreinemachers, K. Stahr, and G. Clemens (Berlin: Springer), 281–317. doi: 10.1007/978-3-642-33377-4_8

Raymond, M., and Rousset, F. (1995). GENEPOP Version 4.0: population genetics software for exact tests and ecumenicism. *J. Hered.* 86, 248–249. doi: 10.1093/oxfordjournals.jhered.a111573

Reed, D. H., and Frankham, R. (2003). Correlation between Fitness and Genetic Diversity. *Conserv. Biol.* 17, 230–237. doi: 10.1046/j.1523-1739.2003.01236.x

Rice, W. R. (1989). Analyzing tables of statistical tests. *Evolution* 43, 223–225. doi: 10.2307/2409177

Rohlf, F. J. (2005). *NTSYS-pc: Numerical Taxonomy and Multivariate Analysis System, Version 2.2*. Setauket: Exeter Software.

Sambrook, J. D., and Russell, W. (2000). *Molecular cloning: a laboratory manual, 2nd edn*. New York: Cold Spring Harbor Laboratory Press.

Sato, M., Kawamata, K., Zaslavskaya, N., Nakamura, A., Ohta, T., Nishikiori, T., et al. (2005). Development of microsatellite markers for Japanese scallop (*Mizuhopecten yessoensis*) and their application to a population genetic study. *Mar. Biotechnol.* 7, 713–728. doi: 10.1007/s10126-004-0127-8

Song, L., Xu, W., Li, C., Li, H., Wu, L., Xiang, J., et al. (2006). Development of expressed sequence tags from the bay scallop, *Argopecten irradians irradians*. *Mar. Biotechnol.* 8, 161–169. doi: 10.1007/s10126-005-0126-4

Tan, K. S., Leng, X., Zhao, Y., Hongxing, L., Cheng, D., Ma, H., et al. (2019). Amino acid variations in polymorphic noble scallops, *Chlamys nobilis*. *J. Food Process. Preserv.* 43:e14262.

Tan, K. S., Zhang, H. K., and Zheng, H. P. (2020b). Selective breeding of edible bivalves and its implication of global climate change. *Rev. Aquac.* 4, 2559–2572. doi: 10.1111/raq.12458

Tan, K. S., Zhang, H. K., Lim, L. S., and Zheng, H. (2020a). Selection breeding program of Nan'ao Golden Scallop *Chlamys nobilis* with higher nutritional

values and less susceptible to stress. *Aquaculture* 517:734769. doi: 10.1016/j.aquaculture.2019.734769

Thai, B. T., Burridge, C. P., and Austin, C. M. (2007). Genetic diversity of common carp (*Cyprinus carpio* L.) in Vietnam using four microsatellite loci. *Aquaculture* 269, 174–186. doi: 10.1016/j.aquaculture.2007.05.017

Williams, S. T., and Benzie, J. A. H. (1998). Evidence of a biogeographic break between populations of a high dispersal starfish: congruent regions within the Indo-West pacific defined by color morphs, mtDNA, and Allozyme Data. *Evolution* 52, 87–99. doi: 10.2307/2410923

Wright, S. (1978). *Evoulution And The Genetics Of Populations, Vol Iv: Variability Within And Among Natural Populations*. Chicago: University of Chicago Press.

Yeh, F. C., Yang, R., and Boyle, T. (1999). *A Microsoft Window Based Freeware for Population Genetic Analysis. Version 1.31*. Canada: University of Alberta.

Yuan, T., He, M. X., and Huang, L. M. (2009). Intraspecific genetic variation in mitochondrial 16S rRNA and COI genes in domestic and wild populations of Huaguizhikong scallop *Chlamys nobilis* Reeve. *Aquaculture* 289, 19–25. doi: 10.1016/j.aquaculture.2009.01.004

Zhan, A. B., Hu, J. J., Hu, X. L., Zhou, Z., Hui, M., Wang, S., et al. (2009). Fine-Scale Population Genetic Structure of Zhikong Scallop (*Chlamys farreri*): do Local Marine Currents Drive Geographical Differentiation?. *Mar. Biotechnol.* 11, 223–235. doi: 10.1007/s10126-008-9138-1

Conflict of Interest: The authors declare that the research was conducted in the absence of any commercial or financial relationships that could be construed as a potential conflict of interest.

Publisher's Note: All claims expressed in this article are solely those of the authors and do not necessarily represent those of their affiliated organizations, or those of the publisher, the editors and the reviewers. Any product that may be evaluated in this article, or claim that may be made by its manufacturer, is not guaranteed or endorsed by the publisher.

frontiers in Marine Science

ORIGINAL RESEARCH
published: 30 August 2021
doi: 10.3389/fmars.2021.725430

Gonad Transcriptome Analysis of the Razor Clam (*Sinonovacula constricta*) Revealed Potential Sex-Related Genes

Hanhan Yao[1,2], Zhihua Lin[2,3], Yinghui Dong[2], Xianghui Kong[2], Lin He[2] and Liangyi Xue[1]**

[1] College of Marine Sciences, Ningbo University, Ningbo, China, [2] Zhejiang Key Laboratory of Aquatic Germplasm Resources, Zhejiang Wanli University, Ningbo, China, [3] Institute of Mariculture Breeding and Seed Industry, Zhejiang Wanli University, Ningbo, China

OPEN ACCESS

Edited by:
Yuehuan Zhang, South China Sea Institute of Oceanology, Chinese Academy of Sciences, China

Reviewed by:
Xiaoting Huang, Ocean University of China, China
Zhiguo Dong, Jiangsu Ocean University, China

***Correspondence:**
Yinghui Dong
dongyinghui118@126.com
Liangyi Xue
xueliangyi@nbu.edu.cn

Specialty section:
This article was submitted to Marine Fisheries, Aquaculture and Living Resources, a section of the journal Frontiers in Marine Science

Received: *15 June 2021*
Accepted: *11 August 2021*
Published: *30 August 2021*

Citation:
Yao H, Lin Z, Dong Y, Kong X, He L and Xue L (2021) Gonad Transcriptome Analysis of the Razor Clam (Sinonovacula constricta) Revealed Potential Sex-Related Genes. Front. Mar. Sci. 8:725430. doi: 10.3389/fmars.2021.725430

The razor clam, *Sinonovacula constricta* is a commercially important bivalve in the western Pacific Ocean, yet little is known about the mechanisms of sex determination/differentiation and gametogenesis. In the present study, the comparative transcriptome analysis of adult gonads (female gonads and male gonads) was conducted to identify potential sex-related genes in *S. constricta*. The number of reads generated for each target library (three females and three males) ranged from 31,853,422 to 37,750,848, and 20,489,472 to 26,152,448 could be mapped to the reference genome of *S. constricta* (the map percentage ranging from 63.71 to 71.48%). A total of 8,497 genes were identified to be differentially expressed between the female and male gonads, of which 4,253 were female-biased (upregulated in females), and 4,244 were male-biased. Forty-five genes were identified as potential sex-related genes, including *DmrtA2*, *Sox9*, *Fem-1b,* and *Fem-1c* involved in sex determination/differentiation and *Vg, CYP17A1*, *SOHLH2*, and *TSSK* involved in gametogenesis. The expression profiles of 12 genes were validated by qRT-PCR, which further confirmed the reliability and accuracy of the RNA-Seq results. Our results provide basic information about the genes involved in sex determination/differentiation and gametogenesis, and pave the way for further studies on reproduction and breeding in *S. constricta* and other marine bivalves.

Keywords: *Sinonovacula constricta*, gonad, transcriptome analysis, sex determination/differentiation, gametogenesis

INTRODUCTION

The razor clam, *Sinonovacula constricta* is a marine bivalve, living in the lower to mid intertidal zones along the western Pacific Ocean coast (Morton, 1984; Wang and Xu, 1997). Razor clam farming began almost 500 years ago in southeastern China, particularly in the coastal areas of Fujian and Zhejiang Province (Wang et al., 1993). In China, *S. constricta* has become one of the most commercially important cultured clam species and has huge market potential. Therefore, it is urgent to further improve the technique in the field of artificial propagation and culture of this

species. For the *S. constricta* selection program, the aim is to construct inbred lines with a variety of traits, such as rapid growth, that underlie successful reproduction.

Compared with other economically important molluscan species, *S. constricta* is diecious (i.e., with fixed gender; individuals do not change sex), and the gonad maturation period is from September to October (Wu and Xu, 2000). Furthermore, it is difficult to differentiate between female and male clams with external morphological characteristics, especially before sex maturity (Wang et al., 1993). Therefore, gonadal maturity and synchronicity cannot be estimated by appearance, yet they are important factors for successful artificial reproduction. In the artificial reproduction conditions of bivalves, the successful hatching of selected spat relies on production of gametes and embryos from synchronous breeders. Therefore, it is essential to achieve genetic improvement for controlled reproduction, which depends on understanding molecular mechanisms and factors that control reproduction (Vahirua-Lechat et al., 2008; Moullac et al., 2013). However, the mechanisms that underlie gonad development and sex determination/differentiation in *S. constricta* are poorly understood, and there is no gene yet identified as an actor involved in gonad development or sex determination.

Gender is the product of sex determination/differentiation. Genetic or environmental processes that establish the gender of an organism, lead to specific molecular cascades, which can change an undifferentiated gonad into an ovary or a testis (Penman and Piferrer, 2008; Piferrer and Guiguen, 2008). Previous genetic studies have shown that some genes expressed in a sexually dimorphic manner in the progress of activation of the ovarian or testis pathway or repression of the alternative pathway, and this process determines the resulting sex or gonad development in model organisms (Piferrer and Guiguen, 2008). In bivalves, studies have identified some genes related to sex determination/differentiation or gametogenesis, for example, *Dmrt* (Doublesex- and mab-3-related transcription factor) and *SoxE* involved in male determination in *Crassostrea gigas* (Naimi et al., 2009a; Santerre et al., 2014), and *Foxl2* and *Beta-catenin* involved in female determination in *Chlamys farreri* (Liu et al., 2012; Li et al., 2014). In recent years, transcriptome sequencing analysis has been widely used to screen for potentially sex-related genes in bivalves. In *C. gigas*, genes involved in sex-determining pathways, such as *SoxH* and *Foxl2* were identified by male and female gonad transcriptome analysis (Zhang et al., 2014). In *Pinctada margaritifera*, genes such as *Dmrt*, *Fem-1*, *Foxl2,* and *Vitellogenin* (*Vg*) were identified as potential sex differentiation/determining genes based on transcriptional change in male and female gonads at different development stages (Teaniniuraitemoana et al., 2014). In *Patinopecten yessoensis*, transcriptome sequencing revealed that the *Foxl2* gene was ovary-biased and *Dmrt1*, *SoxH*, *Fem-1*, and *Sox9* were testis-biased (Yang et al., 2016; Li et al., 2016; Zhou et al., 2019). In *Tegillarca granosa*, genes such as *Sox, Foxl2*, and *Beta-catenin* were identified as sex-related genes from the gonad transcriptome data (Chen et al., 2017). The *Vg* gene was identified to be expressed especially in female gonads in *C. gigas* (Matsumoto et al., 2003), *C. farreri* (Qin et al., 2012), and *P. yessoensis* (Yang et al., 2016). Clearly, studies on sex-related genes not only contribute to improving our knowledge about molecular mechanisms of sex determination/differentiation and gonad development, but also may be applicable to reproductive control of cultured mollusks. However, little is known about the sex-related genes in *S. constricta*.

Recently, the genomic sequence and a large number of transcriptomic data of *S. constricta* have been available (Niu et al., 2013; Ran et al., 2019; Dong et al., 2020), however, the genes related with sex determination/differentiation or gametogenesis were still not identified. In this study, we analyzed the female and male gonadal transcriptomes of *S. constricta* using Illumina sequencing technology, compared expression patterns of differentially expressed genes between female and male gonads, and identified potential sex-related genes. This study aims to identify genes that potentially involved in sex determination/differentiation or gametogenesis. Our results will be useful for further studies on reproduction control and artificial propagation practice in *S. constricta*.

MATERIALS AND METHODS

Animal Sampling and RNA Extraction

Two-year-old mature clams were collected from the Technology Innovation Base of Marine and Fisheries of Ningbo, Zhejiang province, China and used for gonadal transcriptomic sequencing. During the reproduction season, the mature gonads of *S. constricta* are full of sperms or eggs. The gender of clams was confirmed by observing the presence of sperms or eggs under a microscope. Three female and three male clams were selected, and their gonad tissues were sampled and frozen in liquid nitrogen and then stored at −80°C until RNA extraction. The three females were designed as *ScF1*, *ScF2*, and *ScF3* and three males were designed as *ScM1*, *ScM2*, and *ScM3*. Total RNA from each gonad tissue was isolated with Trizol reagent (Invitrogen, United States) according to manufacturer's instructions. DNase I was used to remove DNA contamination from the isolated RNA, and the RNA quantity and quality were evaluated by an Agilent 2100 Bioanalyzer (Agilent Technologies, Santa Clara, United States).

cDNA Library Construction, Sequencing, and Reference-Based Assembly

Six cDNA libraries were constructed according to the standard protocol provided by Biomarker Technologies Co. (Beijing, China). Briefly, mRNA was purified from total RNA with oligo (dT) magnetic beads and fragmented with divalent cations buffer under elevated temperature. First-strand cDNA was generated using random hexamer-primed reverse transcription followed by the synthesis of second-strand cDNA using RNase H and DNA polymerase I. Then the double-strand cDNA was purified and washed with elution buffer followed by end reparation, dA-tailing and ligated to sequencing adapters. Afterward, adaptor-ligated fragments were purified, and suitable fragments were chosen as templates for PCR amplification. The prepared cDNA libraries

were sequenced on the Illumina HiSeq 2500 platform (San Diego, United States) with 150 bp paired-end model.

The raw reads from the six samples were pre-processed by trimming the adaptor sequences and filtering the ambiguous or low-quality short reads with software (Grabherr et al., 2011). Then the resulting high-quality reads from all samples were mapped to the reference genome of *S. constricta* (WSYO00000000.1) using HISAT2 (Kim et al., 2015). String Tie software (Shen et al., 2014) were used to assemble mapped reads and compared with reference genome annotation to discover novel genes. All novel genes were subjected to annotation with different databases, including Swiss-Prot,[1] NR (NCBI non-redundant protein database),[2] GO (Gene Ontology), and KEGG (Kyoto Encyclopedia of Genes and Genomes).[3] BLASTX searches were conducted in the NR database and Swiss-Prot database with an *e*-value threshold of 1E–5.

Sample Relationship Analysis

The correlation coefficient between biological replicates was used to evaluate sample repeatability, and low correlation sample was removed for further analysis. In order to study the global transcriptomic differences and correlation among samples from the two sexes, Principal component analysis (PCA) was conducted and a heat map was generated. PCA was performed on the basic of the average fragments per kilobase of transcript per million mapped reads (FPKM) values for all expressed genes in each sample, and sample repeatability analysis was presented via heat map using R scripts.

Analysis of DEGs (Differentially Expressed Genes) and Function Enrichment

Gene expression level was generally estimated by mapping clean reads to the trinity transcript assembly by RSEM for each sample (Li and Dewey, 2011). Meanwhile, the gene expression level was presented in a normalized expressed value as FPKM. Afterward, reconstruction of transcript assemblies was performed by the reference genome annotation-based transcripts assembly program within the Cufflinks software package to obtain a comprehensive set of transcripts for further differential analysis. The DESeq2 R package was used to identify differentially expressed genes (DEGs) between the two sexes (Anders and Huber, 2010). DEGs were defined as |Log2FoldChange| $>$ 1 and a false-discovery rate $<$ 0.01. The transcriptional pattern variations between the two sexes were assessed by DEG union, and R scripts were used to generate a heat map of the DEGs.

For enrichment analysis, all DEGs were mapped to terms in the KEGG and GO databases using BLAST algorithm with an *E*-value of $\leq$ 1e–5, and the significantly ($P < 0.05$) enriched KEGG and GO terms in DEGs were identified compared with the transcriptome background.

[1]http://www.ebi.ac.uk/swissprot/

[2]http://www.ncbi.nlm.nih.gov/

[3]http://www.genome.jp/kegg/

Gene Expression Analysis by Quantitative Real-Time PCR (qRT-PCR)

To validate the transcriptome sequencing data and the genes that might be potential sex-related genes obtained from DESeq analysis, 12 DEGs were chosen and quantified using quantitative real-time PCR (qRT-PCR). Total RNA was first extracted from each sample by using Trizol Reagent (Invitrogen), and cDNA was then synthesized using the PrimeScript^{TM} RT reagent Kit with gDNA Eraser (Takara, Japan). Finally, qRT-PCR was performed using iTaq Universal SYBR Green Supermix (Bio-Rad, United States) according to manufacturer's instructions on an ABI 7500 Fast Real-time PCR System (Applied Biosystems, United States). The 18S rRNA gene was chosen as the reference gene to serve as an internal control. The 12 pairs of prime sequences used for qRT-PCR analysis were listed in **Table 1**. Each 20 μL reaction system contained the following components: 10 μL iTaq Universal SYBR Green Supermix, 1 μL each primer, 0.8 μL cDNA, and 7.2 μL deionized water. The procedure of qRT-PCR was set as following: 94°C for 20 s and 40 cycles of 94°C for 3 s, 60°C for 15 s, and 72°C for 10 s. The gene relative expression level was calculated with the $2^{-\Delta\Delta ct}$ methods, and the results were compared using one-way analysis of variance in SPSS 20.0 (SPSS, United States). $P < 0.05$ was considered to be statistically significant. The fold changes of 12 genes in female samples vs. male samples were calculated via FPKM, and the $\log_2$FoldChange values of these genes obtained by RNA-Seq and qRT-PCR were used for graphical presentation.

To detect tissue expression pattern of some DEGs, eight tissues, including hepatopancreas, gill, mantle, siphon, adductor muscle, foot, female gonad and male gonad, were collected from three female and three male individuals, respectively, at mature stage. And gene expressions levels were analyzed by qRT-PCR followed the aforementioned procedure.

Sequence Analysis of Sex-Related Genes

The amino acid sequences used for sequence analysis were all retrieved from GenBank. Protein domain structure analysis was performed with SMART software. Multiple sequence alignments were performed by the ClustalW2 program and phylogenetic trees with bootstrap values were constructed with MEGA 7.0 software using the neighbor-joining method. The numbers in the branches of phylogenetic trees represent the bootstrap values from 1,000 replicates, and all the sequence GenBank accession numbers were listed in **Supplementary Table 1**.

RESULTS

Sequence Analysis and Gonad Transcriptome Assembly

To better understand the mechanism of sex determination/differentiation and gametogenesis in *S. constricta*, a comparative transcriptomic analysis was conducted. Six cDNA libraries (Female: *ScF1*, *ScF2*, and *ScF3*; Male: *ScM1*, *ScM2*, and *ScM3*) were sequenced and assembled. The number of reads generated for each library ranged from 31,853,422 to 37,750,848,

with Q30 values ranging from 94.34 to 94.79% (**Table 2**). Among the clean reads, the number of reads that could be mapped to the reference genome ranged from 20,489,472 to 26,152,448, and the percentage of clean reads ranged from 63.71 to 71.48% in the different libraries (**Table 2**). After alignment with the reference genome, 30,651 genes (including 10,092 novel genes) were obtained from global gonad transcriptomes, and 24,198 genes (including 5,279 novel genes) were function-annotated in the GO, NR, KEGG and Swiss-Prot databases. We deposited the transcriptome data into the NCBI Sequence Read Archive (SRA) under accession numbers SRR9937008–SRR9937013.

DEGs Identification and Function Enrichment Analysis

PCA revealed strong clustering associated with sex, and there were obvious differences in transcript expression between ovaries and testis excluding the *ScM1* sample (**Figure 1A**). Meanwhile, a heat map plot for sample relationship analysis also showed that sex identification of samples was exact, except for the *ScM1* sample (**Figure 1B**). The Pearson's correlation coefficient (r^2) were 0.102 and 0.264 between *ScM1* and *ScM2*, *ScM1,* and *ScM3*, respectively, with low coefficient, so the RNA-Seq data from the *ScM1* sample were excluded from further analysis.

For the differential expression analysis, 8,497 DEGs were identified between female gonad group and male gonad group. Compared to female gonad group, 4,244 genes were significantly up-regulated in male gonad group, accounting for 49.95% of all significant DEGs, and 4,253 genes were significantly down-regulated in male gonad group, accounting for 50.05% of all significant DEGs (**Figure 2**). Of all the significant DEGs, 6,823 genes were function-annotated in the GO, Swiss-Prot, KEGG and NR databases by BLASTX with a cut-off *E*-value of 1×10^{-5}.

To explore the potential functions of these DEGs in sex determination/differentiation and gametogenesis, GO and KEGG pathway enrichment analyses were performed.

TABLE 1 | The information of genes validated by qRT-PCR.

Gene ID	Gene name	Annotation	Primer sequence(5′–3′)
ctg423.9/MZ440691	*DmrtA2*	Doublesex and mab-3 related transcription factor A2-like protein	F: ACACCGAAATGTGCCAGA R: TCCCTCCAGCGACAATAA
ctg57.8/MZ440689	*Fem-1b*	Feminization-1b	F: TTCTTGGCGGAATGGACG R: TCGGATGTCTTGGTGGGC
ctg186.37/MZ440688	*Fem-1c*	Protein fem-1 homolog C-like	F: CAGATTTGGAACAGGTCGGAT R: AGATGCTGCTCTCAGTGGTGTT
ctg163.27/MZ440690	*Sox9*	Transcription factor SOX-9-like	F: ACCCACAAGCCCAGCCTAT R: GCGAGGTTGCCTTGGAAA
novel gene_19266	*CYP17A1*	Steroid 17-alpha-hydroxylase/17,20 lyase isoform X1	F: GGTGGCTCTCATTTGTGGTCTT R: AAGGCAGTCGTGATGTCGTTG
ctg318.17	*Smoktcr*	Sperm motility kinase Tcr mutant form-like	F: TGACCCCGTGTTCTGTAATG R: ATGGCACTGAACGGAATAGC
ctg1.91	*TSSK*	Testis-specific serine/threonine kinase	F: CCCGTTGATGTGAAGAAGGT R: ACTTTGAAAATCTCGTGGCG
ctg674.14	*GATA-7*	GATA zinc finger domain-containing protein 7-like	F: CGCACGCACCGCATTCAC R: ATGAGACGCTTCCGCCCG
novel gene _31922	*SOHLH2*	Spermatogenesis- and oogenesis-specific basic helix-loop-helix-containing protein 2	F: AGGGAGCGTATCAAGGACAGC R: TTGCCCTTCCTGTTGAAAATG
novel gene _13121	*FoxA1*	Forkhead box protein A1-A-like	F: GGGGTGGATAAGGAGAGTGG R: TGGGGTCCTGAAGCGATG
ctg1559.4	*Beta-catenin*	Beta-catenin	F: AGACCCTCTTCCAGCGTTTC R: GGCTTCACACAGGAACAGGT
novel gene _30040	*Vg*	Vitellogenin	F: CAGATGTGGTGTTAGAGATGGAAT R: GGACATACGAGAATGAGGTAGGTT
	18S rRNA		F: TCGGTTCTATTGCGTTGGTTTT R: CAGTTGGCATCGTTTATGGTCA

TABLE 2 | Summary statistics of gonad transcriptome sequencing for *S. constricta* from ovary and testis.

Sample ID	Female			Male		
	ScF1	ScF2	ScF3	ScM1	ScM2	ScM3
Clean reads	36,051,818	37,073,896	37,750,848	33,338,138	31,853,422	32,159,464
Base pairs	4,533,013,162	4,662,926,212	4,746,412,276	4,193,274,532	4,007,164,874	4,045,487,056
Mapped reads	25,768,615	25,789,370	26,152,448	22,453,357	20,553,483	20,489,473
Mapped percentage (%)	71.48%	69.56%	69.28%	67.35%	64.53%	63.71%

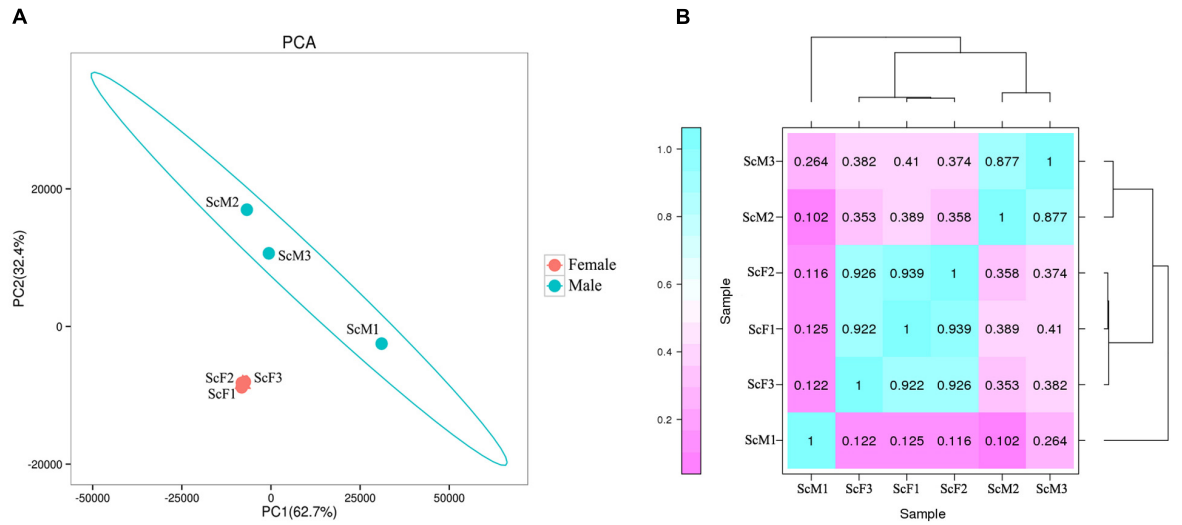

FIGURE 1 | Expression pattern analysis of gonad samples in *S. constricta.* **(A)** Principal components analysis (PCA) showed the strong clustering associated with sex except for *ScM1*. **(B)** Sample correlation heatmap plot revealed exact sex identification except for *ScM1*. Dark green represents strong correlation and dark pink represents weak correlation, and the number in each column and row correspond to the correlation coefficient of one sample with the other five samples including itself.

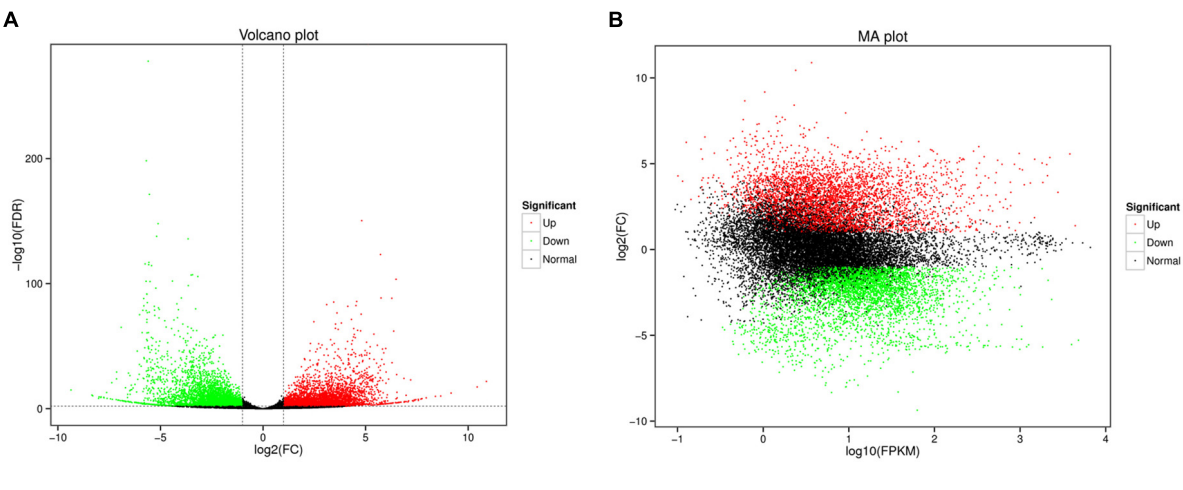

FIGURE 2 | Volcano plot **(A)** and MA plot **(B)** of DEGs (Green dots represented downregulated genes, the red dots represented upregulated genes).

GO functional enrichment analysis showed that 2,746 DEGs had a GO ID and could be categorized into 1,965 functional groups in three main categories: biological process, cellular component, and molecular function. Additionally, 151 GO terms were significantly enriched ($P < 0.05$). Biological process GO terms related to DNA repair (GO:0006281), DNA replication (GO:0006260), and nucleic acid phosphodiester bond hydrolysis (GO:0090305) were significantly enriched ($P < 0.05$), as were molecular function GO terms related to ATP binding (GO:0005524) and nucleic acid binding (GO:0003676) and cell cellular component GO terms related to nucleus (GO:0005634), catalytic step 2 spliceosome (GO:0071013), and Cdc73/Paf1 complex (GO:0016593) (**Figure 3**).

In the KEGG analysis, 1,364 DEGs had KEGG assignations and were associated with 221 pathways. **Figure 4** shows the top 20 enriched pathways. DNA replication, nucleotide excision repair, spliceosome, Fanconi anemia pathway, lysosome, RNA transport, and carbon metabolism were significantly enriched in KEGG pathways ($P < 0.05$), which showed patterns similar to those of the GO terms. Specifically, lysosome, endocytosis, phagosome, sphingolipid metabolism, carbon metabolism, and glycerophospholipid metabolism were significantly enriched in male gonad group ($P < 0.05$) (**Figure 4A**), whereas RNA transport, spliceosome, pyrimidine metabolism, ubiquitin mediated proteolysis, Fanconi anemia pathway, DNA replication, and nucleotide excision repair were significantly enriched in female gonad group ($P < 0.05$) (**Figure 4B**). Some of the

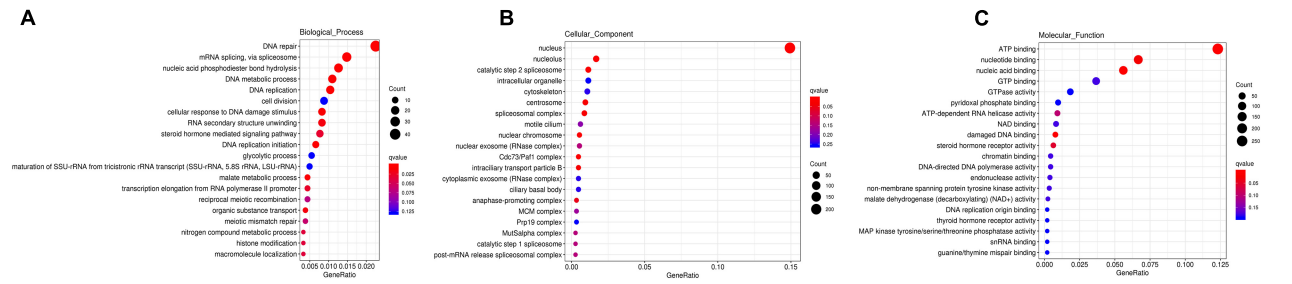

FIGURE 3 | GO functional enrichment of DEGs in biological process **(A)**, cellular component **(B)**, and molecular function **(C)**, respectively. The bigger the Rich factor or the smaller the *q*-value both indicates the more significant GO terms, and the bigger circle size indicates the higher number of genes.

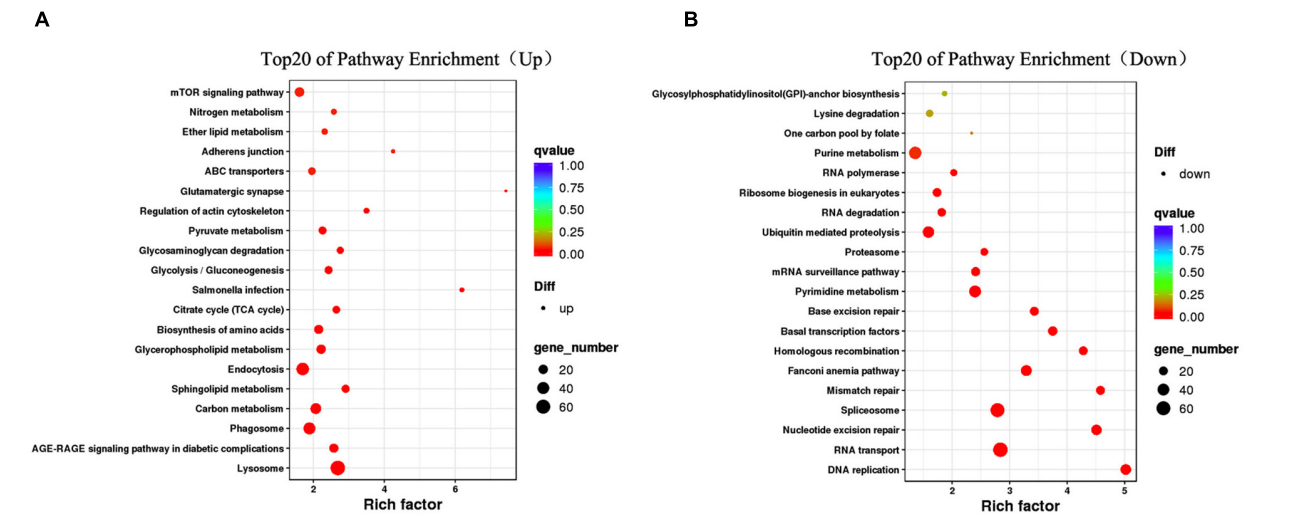

FIGURE 4 | Top20 KEGG pathway enrichment of upregulated DEGs **(A)** and downregulated DEGs **(B)**. The bigger the Rich factor or the smaller the *q*-value both indicates the more significant GO terms, and the bigger circle size indicates the higher number of genes.

DEGs were enriched in the progesterone-mediated oocyte maturation, estrogen signaling pathway, oocyte meiosis, oxytocin signaling pathway, ovarian steroidogenesis, mTOR signaling pathway, FoxO signaling pathway, Wnt signaling pathway, GnRH signaling pathway, ubiquitin-mediated proteolysis, and insulin secretion, which are known to be involved in male and female germ cell development. Some of these GO term and KEGG pathway enrichments were closely related to sex determination/differentiation or gametogenesis. At least 45 genes were identified as sex-related genes that might be involved in sex determination/differentiation or gametogenesis, and most of them were enriched in the GO function terms and KEGG pathways mentioned above (**Supplementary Table 2**).

Identification of DEGs Related to Sex Determination/Differentiation and Gonad Development

A heat map illustrating the hierarchical clustering of the genes differentially expressed between female and male gonads was conducted to visualize the overall gene expression pattern, and four clusters with similar gene expression patterns were generated (**Figure 5**). From the clusters, a catalog of 45 genes potentially involved in sex-determination/differentiation or gametogenesis was generated (**Supplementary Table 1**). The roles of these genes are unknown in *S. constricta*, but most of them have been identified as playing important roles in sex-determination/differentiation or gametogenesis in other organisms.

Cluster 1 included 277 genes, of which 41 genes showed significant similarities to known proteins, and 64 genes possessed GO assignations. And several genes known to be involved in male sex determination/differentiation were identified, including *Fem-1b* (*Fem-1b*, ctg57.8) and *Fem-1c* (*Fem-1c*, ctg186.37). Genes such as *E3 ubiquitin-protein ligase R2-like* (*R2,* novel gene_12556) and *sperm motility kinase Tcr mutant form-like* (*Smoktcr*, ctg318.17 and ctg318.18) were also found, and they have been described as playing roles in spermatogenesis.

In cluster 2(including 2,545 genes), *Beta-catenin* (*Beta-catenin,* ctg1559.4, and ctg1559.5) and *3-oxo-5-alpha-steroid 4-dehydrogenase 1* (*SRD5A1*, ctg350.13) were detected, and they are known to be involved in sex determination/differentiation. Genes

FIGURE 5 | Heatmap of DEGs in female and male gonads. Different columns represent different samples, different rows represent different genes, and the colors represent the gene expression levels [log10(FPKM + 0.000001)] in the samples. Green represents highly expressed genes, and red represents weakly expressed genes.

involved in oogenesis and oocyte maturation were also found, including *mitotic apparatus protein p62-like isoform X2* (MP62, ctg197.11) and *Lis1* (*Lis1*, ctg955.10). Some genes involved in catalyzing steroid biosynthesis and metabolism were also found, such as *17beta-HSD14* gene, which is of great importance to gametogenesis.

In cluster 3 (including 323 genes), we identified genes encoding proteins involved in spermatogenesis and oogenesis,

such as *spermatogenesis- and oogenesis-specific basic helix-loop-helix-containing protein 2* (*SOHLH2*, novel gene _31922) and *spermatogenesis-associated protein 24-like* (*SPATA24*, ctg9357.1). A few genes implicated in glycoprotein biosynthesis and metabolism were also found, such as *vitellogenin* (*Vg*, novel gene _30040) and *vitellogenin-6* (*Vg-6*, novel gene _30041), which are important for female gonad development.

Of the 5352 genes in cluster 4, a large number of genes were found to be differentially expressed between females and males and involved in oogenesis or spermatogenesis. Genes potentially involved in male sex determination included *double sex and mab-3 related transcription factor A2-like protein* (*DmrtA2*, ctg423.9) and *transcription factor Sox-9-like* (*Sox9*, ctg163.27). Genes implicated in spermatid differentiation and development, including *meiotic recombination protein SPO11-like* (*SPO11*, ctg915.3) and *testis-specific serine/threonine-protein* (*TSSK*, ctg1.91; *TSSK1*, ctg1.92; *TSSK4*, ctg207.28), were found, as were genes associated with oogenesis, including *cytochrome P450 26A1*(*CYP26A1*, ctg146.9) and *steroid 17-alpha-hydroxylase/17,20 lyase-like* (*CYP17A1*, ctg67.144). *Serine-protein kinase ATM-like isoform X2* (*ATM*, ctg637.23), which is involved in female gamete generation and oocyte development, was also identified.

Gene Expression and Sequence Analysis of Sex-Related Genes

Twelve genes were chosen for qRT-PCR analysis to validate the differential expression results identified by RNA-Seq. qRT-PCR results showed that the expression levels of *DmrtA2*, *Sox9*, *Fem-1b*, *Fem-1c*, *CYP17A1, Smoktcr, TSSK*, and *GATA-7* in male gonads were significantly higher than those in female gonads ($P < 0.05$, **Figure 6A**), whereas *SOHLH2, FoxA1*, *Beta-catenin*, and *Vg* were significantly highly expressed in female gonads than in male gonads ($P < 0.05$, **Figure 6B**). The expression patterns of these DEGs validated by qRT-PCR were generally consistent with the RNA-Seq results (**Figure 7**), which further confirmed the reliability and accuracy of the RNA-Seq data.

To investigate potential sex-related genes of *S. constricta*, four crucial genes *DmrtA2*, *Sox9*, *Fem-1b,* and *Fem-1c* were further examined and analyzed, and named *ScDmrtA2*, *ScSox9*, *ScFem-1b,* and *ScFem-1c* in *S. constricta*, respectively.

ScDmrtA2

A full-length transcript of *ScDmrtA2* (GenBank no.: MZ440691) was identified with an opening reading frame (ORF) of 1,170 bp encoding 389 amino acids. The deduced amino acids contain the DM domain (34–87 aa) consensus sequences (**Figure 8A1**). The phylogenetic tree showed that ScDmrtA2 was first clustered with DmrtA2 of *Hyriopsis cumingii*, and then grouped with the clade including scallops (*Pecten maximus* and *Mizuhopecten yessoensis*) and oysters (*C. gigas* and *Crassostrea virginica*). Finally, the molluscan DmrtA2 clade was clustered with the vertebrate DmrtA2 clade (**Figure 8A2**). Expression profile of *ScDmrtA2* in different adult tissues revealed that *ScDmrtA2* expressed significantly higher in mantle and gill ($P < 0.05$) than other tissues, and the expression level in male gonads is also significantly higher than that in female gonads ($P < 0.05$) (**Figure 8A3**).

ScSox9

ScSox9 (GenBank no.: MZ440690) was identified with ORF of 1,458 bp encoding 485 aa. An HMG domain consensus sequences were found from 76 to 146 aa in the deduced amino acids (**Figure 8B1**). The phylogenetic tree showed that ScSox9 was clustered with Sox9 of mollusks with the high bootstrap support (92), and then clustered with Sox9 of vertebrate species (bootstrap support 100) (**Figure 8B2**). Tissue expression analysis showed that *ScSox9* was expressed in all nine examined tissues, and expressed significantly higher in foot and adductor muscle than in other tissues ($P < 0.05$) (**Figure 8B3**). Meanwhile, the relative expression level of *ScSox9* in male gonads is about 4.25 folds higher than in female gonads.

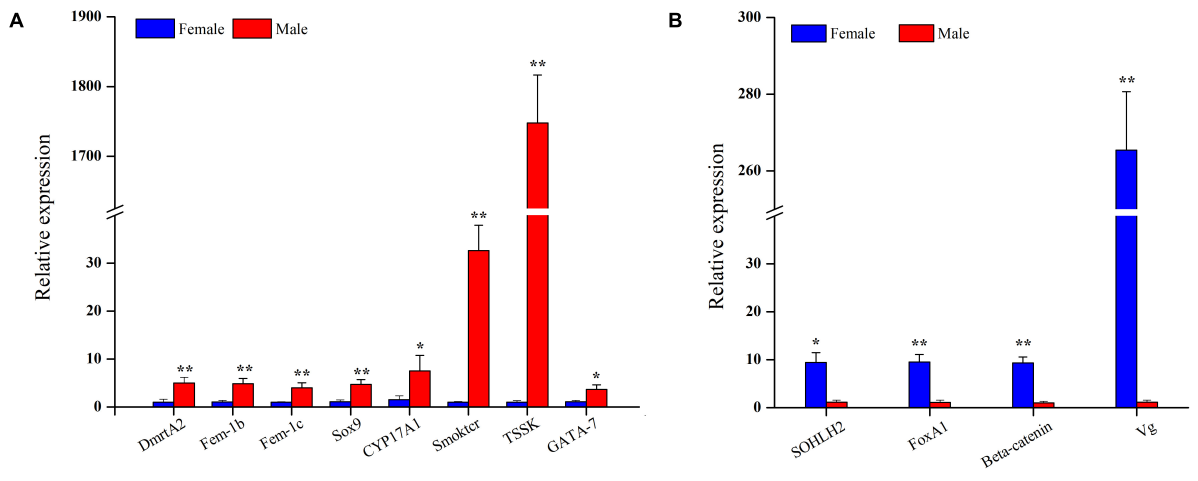

FIGURE 6 | Relative expression level of male-biased genes **(A)** and female-biased genes **(B)** between female and male gonads in *S. constricta* ($n = 4$). Significant differences between female and male gonads are indicated with an asterisk for $P < 0.05$, and with two asterisks for $P < 0.01$.

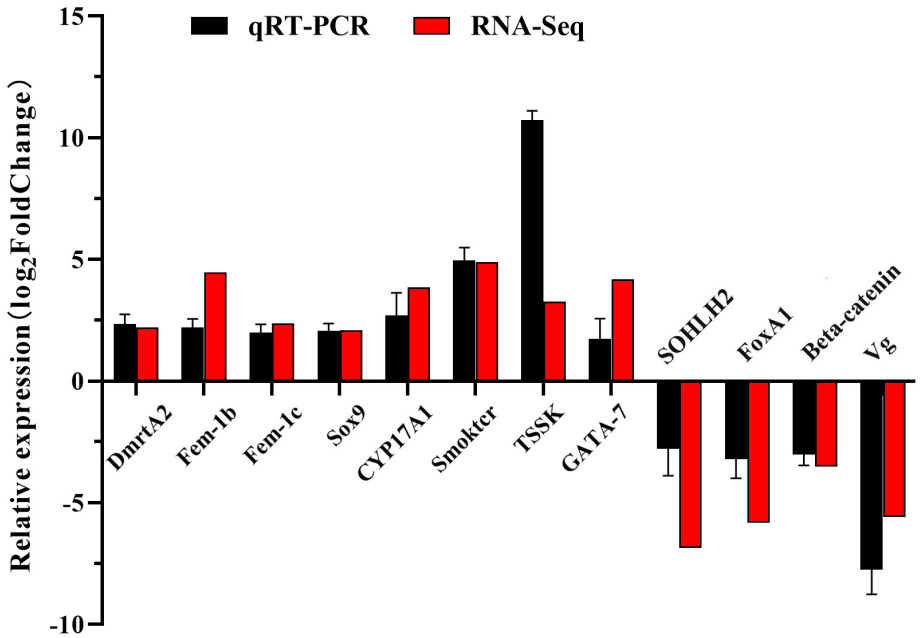

FIGURE 7 | qRT-PCR and RNA-seq validation results. Expression comparisons of 12 sex-biased gene in female and male gonads in *S. constricta*. The *Y*-axis represented log_2FoldChange determined by qRT-PCR and RNA-seq. The mean values and error bars were obtained from three biological and three technical replicates for qRT-PCR results.

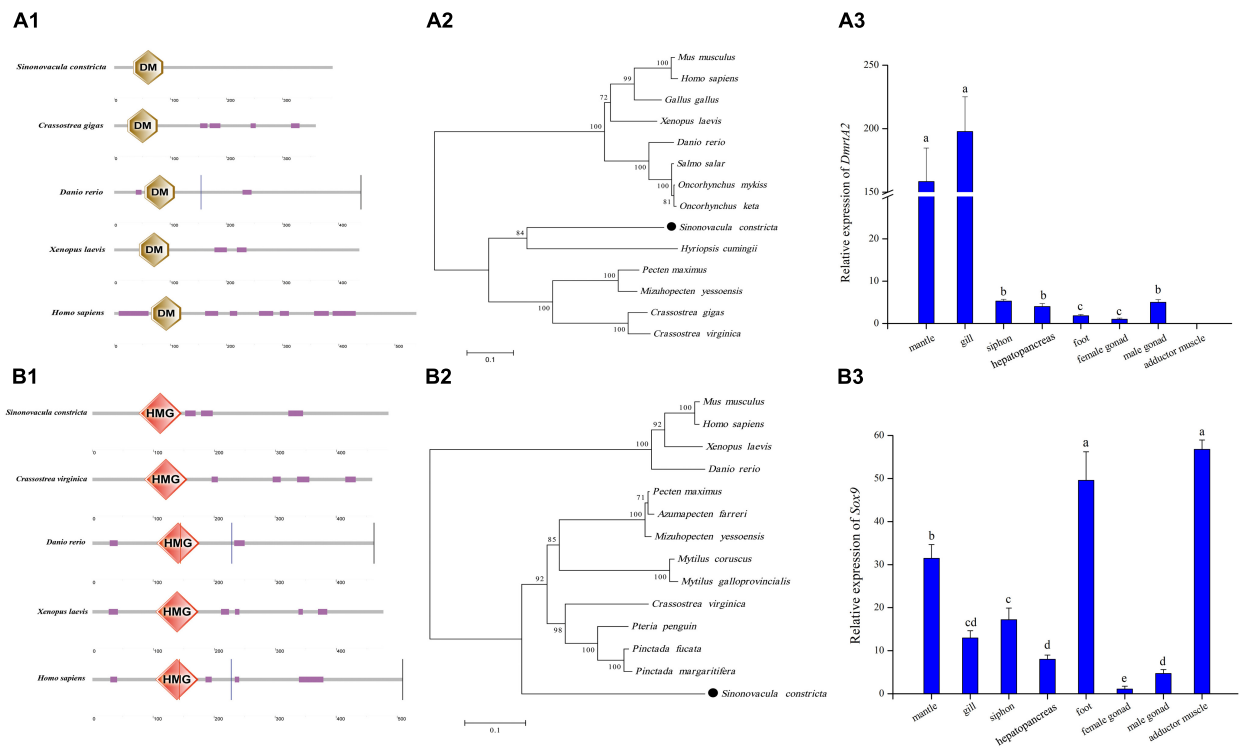

FIGURE 8 | Analysis of ScDmrtA2 and ScSox9 protein domains and their expression profile in adult tissues with standard deviation as error bars (n = 3) in *S. constricta*. **(A1)** DmrtA2 domain structures of razor clam and selected model species. **(A2)** The phylogenetic tree generated with DmrtA2 proteins. **(A3)** Relative expression level of *ScDmrtA2* in adult tissues. **(B1)** Sox9 domain analysis of razor clam and other model species. **(B2)** The phylogenetic tree generated using Sox9 proteins. **(B3)** Expression profile of *ScSox9* in adult tissues.

ScFem-1b and ScFem-1c

Two Fem-1 family genes, Fem-1b (GenBank no.: MZ440689) and Fem-1c (GenBank no.: MZ440688), were identified with complete ORF sequences of 1,911 and 1,869 bp, respectively. The deduced amino acid sequences of Fem-1b and Fem-1c were 636 and 622 aa, respectively, both of which contain seven ankyrin (ANK) repeats at N-terminus and two ankyrin repeats at C-terminus. The ANK repeats are characteristics of the Fem family proteins (**Figures 9A1,A2**). The phylogenetic tree showed that ScFem-1b and ScFem-1c had closer relationships to other mollusks, and were both grouped with mollusks with high bootstrap support (Fem1b 92 and Fem-1c 100), respectively (**Figure 9B**). Both *ScFem-1b* and *ScFem-1c* were expressed in all tissues, and both of them expressed at highest level in male gonads among all detected tissues (P<0.05) (**Figures 9C1,C2**).

DISCUSSION

By analyzing the female and male gonad transcriptome of *S. constricta*, we identified at least 45 sex-related genes, including *DmrtA2*, *Sox9*, *Fem-1b*, *Fem-1c*, and *Beta-catenin* potentially involved in sex determination or differentiation, and *Vg*, *CYP17A1, TSSK,* and *SOHLH2* potentially involved in gametogenesis.

Potential Sex Determination/Differentiation Genes in *S. constricta*

Four potential male sex determining genes (*DmrtA2*, *Sox9*, *Fem-1b*, and *Fem-1c*) were all expressed significantly higher in male gonads than in female gonads (P < 0.05). In vertebrates, *Dmrt* is an important gene involved in sex determination/differentiation, which is a transcription factor and contains a characteristic zinc finger DM domain (Guo et al., 2005; Kopp, 2012). Mammals have at least seven DM domain genes, most of them showed obvious gonadal expression (Xu et al., 2013). *DmrtA2* belongs to *Dmrt* family, and was expressed specially in testis in human, which suggested *DmrtA2* might be involved in sexual development (Ottolenghi et al., 2002). In adult zebrafish, *DmrtA2* was specially expressed in testis, ovary and brain, and the expression level is higher in testis than in ovary (Guo et al., 2004). Furthermore, zebrafish *DmrtA2* expression was restricted in developing germ cells and brain, especially in spermatogonia, spermatocytes, spermatids, and sperm cells, which suggested that *DmrtA2* was potentially involved in gonadal development and spermatogenesis (Guo et al., 2004; Xu et al., 2013). In this study, compared to female gonads, we detected significant elevation of *DmrtA2* gene expression in the testis of *S. constricta*, which might be involved in male gonad development and spermatogenesis, and this would be consistent with the patterns in zebrafish. *ScDmrtA2* were also detected to express significantly higher in mantle and gill than in other tissues (P < 0.05), and Yu et al. (2009) also found high expression of *DmrtA2* in mantle, gill, digestive diverticulum and adductor muscle besides male and female gonads in *Pinctada matensii*, suggesting that *DmrtA2* might exert other functions in mollusks.

We also found that the *Sox9* gene, a homolog of the *SoxE* gene, was male-biased and therefore might be a potential sex determination gene in *S. constricta*. The transcription factor *Sox9* containing an HMG domain, is a key gene in the mammalian testis determining pathway, and plays important roles in male gonadic differentiation and maintenance (Wagner et al., 1994; Knower et al., 2011). In *P. margaritifera*, the *Sox9* gene was also identified as a potential sex determination gene (Teaniniuraitemoana et al., 2014). The expression profiles of *SoxE* in *C. gigas* suggested its important roles in early sex differentiation (Santerre et al., 2014).

Fem-1 gene, as a sex-determining gene for male body development and spermatogenesis, was first discovered in

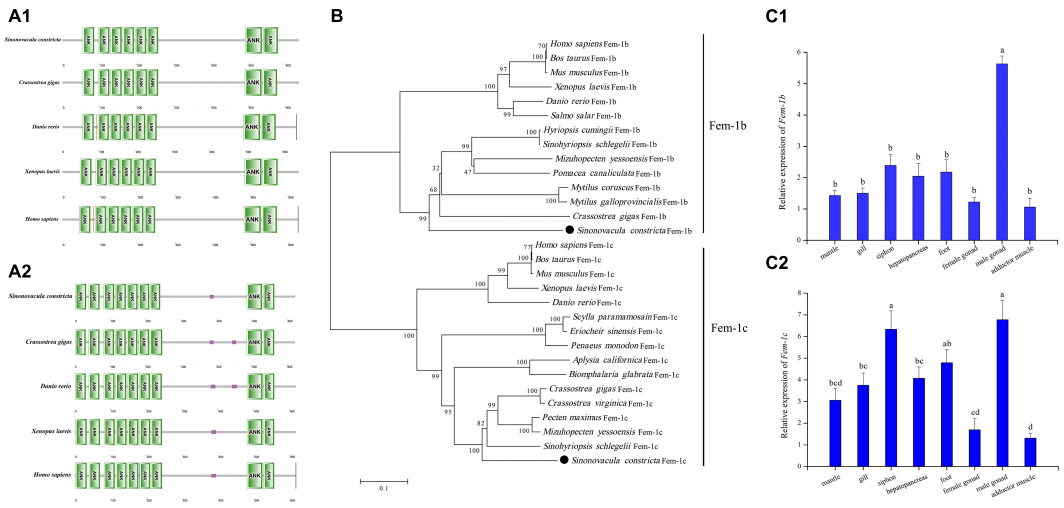

FIGURE 9 | Sequence analysis of ScFem-1b and ScFem-1c and their expression profile in adult tissues with standard deviation as error bars (n = 3). Domain analysis of ScFem-1b **(A1)** and ScFem-1c **(A2)** with that of other model species. The phylogenetic tree of Fem-1b and Fem-1c proteins **(B)**. Expression profile of *ScFem-1b* **(C1)** and *ScFem-1c* **(C2)** in adult tissues.

Caenorhabditis elegans (Ventura-Holman et al., 1998). In vertebrates, the *Fem-1* family contains three conservative members: *Fem-1a*, *Fem-1b*, and *Fem-1c*, which are able to feminize nematode sex differentiation (Ventura-Holman and Maher, 2000; Krakow et al., 2001; Ventura-Holman et al., 2003). The *Fem-1* gene identified in *P. margaritifera* was thought to be related to sex determination (Teaniniuraitemoana et al., 2014), and the *Fem-1c* gene in *P. yessoensis* showed upregulated expression in females (Yang et al., 2016). Using both qRT-PCR and RNA-Seq, we observed significant increases in mRNA levels of the *Fem-1b* and *Fem-1c* genes in male gonads of *S. constricta*, which suggested their functions in sex determination/differentiation.

FoxA1, *FoxD2*, and *Beta-catenin* were also identified to be involved in the female sex determination/differentiation in *S. constricta*. Fox gene family members are transcription factors and some of which play important roles in ovarian development (Shimeld et al., 2010). For example, the *Foxl2* gene has been found to be involved in ovary differentiation and maintenance in vertebrates (Ottolenghi, 2005; Uhlenhaut et al., 2009). In mollusks, the *Foxl2* gene has been identified in *C. farreri* (Liu et al., 2012), *C. gigas* (Naimi et al., 2009b; Zhang et al., 2014), *P. yessoensis* (Li et al., 2016; Yang et al., 2016), and *P. margaritifera* (Teaniniuraitemoana et al., 2014), and it is thought to be a master regulator of female sex determination or ovarian maintenance. However, we did not find the *Foxl2* gene in our RNA-Seq results of *S. constricta*, although *FoxA1* and *FoxD2* were present and ovary-biased. In the canonical Wnt signaling pathway, *Beta-catenin* is a key transcriptional regulator and is essential for ovarian development and maintenance in mammals (Liu et al., 2009). *Beta-catenin* was found to be localized in the oocytes of the ovary, and its expression was significantly high in the ovaries in *C. farreri* (Li et al., 2014). Here, *Beta-catenin* was expressed in both male and female gonads, however, its expression level was significantly higher in the ovaries than in the testis, which suggested *Beta-catenin* might play important roles in ovarian differentiation and maintenance in *S. constricta*.

Identification of Genes Involved in Gametogenesis

In our study, some genes putatively involved in oogenesis and spermatogenesis were also identified. For example, *Vg*, *Vg-6*, and *SOHLH2* were female-biased, and *CYP17A1*, *TSSK*, *TSSK1*, and *TSSK4* were male-biased in *S. constricta*. *Vg* or *Vg-6* as the storage protein and non-polar molecular carrier has been speculated to be involved in combining and transferring proteins, lipids, carotenoids and vitamin to oocytes during oogenesis (Wallace, 1985). In *C. farreri* and *C. gigas*, *Vg* was found to be specifically expressed in ovaries (Matsumoto et al., 2003; Qin et al., 2012). In *S. constricta*, the expression levels of *Vg* and *Vg-6* were significantly higher in ovaries than in testis, suggesting their important roles in oocyte development. *SOHLH2* is a universal transcription regulator of both male and female germline differentiation, with distinct and sex-specific downstream pathways that induce genes important to spermatogonia differentiation and coordinate oocyte differentiation without affecting meiosis I (Suzuki et al., 2011; Shin et al., 2017). In *S. constricta*, *SOHLH2* was expressed in both male and female gonads, with significantly higher expression in female gonads.

CYP17A1, a cytochrome P450 monooxygenase, is involved in the biosynthesis of steroid hormones, such as corticoid and androgen, which occurred in adrenal glands and gonads. Therefore, it indicates that *CYP17A1* is involved in gonad development (Yoshimoto et al., 2016). *TSSK*, *TSSK1*, and *TSSK4* exhibited high expression levels in male gonads of *S. constricta*. *TSSK* family members play important roles in cytoplasm reconstruction at the late stage of spermatogenesis. Knockout of *TSSK1* would result in spermatogonial or spermatocytic apoptosis deficiencies in mouse (Shang et al., 2010; Jha et al., 2013). Therefore, *TSSK*, *TSSK1*, and *TSSK4* were characterized as male-specific genes in adult mature gonads, indicating their important roles in spermatogenesis.

CONCLUSION

In conclusion, we identified 45 sex-related genes that might be potentially involved in sex determination/differentiation or gametogenesis in *S. constricta*. These genes included *DmrtA2*, *Sox9*, *Fem-1b,* and *Fem-1c* for sex determination/differentiation and *Vg, CYP17A1*, *SOHLH2*, and *TSSK* for gametogenesis. Identification of sex-related genes not only contributes to our understanding of reproduction in *S. constricta*, but also may be applicable to developing methods to control reproduction to support sustainable development of the clam farming.

DATA AVAILABILITY STATEMENT

The datasets presented in this study can be found in online repositories. The Illumina transcriptome raw data are available in the Sequence Read Archive (SRA) database at NCBI under accession number SRR9937008-SRR9937010 for female gonad and SRR9937011-SRR9937013 for male gonad of *S. constricta*. The names of the repository/repositories and accession number(s) can be found below: NCBI Genbank, accession numbers: MZ440688, MZ440689, MZ440690, and MZ440691.

AUTHOR CONTRIBUTIONS

YD and ZL conceived the project. XK collected the samples. HY, YD, and LH conducted the gonad transcriptome assembly, annotation, and transcriptome analysis. HY wrote the manuscript. LX revised the manuscript. All authors read and approved the manuscript.

FUNDING

This research was supported by the National Key Research and Development Program of China (2018YFD0901405), the National Natural Science Foundation of China (31902393), the National Marine Genetic Resource Center Program, the Ningbo

Major Project of Science and Technology (2019B10005), and the China Agriculture Research System of MOF and MARA.

ACKNOWLEDGMENTS

We sincerely thank Hongqiang Xu for the sample collection, Dr. Wenfang Dai for her suggestions on data analysis, and we thank Dr. Jianfeng Ren for editing our manuscript.

SUPPLEMENTARY MATERIAL

The Supplementary Material for this article can be found online at: https://www.frontiersin.org/articles/10.3389/fmars.2021.725430/full#supplementary-material

Supplementary Table 1 | Forty-five sex-related genes identified in *S. constricta*.

Supplementary Table 2 | The information sequences used in this study.

REFERENCES

Anders, S., and Huber, W. (2010). Differential expression analysis for sequence count data. *Genome Biol.* 11:R106. doi: 10.1038/npre.2010.4282.1

Chen, C., Xiao, G. Q., Chai, X. L., Lin, X. G., Fang, J., and Teng, S. S. (2017). Transcriptome analysis of sex-related genes in the blood clam *Tegillarca granosa*. *PLoS One* 12:e0184584. doi: 10.1371/journal.pone.0184584

Dong, Y. H., Zeng, Q. F., Ren, J. F., Yao, H. H., Lv, L. Y., He, L., et al. (2020). The chromosome-level genome assembly and comprehensive transcriptomes of the razor clam (*Sinonovacula constricta*). *Front. Genet.* 11:664. doi: 10.3389/fgene.2020.00664

Grabherr, M. G., Haas, B. J., Yassour, M., Levin, J. Z., Thompson, D. A., Amit, I., et al. (2011). Full-length transcriptome assembly from RNA-Seq data 481 without a reference genome. *Nat. Biotechnol.* 29, 644–652. doi: 10.1038/nbt.1883

Guo, Y., Cheng, H., Huang, X., Gao, S., Yu, H., and Zhou, R. (2005). Gene structure, multiple alternative splicing, and expression in gonads of zebrafish Dmrt1. *Biochem. Biophys. Res. Commun.* 330, 950–957. doi: 10.1016/j.bbrc.2005.03.066

Guo, Y., Qin, L., Shang, G., Xiang, Z., and Zhou, R. (2004). Molecular cloning, characterization, and expression in brain and gonad of Dmrt5 of zebrafish. *Biochem. Biophys. Res. Commun.* 324, 569–575. doi: 10.1016/j.bbrc.2004.09.085

Jha, K. N., Coleman, A. R., Wong, L., Salicioni, A. M., Howcroft, E., and Johnson, G. R. (2013). Heat shock protein 90 functions to stabilize and activate the testis-specific serine/threonine kinases, a family of kinases essential for male fertility. *J. Biol. Chem.* 288, 16308–16320. doi: 10.1074/jbc.M112.400978

Kim, D., Langmead, B., and Salzberg, S. L. (2015). HISAT: a fast spliced aligner with low memory requirements. *Nat. Methods* 12, 357–360. doi: 10.1038/NMETH.3317

Knower, K. C., Kelly, S., Ludbrook, L. M., Bagheri-Fam, S., Sim, H., Bernard, P., et al. (2011). Failure of SOX9 regulation in 46XY disorders of sex development with SRY, SOX9 and SF1 mutations. *PLoS One* 6:e17751. doi: 10.1371/journal.pone.0017751

Kopp, A. (2012). Dmrt genes in the development and evolution of sexual dimorphism. *Trends Genet.* 28, 175–184. doi: 10.1016/j.tig.2012.02.002

Krakow, D., Sebald, E., King, L. M., and Cohn, D. H. (2001). Identification of human *FEM1A*, the ortholog of a *C. elegans* sex-differentiation gene. *Gene* 279, 213–219. doi: 10.1016/S0378-1119(01)00756-9

Li, B., and Dewey, C. N. (2011). RSEM: accurate transcript quantification from RNA-seq data with or without a reference genome. *BMC Bioinformatics* 12:323. doi: 10.1186/1471-2105-12-323

Li, H., Zhang, Z., Bi, Y., Yang, D., Zhang, L., and Liu, J. (2014). Expression characteristics of beta-catenin in scallop *Chlamys farreri* gonads and its role as a potential upstream gene of dax1 through canonical wnt signalling pathway regulating the spermatogenesis. *PLoS One* 9:e115917. doi: 10.1371/journal.pone.0115917

Li, Y., Zhang, L., Sun, Y., Ma, X. L., Wang, J., Li, R. J., et al. (2016). Transcriptome sequencing and comparative analysis of ovary and testis identifies potential key sex-related genes and pathways in scallop *Patinopecten yessoensis*. *Mar. Biotechnol.* 18, 453–465. doi: 10.1007/s10126-016-9706-8

Liu, C. F., Bingham, N., Parker, K., and Yao, H. H. (2009). Sex-specific roles of beta-catenin in 794 mouse gonadal development. *Hum. Mol. Genet.* 18, 405–417.

Liu, X. L., Zhang, Z. F., Shao, M. Y., Liu, J. G., and Muhammad, F. (2012). Sexually dimorphic expression of foxl2 during gametogenesis in scallop *Chlamys farreri*, conserved with vertebrates. *Dev. Genes Evol.* 222, 279–286. doi: 10.1007/s00427-012-0410-z

Matsumoto, T., Nakamura, A. M., Mori, K., and Kayano, T. (2003). Molecular characterization of a cDNA encoding putative vitellogenin from the Pacific oyster *Crassostrea gigas*. *Zool. Sci.* 20, 37–42. doi: 10.2108/zsj.20.37

Morton, B. (1984). The functional morphology of *Sinonovacula constricta* with a discussion on the taxonomic status of the Novaculininae (Bivalvia). *J. Zool. Lond.* 202, 299–325. doi: 10.1111/j.1469-7998.1984.tb05085.x

Moullac, L. G., Soyez, C., Sham-Koua, M., Levy, P., Moriceau, J., Vonau, V., et al. (2013). Feeding the pearl oyster *Pinctada margaritifera* during reproductive conditioning. *Aquac. Res.* 44, 404–411. doi: 10.1111/j.1365-2109.2011.03045.x

Naimi, A., Martinez, A. S., Specq, M. L., Diss, B., Mathieu, M., and Sourdaine, P. (2009a). Molecular cloning and gene expression of Cg-Foxl2 during the development and the adult gametogenetic cycle in the oyster *Crassostrea gigas*. *Comp. Biochem. Physiol. B Biochem. Mol. Biol.* 154, 134–142. doi: 10.1016/j.cbpb.2009.05.011

Naimi, A., Martinez, A. S., Specq, M. L., Mrac, A., Diss, B., Mathieu, M., et al. (2009b). Identification and expression of a factor of the DM family in the oyster *Crassostrea gigas*. *Comp. Biochem. Phys. A* 152, 189–196. doi: 10.1016/j.cbpa.2008.09.019

Niu, D., Wang, L., Sun, F., Liu, Z., and Li, J. (2013). Development of molecular resources for an intertidal clam, *Sinonovacula constricta*, using 454 transcriptome sequencing. *PLoS One* 8:e67456. doi: 10.1371/journal.pone.0067456

Ottolenghi, C. (2005). Foxl2 is required for commitment to ovary differentiation. *Hum. Mol. Genet.* 14, 2053–2062. doi: 10.1093/hmg/ddi210

Ottolenghi, C., Fellous, M., Barbieri, M., and McElreavey, K. (2002). Novel paralogy relations among human chromosomes support a link between the phylogeny of doublesex-related genes and the evolution of sex determination. *Genomics* 79, 333–343. doi: 10.1006/geno.2002.6711

Penman, D. J., and Piferrer, F. (2008). Fish gonadogenesis. Part I: genetic and environmental mechanisms of sex determination. *Rev. Fish. Sci.* 16, 16–34. doi: 10.1080/10641260802324610

Piferrer, F., and Guiguen, Y. (2008). Fish gonadogenesis. Part II: molecular biology and genomics of sex differentiation. *Rev. Fish. Sci.* 16, 35–55. doi: 10.1080/10641260802324644

Qin, Z., Li, Y., Sun, D., Shao, M., and Zhang, Z. (2012). Cloning and expression analysis of the vitellogenin gene in the scallop *Chlamys farreri* and the effects of estradiol-17b on its synthesis. *Invertebr. Biol.* 131, 312–321. doi: 10.1111/ivb.12006

Ran, Z., Li, Z., Yan, X., Liao, K., Kong, F., Zhang, L., et al. (2019). Chromosome-level genome assembly of the razor clam *Sinonovacula constricta* (Lamarck, 1818). *Mol. Ecol. Resour.* 19, 1647–1658. doi: 10.1111/1755-0998.13086

Santerre, C., Sourdaine, P., Adeline, B., and Martinez, A. S. (2014). Cg-SoxE and Cg-β-catenin, two new potential actors of the sex-determining pathway in a hermaphrodite lophotrochozoan, the Pacific oyster *Crassostrea gigas*. *Comp. Biochem. Physiol. A Mol. Integr. Physiol.* 167, 68–76. doi: 10.1016/j.cbpa.2013.09.018

Shang, P., Baarends, W. M., Hoogerbrugge, J., Ooms, M., Cappellen, W. A., Antonius, A. W., et al. (2010). Functional transformation of the chromatoid body in mouse spermatids requires testis-specific serine/threonine kinases. *J. Cell. Sci.* 123, 331–339. doi: 10.1242/jcs.059949

Shen, S., Park, J. W., Lu, Z. X., Lin, L., Henry, M. D., Wu, Y. N., et al. (2014). rMATS: robust and flexible detection of differential alternative splicing from

replicate RNA-seq data. *Proc. Natl. Acad. Sci. U.S.A.* 111, E5593–E5601. doi: 10.1073/pnas.1419161111

Shimeld, S. M., Boyle, M. J., Brunet, T., Luke, G. N., and Seaver, E. C. (2010). Clustered Fox genes in lophotrochozoans and the evolution of the bilaterian Fox gene cluster. *Dev. Biol.* 340, 234–248. doi: 10.1016/j.ydbio.2010.01.015

Shin, Y. H., Ren, Y., Suzuki, H., Golnoski, K. J., Ahn, H. W., Mico, V., et al. (2017). Transcription factors SOHLH1 and SOHLH2 coordinate oocyte differentiation without affecting meiosis I. *J. Clin. Invest.* 127, 2106–2117. doi: 10.1172/JCI90281

Suzuki, H., Ahn, H. W., Chu, T., Bowden, W., Gassei, K., Orwig, K., et al. (2011). SOHLH1 and SOHLH2 coordinate spermatogonial differentiation. *Dev. Biol.* 361, 301–312. doi: 10.1016/j.ydbio.2011.10.027

Teaniniuraitemoana, V., Huvet, A., Levy, P., Klopp, C., Lhuillier, E., Gaertner-Mazouni, N., et al. (2014). Gonad transcriptome analysis of pearl oyster *Pinctada margaritifera*: identification of potential sex differentiation and sex determining genes. *BMC Genomics* 15:491. doi: 10.1186/1471-2164-15-491

Uhlenhaut, N. H., Jakob, S., Anlag, K., Eisenberger, T., Sekido, R., Kress, J., et al. (2009). Somatic sex reprogramming of adult ovaries to testes by FOXL2 ablation. *Cell* 139, 1130–1142. doi: 10.1016/j.cell.2009.11.021

Vahirua-Lechat, I., Laure, F., LeCoz, J. R., Bianchini, J. P., Bellais, M., and Le Moullac, G. (2008). Changes in fatty acid and sterol composition during oogenesis in the pearl oyster *Pinctada margaritifera*. *Aquac. Res.* 39, 1739–1746. doi: 10.1111/j.1365-2109.2008.02050.x

Ventura-Holman, T., Lu, D., Si, X., Izevbigie, E. B., and Maher, J. F. (2003). The Fem1c genes: conserved members of the Fem1 gene family in vertebrates. *Gene* 314, 133–139. doi: 10.1016/S0378-1119(03)00712-1

Ventura-Holman, T., and Maher, J. F. (2000). Sequence, organization, and expression of the human FEM1B gene. *Biochem. Biophys. Res. Commun.* 267, 317–320. doi: 10.1006/bbrc.1999.1942

Ventura-Holman, T., Seldin, M. F., Li, W., and Maher, J. F. (1998). The murine fem1 gene family: homologs of the *Caenorhabditis elegans* sex-determination protein FEM-1. *Genomics* 54, 221–230. doi: 10.1111/j.1365-2109.2008.02050.x

Wagner, T., Wirth, J., Meyer, J., Zabel, B., Held, M., Zimmer, J., et al. (1994). Autosomal sex reversal and campomelic dysplasia are caused by mutations in and around the SRY-related gene SOX9. *Cell* 79, 1111–1120. doi: 10.1016/0092-8674(94)90041-8

Wallace, R. A. (1985). "Vitellogenesis and oocyte growth in nonmammalian vertebrates," in *Oogenesis Developmental Biology*, Vol. 1, ed. L. W. Browder (Boston MA: Springer), 127–177. doi: 10.1007/978-1-4615-6814-8-3

Wang, R. C., Wang, Z. P., and Zhang, J. Z. (1993). *Marine Shellfish Aquaculture*. Qingdao: Qingdao Ocean University Press, 322–324.

Wang, W. X., and Xu, Z. Z. (1997). Larval swimming and postlarval drifting behavior in the infaunal bivalve *Sinonovacula constricta*. *Mar. Ecol. Prog. Ser.* 148, 71–81. doi: 10.3354/meps148071

Wu, H. X., and Xu, A. G. (2000). A test on artificial cultivation of *Sinonovacula constricta* (Lamark). *Mar. Sci.* 24, 15–17.

Xu, S., Xia, W., Zohar, Y., and Gui, J. F. (2013). Zebrafish *dmrta2* regulates the expression of cdkn2c in spermatogenesis in the adult testis. *Biol. Reprod.* 88:14. doi: 10.1095/biolreprod.112.105130

Yang, D., Yin, C., Chang, Y. Q., Dou, Y., Hao, Z. L., and Ding, J. (2016). Transcriptome analysis of male and female mature gonads of Japanese scallop *Patinopecten yessonsis*. *Genes Genomics* 38, 1041–1052. doi: 10.1007/s13258-016-0449-8

Yoshimoto, F. K., Gonzalez, E., Auchus, R. J., and Guengerich, F. P. (2016). Mechanism of 17α,20-lyase and new hydroxylation reactions of human cytochrome P450 17A1. *J. Biol. Chem.* 291, 17143–17164. doi: 10.1074/jbc.M116.732966

Yu, F. F., Gui, J. F., Zhou, L., Wang, M. F., and Yu, X. Y. (2009). Cloning and expression characterization of Dmrt5 in *Pinctada Martensii*. *Acta. Hydrobiol. Sin.* 33, 844–850. doi: 10.3724/SP.J.0000.2009.50844

Zhang, N., Xu, F., and Guo, X. (2014). Genomic analysis of the Pacific oyster (*Crassostrea gigas*) reveals possible conservation of vertebrate sex determination in a mollusc. *G3 (Bethesda)* 4, 2207–2217. doi: 10.1534/g3.114.013904

Zhou, L. Q., Liu, Z. H., Dong, Y. H., Sun, X. J., Wu, B., Yu, T., et al. (2019). Transcriptomics analysis revealing candidate genes and networks for sex differentiation of Yesso scallop (*Patinopecten yessoensis*). *BMC Genomics* 20:671. doi: 10.1186/s12864-019-6021-6

Conflict of Interest: The authors declare that the research was conducted in the absence of any commercial or financial relationships that could be construed as a potential conflict of interest.

Publisher's Note: All claims expressed in this article are solely those of the authors and do not necessarily represent those of their affiliated organizations, or those of the publisher, the editors and the reviewers. Any product that may be evaluated in this article, or claim that may be made by its manufacturer, is not guaranteed or endorsed by the publisher.

frontiers in Marine Science

ORIGINAL RESEARCH
published: 06 September 2021
doi: 10.3389/fmars.2021.742330

A Genome-Wide Association Study Identifies Candidate Genes Associated With Shell Color in Bay Scallop *Argopecten irradians irradians*

Xinghai Zhu[1†], *Junhao Zhang*[1†], *Xiujiang Hou*[1], *Pingping Liu*[1], *Jia Lv*[1], *Qiang Xing*[1,2*], *Xiaoting Huang*[1,2], *Jingjie Hu*[1,3] *and Zhenmin Bao*[1,2]

[1] *MOE Key Laboratory of Marine Genetics and Breeding, College of Marine Life Sciences, Ocean University of China, Qingdao, China,* [2] *Laboratory for Marine Fisheries Science and Food Production Processes, Qingdao National Laboratory for Marine Science and Technology, Qingdao, China,* [3] *Laboratory of Tropical Marine Germplasm Resources and Breeding Engineering, Sanya Oceanographic Institution of the Ocean University of China, Sanya, China*

OPEN ACCESS

Edited by:
Yuehuan Zhang, South China Sea Institute of Oceanology, Chinese Academy of Sciences, China

Reviewed by:
Weiwei You, Xiamen University, China
Hao Zhen Lin, Dalian Ocean University, China

***Correspondence:**
Qiang Xing
qiangxing@ouc.edu.cn

[†] *These authors have contributed equally to this work*

Specialty section:
This article was submitted to Marine Fisheries, Aquaculture and Living Resources, a section of the journal Frontiers in Marine Science

Received: *16 July 2021*
Accepted: *11 August 2021*
Published: *06 September 2021*

Citation:
Zhu X, Zhang J, Hou X, Liu P, Lv J, Xing Q, Huang X, Hu J and Bao Z (2021) A Genome-Wide Association Study Identifies Candidate Genes Associated With Shell Color in Bay Scallop Argopecten irradians irradians. Front. Mar. Sci. 8:742330. doi: 10.3389/fmars.2021.742330

Molluscan shell color has consistently drawn attention for its abundant diversity and commercial use in shellfish breeding projects. Recently, two new strains of bay scallop (*Argopecten irradians irradians*) with different shell colors as marked phenotypic traits have been artificially bred to improve their economic values; however, the inheritance mechanism of their shell pigmentation is still unclear. In this study, a genome-wide association study (GWAS) was conducted to determine the genetic basis of shell color in bay scallops utilizing 29,036 high-quality single-nucleotide polymorphisms (SNPs) derived from 80 purple-red (PP) and 80 black-brown (BP) shell color individuals. The result of the GWAS showed that 469 SNPs ($p < 1.72E{-}6$) significantly associated with shell color were mainly distributed in chromosome 7. The top three SNPs (i.e., chr7-12764003, chr7-13213864, and chr7-11899306) are located in the genic region of *G-protein-coupled receptor-like 101* (*GRL101*), *polyketide synthase 1* (*PKS1*), and *phosphoinositide phospholipase C* (*PLC1*), which have been widely reported to be involved in pigmentation. Successfully, the top three SNPs were verified in another non-breeding bay scallop population. Furthermore, Gene Ontology (GO) and Kyoto Encyclopedia of Genes and Genomes (KEGG) pathway analyses obtained 38 GO terms covering 297 genes and aggregating pathways involving 252 annotated genes. Specifically, the expression profiles of the top three identified candidate genes were detected in mantles of PP and BP individuals by real-time quantitative reverse transcription PCR. The significantly higher expression levels of *GRL101* (6.43-fold) and *PLC1* (6.48-fold) in PP, and *PKS1* (12.02-fold) in BP implied that *GRL101* and *PLC1* potentially functioned in PP shell coloration, and black pigmentation in BP might be principally regulated by *PKS1*. Our data provide valuable information for deciphering the phenotype differences of shell color in the bay scallop.

Keywords: genome-wide association study, *Argopecten irradians irradians*, shell color, single nucleotide polymorphism, candidate genes

INTRODUCTION

The shell of mollusks with diverse forms and alternative colors has always appealed to consumers and scientists (Comfort, 1950). Shell color of marine mollusks, an obvious and marked genetic-based phenotypic trait, has been proven to be closely related to production traits (Cong et al., 2014; Zhang et al., 2016). Therefore, shell color has been widely applied in the selective breeding project of economic shellfish, such as oysters (Xu et al., 2019; Han et al., 2020), mussels (Innes and Leslie, 1977; Li et al., 2014), scallops (Petersen et al., 2012; Ding et al., 2015), clams (Zhang et al., 2018; Nie et al., 2020), and abalones (Liu et al., 2007; Hoang et al., 2017). To reveal the mechanism of shell color formation, several investigations have been conducted and found multiple factors, ranging from environmental factors to inner genetic factors, contributing to the higher variability of shell color in mollusks (Underwood and Creese, 1976; Kraeuter et al., 1984). For example, researches demonstrated that water temperature differences (Heller, 1992), salinity variations (Sokolova and Berger, 2000), and diet sources (Marchais et al., 2017) could affect shell color formation in mollusks. On the aspect of genetic basis, shell color has been demonstrated to be determined by one or a small number of major gene(s) in some shellfish species (Cole, 1975; Palmer, 1985). For instance, experimental crosses of Manila clam, *Ruditapes philippinarum,* verified that pigmented coloration in two valves is controlled by at least two genes (Peignon et al., 1995). In noble scallop *Chlamys nobilis*, a one-locus-three-allele model was proposed to elucidate the distribution of four different color variants, and the brown shell color is controlled by a recessive allele distinct from the other colors (Zheng et al., 2013). Investigation in Pacific oyster, *Crassostrea gigas,* demonstrated that shell pigmentation is controlled by two genetic loci, with one responsible for the secretion of pigments and the other responsible for the distribution mode of pigmentation (Xu et al., 2019). Furthermore, transcriptomes and digital gene expression analysis of four different color clams, *Meretrix meretrix,* suggested that several potential genes and the Notch pathway played a crucial role in its shell color patterning (Yue et al., 2015). The same method was also exerted in two extreme color phenotypes of Yesso scallop, *Patinopecten yessoensis,* and 25 significantly differential expression genes were identified for unraveling shell color differences (Sun et al., 2016). These researches provided pivotal loci/genes responsible for the formation of shell coloration and served as candidate markers for mollusks breeding projects.

Biological pigments are considered as the key element of shell color diversity, and the distinct color is perceived because of different types of pigments, such as melanins, porphyrins, tetrapyrroles, and carotenoids, which had been identified in shellfish shells (Comfort, 1951; Stemmer and Nehrke, 2014). Melanins were first derived by oxidation and polymerization of tyrosine in animals or phenolic compounds in lower organisms (D'Iischia et al., 2013). Using the ultraviolet and infrared radiation spectral analysis, melanin was confirmed as the black pigment extracted from the scars where adductor muscle jointed shells in oysters (Hao et al., 2015). Eumelanin and pheomelanin, two forms of melanin, were verified to comprise the dark brown shell pigments with ∼76.6 and 23.4% components *via* spectrophotometry scanning and high-performance liquid chromatography in Yesso scallop (Sun et al., 2017). As for porphyrins, the cyclic structure of tetrapyrroles is often associated with red, brown, or purple shell coloration (Comfort, 1951). Investigation *via* modern chemical and multimodal spectroscopic techniques of shell pigments in marine snails *Clanculus pharaonius* and *Clanculus margaritarius* showed that pink-red dots and lines in shells were caused by porphyrins (Williams et al., 2016). Furthermore, carotenoids were regarded as the principal substance that presented orange adductor muscle and shell color in scallop since their first identification in the adductor muscle of rare orange Yesso scallop variants (Li et al., 2010). Subsequent analysis in reddish-orange and brown shell-color Yesso scallops identified candidate genes involved in carotenoid metabolism during shell color formation (Zhao et al., 2017). A similar result was also reported in noble scallop populations, in which individuals with orange shell color contained dramatically higher carotenoid content compared with the brown ones (Zheng et al., 2010).

The bay scallop, *Argopecten irradians irradians*, is polymorphic for shell color (purple, orange, yellow, or white) and possesses advantages of fast growth and high production in aquaculture (Shumway and Parsons, 2006; Wang et al., 2007). Selective breeding of bay scallops for better growth and tolerance performance has been consecutively conducted for generations from the 1980s in China (Zheng et al., 2004, 2011; Wang et al., 2017). Specifically, a potential phenotypic correlation between shell color and growth traits has been observed in artificially bred bay scallops (Wang et al., 2020). Consequently, understanding the genetic mechanism of shell color in bay scallops is of theoretical and economic importance. The first comprehensive classification of shell color based on experimental crosses in bay scallop showed that three background colors, six pattern colors, and the diversity of shell colors were under genetic control (Kraeuter et al., 1984; Elek and Adamkewicz, 1990). Subsequent study of shell color inheritance in selfing families found that orange or yellow parents produced both colorful and white progeny with a ratio of ∼3:1, implying that shell color in bay scallops was controlled by one locus being dominant. Furthermore, one amplified fragment length polymorphism (AFLP) marker was successfully identified in orange and white shell color bay scallops through genetic linkage analysis (Qin et al., 2007). Considering the large polymorphism of shell color in bay scallop, further genome-wide researches is still needed to identify the comprehensive candidate loci/genes and to explore the potential molecular mechanism.

Genome-wide association study (GWAS) is an accurate and powerful tool to identify novel genetic variants loci underlying complex traits and has been broadly applied in various fields (Zhao et al., 2011; Kim et al., 2012; Sukumaran and Yu, 2014; Ikeda et al., 2018; Ning et al., 2019). Investigations using GWAS have already successfully deciphered genetic variants of coloration traits, in which the identified specific markers could be potentially beneficial for selective breeding. For instance, a strong candidate locus, in *arabidopsis pseudo-response regulator 2-like*

(*APRR2*) that regulates the accumulation of green pigments, was identified in melon and watermelon *via* GWAS (Oren et al., 2019). Information of two colors of single-nucleotide polymorphisms (SNPs) in French Saanen goats could be used to remove the undesired colored goats through molecular marker-assisted breeding (Martin et al., 2016). Furthermore, five potential loci related to carotenoid biosynthesis were identified in maize (*Zeamays* L.); therefore, a greater abundance of carotenoids accompanied by the deeper orange color of the kernel was potentially obtained (Owens et al., 2019). A similar GWAS result has also been concluded in Yesso scallop, in which three candidate genes (i.e., *LDLR*, *FRIS*, and *FRIY*) were detected around the two most significant potential loci and were proven to be involved in carotenoid metabolism in reddish-orange shell individuals (Zhao et al., 2017). These GWAS results not only provide a list of candidate loci/genes to be functionally validated but also offer an efficient approach for deciphering the genetic architecture of complex traits and selecting the breeding strategy.

This study aimed to identify significant SNP makers associated with shell color (purple-red and black-brown) in two new strains of bay scallops by performing GWAS, with the aid of whole-genome sequence databases of *A. irradians irradians* (unpublished data). The top three SNPs that dominantly control the shell color formation were further analyzed in their located candidate genes and then verified in another population. Gene Ontology (GO) and Kyoto Encyclopedia of Genes and Genomes (KEGG) pathway analyses were conducted to reveal the potential molecular mechanism in bay scallop shell coloration. Finally, we investigated the expression levels of the top three candidate genes in bay scallop mantles to detect their vital roles in shell coloration and to provide valuable information for the efficient selective breeding of shell color strains in bay scallop.

MATERIALS AND METHODS

Scallop Materials and Miso-RAD Library Construction

Two strains of healthy bay scallops with nearly 9-month-old, namely, the purple-red shell color population (PP) ($N > 500$) and the black-brown shell color population (BP) ($N > 500$), were used as samples in 2016. The shell color trait of both strains is genetically stable due to the genomic selection of four consecutive generations from 2012 to 2015 by our group (**Figure 1**). Samples were collected from artificial scallop-rearing substrates at Qingdao Jinshatan Fishery Group Co. Qingdao (35°97′23 N, 120°27′28 E, Shandong Province). Subsequently, we randomly selected scallop samples ($N = 80$) from each group based on their shell color. Gills were removed from each scallop according to the procedure of Mao et al. (2013) and then preserved in 100% ethanol at −20°C before genetic analysis. Our experiments were conducted according to the guidelines and regulations established by the Ocean University of China and the local government.

Genomic DNA was extracted from the gill using a standard phenol-trichloromethane method (Sambrook et al., 1989).

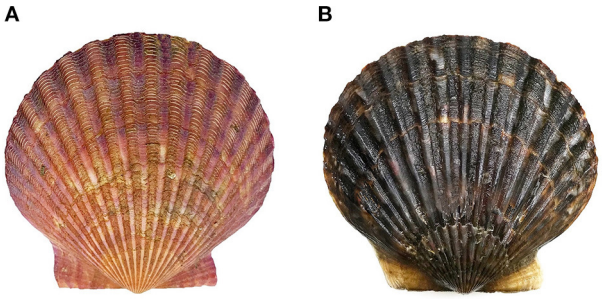

FIGURE 1 | (A) The purple-red shell color (PP) and **(B)** black-brown shell color (BP) bay scallops *Argopecten irradians*.

Subsequently, Miso-RAD libraries were constructed by using 80 PP and 80 BP individuals, following the protocol developed by Wang et al. (2016). On summarizing, genomic DNA of the 160 selected bay scallop individuals was digested with BsaXI (New England BioLabs, MA, USA, Cat. no. R0609) at 37°C for 45 min. Adaptor ligation, PCR amplification, digestion, and ligation were followed and after which every five DNA fragments were set as one group (barcoding and pooling). MinElute PCR Purification Kit (Qiagen, Hilden, Germany, Cat. no. 28004) was used to purify each product that concatenated five tags from five samples after performing amplification for two times. The 32 libraries were then pooled to run double-end sequencing on the Illumina Hiseq2000 system (San Diego, USA).

Sequence Data Processing and Genotyping

Raw reads were first preprocessed to eliminate paired-end (PE) reads with ambiguous base calls (N), long homopolymer regions (>10 bp), or excessive low-quality bases (>20% of bases with quality score <10) to obtain high-quality reads. PEAR software (Zhang J. et al., 2014) was exerted to assemble the forward and reverse reads. The merged reads containing five tags were divided into single-tag datasets by using homemade Perl script, and *via* SOAP software (Li et al., 2009), each tag was subsequently aligned to the chromosome-level reference bay scallop genome (unpublished data) that was constructed by our group. The RADtyping software (Fu et al., 2013) was employed in the genotyping analysis of sequencing data. The selective rules of markers included polymorphism, sufficient genotype rate (with available genotype over 80% progenies), and minor allele frequency (MAF) higher than 0.05. Then, the qualified markers were used for downstream analysis.

Genome-Wide Association Study and Candidate Gene Searching

To reduce the false-positive rate, the population genomic structure analysis was performed to provide a population membership matrix through Admixture software 1.3 (Alexander et al., 2009), and a kinship matrix was estimated by TASSEL 5.0 (Bradbury et al., 2007). Association analysis between genotypes and shell colors was conducted using PLINK software 1.9 (Chang

et al., 2015) by employing the logistic regression model with these two covariates to detect the associate SNPs. The statistic *p*-value for each SNP was calculated and summarized in ascending order. The threshold *p*-value for genome-wide significance was calculated using the Bonferroni correction based on the number of qualified makers (Johnson et al., 2010). When an SNP scored less than the significance cutoff (1.72E−6), the sequence of each maker was extracted and used as a query to exert BLASTN (Altschul et al., 1997) to search the draft genome of *A. irradians irradians* (unpublished data) that were annotated by the protein database NR. In addition, the Manhattan plot was drawn by an R package named "ggplot," and these potential SNPs ($p < 1.00E{-}5$) were captured to conduct bioinformatics analysis, including GO function annotation and KEGG pathway enrichment analyses (http://www.omicshare.com/tools).

SNP Verification

To further evaluate the accuracy of GWAS, the top three SNPs (*p*-value < 1.00E−17) were selected to verify in the 30 purple-red shell color samples and 30 black-brown shell color samples collected from another separate bay scallop population ($N > 500$) in the sea area of Huangdao District, Qingdao, Shandong Province, in 2018. Striated muscles of the above 60 individuals were separately sampled and preserved at −80°C for subsequent analysis. The primer sequences are provided in **Table 1**. The PCR of fragments containing the above three SNPs was carried out as follows: 2 μl of template DNA (50 ng/μl), 15 μl of Q5 High-Fidelity 2× Master Mix (New England BioLabs, MA, USA, Cat. no. M0492S), 0.5 μl (10 pmol/μl) of each forward and reverse primer, and sterile water up to 30 μl volume was added for amplifying. The related parameters in the PCR system for three primers were pre-denaturing under 98°C for 30 s, then denaturing under 98°C for 10 s, annealing under 56°C for 15 s, and extending under 72°C for 10 s, respectively. After 28 cycles, the sample was extended under 72°C for 2 min. The PCR products were sequenced using the Sanger method by Sangon Biotech (Shanghai, China). Sequences amplified by the primers were compared among the 60 scallops (30 PP and 30 BP, respectively) using the ClustalW2 multiple alignment program (http://www.ebi.ac.uk/Tools/msa/clustalw2/). When a mutation was detected, comparisons of genotype frequencies between the PP and BP were performed using Fisher's exact test to identify the shell color-associated mutation. *p*-values < 0.05 were considered statistically significant.

Candidate Gene Evaluation

To compare the differences in the expression levels of genes which are the top three SNPs annotated between PP and BP, 30 PP and 30 BP individuals from another non-breeding bay scallop population ($N > 500$) were randomly recruited, and the mantle was sampled in the sea area of Huangdao District, Qingdao, Shandong Province, in 2020. Total RNA of the sampled mantles was isolated following the method described by Hu et al. (2006) and then digested with DNaseI (Takara, Shiga, Japan). The concentration and purity of the RNA were determined using a Nanovue Plus spectrophotometer (GE Healthcare, Piscataway, NJ, USA), and the RNA integrity was assessed by agarose gel electrophoresis. The first-strand cDNA was synthesized according to the protocol of the manufacturer using Moloney murine leukemia virus (MMLV) reverse transcriptase (Thermo, Wilmington, USA) in a 20 μl volume with 2 μg of each total RNA sample as the template and 0.5 μg of oligo (dT)18 (Takara Biotechnology, Liaoning, China) as the primer. The mixture was denatured at 65°C for 5 min and then chilled immediately on ice. After adding the reverse transcriptase, reaction buffer, and dNTPs, cDNA was amplified under the following conditions: 42°C for 90 min and 72°C 10 min. The cDNA was stored at −20°C and diluted to 5 ng/μl for use as the template in the real-time quantitative reverse transcription PCR (qRT-PCR). Data from the qRT-PCR were obtained and the gene expression level is shown as the fold change. The statistical analysis of the data was performed with SPSS software (version 21.0) *via* an independent sample *t*-test. Differences were considered significant at $p < 0.05$.

TABLE 1 | Primer sequences used in this study.

SNP/Gene	Primers sequence	Note
chr7-12764003	F: 5′-TCCCAGTAGAAGTCGCACAC-3′ R: 5′-GCCTAAAGCCATACAAAACG-3′	SNP verification
chr7-13213864	F: 5′-CATAGAGAACGCGTAAAGGCGGATC-3′ R: 5′-GCTGGCAAGTCAGGACAAAGAAGGG-3′	SNP verification
chr7-11899306	F: 5′-CTTGATCGGCAGAGATAATTTAACA-3′ R: 5′-ATTCCCCAATGAGAGCCCACT-3′	SNP verification
GRL101	F: 5′-CTACTGGCACAACTACTCCATAC-3′ R: 5′-CTCGTGCAGAAACTCGATACA−3′	qRT-PCR
PKS1	F: 5′-AACTTACTGGGTCCATCACTTAC−3′ R: 5′-CATGGACGACTCACCAATTCT−3′	qRT-PCR
PLC1	F: 5′-CATGGGTCAGGTGGTTATGT-3′ R: 5′-CGTTCATCGCCTCCTGTATAA-3′	qRT-PCR

SNP, single-nucleotide polymorphism.

RESULTS

Sequencing Data

In total, sequencing of 32 Miso-RAD libraries produced 447,286,098 reads (GenBank: PRJNA689862), and the average sequencing depth was 22.32 × with 2,795,538 reads per individual. After quality control, we obtained 219,383,262 high-quality reads, and an average of 42.49% of high-quality reads in each individual was uniquely mapped to the bay scallop genome (unpublished data) by SOAP. Eventually, a total of 211,728 SNPs were genotyped in 160 scallop samples (80 PP and 80 BP) *via* RADtyping.

Genomic Regions Associated with Shell Color

A total of 211,728 SNP markers obtained from 160 bay scallop individuals were exerted to quality control performed by PLINK software. After quality filtering (call rate > 80% and MAF > 5%), a set of 29,036 qualified SNPs were successfully assigned to the 16 chromosomes of bay scallop and used for

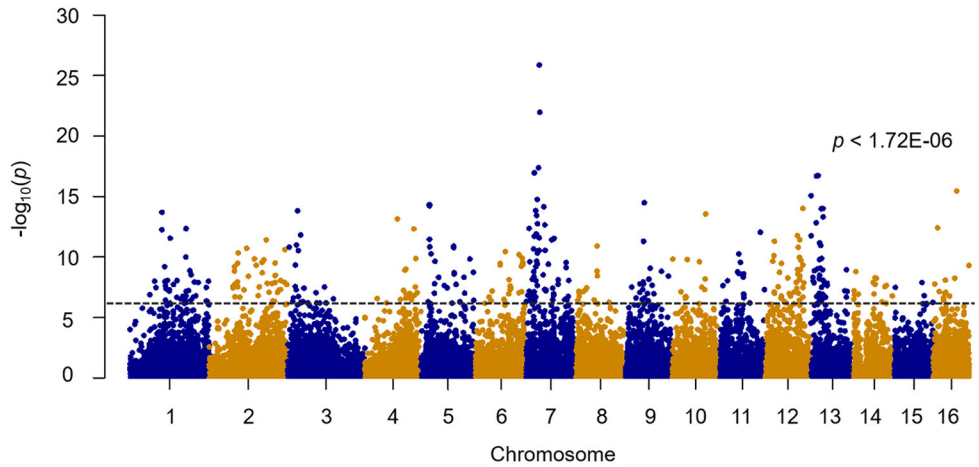

FIGURE 2 | Genome-wide association study (GWAS) of shell color with 29,036 single-nucleotide polymorphisms (SNPs) in bay scallops ($p < 1.72E{-}06$).

TABLE 2 | Information of the top eight SNPs associated with bay scallop shell color.

SNP	Allele 1	Allele 2	F_PP[a]	F_BP[b]	*p*-value	Position (bp)
chr7-12764003	G	A	0.7937	0.03125	1.36E-26	12,764,003
chr7-13213864	T	A	0.8481	0.06579	1.07E-22	13,213,864
chr7-11899306	T	C	0.7812	0.0375	4.17E-18	11,899,306
chr7-7814275	C	A	0.7792	0.04464	1.10E-17	7,814,275
chr13-7315277	A	C	0.1284	0	1.84E-17	7,315,277
chr13-5594794	A	T	0.1062	0.025	2.02E-17	5,594,794
chr16-23189193	T	C	0.1076	0.01875	3.55E-16	23,189,193
chr13-253787	A	G	0.225	0.2623	8.49E-16	253,787

[a] *Allele frequency in PP.*
[b] *Allele frequency in BP.*

further genome-wide analysis (**Figure 2**). Genetic clustering illustrated that the admixed ancestry of PP and BP was shown for $K = 2$, with kinship coefficients varying from 0 to 0.02 between PP and BP individuals, then the corresponding components were brought as covariates. After conducting Bonferroni correction and 0.05 cutoff ($p < 1.72E{-}6$), we detected 469 SNPs significantly associated with shell color, and 285 of these 27 bp tags could be directly annotated in the bay scallop genome. Furthermore, the $-\log_{10}$ (*p*-value) values of the top eight SNPs with a significant association of shell color were higher than 15, and these top eight SNPs were mainly distributed in chromosome 7 (**Table 2**). Specifically, the top eight loci were separately located at the genic regions of *GRL101* (*G-protein-coupled receptor-like 101*), *PKS1* (*polyketide synthase 1*), *PLC1* (*phosphoinositide phospholipase C*), *GLRA1* (*glycine receptor subunit alpha-1-like*), *COL4* (*zinc finger protein constants-like 4*), *CL1* (*cathepsin L1-like*), and gene *LOC110449017* (not yet characterized), as well as at an intergenic region (where SNP Chr13-253787 anchored).

Among these, the top three loci were distributed in the genic region of chromosome 7 (**Figure 3**). More specifically, SNP chr7-12764003 was mapped to location 41 bp in the coding sequence (CDS) 7 of *GRL101*, and SNP chr7-13213864 was cited in position 1,347 bp in CDS 5 of *PKS1*. For chr7-11899306, an SNP was located at position 14,136 bp in the first intron of *PCL1*. Subsequently, the top three SNPs were selected to be verified by sequencing the PCR products using the Sanger method by Sangon Biotech (Shanghai, China).

SNP Verification

All the top three SNPs provided by the GWAS results were successfully verified by Sanger sequencing in another separate bay scallop population. The allele and genotype frequency of these three SNP markers are shown in **Table 3**. For SNP chr7-12764003, dimorphic alleles could be observed, with AA and GG presenting in PP and BP, respectively. As for SNP chr7-13213864, the genotype of AA (100%) was only observed in PP, while another two genotypes of TT and AT were present in BP, with frequencies of 76.67 and 23.33%, respectively. Besides, the genotype is varied in SNP chr7-11899306 (for CC, TT, CT; 76.67, 0, 23.33% in PP and 6.67, 63.33, 30% in BP, respectively). Comparison between PP and BP individuals showed that genotype frequencies of the above three SNP markers were significantly different ($p < 0.05$). These results support that the verified SNPs

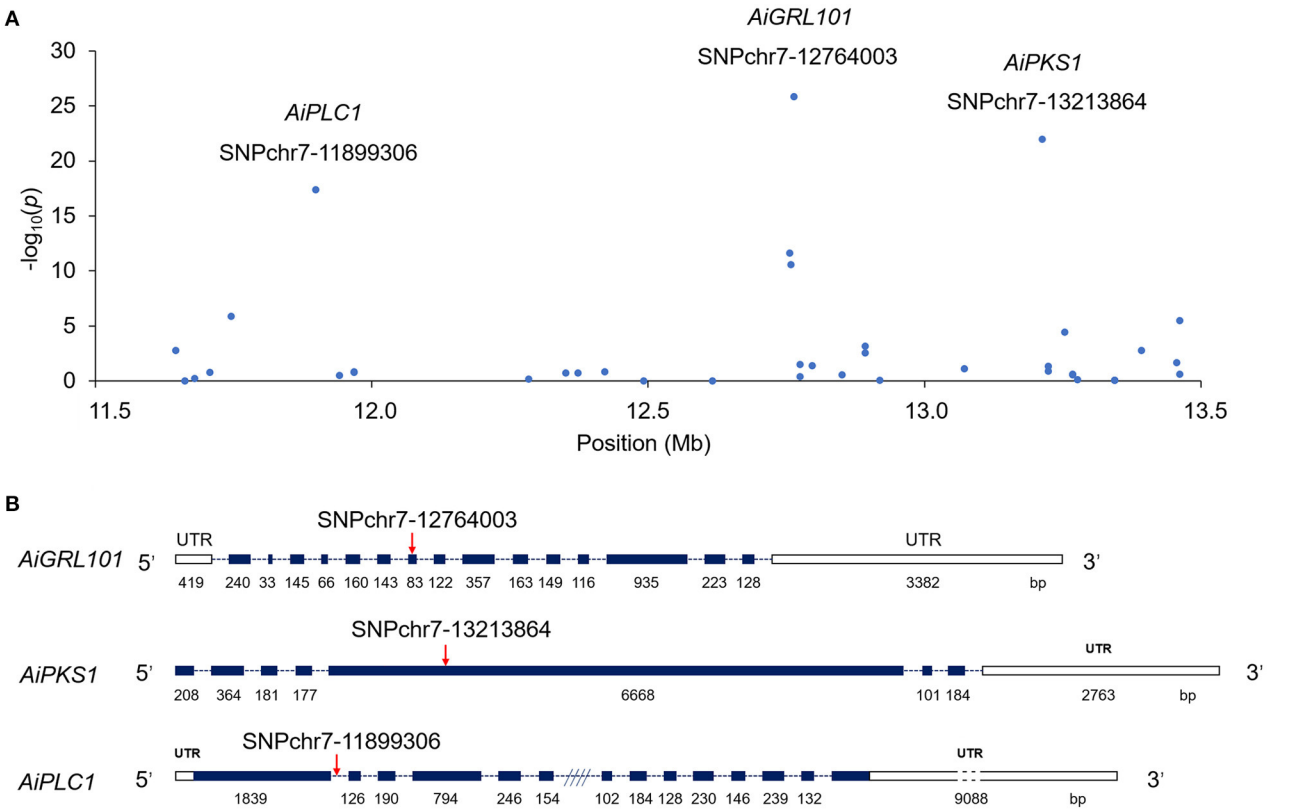

FIGURE 3 | A few neighboring SNP loci on chromosome 7 are independently associated with shell color in the bay scallop. **(A)** The genic structure of *AiGRL101, AiPKS1,* and *AiPLC1.* **(B)** The blank boxes indicate the 5′UTRs and 3′UTRs (untranslated region); the dark blue boxes represent coding sequence (CDS); the dotted lines indicate the introns; and the red arrows indicate the verified SNPs in responding genes. The CDS are shown relative to their lengths and the SNPs are marked in the accurate positions in the genic sequences.

TABLE 3 | Comparison of genotype frequencies of the top three SNPs between PP ($N = 30$) and BP ($N = 30$) bay scallops.

SNP	Location	Locus	Genotype	Number of scallop		Fisher's exact test *p*-value
				PP	BP	
chr7-12764003	Exon	A = G	AA	30	0	<2.20E-16
			GG	0	30	
chr7-13213864	Exon	A > T	AA	30	0	0.010540
			TT	0	23	
			AT	0	7	
chr7-11899306	Intron	C > T	CC	27	2	0.001293
			TT	0	19	
			CT	3	9	

might be involved in shell color formation of bay scallop PP and BP.

GO and KEGG Analyses of Candidate Genes

After a widely used and less-stringent threshold *p*-value < 1.00E−5 (Marigorta et al., 2018), we obtained 713 significant SNPs annotated in 374 unigenes. Subsequently, GO function annotation and KEGG pathway enrichment were applied to excavate the potential association between these genes and shell color. Results displayed that 38 GO terms were classified into the biological process (BP), cellular component (CC), and molecular function (MF) under level 2 covering 297 genes (**Figure 4**). In detail, genes related to the cellular process (105 genes), single-organism process (94 genes), and metabolic process (68 genes) showed remarkable terms in BP. Genes related to the membrane (53 genes) displayed the notable term in

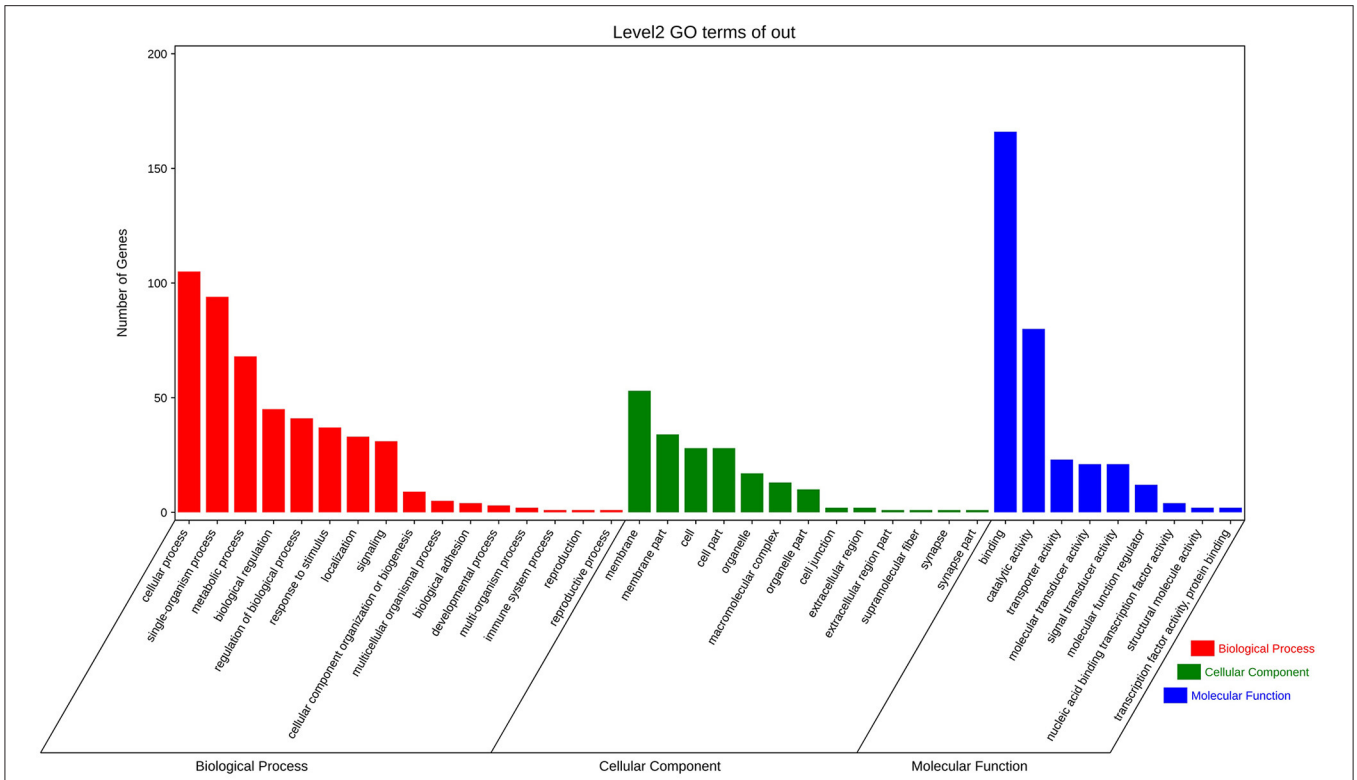

FIGURE 4 | The summary of Gene Ontology (GO) function annotation analysis for candidate genes that comprised significant SNPs ($p < 1.00E{-}5$). Each term describes the function of the gene cluster, and the length of colored bars represents the difference of the number of genes.

CC. Genes associated with binding (166 genes) and catalytic activity (80 genes) were highly presented in MF (**Figure 4**). In terms of KEGG pathway enrichment analysis, a total of 252 genes were acquired annotations and involved in 44 pathways (**Figure 5**). The above candidate genes were chiefly distributed in metabolism (69 genes), genetic information processing (15 genes), environmental information process (55 genes), cellular process (38 genes), organismal systems (90 genes), and human disease (97 genes) (**Figure 5**). Specifically, signal transduction (37 genes), global and overview maps (29 genes), infectious diseases (23 genes), cancers (21 genes), and endocrine system (19 genes) were mainly presented. Overall, the result indicated that the extracted GO terms and KEGG pathway are closely related to cellular process, membrane, signaling, and binding, and these possible molecular mechanisms may attribute to the shell color formation.

Expression Patterns of the Top Three Genes

Annotation results showed that the top three SNPs were located in three genes, including *GRL101* (chr7-12764003), *PKS1* (chr7-13213864), and *PLC1* (chr7-11899306), which were further selected for comparing their expression differences in mantles between PP and BP individuals. As shown in **Figure 6**, the expression profiles of the three target genes were ubiquitous in both PP and BP individuals but exhibited distinct expression patterns. Specifically, an extremely significant higher (6.43-fold, $p < 0.01$) expression level of *GRL101* was detected in PP than that in BP. A similar phenomenon was also observed in *PLC1*, which displayed a prominently increasing expression level in PP (6.48-fold, $p < 0.05$) compared with BP. On the contrary, the expression of *PSK1* was notably correlated with black-brown shell color rather than purple-red shell color (12.02-fold of BP compared with PP). Overall, in the bay scallop, the significantly higher expression profiles of *GRL101* and *PLC1* were detected in PP, implying that they may play a pivotal role in purple-red shell formation. Besides, *PSK1* is principally expressed in BP instead of PP, suggesting that it may involve black-brown pigmentation during shell formation.

DISCUSSION

Aquaculture breeding researches have confirmed that color trait in most aquaculture species is heritable, including red/white flesh color in salmon (Iwamoto et al., 1990), carapace/hepatopancreas color in crab (Li Q. et al., 2019), black/white shell color in oyster (Xu et al., 2019), white/orange in scallop adductor muscle (Li X. et al., 2019), etc. Particularly, the bay scallop is polymorphic for the background color of the shell and presents a highly variable distribution of overlying pigments (Clarke, 1965). Although previous investigations showed one or several major genes contributed to shell color diversity of bay scallop

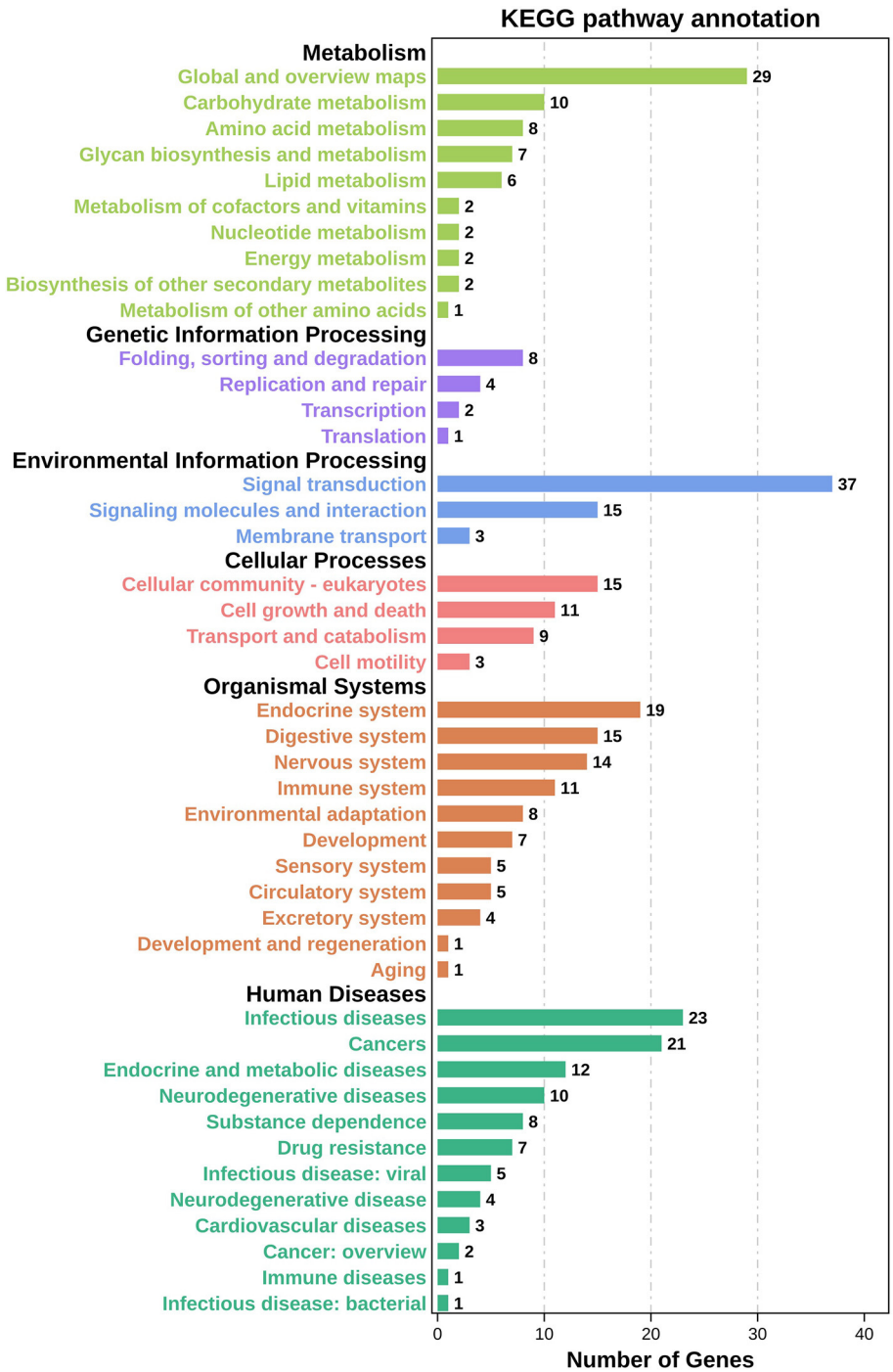

FIGURE 5 | The summary of Kyoto Encyclopedia of Genes and Genomes (KEGG) pathway enrichment analysis performed for biological process, cellular component, and molecular function. Functional annotation of candidate selective genes that comprised significant SNPs ($p < 1.00E{-}5$).

(Adamkewicz and Castagna, 1988; Qin et al., 2007; Teng et al., 2018), the precise loci/genes for specific color difference and the mechanism underneath shell color formation in bay scallop are elusive. With rapid development in biotechnology, constantly upgraded methods for studying shell color polymorphisms in bay scallop would dredge out specific genes behind target trait. GWAS has been proven to be an efficient approach to elucidate the genetic variations related to complex phenotypes and to identify the pivotal candidate genes of target economic traits, thereby providing referential makers for the selective breeding

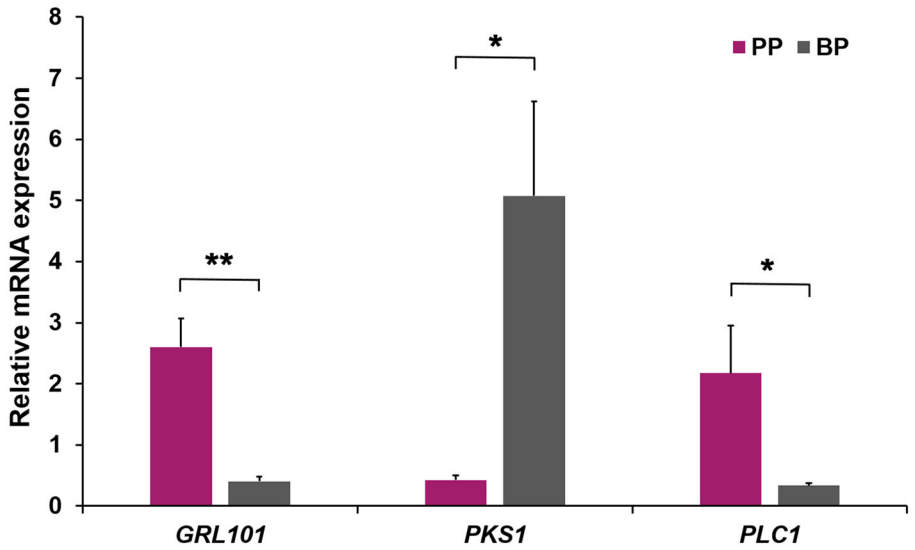

FIGURE 6 | The relative expression levels of *GRL101*, *PKS1,* and *PLC1* in the mantle of PP and BP bay scallops. Three replicates were performed for each adult mantle, and three technical replicates were conducted for each PCR. The comparison of the expression levels of *GRL101*, *PKS1,* and *PLC1* in the mantle of PP and BP bay scallops was performed using an independent sample *t*-test. * and ** indicate statistically significant differences ($p < 0.05$ and $p < 0.01$, respectively).

projects (Luo et al., 2012). By this method, 469 SNPs that displayed statistically significant differences between PP and BP were identified in our research. As the Manhattan plot displayed, the top value of $-\log_{10}$ (*p*-value) reached nearly 26, which is much more stringent than 5.8 ($p < 1.72\text{E}{-}06$) that referred to Bonferroni correction, demonstrating that our result is reliable (false positives are rare). Intriguingly, most of the significant SNPs associated with shell color were primarily allocated in chromosome 7 of bay scallop. With the similarity to that in Yesso scallop, the major SNPs associated with shell color were located in chromosome 11 (Zhao et al., 2017), and almost all the significant SNPs associated with carotenoid coloration in scallop adductor muscle were distributed in chromosome 8 (Li X. et al., 2019). Based on the fact that most qualitative traits are typically determined by one or several pivotal loci/genes, we speculated that color variants in scallop were potentially regulated by limited candidate loci/genes gathered closely in association with the genomic region(s) of the specific linkage group. In addition, the tandem or proximal (in a nearby chromosomal region but not adjacent) locations may not only facilitate coordinate expressions of candidate genes but also guarantee efficient expression regulations by pivotal loci.

The top three SNPs with a *p*-value <1.00E−17 were successfully verified in another separate population *via* Sanger sequencing. The extremely significant ($p < 0.01$) or significant ($p < 0.05$) differences of the three selected loci between PP and BP suggested that these SNPs might be responsible for shell color formation and potentially used as selective breeding markers in shell color-specific projects of bay scallop. In addition, the top eight SNPs ($p < 1.00\text{E}{-}15$) were principally and separately located in genes (exon or intron) except on locus (SNP chr13-253787) located in intergenic regions. A similar phenomenon has also been concluded in the shell color of the Yesso scallop (Zhao et al., 2017). The above results revealed that color traits in scallops may be principally controlled by the coding regions (where SNPs are located) of most critical candidate genes (Cargill et al., 1999) and meanwhile regulated through crucial SNPs within introns or intergenic regions *via* transcriptional regulation (Sturm et al., 2008; Visser et al., 2014).

Bay scallop shell color significance-associated candidate genes, namely, *GRL101*, *PKS1,* and *PLC1,* where the top three SNPs were located, were further selected for comparing their expression differences between PP and BP individuals. The scallop mantle constantly contacts with the shell; therefore, the mantle is considered to manufacture and transport pigments to the shell along the growing edge during shell formation (Fowler et al., 1992). Upon this basis, further expression patterns of the top three candidate genes were characterized in the mantle of PP and BP individuals, respectively. In this study, the mRNA expression level of *GRL101* in PP was over six times that in BP ($p < 0.05$), suggesting GRL101 might function in purple-red shell coloration. As reported, GRL101 belongs to the G-protein-coupled receptors (GPCRs) superfamily (Karnik et al., 2003) that exerts multifunctions, such as a variety of hormones and neurotransmitters regulation (Nilaweera et al., 2006, 2008; Rosenbaum et al., 2009). Specifically, a set number of GPCRs were proven to be involved in pigments formation, known as responding to red-pigment concentrating hormone (RPCH) in *Carcinus maenas* (Alexander et al., 2018) and interceding pigment granule dispersion in *Xenopus laevis* melanophores (Teh and Sugden, 2001). Furthermore, GPCRs activated by chromatophores can affect pigment redistribution to alter the color appearance of the animal (Lerner, 1994). In particular, visual pigment rhodopsin (the first order of GPCRs) performs functions on the absorption and conversion of light into chemical signals (Smith, 2010). Based on this, our results implied that

GRL101 involved and functioned in the purple-red color shell formation of bay scallop, whereas GRL101 protein was regarded as an orphan receptor performing an uncertain function that was extensively explored in humans (Gene ID: 83550), mice (Gene ID: 245424), sea urchins (Gene ID: 115922752), king scallops (Gene ID: 117318188), and other species. Whether the GRL101 in the bay scallop is also considered an orphan receptor still needs to be further investigated. Coincidently, the majority of GPCRs were coupled to the phosphoinositide signaling pathway where the third candidate gene *PLC1* played a pivotal role (Tobin, 1997). Previous researches reported that PLC1 has been classified into an important class of enzymes involved in lipids-related signaling in plants (Rupwate and Rajasekharan, 2012) and acted as signal transducers to generate messengers participating in lipid metabolism in mammals (Essen et al., 1996). Furthermore, the lipid-related genes were proved to be closely associated with carotenoids (Zhang Y. et al., 2014) that contributed to the formation of reddish-orange shells in Yesso scallop (Zhao et al., 2017). Hence, it might then make sense that much higher expression of *PLC1* detected in PP individuals leads to the accumulation of carotenoid which in turn resulted in a red-colored shell. Therefore, our results suggest that *PLC1* might be related to lipid-associated carotenoid absorption and/or transportation. Collectively, we speculated that *GRL101* might perform a common feature of coloration-related *GPCRs* and activate *PLC1* in the phosphoinositide signaling pathway to affect lipid metabolism, including lipid-associated carotenoid regulation, resulting in the purple-red visualization of PP.

Another candidate gene *PKS1* belongs to polyketide synthase-related genes (Moriwaki et al., 2004), and the ancient and diversified family members have been well studied in animal fatty acid synthase (Kroken et al., 2003). As reported, plenty of microorganisms employed *PKS* to produce pigments and other products of intermediate metabolism (Hutchinson, 2003). For example, the biosynthesis of black pigment melanin derived by *PKS1* was reported in *Colletotrichum lagenarium* (Takano et al., 1995) and *Aspergillus fumigatus* (Heinekamp et al., 2013), respectively. Unlike *PKS1* as the pivotal component in melanin biosynthesis in microorganisms, melanin biosynthesis in various tissues of vertebrates was prevailingly affected by *tyrosinase* genes (Sato et al., 2001). Similarly, melanin biosynthesis was more inclined to be regulated by tyrosinase that contributes to black-brown shell pigmentation in most mollusks (Bai et al., 2013; Sun et al., 2015). However, our study showed that a higher expression level (12.02-fold, $p < 0.05$) of *PKS1* in the black-brown shell individuals was observed than that in purple-red ones; therefore, we speculated that black pigmentation in BP might be regulated by *PKS1* as it functioned in microorganisms. Although melanin synthesis in scallop has not been reported yet, the typical biosynthesis pathway (in which tyrosinase is involved) as an alternative method seems worth further study.

Generally, causal SNPs were identified to be strongly associated with target traits, especially the SNPs that were located in the coding region would affect traits directly by changing their encoding amino acid and therefore resulting in the alteration of protein (Seong et al., 2011). However, in this study, the two most significant SNPs, namely, chr7-12764003, and chr7-13213864, were separately located in the CDS of *AiGRL101* and *AiPSK1*, caused synonymous mutations in target amino acids. We speculated that SNPs located in the CDS of *AiGRL101* and *AiPSK1* might not control the scallop shell coloration directly *via* mutation of amino acids, but mediate regulating candidate genes by affecting codon bias (Plotkin and Kudla, 2011), translation efficiency (Miyuki and Kentaro, 2013), mRNA secondary structure stability (Chamary and Hurst, 2005), and splicing (Li et al., 2020). Furthermore, linkage disequilibrium (LD) analysis of the three closely arranged SNPs (**Figure 2**) *via* MEGA (Version 10.1.8) (Sudhir et al., 2018) showed that LD coefficient r^2 between each pair of SNPs was higher than 0.7 (ranged from 0.72 to 0.78), demonstrating that shell color in bay scallop may be regulated by closely linked major SNPs and/or specific interactions among them which potentially affect the expression of candidate genes resulting in shell color formation and differentiation. Further research is needed for investigating the potential molecular mechanism of synonymous mutation of CDS in candidate genes and interactions of target genes in regulating shell coloration of bay scallops.

Furthermore, 713 SNPs ($p < 1.00E{-}5$) significantly associated with bay scallop shell color were mapped to 374 unigenes, followed by GO function annotation and KEGG pathway enrichment for elucidating their important molecular mechanism (Wang et al., 2019). GO function annotation in this study primarily participated in cellular process, membrane, and binding function, which is similar to previous research that cellular process and binding are the largest group of biological process and molecular function in the transcriptomic analysis of red/white-colored valves of moon scallop (Huang et al., 2015), as well as different shell color lines in Yesso scallop (Ding et al., 2015). Furthermore, transcriptome sequencing of orange shell color bay scallops revealed that differentially expressed genes were mainly annotated in signal transduction, metabolism, human diseases, and organismal systems (Teng et al., 2018) and that is in accordance with our result of KEGG pathway analysis. Taken together, the above results suggest that the shell color of the bay scallop is not only dominated by several loci/genes but also modified by plenty of related minor loci/genes.

CONCLUSION

We identified SNPs associated with the purple-red and black-brown shell colors bay scallop through GWAS. The genomic regions associated with shell color were mainly located in chromosome 7. The top three SNPs were located in the genic region of *GRL101*, *PKS1,* and *PLC1* and successfully verified in another separate population. Expression patterns analyses suggested that *GRL101* and *PLC1* potentially functioned in purple-red shell coloration, and black pigmentation in BP might be principally regulated by *PKS1*. GO function annotation

and KEGG pathway enrichment analyses revealed the possible molecular mechanism of shell color formation. Taken together, this evidence collectively provides valuable information for deciphering the phenotype differences of shell color and helps in the molecular marker-assisted breeding in bay scallops.

DATA AVAILABILITY STATEMENT

The datasets generated for this study can be found in online repositories. The names of the repository/repositories and accession number(s) can be found below: NCBI GenBank (accession number: PRJNA689862).

ETHICS STATEMENT

The animal study was reviewed and approved by Ocean University of China.

AUTHOR CONTRIBUTIONS

QX, JH, and ZB conceived and designed the experiments. XZ, JZ, and XHo collected the samples. QX, XZ, PL, and JL performed the experiments. XZ, QX, JZ, and XHu analyzed the data. QX and XZ wrote the manuscript. All authors have read and approved the final manuscript. All authors contributed to the article and approved the submitted version.

FUNDING

This work was supported by the National Natural Science Foundation of China-Shandong Joint Fund (U1706203), the Earmarked Fund for Agriculture Seed Improvement Project of Shandong Province (2020LZGC016), Sanya Yazhou Bay Science and Technology City (SKJC-KJ-2019KY01), and the China Agriculture Research System of MOF and MARA.

REFERENCES

Adamkewicz, L., and Castagna, M. (1988). Genetics of shell color and pattern in the bay scallop *Argopecten irradians*. *J. Heredity* 79, 14–17. doi: 10.1093/oxfordjournals.jhered.a110436

Alexander, D. H., Novembre, J., and Lange, K. (2009). Fast model-based estimation of ancestry in unrelated individuals. *Genome Res.* 19, 1655–1664. doi: 10.1101/gr.094052.109

Alexander, J. L., Oliphant, A., Wilcockson, D. C., Audsley, N., Down, R. E., Lafont, R., et al. (2018). Functional characterization and signaling systems of corazonin and red pigment concentrating hormone in the green shore crab, *Carcinus maenas*. *Front. Neurosci.* 11:752. doi: 10.3389/fnins.2017.00752

Altschul, S. F., Madden, T. L., Schäffer, A. A., Zhang, J., Zhang, Z., Miller, W., et al. (1997). Gapped BLAST and PSI-BLAST: a new generation of protein database search programs. *Nucleic Acids Res.* 25, 3389–3402. doi: 10.1093/nar/25.17.3389

Bai, Z., Zheng, H., Lin, J., Wang, G., and Li, J. (2013). Comparative analysis of the transcriptome in tissues secreting purple and white nacre in the pearl mussel *Hyriopsis cumingii*. *PLoS ONE* 8:e53617. doi: 10.1371/journal.pone.0053617

Bradbury, P. J., Zhang, Z., Kroon, D. E., Casstevens, T. M., Ramdoss, Y., and Buckler, E. S. (2007). TASSEL: software for association mapping of complex traits in diverse samples. *Bioinformatics* 23, 2633–2635. doi: 10.1093/bioinformatics/btm308

Cargill, M., Altshuler, D., Ireland, J., Sklar, P., Ardlie, K., Patil, N., et al. (1999). Characterization of single-nucleotide polymorphisms in coding regions of human genes. *Nat. Genet.* 22, 231–238. doi: 10.1038/10290

Chamary, J. V., and Hurst, L. D. (2005). Evidence for selection on synonymous mutations affecting stability of mRNA secondary structure in mammals. *Genome Biol.* 6:R75. doi: 10.1186/gb-2005-6-9-r75

Chang, C. C., Chow, C. C., Tellier, L. C., Vattikuti, S., Purcell, S. M., and Lee, J. J. (2015). Second-generation PLINK: rising to the challenge of larger and richer datasets. *Gigascience* 4:7. doi: 10.1186/s13742-015-0047-8

Clarke, A. H. (1965). The scallop superspecies *Aequipecten irradians* (Lamarck). *Malacologia* 2:161–168.

Cole, T. J. (1975). Inheritance of juvenile shell colour of the oyster drill *Urosalpinx cinerea*. *Nature* 257, 794–795. doi: 10.1038/257794a0

Comfort, A. (1950). Acid-soluble pigments of molluscan shells. 5. Identity of some subsidiary fractions derived from *Pinctada vulgaris*. *Biochem. J.* 47, 254–255. doi: 10.1042/bj0470254

Comfort, A. (1951). The pigmentation of molluscan shells. *Biol. Rev.* 26, 285–301. doi: 10.1111/j.1469-185X.1951.tb01358.x

Cong, R., Kong, L., Yu, H., and Li, Q. (2014). Association between polymorphism in the insulin receptor-related receptor gene and growth traits in the Pacific oyster *Crassostrea gigas*. *Biochem. Syst. Ecol.* 54, 144–149. doi: 10.1016/j.bse.2014.02.003

D'Iischia, M., Wakamatsu, K., Napolitano, A., Briganti, S., Garcia-Borron, J. C., Kovacs, D., et al. (2013). Melanins and melanogenesis: methods, standards, protocols. *Pigm. Cell Melanoma Res.* 26, 616–633. doi: 10.1111/pcmr.12121

Ding, J., Zhao, L., Chang, Y., Zhao, W., Du, Z., and Hao, Z. (2015). Transcriptome sequencing and characterization of Japanese scallop *Patinopecten yessoensis* from different shell color lines. *PLoS ONE* 10:e0116406. doi: 10.1371/journal.pone.0116406

Elek, J., and Adamkewicz, S. L. (1990). Polymorphism for shell color in the Atlantic bay scallop *Argopecten irradians* (Lamarck) (Mollusca: Bivalvia) on Martha's Vineyard island. *Am. Malacol. Bull.* 7, 117–126.

Essen, L. O., Perisic, O., Cheung, R., Katan, M., and Williams, R. L. (1996). Crystal structure of a mammalian phosphoinositide-specific phospholipase Cδ. *Nature* 380, 595–602. doi: 10.1038/380595a0

Fowler, D. R., Meinhardt, H., and Prusinkiewicz, P. (1992). Modeling seashells. *Acm Siggraph Comput. Graph.* 26, 379–387. doi: 10.1145/142920.134096

Fu, X., Dou, J., Mao, J., Su, H., Jiao, W., Zhang, L., et al. (2013). RADtyping: an integrated package for accurate *de novo* codominant and dominant RAD genotyping in mapping populations. *PLoS ONE* 8:e79960. doi: 10.1371/journal.pone.0079960

Han, Z., Li, Q., Liu, S., and Kong, L. (2020). Crossbreeding of three different shell color lines in the Pacific oyster reveals high heterosis for survival but low heterosis for growth. *Aquaculture* 529:735621. doi: 10.1016/j.aquaculture.2020.735621

Hao, S., Hou, X., Wei, L., Li, J., Li, Z., and Wang, X. (2015). Extraction and identification of the pigment in the adductor muscle scar of pacific oyster *Crassostrea gigas*. *PLoS ONE* 10:e0142439. doi: 10.1371/journal.pone.0142439

Heinekamp, T., Thywißen, A., Macheleidt, J., Keller, S., Valiante, V., and Brakhage, A. A. (2013). *Aspergillus fumigatus* melanins: interference with the host endocytosis pathway and impact on virulence. *Front. Microbiol.* 3:440. doi: 10.3389/fmicb.2012.00440

Heller, J. (1992). Shell colour variation in *Bullia digitalis*, a sand-dwelling, intertidal whelk (Gastropoda: Prosobranchia). *Biol. J. Linn. Soc.* 46, 247–258. doi: 10.1111/j.1095-8312.1992.tb00863.x

Hoang, T. H., Stone, D. A., Duong, D. N., Bansemer, M. S., Harris, J. O., and Qin, J. G. (2017). Colour change of greenlip abalone (*Haliotis laevigata* Donovan) fed formulated diets containing graded levels of dried macroalgae meal. *Aquaculture* 468, 278–285. doi: 10.1016/j.aquaculture.2016.10.027

Hu, X., Bao, Z., Hu, J., Shao, M., Zhang, L., Bi, K., et al. (2006). Cloning and characterization of tryptophan 2, 3-dioxygenase gene of Zhikong scallop *Chlamys farreri* (Jones and Preston 1904). *Aquac. Res.* 37, 1187–1194. doi: 10.1111/j.1365-2109.2006.01546.x

Huang, R., Zheng, Z., Wang, Q., Zhao, X., Deng, Y., Jiao, Y., et al. (2015). Mantle branch-specific RNA sequences of moon scallop *Amusium pleuronectes* to identify shell color-associated genes. *PLoS ONE* 10:e0141390. doi: 10.1371/journal.pone.0141390

Hutchinson, C. R. (2003). Polyketide and non-ribosomal peptide synthases: falling together by coming apart. *Proc. Nat. Acad. Sci.* 100, 3010–3012. doi: 10.1073/pnas.0730689100

Ikeda, M., Takahashi, A., Kamatani, Y., Okahisa, Y., Kunugi, H., Mori, N., et al. (2018). A genome-wide association study identifies two novel susceptibility loci and trans population polygenicity associated with bipolar disorder. *Mol. Psychiatry* 23, 639–647. doi: 10.1038/mp.2016.259

Innes, D. J., and Leslie, E. H. (1977). Inheritance of a shell-color polymorphism in the mussel. *J. Heredity* 68, 203–204. doi: 10.1093/oxfordjournals.jhered.a108814

Iwamoto, R. N., Myers, J. M., and Hershberger, W. K. (1990). Heritability and genetic correlations for flesh coloration in pen-reared coho salmon. *Aquaculture* 86, 181–190. doi: 10.1016/0044-8486(90)90111-Y

Johnson, R. C., Nelson, G. W., Troyer, J. L., Lautenberger, J. A., Kessing, B. D., Winkler, C. A., et al. (2010). Accounting for multiple comparisons in a genome-wide association study (GWAS). *BMC Genomics* 11:724. doi: 10.1186/1471-2164-11-724

Karnik, S. S., Gogonea, C., Patil, S., Saad, Y., and Takezako, T. (2003). Activation of G-protein-coupled receptors: a common molecular mechanism. *Trends Endocrinol. Metabol.* 14, 431–437. doi: 10.1016/j.tem.2003.09.007

Kim, H. C., Lee, J. Y., Sung, H., Choi, J. Y., Park, S. K., Lee, K. M., et al. (2012). A genome-wide association study identifies a breast cancer risk variant in *ERBB4* at 2q34: results from the Seoul Breast Cancer Study. *Breast Cancer Res.* 14:R56. doi: 10.1186/bcr3158

Kraeuter, J., Adamkewicz, L., Castagna, M., Wall, R., and Karney, R. (1984). Rib number and shell color in hybridized subspecies of the Atlantic bay scallop, *Argopecten irradians*. *Nautilus* 98, 17–20.

Kroken, S., Glass, N. L., Taylor, J. W., Yoder, O. C., and Turgeon, B. G. (2003). Phylogenomic analysis of type I polyketide synthase genes in pathogenic and saprobic ascomycetes. *Proc. Nat. Acad. Sci.* 100, 15670–15675. doi: 10.1073/pnas.2532165100

Lerner, M. R. (1994). Tools for investigating functional interactions between ligands and G-protein-coupled receptors. *Trends Neurosci.* 17, 142–146. doi: 10.1016/0166-2236(94)90087-6

Li, M., Lu, X., Dong, J., Yao, Z., Wu,. Y., Rao,. H., et al. (2020). A synonymous mutation in exon 39 of *FBN1* causes exon skipping leading to Marfan syndrome. *Genomics* 112, 3856–3861. doi: 10.1016/j.ygeno.2020.06.024

Li, N., Hu, J., Wang, S., Cheng, J., Hu, X., Lu, Z., et al. (2010). Isolation and identification of the main carotenoid pigment from the rare orange muscle of the Yesso scallop. *Food Chem.* 118, 616–619. doi: 10.1016/j.foodchem.2009.05.043

Li, Q., Liu, Q., Zhang, C., Cheng, Y., and Wu, X. (2019). Can color-related traits in the Chinese mitten crab (*Eriocheir sinensis*) be improved through quantitative genetic inheritance? *Aquaculture* 512:734355. doi: 10.1016/j.aquaculture.2019.734355

Li, R., Yu, C., Li, Y., Lam, T. W., Yiu, S. M., Kristiansen, K., et al. (2009). SOAP2: an improved ultrafast tool for short read alignment. *Bioinformatics* 25, 1966–1967. doi: 10.1093/bioinformatics/btp336

Li, X., Bai, Z., Luo, H., Wang, G., and Li, J. (2014). Comparative analysis of total carotenoid content in tissues of purple and white inner-shell color pearl mussel, *Hyriopsis cumingii*. *Aquacult. Int.* 22, 1577–1585. doi: 10.1007/s10499-014-9766-6

Li, X., Wang, S., Xun, X., Zhang, M., Wang, S., Li, H., et al. (2019). A carotenoid oxygenase is responsible for muscle coloration in scallop. *Biochimica et Biophysica Acta (BBA)—Molecul. Cell Biol. Lipids* 1864, 966–975. doi: 10.1016/j.bbalip.2019.03.003

Liu, X., Wu, F., and Zhang, G. (2007). Genetic basis of tangerine shell color variation in the Pacific abalone, *Haliotis discus hannai*. *Aquaculture* 272:S286. doi: 10.1016/j.aquaculture.2007.07.127

Luo, W., Cheng, D., Chen, S., Wang, L., Li, Y., Ma, X., et al. (2012). Genome-wide association analysis of meat quality traits in a porcine large white × minzhu intercross population. *Int. J. Biol. Sci.* 8:580. doi: 10.7150/ijbs.3614

Mao, J., Lv, J., Miao, Y., Sun, C., Hu, L., Zhang, R., et al. (2013). Development of a rapid and efficient method for non-lethal DNA sampling and genotyping in scallops. *PLoS ONE* 8:e68096. doi: 10.1371/journal.pone.0068096

Marchais, V., Jolivet, A., Herv,é, S., Roussel, S., Schöne, B. R., Grall, J., et al. (2017). New tool to elucidate the diet of the ormer *Haliotis tuberculata* (L.): Digital shell color analysis. *Mar. Biol.* 164:71. doi: 10.1007/s00227-017-3103-3

Marigorta, U. M., Rodríguez, J. A., Gibson, G., and Navarro, A. (2018). Replicability and prediction: lessons and challenges from GWAS. *Trends Gene.* 34, 504–517. doi: 10.1016/j.tig.2018.03.005

Martin, P. M., Palhiere, I., Ricard, A., Tosser-Klopp, G., and Rupp, R. (2016). Genome wide association study identifies new loci associated with undesired coat color phenotypes in Saanen goats. *PLoS ONE* 11:e0152426. doi: 10.1371/journal.pone.0152426

Miyuki, T., and Kentaro, M. (2013). Directed evolution study unveiling key sequence factors that affect translation efficiency in *Escherichia coli*. *J. Biosci. Bioeng.* 116, 540–545. doi: 10.1016/j.jbiosc.2013.05.013

Moriwaki, A., Kihara, J., Kobayashi, T., Tokunaga, T., Arase, S., and Honda, Y. (2004). Insertional mutagenesis and characterization of a polyketide synthase gene (*PKS1*) required for melanin biosynthesis in *Bipolaris oryzae*. *FEMS Microbiol. Lett.* 238, 1–8. doi: 10.1111/j.1574-6968.2004.tb09729.x

Nie, H., Jiang, K., Jiang, L., Huo, Z., Ding, J., and Yan, X. (2020). Transcriptome analysis reveals the pigmentation related genes in four different shell color strains of the Manila clam *Ruditapes philippinarum*. *Genomics* 112, 2011–2020. doi: 10.1016/j.ygeno.2019.11.013

Nilaweera, K. N., Ozanne, D., Wilson, D., Mercer, J. G., Morgan, P. J., and Barrett, P. (2006). G protein-coupled receptor 101 mRNA expression in the mouse brain: altered expression in the posterior hypothalamus and amygdala by energetic challenges. *J. Neuroendocrinol.* 19, 34–45. doi: 10.1111/j.1365-2826.2006.01502.x

Nilaweera, K. N., Wilson, D., Bell, L., Mercer, J. G., Morgan, P. J., and Barrett, P. (2008). G protein-coupled receptor 101 mRNA expression in supraoptic and paraventricular nuclei in rat hypothalamus is altered by pregnancy and lactation. *Brain Res.* 1193, 76–83. doi: 10.1016/j.brainres.2007.11.048

Ning, X., Li, X., Wang, J., Zhang, X., Kong, L., Meng, D., et al. (2019). Genome-wide association study reveals *E2F3* as the candidate gene for scallop growth. *Aquaculture* 511:734216. doi: 10.1016/j.aquaculture.2019.734216

Oren, E., Tzuri, G., Vexler, L., Dafna, A., Meir, A., Faigenboim, A., et al. (2019). The multi-allelic *APRR2* gene is associated with fruit pigment accumulation in melon and watermelon. *J. Exp. Bot.* 70, 3781–3794. doi: 10.1093/jxb/erz182

Owens, B. F., Mathew, D., Diepenbrock, C. H., Tiede, T., Wu, D., Mateos-Hernandez, M., et al. (2019). Genome-wide association study and pathway-level analysis of kernel color in maize. *G3: Genes, Genomes, Genetics* 9, 1945–1955. doi: 10.1534/g3.119.400040

Palmer, A. R. (1985). Genetic basis of shell variation in *Thais emarginata* (Prosobranchia, Muricacea). *I. Banding in populations from Vancouver Island. The Biological Bulletin* 169, 638–651. doi: 10.2307/1541306

Peignon, J. M., Gerard, A., Naciri, Y., Ledu, C., and Phelipot, P. (1995). Analysis of shell colour determinism in the Manila clam *Ruditapes philippinarum*. *Aquat. Living Resour.* 8, 181–189. doi: 10.1051/alr:1995015

Petersen, J. L., Baerwald, M. R., Ibarra, A. M., and May, B. (2012). A first-generation linkage map of the Pacific lion-paw scallop (*Nodipecten subnodosus*): Initial evidence of QTL for size traits and markers linked to orange shell color. *Aquaculture* 350, 200–209. doi: 10.1016/j.aquaculture.2012.03.039

Plotkin, J. B., and Kudla, G. (2011). Synonymous but not the same: the causes and consequences of codon bias. *Nat. Rev. Genet.* 12, 32–42. doi: 10.1038/nrg2899

Qin, Y., Liu, X., Zhang, H., Zhang, G., and Guo, X. (2007). Identification and mapping of amplified fragment length polymorphism markers linked to shell color in bay scallop, *Argopecten irradians* (Lamarck, 1819). *Marine Biotechnol.* 9, 66–73. doi: 10.1007/s10126-006-6076-7

Rosenbaum, D. M., Rasmussen, S. G., and Kobilka, B. K. (2009). The structure and function of G-protein-coupled receptors. *Nature* 459, 356–363. doi: 10.1038/nature08144

Rupwate, S. D., and Rajasekharan, R. (2012). Plant phosphoinositide-specific phospholipase C: an insight. *Plant Signal. Behav.* 7, 1281–1283. doi: 10.4161/psb.21436

Sambrook, J., Fritsch, E. F., and Maniatis, T. (1989). *Molecular Cloning: A Laboratory Manual*, Second Edition. Cold Spring Harbor Laboratory Press.

Sato, S., Tanaka, M., Miura, H., Takeuchi, T., Yamamoto, H., Ikeo, K., et al. (2001). Functional conservation of the promoter regions of vertebrate tyrosinase genes. *J. Investigat. Dermatol. Sympo. Proceed.* 6, 10–18. doi: 10.1046/j.0022-202x.2001.00008.x

Seong, J., Dong, S. S., Park, K. D., Lee, H. K., and Hong, S. K. (2011). Identification and analysis of MC_4R polymorphisms and their association with

economic traits of Korean cattle (Hanwoo). *Mol. Biol. Rep.* 39, 3597–3601. doi: 10.1007/s11033-011-1133-3

Shumway, S. E., and Parsons, J. (2006). Scallops: biology, ecology and aquaculture new edition. *Developm. Aquacult. Fisher. Sci.* 35. doi: 10.1016/0022-0981(92)90183-B

Smith, S. O. (2010). Structure and activation of the visual pigment rhodopsin. *Annu. Rev. Biophys.* 39, 309–328. doi: 10.1146/annurev-biophys-101209-104901

Sokolova, I. M., and Berger, V. J. (2000). Physiological variation related to shell colour polymorphism in White Sea *Littorina saxatilis*. *J. Exp. Mar. Biol. Ecol.* 245, 1–23. doi: 10.1016/S0022-0981(99)00132-X

Stemmer, K., and Nehrke, G. (2014). The distribution of polyenes in the shell of *Arctica islandica* from North Atlantic localities: a confocal Raman microscopy study. *J. Molluscan Stud.* 80, 365–370. doi: 10.1093/mollus/eyu033

Sturm, R. A., Duffy, D. L., Zhao, Z. Z., Leite, F. P., Stark, M. S., Hayward, N. K., et al. (2008). A single SNP in an evolutionary conserved region within intron 86 of the *HERC2* gene determines human blue-brown eye color. *Am. J. Hum. Genetics* 82, 424–431. doi: 10.1016/j.ajhg.2007.11.005

Sudhir, K., Glen, S., Li, M., Christina, K., and Koichiro, T. (2018). MEGA X: Molecular evolutionary genetics analysis across computing platforms. *Mol. Biol. Evol.* 35, 1547–1549. doi: 10.1093/molbev/msy096

Sukumaran, S., and Yu, J. (2014). Association mapping of genetic resources: achievements and future perspectives. *Genom. Plant Genetic Resourc.* 1, 207–235. doi: 10.1007/978-94-007-7572-5_9

Sun, X., Liu, Z., Zhou, L., Wu, B., Dong, Y., and Yang, A. (2016). Integration of next generation sequencing and EPR analysis to uncover molecular mechanism underlying shell color variation in scallops. *PLoS ONE* 11:e0161876. doi: 10.1371/journal.pone.0161876

Sun, X., Wu, B., Zhou, L., Liu, Z., Dong, Y., and Yang, A. (2017). Isolation and characterization of melanin pigment from Yesso scallop *Patinopecten yessoensis*. *J. Ocean Univ. China* 16, 279–284. doi: 10.1007/s11802-017-3162-6

Sun, X., Yang, A., Wu, B., Zhou, L., and Liu, Z. (2015). Characterization of the mantle transcriptome of yesso scallop (*Patinopecten yessoensis*): identification of genes potentially involved in biomineralization and pigmentation. *PLoS ONE* 10:e0122967. doi: 10.1371/journal.pone.0122967

Takano, Y., Kubo, Y., Shimizu, K., Mise, K., Okuno, T., and Furusawa, I. (1995). Structural analysis of *PKS1*, a polyketide synthase gene involved in melanin biosynthesis in *Colletotrichum lagenarium*. *Molecul. Gene. Genet. MGG* 249, 162–167. doi: 10.1007/BF00290362

Teh, M. T., and Sugden, D. (2001). An endogenous 5-HT7 receptor mediates pigment granule dispersion in *Xenopus laevis* melanophores. *Br. J. Pharmacol.* 132, 1799–1808. doi: 10.1038/sj.bjp.0703988

Teng, W., Cong, R., Que, H., and Zhang, G. (2018). *De novo* transcriptome sequencing reveals candidate genes involved in orange shell coloration of bay scallop *Argopecten irradians*. *J. Oceanol. Limnol.* 36, 1408–1416. doi: 10.1007/s00343-018-7063-3

Tobin, A. B. (1997). Phosphorylation of phospholipase C-coupled receptors. *Pharmacol. Therapeut.* 75, 135–151. doi: 10.1016/S0163-7258(97)00053-3

Underwood, A. J., and Creese, R. G. (1976). Observations on the biology of the trochid gastropod *Austrocochlea constricta* (Lamarck) (Prosobranchia). II. The effects of available food on shell-banding pattern. *J. Experim. Marine Biol. Ecol.* 23, 229–240. doi: 10.1016/0022-0981(76)90022-8

Visser, M., Palstra, R. J., and Kayser, M. (2014). Human skin color is influenced by an intergenic DNA polymorphism regulating transcription of the nearby *BNC2* pigmentation gene. *Hum. Mol. Genet.* 23, 5750–5762. doi: 10.1093/hmg/ddu289

Wang, C., Liu, B., Liu, X., Ma, B., Zhao, Y., Zhao, X., et al. (2017). Selection of a new scallop strain, the Bohai Red, from the hybrid between the bay scallop and the Peruvian scallop. *Aquaculture* 479, 250–255. doi: 10.1016/j.aquaculture.2017.05.045

Wang, L., Zhang, H., Song, L., and Guo, X. (2007). Loss of allele diversity in introduced populations of the hermaphroditic bay scallop *Argopecten irradians*. *Aquaculture* 271, 252–259. doi: 10.1016/j.aquaculture.2007.06.020

Wang, S., Liu, P., Lv, J., Li, Y., Cheng, T., Zhang, L., et al. (2016). Serial sequencing of isolength RAD tags for cost-efficient genome-wide profiling of genetic and epigenetic variations. *Nat. Protoc.* 11, 2189–2200. doi: 10.1038/nprot.2016.133

Wang, X., Ding, S., Yin, D., Song, J., and Chang, Y. (2020). Response to selection for growth in the second generation of two shell color lines of the bay scallop *Argopecten irradians*. *Aquaculture* 528:735536. doi: 10.1016/j.aquaculture.2020.735536

Wang, Y., Liu, L., and Chen, Z. (2019). Transcriptome profiling of cervical cancer cells acquired resistance to cisplatin by deep sequencing. *Artific. Cells Nanomed. Biotechnol.* 47, 2820–2829. doi: 10.1080/21691401.2019.1637882

Williams, S. T., Ito, S., Wakamatsu, K., Goral, T., Edwards, N. P., Wogelius, R. A., et al. (2016). Identification of shell colour pigments in marine snails *Clanculus pharaonius* and *C. margaritarius (Trochoidea; Gastropoda)*. PLOS ONE 11, e0156664. doi: 10.1371/journal.pone.0156664

Xu, C., Li, Q., Yu, H., Liu, S., Kong, L., and Chong, J. (2019). Inheritance of shell pigmentation in Pacific oyster *Crassostrea gigas*. *Aquaculture* 512:734249. doi: 10.1016/j.aquaculture.2019.734249

Yue, X., Nie, Q., Xiao, G., and Liu, B. (2015). Transcriptome analysis of shell color-related genes in the clam *Meretrix*. *Marine Biotechnol.* 17, 364–374. doi: 10.1007/s10126-015-9625-0

Zhang, G., Zhang, W., Ye, R., Fang, A., Ren, G., Zheng, R., et al. (2016). Analysis of selective breeding of nacre color in two strains of *Hyriopsis cumingii* Lea based on the cielab colorspace. *J. Shellfish Res.* 35, 225–229. doi: 10.2983/035.035.0124

Zhang, J., Kobert, K., Flouri, T., and Stamatakis, A. (2014). PEAR: a fast and accurate Illumina Paired-End reAd mergeR. *Bioinformatics* 30, 614–620. doi: 10.1093/bioinformatics/btt593

Zhang, S., Wang, H., Yu, J., Jiang, F., Yue, X., and Liu, B. (2018). Identification of a gene encoding microphthalmia-associated transcription factor and its association with shell color in the clam *Meretrix petechialis*. *Comparat. Biochem. Physiol. Part B: Biochem. Molecul. Biol.* 225, 75–83. doi: 10.1016/j.cbpb.2018.04.007

Zhang, Y., Zhang, L., Sun, J., Qiu, J., Hu, X., Hu, J., et al. (2014). Proteomic analysis identifies proteins related to carotenoid accumulation in Yesso scallop (*Patinopecten yessoensis*). *Food Chem.* 147, 111–116. doi: 10.1016/j.foodchem.2013.09.078

Zhao, J., Gupta, S., Seielstad, M., Liu, J., and Thalamuthu, A. (2011). Pathway-based analysis using reduced gene subsets in genome-wide association studies. *BMC Bioinform.* 12:17. doi: 10.1186/1471-2105-12-17

Zhao, L., Li, Y., Li, Y., Yu, J., Liao, H., Wang, S., et al. (2017). A genome-wide association study identifies the genomic region associated with shell color in Yesso scallop, *Patinopecten yessoensis*. *Marine Biotechnol.* 19, 301–309. doi: 10.1007/s10126-017-9751-y

Zheng, H., Liu, H., Zhang, T., Wang, S., Sun, Z., Liu, W., et al. (2010). Total carotenoid differences in scallop tissues of *Chlamys nobilis* (Bivalve: Pectinidae) with regard to gender and shell colour. *Food Chem.* 122, 1164–1167. doi: 10.1016/j.foodchem.2010.03.109

Zheng, H., Xu, F., and Zhang, G. (2011). Crosses between two subspecies of bay scallop *Argopecten irradians* and heterosis for yield traits at harvest. *Aquac. Res.* 42, 602–612. doi: 10.1111/j.1365-2109.2010.02657.x

Zheng, H., Zhang, G., Liu, X., Zhang, F., and Guo, X. (2004). Different responses to selection in two stocks of the bay scallop, *Argopecten irradians* Lamarck (1819). *J. Exp. Mar. Biol. Ecol.* 313, 213–223. doi: 10.1016/j.jembe.2004.04.015

Zheng, H., Zhang, T., Sun, Z., Liu, W., and Liu, H. (2013). Inheritance of shell colours in the noble scallop *Chlamys nobilis* (Bivalve: Pectinidae). *Aquac. Res.* 44, 1229–1235. doi: 10.1111/j.1365-2109.2012.03124.x

Conflict of Interest: The authors declare that the research was conducted in the absence of any commercial or financial relationships that could be construed as a potential conflict of interest.

Publisher's Note: All claims expressed in this article are solely those of the authors and do not necessarily represent those of their affiliated organizations, or those of the publisher, the editors and the reviewers. Any product that may be evaluated in this article, or claim that may be made by its manufacturer, is not guaranteed or endorsed by the publisher.

frontiers in Marine Science

ORIGINAL RESEARCH
published: 09 September 2021
doi: 10.3389/fmars.2021.741230

Chromosome Identification and Cytogenetic Map Construction of Zhikong Scallop (*Chlamys farreri*) Based on Fluorescence *in situ* Hybridization

Liping Hu[1,2], *Liming Jiang*[1,2], *Qiang Xing*[1,3], *Zujing Yang*[1,3]*, *Qiang Zhao*[2], *Liyong Wang*[2], *Xiaoting Huang*[1,3]* and *Zhenmin Bao*[1,3]

[1] MOE Key Laboratory of Marine Genetics and Breeding, College of Marine Life Sciences, Ocean University of China, Qingdao, China, [2] Yantai Marine Economic Research Institute, Yantai, China, [3] Laboratory for Marine Fisheries Science and Food Production Processes, Qingdao National Laboratory for Marine Science and Technology, Qingdao, China

OPEN ACCESS

Edited by:
Yuehuan Zhang,
South China Sea Institute of Oceanology, Chinese Academy of Sciences (CAS), China

Reviewed by:
Bin Xia,
Qingdao Agricultural University, China
Zhenming Lv,
Zhejiang Ocean University, China

***Correspondence:**
Zujing Yang
yzj@ouc.edu.cn
Xiaoting Huang
xthuang@ouc.edu.cn

Specialty section:
This article was submitted to Marine Fisheries, Aquaculture and Living Resources, a section of the journal Frontiers in Marine Science

Received: 14 July 2021
Accepted: 09 August 2021
Published: 09 September 2021

Citation:
Hu L, Jiang L, Xing Q, Yang Z, Zhao Q, Wang L, Huang X and Bao Z (2021) Chromosome Identification and Cytogenetic Map Construction of Zhikong Scallop (Chlamys farreri) Based on Fluorescence in situ Hybridization. Front. Mar. Sci. 8:741230. doi: 10.3389/fmars.2021.741230

Zhikong scallop (*Chlamys farreri*) is a bivalve species with broad economic and biological value, and an essential species of aquaculture in North China. Recently, efforts have been made to improve knowledge of genome, genetics, and cytogenetics, which is devoted to develop the molecular breeding project for the scallop. In this study, we constructed a cytogenetic map and identified all chromosomes of *C. farreri* using fluorescence *in situ* hybridization (FISH). A total of 100 Bacterial Artificial Chromosome (BAC) clones and 27 fosmid clones, including 58 microsatellite marker-anchored BAC clones, 4 genes-anchored BAC clones, 38 random BAC clones, 22 repetitive sequences-anchored fosmid clones, and 5 gene-anchored fosmid clones, were tested as probes, and 69 of them produced specific and stable signal on one pair of chromosomes. Then, multiple co-hybridizations were conducted to distinguish all the submetacentric and subtelocentric chromosomes with similar morphology by the abovementioned chromosome-specific markers. On this basis, a cytogenetic map of *C. farreri* containing 69 clones was constructed by co-hybridization and karyotype analysis. The markers covered all 19 pairs of chromosomes, and the average number of markers on each chromosome was 3.6. The cytogenetic map provides a platform for genetic and genomic analysis of *C. farreri*, which facilitates the molecular breeding project of *C. farreri* and promotes the comparative studies of chromosome evolution in scallops and even bivalves.

Keywords: *Chlamys farreri*, chromosome identification, cytogenetic map, FISH, BAC, fosmid

INTRODUCTION

Chromosome identification is an important part of genome research, which provides a broad view of chromatin structure organization. Traditionally, chromosome morphological characteristics (e.g., chromosome relative lengths and arm ratios) and banding techniques (e.g., C-banding, G-banding, and NORs-banding) have shown to be a powerful utility for the chromosome identification in many animal and plant species (Xu and Shi, 2007; Ocalewicz et al., 2008). However,

these procedures have proven to be difficult in scallops and other bivalve species (Insua et al., 1998; Gajardo et al., 2002; Huang et al., 2007a,b), which were mainly due to the lack of cultured cells for the preparation of high-quality elongated chromosomes.

The development of fluorescence *in situ* hybridization (FISH) is a significant step toward chromosome identification, and FISH is a well-established approach for determining the location and relative order of DNA sequences in chromosomes (Zhang et al., 2008a; Merlo et al., 2021). The initial probes used as landmarks for chromosome distinguish were repetitive sequences, mainly including satellite sequences (Wang et al., 2001; Zhang et al., 2008a), ribosomal DNA (Zhang et al., 1999; Xu et al., 2001; Huang et al., 2007a,b), and histone genes (Eirín-López et al., 2002, 2004; Zhang et al., 2007a). However, these repetitive sequence probes could identify only partial chromosomes. Mapping using large-insert DNA genomic clones [e.g., P1, fosmid, and bacterial artificial chromosome (BAC)] as probes for FISH provided an alternative approach that has been successfully used in some shellfish species. Wang et al. (2005) accomplished the identification of seven pairs of chromosomes of eastern oysters by using P1 clones as FISH probes. Zhang et al. (2008a) successfully distinguished eight pairs of chromosomes of *Chlamys farreri* using eight fosmid clones. Li et al. (2016) and Yang et al. (2016) identified six and five pairs of chromosomes of *Patinopecten yessoensis* by six and eight fosmid clones, respectively. In some plant species, especially in those species with relatively small chromosomes, BAC-FISH had played an important role in chromosome identification and cytogenetic researches (Wang et al., 2007; Wai et al., 2010; Lee et al., 2020; Mendoza et al., 2020). In white campion *Silene latifolia*, 12 pairs of chromosomes were distinguished by the simultaneous hybridization of five BAC clones and three repetitive sequences on mitotic chromosomes (Lengerova et al., 2004). Furthermore, based on FISH, the integration of genetic and cytogenetic maps was carried out in many organisms, such as *Bombyx mori* (Yoshido et al., 2005), *C. farreri* (Feng et al., 2014), *Scophthalmus maximus* (Taboada et al., 2014), *P. yessoensis* (Yang et al., 2019), and some plants (Wang et al., 2006; Xiong et al., 2010; Dong et al., 2018; Yurkevich et al., 2021), which assisted the chromosome identification and evolution researches in the abovementioned species.

Zhikong scallop (*C. farreri*, Jones et Preston 1904), distributing along the sea coast of China, Japan, Korea, and Sakhalin in Russia, is one of the main mariculture species in China. It possessed the typical chromosome number for Pectinidae ($2n = 38$), which was considered the closest representative of the ancestral karyotype of Pectinidae (Wang and Guo, 2004). Chromosome morphological characteristics revealed that the chromosomes of *C. farreri* were continuous in size. In addition to three pairs of typical metacentric chromosomes, *C. farreri* had 16 pairs of submetacentric and/or subtelocentric chromosomes appearing similar in morphology (Wang and Guo, 2004; Huang et al., 2006). In recent years, the genomic resources of *C. farreri*, such as BAC libraries (Zhang et al., 2008b; Cheng, 2010), fosmid libraries (Zhang et al., 2007b), and genome (Li et al., 2017), are available. Some chromosomes of *C. farreri* had been distinguished by FISH using repetitive sequences or large-insert DNA clones as probes (Huang et al., 2006, 2012; Zhang et al., 2007a, 2008b; Huan et al., 2009a,b; Feng et al., 2014). However, it is still difficult to identify all 19 chromosomes of *C. farreri* based on the present FISH results of these probes. Until now, a complete set of chromosome-specific DNA markers have not been developed for this species.

In this study, chromosome-specific BAC and fosmid clones were selected as probes to accomplish the chromosome identification and cytogenetic map construction of *C. farreri* by multiple FISH. Among them, each chromosome of *C. farreri* could be identified by co-hybridization and karyotype analysis. The integrated cytogenetic map will contribute to further characterization and application of the *C. farreri* genome.

MATERIALS AND METHODS

Scallop Chromosome Preparation

Zhikong scallop (*C. farreri*) trochophore larvae were obtained from an aquatic hatchery in Rongcheng, Shandong Province, China. Metaphase was prepared according to the methods described by Huang et al. (2006). Briefly, larvae were treated with colchicines (0.01%) in seawater for 2 h at room temperature, then exposed to 0.075 M KCl solution for 20 min, and, finally, fixed three times (15 min each) in the fresh Carnoy's solution (ethanol:glacial acetic acid, 3:1 v/v). The fixed larvae were dissociated into a cell suspension using 50% acetic acid and then dropped onto hot-wet slides and air-dried.

Probe Selection and Labeling

The chosen clones for testing signal specificity in FISH studies included microsatellite marker-anchored BAC clones, genes-anchored BAC clones, random BAC clones, repetitive sequences-anchored fosmid clones, and genes-anchored fosmid clones. All BAC clones used in the FISH analysis were screened from the *C. farreri* *Hind*III-BAC (BH) and *Bam*HI-BAC (BB) libraries (Cheng, 2010), and the microsatellite markers contained in the BAC clones were selected based on the SSR genetic map of *C. farreri* (Zhan et al., 2009). All fosmid clones used in the FISH analysis were selected according to the information from pair-end sequencing results of the fosmid library of *C. farreri* (Zhang et al., 2007b). BAC and fosmid DNA were isolated *via* the standard laboratory methods (Sambrook et al., 1989) and then labeled with digoxigenin (Dig)-11-2'-deoxyuridine 5'-triphosphate (dUTP) or biotin-16-dUTP by Dig- or biotin-nick translation mix (Roche, American) according to the instructions of the manufacturer.

FISH and Co-hybridization

The FISH experiments were performed following the methods published by Huang et al. (2007b). Chromosome slides were pretreated with RNase A (100 μg/ml) in 2× saline sodium citrate buffer (SSC) at 37°C for 1 h, followed by pepsin (0.005%) in 10 mM HCl at 37°C for 10 min. Chromosome slides were denatured in 70% formamide mixed with 2× SSC at 75°C for 2 min, immediately dehydrated in a chilled ethanol series (70, 90, and 100%) for 5 min each, and then air-dried. Hybridization mixture consisted of 10–15 ng/μl Dig-11-dUTP and/or biotin-16-dUTP labeled BAC or fosmid DNAs, 50% deionized formamide, 10% dextran sulfate, and 2× SSC. The hybridization mixture was denatured at 90°C for 5 min and immediately cooled

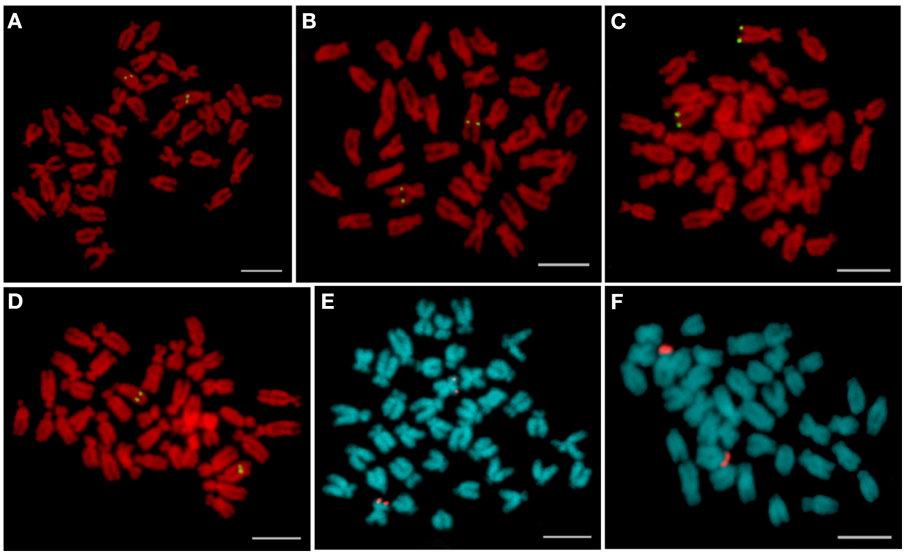

FIGURE 1 | Representative fluorescence *in situ* hybridization (FISH) pattern of bacterial artificial chromosome (BAC) and fosmid clones on mitotic metaphase chromosomes of *Chlamys farreri*. **(A)** BH1060G11 containing microsatellite marker CFLD034; **(B)** BH565D6 containing microsatellite marker CFMSM014; **(C)** BB240C9 containing *Dmrt4* gene; **(D)** random BAC clone BH60F12; **(E)** F421B9 containing repetitive sequences; and **(F)** F541H2 containing *Hsp22* gene. Scale bars = 5 μm.

on ice. A denatured probe was then applied onto the slide, and DNA-DNA *in situ* hybridization was carried out in a moist chamber at 37°C for 16–18 h. Then, slides were washed in 50% formamide in 2× SSC at 37°C for 10 min, in 1× SSC at 37°C three times (5 min each), and in 2× SSC at room temperature for 5 min. Dig-labeled and biotin-labeled probes were detected using anti-digoxigenin-rhodamine (Roche, American) and fluorescein isothiocyanate (FITC)-conjugated avidin D cell sorter (DOS) (Vector, American), respectively. Chromosomal DNAs were then counterstained with 4,6-diamidino-2-phenylindole (DAPI) or 1.5 μg/ml propidium iodide (PI) at 37°C for 10 min. Hybridization signals were visualized, and images were recorded using a (Leica, Germany) DM4000B microscope equipped with an epifluorescence system and a charge coupled device (CCD) camera. At least 10 metaphases were examined for each probe and karyotype analysis, and the chromosomal pairs marked by clones were classified based on the Levan's criteria (Levan et al., 1964). Then, clones within distinct signals and discernable chromosomal location were selected for co-hybridization with other clones.

For co-hybridization, probes labeled with Dig- and biotin- were pooled for hybridization, and other protocol was the same as that for regular hybridization mentioned earlier.

RESULTS

Development of Chromosome-Specific Cytogenetic Markers

After screening the BAC libraries of *C. farreri*, 58 microsatellite marker-anchored BAC clones and 4 genes-anchored BAC clones were obtained. Meanwhile, according to the information of pair-end sequences of the fosmid clones, 22 repetitive sequences-anchored clones and 5 genes-anchored clones were selected. In addition, 38 random BAC clones were also tested as a probe for FISH. In total, 127 BAC and fosmid clones were isolated and hybridized on mitotic metaphase chromosomes. Among them, 72 clones could successfully map on the chromosomes, and a total of 69 clones, including 58 BACs and 11 fosmids, could produce specific FISH signals on one pair of chromosomes. These BAC and fosmid clones producing unambiguous and reproducible FISH signals were used as chromosome-specific markers. As shown in **Figure 1A**, BAC clone BH1060G11 containing microsatellite marker CFLD034 hybridized to the middle of the long arm of a big pair of subtelocentric chromosomes. BAC clone BH565D6 containing microsatellite marker CFMSM014 was mapped to the long arm of a pair of submetacentric chromosomes, about two-fifth of the long arm away from the centromere (**Figure 1B**). FISH with BAC clone BB240C9 containing *Dmrt4* gene revealed one single locus on the telomeric region of the long arm of a pair of submetacentric chromosomes (**Figure 1C**). The random BAC clone BH60F12 was located on the long arm of a pair of subtelocentric chromosomes, about four-fifth of the long arm away from the centromere (**Figure 1D**). In addition, fosmid clone F421B9 containing tandemly repetitive DNAs showed distinct signals on the telomeric region of the short arm of a pair of metacentric chromosomes (**Figure 1E**). Hybridization with fosmid clone F541H2 containing heat shock protein (*Hsp22*) gene (**Figure 1F**) revealed intensive signals on the short arm of a pair of subtelocentric chromosomes. The FISH results of all the isolated chromosome-specific clones were summarized in **Table 1**.

TABLE 1 | Sequence information and hybridization results of 69 chromosome-specific markers in the cytogenetic map of *Chlamys farreri*.

Chr. No.	Clone name	Information of clone	Location of signals		Clone reference
			Chr. type	Arm type	
1	BB34D10	Random BAC clone	m	p	In this study
	F418E2	Forward and reverse sequences show partial identity (2008)	m	p	In this study
	F411D6	Containing tandem repeats with unit length of 27bp at both ends	m	q	In this study
	BH984B5	Containing microsatellite marker CFMSP003 from LG14	m	q	Feng et al., 2014
	BB105B2	Containing microsatellite marker CFJD047 from LG14	m	q	Feng et al., 2014
2	F421B9	Forward and reverse sequences are repeats and show highly similar	m	p	In this study
	BB311A9	Containing microsatellite marker CFFD048 from LG4	m	q	Feng et al., 2014
3	BB98C5	Random BAC clone	m	p	Feng et al., 2014
4	F400H6	Forward sequence significantly hit to histone H4 gene	sm	P	Zhang et al., 2008b
	BH565D6	Containing microsatellite marker CFMSM014 from LG16	sm	q	Feng et al., 2014
	F409B11	Forward and reverse sequences show partial identity	sm	q	In this study
5	BH1003H1	Random BAC clone	sm	q	In this study
	BB324B4	Random BAC clone	sm	q	In this study
	F420E3	Both end sequences showing identity are tandem repeats with unit length of 39 bp	sm	q	In this study
6	BB34D12	Random BAC clone	sm	p	In this study
	F458F11	Forward sequence significantly hit to histone H1 gene	sm	q	Zhang et al., 2008b
	BH64A4	Random BAC clone	sm	q	In this study
	BB233G7	Containing microsatellite marker CFOD062 from LG13	sm	q	Feng et al., 2014
7	BH799B12	Containing microsatellite marker CFHD004 from LG3	sm/st	p	Feng et al., 2014
	BH1049A9	Containing microsatellite marker CFFD093 from LG3	sm/st	q	Feng et al., 2014
	BB240C9	Containing male sex-related (*Dmrt4*) gene	sm/st	q	In this study
8	BH1304E11	Containing microsatellite marker CFLD006 from LG1	sm	q	Feng et al., 2014
	BH1162H2	Containing microsatellite marker CFFD143 from LG1	sm	q	Feng et al., 2014
	BH983A4	Random BAC clone	sm	q	In this study
	BH60B1	Random BAC clone	sm	q	In this study
9	BB24F11	Random BAC clone	st	p	
	BB199E2	Random BAC clone	st	q	In this study
	BH1060G11	Containing microsatellite marker CFLD034 from LG7	st	q	In this study
	BH431C4	Containing microsatellite marker CFE15 from LG19	st	q	Feng et al., 2014
10	BH793B11	Containing microsatellite marker CFKD077 from LG2	st	p	Feng et al., 2014
	BB69B10	Containing microsatellite marker CFFD041 from LG16	st	p	Feng et al., 2014
	F408A12	Both end sequences significantly hit to 18S rRNA gene	st	p	Zhang et al., 2008b
	F541H2	Forward sequence significantly hit to heat shock protein (*Hsp22*) gene	st	p	In this study
	F393C3	Forward sequences are tandem repeats with unit length of 155 bp	st	p	In this study
	BH323B5	Random BAC clone	st	p	In this study
	BB34A12	Random BAC clone	st	q	In this study
	BH783B4	Containing microsatellite marker CFBD213 from LG2	st	q	Feng et al., 2014
	BH1285H8	Containing microsatellite marker CFBD170 from LG6	st	q	Feng et al., 2014
11	BH885H2	Containing microsatellite marker CFKD091 from LG12	st	p	Feng et al., 2014
	BB224B4	Containing microsatellite marker CFKD096 from LG12	st	p	Feng et al., 2014
	BH1053D8	Random BAC clone	st	q	In this study
	BH1003G1	Containing microsatellite marker CFBD224 from LG18	st	q	Feng et al., 2014
12	BB32G4	Containing microsatellite marker CFCD134 from LG7	st	q	In this study
	BB138G5	Containing microsatellite marker CFLD047 from LG8	st	q	In this study
	BB29H9	Random BAC clone	st	q	In this study
13	BH1291D12	Containing microsatellite marker CFFD110 from LG7	st	q	Feng et al., 2014
	BB312B11	Containing microsatellite marker KD022 from LG13	st	q	Feng et al., 2014
14	BH1308F7	Containing microsatellite marker CFLD137 from LG3	st	p	In this study
	BH986B2	Containing microsatellite marker CFAD184 from LG18	st	q	Feng et al., 2014

(Continued)

TABLE 1 | Continued

Chr. No.	Clone name	Information of clone	Location of signals		Clone reference
			Chr. type	Arm type	
	BH966F2	Containing microsatellite marker CFCD172 from LG8	st	q	Feng et al., 2014
	BB27C6	Containing microsatellite marker CFFD167 from LG10	st	q	In this study
	BH60F12	Random BAC clone	st	q	In this study
15	BH60F1	Random BAC clone	st	p	In this study
	BB75B6	Containing microsatellite marker CFFBD204 from LG11	st	p	Feng et al., 2014
	BH1308E3	Containing microsatellite marker CFBD193 from LG11	st	q	Feng et al., 2014
	BB23H9	Containing microsatellite marker CFCD104 from LG6	st	q	In this study
	BH569G6	Random BAC clone	st	q	In this study
16	BH1261C3	Containing microsatellite marker CFOD056 from LG17	st	q	Feng et al., 2014
	BB239F4	Random BAC clone	st	q	In this study
	BH368F12	Containing microsatellite marker CFLD144 from LG17	st	q	Feng et al., 2014
17	F410G10	Containing tandem repeats with unit length of 25 bp at both ends	st	p	In this study
	BH64E8	Random BAC clone	st	p	In this study
	BH1002C5	Containing sex-related (*Q-dx*) gene	st	p	In this study
	BB239A6	Containing microsatellite marker CFLD060 from LG19	st	q	Feng et al., 2014
18	BH60A1	Random BAC clone	st	p	In this study
	BB105A1	Containing microsatellite marker CFFD144 from LG5	st	p	Feng et al., 2014
	BB86D4	Containing microsatellite marker CFAD018 from LG5	st	q	Feng et al., 2014
19	BB235A11	Containing microsatellite marker CFID005 from LG15	st	q	Feng et al., 2014
	BB39F11	Containing microsatellite marker CFJD077 from LG10	st	q	Feng et al., 2014

Chr, chromosome; BH, HindIII-BAC library; BB, BamHI-BAC library; F, Fosmid library; m, metacentric chromosomes; sm, submetacentric chromosomes; st, subtelocentric chromosomes; p, short arm of chromosome; q, long arm of chromosome; LG, linkage group.

Identification of All Chromosomes

Three pairs of typical metacentric chromosomes of *C. farreri* could be identified by their distinct size, as shown in **Figure 2**. The largest one was named as Chr. 1, then the middle one as Chr. 2, and the smallest one as Chr. 3.

Due to the other 16 pairs of submetacentric and subtelocentric chromosomes appeared similar in morphology and continuous in size, at least 15 chromosome-specific markers are required to distinguish them. Among the 69 clones showing unambiguous unique FISH signals in the earlier results, 15 most reliable representations from the 15 pairs of submetacentric and subtelocentric chromosomes, which were shown to be located on the same type or similar size of chromosomes (**Figure 3**), were selected for multiple two-color FISH. As shown in **Supplementary Figure 1-1a**, three clones of F409B11, F420E3, and F458F11 were hybridized to three different pairs of submetacentric chromosomes, and we named the three chromosomes as Chr. 4 (**Figure 3A**), Chr. 5 (**Figure 3B**), and Chr. 6 (**Figure 3C**), respectively. The co-hybridization with the mixed probes containing F409B11, F420E3, F458F11, and BH1049A9 (**Supplementary Figure 1-1b**) revealed that BAC clone BH1049A9 located another submetacentric/subtelocentric chromosomes, which were different from Chr. 4–6, and we named it as Chr. 7 (**Figure 3D**). **Supplementary Figures 1-1c,d** show that BH1304E11 was mapped on one small pair of submetacentric chromosomes differing from Chr. 4–7, and this chromosome was named for Chr. 8 (**Figure 3E**).

Fluorescence *in situ* hybridization with BH1060G11, F409B11 (Chr. 4), and F420E3 (Chr. 5) (**Supplementary Figure 1-1e**) revealed that BH1060G11 was mapped on a big pair of a subtelocentric chromosome instead of submetacentric Chr. 4 and Chr. 5, although these three pairs of chromosomes showed similar size. The subtelocentric chromosome mapped with BH1060G11 was named as Chr. 9 (**Figure 3F**). Similarly, **Supplementary Figures 1-1f,g** show that clone F408A12 was assigned to another big pair of subtelocentric chromosomes named as Chr. 10 (**Figure 3G**) differing from Chr. 9 and Chr. 8. Clone BH1003G1 was located on a pair of submetacentric/subtelocentric chromosomes, and the co-hybridizations of this clone and F458F11 (Chr. 6) (**Supplementary Figure 1-1j**), this clone and BH1049A9 (Chr. 7) (**Supplementary Figure 1-1h**), as well as this clone and BH1060G11 (Chr. 9) and F408A12 (Chr. 10) (**Supplementary Figure 1-1i**) confirmed the different chromosome assignments of BH1003G1, and we named this chromosome as Chr. 11 (**Figure 3H**). BB32G4, BH60F1, BH1003G1 (Chr. 11), and F408A12 (Chr. 10) were hybridized to four different pairs of chromosomes (**Supplementary Figures 1-1k,l**), and the chromosome hybridized by BB32G4 was named as Chr. 12 (**Figure 3I**). BH1291D12 was located on another pair of subtelocentric

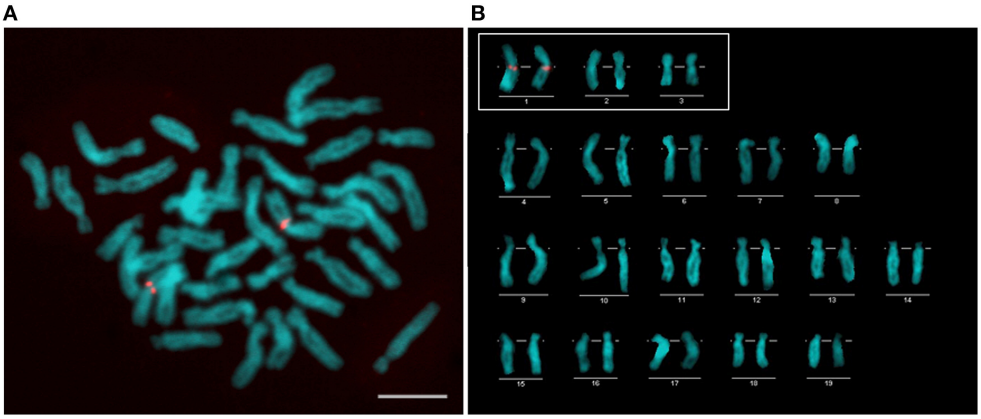

FIGURE 2 | FISH mapping of F411D6 containing tandem repeats **(A)** and karyotype **(B)** of *C. farreri* after 4,6-diamidino-2-phenylindole (DAPI) staining. The chromosomes in the white box are three pairs of metacentric chromosomes. Scale bars = 5 μm.

chromosomes differing from Chr. 9–12 by the co-hybridization of BH1291D12, BH1060G11 (Chr. 9), and BB32G4 (Chr. 12) (**Supplementary Figure 1-1m**), BH1291D12 and F408A12 (Chr. 10) (**Supplementary Figure 1-1n**), as well as BH1291D12 and BH1003G1 (Chr. 11) (**Supplementary Figure 1-1o**), and this pair of chromosomes was named as Chr. 13 (**Figure 3J**). **Supplementary Figures 1-2(a–c)** revealed that clones BH60F12, BH1291D12 (Chr. 13), BB32G4 (Chr. 12), BH1003G1 (Chr. 11), and BH60F1 were assigned to different subtelocentric chromosomes, and the BH60F12-locating chromosome was slightly smaller than Chr. 13, and it was named as Chr. 14 (**Figure 3K**). Clone BH60F1 confirmed its location at another subtelocentric chromosome [named as Chr. 15 (**Figure 3L**)] by the co-hybridization results of this clone with the other clones mapped to the identified subtelocentric chromosomes, as shown in **Supplementary Figures 1-1(k,l)**, **1-2(c,d)**. The clone BB239F4 had an assignment of the subtelocentric chromosome, named as Chr. 16 (**Figure 3M**), which were different from Chr. 9–15, which were revealed by the co-hybridization results of BB239F4 and BH60F1 (Chr. 15) (**Supplementary Figure 1-2e**), BB239F4 and BH60F12 (Chr. 14) (**Supplementary Figure 1-2f**), BB239F4, BH1291D12 (Chr. 13), and BH1060G11 (Chr. 11) (**Supplementary Figure 1-2g**), BB239F4 and BB32G4 (Chr. 12) (**Supplementary Figure 1-2h**), as well as BB239F4, F408A12 (Chr. 10), and BH1060G11 (Chr. 9) (**Supplementary Figure 1-2i**). BH64E8 and BH60A1 were readily mapped on two pairs of small subtelocentric chromosomes (**Supplementary Figure 1-2o**), and the co-hybridization analysis revealed that they could separate these two pairs of chromosomes from the other small subtelocentric chromosomes involving Chr. 16, 15, 14, and 13, as shown in **Supplementary Figures 1-2(j–n)**. These two small subtelocentric chromosomes were named as Chr. 17 (**Figure 3N**) and Chr. 18 (**Figure 3O**), respectively. Since 15 of the 16 submetacentric and subtelocentric chromosomes with similar morphology and size had been identified, the remaining one would be automatically distinguished, and it was named as Chr. 19.

Based on the abovementioned data, all the 19 chromosomes of *C. farreri* were successfully distinguished and named for the first time.

Construction of a Cytogenetic Map

The establishment of representative chromosome-specific cytogenetic markers allowed to construct a cytogenetic map of *C. farreri*. The main strategy was to do the co-localization analysis of the newly developed chromosome-specific markers and the representative chromosome-specific markers on the same chromosome.

By using this strategy, fosmid clone F418E2, BAC clones BB34D10, BH984B5, and BB105B2 were all hybridized to Chr. 1, and BB34D10 was located on the telomeric region of the short arm of Chr. 1, F418E2 was on the middle of one arm of this chromosome, while BH984B5 and BB105B2 were mapped to about middle and telomeric region of the other arm of Chr. 1, respectively (**Figures 4A–C**). The co-hybridizations of F458F11, BB34D12, and BB233G7 (**Figure 4D**), as well as BB34D12 and BH64A4 (**Figure 4E**), revealed that these clones were all assigned to Chr. 6. Among them, BB34D12 was located near the telomeric region of the short arm, the other three clones were all mapped to the long arm, which were close to the centromere (F458F11 and BH64A4), and about telomeric region of Chr. 6 (BB233G7). As shown in **Figure 4F**, BH1049A9 and BB240C9 were observed as located near the centromere and at the telomeric region of the long arm of Chr. 7, respectively. Clone BH799B12 was also mapped to Chr. 7, and it was located about midway on the short arm of this chromosome. The co-hybridization of BH1304E11 and BH60B1 confirmed their locations on Chr. 8, near the centromere and about four-fifth of the long arm away from the centromere, respectively (**Figure 4G**). BH1162H2 was mapped to the location that was near the BH1304E11 on the same chromosome. The chromosomal locations of F541H2, F393C3, BB69B10, BH323B5, and BH1285H8 were analyzed by simultaneously hybridizing with the representative clone of Chr. 10 (F408A12). Five clones

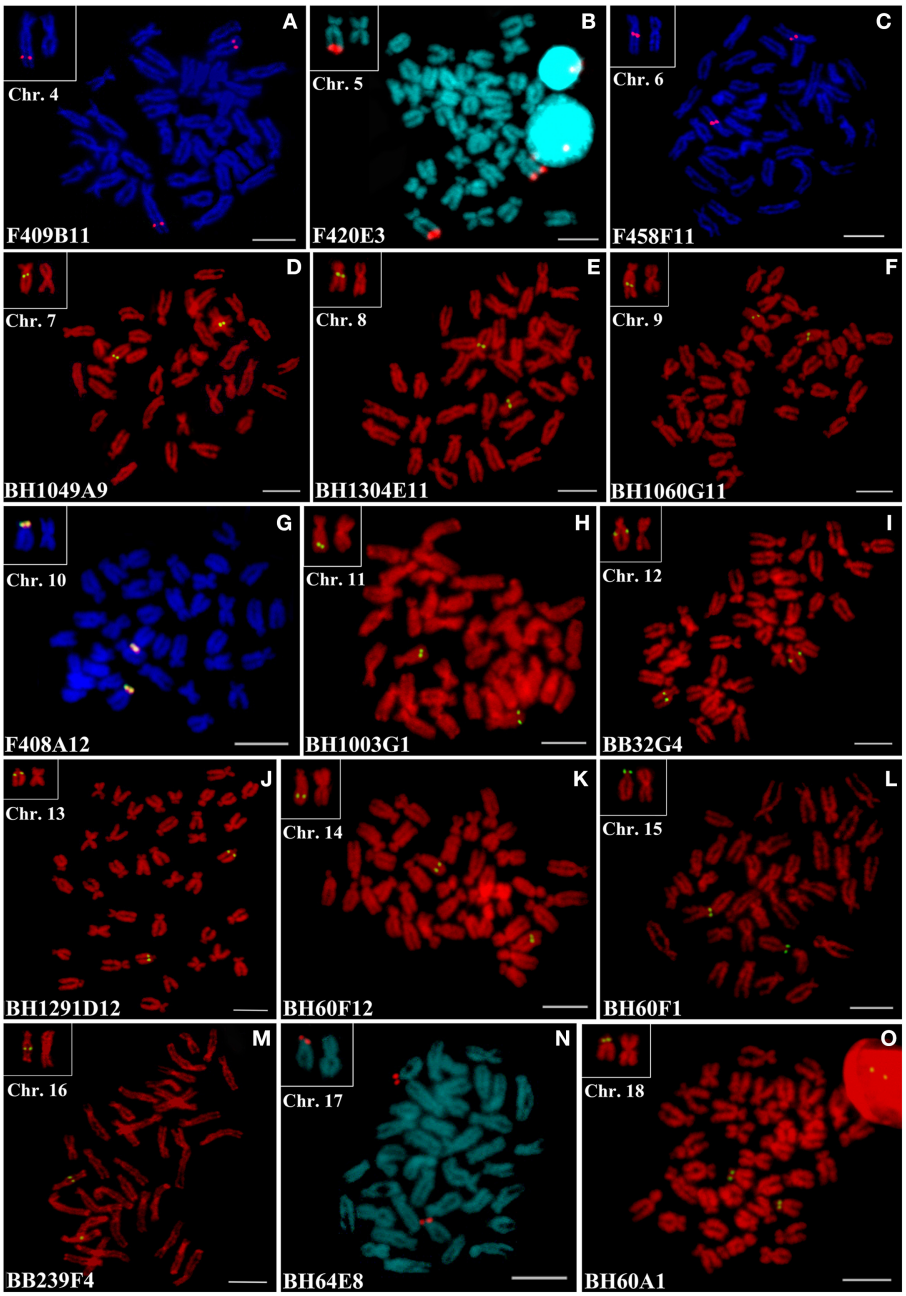

FIGURE 3 | FISH results of 15 reliable representations from the 15 pairs of submetacentric and subtelocentric chromosomes of *C. farreri*. The chromosomes in the white box are the chromosome with specific signal and the largest metacentric chromosome. Scale bars = 5 μm.

of F541H2, F393C3, BB69B10, BH323B5, and F408A12 were all located on the short arm of Chr. 10, and their relative order on the chromosome was not unambiguous on the highly condensed metaphase chromosomes (**Figures 4H–J**). Clone BH1285H8 produced bright signals on the long arm of Chr. 10, about one-fourth from the centromere (BH1285H8, **Figure 4K**). BH60F12 and BH 966F2 were hybridized on the same chromosome with BH986B2, and they were all located on the long arm of Chr. 14 (**Figures 4L,M**). Of which, BH986B2 was mapped to near the centromeric region, BH 966F2 was on the middle of the long arm, and BH60F12 was about three-fourth from the centromere. BAC clones BH60F1 and BB75B6 were both located at the end of the short arm of Chr. 15 (**Figure 4N**). BH1308E3 was also mapped to Chr. 15 by co-hybridization with BB75B6, and it was

hybridized near the centromeric region of the long arm. BH64E8 and BH1002C5 were simultaneously located on the short arm of Chr. 17, and it was difficult to distinguish their chromosomal locations (**Figure 4O**).

Referring to the FISH results of a single specific probe, 69 clones could produce positive signals on a single chromosome. However, for some of them, especially those producing high background, it was difficult to achieve the co-hybridization of multiple clones because the FISH condition of these clones was different. We determined the chromosomal locations of these clones by the karyotype analysis based on their one-color FISH. In summary, all the available data were used for the construction of the karyotype ideogram of *C. farreri*, which indicated the FISH mapping of 69 cytogenetic markers (**Figure 5**). All the information on these 69 markers is provided in **Table 1**. The cytogenetic markers on different chromosomes were different, with 3.6 as an average number of markers. Of which, Chr. 10 has the most number of markers which was nine, and Chr. 3 has the least number of markers which was one.

DISCUSSION

Cytogenetic researches rely on accurate chromosome identification, which is also the first step in understanding the genome organization of a species. Unfortunately, it is still a challenge to identify all the individual chromosomes of *C. farreri*. The studies of karyotype, silver staining, and fluorescent staining (PI and DAPI) offered limited information for the reliably distinguishing *C. farreri* chromosomes (Huang et al., 2006; Xu et al., 2011). Based on the large-insert genomic DNA libraries (e.g., fosmid and BAC), FISH is an efficient method to accomplish the chromosome-specific identification. Zhang et al. (2008a) have successfully identified eight chromosomes of *C. farreri* by using eight fosmid clones as FISH probes, among which five clones were simultaneously located on different chromosomes by two-color co-hybridization. Combining these results, in this study, we isolated some chromosome-specific fosmid clones from the *C. farreri* fosmid library (Zhang et al., 2007b). In addition, a large number of chromosome-specific BAC clones were also isolated from the *C. farreri* BH and BB libraries (Cheng, 2010). These were the basis for identifying individual chromosome and constructing the cytogenetic map of *C. farreri*.

In many plant species, chromosomes were arranged based on their lengths in conventional karyotyping, with the longest one as the first chromosome and the shortest one as the last chromosome, although the chromosome numbering systems were not unified. In the potato karyotyping, the chromosomes distinguished based on the Giemsa-banding patterns were named either numerically, from chromosome 1 to chromosome 12 (Pijnacker and Ferwerda, 1984), or alphabetically, from chromosome A to chromosome L (Wagenvoort et al., 1994). Moreover, the pachytene chromosomes of potatoes were named using a Roman number system (Yeh and Peloquin, 1965). Unfortunately, there has been no unambiguous numbering and naming for all the chromosomes of *C. farreri* due to the lack of accurate chromosomal markers. In some species, such as sorghum (Kim et al., 2002, 2005), silkworm (Yoshido et al., 2005), alpaca (Mendoza et al., 2020), and *Senegalese sole* (Merlo et al., 2021), all chromosomes could be identified by simultaneous FISH of a cocktail of landed large-insert DNA clones and/or repetitive DNA probes. In this study, we successfully distinguished all the 19 chromosomes of *C. farreri* through multiple two-color FISH and numbered them based on the chromosome-specific markers aided by the chromosomal morphology and lengths. They were arranged with the three metacentric chromosomes being chromosomes 1–3 from the longest one to the shortest one, following the five submetacentric chromosomes being chromosomes 4–8 from the longest one to the shortest one, and then all the subtelocentric chromosomes being chromosomes 9–19. In addition, our studies confirmed that this naming system could apply to the species with a large number of chromosomes as well as having difficulty in identifying individual chromosome using traditional karyotype and banding methods.

The chromosome assignment of large-insert DNA clones containing genetic markers provided bases not only for the chromosome identification but also for the integration of cytological and genetic linkage maps. Some species have been conducted multiple linkage maps, but it is still difficult to compare or integrate the different linkage groups due to the lack of a common nomenclature system for linkage groups. Actually, the problem could be solved by unifying the linkage groups and chromosomes, which could be accomplished by the chromosomal location of the large-insert DNA clones containing genetic markers (Mendes et al., 2020). In many plant species, the FISH mapping of BAC clones containing amplified fragment length polymorphism (AFLP) or microsatellite genetic markers accomplished the recognition of chromosomes as well as the integration of linkage groups and chromosomes (Kim et al., 2002, 2005; Tang et al., 2009; Yurkevich et al., 2021). Similar research was also reported in the scallop species of *P. yessoensis*, and the 19 LGs were successfully assigned to 19 pairs of chromosomes by SNP-anchored fosmid clones, which achieving chromosome recognition and integration of genetic and cytogenetic map (Yang et al., 2019). In addition, the distributions of microsatellite markers in some plant species were observed that they were specific and correlated with certain chromosomal organizations (e.g., euchromatin, heterochromatin, and centromeres) (Cuadrado et al., 2008). With the aid of chromosome-specific markers, we could locate more molecular markers on the chromosomes to understand chromosomal structures.

The integration of cytogenetic and genomic data had advanced our understanding of the genomic structure and evolution of the organism. In mandarin *Citrus reticulata*, the BAC-FISH of 18 BAC clones established correlations between mandarin scaffolds and chromosomes, allowing further structural genomic and comparative study with the sweet orange genome (Mendes et al., 2020). In Siberian sturgeon *Acipenser baerii* with polyploidy genome, a detailed chromosomal map consisted of starlet-specific repeats and chromosomal probes reconstructed the evolutionary reorganizations of 11 ancestral chromosomes after Ac1R and Ac2R (Biltueva et al., 2020). A cytogenetic map of *C. farreri* was constructed for the first time by FISH with probes of clones, such as microsatellite-anchored

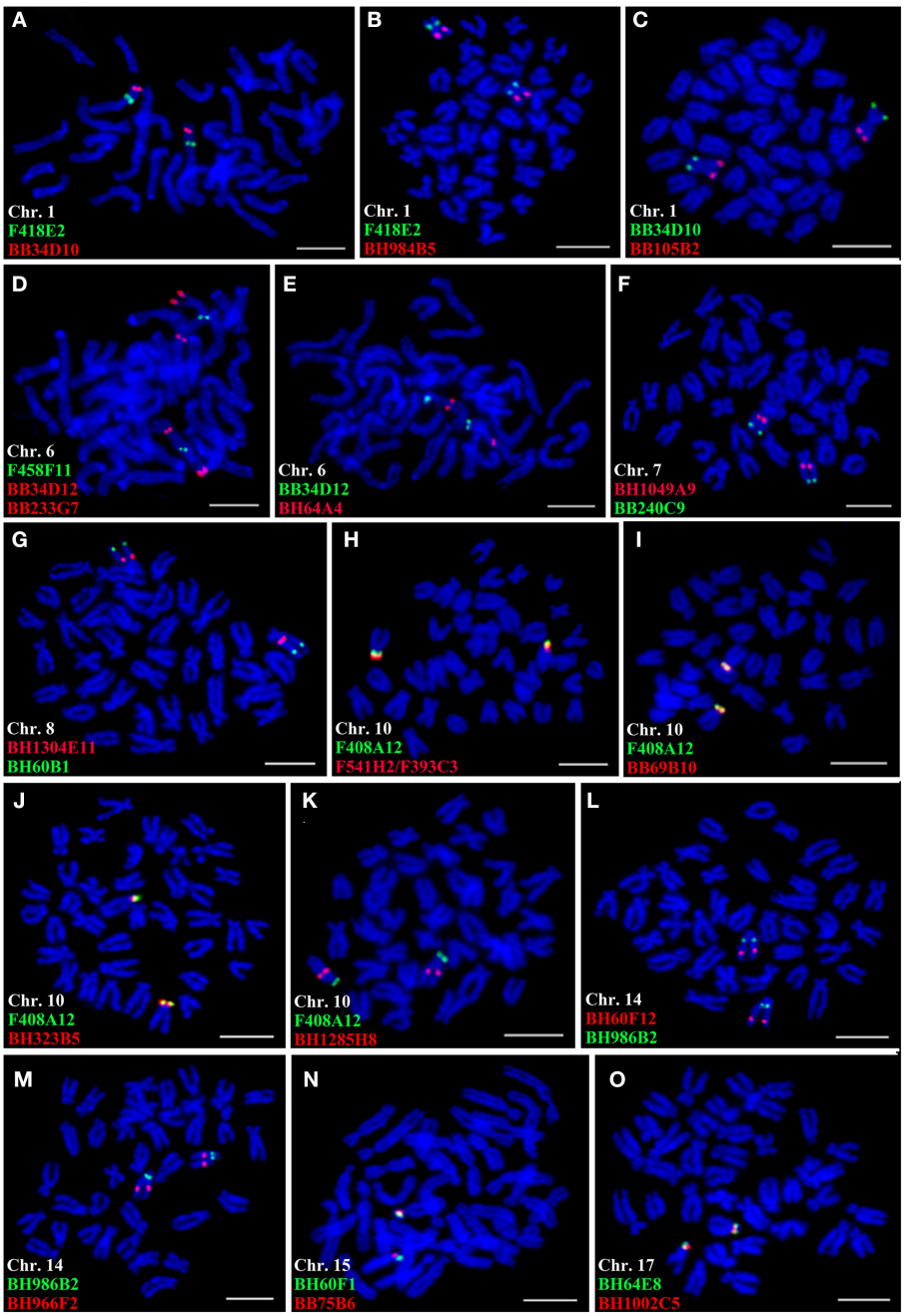

FIGURE 4 | Co-hybridization of the clones on the same chromosomes. Red and green signals correspond to digoxigenin (Dig)- and biotin-labeled probes, respectively. Scale bars = 5 μm.

BAC clones, random BAC clones, repetitive DNA fosmid clones, genes-anchored BAC, and fosmid clones. All the mapped BAC and fosmid clones could be developed as sequence-tagged sites for further unification of the cytogenetic, physical, and genetic maps. The use of these markers is highly reproducible and does not require any specific stages of chromosome preparation which is required for traditional bandings. FISH with the chromosome-specific cytogenetic markers is the certain method for chromosome identification and construction of a cytogenetic map of *C. farreri*. In addition, the *C. farreri* genome contained numerous repetitive sequences which led to difficulties in genome assembly. The ability to identify the position of the repetitive sequence on the chromosomes of *C. farreri* would enable us to fill those gaps in the genome.

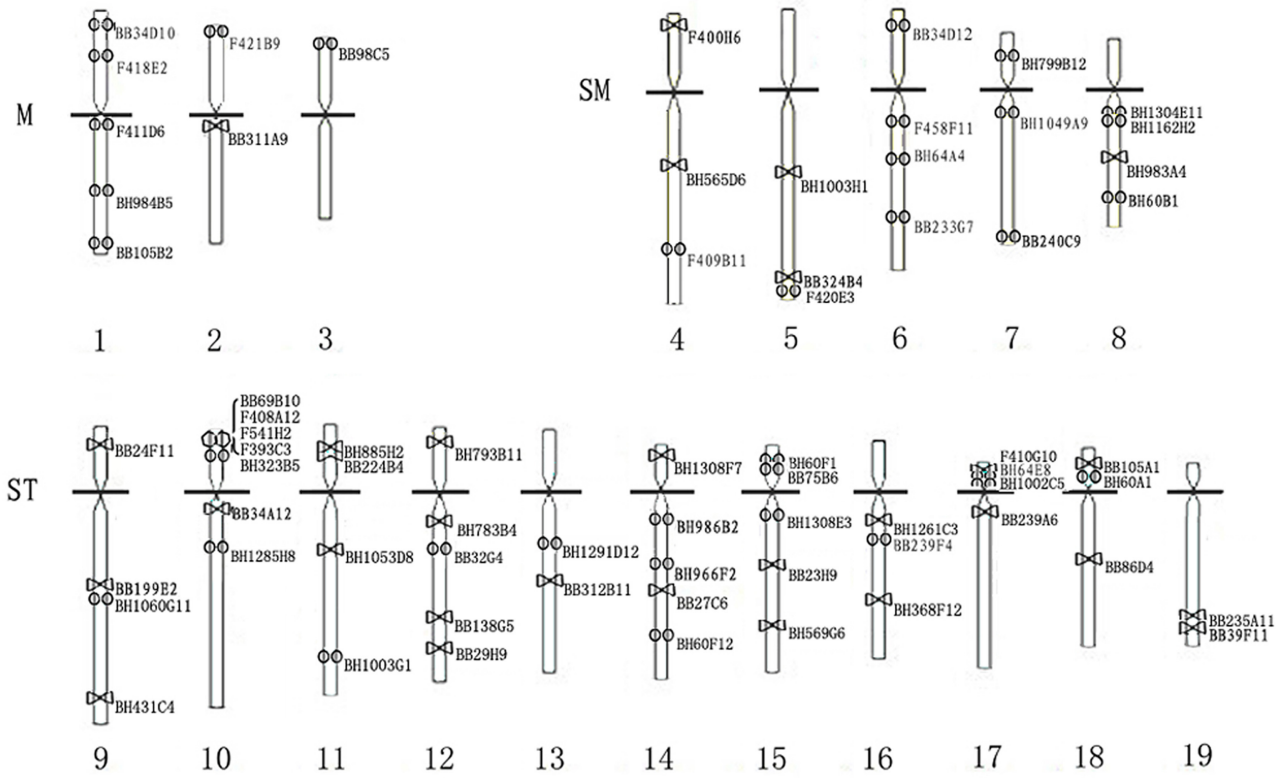

FIGURE 5 | Karyotype ideogram of *C. farreri* showing chromosome assignment of 69 markers. The circles represent the loci of the markers that have been confirmed by co-hybridization. The triangles represent the loci of the markers determined by the karyotype analysis.

CONCLUSION

The cytogenetic mapping will facilitate accurate assembly of the genome and understanding the genome organization of *C. farreri*, and enable comparative cytogenetic research of the bivalve.

DATA AVAILABILITY STATEMENT

The original contributions presented in the study are included in the article/**Supplementary Material**, further inquiries can be directed to the corresponding authors.

AUTHOR CONTRIBUTIONS

LH, XH, and ZB conceived and designed the experiments. QX, QZ, and LW collected the samples. LH, LJ, and QX performed the experiments. LH, ZY, and XH analyzed the data. LH wrote the manuscript. All authors have read and approved the final manuscript.

FUNDING

This study was supported by the grants of the Chinese Ministry of Science and Technology through the National Key Research and Development Program of China (2018YFD0901402 and 2018YFD0900304), the Yantai Science and Technology Project (2020MSGY063), the China Agriculture Research System of MOF and MARA, and the Earmarked Fund for Agriculture Seed Improvement Project of the Shandong Province (2020LZGC016).

SUPPLEMENTARY MATERIAL

The Supplementary Material for this article can be found online at: https://www.frontiersin.org/articles/10.3389/fmars.2021.741230/full#supplementary-material

Supplementary Figures 1-1 and 1-2 | Co-hybridization of the markers on different chromosomes. Red and green signals correspond to Dig- and biotin-labeled probes, respectively. Scale bars = 5 μm.

REFERENCES

Biltueva, L. S., Prokopov, D. Y., Romanenko, S. A., Interesova, E. A., Schartl, M., and Trifonov, V. A. (2020). Chromosome distribution of highly conserved tandemly arranged repetitive DNAs in the Siberian Sturgeon (*Acipenser baerii*). *Genes* 11:1375. doi: 10.3390/genes11111375

Cheng, J. (2010). *Construction and Application Analysis of Large Fragment Genomic Libraries of Zhikong Scallop (Chlamys farreri)*. Diss. Ocean University of China.

Cuadrado, A., Cardoso, M., and Jouve, N. (2008). Physical organisation of simple sequence repeats (SSRs) in Triticeae: structural, functional and evolutionary implications. *Cytogenet. Genome Res.* 120, 210–219. doi: 10.1159/000121069

Dong, G., Shen, J., Zhang, Q., Wang, J., Yu, Q., Ming, R., et al. (2018). Development and applications of chromosome-specific cytogenetic BAC-FISH probes in *S. spontaneum*. *Front. Plant Sci.* 9:218. doi: 10.3389/fpls.2018.00218

Eirín-López, J. M., González-Tizón, A. M., Martínez, A., and Méndez, J. (2002). Molecular and evolutionary analysis of mussel histone genes (*mytilus* spp): possible evidence of an "orphon origin" for H1 histone genes. *J. Mol. Evol.* 55, 272–283. doi: 10.1007/s00239-002-2325-1

Eirín-López, J. M., Ruiz, M. F., González-Tizón, A. M., Martínez, A., Sánchez, L., and Méndez, J. (2004). Molecular evolutionary characterization of the mussel *mytilus* histone multigene family: first record of a tandemly repeated unit of five histone genes containing an h1 subtype with "orphon" features. *J. Mol. Evol.* 58, 131–144. doi: 10.1007/s00239-003-2531-5

Feng, L., Hu, L., Fu, X., Liao, H., Li, X., Zhan, A., et al. (2014). An integrated genetic and cytogenetic map for Zhikong scallop, *Chlamys farreri*, based on microsatellite markers. *PLoS ONE* 9:e92567. doi: 10.1371/journal.pone.0092567

Gajardo, G., Parraguez, M., and Colihueque, N. (2002). Karyotype analysis and chromosome banding of the Chilean-Peruvian scallop *Argopecten purpuratus* (Lamarck, 1819). *J. Shellfish Res.* 21, 585–590.

Huan, P., Zhang, X., Li, F., Zhang, Y., Zhao, C., Liu, B., et al. (2009a). Chromosomal localization of heat shock protein 70 (HSP70) gene in Zhikong scallop *Chlamys farreri* using BAC-FISH. *Mar. Sci.* 33, 10–15. doi: 10.1016/S1874-8651(10)60079-8

Huan, P., Zhang, X., Li, F., Zhang, Y., Zhao, C., Liu, B., et al. (2009b). Chromosomal localization and development of SNP markers of a serine protease gene in Farrer's scallop (*Chlamys farreri*). *Hereditas* 31, 1241–1247. doi: 10.3724/SP.J.1005.2009.01241

Huang, C., Huan, P., Zhang, X., and Xiang, J. (2012). Chromosomal localization of NDPK gene in Zhikong scallop *Chlamys farreri* using BAC-FISH. *Mar. Sci.* 36, 1–5. Available online at: https://xueshu.baidu.com/usercenter/paper/show?paperid=9bd6e080843f2fdea7474c7bfb505fab

Huang, X., Bao, Z., Bi, K., Hu, J., Zhang, C., Zhang, Q., et al. (2006). Chromosomal localization of the major ribosomal RNA genes in scallop *Chlamys farreri*. *Acta Oceanol. Sin.* 25, 108–115. doi: 10.1016/j.marchem.2005.09.003

Huang, X., Hu, J., Hu, X., Zhang, C., Zhang, L., Wang, S., et al. (2007a). Cytogenetic characterization of the bay scallop, *Argopecten irradians irradians*, by multiple staining techniques and fluorescence in situ hybridization. *Genes Genet. Syst.* 82, 257–263. doi: 10.1266/ggs.82.257

Huang, X., Hu, X., Hu, J., Zhang, L., Wang, S., Lu, W., et al. (2007b). Mapping of ribosomal DNA and (TTAGGG)n telomeric sequence by FISH in the bivalve *Patinopecten yessoensis*. *J. Mollus Stud.* 73, 393–398. doi: 10.1093/mollus/eym036

Insua, A., López-Piñón, M. J., and Méndez, J. (1998). Characterization of *Aequipecten opercularis* (Bivalvia: Pectinidae) chromosomes by different staining techniques and fluorescent in situ hybridization. *Genes Genet. Syst.* 73, 193–200. doi: 10.1266/ggs.73.193

Kim, J. S., Childs, K. L., Islam-Faridi, M. N., Menz, M. A., Klein, R. R., Klein, P. E., et al. (2002). Integrated karyotyping of sorghum by in situ hybridization of landed BACs. *Genome* 45, 402–412. doi: 10.1139/g01-141

Kim, J. S., Klein, P. E., Klein, R. R., Price, H. J., Mullet, J. E., and Stelly, D. M. (2005). Chromosome identification and nomenclature of *Sorghum bicolor*. *Genetics* 169, 1169–1173. doi: 10.1534/genetics.104.035980

Lee, L. S., Navarro-Domínguez, B. M., Wu, Z., Montiel, E. E., Badenhorst, D., Bista, B., et al. (2020). Karyotypic evolution of sauropsid vertebrates illuminated by optical and physical mapping of the painted turtle and slider turtle genomes. *Genes* 11:928. doi: 10.3390/genes11080928

Lengerova, M., Kejnovsky, E., Hobza, R., Macas, J., Grant, S. R., and Vyskot, B. (2004). Multicolor FISH mapping of the dioecious model plant, *Silene latifolia*. *Theor. Appl. Genet.* 108, 1193–1199. doi: 10.1007/s00122-003-1568-6

Levan, A., Fredga, K., and Sandberg, A. A. (1964). Nomenclature for centromeric position on chromosomes. *Hereditas* 52, 201–220. doi: 10.1111/j.1601-5223.1964.tb01953.x

Li, X., Yang, Z., Liao, H., Zhang, Z., Huang, X., and Bao, Z. (2016). Chromosomal mapping of tandem repeats in the Yesso scallop, *Patinopecten yessoensis* (Jay, 1857), utilizing fluorescence *in situ* hybridization. *Comp. Cytogenet.* 10, 157–169. doi: 10.3897/CompCytogen.v10i1.7391

Li, Y., Sun, X., Hu, X., Xun, X., Zhang, J., Guo, X., et al. (2017). Scallop genome reveals molecular adaptations to semi-sessile life and neurotoxins. *Nat. Commun.* 8:1721. doi: 10.1038/s41467-017-01927-0

Mendes, S., Régis, T., Terol, J., Soares Filho, W. D. S., Talon, M., and Pedrosa-Harand, A. (2020). Integration of mandarin (*Citrus reticulata*) cytogenetic map with its genome sequence. *Genome* 63, 437–444. doi: 10.1139/gen-2020-0046

Mendoza, M. N., Raudsepp, T., More, M. J., Gutiérrez, G. A., and Ponce de León, F. A. (2020). Cytogenetic mapping of 35 new markers in the Alpaca (*Vicugna pacos*). *Genes* 11:522. doi: 10.3390/genes11050522

Merlo, M. A., Portela-Bens, S., Rodríguez, M. E., García-Angulo, A., Cross, I., Arias-Pérez, A., et al. (2021). A comprehensive integrated genetic map of the complete karyotype of *Solea senegalensis* (Kaup 1858). *Genes* 12:49. doi: 10.3390/genes12010049

Ocalewicz, K., Penman, D. J., and Babiak, I. (2008). Variation in size and location of the Ag-NOR in the Atlantic halibut (*Hippoglossus hippoglossus*). *Genetica* 133, 261–267. doi: 10.1007/s10709-007-9209-7

Pijnacker, L. P., and Ferwerda, M. A. (1984). Giemsa C-banding of potato chromosomes. *Genome* 26, 415–419. doi: 10.1139/g84-067

Sambrook, J., Fritsch, E. F., Maniatis, T. (1989). *Molecular Cloning: A Laboratory Manual*. Cold Spring Harbor, NY: Cold Spring Harbor Laboratory Press.

Taboada, X., Pansonato-Alves, J. C., Foresti, F., Martínez, P., Viñas, A., Pardo, B. G., et al. (2014). Consolidation of the genetic and cytogenetic maps of turbot (*Scophthalmus maximus*) using FISH with BAC clones. *Chromosoma* 123, 281–291. doi: 10.1007/s00412-014-0452-2

Tang, X., de Boer, J. M., van Eck, H. J., Bachem, C., Visser, R. G., and de Jong, H. (2009). Assignment of genetic linkage maps to diploid *Solanum tuberosum* pachytene chromosomes by BAC-FISH technology. *Chromosome Res.* 17, 899–915. doi: 10.1007/s10577-009-9077-3

Wagenvoort, M., Rouwendal, G. J. A., and Kuiper-Groenwold, G., Vries-van, Hulten. (1994). Chromosome identification in potato trisomics (2n=2x+1=25) by conventional staining, Giemsa C-banding and non-radioactive in situ hybridization. *Cytologia* 59, 405–417. doi: 10.1508/cytologia.59.405

Wai, C. M., Ming, R., Moore, P. H., Paull, R. E., and Yu, Q. (2010). Development of chromosome-specific cytogenetic markers and merging of linkage fragments in Papaya. *Trop. Plant Biol.* 3, 171–181. doi: 10.1007/s12042-010-9054-1

Wang, C. J. R., Harper, L., and Cande, W. Z. (2006). High-resolution single-copy gene fluorescence in situ hybridization and its use in the construction of a cytogenetic map of maize chromosome 9. *Plant Cell* 18, 529–544. doi: 10.2307/20076617

Wang, K., Guo, W., and Zhang, T. (2007). Development of one set of chromosome-specific microsatellite-containing BACs and their physical mapping in *Gossypium hirsutum* L. *Theor. Appl. Genet.* 115, 675–682. doi: 10.1007/s00122-007-0598-x

Wang, Y., and Guo, X. (2004). Chromosomal rearrangement in Pectinidae revealed by rRNA loci and implications for bivalve evolution. *Biol. Bull.* 207, 247–256. doi: 10.2307/1543213

Wang, Y., Xu, Z., and Guo, X. (2001). A centromeric satellite sequence in the Pacific oyster (*Crassostrea gigas* Thunberg) identified by fluorescence in situ hybridization. *Mar. Biotechnol.* 3, 486–492. doi: 10.1007/s10126-001-0063-3

Wang, Y., Xu, Z., Pierce, J. C., and Guo, X. (2005). Characterization of eastern oyster (*Crassostrea virginica* Gmelin) chromosomes by fluorescence in situ hybridization with bacteriophage P1 clones. *Mar. Biotechnol.* 7, 207–214. doi: 10.1007/s10126-004-0051-y

Xiong, Z., Kim, J. S., and Pires, J. C. (2010). Integration of genetic, physical, and cytogenetic maps for *Brassica rapa* chromosome A7. *Cytogenet. Genome Res.* 129, 190–198. doi: 10.1159/000314640

Xu, J., Ren, X., Bao, Z., Wang, S., Hu, L., and Huang, X. (2011). DAPI-banding and PI-banding of Zhikong scallop (*Chlamys farreri*). *Periodical of Ocean University of China* 4, 77–80. doi: 10.3724/SP.J.1011.2011.00415

Xu, J., and Shi, J. (2007). C banding and fluorescent banding pattern of the chromosomes of *Cunninghamia lanceolate*. *Mol. Plant Breed.* 4, 515–520.

Xu, Z., Guo, X., Gaffney, P. M., and Pierce, J. C. (2001). Chromosomal location of themajor ribosomal RNA genes in *Crassostrea virginica* and *Crassostrea gigas*. *Veliger* 44, 79–83. doi: 10.3901/JME.2001.02.079

Yang, Z., Li, X., Liao, H., Hu, L., Peng, C., Zhang, Z., et al. (2019). A molecular cytogenetic map of scallop (*Patinopecten yessoensis*). *Mar. Biotechnol.* 21, 731–742. doi: 10.1007/s10126-019-09918-6

Yang, Z., Li, X., Liao, H., Hu, L., Zhang, Z., Zhao, B., et al. (2016). Physical mapping of immune-related genes in Yesso scallop (*Patinopecten yessoensis*) using fluorescent in situ hybridization. *Comp. Cytogenet.* 10, 529–541. doi: 10.3897/CompCytogen.v10i4.10047

Yeh, B. P., and Peloquin, S. J. (1965). Pachytene chromosomes of the potato (*Solanum tuberosum*, Group Andigena). *Am. J. Bot.* 52, 1014–1020.

Yoshido, A., Bando, H., Yasukochi, Y., and Sahara, K. (2005). The *Bombyx mori* karyotype and the assignment of linkage groups. *Genetics* 170, 675–685. doi: 10.1534/genetics.104.040352

Yurkevich, O. Y., Samatadze, T. E., Selyutina, I. Y., Romashkina, S. I., Zoshchuk, S. A., Amosova, A. V., et al. (2021). Molecular cytogenetics of eurasian species of the genus *Hedysarum* L.(Fabaceae). *Plants* 10, 89. doi: 10.3390/plants10010089

Zhan, A., Hu, J., Hu, X., Hui, M., Wang, M., Peng, W., et al. (2009). Construction of microsatellite-based linkage maps and identification of size-related quantitative trait loci for Zhikong scallop (*Chlamys farreri*). *Anim. Genet.* 40, 821–831. doi: 10.1111/j.1365-2052.2009.01920.x

Zhang, L., Bao, Z., Cheng, J., Li, H., Huang, X., Wang, S., et al. (2007b). Fosmid library construction and initial analysis of end sequences in Zhikong scallop (*Chlamys farreri*). *Mar. Biotechnol.* 9, 606–612. doi: 10.1007/s10126-007-9014-4

Zhang, L., Bao, Z., Wang, S., Hu, X., and Hu, J. (2008a). FISH mapping and identification of Zhikong scallop (*Chlamys farreri*) chromosomes. *Mar. Biotechnol.* 10, 151–157. doi: 10.1007/s10126-007-9045-x

Zhang, L., Bao, Z., Wang, S., Huang, X., and Hu, J. (2007a). Chromosome rearrangements in Pectinidae (Bivalvia: Pteriomorphia) implied based on chromosomal localization of histone H3 gene in four scallops. *Genetica* 130, 193–198. doi: 10.1007/s10709-006-9006-8

Zhang, Q., Yu, G., Cooper, R. K., and Tiersch, T. R. (1999). Chromosomal location by fluorescence in situ hybridization of the 28S ribosomal RNA gene of the eastern oyster. *J. Shellfish Res.* 18, 431–435.

Zhang, Y., Zhang, X., Scheuring, C. F., Zhang, H., Li, F., and Xiang, J. (2008b). Construction of bacterial artificial chromosome libraries for Zhikong scallop *Chlamys farreri*. *Chin J Oceanol Limn* 26, 215–218. doi: 10.1007/s00343-008-0215-0

Conflict of Interest: The authors declare that the research was conducted in the absence of any commercial or financial relationships that could be construed as a potential conflict of interest.

Publisher's Note: All claims expressed in this article are solely those of the authors and do not necessarily represent those of their affiliated organizations, or those of the publisher, the editors and the reviewers. Any product that may be evaluated in this article, or claim that may be made by its manufacturer, is not guaranteed or endorsed by the publisher.

frontiers in Marine Science

ORIGINAL RESEARCH
published: 16 September 2021
doi: 10.3389/fmars.2021.746026

Characterization and Function Analysis of β, β-carotene-9′, 10′-oxygenase 2 (*BCDO2*) Gene in Carotenoid Metabolism of the Red Shell Hard Clam (*Meretrix meretrix*)

Lulu Fu[1,2], *Heming Shi*[2], *Wenfang Dai*[2,3], *Hanhan Yao*[2]*, *Yongbo Bao*[2], *Zhihua Lin*[2,3] *and Yinghui Dong*[2]*

[1] College of Fisheries, Henan Normal University, Xinxiang, China, [2] Zhejiang Key Laboratory of Aquatic Germplasm Resources, College of Biological & Environmental Sciences, Zhejiang Wanli University, Ningbo, China, [3] Ninghai Institute of Mariculture Breeding and Seed Industry, Zhejiang Wanli University, Ningbo, China

OPEN ACCESS

Edited by:
Liqiang Zhao,
Guangdong Ocean University (GDOU), China

Reviewed by:
Zhe Zheng,
Guangdong Ocean University (GDOU), China
Hao Song,
Institute of Oceanology, Chinese Academy of Sciences (CAS), China

***Correspondence:**
Hanhan Yao
yaohanhan1020@126.com
Yinghui Dong
dongyinghui118@126.com

Specialty section:
This article was submitted to Marine Fisheries, Aquaculture and Living Resources, a section of the journal Frontiers in Marine Science

Received: 23 July 2021
Accepted: 19 August 2021
Published: 16 September 2021

Citation:
Fu L, Shi H, Dai W, Yao H, Bao Y, Lin Z and Dong Y (2021) Characterization and Function Analysis of β, β-carotene-9′, 10′-oxygenase 2 (BCDO2) Gene in Carotenoid Metabolism of the Red Shell Hard Clam (Meretrix meretrix). Front. Mar. Sci. 8:746026. doi: 10.3389/fmars.2021.746026

The relationship between carotenoid and shellfish shell color has gained increasing attention. β, β-carotene-9′,10′-oxygenase 2 (BCDO2) is a key enzyme in animal carotenoid metabolism, and its accumulation affects the change in body color, as demonstrated in mammals, birds, and fish. However, it is unclear whether BCDO2 is involved in the formation of the red shell color of clam. To explore the molecular structure and biological function of *BCDO2* gene in the process of carotenoids accumulation, in this study, the *BCDO2* from hard clam *Meretrix meretrix* (designated as *Mm-BCDO2*) was cloned and characterized, and the single-nucleotide polymorphisms (SNPs) associated with shell color were detected. The results of qRT-PCR indicated that *Mm-BCDO2* gene was expressed in all six tested tissues, and the expression of mantle was significantly higher than other tissues ($P < 0.05$). The association analysis identified 20 SNPs in the exons of *Mm-BCDO2*, among which three loci (i.e., c.984A > C, c.1148C > T, and c.1187A > T) were remarkably related ($P < 0.05$) to the shell color of clam. The western blot analysis revealed that the expression level of Mm-BCDO2 in the mantle of red shell clams was stronger than that of white shell clams ($P < 0.05$). Further, the immunofluorescence analysis indicated that the single-layer columnar cells at the edge of the mantle were the major sites for the Mm-BCDO2 secretion. This study explored the potential impacts of *BCDO2* gene on the shell color of *M. meretrix*, which provided a theoretical basis for a better understanding of the important role of *BCDO2* in carotenoid metabolism.

Keywords: *Meretrix meretrix*, *BCDO2*, carotenoids, shell color, SNP

INTRODUCTION

Carotenoids are a class of fat-soluble pigments, which can be classified into two groups: the xanthophylls (oxygenated-contained group) and the carotenes (hydrocarbons without oxygenated group) (Wu et al., 2016). It has been reported that carotenoids play an important role in various aspects of animal life. For example, it acts as precursors of vitamin A and antioxidants to involve

in host physiological response (Svensson and Wong, 2011; Milani et al., 2017). The zeaxanthin, lutein, and astaxanthin have a positive effect on antioxidant and light filtering by preventing vision loss and eye diseases (Li et al., 2017), hence protecting the eyesight to a certain extent (Felix et al., 2011). Moreover, carotenoids and their derivatives are involved in the coloration of feathers, skin, and shells, which play a signal role in mate selection, social competition, and species recognition (Blount and Mcgraw, 2008).

Notably, animals that are unable to *de novo* synthesize carotenoids can get them from the diet (Zheng et al., 2010). The metabolic process of carotenoids in animals includes a series of metabolic reactions. Enzyme degradation is the key step for the utilization of carotenoids. So far, two types of carotene oxygenase, β-carotene 15, 15′-monooxygenase (BCMO1) and β-carotene 9′, 10′-dioxygenase (BCDO2), have been identified in vertebrates (Wu et al., 2016). BCMO1 is a key enzyme that converts β-carotene into vitamin A. Most β-carotene is symmetrically cleaved to form metabolites under the action of BCMO1 (Georg et al., 2010). BCDO2 displays broad substrate specificity and can cleave β-carotene, generating beta-10′-apocarotenal and beta-ionone; contrarily, beta-10′-apocarotenal can be cleaved by BCMO1 to produce retinaldehyde and downstream derivatives including retinol and retinoic acid (Seña et al., 2016; Jin et al., 2020). In addition, BCMO1 catalyzes the asymmetric cleavage of xanthophylls to generate rosafluene and ionone (Seña et al., 2016). Studies have found that the expression level of *BCDO2* affects the body color of animals (Eriksson et al., 2008). Similarly, researches on the body surface color of wall lizard have showed that the content of lutein and zeatin is remarkably higher in yellow skin lizard compared with that in white skin lizard, which corresponds to the significantly lower expression level of *BCDO2* in yellow skin lizard (Andrade et al., 2019). Genetic studies on the effect of *BCDO2* mutations on "yellow fat" phenotype in cattle, sheep, and chicken have showed that *BCDO2* is implicated in the carotenoid homeostasis of milk color, fat color, and skin color (Eriksson et al., 2008; Berry et al., 2009; Tian et al., 2009; Vge and Boman, 2010). Genetic disruption (low-temperature expression and detergent choice) of *BCDO2* can significantly affect binding and turnover rates of the recombinant enzymes with various xanthophyll substrates and then increase the concentration of dietary pigment in plasma and blood of the mice (Babino et al., 2015).

Currently, researches on the role of carotenoids on the coloring of tissues and shells have been reported in *Meretrix meretrix* (Lin and Dong, 2015; Cui et al., 2018), *Crassostrea gigas* (Ge et al., 2016; Wang et al., 2016, 2018), *Pinctada fucata* (Zhang et al., 2019), *Hyriopsis cumingii* (Li et al., 2014b), *Paphia textile* (Deng et al., 2018), *Chlamys nobilis* (Zheng et al., 2010), and *Exopalaemon carinicauda* (Jin et al., 2020). The hard clam (*M. meretrix*) mainly distributed in the coastal area of Asia is one of the most important commercially cultured bivalves in China (Lin, 2015). Notably, clam shell displays two kinds of typical and differentiated colors, including white and red (Lin, 2015). The Raman spectra of the shell layer of *M. meretrix* showed that the characteristic peaks of the carotenoids of the red shell clams are stronger than those of the white shell clams (Zhan, 2015). And the total carotenoid content in the marginal membrane of the red clam mantle is about 3.4 times that of the white clam, which is a very significant difference (Qi, 2014). Especially, the ability of individual clams to ingest, absorb, and metabolize carotenoids is different, which may be one of the main reasons for the difference in shell color (Meilisza et al., 2017). However, it is unclear whether this difference attributes to the expression of the *BCDO2* gene in *M. meretrix*. To address this gap, the expression level of the *BCDO2* gene was compared between red and white shell color *M. meretrix*. Further, we investigated the distribution and SNPs of the *BCDO2* gene in the two groups. Our findings will provide valuable information for further studies on the mechanism of clam shell color formation.

MATERIALS AND METHODS

Ethics Statement

The adult hard clams (*M. meretrix*) at the age of 2 years were collected from the genetic breeding research center of Zhejiang Wanli University, China. All experimental procedures were approved by the Institutional Animal Care and Use Committee (IACUC) of Zhejiang Wanli University, China.

Sample Collection and Preparation

Six tissues including gill, siphon, digestive gland, adductor muscle, mantle, and foot were dissected, frozen immediately in liquid nitrogen, and then stored at −80°C.

RNA Extraction and cDNA Synthesis

Total RNA was extracted from the foot, mantle, digestive gland, siphon, gill, and adductor muscle by using the Trizol method. The first-strand cDNA was synthesized using the prime script RT reagent kit with gDNA Eraser (TAKARA, Japan) according to the instructions of the manufacturer. In brief, the amplification reactions were performed in a 20 μL volume containing 7 μL tissue RNA (1,500 μg/μL), 1 μL gDNA eraser, 2 μL 5× gDNA eraser buffer, 1 μL prime script RT enzyme mix 1, 4 μL 5× prime script buffer 2, 1 μL RT prime mix, and 4 μL RNase free dH_2O. The first-strand cDNA was synthesized by incubating the mixture at 42°C for 2 min, 37°C for 15 min, and finally, heating at 85°C for 5 s.

Cloning of Full-Length cDNA

The expressed sequence tag (EST) homologous to *Mm-BCDO2* was detected through the cDNA library of *M. meretrix* (GenBank accession no. SRX023927). A pair of gene-specific primers, *Mm-BCDO2*-F and *Mm-BCDO2*-R (**Table 1**), was designed on the basis of EST sequence of *Mm-BCDO2* gene. The PCR amplification was synthesized following the instructions of SMARTer^{TM} RACE cDNA amplification kit (Clontech, San Francisco, USA). The RACE PCR was performed in a 25 μL volume, which contained DEPC water, 10× advantage 2 PCR buffer, 10 mM of dNTPs, 10 μM of gene-specific primer, 10× universal primer A mix (UPM), 1 μL of diluted RACE cDNA, and 50× advantage 2 polymerase mix. The amplification was carried out as follows: 5 cycles of 94°C for 30 s, 72°C for 3 min; 5 cycles of 94°C for 30 s, 70°C for 30 s, 72°C for 3 min; and 25 cycles of 94°C for 30 s, 68°C for 30 s, 72°C 3 min. PCR products were examined on 1.0% agarose gels and purified by gel extraction kit (Tiangen,

TABLE 1 | Primers and sequences used in this experiment.

Primer	Primer sequence 5′-3′	Applications
Mm-BCDO2-F	AAGGAATGGGCAGCGGATGACTGTTAC	3′ RACE
Mm-BCDO2-R	GCGTCCACCACCAACAAGAAAGCA	5′ RACE
Mm-BCDO2-F1	GACCTTGCCCACACCAG	cDNA identification
Mm-BCDO2-R1	CATCATTTTGTTCAGCCAGA	cDNA identification
Mm-BCDO2-SNP-F	ACAGAAATGGACCGGGC	SNP detection
Mm-BCDO2-SNP-R	TCCTTCATAGATCTTGCGTCCAC	SNP detection
Mm-BCDO2-qRT-F	CATACGAGGATAACGGTCACG	qRT-PCR
Mm-BCDO2-qRT-R	TTTCCGCTTTGGCTGCTG	qRT-PCR
18s-F	CTTTCAAATGTCTGCCCTATCAACT	qRT-PCR
18s-R	TCCCGTATTGTTATTTTTCGTCACT	qRT-PCR

Beijing, China). The purified PCR products were cloned into pEasy-T1 (Trans, Beijing, China), and T1 vector was transformed into *E. coli* DH5a, and the positive plasmids were selected and sequenced. A pair of gene-specific primers, *Mm-BCDO2*-F1 and *Mm-BCDO2*-R1 (**Table 1**), was designed based on the full-length cDNA sequence and used to confirm the accuracy of cloning and sequencing of *Mm-BCDO2*.

Sequence and Phylogenetic Analysis

The cDNA sequence was assembled using the BLASTX search program of the National Center for Biotechnology Information (NCBI). The open reading frame (ORF) of *Mm-BCDO2* cDNA was identified using the ORF Finder program from NCBI. The theoretical isoelectric point (p*I*) and molecular weight (Mw) of Mm-BCDO2 protein were calculated using Compute p*I*/Mw Tool. Conserved domain of the deduced Mm-BCDO2 was predicted by simple modular architecture research tool (SMART). Tertiary structure of the amino acid sequence of deduced Mm-BCDO2 was analyzed using the SWISSMODEL tool. Multiple alignments of BCDO2 proteins between *M. meretrix* and other species were performed using ClustalW2 program. A phylogenetic tree was constructed by the neighbor-joining (NJ) method with MEGA X software.

Quantitative Expression Analysis

The mRNA expression levels of *Mm-BCDO2* at different adult tissues ($n = 4$, four sets of samples per tissue) were analyzed by real-time quantitative reverse transcription PCR (qRT-PCR). A pair of gene-specific primers, *Mm-BCDO2* qRT-F/R (**Table 1**), was used to quantitatively detect the expression level of *Mm-BCDO2* with 18S rRNA as an internal reference. The qRT-PCR was performed in 12 μL of iTaq universal SYBR green super mix (Bio-Rad, Beijing, China), 7.2 μL deionized water, 0.8 μL of the first-strand cDNA, and 1 μL of each primer. The amplification was carried out at the following condition: incubation of 20 s at 94°C; 40 cycles of 3 s at 94°C, 15 s at 60°C, and 10 s at 72°C; and a final extension of 7 min at 72°C. All amplifications were performed in triplicate as biological replicates, and negative controls were run in the absence of cDNA templates. The $2^{-\Delta\Delta CT}$ method was used to analyze the expression level of *Mm-BCDO2*. The expression levels of *Mm-BCDO2* among different tissues and between red and white shell clam groups were compared using the one-way ANOVA and Student's *t*-tests, respectively.

SNPs of *Mm-BCDO2* and Their Association With Clam Shell Color

A pair of primers, *Mm-BCDO2*-SNP-F/R (**Table 1**), was designed based on the cDNA sequence of *Mm-BCDO2* gene; 180 adult hard clams at 2 years of age were used for the SNP detection, collected from one population in Ningbo, Zhejiang Province, China. Total RNA was extracted from the mantle of clams, and then, the cDNA was synthetized using the methods described above. SNPs were detected by directly sequencing the PCR products using Sanger technology and the ABI3730 platform (Applied Biosystems, Foster City, CA, USA). The SNP genotypes were analyzed by using the Mutation Surveyor software version 4.0.8. The software PopGen32 was used to identify deviations from Hardy–Weinberg equilibrium and polymorphism information content (*PIC*) of significantly different SNP sites. The associated loci linkage disequilibrium (*LD*) was analyzed by the SHEsis online (http://analysis.bio-x.cn/myAnalysis.php). The difference in the genotype frequency of SNP locus between red and white shell clam populations was examined using the chi-square (χ^2) text. The correlation between the SNPs of *Mm-BCDO2* and clam shell color traits was analyzed by using the SPSS software version 20.0. The one-way ANOVA was adopted to compare the difference among different genotypes.

Immunofluorescence Analysis

The marginal tissues of the mantle and digestive gland were chosen from red and white shell clams, respectively. These samples were fixed with 4% paraformaldehyde, then dehydrated by gradient ethanol and xylene/*n*-butanol transparent, and paraffin-embedded sections (thickness 4 μm) were prepared. After baking, the tissue slices were deparaffinized with xylene, rehydrated with gradient ethanol, washed with PBS, and retrieved with EDTA antigen. Sections were then blocked for 1 h in blocking solution (5% albumin from bovine serum) at room temperature, followed by primary antibody (antibody rabbit anti-Mm-BCDO2, produced privately by HuaBio, Zhejiang, 1:200) incubation (overnight, 4°C). Primary antibody was detected by secondary antibodies Alexa Fluor 488 donkey anti-rabbit immunoglobulin G (Invitrogen, Carlsbad, California, U.S.) and diluted at 1:150. Nuclei were stained with DAPI (Beyotime, Shanghai, China). The cells were observed and photographed under a fluorescence microscope (Nikon Eclipse 80i, Tokyo, Japan).

Western Blot Detection

The mantle and digestive gland tissues were dissected from red and white shell clams, respectively. The samples were added with

an appropriate amount of RIPA lysate and then homogenized. The suspension was collected to measure protein concentration by BCA method, configured SDS-PAGE gel with appropriate concentration and loaded the same amount. The protein glue with the target protein was transferred to PVDF membrane and then blocked for 1 h in blocking solution (5% skimmed milk powder solution) at room temperature, followed by primary antibody (antibody rabbit anti-Mm-BCDO2, produced privately by HuaBio, Zhejiang, 1:1,000) incubation (overnight, 4°C). Primary antibody was bound by secondary antibodies [anti-rabbit labeled with biotin HRP (1:8,000)] for 1 h. ECL luminescent substrate mixture was dropped on the PVDF membrane. The proteins were observed and photographed under gel imagers (Bio-Rad, Beijing, China).

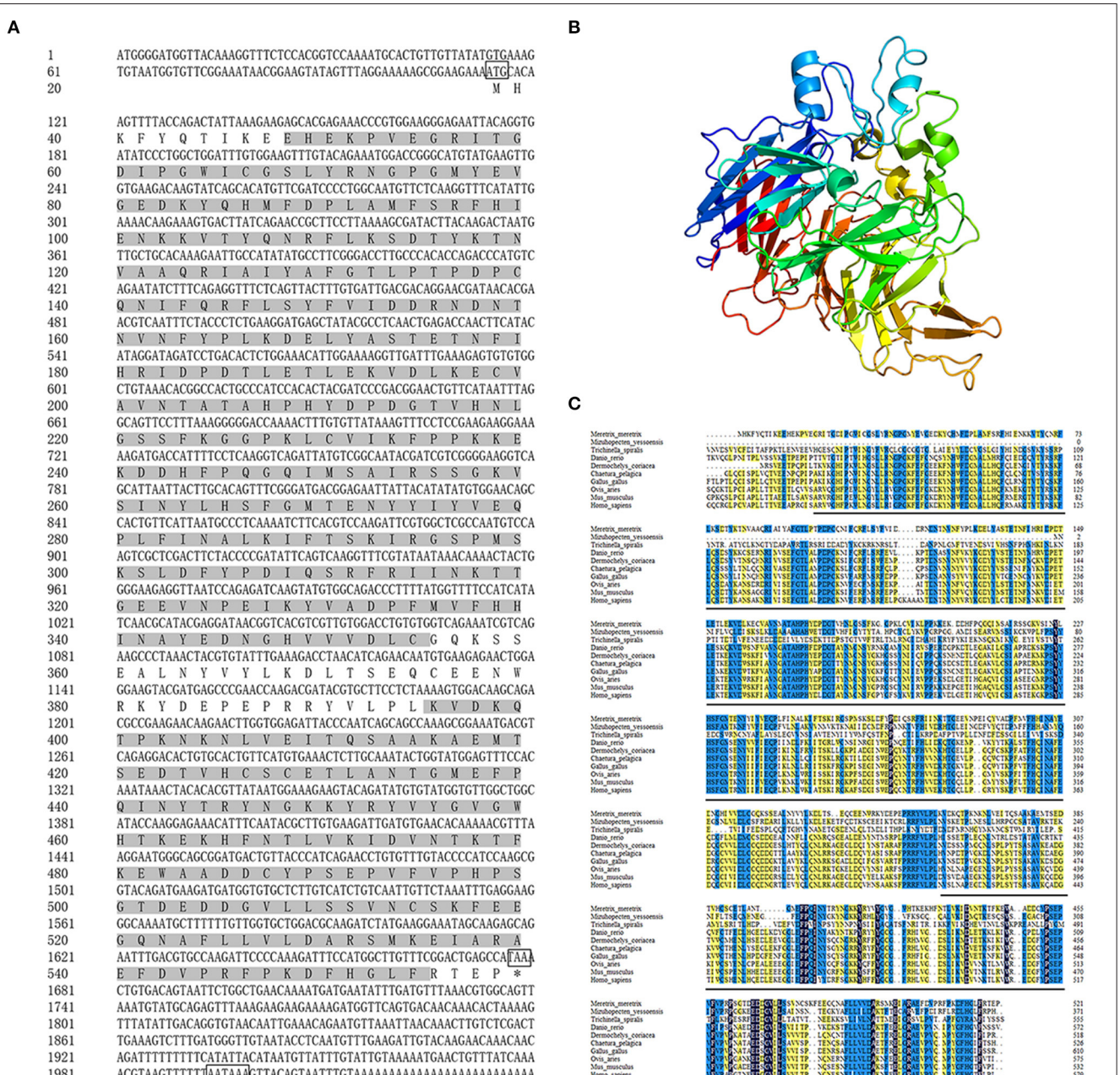

FIGURE 1 | The information of the *Mm-BCDO2* gene. **(A)** The full length of cDNA and deduced amino acid sequence of *Mm-BCDO2*. The frames represented the start codon, the stop codon, and polyadenylation signal. The gray background fill is the functional domain of RPE65. **(B)** The structure of Mm-BCDO2 protein. The arrow structure elements are β-strand, the helical structure elements are α-helix, and the others are random coils and turns. **(C)** Multiple alignments of amino acid sequences of BCDO2 from *M. meretrix* and other model species. Among these, the completely (=100%), strongly (≥75%), and weakly (≥50%) conserved residues are shaded in black, blue, and yellow, respectively. The black line represents the domain RPE65.

RESULTS

Molecular Characterization of *Mm-BCDO2*

The full-length cDNA of *Mm-BCDO2* gene was 2,040 bp, including a 5' untranslated region (UTR) of 113 bp, an open reading frame (ORF) of 1,566 bp that encoded 521 amino acids, and a 3' UTR of 361 bp existing a tail signal (AATAAA) after terminator codon (**Figure 1A**). Based on the amino acid sequence encoded by the *BCDO2* gene, the protein molecular weight was predicted to be 60.06 kDa, corresponding isoelectric point (p*I*) = 5.83, including a RPE65 domain (11–308, 356–517 aa). Mm-BCDO2 was a hydrophilic protein with a large proportion of polar amino acids. Protein structure prediction showed that Mm-BCDO2 protein composed of 9 α helices, 38 β-sheets, and a large number of random coils and had the typical characteristics of RPE65 protein family with a cleft and a right-handed twisted anti-parallel β-barrel (**Figure 1B**). The multiple comparisons between the BCDO2 of mollusks and model animals showed that Mm-BCDO2 had a relatively low similarity with other species (15−44%). Among them, Mm-BCDO2 had the highest homology with *Tauraco erythrolophus* (43.36%), the lowest homology with *Trichinella spiralis* (15.15%), and the homology with shellfish *Mizuhopecten yessoensis* (27.34%) (**Figure 1C**).

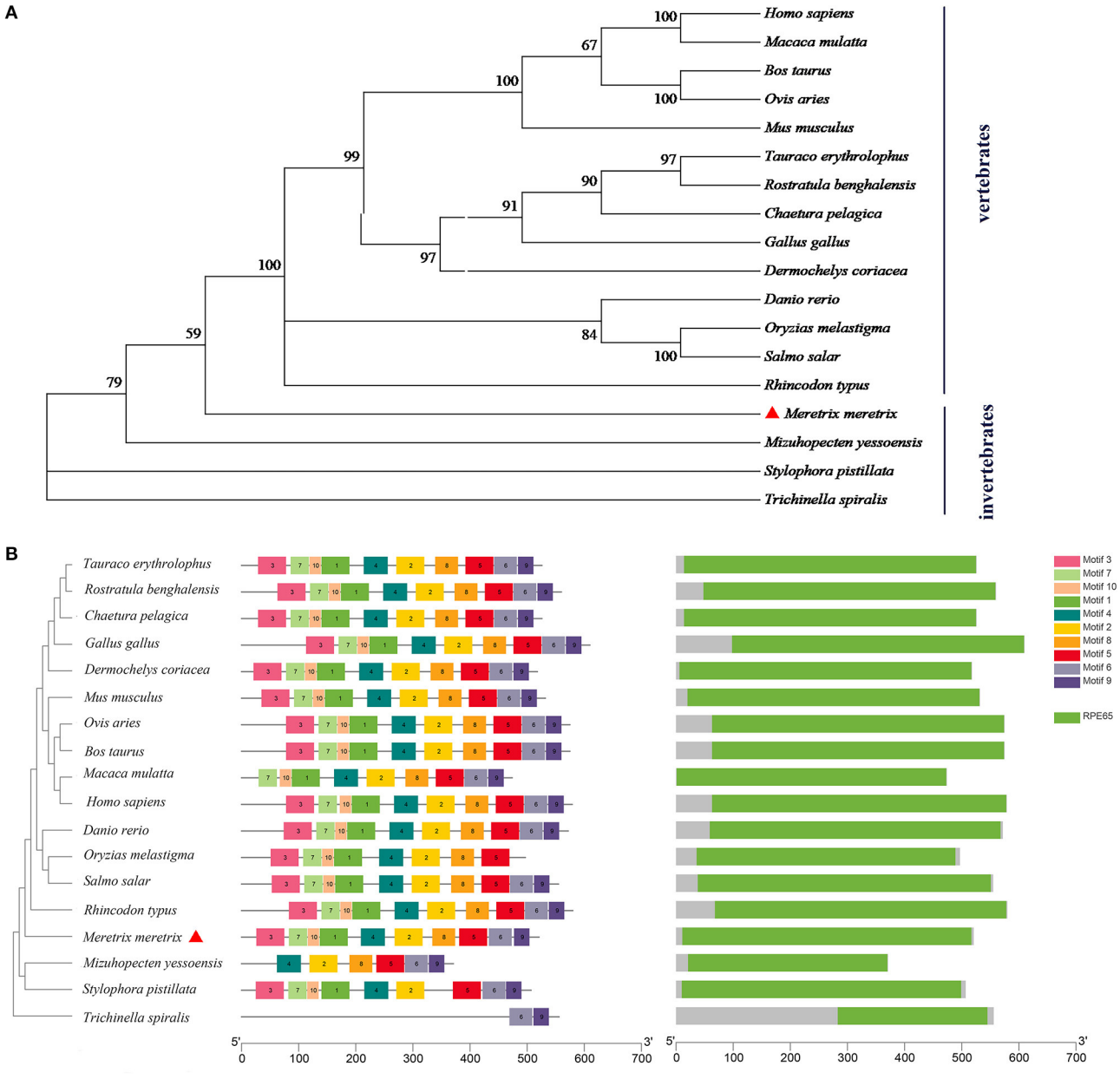

FIGURE 2 | Analysis of evolutionary relationship among species. **(A)** Phylogenetic tree analysis of BCDO2 protein between *M. meretrix* and other species. **(B)** The structure of BCDO2 of *M. meretrix*, other bivalves and vertebrates.

The phylogenetic tree showed that the BCDO2 proteins from vertebrates were clustered together as one branch, while that from *M. meretrix* and other invertebrates were gathered into one branch (**Figure 2A**). Eighteen BCDO2 protein sequences were analyzed and identified 10 conserved motifs, ranging in length from 6 to 50 amino acid residues. Most of the BCDO2 proteins contained motif 1–10 with the exception of *M. yessoensis*, *Stylophora pistillata,* and *T. spiralis*. The domain prediction analysis showed that there was a PRE65 functional domain in all tested vertebrates and invertebrates except *T. spiralis* (**Figure 2B**), indicating that the functions between them might be extremely similar.

High mRNA expression levels of *Mm-BCDO2* were observed in the mantle and foot, followed by the digestive gland, siphon, adductor muscle, and gill (**Figure 3**). Notably, the expression level of *Mm-BCDO2* was significantly higher ($P < 0.05$) in the mantle of red shell clams than that of white shell clams (**Figure 3**).

Associations Between the SNP of *Mm-BCDO2* and Shell Color of Clam

A total of 20 polymorphic loci were screened in the coding sequence of *Mm-BCDO2* (**Supplementary Table 1**), of which three SNPs (c.984A > C, c.1148C > T, and c.1187A > T) were significantly associated with clam shell color formation (**Table 2**). The c.984A>C and c.1187A>T sites were non-synonymous mutations, which led to the mutation of amino acids from Lys to Gln and from Lys to Asn, respectively. The c.1148C>T site was a synonymous mutation. Statistical analysis of the mutation types of SNP sites found that there existed conversion and transversion types in the SNP of *Mm-BCDO2* exons (**Table 3**).

Both c.1148 C>T and c.1187 A>T were low polymorphism sites, while c.984 A>C was a moderate polymorphism site in the red shell clams. On the contrary, all the three SNPs were moderately polymorphic sites in the white shell clams (**Table 4**). The range of observed heterozygosity (H_o) and expected heterozygosity (H_e) in the red shell clams was 0.193–0.237 and 0.232–0.468, respectively, whereas the range of H_o and H_e in the white shell clams was 0.146–0.265 and 0.335–0.497, respectively. Further, the linkage disequilibrium results showed that the three sites were strongly linked ($D' > 0.75$; **Table 5**).

Three-locus haplotypes consisting of three SNPs were constructed to estimate the haplotype frequencies using SHEsis software. The analytical results showed that ACA was a common haplotype. CCA, CCT, and CTT haplotype frequencies for these three polymorphisms showed significant differences between the red shell and white shell ($P < 0.05$; **Table 6**).

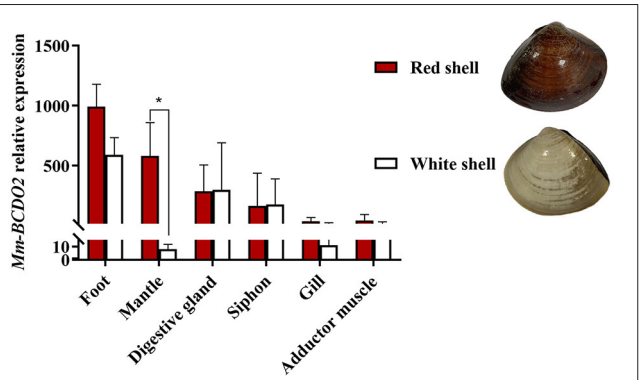

FIGURE 3 | Relative expression levels of *Mm-BCDO2* in different tissues from *M. meretrix*. Significant differences between red shell and white shell are indicated with an asterisk for $P < 0.05$.

Distribution of Mm-BCDO2 Protein in the Mantle and Digestive Gland

The immunofluorescence was used to assess the subcellular distribution of Mm-BCDO2 in the mantle and digestive gland

TABLE 3 | Variation type of the SNPs of *Mm-BCDO2* gene.

Variation type	Genotype	Sites	Total number
Transition	GA	500, 1,047, 1,406, 1,436, 1,454, 1,496	6
	CT	1,148, 1,211, 1,403, 1,439, 1,589	5
Transversion	TA	663, 707, 1,118, 1,187, 1,535	5
	AC	899, 984, 1,376, 1,376	4

TABLE 2 | Analysis of association between the SNPs of *Mm-BCDO2* and clam shell color.

Locus	Genotype	Number (Genotype frequency)		Allele	Allele frequency		χ^2 (*P*-value)
		Red shell	White shell		Red shell	White shell	
c.984A>C	AA	69 (51.11)	72 (47.68)	A	62.96	54.97	6.855 (0.032)*
	AC	32 (23.7)	22 (14.57)	C	37.04	45.03	
	CC	34 (25.19)	57 (37.75)				
c.1148C>T	CC	104 (77.04)	107 (70.86)	C	86.67	79.14	7.228 (0.027)*
	CT	26 (19.26)	25 (16.56)	T	13.33	20.86	
	TT	5 (3.7)	19 (12.58)				
c.1187A>T	AA	100 (74.07)	85 (56.29)	A	85.19	69.54	16.026 (0.0003)**
	AT	30 (22.22)	40 (26.49)	T	14.81	30.46	
	TT	5 (3.7)	26 (17.22)				

Significant differences between red shell and white shell are indicated with an asterisk for $P < 0.05$, and with two asterisks for $P < 0.01$.

TABLE 4 | Polymorphic parameters of the SNP loci of *Mm-BCDO2* gene.

Strain	Locus	Ho	He	Ne	PIC
Red shell color	c.984 A>C	0.237	0.468	1.874	0.358
	c.1148 C>T	0.193	0.232	1.301	0.204
	c.1187 A>T	0.222	0.253	1.338	0.220
White shell color	c.984 A>C	0.146	0.497	1.981	0.373
	c.1148 C>T	0.172	0.335	1.502	0.278
	c.1187 A>T	0.265	0.425	1.735	0.334

TABLE 5 | Linkage disequilibrium analysis among three SNP of *Mm-BCDO2* gene.

Locus	c.984A>C	c.1148C>T	c.1187A>T
c.984 A>C		1.000 (1.000)	1.000 (1.000)
c.1148 C>T	0.262 (0.328)		1.000 (1.000)
c.1187 A>T	0.296 (0.543)	0.885 (0.543)	

The value above the diagonal represents D′, and the value below the diagonal represents R^2. The number outside the parentheses and inside the parentheses is the linkage disequilibrium analysis of red and white shell clams, respectively.

TABLE 6 | Haplotype analysis of three SNPs of *Mm-BCDO2* gene.

Haplotype sequence	All subjects	Red shell (frequency)	White shell (frequency)	χ^2 (*P*-value)
ACA	336	166.00 (0.550)	170.00 (0.630)	3.760 (0.052)
CCA	103	43.00 (0.142)	60.00 (0.222)	6.156 (0.013*)
CCT	33	29.00 (0.096)	4.00 (0.015)	17.298 (0.000**)
CTT	100	64.00 (0.212)	36.00 (0.133)	6.102 (0.013*)
CTA	0	0.00 (0.000)	0.00 (0.000)	

Significant differences between red shell and white shell are indicated with an asterisk for $P < 0.05$, and with two asterisks for $P < 0.01$.

of red and white shell clams. The result revealed that the Mm-BCDO2 was an extranuclear enzyme (**Figure 4**). According to the green fluorescence signal, the expression level of Mm-BCDO2 protein in single-layer columnar cells at the edge of the mantle of red clam was higher than that of white clam, but there was no difference in the muscle fibers scattered in the middle of the mantle (**Figure 4A**). Mm-BCDO2 was expressed on the glandular epithelium of digestive gland, while there was no difference in the expression level of Mm-BCDO2 between red and white shell clams (**Figure 4B**).

Expression of Mm-BCDO2 Protein in the Mantle and Digestive Gland

Western blot analysis of the Mm-BCDO2 protein in the mantle and digestive gland showed that the target band appeared at the predicted molecular weight. There was no significant difference in the expression level of BCDO2 in the digestive gland between red and white shell clams (**Figure 5A**). Conversely, Mm-BCDO2 was highly expressed in the mantle of the red shell clams compared with that of the white shell clams ($P < 0.05$; **Figure 5B**).

DISCUSSION

Studies on mammals, fish, and birds have revealed that *BCDO2* can control carotenoid homeostasis, thereby affecting changes in body surface color or tissue color (Amengual et al., 2013; Costabile et al., 2016). In this study, the full-length cDNA sequence of *Mm-BCDO2* was successfully cloned. Further, *Mm-BCDO2* displayed low identity in sequence size with other species such as mammal and shellfish, but all of them contained the RPE65 domain. It is still controversial whether the function of *BCOD2* gene is conserved in evolution. For example, RPE65 was molecularly identified as the first member of the vertebrate carotenoid cleavage dioxygenase family member (Hamel et al., 1993) and initially characterized as retinoid-binding protein rather than an enzyme catalyst (Gollapalli et al., 2003; Mata et al., 2004). Some studies question whether there exist the BCDO2 enzyme that produces vitamin A (Hansen and Maret, 1988). It has been reported that *BCDO2* gene encodes an enzymatically active protein, but it showed no carotenoid cleavage activity in human (Li et al., 2014a; Seña et al., 2016). Indeed, studies have proved that BCDO2 is a catalytically competent enzyme and displays broad substrate specificity by transferring human *BCDO2* splice variants into ARPE-19 cells and *E. coli* (Thomas et al., 2020). Furthermore, primate BCDO2 displayed a conserved structural fold and enzymatic function (Babino et al., 2015). Consistently, the *BCDO2* gene in vertebrate was conserved in evolution, while that in invertebrate was quite different here. Therefore, whether the function of *BCDO2* gene is conserved in evolution needs to be further explored.

Increasing studies have shown that the polymorphism of *BCDO2* gene is related to color traits (Wu et al., 2020). For instance, the nonsense mutations of *BCDO2* gene in the cattle lead to increased carotenoids in milk (Berry et al., 2009), while the yellow fat traits of sheep and rabbit are correlated with mutations in the coding region of *BCDO2* gene (Vge and Boman, 2010; Strychalski et al., 2015, 2019; Niu et al., 2016). In addition, studies have found that some polymorphic loci of *BCDO2* gene are completely linked to the skin color traits of chickens (Eriksson et al., 2008; Xu et al., 2017). These findings reveal that *BCDO2* mutations cause the alterations in its function on mediating carotenoids cleavage. Non-synonymous single-nucleotide polymorphisms (SNPs) result in changes in the encoded amino acids, which in turn may affect the function of corresponding proteins (Katsonis et al., 2015; Cao et al., 2016). This is considered to be an important cause that leads to changes in animal phenotypes. In this study, the positions c.984 A>C and c.1187 A>T were non-synonymous mutations, and the position Lys984Gln caused the amino acid coded to be mutated from positively charged to uncharged, which was located near the conservative site. Similarly, the site Lys1187Asn led to the amino acid mutation from positively charged to negatively charged, which was located in the starting region of the functional domain. Three haplotype frequencies for these three polymorphisms showed significant differences between red shell clams and white shell clams ($P < 0.05$). We think the different genotypes of the three SNPs may associate with mRNA stability or affect *Mm-BCDO2* gene expression through

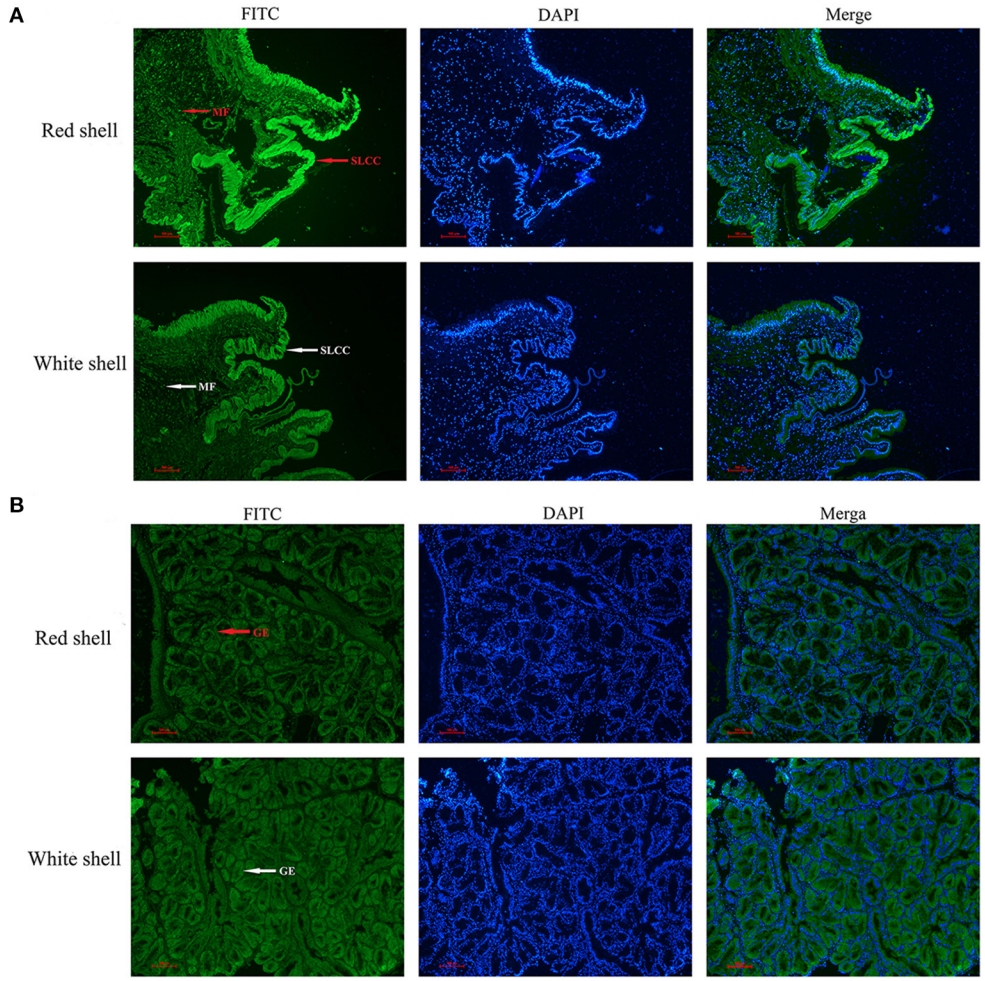

FIGURE 4 | Distribution of BCDO2 in the mantle and digestive gland from red and white shell *M. meretrix*, respectively. **(A)** Localization of BCDO2 in single-layer columnar cells (SLCC) and muscle fibers (MF) of the mantle. **(B)** Localization of BCDO2 in glandular epithelium (GE) of digestive gland. Green fluorescence signal, FITC; blue fluorescence signal, DAPI.

interaction with other transcription factors that would disturb carotenoids metabolism. It has been shown that changes in the charge of amino acids can lead to changes in redox intensity (Jiao et al., 2016). Consistent with the notion, a non-synonymous mutation in the *BCDO2* gene was found to disrupt the carotenoid cleavage activity of the enzyme in a study of the coloration mechanism on birds, thereby causing a significant increase in the concentration of intact carotenoids in tissues (Anna et al., 2020). These findings suggest that *BCDO2* gene plays an important role in the accumulation of carotenoids in animal tissues. Therefore, we speculate that changes of amino acid at multiple sites may affect the spatial collision between the side chain of corresponding site of the clam BCDO2 protein and the surrounding side chain, thereby changing the protein structure or causing protein folding defects, which in turn altered enzyme activities and resulted in different metabolic capabilities between red and white shell clams. Intriguingly, there was a strong linkage between c.984 A>C and c.1187 A>T, which could be inherited stably and could be an important target of selection in the evolution of color traits.

Changes in gene expression are the basis for differential phenotypes between the same species (Fallahshahroudi et al., 2018). In this study, the *Mm-BCDO2* gene was expressed in all six tested tissues, with significantly higher expression in the mantle of red shell clams than white shell clams, and there was no difference in the digestive gland. These findings were further verified by western blot and immunofluorescence analysis. Consistently, the expression level of *BCDO2* gene in the red feathers and beaks of *Quelea quelea* was significantly higher than that in the pale yellow feathers and beaks of the population (Walsh et al., 2012). The expression level of *BCDO2* decreased in the skin, muscle, and adipose tissue of the white leghorn compared with that of the *Red Junglefowl*, but no change was observed in the liver and other internal organs. It has been proposed that the expression level of *BCDO2* gene in the livers did not decrease because BCDO2 was not sensitive to the

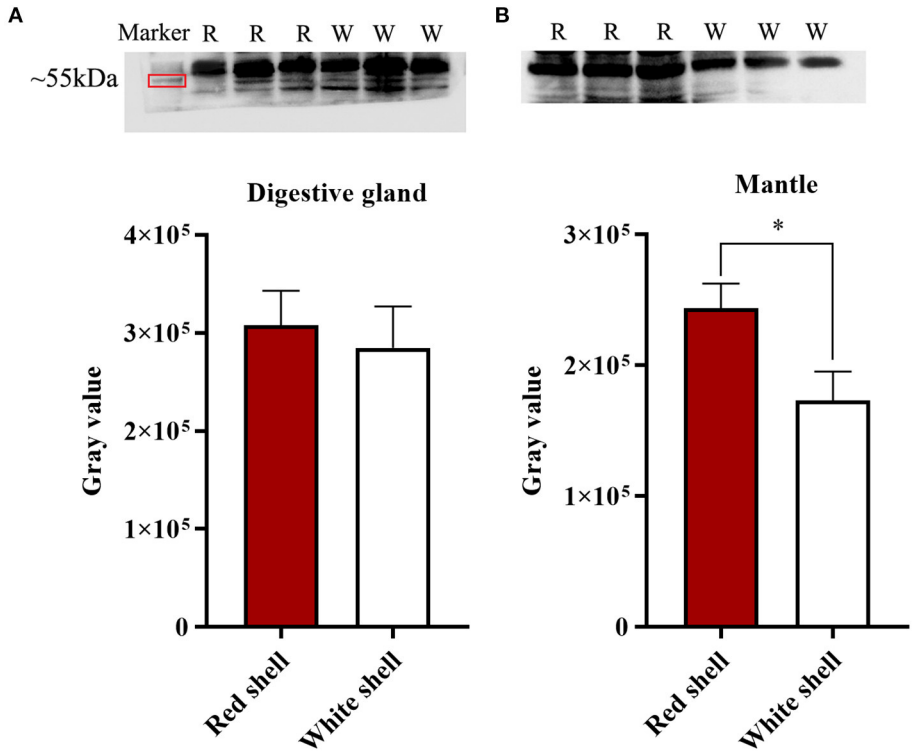

FIGURE 5 | Western blotting analysis of Mm-BCDO2 protein in the digestive gland **(A)** and mantle **(B)** of red and white shell clams. Significant differences between red shell and white shell are indicated with an asterisk for $P < 0.05$.

toxicity of excess carotenoids (Fallahshahroudi et al., 2019). On the contrary, the transcript levels of *BCDO2-l* gene was elevated in the white Chinook salmon compared with that in the red Chinook salmon (Lehnert et al., 2019). The protection of cells against apoptosis induced by carotenoid is strictly dependent on BCDO2 enzymatic function (Lobo et al., 2012). Our previous study on the clam shell color found that the genes and proteins that are related to carotenoid transport were significantly higher in the red shell clams than that in the white shell clams (Zhan, 2015). Therefore, we speculate that there are two explanations for this phenomenon. On the one hand, it is to prevent excessive carotenoid accumulation in the body from causing cellular oxidative stress, which will have side effects on the body, so more carotene oxygenases are needed to decompose carotenoids. Previous studies in mice have shown that high concentration of carotenoids can force the expression of the *BCDO2* gene, so the high-level expression of carotene oxygenase in the body can balance the carotenoid concentration without causing oxidative stress (Babino et al., 2015). On the other hand, it may be that the body needs to metabolize carotenoids to show different colors (red, yellow, etc.). "Red" pigments are instead often metabolically derived from the yellow precursors, typically by oxygenation (also known as allylic oxidation), adding double-bonded oxygen atoms ("keto-groups") to the end rings, thereby shifting the absorptance λ max toward longer wavelengths (Britton, 1995). For example, researchers have found that some birds produce red feathers by metabolizing carotenoids into derived keto carotenoids, while other birds produce red feathers by depositing high concentrations of yellow dietary carotenoids (Andersson et al., 2006). And the method of depositing carotenoids in clams needs further research.

In summary, we characterized the cDNA of *Mm-BCDO2* and analyzed the relationship between its sequence characteristics and phylogenetic trait. The expression level of *Mm-BCDO2* gene was significantly higher in the mantle of the red shell clams than that in the white shell clams. Moreover, the association analysis identified three shell color-related SNPs in the exons of *Mm-BCDO2*. Among them, the non-synonymous mutations of c.984 A>C and c.1187 A>T sites may be correlated with the accumulation of carotenoids. Overall, these findings contribute to understanding the role of *Mm-BCDO2* gene in the formation of shell color via regulating carotenoid levels and provide molecular marker for shell color breeding in *M. meretrix*.

DATA AVAILABILITY STATEMENT

The datasets presented in this study can be found in online repositories. The names of the repository/repositories and accession number(s) can be found in the article/**Supplementary Material**.

ETHICS STATEMENT

This animal study was reviewed and approved by the Institutional Animal Care and Use Committee (IACUC) of Zhejiang Wanli University, China.

AUTHOR CONTRIBUTIONS

YD, HY, and ZL designed the study. LF performed the experiments under the support of YB. LF, HS, WD, and YD analyzed the data and wrote the manuscript. All authors read and approved the manuscript.

FUNDING

This work was supported by the National Natural Science Foundation of China (31772846), National Key Research and Development Program of China (2018YFD0901404), Ningbo Major Project of Science and Technology (2019B10005), Zhejiang Provincial First-Class Discipline of Bioengineering-A (ZS2019001), and National Marine Genetic Resource Center Program.

SUPPLEMENTARY MATERIAL

The Supplementary Material for this article can be found online at: https://www.frontiersin.org/articles/10.3389/fmars.2021.746026/full#supplementary-material

REFERENCES

Amengual, J., Widjaja Adhi, M., Rodriguez Santiago, S., Hessel, S., Golczak, M., Palczewski, K., et al. (2013). Two carotenoid oxygenases contribute to mammalian provitamin a metabolism. *J. Biol. Chem.* 288, 34081–34096. doi: 10.1074/jbc.M113.501049

Andersson, S., Prager, M., and Johansson, E. (2006). Carotenoid content and reflectance of yellow and red nuptial plumages in widowbirds (*Euplectes spp.*). *Func. Ecol.* 21, 272–281. doi: 10.1111/j.1365-2435.2007.01233.x

Andrade, P., Pinho, C., Pérezide Lanuza, G., Afonso, S., Brejcha, J., Rubin, C. J., et al. (2019). Regulatory changes in pterin and carotenoid genes underlie balanced color polymorphisms in the wall lizard. *Proc. Natl. Acad. Sci. U.S.A.* 116, 5633–5642. doi: 10.1073/pnas.1820320116

Anna, G. M., Toomey, M., Araújo, P., Lopes, R. J., Sandra, A., Myers, C. A., et al. (2020). Genetic basis of de novo appearance of carotenoid ornamentation in bare parts of canaries. *Mol. Biol. Evol.* 37, 1317–1328. doi: 10.1093/molbev/msaa006

Babino, D., Palczewski, G., Widjaja-Adhi, M., Kiser, P. D., and Lintig, J. V. (2015). Characterization of the role of β-carotene 9,10-dioxygenase in macular pigment metabolism. *J. Biol. Chem.* 290, 24844–24857. doi: 10.1074/jbc.M115.668822

Berry, S. D., Davis, S. R., Beattie, E. M., Thomas, N. L., Burrett, A. K., Ward, H. E., et al. (2009). Mutation in bovine β-carotene oxygenase 2 affects milk color. *Genetics* 182, 923–926. doi: 10.1534/genetics.109.101741

Blount, J. D., and Mcgraw, K. J. (2008). "Signal functions of carotenoid colouration," in *Carotenoids,* ed B. George (Basel: Birkhäuser), 213–236. doi: 10.1007/978-3-7643-7499-0_11

Britton, G. (1995). Structure and properties of carotenoids in relation to function. *FASEB. J.* 9,1551–1559. doi: 10.1096/fasebj.9.15.8529834

Cao, R., Shi, Y., Chen, S., Ma, Y., Chen, J., Yang, J., et al. (2016). DbSAP: Single amino-acid polymorphism database for protein variation detection. *Nucleic Acids Res.* 45, 827–832. doi: 10.1093/nar/gkw1096

Costabile, B. K., Kim, Y. K., Iqbal, J., Zuccaro, M. V., Wassef, L., Narayanasamy, S., et al. (2016). Beta-apo-10′-carotenoids modulate placental microsomal triglyceride transfer protein expression and function to optimize transport of intact beta-carotene to the embryo. *J. Biol. Chem.* 291, 18525–18535. doi: 10.1074/jbc.M116.738336

Cui, B., Dong, Y., Zhao, J., Hu, L., LI, X., Yao, H., et al. (2018). Cloning and expression analysis of SRBI gene in different shell-color strains of *Meretrix meretrix*. *Acta Hydrobiol. Sin.* 42, 488–493. doi: 10.7541/2018.061

Deng, S. Z., Li, Q. C., Han, F., Zhang, X. L., Cai, M. Y., Zhang, J., et al. (2018). Analysis of total carotenoid content with different tissues or genders in *Paphia textzle*. *Mar. Bull.* 37, 165–168, 208. doi: 10.11840/j.issn.1001-6392.2018.02.006

Eriksson, J., Larson, G., Gunnarsson, U., Bed'Hom, B., Tixier-Boichard, M., Strömstedt, L., et al. (2008). Identification of the yellow skin gene reveals a hybrid origin of the domestic chicken. *PLoS Genet.* 4:e1000010. doi: 10.1371/journal.pgen.1000010

Fallahshahroudi, A., Løtvedt, P., Bélteky, J., Altimiras, J., and Jensen, P. (2018). Changes in pituitary gene expression may underlie multiple domesticated traits in chickens. *Heredity* 122, 195–204. doi: 10.1038/s41437-018-0092-z

Fallahshahroudi, A., Sorato, E., Altimiras, J., and Jensen, P. (2019). The domestic BCO2 allele buffers low-carotenoid diets in chickens: possible fitness increase through species hybridization. *Genetics* 212, 1445–1452. doi: 10.1534/genetics.119.302258

Felix, M. B., Snodderly, D. M., Johnson, E. J., Schalch, W., Korepcke, W., Gerss, J., et al. (2011). Nutritional manipulation of primate retinas, V: effects of lutein, zeaxanthin, and n-3 fatty acids on retinal sensitivity to blue-light-induced damage. *Invest. Ophthalmol. Vis. Sci.* 52, 3934–3942. doi: 10.1167/iovs.10-5898

Ge, J. L., Li, Q., and Yu, H. (2016). Selection response in mass selection of golden shell Pacific oyster (*Crassostrea gigas*). *J. Fish. China* 40, 95–100. doi: 10.11964/jfc.20150409829

Georg, L., Jennifer, L., and Gerald, R. (2010). Molecular and dietary regulation of β,β-carotene 15,15′-monooxygenase 1 (BCMO1). *Arch. Insect Biochem.* 502, 8–16. doi: 10.1016/j.abb.2010.06.032

Gollapalli, D. R., Maiti, P., and Rando, R. R. (2003). RPE65 operates in the vertebrate visual cycle by stereospecifically binding all-trans-retinyl esters. *Biochemistry* 42:11824–30. doi: 10.1021/bi035227w

Hamel, C. P., Tsilou, E., Pfeffer, B. A., Hooks, J. J., Detrick, B., and Redmond, T. M. (1993). Molecular cloning and expression of RPE65, a novel retinal pigment epithelium-specific microsomal protein that is post-transcriptionally regulated *in vitro*. *J. Biol. Chem.* 268, 15751–15757. doi: 10.1016/S0021-9258(18)82319-5

Hansen, S., and Maret, W. (1988). Retinal is not formed in vitro by enzymatic central cleavage of beta-carotene. *Biochemistry* 27, 200–206. doi: 10.1021/bi00401a030

Jiao, J., Yang, X., Jin, L., Gao, J., Yang, Z., Xiao, Y., et al. (2016). Conservative and variability of the important functional sites in a laccase from *bacillus subtilis*. *Chem. J. Chin. Univer.* 37, 1320–1327. doi: 10.7503/cjcu20160092

Jin, Y., Yu, Y., Zhang, C., Li, S., Zhang, X., and Li, F. (2020). Characterization and function analysis of the beta-carotene oxygenase-like genes in carotenoids metabolism of the ridgetail white prawn *exopalaemon carinicauda*. *Front. Physiol.* 11:745–760. doi: 10.3389/fphys.2020.00745

Katsonis, P., Koire, A., Wilson, S. J., Hsu, T. K., Lua, R. C., Wilkins, A. D., et al. (2015). Single nucleotide variations: biological impact and theoretical interpretation. *Protein Sci.* 23, 1650–1666. doi: 10.1002/pro.2552

Lehnert, S. J., Christensen, K. A., Vandersteen, W. E., Sakhrani, D., and Devlin, R. H. (2019). Carotenoid pigmentation in salmon: variation in expression at BCO2-l locus controls a key fitness trait affecting red coloration. *Proc. R. Soc. B.* 286, 20191588–20191596. doi: 10.1098/rspb.2019.1588

Li, B., Vachali, P. P., Gorusupudi, A., Shen, Z., Sharifzadeh, H., Besch, B. M., et al. (2014a). Inactivity of human β,β-carotene-9',10'-dioxygenase (BCO2) underlies retinal accumulation of the human macular carotenoid pigment. *Proc. Natl. Acad. Sci. U.S.A.* 111, 10173–10178. doi: 10.1073/pnas.1402526111

Li, B., Vachali, P. P., Shen, Z., Gorusupudi, A., Nelson, K., Besch, B. M., et al. (2017). Retinal accumulation of zeaxanthin, lutein, and β-carotene in mice deficient in carotenoid cleavage enzymes. *Exp. Eye. Res.* 159, 123–131. doi: 10.1016/j.exer.2017.02.016

Li, X., Bai, Z., Luo, H., Wang, G., and Li, J. (2014b). Comparative analysis of total carotenoid content in tissues of purple and white inner-shell color pearl mussel, *Hyriopsis cumingii*. *Aquacult. Int.* 22, 1577–1585. doi: 10.1007/s10499-014-9766-6

Lin, Z. (2015). *Biology and Culture Technology of Meretrix meretrix*. Beijing: Science Press Beijing.

Lin, Z. H., and Dong, Y. H. (2015). *Meretrix meretrix* "Wanlihong". *China Fish.* 479, 72–74.

Lobo, G. P., Isken, A., Hoff, S., Babino, D., and Lintig, J. V. (2012). BCDO2 acts as a carotenoid scavenger and gatekeeper for the mitochondrial apoptotic pathway. *Development* 139, 2966–2977. doi: 10.1242/dev.079632

Mata, N. L., Moghrabi, W. N., Lee, J. S., Bui, T. V., Radu, R. A., Horwitz, J., et al. (2004). RPE65 is a retinyl ester binding protein that presents insoluble substrate to the isomerase in retinal pigment epithelial cells. *J. Biol. Chem.* 279, 635–643. doi: 10.1074/jbc.M310042200

Meilisza, N., Jusadi, D., Zairin, M., Artika, I. M., Utomo, N. P., Kadarini, T., et al., (2017). Digestibility, growth and pigmentation of astaxanthin, canthaxanthin or lutein diets in Lake Kurumoi rainbowfish, Melanotaenia parva (Allen) cultured species. *Aquac. Res.* 48, 1–9. doi: 10.1111/are.13372

Milani, A., Basirnejad, M., Shahbazi, S., and Bolhassani, A. (2017). Carotenoids: biochemistry, pharmacology and treatment. *Br. J. Pharmacol.* 174, 1290–1324. doi: 10.1111/bph.13625

Niu, Y., Jin, M., Li, Y., Li, P., and Chen, Y. (2016). Biallelic b-carotene oxygenase 2 knockout results in yellow fat in sheep via CRISPR/Cas9. *Anim. Genet.* 48, 242–244. doi: 10.1111/age.12515

Qi, X. Y. (2014). *The analysis of molecular mechanisms of shell color formation for Meretrix meretrix (dissertation)*. Ningbo University, Ningbo, Zhejiang.

Seña, C. D., Jian, S., Narayanasamy, S., Riedl, K. M., Yan, Y., Curley, R. W., et al. (2016). Substrate specificity of purified recombinant chicken β-carotene 9′,10′-oxygenase (bco2). *J. Biol. Chem.* 291, 14609–14619. doi: 10.1074/jbc.M116.723684

Strychalski, J., Brym, P., Czarnik, U., and Gugoek, A. (2015). A novel AAT-deletion mutation in the coding sequence of the BCO2 gene in yellow-fat rabbits. *J. Appl. Genet.* 56, 535–537. doi: 10.1007/s13353-015-0290-9

Strychalski, J., Gugoek, A., Brym, P., Antoszkiewicz, Z., and Chwastowska-Siwiecka, I. (2019). Polymorphism of the BCO2 gene and the content of carotenoids, retinol, and α-tocopherol in the liver and fat of rabbits. *Rev. Bras. Zool.* 48:e20180243. doi: 10.1590/rbz4820180243

Svensson, P. A., and Wong, B. B. M. (2011). Carotenoid-based signals in behavioural ecology: a review. *Behaviour* 148, 131–189. doi: 10.1163/000579510X548673

Thomas, L. D., Bandara, S., Parmar, V. M., Srinivasagan, R., Khadka, N., Golczak, M., et al. (2020). The human mitochondrial enzyme BCO2 exhibits catalytic activity toward carotenoids and apocarotenoids. *J. Biol. Chem.* 295, 15553–15565. doi: 10.1074/jbc.RA120.015515

Tian, R., Pitchford, W. S., Morris, C. A., Cullen, N. G., and Bottema, C. D. K. (2009). Genetic variation in the β, β-carotene-9′, 10′-dioxygenase gene and association with fat colour in bovine adipose tissue and milk. *Anim. Genet.* 41, 253–259. doi: 10.1111/j.1365-2052.2009.01990.x

Vge, D. I., and Boman, I. A. (2010). A nonsense mutation in the beta-carotene oxygenase 2 (BCO2) gene is tightly associated with accumulation of carotenoids in adipose tissue in sheep (*Ovis aries*). *BMC Genet.* 11:10–16. doi: 10.1186/1471-2156-11-10

Walsh, N., Dale, J., Mcgraw, K. J., Pointer, M. A., and Mundy, N. I. (2012). Candidate genes for carotenoid coloration in vertebrates and their expression profiles in the carotenoid-containing plumage and bill of a wild bird. *Proc. Soc. B.* 279, 58–66. doi: 10.1098/rspb.2011.0765

Wang, J., Li, Q., Zhong, X., Song, J., Kong, L., and Yu, H. (2018). An integrated genetic map based on EST-SNPs and QTL analysis of shell color traits in Pacific oyster *Crassostrea gigas*. *Aquaculture* 492, 226–236. doi: 10.1016/j.aquaculture.2018.04.018

Wang, X. L., Li, Q., and Kong, L. F. (2016). Construction and comparison of growth and survival among different golden shell families of Pacific oyster (*Crassostrea gigas*). *J. Fish. China* 40, 1683–1693. doi: 10.11964/jfc.20150810050

Wu, J., Chen, G., Lin, Z., Yin, Y., Chen, H., Chen, J., et al. (2020). Polymorphism of BCO2 gene and its correlation with skin yellowness in partridge chickens. *China Poult.* 42, 12–18. doi: 10.3389/fphys.2021.585089

Wu, L., Guo, X., Wang, W., Medeiros, D. M., Clarke, S. L., Lucas, E. A., et al. (2016). Molecular aspects of β, β-carotene-9′, 10′-oxygenase 2 in carotenoid metabolism and diseases. *Exp. Biol. Med.* 241, 1879–1887. doi: 10.1177/1535370216657900

Xu, J., Lin, S., Gao, X., Nie, Q., and Zhang, X. (2017). Mapping of id locus for dermal shank melanin in a Chinese indigenous chicken breed. *J. Genet.* 96, 977–983. doi: 10.1007/s12041-017-0862-z

Zhan, Y. L. (2015). *Identification of shell color and the related gene and microRNA research of Meretrix meretrix (dissertation)*. Zhejiang Wanli University, Ningbo, Zhejiang.

Zhang, B., Zhu, C., Meng, Z., Liu, B., and Yu, D. (2019). Carotenoids in pearl oyster *Pinctada fucata*: the tissue distribution and correlation to color parameters. *Pak. J. Zool.* 51, 1655–1661. doi: 10.17582/journal.pjz/2019.51.5.1655.1661

Zheng, H., Liu, H., Tao, Z., Wang, S., Sun, Z., Liu, W., et al., (2010). Total carotenoid differences in scallop tissues of Chlamys nobilis (Bivalve: Pectinidae) with regard to gender and shell colour. *Food Chem.* 122, 1164–1167. doi: 10.1016/j.foodchem.2010.03.109

Conflict of Interest: The authors declare that the research was conducted in the absence of any commercial or financial relationships that could be construed as a potential conflict of interest.

Publisher's Note: All claims expressed in this article are solely those of the authors and do not necessarily represent those of their affiliated organizations, or those of the publisher, the editors and the reviewers. Any product that may be evaluated in this article, or claim that may be made by its manufacturer, is not guaranteed or endorsed by the publisher.

frontiers in Marine Science

ORIGINAL RESEARCH
published: 29 September 2021
doi: 10.3389/fmars.2021.731517

Transcriptome Profiling Based on Different Time Points After Hatching Provides a Core Set of Gene Resource for Understanding Larval Immune Response Mechanisms Against *Vibrio anguillarum* Infection in *Amphioctopus fangsiao*

Xiaokai Bao[1†], Yan Li[1†], Jianbai Zhang[2], Xipan Chen[1], Xiaohui Xu[1], Yanwei Feng[1], Guohua Sun[1], Xiumei Liu[3], Bin Li[1,4], Weijun Wang[1,5], Zan Li[1] and Jianmin Yang[1]**

[1] College of Agriculture, Ludong University, Yantai, China, [2] Yantai Marine Economic Research Institute, Yantai, China, [3] College of Life Sciences, Yantai University, Yantai, China, [4] Yantai Haiyu Marine Science and Technology Co., Ltd., Yantai, China, [5] Jiangsu Baoyuan Biotechnology Co., Ltd., Lianyungang, China

Immune defense systems are indispensable for living organisms. Within an immune network, problems with any given link can impact the normal life activities of an organism. *Amphioctopus fangsiao* is a cephalopod that exists widely throughout the world's oceans. Because of its nervous system and locomotive organs, it has become increasingly studied in recent years. *Vibrio anguillarum* is one of the most common pathogenic bacteria in aquaculture organisms. It is highly infectious and can infect almost all aquaculture organisms. *V. anguillarum* infection can cause many adverse biological phenomena, including tissue bleeding. Study the immune response after *V. anguillarum* infection would help us to understand the molecular mechanisms of immune response in aquaculture organisms. In this research, we infected the primary incubation *A. fangsiao* with *V. anguillarum* for 24 h. We analyzed gene expression in *A. fangsiao* larvae via transcriptome profiles at 0, 4, 12, and 24 h after hatching, and 1,385, 734, and 6,109 differentially expressed genes (DEGs) were identified at these three time points. Gene Ontology (GO) and Kyoto Encyclopedia of Genes and Genomes (KEGG) enrichment analyses were used to identify immune-related DEGs. Protein–protein interaction networks were constructed to examine interactions between immune-related genes. Twenty hub genes involved in multiple KEGG signaling pathways or with multiple protein–protein interaction relationships were identified, and their differential expression verified by quantitative RT-PCR. We first studied *V. anguillarum* infection of *A. fangsiao* larvae by means of protein–protein interaction networks. The results provide valuable genetic resources for understanding immunity in molluscan larvae. These data serve as a theoretical basis for the artificial breeding of *A. fangsiao*.

Keywords: *Amphioctopus fangsiao*, *Vibrio anguillarum*, larval growth, transcriptome, protein-protein interaction networks, immunity, infecting

OPEN ACCESS

Edited by:
Yuehuan Zhang,
South China Sea Institute of Oceanology, Chinese Academy of Sciences (CAS), China

Reviewed by:
Jun Li,
South China Sea Institute of Oceanology, Chinese Academy of Sciences (CAS), China
Camino Gestal,
Consejo Superior de Investigaciones Científicas (CSIC), Spain
Xubo Wang,
Ocean University of China, China

***Correspondence:**
Zan Li
lizanlxm@163.com
Jianmin Yang
ladderup@126.com

[†] These authors have contributed equally to this work and share first authorship

Specialty section:
This article was submitted to Marine Fisheries, Aquaculture and Living Resources, a section of the journal Frontiers in Marine Science

Received: *27 June 2021*
Accepted: *06 September 2021*
Published: *29 September 2021*

Citation:
Bao X, Li Y, Zhang J, Chen X, Xu X, Feng Y, Sun G, Liu X, Li B, Wang W, Li Z and Yang J (2021) Transcriptome Profiling Based on Different Time Points After Hatching Provides a Core Set of Gene Resource for Understanding Larval Immune Response Mechanisms Against Vibrio anguillarum Infection in Amphioctopus fangsiao. Front. Mar. Sci. 8:731517. doi: 10.3389/fmars.2021.731517

INTRODUCTION

As a new research direction, mollusks have received extensive attention recently because of their complex immune responses and molecular mechanisms (Sokolova, 2009; Wang et al., 2019). organism growth is inseparable from immune response, and loss of immunity leads to disease and even death, suggesting that immune response is a core factor of the growth of organisms (Rowley and Powell, 2007; Barcia and Ramos-Martínez, 2011; Wang et al., 2019). The larval is a relatively vulnerable stage in life (Ginger et al., 2013; Kaplan et al., 2013). Growth quality among larvae directly affects the quality of life of the adult, impacting characteristics including vitality and physique. The immune functions of larvae are important to the growth process. It is well known that organisms have a higher ability to resist invasion by external pathogens when the numbers and activity of their immune cells are high. Therefore, immune function can effectively protect larvae of organisms, maintaining their normal growth (Wang et al., 2013; Matozzo, 2016).

As a marine mollusk, *Amphioctopus fangsiao* is widely distributed along the coasts of the Pacific, the Yellow Sea, and the Bohai Sea. Due to the difficulties associated with catching wild *A. fangsiao*, numbers of *A. fangsiao* bred in captivity have gradually risen in recent years. However, whether *A. fangsiao* is wild or bred the larvae are vulnerable to a variety of pathogens including bacteria and viruses (Budelmann, 1994; Wei et al., 2015, 2018). *Vibrio anguillarum* is a gram-positive bacterium that can cause many popular diseases in aquaculture animals. In recent years, multiple studies have confirmed *V. anguillarum* infections in many fish species, including *Salmo salar* and *Paralichthys olivaceus* (Hoel et al., 1997; Li et al., 2015; Bao et al., 2019). *V. anguillarum* can infect bivalve and gastropod such as *Chlamys nobilis* and *Haliotis gigantea* (Cong et al., 2008; Iehata et al., 2009; Zhang et al., 2016). When aquaculture organisms are infected by *V. anguillarum*, they display red gills, muscle bleeding, mucosal tissue decay, and other symptoms, ultimately leading to significant losses to the aquaculture industry. *V. anguillarum* infection requires certain conditions, and the incidence rate of *V. anguillarum* infection tends to be higher in poor environments or among injured or stimulated organisms (Vázquez et al., 2006; Zhou et al., 2010; Nie et al., 2017). Although there are widely studies on the infection of *V. anguillarum* in fish, bivalve, and gastropod, there are still few studies have been conducted on the infection of mollusks, especially cephalopods. The pathogenic mechanisms of *V. anguillarum* in cephalopods are still unclear, and require further study.

Transcriptome sequencing technology has recently become an important method for studying differences between individuals of the same species. To aid in assessing biological immune response mechanisms, transcriptome sequencing can analyze differences in gene expression between different individuals or tissues (Zhao et al., 2012; Silva et al., 2013; Zhang et al., 2018). It can help identify important immune genes and further study biological immune response mechanisms. Previous researches have carried out transcriptome analyses of aquatic mollusks such as *Pinctada martensii* (Zhao et al., 2012), *Biomphalaria glabrata* (Silva et al., 2013), *Haliotis diversicolor* (Zhang et al., 2018), *Octopus vulgaris* (Castellanos-Martínez et al., 2014), and *Euprymna tasmanica* (Salazar et al., 2015; Schultz and Adema, 2017). The transcriptome analyses of *A. fangsiao* is still lacking, which need a lot of experiments to explore.

In this research, we infected the primary incubation *A. fangsiao* larvae with *V. anguillarum* for 24 h. We then took *A. fangsiao* larvae at 0, 4, 12, and 24 h after hatching for transcriptome sequencing and bioinformatics analyses, including gene function annotation, differentially expressed genes (DEGs) analysis, Gene Ontology (GO) functional enrichment analysis, Kyoto Encyclopedia of Genes and Genomes (KEGG) functional enrichment analysis, and immune-related protein–protein interaction network studies. We identified and verified 20 differentially expressed hub genes using quantitative RT-PCR. These results revealed the immunity of *A. fangsiao* larvae after infection with *V. anguillarum*, providing a valuable resource for understanding immune response mechanisms in mollusks, and laying a foundation for exploring the immune response mechanisms of other mollusks.

MATERIALS AND METHODS

Ethics Statement

Amphioctopus fangsiao samples were obtained from a commercial hatchery. This research was conducted in accordance with the protocols of the Institutional Animal Care and Use Committee of the Ludong University (protocol number LDU-IRB20210308NXY) and the China Government Principles for the Utilization and Care of Invertebrate Animals Used in Testing, Research, and Training (State Science and Technology Commission of the People's Republic of China for No. 2, October 31, 1988[1]).

Sample Collection and RNA Preparation

The wild parent used in these experiments were obtained from the Rizhao Sea area. After spawning, the eggs were protected and incubated by female parent *A. fangsiao*. During the incubation process, the seawater temperature was maintained at 19–20.8°C, and the incubation lasted approximately 29 days. After hatching, larvae were temporarily cultured in floating seawater containing 1×10^7 CFU/mL *V. anguillarum* for 24 h. Primary incubation larvae were collected and stored for 4, 12, and 24 h in liquid nitrogen until RNA was extracted using the TRIzol method.

Nine larvae from primary incubation were randomly selected from each time point for RNA extraction: *A. fangsiao* larvae infected for 0 h (Oo-C), *A. fangsiao* larvae infected for 4 h (Oo-4h), *A. fangsiao* larvae infected for 12 h (Oo-12h), and *A. fangsiao* larvae infected for 24 h (Oo-24h). At each time point, equal molar masses of RNA from any three of nine larvae were pooled into one replicate to provide a template for the construction of the transcriptome library; any three of the remaining six larvae were pooled into the second

[1]http://www.gov.cn/gongbao/content/2011/content_1860757.htm

replicate; and the final three larvae were pooled into the third replicate. Remaining RNA was retained for subsequent quantitative RT-PCR verification.

Library Construction and Illumina Sequencing

Library construction was carried out according to a method described by Li et al. (2017). Finally, we sequenced each sample using an Illumina HiSeq 4000 platform.

Gene Expression Level Analysis and Functional Annotation

A reference sequence was obtained by splicing Trinity with RSEM, and clean reads were mapped to this reference sequence. We then obtained the number of read counts for each sample that mapped to each gene. The read count was transformed into fragments per kilobase of transcript per million mapped reads (FPKM) to analyze the gene expression and abundance, and expression levels of samples were positively correlated with FPKM. The unigenes were annotated by searching the sequences against the NR, NT, GO, SwissProt, and KOG databases using BLASTX with a cut-off of E value $\leq$ 1e-5. Meanwhile, we annotated unigenes into Pfam database with Hmmer 3.0 package (E value ≤ 0.01).

Differentially Expressed Genes Screening and Analysis

Differentially expressed genes were screened out using the DESeq2 package for R as a negative binomial distribution model. First of all, data were imported for building the dds model, and then the DESeq function was used to estimate the dispersion of the samples. After that, the difference in gene expressions was analyzed by this package. Finally, DEGs with q-value ≤ 0.05 and $|\log2 \text{ fold change}| \geq 1$ were screened out (Love et al., 2014; Ho et al., 2017). Significant DEGs in each time point were screened by GO functional enrichment analysis to obtain GO terms and distribution of DEGs. Statistical analyses of DEGs were conducted. To further understand functions of DEGs, KEGG signaling pathway analysis was performed for up- and down-regulated genes, and we annotated immune pathways involving DEGs. Finally, we screened the signaling pathways in which DEGs were significantly enriched, and species and numbers of DEGs in these pathways were counted.

Trend Analysis

Through trend analysis, we understood the change trend of gene expression over time. STEM was used to analyze the expressing trend of DEGs, and cluster trends in gene expression quantity. The parameters were set as follows: the Maximum Unit Change in model profiles between time points is 1; maximum output profiles number is 20 (similar profiles will be merged); minimum ratio of fold change of DEGs is no less than 2.0; the criterion for screening trends with significant differences is p-value ≤ 0.05 (Ernst and Bar-Joseph, 2006). Trend analysis showed the expressing trend of genes in the process of larval growth after infection, and predicted the future trend, which can help us explore the relationship between immunity and larval growth of *A. fangsiao* after infection.

Functional Protein Association Network Construction

We used STRING v11.0 with default parameters to construct protein–protein interaction networks to further explore gene relationships in immune regulation pathways (Damian et al., 2018).

Quantitative RT-PCR Validation

We verified the accuracy of our RNA-Seq results using quantitative RT-PCR to validate 20 selected genes (**Supplementary Table 1**). Three biological replicates of each time point were used in the experiment. Primer Premier 5.0 was used to design gene-specific primers. **Table 1** lists the 20 selected genes and their corresponding primer sequences. We evaluated the stability of *GAPDH*, β-*actin,* and *18S* genes in different tissues and embryo development stages of *A. fangsiao*. The expression level of *A. fangsiao* β-*actin* tended to be stable, and it was used as an endogenous control in this experiment. Quantitative RT-PCR was performed according to a method described by Li et al. (2019).

RESULTS

Sequencing Results and Quality Assessment

Samples at four time points were sequenced by RNA-Seq. The overview of sequencing results is provided in **Table 2**. Raw sequencing reads were submitted to Sequence Read Archive in NCBI; the SRA accession numbers were SRR15204591, SRR15204592, SRR15204593, SRR15204594, SRR15204595, SRR15204596, SRR15204597, SRR15204598, SRR15204599, SRR15204600, SRR15204601, and SRR15204602[2].

Differential Expression Analysis

Through differential expression analysis, we identified 1,385, 734, and 6,109 DEGs at 4, 12, and 24 h after infecting compared with primary incubation larvae. Among these, 480 DEGs were up-regulated, and 905 DEGs were down-regulated at 4 h after infection; 338 DEGs were up-regulated, and 396 DEGs were down-regulated at 12 h after infection; 1,685 DEGs were up-regulated, and 4,424 DEGs were down-regulated at 24 h after infection (**Figure 1** and **Supplementary Tables 2–4**). A Venn diagram shows all DEGs after infecting. Because DEGs at each of the three time points might be key genes affecting immunity in *A. fangsiao* larvae, their union set (7,019 DEGs) was selected for subsequent analysis (**Figure 2** and **Supplementary Table 5**). The heatmap (**Figure 3** and **Supplementary Table 6**) intuitively shows the clustering distribution of these DEGs.

[2]https://www.ncbi.nlm.nih.gov/Traces/study/?acc=SAMN20309867&o=acc_s%3Aa

TABLE 1 | Primer list for quantitative RT-PCR verification.

Gene name	Forward primer (5′-3′)	TM (°C)	Reverse primer (5′-3′)	TM (°C)	Amplicon length (bp)
ATM	TTGACTTGCTGCGTTCTC	60	ACCTCTCCGACTGTCTATTC	60	105
AXIN1	GTGAATAGGTGCGTCCTTAC	60	TAGCAGTCTTGATGGCATTC	60	106
CASP3	TCCAGGGACAGTGGAATAG	60	GTTATGCACGATGCTGGT	60	105
COL1A1	CCTTCGTTTCTTATCTCTTGCC	61	GTGTGTGCTTGTGTGTGTAA	61	185
COL1A2	CAGGAGGCACTGGTTAAAG	60	ACAAGTTCTCCGGCTTTG	60	139
COL2A1	TTGCGTCTCCGTCACTTA	61	TGGAGCACCACCTTTAGT	60	111
COL4A1	CACTCTGCCGAGGAAATATG	60	GCCAAGTCCTTGACAGTTTA	60	101
COL4A4	GTCTTACTGGAGAACGTTGAG	60	CACCAATGCGACCATCTT	60	120
CREBBP	TTTGTATCCGCCTTGTAGTG	60	CAAGGAGAGGAAGTGGAATTAG	60	115
GART	GAGAGGCTCAACACCAATC	60	GCTTGAACACATTGCTTACC	60	107
ITGA4	CTTCCAACTGGAGCCTATTAAG	60	AGCATGACTGGGATGTACT	60	124
MAPK14	CGCATCTGTAACTCCCTTTC	60	GACACGTCACTGCTTCTATT	60	119
MTOR	GATTGTCCCACCACCTCTA	60	CAGCTTGCCACCTTGATTA	60	100
NFKB1	CCACTTGGCTGTTGTTACT	60	AAGTCTCCATCCCGACAA	60	126
PIK3CB	CTGGCATCCTTATGCTTCTT	60	GTTCTATCCCAACGGACTTG	60	140
PLCG1	TTCCCATGGAACCATTTCTC	60	CCGAACAAGACGAAGATCAA	60	100
PTK2	CAGTTTGACCACCCTCATATC	60	TGTAAATAAGCCCGCATCTC	60	110
RAC1	TAGCAAGACCCTGAGGATAG	60	TATTGGTCGGCACGAAAC	60	102
WNT4	GGCATGCAGTACCCATATAC	60	CGCACCTCTTTCCAGTTT	60	165
WNT5A	TGGCATGTGGTCGTAATG	60	TACAGAGTGGAGAGGTATGG	60	122

Differentially Expressed Genes Expression Trend

STEM was used to analyze trends in 7,019 DEGs. The results showed that DEGs were divided into 20 expression trends, involving six significantly enriched ones (**Figure 4**). Their *p*-value were less than 0.05, and 4,940 DEGs were differentially expressed in these trends. Among them, profile 0 (**Figure 4D**) is the most significant trend, and profile 9 (**Figure 4C**) has the most genes expressed in this trend.

Gene Ontology and Kyoto Encyclopedia of Genes and Genomes Enrichment Analysis of Differentially Expressed Genes

We identified the top ten level-3 terms of the three categories (biological process: 352 level-3 subclasses, molecular function: 107 level-3 subclasses, and cellular component: 84 level-3 subclasses) (**Figure 5** and **Supplementary Table 7**) by GO functional enrichment analysis. For instance, the signal transduction term and the cell differentiation term in biological process were closely related to immunity. Similarly, KEGG enriched DEGs in different pathways guided us to further understand the functions of these genes. Of 7,019 DEGs, 1,548 DEGs were enriched in 263 level-2 KEGG class pathways (**Figure 6** and **Supplementary Table 8**). **Table 3** showed the 20 immune-related pathways that were significantly enriched including biosynthesis of antibiotics signaling pathway, Wnt signaling pathway, and PI3K-Akt signaling pathway. Because some DEGs were involved in the regulation of multiple signal pathways, we finally obtained 208 genes enriched in 20 immune-related pathways for follow-up analyses.

TABLE 2 | Summary of sequencing results.

Sample	Raw reads	Clean reads	Q20 (%)	Q30 (%)	GC (%)
Oo-C-1	50,581,378	49,165,388	97.54	93.27	40.62
Oo-C-2	49,281,546	46,846,720	97.42	93.07	39.91
Oo-C-3	55,727,122	53,007,342	97.39	92.94	40.58
Oo-4h-1	43,683,716	40,502,546	97.38	92.93	40.15
Oo-4h-2	50,981,374	47,814,924	97.47	93.15	40.63
Oo-4h-3	44,781,414	41,833,784	97.30	92.78	40.37
Oo-12h-1	42,605,216	40,522,842	97.72	93.70	40.58
Oo-12h-2	54,564,714	51,170,578	97.30	92.72	40.52
Oo-12h-3	56,997,500	53,933,392	97.61	93.42	40.56
Oo-24h-1	51,418,618	49,235,968	97.71	93.67	40.37
Oo-24h-2	60,787,322	58,211,806	97.52	93.20	40.78
Oo-24h-3	63,795,232	61,219,086	97.57	93.32	40.71

Construction of Immune-Related Protein Interaction Networks

Proteins are important components of all cells and tissues in living organisms. All important parts of an organism require functional proteins, which are the main mediators of the activities of life. Construction of protein–protein interaction networks can help reveal the key genes involved in immune processes. We constructed protein–protein interaction networks using the protein sequences encoded by 208 genes in 20 significantly enriched immune-related signaling pathways. **Figure 7** shows these networks. Among this figure, the CASP gene had the highest number of protein-protein interactions, and the other 5 genes including AXN1, CREBBP, MTOR, PTK2, and WNT5A were interacted with more than 20 proteins. Relevant parameter information of them was listed in **Table 4**. There were 148 nodes and 622 edges in the network, and each node was interacted with

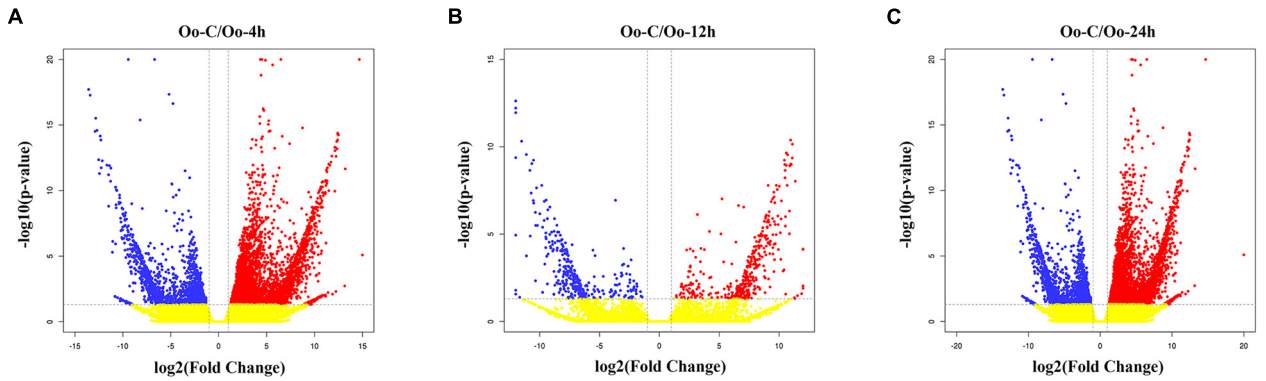

FIGURE 1 | (A) Volcano plot of DEGs distribution trends between Oo-C and Oo-4h. Each dot stands for a gene. Red dots indicate up-regulated DEGs; blue dots are down-regulated DEGs; and yellow dots stand for the genes with no difference. **(B)** Volcano plot of DEGs distribution trends between Oo-C and Oo-12h. **(C)** Volcano plot of DEGs distribution trends between Oo-C and Oo-24h.

an average of 8.41 nodes. The clustering coefficient was 0.466, and the *p*-value of this network was $\leq$ 1.0e-16.

Acquisition and Validation of Key Differentially Expressed Genes Related to Immune Processes

This research focused on interactions between key immune-related genes. Twenty key DEGs (**Table 5**) involved in multiple signaling pathways or multiple interaction relationships were obtained from KEGG pathway analysis and protein–protein interaction networks. These were then used to explore interaction mechanisms between them. The 20 key genes were divided into five categories as follows: Collagen family, Wnt signaling pathway, biosynthesis of antibiotics signaling pathway, tumor necrosis factor (TNF) signaling pathway, and other important immune-related genes. To verify the accuracy of these key genes, we used quantitative RT-PCR to quantitatively assess the relative expression of 20 immune-related genes at each time point identified as DEGs by RNA-Seq. Quantitative RT-PCR results showed that all DEGs measured were single products. A comparison of gene expression profiles by RNA-Seq and quantitative RT-PCR (**Figure 8**) indicated that the quantitative RT-PCR results correlated significantly with the RNA-Seq results, and the two methods presented the same trend pattern.

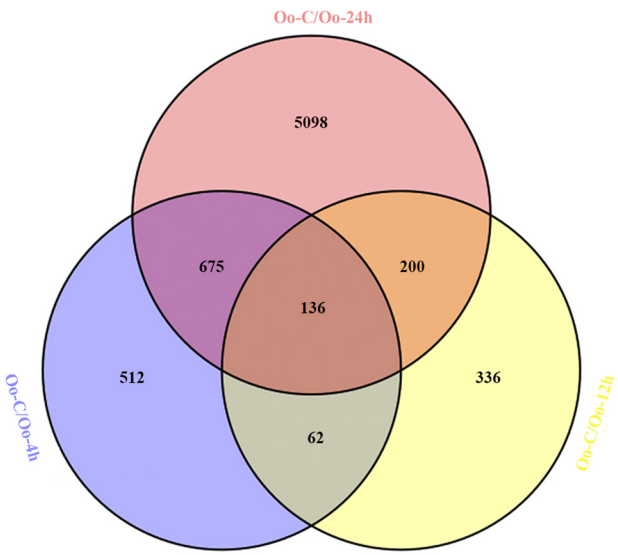

FIGURE 2 | The Venn diagram shows the overlap of the DEGs at 4 h (blue), 12 h (yellow), and 24 h (red) after infecting.

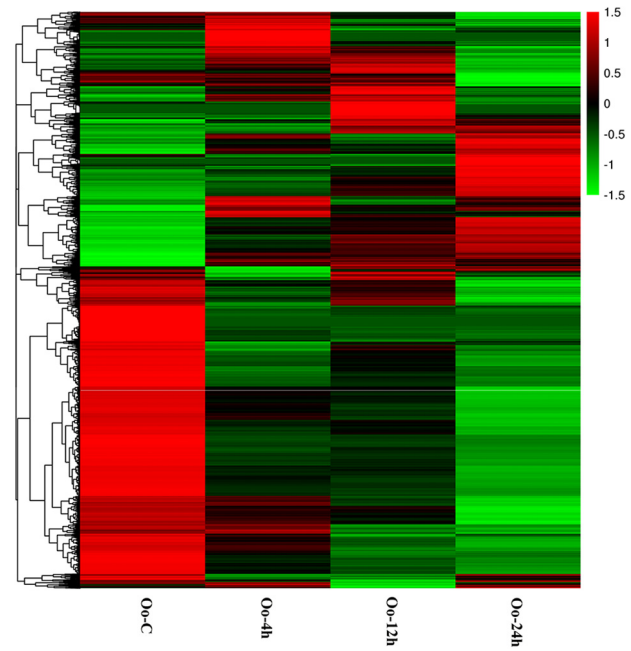

FIGURE 3 | Heatmap analysis of hierarchical clustering of DEGs at four time points. Each row represents one gene, and each column stands for a time point. The colors range from green to red, indicating the level of expression from low to high.

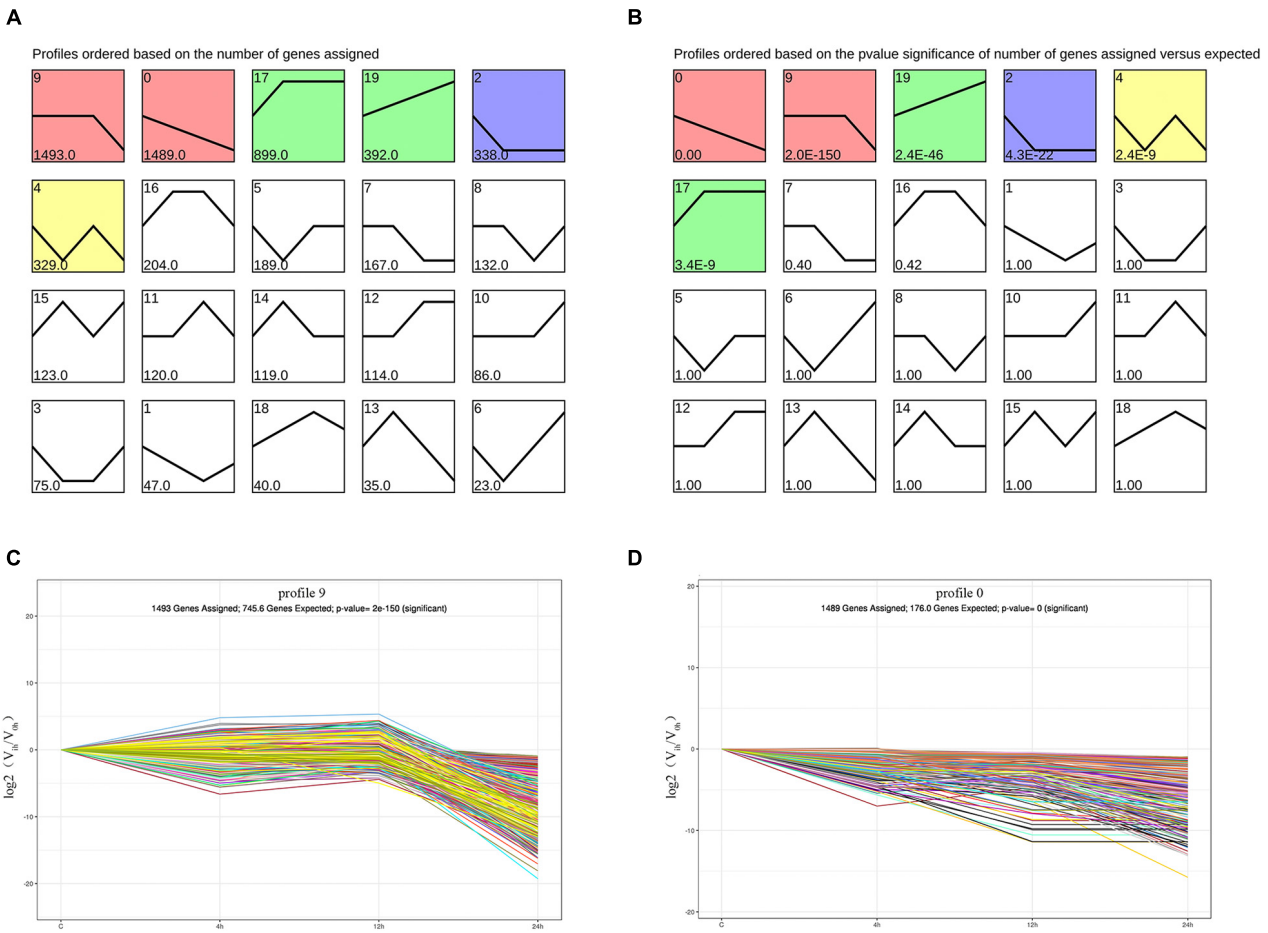

FIGURE 4 | Trend analysis was used to analysis the trend changes of DEGs. **(A)** Trend analysis results sorted by the number of enriched DEGs. **(B)** Trend analysis results sorted by *p*-value. **(C)** The expression trend of DEGs in profile 9. The *x*-axis lists the time point after hatching; the *y*-axis indicates log2(fold change). **(D)** The expression trend of DEGs in profile 0.

DISCUSSION

The Purpose and Significance of This Research

Amphioctopus fangsiao has become increasingly popular because of its rich nutritional value and delicious meat. As an economically important species employed in mariculture, the artificial breeding of *A. fangsiao* has been well concerned (Iehata et al., 2009; Zhang et al., 2016; Li et al., 2019). The larval growth stage is very important for *A. fangsiao*, which determines whether the adult can grow healthily. The larvae of aquaculture organisms are easily infected by a variety of pathogens, which can seriously hinder aquaculture development (Barcia and Ramos-Martínez, 2011; Wang et al., 2019). Research into biological immune responses to bacterial infection will help breeders to prevent and mitigate bacterial infections. We infected primary incubation larvae for 24 h with *V. anguillarum*, and identified the changes of the biological immune response mechanisms. We identified 7,019 DEGs and believed that these genes have an important relationship with the immune response mechanisms of *A. fangsiao* larvae. A heatmap showed that there were significant differences in immunity with increase in *A. fangsiao* larvae infection time. The results of trend analysis showed that the six of the 20 trends were significantly enriched, and half of DEGs were expressed in these trends, indicating significant differences in the immunity after larval infection. KEGG enrichment analysis obtained 20 immune-related pathways enriched in DEGs, which were interacted with each other and shared biological immune functions. Finally, we used 208 genes in these pathways to construct protein–protein interaction networks to understand immune response mechanisms of *A. fangsiao* larvae.

Trend Analysis of Differentially Expressed Genes

The results of the trend analysis in **Figure 4** indicated that profile 9 trend had the largest number of DEGs, and the significance of profile 0 trend was the highest. Among them, the gene expression trends showed continuously down-regulation and from stable to down, respectively, which were inconsistent with the expectation of our experiment. Therefore, we conducted

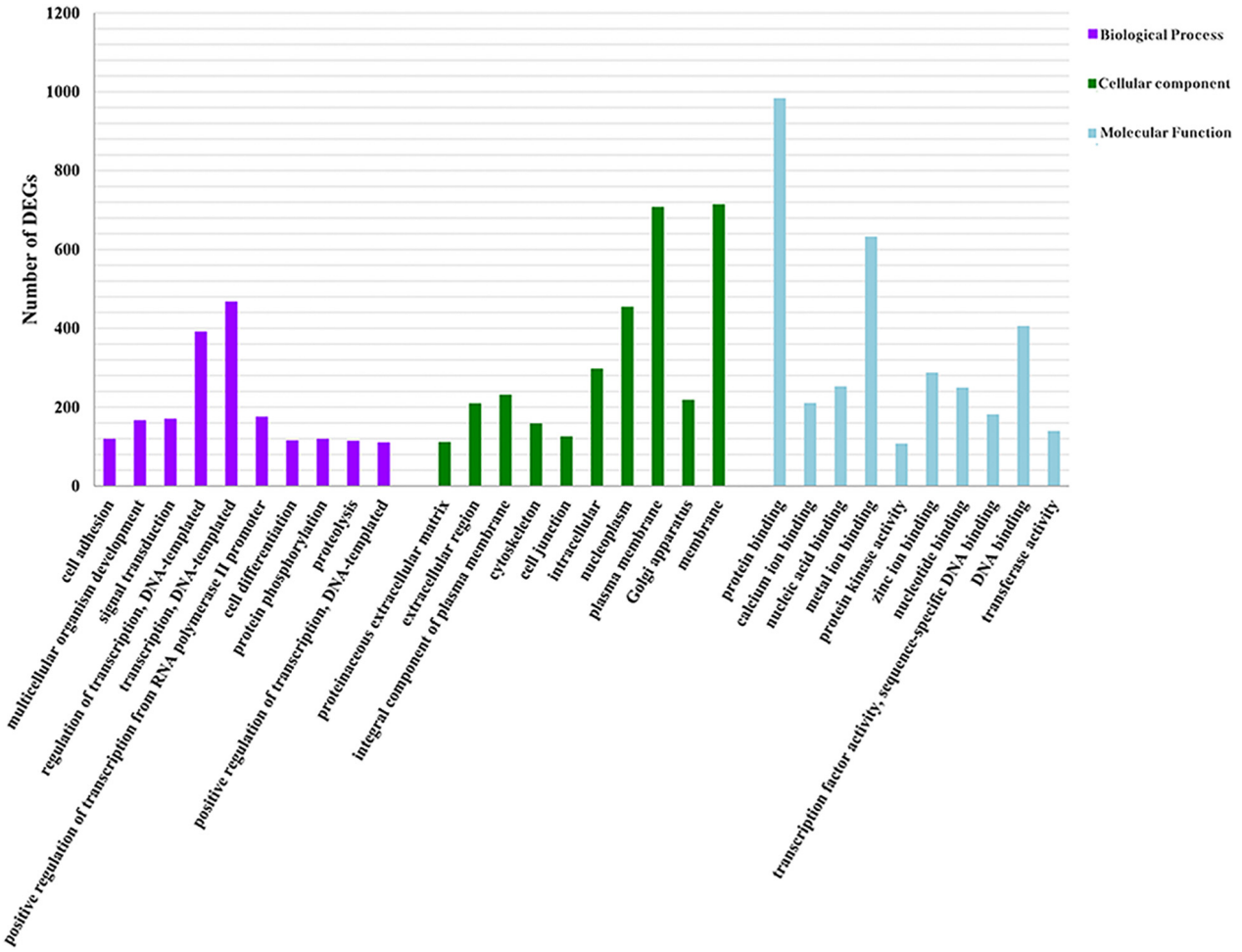

FIGURE 5 | GO analysis of DEGs. Distribution of level-3 GO annotation among the three categories. The *y*-axis represents the corresponding number of DEGs; the *x*-axis stands for the gene function classification based on GO.

GO and KEGG enrichment analyses of the genes involved to further explore the causes. In our analysis, we found that these genes were mainly involved in metabolic processes, including protein digestion and absorption signaling pathway, insulin signaling pathway, and cell adhesion term (Curtis et al., 1978; Lee and Pilch, 1994; Schepis et al., 2012; Brezas and Hardy, 2020). These results showed that the metabolic capacity of *A. fangsiao* larvae decreased gradually in the course of infection. Meanwhile, 1,291 DEGs in profile 17 and profile 19 were up-regulated. We used DEGs from these two profiles for GO and KEGG enrichment analyses, and identified a number of immune-related terms and pathways. For instance, positive regulation of JNK cascade term, biosynthesis of antibiotics signaling pathway, and NF-kappa B signaling pathway were significantly enriched. The JNK cascade is a key step in cell apoptosis mediated by the NF- kappa B signaling pathway, which is involved in the apoptosis process of diseased cells (Bubici et al., 2004; Lanna et al., 2017). NF-κB is involved in the regulation of immunity, lymphocyte development, and tumorigenesis (Bubici et al., 2004; Sun, 2017). Antibiotics can effectively resist the invasion of bacteria, and their synthesis can improve biological resistance (Bulfon et al., 2020). In conclusion, although the DEGs for the two most critical trends were down-regulated, they were highly correlated with metabolism. The results indicated that the metabolism of larvae was affected and had a downward trend after infection. The other DEGs in two up-regulated trends were more associated with immunity, suggesting that the immune response of *A. fangsiao* larvae increased gradually with the prolongation of infection. Above results revealed significant changes in the responses of *A. fangsiao* after infection. The complex mechanisms of *A. fangsiao* after infection need to be further studied and discussed in the future.

Enrichment Analysis of Immune-Related Kyoto Encyclopedia of Genes and Genomes Signaling Pathways and Gene Ontology Terms

Many immune-related terms and pathways were yielded through GO and KEGG enrichment analyses, including signal

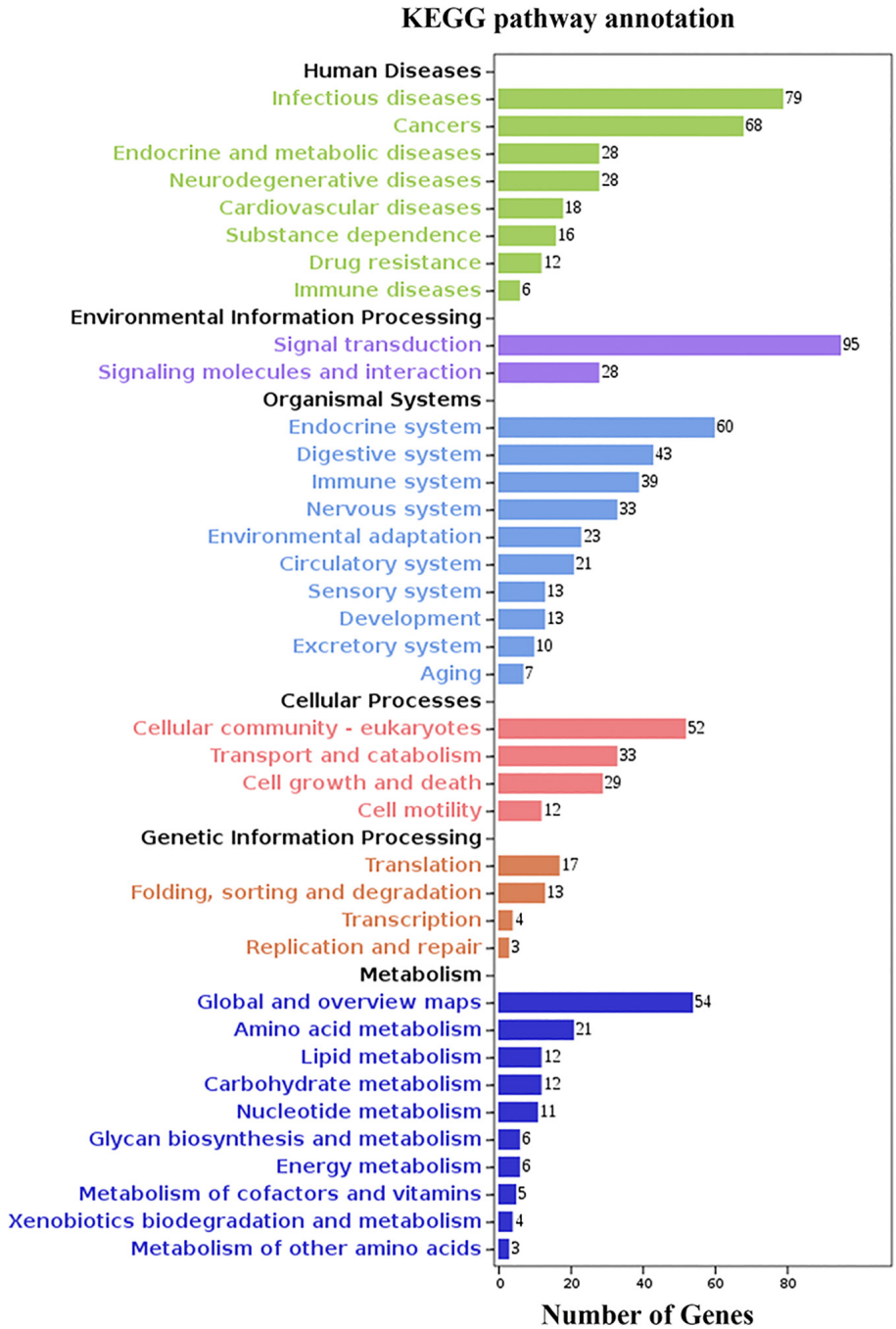

FIGURE 6 | KEGG analysis of DEGs. The *y*-axis indicates level-2 KEGG classes; the *x*-axis represents the corresponding number of DEGs.

transduction term, cell differentiation term, biosynthesis of antibiotics signaling pathway, TNF signaling pathway, and other key terms and pathways. These terms and pathways were vital in biological immunity, indicating that there were a large number of immune-related genes in the larvae infected with *V. anguillarum*, and thus resulted in complex immune responses in the larvae. A comprehensive analysis of the enriched KEGG pathways and GO terms contributes to investigate the molecular mechanisms and immune systems changes of *A. fangsiao* larvae after infection with *V. anguillarum*, thereby aiding our artificial breeding work.

Speculation of Hub Genes

Proteins are the basis of biological activities, and their interactions maintain the growth and development of organisms. We used 208 key DEGs identified in immune-related pathways to construct protein–protein interaction networks. The results

TABLE 3 | Summary of 20 significant immune-related signaling pathways.

Pathways	Number of DEGs
Pathways in cancer	52
PI3K-Akt signaling pathway	45
Biosynthesis of antibiotics	31
Wnt signaling pathway	28
Transcriptional misregulation in cancer	20
TNF signaling pathway	18
Inflammatory mediator regulation of TRP channels	15
Proteoglycans in cancer	14
Chemokine signaling pathway	13
Bacterial invasion of epithelial cells	11
Apoptosis	10
NF-kappa B signaling pathway	9
Natural killer cell mediated cytotoxicity	8
Leukocyte transendothelial migration	7
p53 signaling pathway	6
Toll-like receptor signaling pathway	5
Central carbon metabolism in cancer	4
T cell receptor signaling pathway	4
NOD-like receptor signaling pathway	3
MicroRNAs in cancer	2

suggested that interactions between these proteins was greater than expected relative to a randomly selected a group of proteins of similar size from the genome. This conclusion proves that above proteins cooperate in carrying out coordinated functions. We thus suggested that nodes with more edges were hub proteins in immune response. The genes corresponding to these hub proteins were identified as hub genes for further studies and verification.

Functional Analysis of Kyoto Encyclopedia of Genes and Genomes Signaling Pathways and Hub Genes

Transcriptome profiling was analyzed to compare the changes of immune response mechanisms in *A. fangsiao* larvae infected with *V. anguillarum* within 24 h. This helps us to further understand the *A. fangsiao* larval immune response to *V. anguillarum* infection with the growth of them. Finally, we speculatively identified 20 hub genes involved in multiple protein–protein interaction relationships or KEGG signaling pathways, and these hub genes, KEGG signaling pathways, and immune differences at each time point were investigated.

Collagen Family

Collagen is one of the most abundant proteins in the organisms. It is an important part of extracellular matrix, and plays a regulatory role in tissue structure. Its subunits directly affect cell phenotypes by mediating cell differentiation and apoptosis via relevant signaling pathways (Brondijk et al., 2010; Jürgensen et al., 2020). Collagen also acts as a major part in the immune system. When cells are stimulated by bacteria, collagen receptors are responsive to change the extracellular environment, thus indirectly regulating the activities of immune cells to resist the invasion of bacteria (Kresina et al., 1984; Aragona et al., 1998; Brondijk et al., 2010). In this study, five key genes involved in the immune response of collagen family (COL1A1, CoL1A2, COL2A1, COL4A1, and COL4A4) were identified. Among them, COL1A1 and COL2A1 presented the most obvious effect on enhancing the biological resistance to external invasion through the protection of bones, kidney, skin, and other organs. The lack of collagens in the organisms can lead to osteogenic and skin damages, which can reduce the immunity of organisms indirectly (Kuppevelt et al., 1995; Takai et al., 2001; Makino et al., 2010). In our study, the five genes in collagen family were enriched significantly, indicating an obvious bacteriological stimulation effect. Collagen family may be an important part to regulate the biological immune functions. In the above five genes, COL1A1 and COL2A1 were significantly up-regulated with the prolongation of infection time. This result indicated that *A. fangsiao* larvae had a strong immunity to effectively resist the invasion of pathogens. The other three genes were continuously down-regulated within 24 h of infection, the specific reasons need additional explorations.

Wnt Signaling Pathway

Wnt is an important immune regulatory protein widely existing in various organisms. It participates in the immune response of multiple organs and acts a key role in maintaining tissue homeostasis (Famili et al., 2016). The Wnt signaling pathway can be divided into two subtypes: typical Wnt signaling pathway and atypical Wnt signaling pathway. The interaction between these two pathways regulates the growth, proliferation, differentiation, and apoptosis of immune cells, which can affect multiple immune responses of organisms (Naskar et al., 2014; Yu et al., 2014; Chae and Bothwell, 2018). Moreover, the Wnt signaling pathway is responsible for maintaining homeostasis through repairing damaged tissues and regulating the inflammatory response, which plays a role in the resistance and treatment of some immune diseases (Staal et al., 2008; Pai et al., 2017; Ruan et al., 2021). In this study, the Wnt signaling pathway was significantly enriched, and multiple DEGs including TBL1XR1, ROCK2, and CSNK1A1 were enriched in this pathway. They are the key factors in the immune system, and play a significant role in immune regulation during larval growth. Meanwhile, these genes are functional in the resistance of larvae against the invasion of pathogens and promote the normal growth of organisms (Puigvert et al., 2013; Nikola et al., 2017; Venturutti et al., 2020). Their up-regulation after larval infection suggested the improved immune ability of *A. fangsiao* larvae after being infected with bacteria.

Biosynthesis of Antibiotics Signaling Pathway

Antibiotics are a class of metabolites produced in the life of higher animals, plants, and fungi, which have the ability to resist the invasion of pathogens. They can affect the growth of organisms by regulating cell growth and apoptosis (Pomorska-Mól and Pejsak, 2012; Herman, 2020). Biosynthesis of antibiotics can improve the ability of organisms to resist bacterial infection and increase the resistance of larvae. When organisms are invaded by

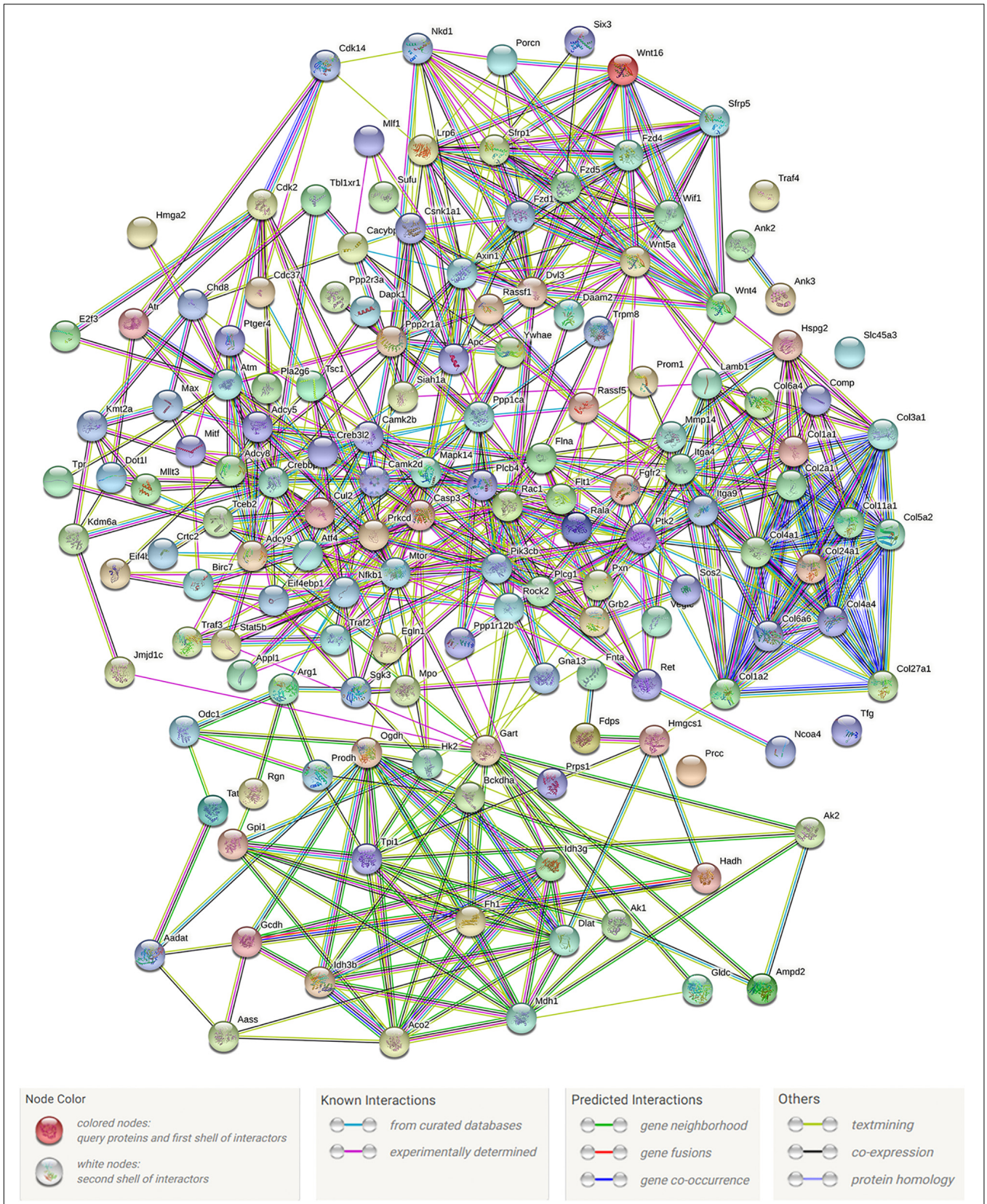

FIGURE 7 | Immune-related protein–protein interaction networks. Network nodes stand for proteins. The legend represents the relationships between nodes.

TABLE 4 | Network statistics of immune-related proteins.

Network statistics	
Number of nodes	148
Number of edges	622
Average node degree	8.41
Clustering coefficient	0.466
Expected number of edges	223
PPI enrichment *p*-value	1.0E-16

TABLE 5 | Summary of 20 key DEGs.

Gene name (abbreviation)	Gene name (official full name)	Number of KEGG signaling pathways	Number of protein–protein interactions
ATM	ataxia telangiectasia mutated	4	14
AXIN1	Axin 1	2	23
CASP3	caspase 3	3	29
COL1A1	collagen type I alpha 1 chain	1	18
COL1A2	collagen type I alpha 2 chain	1	15
COL2A1	collagen type II alpha 1 chain	1	17
COL4A1	collagen type IV alpha 1 chain	2	15
COL4A4	collagen type IV alpha 4 chain	2	15
CREBBP	CREB binding protein	2	25
GART	phosphoribosylglycinamide formyltransferase	1	19
ITGA4	integrin alpha 4	3	16
MAPK14	mitogen activated protein kinase 14	6	20
MTOR	mechanistic target of rapamycin kinase	2	24
NFKB1	nuclear factor kappa B subunit 1	8	12
PIK3CB	phosphatidylinositol-4,5-bisphosphate 3-kinase catalytic subunit beta	12	14
PLCG1	phospholipase C gamma 1	7	11
PTK2	protein tyrosine kinase 2	5	24
RAC1	Rac family small GTPase 1	1	21
WNT4	Wnt family member 4	2	15
WNT5A	Wnt family member 5A	1	20

external bacteria, antibiotics participate in the immune response, which can help organisms resist invasion, and increase their immunity. Recent studies have shown that antibiotics can treat some immune diseases and prevent immune system disorders (Stevens, 1996; Pomorska-Mól and Pejsak, 2012; Yang et al., 2017). In our study, biosynthesis of antibiotics signaling pathway was significantly enriched, suggesting that antibiotics act as an important part in the immune response of *A. fangsiao* larvae. Many key immune-related genes in this pathway were up-regulated with the growth of infected *A. fangsiao* larvae, indicating that antibiotics can guide a variety of immune responses to eliminate invading pathogens.

Tumor Necrosis Factor Signaling Pathway

As a regulatory factor, TNF exists in various organisms. It can send signals to proteins in the immune system, promote the interaction between immune cells, and enhance the immune ability of organisms (Ferreira et al., 1993; Vielhauer and Mayadas, 2007; Croft, 2009; George et al., 2014; Li et al., 2021). In the immune system, TNF also acts as a signal protein to regulate the release of other cytokines. Moreover, TNF plays an important role in promoting T cell proliferation, interferon expression, and accelerating the efficiency of chemokines (Palanki et al., 2000; Vielhauer and Mayadas, 2007; Lougaris et al., 2017; Li et al., 2021). In our research, multiple immune-related genes including NFKB1, ATF4, and MAP2K4 were significantly enriched in this pathway. NFKB1 plays a major part in the regulation of immune response in organisms, which increases the resistance of organisms by regulating expression levels of proinflammatory factors, and inflammation-related proteins in immune cells. The other two genes are also useful in regulating the immune response of organisms (Sethi et al., 2007; Vielhauer and Mayadas, 2007; Huang et al., 2019). This result suggested that immune genes responded quickly after infection, which increasing the immune activity of *A. fangsiao* larvae, and effectively eliminated the invading pathogens.

Analysis of Three Important Hub Genes

Among all hub genes, CASP3, CREBBP, and PTK2 were enriched in more than two immune-related signaling pathways, and possessed higher numbers of protein–protein interactions. CASP3 is a regulator of cell apoptosis. It can maintain the dynamic balance of cell number and the healthy growth of organisms by regulating the apoptosis of pathological cells and aging cells. The up-regulation of CASP3 is helpful to clear the diseased cells, and improve the survival rate and vitality of organism larvae (Lowe and Lin, 2000; Suzuki et al., 2020). As an acetyltransferase, CREBBP exists widely in lymphocytes of various organisms. It is a key gene regulating immune response, resisting pathogen invasion, and promoting immune cell expression. The low expression or loss of function of CREBBP leads to the disorder of enhancer network and B cell signal, and causes the disorder of expression of other immune cells (Jiang et al., 2016; Zhang et al., 2017; Jia et al., 2018). PTK2 is a protein kinase widely existing in various tissues, and organs of organisms, which acts as an extremely important disease regulator. At the same time, PTK2 is involved in the regulation of cell adhesion and movement, which is conducive to substance transport, and the expression levels of immune genes (Zhang et al., 2017; Yi et al., 2021). In this study, CREBBP was up-regulated within the first 12 h of infection, and slightly down-regulated within the last 12 h, indicating an important role in the immune regulation of *A. fangsiao* larvae after infection. PTK2 was significantly up-regulated within 24 h after infection and down-regulated within 4 to 12 h. The causes of PTK2 down-regulation need to be explained by subsequent studies. The above two genes had obvious effects on larval immunity, which is beneficial for the larvae to resist the invasion of pathogens. However, with the prolongation of infection time, CASP3 was down-regulated. This result is not consistent with our study, which needs additional studies to explain.

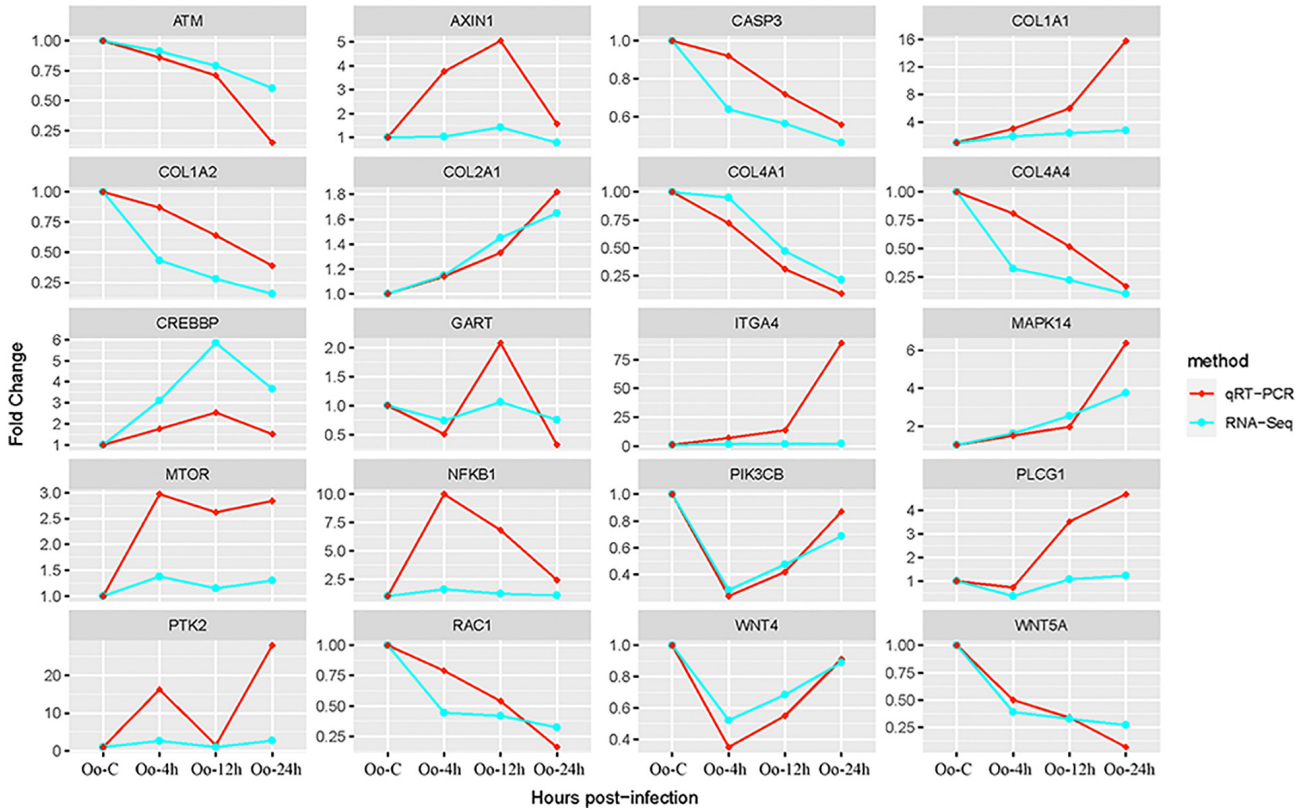

FIGURE 8 | Comparison of expression of 20 hub genes between qRT-PCR and RNA-Seq results. The transcript expression levels of the selected DEGs were each normalized to that of the β-*actin* gene. The *x*-axis represents the growth time after hatching; the *y*-axis stands for Fold change.

Other Hub Genes and Kyoto Encyclopedia of Genes and Genomes Signaling Pathways

In addition to the above hub genes and KEGG signaling pathways, our results identified other key DEGs and pathways involved in *A. fangsiao* larval immunity, including pathways in cancer signaling pathway, NF-kappa B signaling pathway, the PLCG1 gene, the ITGA4 gene, and the MTOR gene. The above two signaling pathways and three genes have been reported to be closely related to the immune response in various organisms (Wang et al., 2008; Thurnher et al., 2013; Darzi et al., 2017; Dieli-Crimi et al., 2018; Hong et al., 2019; Shiseki et al., 2019). The signaling pathways and genes details of the immune response mechanisms of *A. fangsiao* larvae infected with *V. anguillarum* require additional studies to further elucidate mechanistic details.

CONCLUSION

We performed transcriptome analyses of gene expression in primary incubation *A. fangsiao* larvae within 24 h of *V. anguillarum* infection, and established a protein–protein interaction network. Twenty hub DEGs enriched in multiple KEGG signaling pathways or with multiple protein–protein interaction relationships were identified. In our research, protein–protein interaction networks were first used to explore differences on *A. fangsiao* larval immunity. Our results provide valuable genetic resources for understanding the immunity of invertebrate larvae. Meanwhile, the data serve as a foundation for additional research into immune processes in invertebrates.

DATA AVAILABILITY STATEMENT

The original contributions presented in the study are publicly available in NCBI using accession numbers SRR15204591 – SRR15204602 at the following link: https://www.ncbi.nlm.nih.gov/Traces/study/?acc=SAMN20309867&o=acc_s%3Aa.

ETHICS STATEMENT

This research was conducted in accordance with the protocols of the Institutional Animal Care and Use Committee of the Ludong University (protocol number LDU-IRB20210308NXY) and the China Government Principles for the Utilization and Care of Invertebrate Animals Used in Testing, Research, and Training (State Science and Technology Commission of the People's Republic of China for No. 2, October 31, 1988. http://www.gov.cn/gongbao/content/2011/content_1860757.htm).

AUTHOR CONTRIBUTIONS

ZL and JY designed and supervised the study. XB, YL, JZ, XC, XX, and BL prepared the samples. XB, YL, YF, GS, WW, and XL analyzed all sequencing data. XB and ZL wrote the manuscript. All authors have read and approved the final manuscript.

FUNDING

This research was supported by China Agriculture Research System of MOF and MARA, the Natural Science Foundation of Shandong Province (No. ZR2019BC052), the National Natural Science Foundation of China (No. 42006077), and the "Entrepreneurship and Innovation Talents" programme of Jiangsu Province of China.

SUPPLEMENTARY MATERIAL

The Supplementary Material for this article can be found online at: https://www.frontiersin.org/articles/10.3389/fmars.2021.731517/full#supplementary-material

REFERENCES

Aragona, F., D'Urso, L., and Marcolongo, R. (1998). Immunologic Aspects of Bovine Injectable Collagen in Humans. *Eur. Urol.* 33, 129–133. doi: 10.1159/000019544

Bao, P., Sun, X., Liu, Q., Zhang, Y., and Liu, X. (2019). Synergistic effect of a combined live Vibrio anguillarum and Edwardsiella piscicida vaccine in turbot. *Fish Shellfish Immunol.* 88, 84–90. doi: 10.1016/j.fsi.2019.02.014

Barcia, R., and Ramos-Martínez, J. I. (2011). Stress-based modulation of the immune response in molluscan hemocytes: a two-receptor model. *Invertebr. Survival J.* 8, 56–58.

Brezas, A., and Hardy, R. W. (2020). Improved performance of a rainbow trout selected strain is associated with protein digestion rates and synchronization of amino acid absorption. *Sci. Rep.* 10:4678.

Brondijk, T. H. C., Ruiter, T. D., Ballering, J., Wienk, H., Lebbink, R. J., Boelens, R., et al. (2010). Crystal structure and collagen-binding site of immune inhibitory receptor LAIR-1: unexpected implications for collagen binding by platelet receptor GPVI. *Blood* 115, 1364–1373. doi: 10.1182/blood-2009-10-246322

Bubici, C., Papa, S., Pham, C. G., Zazzeroni, F., and Franzoso, G. (2004). NF-κB and JNK: An Intricate Affair. *Cell Cycle* 3, 1524–1529. doi: 10.4161/cc.3.12.1321

Budelmann, B. U. (1994). Cephalopod sense organs, nerves and the brain: Adaptations for high performance and life style. *Mar. Behav. Physiol.* 25, 13–33. doi: 10.1080/10236249409378905

Bulfon, C., Prearo, M., Volpatti, D., Byadgi, O., Righetti, M., Maniaci, M. G., et al. (2020). Resistant and susceptible rainbow trout (Oncorhynchus mykiss) lines show distinctive immune response to Lactococcus garvieae. *Fish Shellfish Immunol.* 105, 457–468. doi: 10.1016/j.fsi.2020.06.040

Castellanos-Martínez, S., Arteta, D., Catarino, S., and Gestal, C. (2014). De Novo Transcriptome Sequencing of the Octopus vulgaris Hemocytes Using Illumina RNA-Seq Technology: Response to the Infection by the Gastrointestinal Parasite Aggregata octopiana. *PLoS One* 9:e107873. doi: 10.1371/journal.pone.0107873

Chae, W., and Bothwell, A. L. M. (2018). Canonical and Non-Canonical Wnt Signaling in Immune Cells. *Trends Immunol.* 39, 830–847. doi: 10.1016/j.it.2018.08.006

Cong, M., Song, L., Wang, L., Zhao, J., Qiu, L., Li, L., et al. (2008). The enhanced immune protection of Zhikong scallop Chlamys farreri on the secondary encounter with Listonella anguillarum. *Compar. Biochem. Physiol. Part B* 151, 191–196. doi: 10.1016/j.cbpb.2008.06.014

Croft, M. (2009). The role of TNF superfamily members in T-cell function and diseases. *Nat. Rev. Immunol.* 9, 271–285. doi: 10.1038/nri2526

Curtis, K. J., Kim, Y. S., Perdomo, J. M., Silk, D. B. A., and Whitehead, J. S. (1978). Protein digestion and absorption in the rat. *J. Physiol.* 274, 409–419.

Damian, S., Gable, A. L., David, L., Junge, A., Wyder, S., Huerta-Cepas, J., et al. (2018). STRING v11: protein-protein association networks with increased coverage, supporting functional discovery in genome-wide experimental datasets. *Nucleic Acids Res.* 47, D607–D613.

Darzi, L., Boshtam, M., Shariati, L., Kouhpayeh, S., Gheibi, A., Rahimmanesh, I., et al. (2017). The silencing effect of miR-30a on ITGA4 gene expression in vitro: an approach for gene therapy. *Res. Pharm. Sci.* 12, 456–464. doi: 10.4103/1735-5362.217426

Dieli-Crimi, R., Martínez-Gallo, M., Franco-Jarava, C., Antolin, M., Blasco, L., Paramonov, I., et al. (2018). Th1-skewed profile and excessive production of proinflammatory cytokines in a NFKB1-deficient patient with CVID and severe gastrointestinal manifestations. *Clin. Immunol.* 195, 49–58. doi: 10.1016/j.clim.2018.07.015

Ernst, J., and Bar-Joseph, Z. (2006). STEM: a tool for the analysis of short time series gene expression data. *BMC Bioinform.* 7:191.

Famili, F., Perez, L. G., Naber, B. A., Noordermeer, J. N., Fradkin, L. G., and Staal, F. J. (2016). The non-canonical Wnt receptor Ryk regulates hematopoietic stem cell repopulation in part by controlling proliferation and apoptosis. *Cell Death Dis.* 7:e2479. doi: 10.1038/cddis.2016.380

Ferreira, S. H., Lorenzetti, B. B., Cunha, F. Q., and Poole, S. (1993). Bradykinin release of TNF-α plays a key role in the development of inflammatory hyperalgesia. *Inflam. Res.* 38, 7–9.

George, P. D. C., Agoramoorthy, G., and Chakraborty, C. (2014). TNF/TNFR: drug target for autoimmune diseases and immune-mediated inflammatory diseases. *Front. Biosci.* 19:1028–1040. doi: 10.2741/4265

Ginger, K., Vera, C., Dineshram, R., Dennis, C., Adela, L., Yu, Z., et al. (2013). Larval and Post-Larval Stages of Pacific Oyster (Crassostrea gigas) Are Resistant to Elevated CO2. *PLoS One* 8:e64147. doi: 10.1371/journal.pone.0064147

Herman, R. A. (2020). Increasing allergy: are antibiotics the elephant in the room? *Allergy Asthma Clin. Immunol.* 16, 35–36.

Ho, X. D., Phung, P., Le, V. Q., Nguyen, V. H., Reimann, E., Prans, E., et al. (2017). Whole transcriptome analysis identifies differentially regulated networks between osteosarcoma and normal bone samples. *Exp. Biol. Med.* 242, 1802–1811. doi: 10.1177/1535370217736512

Hoel, K., Salonius, K., and Lillehaug, A. (1997). Vibrio antigens of polyvalent vaccines enhance the humoral immune response to Aeromonas salmonicida antigens in Atlantic salmon (Salmo salar L.) *Fish Shellfish Immunol.* 7, 71–80. doi: 10.1006/fsim.1996.0063

Hong, B. S., Ryu, H. S., Kim, N., Kim, J., Lee, S., Moon, H., et al. (2019). Tumor suppressor miRNA-204-5p regulates growth, metastasis, and immune microenvironment remodeling in breast cancer. *Cancer Res.* 79, 1520–1534.

Huang, W., Qiu, S., Tong, X., He, Y., Wang, Z., and Dong, Y. (2019). Activating transcription factor 4 is required for high glucose inhibits proliferation and differentiation of MC3T3-E1 cells. *J. Recept. Signal Transduct.* 39, 409–414.

Iehata, S., Inagaki, T., Okunishi, S., Nakano, M., Tanaka, R., and Maeda, H. (2009). Colonization and probiotic effects of lactic acid bacteria in the gut of the abalone Haliotis gigantea. *Fisheries Sci.* 75, 1285–1293. doi: 10.1007/s12562-009-0138-5

Jia, D., Augert, A., Kim, D., Eastwood, E., Wu, N., Kim, K., et al. (2018). Crebbp Loss Drives Small Cell Lung Cancer and Increases Sensitivity to HDAC Inhibition. *Cancer Dis.* 8, 1422–1437. doi: 10.1158/2159-8290.cd-18-0385

Jiang, Y., Ortega-Molina, A., Geng, H., Ying, H., Hatzi, K., Parsa, S., et al. (2016). CREBBP Inactivation Promotes the Development of HDAC3 Dependent Lymphomas. *Cancer Dis.* 7, 38–53. doi: 10.1158/2159-8290.cd-16-0975

Jürgensen, H. J., Putten, S. V., Nørregaard, K. S., Bugge, T. H., Engelholm, L. H., Behrendt, N., et al. (2020). Cellular uptake of collagens and implications for immune cell regulation in disease. *Cell. Mole. Life Sci.* 77, 3161–3176. doi: 10.1007/s00018-020-03481-3

Kaplan, M. B., Mooney, T. A., McCorkle, D. C., and Cohen, A. L. (2013). Adverse Effects of Ocean Acidification on Early Development of Squid (Doryteuthis pealeii) . *PLoS One* 8:e63714. doi: 10.1371/journal.pone.0063714

Kresina, T. F., Rosner, I. A., Goldberg, V. M., and Moskowitz, R. W. (1984). Immunoglobulin G-induced experimental chronic immune synovitis: Cell-mediated immunity to native interstitial collagen molecules and their constituent polypeptide chains. *Cell. Immunol.* 87, 504–516. doi: 10.1016/0008-8749(84)90019-4

Kuppevelt, T. H. V., Veerkamp, J. H., and Timmermans, J. A. H. (1995). Immunoquantification of type I, III, IV and V collagen in small samples of human lung parenchyma. *Internat. J. Biochem. Cell Biol.* 27, 775–782. doi: 10.1016/1357-2725(95)00047-s

Lanna, A., Gomes, D. C. O., Muller-Durovic, B., McDonnell, T., Escors, D., Gilroy, D. W., et al. (2017). A sestrin-dependent Erk/Jnk/p38 MAPK activation complex inhibits immunity during aging. *Nat. Immunol.* 18, 354–363. doi: 10.1038/ni.3665

Lee, J., and Pilch, P. F. (1994). The insulin receptor: structure, function, and signaling. *Am. Physiol.* 266, 319–334.

Li, J., Gao, D., Wang, Q., Wang, J., and Wang, Q. (2015). Efficacy of Vibrio anguillarum antigen administered by intraperitoneal injection route in Japanese flounder, Paralichthys olivaceus (Temminck et Schlegel) *Aquacult. Res.* 36, 1104–1111. doi: 10.1111/j.1365-2109.2005.01327.x

Li, K., Qiu, H., Yan, J., Shen, X., Wei, X., Duan, M., et al. (2021). The involvement of TNF-α and TNF-β as proinflammatory cytokines in lymphocyte-mediated adaptive immunity of Nile tilapia by initiating apoptosis. *Dev. Compar. Immunol.* 115:103884. doi: 10.1016/j.dci.2020.103884

Li, Z., Fan, T., Liu, X., Liu, X., Wang, W., Wang, Q., et al. (2019). Characterization and Functional Study on Octopus ocellatus Interleukin-17. *J. Ocean Univ. China* 18, 1443–1450. doi: 10.1007/s11802-019-4116-y

Li, Z., Liu, X., Liu, J., Zhang, K., Yu, H., He, Y., et al. (2017). Transcriptome profiling based on protein–protein interaction networks provides a core set of genes for understanding blood immune response mechanisms against Edwardsiella tarda infection in Japanese flounder (Paralichthys olivaceus) . *Dev. Compar. Immunol.* 78, 100–113. doi: 10.1016/j.dci.2017.09.013

Lougaris, V., Patrizi, O., Baronio, M., Tabellini, G., Tampella, G., Damiati, E., et al. (2017). NFKB1 regulates human NK cell maturation and effector functions. *Clin. Immunol.* 175, 99–108. doi: 10.1016/j.clim.2016.11.012

Love, M. I., Huber, W., and Anders, S. (2014). Moderated estimation of fold change and dispersion for RNA-seq data with DESeq2. *Genome Biol* 15:550.

Lowe, S. W., and Lin, A. W. (2000). Apoptosis in cancer. *Carcinogenesis* 21, 485–495.

Makino, H., Shikata, K., Wieslander, J., Wada, J., Kashihara, N., Yoshioka, K., et al. (2010). Localization of Fibril/Microfibril and Basement Membrane Collagens in Diabetic Glomerulosclerosis in Type 2 Diabetes. *Diabetic Med.* 11, 304–311. doi: 10.1111/j.1464-5491.1994.tb00276.x

Matozzo, V. (2016). Aspects of eco-immunology in molluscs. *Invertebr. Surv. J.* 13, 116–121.

Naskar, D., Maiti, G., Chakraborty, A., Roy, A., Chattopadhyay, D., and Sen, M. (2014). Wnt5a-Rac1-NF-kB homeostatic circuitry sustains innate immune functions in macrophages. *J. Immunol.* 192, 4386–4397. doi: 10.4049/jimmunol.1302817

Nie, L., Zhou, Q., Qiao, Y., and Chen, J. (2017). Interplay between the gut microbiota and immune responses of ayu (Plecoglossus altivelis) during Vibrio anguillarum infection. *Fish Shellfish Immunol.* 68, 479–487. doi: 10.1016/j.fsi.2017.07.054

Nikola, S., Taeg, O. G., Hyung-Hwan, K., Beaulieu, L. M., Falet, H., Kaminski, K., et al. (2017). Decreased Thromboembolic Stroke but not Atherosclerosis or Vascular Remodeling in Mice with ROCK2-deficient Platelets. *Cardiovas. Res.* 2017, 1307–1317. doi: 10.1093/cvr/cvx071

Pai, S. G., Carneiro, B. A., Mota, J. M., Costa, R., Leite, C. A., Barroso-Sousa, R., et al. (2017). Wnt/beta-catenin pathway: modulating anticancer immune response. *J. Hematol. Oncol.* 10, 101–112.

Palanki, M. S., Erdman, P. E., Gayo-Fung, L. M., Shevlin, G. I., Sullivan, R. W., Suto, M. J., et al. (2000). Inhibitors of NF-kB and AP-1 gene expression: SAR studies on the pyrimidine portion of 2-Chloro-4-trifluoromethylpyrimidine-5-[N-(3′,5′-bis(trifluoromethyl)phenyl)carboxamide]. *J. Med. Chem.* 43, 3995–4004. doi: 10.1021/jm0001626

Pomorska-Mól, M., and Pejsak, Z. (2012). Effects of antibiotics on acquired immunity in vivo – Current state of knowledge. *Polish J. Vet. Aciences* 15, 583–588. doi: 10.2478/v10181-012-0089-0

Puigvert, J. C., Stechow, L. V., Siddappa, R., Pines, A., Bahjat, M., Haazen, L., et al. (2013). Systems biology approach identifies the kinase Csnk1a1 as a regulator of the DNA damage response in embryonic stem cells. *Sci. Signal.* 6:ra5.

Rowley, A. F., and Powell, A. (2007). Invertebrate immune systems specific, quasi-specific, or nonspecific? *J. Immunol.* 179, 7209–7214. doi: 10.4049/jimmunol.179.11.7209

Ruan, Y., Ogana, H., Gang, E., Kim, H. N., and Kim, Y. M. (2021). Wnt Signaling in the Tumor Microenvironment. *Adv. Exp. Med. Biol.* 1270, 107–121. doi: 10.1007/978-3-030-47189-7_7

Salazar, K. A., Joffe, N. R., Dinguirard, N., Houde, P., and Castillo, M. G. (2015). Transcriptome Analysis of the White Body of the Squid Euprymna tasmanica with Emphasis on Immune and Hematopoietic Gene Discovery. *PLoS One* 10:e0119949. doi: 10.1371/journal.pone.0119949

Schepis, A., Sepich, D., and Nelson, W. J. (2012). αE-catenin regulates cell-cell adhesion and membrane blebbing during zebrafish epiboly. *Dev.* 139, 537–546. doi: 10.1242/dev.073932

Schultz, J. H., and Adema, C. M. (2017). Comparative immunogenomics of molluscs. *Dev. Compar. Immunol.* 75, 3–15. doi: 10.1016/j.dci.2017.03.013

Sethi, G., Ahn, K. S., Xia, D., Kurie, J. M., and Aggarwal, B. B. (2007). Targeted Deletion of MKK4 Gene Potentiates TNF-Induced Apoptosis through the Down-Regulation of NF-κB Activation and NF-κB-Regulated Antiapoptotic Gene Products. *J. Immunol.* 179, 1926–1933. doi: 10.4049/jimmunol.179.3.1926

Shiseki, M., Ishii, M., Miyazaki, M., Osanai, S., Wang, Y., Yoshinaga, K., et al. (2019). Reduced PLCG1 expression is associated with inferior survival for myelodysplastic syndromes. *Cancer Med.* 9, 460–468. doi: 10.1002/cam4.2717

Silva, T. M., Melo, E. S., Lopes, A. C. S., Veras, D. L., Duarte, C. R., Alves, L. C., et al. (2013). Characterization of the bacterial microbiota of Biomphalaria glabrata (Say, 1818) (Mollusca: Gastropoda) from Brazil. *Lett. Appl. Microbiol.* 57, 19–25. doi: 10.1111/lam.12068

Sokolova, I. M. (2009). Apoptosis in molluscan immune defense. *Invertebr. Surv. J.* 6, 49–58.

Staal, F. J. T., Luis, T. C., and Tiemessen, M. M. (2008). WNT signalling in the immune system: WNT is spreading its wings. *Nat. Rev. Immunol.* 8, 581–593. doi: 10.1038/nri2360

Stevens, D. L. (1996). Immune modulatory effects of antibiotics. *Curr. Opin. Infect. Dis.* 9, 165–169. doi: 10.1097/00001432-199606000-00007

Sun, S. (2017). The non-canonical NF-κB pathway in immunity and inflammation. *Nat. Rev. Immunol.* 17, 545–558. doi: 10.1038/nri.2017.52

Suzuki, T., Ichii, O., Nakamura, T., Horino, T., Elewa, Y. H. A., and Kon, Y. (2020). Immune-associated renal disease found in caspase 3-deficient mice. *Cell Tissue Res.* 379, 323–335. doi: 10.1007/s00441-019-03084-w

Takai, K. K., Hattori, S., and Irie, S. (2001). Type V collagen distribution in liver is reconstructed in coculture system of hepatocytes and stellate cells; the possible functions of type V collagen in liver under normal and pathological conditions. *Cell Struct. Funct.* 26, 289–302. doi: 10.1247/csf.26.289

Thurnher, M., Gruenbacher, G., and Nussbaumer, O. (2013). Regulation of mevalonate metabolism in cancer and immune cells. *Biochim. et Biophys. Acta* 1831, 1009–1015. doi: 10.1016/j.bbalip.2013.03.003

Vázquez, J. A., Docasal, S. F., Mirón, J., González, M. P., and Murado, M. A. (2006). Proteases production by two Vibrio species on residuals marine media. *J. Industr. Microbiol. Biotechnol.* 33, 661–668.

Venturutti, L., Teater, M., Zhai, A., Chadburn, A., Babiker, L., Kim, D., et al. (2020). TBL1XR1 Mutations Drive Extranodal Lymphoma by Inducing a Pro-tumorigenic Memory Fate. *Cell* 182, 1–20.

Vielhauer, V., and Mayadas, T. N. (2007). Functions of TNF and its receptors in renal disease: distinct roles in inflammatory tissue injury and immune regulation. *Semin. Nephrol.* 27, 286–308.

Wang, L., Qiu, L., Zhou, Z., and Song, L. (2013). Research progress on the mollusc immunity in China. *Dev. Compar. Immunol.* 39, 2–10. doi: 10.1016/j.dci.2012.06.014

Wang, L., Wang, W., Yang, C., Sun, J., and Song, L. (2019). The immune recognition mechanisms in mollucs. *Fish Shellfish Immunol.* 91, 461–462. doi: 10.1016/j.fsi.2019.04.263

Wang, X., Yue, P., Kim, Y. A., Fu, H., Khuri, F. R., and Sun, S. (2008). Enhancing Mammalian Target of Rapamycin (mTOR)–Targeted Cancer Therapy by Preventing mTOR/Raptor Inhibition-Initiated, mTOR/Rictor Independent Akt Activation. *Cancer Res.* 68, 7409–7418. doi: 10.1158/0008-5472.can-08-1522

Wei, X., Xu, J., Yang, J., Liu, X., Zhang, R., Wang, W., et al. (2015). Involvement of a Serpin serine protease inhibitor (OoSerpin) from mollusc Octopus ocellatus in antibacterial response. *Fish Shellfish Immunol.* 42, 79–87.

Wei, X., Zhao, T., Ai, K., Li, H., Jiang, X., Li, C., et al. (2018). Role of scavenger receptor from Octopus ocellatus as a co-receptor of Toll-like receptor in initiation of TLR-NF-kB signaling during anti-bacterial response. *Dev. Compar. Immunol.* 84, 14–27. doi: 10.1016/j.dci.2018.01.023

Yang, J. H., Bhargava, P., McCloskey, D., Mao, N., Palsson, B. O., Collins, J. J., et al. (2017). Antibiotic-Induced Changes to the Host Metabolic Environment Inhibit Drug Efficacy and Alter Immune Function. *Cell Host Microbe* 22, 757–765. doi: 10.1016/j.chom.2017.10.020

Yi, L., Zhou, L., Luo, J., and Yang, Q. (2021). Circ-PTK2 promotes the proliferation and suppressed the apoptosis of acute myeloid leukemia cells through targeting miR-330-5p/FOXM1 axis. *Blood Cells Mole. Dis.* 86:102506. doi: 10.1016/j.bcmd.2020.102506

Yu, B., Chang, J., Liu, Y., Li, J., Kevork, K., Al-Hezaimi, K., et al. (2014). Wnt4 signaling prevents skeletal aging and inflammation by inhibiting nuclear factor-κB. *Nat. Med.* 20, 1009–1017. doi: 10.1038/nm.3586

Zhang, J., Vlasevska, S., Wells, V. A., Nataraj, S., Holmes, A. B., Duval, R., et al. (2017). The CREBBP Acetyltransferase Is a Haploinsufficient Tumor Suppressor in B-cell Lymphoma. *Cancer Dis.* 7, 322–337. doi: 10.1158/2159-8290.cd-16-1417

Zhang, Q., Lu, Y., Zheng, H., Liu, H., and Li, S. (2016). Differential immune response of vitellogenin gene to Vibrio anguillarum in noble scallop Chlamys nobilis and its correlation with total carotenoid content. *Fish Shellfish Immunol.* 50, 11–15. doi: 10.1016/j.fsi.2016.01.001

Zhang, X., Shi, J., Sun, Y., Habib, Y. J., Yang, H., Zhang, Z., et al. (2018). Integrative transcriptome analysis and discovery of genes involving in immune response of hypoxia/thermal challenges in the small abalone Haliotis diversicolor. *Fish Shellfish Immunol.* 84, 609–624. doi: 10.1016/j.fsi.2018.10.044

Zhao, X., Wang, Q., Jiao, Y., Huang, R., Deng, Y., Wang, H., et al. (2012). Identification of Genes Potentially Related to Biomineralization and Immunity by Transcriptome Analysis of Pearl Sac in Pearl Oyster Pinctada martensii. *Mar. Biotechnol.* 14, 730–739. doi: 10.1007/s10126-012-9438-3

Zhou, L., Wang, X., Liu, Q., Wang, Q., Zhao, Y., and Zhang, Y. (2010). A novel multivalent vaccine based on secretary antigen-delivery induces protective immunity against Vibrio anguillarum and Aeromonas hydrophila. *J. Biotechnol.* 146, 25–30. doi: 10.1016/j.jbiotec.2009.12.010

Conflict of Interest: WW was employed by the company Jiangsu Baoyuan Biotechnology Co., Ltd. BL was employed by the company Yantai Haiyu Marine Science and Technology Co., Ltd.

The remaining authors declare that the research was conducted in the absence of any commercial or financial relationships that could be construed as a potential conflict of interest.

Publisher's Note: All claims expressed in this article are solely those of the authors and do not necessarily represent those of their affiliated organizations, or those of the publisher, the editors and the reviewers. Any product that may be evaluated in this article, or claim that may be made by its manufacturer, is not guaranteed or endorsed by the publisher.

frontiers in Marine Science

ORIGINAL RESEARCH
published: 14 October 2021
doi: 10.3389/fmars.2021.744212

The Discovery of Circadian Rhythm of Feeding Time on Digestive Enzymes Activity and Their Gene Expression in *Sinonovacula constricta* Within a Light/Dark Cycle

Yanzi Liu[1,2], Hanhan Yao[2], Tingting Zhou[3], Zhihua Lin[2,3] and Yinghui Dong[2]**

[1] College of Fisheries and Life Science, Shanghai Ocean University, Shanghai, China, [2] Zhejiang Key Laboratory of Aquatic Germplasm Resources, College of Biological and Environmental Sciences, Zhejiang Wanli University, Ningbo, China, [3] Ninghai Institute of Mariculture Breeding and Seed Industry, Zhejiang Wanli University, Ningbo, China

The circadian rhythm has a great impact on the growth, metabolism and development of animals, but little is known about the circadian rhythm of marine bivalves. Understanding of the feeding rhythm is of great significance to increase the yield of razor clam *Sinonovacula constricta*, an economically important bivalve mollusk. The aim of this experiment was to study the effects of circadian rhythm of feeding time on digestive enzymes activities and their gene expression in *S. constricta* within a light (ZT8-ZT20)/dark (ZT20-ZT8) cycle. The present results showed that circadian rhythm of feeding rate (FR) was highly associated with digestive enzyme activities and relative expression of their genes. The highest values of FR were basically observed in the night from ZT0-ZT2 and ZT6-ZT8, which were significantly higher than those values in the daytime from ZT12-ZT14 and ZT18-ZT20 ($P < 0.05$). The digestive enzymes activities displayed the highest values at ZT2 and ZT8, and the lowest at ZT14 and ZT20. Among them, cellulase and pepsin were found to have significantly different activities ($P < 0.05$), rather than amylase and lipase. Notably, the relative expression of digestive enzyme genes shared the similar pattern with the activities of digestive enzymes. The highest values of relative gene expression of *amylase* (*AMY*), *lipase* (*LIP*), *cellulase* (*CEL*), and *pepsin* (*PEP*) were found at ZT2 and ZT8 in the night, while the lowest values were found at ZT14 during the day. It is therefore suggested that the biological clock may regulate the process from feeding to digestion. Furthermore, it might be better to feed at night to reduce cultivating cost and increase economic benefits in the farming industry of *S. constricta*.

Keywords: *Sinonovacula constricta*, circadian rhythm, feeding rate, digestive enzyme, gene expression

OPEN ACCESS

Edited by:
Weiwei You,
Xiamen University, China

Reviewed by:
Xiaolong Gao,
Xiamen University, China
Kwang-Sik Choi,
Jeju National University, South Korea

***Correspondence:**
Hanhan Yao
yaohanhan1020@126.com
Yinghui Dong
dongyinghui118@126.com

Specialty section:
This article was submitted to Marine Fisheries, Aquaculture and Living Resources, a section of the journal Frontiers in Marine Science

Received: *20 July 2021*
Accepted: *20 September 2021*
Published: *14 October 2021*

Citation:
Liu Y, Yao H, Zhou T, Lin Z and Dong Y (2021) The Discovery of Circadian Rhythm of Feeding Time on Digestive Enzymes Activity and Their Gene Expression in Sinonovacula constricta Within a Light/Dark Cycle. Front. Mar. Sci. 8:744212. doi: 10.3389/fmars.2021.744212

INTRODUCTION

The circadian rhythm is a 24-h cyclical change in environmental factors such as light and temperature caused by the rotation of the earth, which has an important impact on the physiology and behavior of organisms (Fustin et al., 2013). The circadian rhythms inside and outside the organism are closely related to the rhythm changes of the external environment. When the rhythm

of environmental factors is changed, the nervous system and endocrine system of animals will change accordingly, leading to changes in their behaviors, lifestyles, and physiological conditions (Wu et al., 2002).

The feeding rhythm of animals affected by cyclical change factors (e.g., light and tide) is essential for the establishment of scientific feeding mode (Mistlberger, 1994; Sanchezvazquez, 1995; Wang, 2004; Connor and Gracey, 2011). Many activities such as feeding, oxygen consumption and digestion have been used to study rhythmic behavior in European oyster *Ostrea edulis*, New Zealand cockle *Austravenus stutchburyi*, clam *Saxidomus purpuratus*, etc (Morton, 1971; Williams and Pilditch, 1997; Kim et al., 2003). Furthermore, the absorption of food after feeding is closely related to the process of digestion and metabolism. Meanwhile, digestive enzyme activity is an important indicator of digestion and absorption capacity, which determines the ability to digest and absorb nutrients for food (Bobrowska et al., 2011; Wu et al., 2013). The relationship between the activity of digestive enzymes and the feeding pattern has been studied in cockle *Cerastoderma edule* (Ibarrola et al., 1998), clam *Ruditapes decussatus* and *Venerupis pullastra* (Albentosa and Moyano, 2008), and scallop *Patinopecten yessoensis* (Li et al., 2010). In addition, some previous studies have found that the activities of digestive enzymes such as pepsin, amylase, cellulase, and lipase are served as indicators that can measure the digestion and absorption of protein and carbohydrates in bivalves (Supannapong et al., 2008; Tizon et al., 2013). For animals, digestion is a complex process that requires signal transduction regulation inside and outside the body. The enzyme-related protein precursor mRNA is regulated to stimulate transcription and synthesis after ingestion, so that the enzyme precursors are released to promote digestion, absorption, and growth (Yúfera et al., 2018). For example, *amylase* (*AMY*) gene is proved to be involved in the growth of razor clam *Sinonovacula constricta* and Pacific oyster *Crassostrea gigas*, while *cellulase* (*CEL*) can improve the digestibility of food and synthesize glucose to provide energy for the body (Meenu et al., 2014; Thongsaiklaing et al., 2014; Rong et al., 2015; Liu et al., 2017). Moreover, *lipase* (*LIP*) gene expression is correlated with feeding status, whereas *pepsin* (*PEP*) has important digestive functions in both vertebrates and invertebrates (Liang et al., 2003). The presence of various forms of pepsin precursors such as *pepsin A* and *pepsin C* may be related to food or feeding habits (Carginale et al., 2004).

S. constricta is an economically and ecologically important benthic marine bivalve, which naturally distributes along the western Pacific coasts of China, Japan, and South Korea (Morton, 2010). It has been widely cultivated in the intertidal zone and estuary waters with more than 400 years of cultivating history in the Zhejiang and Fujian provinces, China (Shen et al., 2013). Due to relatively short production cycle and high productive efficiency, it has been become an important marine aquaculture species in China with 852,925 tons of production in 2018 (FAO, 2020). Food intake is one of the important conditions for increasing the yield of industrial aquaculture (Rønnestad et al., 2013). Good ingestion and efficient digestion of nutrients are necessary to meet the high demand of matter and energy, which are able to support the high-growth rate (Navarro-Guillén et al., 2018). In order to determine the optimal feeding time and increase the growth rate of *S. constricta*, we continuously measured feeding rate, digestive enzyme activity, and relative expression of digestive enzyme genes at different time points in the day and night. The present results will be beneficial for reducing farming cost and increasing farming benefits.

MATERIALS AND METHODS

Experimental Animals

S. constricta were obtained from Ningbo Ocean and Fishery Science and Technology Innovation Base (Ningbo, Zhejiang province). One-year-old adults (n = 60) with an average shell length of (5.9 ± 0.3) cm were collected to culture for a week in seawater within light and dark (L/D) cycles. The lights in the experimental environment were turned on, and shoot them directly into the tank from ZT (Zeitgeber Time) 8-ZT20 to simulate the daytime, and from ZT20-ZT8 to cover the tank with a black cloth to simulate the night. All clams were not fed before the start of the experiment. During the formal experiment, the clams were fed with the live microalgae of *Chaetoceros muelleri* with the concentration of (2.5 ± 0.2) × 10^8 cell/L. The water temperature and salinity were maintained at (25.0 ± 2) °C and (20 ± 1) ppt, respectively. All experimental procedures were approved by the Institutional Animal Care and Use Committee of Zhejiang Wanli University, China.

Feeding Rate Experiment

The clams in similar size were selected and placed into 12 tanks, having five individuals in each tank. The time setting was to divide 24 h into four time periods, including ZT0-ZT2, ZT6-ZT8, ZT12-ZT14, and ZT18-ZT20. For each time point, it corresponded to three parallel tanks. Before the experiment, a preliminary experiment was conducted to determine the concentration of microalgae *C. muelleri*. No clam was placed in the control tank, and the same concentration of algae for tank was used to calculate the loss rate of algae. During the experiment, the water was exchanged at each time point, and the water temperature was kept constant for 3 days.

Before and after each time point, water samples of the experimental groups and control groups were sampled to count the concentration of algae on a blood cell counter. The feeding rate (FR) was calculated according to the following formula:

$$\mathbf{FR} = \boldsymbol{V}(\mathbf{C_{td}}\text{-}\mathbf{C_{td}}\mathbf{S_d}\text{-}\mathbf{C_t})/(\boldsymbol{NT})\text{(Riisgård, 1991)}.$$

$\mathbf{C}_{td}$ and $\mathbf{C}_t$: the algae concentration in the control group and experimental group at the end of the experiment (cells/L), $\boldsymbol{T}$: the experimental time (h), $\boldsymbol{V}$: the volume of the experimental water (L), $\boldsymbol{N}$: the number of experimental clam, $\mathbf{S}_d$: the control bait variation coefficient.

Analysis of Digestive Enzyme Activities

A total of 240 clams with similar sizes were randomly distributed into three tanks (group A, group B, and group C). Samples were obtained at 6 h intervals (ZT2, ZT8, ZT14, and ZT20) after

feeding, having continuous sampling for 3 days. Four individuals were randomly selected from each group, and the visceral mass tissue was dissected and immediately frozen in liquid nitrogen, and stored at −80°C.

The enzyme extracts were prepared to measure the enzyme activities of α-amylase, lipase, cellulase, and pepsin. Each sample was weighed at 100 mg, which was mixed with 0.9 mL of normal saline for mechanically homogenization using an automatic sample rapid grinding machine[1]. The samples were centrifuged at 3,500 rpm for 10 min at 4°C. All samples were kept in ice in order to avoid enzymes denaturation or damage. Enzyme extracts were kept at −20°C until analysis within 24 h.

All enzymatic activity analysis was conducted by using the commercial kits from Nanjing Jiancheng Bioengineering Institute[2]. α-amylase activity as protein per mg of visceral mass reacted with the substrate at 37°C for 30 min to hydrolyze 10 mg amylon and recorded at $OD_{600\ nm}$. The unit of lipase activity was per g tissue protein reacted with methyl resorufin substrate at 37°C and recorded at OD_{580nm}. The cellulase activity as tissue per g catalyzed to 1 μg glucose per minute and recorded at OD_{550nm}. One unit of pepsin activity was defined as tissue protein per mg decomposed into 1 μg amino acid at 37°C per minute and recorded at OD_{660nm}. The protein concentration extracted from the tissue uses the BSA kit[3]. The enzyme activity of α-amylase, lipase, cellulase, and pepsin were all measured according to the standard protocol.

RNA Extraction and Real-Time Quantitative Expression Analysis of Digestive Enzyme Genes

The total RNA was extracted from the visceral mass by using the Trizol reagent following the manufacturer's instructions[4]. The RNA quality was tested by electrophoresis, and the concentration was measured with a nucleic acid detector NanoVue Plus. Total RNA was reverse transcribed to cDNA by RT-PCR kits[5].

The whole predicted coding sequence (CDS) sequences of *AMP*, *LPS*, *CEL*, and *PEP* were obtained from the genome of *S. constricta* (WSYO00000000.1). The primer sequences were designed following the CDS sequences and listed in **Table 1**. The mRNA expression levels per each gene were assessed by qRT-PCR using ChamQ SYBR qPCR Master Mix[6]. The 20 μL reaction volume for amplification contained 10 μL of SYBR qPCR Master Mix, 1 μL of each primer (10 μM), and 8 μL of cDNA sample (10 ng/μL). Initial denaturation was conducted at 95°C for 10 s, followed by 40 cycles at 95°C for 5 s and at 60°C for 30 s. 18S rRNA gene was selected as the housekeeping gene, and the expression levels of *AMP*, *LPS*, *CEL*, and *PEP* gene were normalized to that of 18S rRNA by using the $2^{-\Delta\Delta CT}$ method.

[1]https://www.roche.com/

[2]http://www.njjcbio.com/

[3]https://www.thermofisher.cn/

[4]https://www.sangon.com/

[5]https://www.takarabiomed.com.cn/

[6]http://vazyme.bioon.com.cn/

TABLE 1 | Primer sequences used for qRT-PCR analysis.

Primers	Sequence (5′-3′)	Length (bp)
AMY-F	ACCATCGTCCACCTGTTC	201
AMY-R	CAACAAACTCCGCCTCC	
LPS-F	AGAGTCGGCAAGTTCGTG	223
LPS-R	ATGTCTGCCCAACCTGG	
CEL-F	TGGAGGTGTGGAAGGGA	207
CEL-R	TGTGTCTGCGAAGTGCTGGC	
PEP-F	ACCCCTCCTCAGCCATT	139
PEP-R	GCCTTGTAGGTGGACGAT	
18S-F	TCGGTTCTATTGCGTTGGTTTT	180
18S-R	CAGTTGGCATCGTTTATGGTCA	

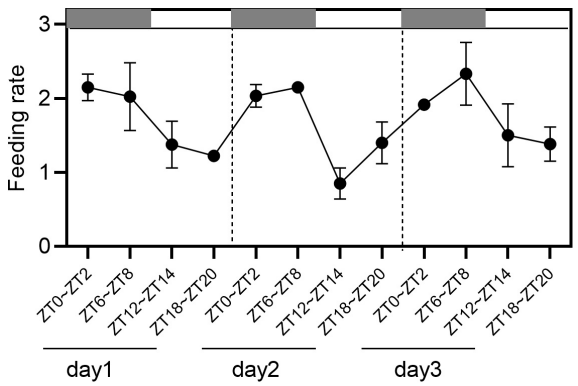

FIGURE 1 | The results of feeding rate in 12 h light/12 h dark (L/D) cycles during 3 days. Values are represented as means ± SD (n = 3). The gray grid represents the dark time point.

Statistical Analysis

Data were presented as the means ± standard deviation, and one-way ANOVA analysis were used to compare the difference in food intake ratio, digestive enzyme activity and digestive enzyme gene expression at different time points in the day and night. GraphPad prism 8 software was used to statistically analysis. $P < 0.05$ was considered statistically as the significant difference, and $P < 0.01$ as the extremely significant difference.

RESULTS

Analysis of Diurnal Difference of Feeding Rate

Under the condition of 12 h light/12 h dark (L/D) cycles, the food intake rates at ZT0-ZT2 and ZT6-ZT8 during the night were higher than those at ZT12-ZT14 and ZT18-ZT20 during the day, indicating an obvious circadian rhythm of feeding (**Figure 1**). For the first day at ZT0-ZT2 and ZT18-ZT20, the food intake rates were 2.15×10^8 (cells/h) and 1.225×10^8 (cells/h). For the second day at ZT6-ZT8 and ZT12-ZT14, the food intake rates were 2.03×10^8 (cells/h) and 0.85×10^8 (cells/h). For the third day at ZT6-ZT8 and ZT18-ZT20, the food intake rates were 2.33×10^8 (cells/h) and 1.38×10^8 (cells/h). In total, the highest and lowest

TABLE 2 | Results of one-way ANOVA analysis of feeding rate under the diurnal cycle.

Feeding rate	1 days				2 days				3 days			
	MS	*df*	*F*	*P*	MS	*df*	*F*	*P*	MS	*df*	*F*	*P*
Between ZT	0.639	3	13.50	0.0017**	1.093	3	49.47	<0.0001**	0.561	3	6.795	0.0137*
Within ZT	0.0473	8			0.221	8			0.083	8		

*Asterisks indicate significant differences: *P < 0.05 and **P < 0.01.*

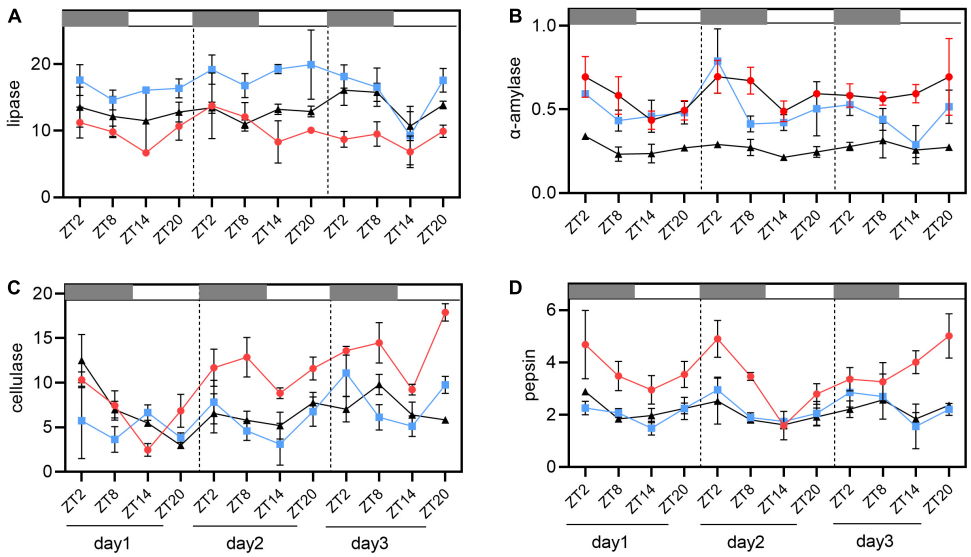

FIGURE 2 | Analysis of four digestive enzyme activities in 12 h light/12 h dark (L/D) cycles during 3 days. **(A)** Lipase activity diagram. **(B)** α-amylase activity diagram. **(C)** Cellulase activity diagram. **(D)** Pepsin activity diagram. Values are represented as means ± SD (n = 4). Group A, B, C are three parallel tanks with the same cultivating conditions, and the red circle represents Group A, the blue square represents Group B and black triangle represents Group C. The gray grid represents the dark time point.

ingestion points were significantly different in the experimental period by one-way ANOVA analysis ($P < 0.05$), with 1.69–2.39 times between them (**Table 2**).

The Circadian Rhythm of Four Digestive Enzyme Activities

The results of α-amylase, lipase, cellulase, and pepsin activities (expressed as U mg^{-1}) were shown in **Figure 2** and **Table 3**. These four enzymes have a diurnal variation trend in group A, B, C. The activities of lipase reached the highest value at ZT20 and ZT2, followed by low levels of activity between ZT8 and ZT14. Among all these four enzymes, the activities of lipase were significantly lower than those of other enzymes ($P < 0.05$). However, only part of the results detected significant differences between the highest and lowest points of lipase activities (**Table 3** and **Figure 2A**). For α-amylase, the maximum values of enzyme activities were generally detected at ZT20 and ZT2, while the minimum values were found at ZT8 and ZT14. Nevertheless, α-amylase activities during the whole day and night cycle were statistically different between time periods, but it was only partially present (**Table 3** and **Figure 2B**). As indicated, cellulase and pepsin had the highest activities, displaying the same changing trend ($P < 0.05$, **Table 3** and **Figures 2C,D**). Basically, the enzyme activities were found to be higher in the dark (ZT20-ZT8) than those in the light (ZT8-ZT20).

Relative Expression of Four Digestive Enzyme Genes

The results of relative expression of digestive enzyme genes were shown in **Figure 3**. The relative expression of *AMY*, *LPS*, *CEL*, and *PEP* had a regular trend from high to low levels from ZT2 to ZT20 of 3 days, with no significant change in diurnal fluctuations. The relative expression of *LPS* had the highest expression level at ZT2 and ZT8, the lowest expression at ZT14 (**Figure 3A**). Meanwhile, *AMY* was detected to be the highest at ZT2 and the lowest at ZT14 (**Figure 3B**). Similarly, the gene expression of *CEL* was found to be the highest at ZT2 and the lowest at ZT14 (**Figure 3C**). Consistently, *PEP* showed the highest expression level at ZT2 and the lowest expression at ZT14 and ZT20 (**Figure 3D**).

DISCUSSION

For most organisms, circadian rhythm is affected by endogenous factors and external environmental factors

TABLE 3 | Results of one-way ANOVA analysis of digestive enzyme activity under the diurnal cycle.

Digestive enzyme	Group	1 days			2 days			3 days		
		MS	*F*	*P*	MS	*F*	*P*	MS	*F*	*P*
α-amylase bZT/wZT	A	0.0362/0.0081	4.448	0.0406*	0.0295/0.0052	5.63	0.0226*	0.0101/0.0145	0.7008	0.5776
	B	0.0147/0.0040	3.72	0.061	0.0936/0.0138	6.786	0.0137*	0.0362/0.005	7.252	0.0114*
	C	0.0074/0.0013	5.671	0.022*	0.0033/0.0093	3.543	0.0677	0.0017/0.0032	0.5499	0.6622
Lipase bZT/wZT	A	12.32/1.308	9.417	0.005**	16.66/5.527	3.015	0.0942	5.648/1.961	2.88	0.1029
	B	4.54/2.417	1.878	0.2116	5.692/5.07	1.123	0.396	51.1/5.248	9.738	0.0048**
	C	2.339/6.736	0.347	0.792	3.217/0.3558	9.042	0.006**	18.51/1.838	10.07	0.0043**
Cellulase bZT/wZT	A	31.74/1.791	17.72	0.0007**	8.832/3.394	2.602	0.1243	38.26/0.9671	39.56	<0.0001**
	B	5.283/2.831	1.866	0.2137	14.45/3.256	4.438	0.0408*	29.01/2.822	10.28	0.004**
	C	48.9/2.509	19.49	0.0005**	4.717/2.27	2.078	0.1816	9.341/0.928	1.07	0.0043**
Pepsin bZT/wZT	A	1.589/0.4292	3.701	0.0616	5.721/0.2232	25.63	0.0002**	1.953/0.2985	6.545	0.0151*
	B	0.3937/0.0769	5.122	0.0288*	0.8881/0.1158	7.673	0.0097**	1.181/0.2887	4.091	0.0493*
	C	0.6492/0.0234	27.74	0.0001**	0.4604/0.1137	4.049	0.0505	0.286/0.02271	12.59	0.0021**

*Asterisks indicate significant differences: *P < 0.05 and **P < 0.01.*
bZT/wZT stands for between ZT and within ZT. All the df values of bZT were three. All the df values of wZT were eight.

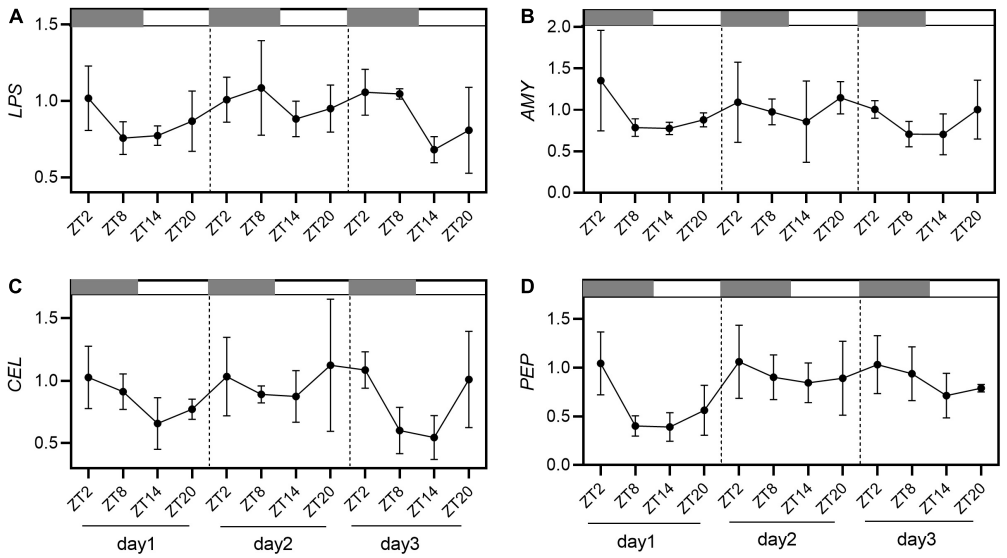

FIGURE 3 | Relative gene expression of *LPS* **(A)**, *AMY* **(B)**, *CEL* **(C)**, and *PEP* **(D)** in 12 h light/12 h dark (L/D) cycles during 3 days. Values are represented as means ± SD (n = 4). The gray grid represents the dark time point.

(Mata-Sotres et al., 2016). Under natural light conditions, the behavior of most animals is divided into two types: diurnal and nocturnal. Understanding and clarifying the circadian rhythm can provide a scientific basis for revealing accurately the laws and inner mechanisms of many life phenomena. Although the feeding rhythm is of great significance for establishing a scientific feeding mode to farmed animals, there are few studies on the feeding rhythm and their mechanisms in aquatic animals. In fish, as reported, the Gilthead sea bream *Sparus aurata* showed an feeding rhythm during the day under a light/dark condition (Mata-Sotres et al., 2015). In contrast, the Japanese prawn *Pen*aeus *japonicus* feeds at night under the same conditions (Reymond and Lagardère, 1990). In mollusks, many species showed similar feeding and metabolic rhythm. For example, Manila clam *Ruditapes philippinarum* exhibited a 24 h circadian rhythm of feeding rates, having a higher feeding rate at night than that in the day (Jiang et al., 2009). A study on circadian feeding activity and digestive physiology in the abalone *Haliotis discus hannai* found that the percentages of ingesting food were significantly higher at night than in the daytime, demonstrating their nocturnal characteristics (Gao et al., 2021). An obvious circadian rhythm in water filtration rate was also found in the scallop *Chlamys farreri*, which had a significantly higher water filtration rate at night than that in daytime (Du et al., 2012). In *S. constricta*, the obvious diurnal changes in food intake rates were proved by the energy budget study (Li et al., 2006). In the present study, we found that the feeding rate of razor clam in dark was significantly higher than that in light, speculating

that there may be a circadian rhythm of feeding, which is indirectly regulated by biological clock genes. Additionally, the highest feeding point of mollusks at night may be related to avoiding being preyed by predators. Moreover, some studies in aquatic animals have found that light is the most important external factor influencing the feeding activity and different modes of light conditions will reduce the intake of food (Li et al., 2010). Especially, for the nocturnal animals that forage at night, light inhibits their feeding behavior. However, the long-term evolutionary internal biological clock can regulate the life patterns of animals, which may control the time and amount of consumed food (Annie et al., 1999). These findings may thus help us optimize the feeding time and frequency in clam aquaculture.

The degree of digestion is derived from the intestinal transport factor and digestive enzyme activity that reflects the digestion and absorption capacities of intestinal tract (Mata-Sotres et al., 2015; Navarro-Guillén et al., 2015). Generally, there is a close relationship between the digestive enzyme activity and feeding behavior, which the increase of digestive enzyme activity is several hours earlier than the time of peak feeding, suggesting that the early enzyme secretion can optimize the percentages of digestion and absorption, and reduce the risk of predation due to shortened feeding time. For nocturnal animals, even under an unnatural light/dark cycle, the digestive enzyme activity is prone to be higher at night than in the daytime. In the current study, the light/dark cycle and feeding rate had a significant impact on four digestive enzyme activities in the visceral mass of *S. constricta*, including α-amylase, lipase, cellulase, and pepsin. The vitality of digestive enzymes after the increase of food intake in ZT2 and ZT8 at night is significantly higher than that in low food intake ZT14 and ZT20 in the daytime, demonstrating that food digestion has a circadian rhythm behavior. There is also the same finding that the production of digestive enzymes increased significantly after increasing food intake, like in *C. edule* (Ibarrola et al., 1998) and clam *R. philippinarum* (Houki and Tomohiko, 2020). However, relatively speaking, lipase activity is significantly lower than the other three. Numerous studies have shown that carnivorous animals have higher lipase content than omnivorous and herbivorous animals, and those with high lipase content are generally seen in animals with mature intestines, lipid hydrolysis mainly occurs in the pyloric caeca and/or proximal intestine (Caruso et al., 2009; Tengjaroenku et al., 2000). The razor clam, as a filter-feeding shellfish, has an incompletely differentiated intestine, which the ability to hydrolyze lipids is weak.

The expression of digestive enzyme genes is strongly correlated to their enzyme activities, which directly reflect the digestive physiology of aquatic animals. Existing research has shown that the increase of enzyme genes expression at night was the regulation of translation process and may be the anticipation of next food intake (José Antonio et al., 2016). A recent research on the feeding and digestion physiology of abalone *H. discus hannai* under the light/dark cycle found that digestive enzymes and feeding related genes were significantly higher at night than during the day with rhythmic 24 h oscillations (Gao et al., 2021). In this research, the mRNA levels of four key digestive enzyme genes (*AMY*, *LPS*, *CEL*, and *PEP*) by qRT-PCR during the light/dark cycles were basically consistent with the production of their enzymes. Furthermore, the genes expression showed a periodic pattern of high at night and low during the day for consecutive 3 days, indicating that circadian rhythm may be the internal mechanism that was regulated by circadian clock genes (Paredes et al., 2014; Qin et al., 2020). Then the circadian clock genes may regulate the expression of *AMY*, *LPS*, *CEL*, and *PEP*, thereby participating indirectly in the feeding and digestion activities of *S. constricta*. Although the similar trends of gene expression and activities of key digestive enzymes, and feeding rates in this experiment were discovered, deep understanding of their corresponding relationships still need a lot of in-depth and meticulous research.

CONCLUSION

The feeding rate, digestive enzyme activities and relative expression of their genes all had a circadian rhythm in *S. constricta*, which it can be basically determined that ZT0-ZT2 will reach the peak at night and ZT12-ZT14 will reach the lowest value during the day from feeding to digestion. Therefore, it can be speculated that razor clams have higher nighttime activities than during the day, suggesting that the feeding time in the industrial farming can be arranged at night to reduce cultivating costs and increase farming benefits.

DATA AVAILABILITY STATEMENT

The datasets presented in this study can be found in online repositories. The names of the repository/repositories and accession number(s) can be found in the article/**Supplementary Material**.

ETHICS STATEMENT

The adult hard clams *Sinonovacula constricta* at the age of 1 year were collected from the genetic breeding research center of Zhejiang Wanli University, China. All experimental procedures were approved by the Institutional Animal Care and Use Committee (IACUC) of Zhejiang Wanli University, China.

AUTHOR CONTRIBUTIONS

HY and YD conceived and designed the project. TZ collected the samples and contributed reagents. YL performed the experiments and data analysis, and wrote and revised the manuscript. All authors read and approved the final manuscript.

FUNDING

This work was supported by the National Natural Science Foundation of China (31902393), National Key Research

and Development Program of China (2018YFD0901405 and 2020YFD0900802), Zhejiang Major Program of Science and Technology (2021C02069-7), Ningbo Major Project of Science and Technology (2019B10005), and National Marine Genetic Resource Center Program.

SUPPLEMENTARY MATERIAL

The Supplementary Material for this article can be found online at: https://www.frontiersin.org/articles/10.3389/fmars.2021.744212/full#supplementary-material

REFERENCES

Albentosa, M., and Moyano, F. J. (2008). Influence of nutritional stress on digestive enzyme activities in juveniles of two marine clam species, *Ruditapes decussatus* and *Venerupis pullastra*. *J. Sea Res.* 59, 249–258. doi: 10.1016/j.seares.2008.02.004

Annie, M., Stephen, C. B., and Jean-Franois, H. (1999). Daily burrowing cycle and feeding activity of juvenile sea cucumbers *Holothuria scabra* in response to environmental factors. *J. Exp. Mar. Biol. Ecol.* 239, 125–156. doi: 10.1016/S0022-0981(99)00034-9

Bobrowska, B., Tokrz, A., Białek, S., and Seweryn, M. (2011). Effect of dietary supplementation on the prognostic value of urinary and serum 8-isoprostaglandin F2α in chemically-induced mammary carcinogenesis in the rat. *Lipids Health Dis.* 10:40. doi: 10.1186/1476-511X-10-40

Carginale, V., Trinchella, F., Capasso, C., Scudiero, R., Riggio, M., and Parisi, E. (2004). Adaptive evolution and functional divergence of pepsin gene family. *Gene* 333, 81–90. doi: 10.1016/j.gene.2004.02.011

Caruso, G., Denaro, M. G., and Genovese, L. (2009). Digestive enzymes in some teleost species of interest for mediterranean aquaculture. *Open Fish Sci. J.* 2, 74–86. doi: 10.2174/1874401X00902010074

Connor, K. M., and Gracey, A. Y. (2011). Circadian cycles are the dominant transcriptional rhythm in the intertidal mussel *Mytilus californianus*. *Proc. Natl. Acad. Sci. U.S.A.* 108, 16110–16115. doi: 10.1073/pnas.1111076108

Du, M. R., Fang, J. G., Mao, Y. Z., Zhang, J. H., Ge, C. Z., Jiang, Z. J., et al. (2012). Diurnal rhythm of filtration rate of Zhikong scallop *Chlamys farreri* veliger and spat. *Prog. Fish. Sci.* 33, 73–77.

FAO (2020). *Fishery and Aquaculture Statistics 2018.* Available online at: http://www.fao.org/fishery/statistics/yearbook/en (accessed September 1, 2021).

Fustin, J. M., Doi, M., Yamaguchi, Y., Hida, H., Nishimura, S., and Yoshida, M. (2013). RNA-methylation-dependent RNA processing controls the speed of the circadian clock. *Cell* 155, 793–806. doi: 10.1016/j.cell.2013.10.026

Gao, X. L., Pang, G. W., Luo, X., You, W. W., and Ke, C. H. (2021). Effects of light cycle on circadian feeding activity and digestive physiology in *Haliotis discus hannai*. *Aquaculture* 539:736642. doi: 10.1016/j.aquaculture.2021.736642

Houki, S., and Tomohiko, K. (2020). Feeding and digestion periodicity of Manila clam *Ruditapes philippinarum* in natural intertidal and subtidal zones estimated from the morphological condition of the crystalline style. *J. Molluscan Stud.* 86, 361–371.

Ibarrola, I., Larretxea, X., Iglesias, J. I. P., Urrutia, M. B., and Navarro, E. (1998). Seasonal variation of digestive enzyme activities in the digestive gland and the crystalline style of the common cockle *Cerastoderma edule*. *Comp. Biochem. Physiol.* 121, 25–34. doi: 10.1016/S1095-6433(98)10097-1

Jiang, S. L., Zhao, C. M., Wang, Y. H., Yin, H., Sun, Y., and Shi, X. Y. (2009). Effects of water temperature, shell length and the concentration of algae on the ingestion rate of *Ruditapes philippinarum*. *Prog. Fish. Sci.* 30, 78–83.

José Antonio, M. S., Francisco, J. M., and Gonzalo, M. R. (2016). Daily rhythms of digestive enzyme activity and gene expression in gilthead seabream (*Sparus aurata*) during ontogeny. *Comp. Biochem. Physiol. A Mol. Integr. Physiol.* 197, 43–51.

Kim, W. S., Huh, H. T., Je, J. G., and Han, K. N. (2003). Evidence of two-clock control of endogenous rhythm in the Washington clam, *Saxidomus purpuratus*. *Mar. Biol.* 142, 305–309. doi: 10.1007/s00227-002-0952-0

Li, B., Chen, B., Qi, Z. H., Jiang, Z., Zhang, J., and Fang, J. (2010). Relationship between differential retention of *Escherichia coli* and *Enterococcus faecalis* and variations in enzyme activity in the scallop *Patinopecten yessoensis*. *Mar. Pollut. Bull.* 60, 1600–1605. doi: 10.1016/j.marpolbul.2010.03.017

Li, D. X., Li, T. W., Su, X. R., Lin, Z. H., Chai, X. L., and Fang, J. (2006). Energy budgets of *Sinonovacula constricta*. *Fish. Sci.* 25, 401–404.

Liang, X. F., Bai, J. J., Lao, H. H., Li, G. S., Zhou, T. H., and Hiroshi, Y. O. (2003). Nutritional regulaition of lipoprotein lipase gene experssion and visceral fat deposition in red set bream (*Pagrus major*). *Oceanologia Et Limnologiia Sinica* 34, 625–630. doi: 10.3321/j.issn:0029-814X.2003.06.006

Liu, C. S., Dong, Y. H., Xue, Q. G., and Lin, Z. H. (2017). Association of α-amylase gene with growth traits in the razor clam *Sinonovacula*. *Invertebrate Surviv. J.* 14, 494–504.

Mata-Sotres, A., Yufera, J., Manuel, J. M., and Martinez-Rodriguez, G. (2016). Daily rhythms of digestive enzyme activity and gene expression in gilthead seabream (*Sparus aurata*) during ontogeny. *Comp. Biochem. Physiol. A* 197, 43–51.

Mata-Sotres, J. A., Martínez-Rodríguez, G., Pérez-Sánchez, J., Martínez-Rodríguez, G., Pérez-Sánchez, J., and Sánchez-Vázquez, F. J. (2015). Daily rhythms of clock gene expression and feeding behavior during the larval development in gilthead seabream, *Sparus aurata*. *Chronobiol. Int.* 32:1061. doi: 10.3109/07420528.2015.1058271

Meenu, K., Singh, G., and Vishwakarma, R. A. (2014). "Chapter 22-molecular mechanism of cellulase production systems in trichoderma," in *Biotechnology and Biology of Trichoderma*, eds A. Herrera-Estrella, R. S. Upadhyay, I. Druzhinina, M.Tuohy, M. Schmoll, V. G. Gupta (Philadelphia, PA: Elsevier Science), 319–324. doi: 10.1016/B978-0-444-59576-8.00022-9

Mistlberger, R. E. (1994). Circadian food-anticipatory activity: formal models and physiological mechanisms. *Neurosci. Biobehav. Rev.* 18, 171–195. doi: 10.1016/0149-7634(94)90023-x

Morton, B. (1971). The diurnal rhythm and tidal rhythm of feeding anddigestion in *Ostrea edulis*. *Biol. J. Linn. Soc.* 3, 329–342. doi: 10.1111/j.1095-8312.1971.tb00526.x

Morton, B. (2010). The functional morphology of *Sinonovacula constricta* with a discussion on the taxonomic status of the Novaculininae (Bivalvia). *Proc. Zool. Soc. Lond.* 202, 299–325. doi: 10.1111/j.1469-7998.1984.tb05085.x

Navarro-Guillén, C., Conceio, L. E. C., Pinto, W., Siguero, I., and Yúfera, M. (2018). Fast growing greater amberjack post-larvae require a high energy-high protein weaning diet. *Aquaculture* 499, 195–202. doi: 10.1016/j.aquaculture.2018.09.037

Navarro-Guillén, C., Moyano, F. J., and Yúfera, M. (2015). Diel food intake and digestive enzyme production patterns in *Solea senegalensis* larvae. *Aquaculture* 435, 33–42. doi: 10.1016/j.aquaculture.2014.09.017

Paredes, J. F., Vera, L. M., Martinez-Lopez, F. J., Navarro, I., and Sánchez, V. F. J. (2014). Circadian rhythms of gene expression of lipid metabolism in gilthead seabream liver: synchronisation to light and feeding time. *Chronobiol. Int.* 31, 613–626. doi: 10.3109/07420528.2014.881837

Qin, C. J., Sun, J. X., Wang, J., Han, Y., and Hu, P. (2020). Discovery of differentially expressed genes in the intestines of *Pelteobagrus vachellii* within a light/dark cycle. *Chronobiol. Int.* 37, 339–352. doi: 10.1080/07420528.2019.1690498

Reymond, H., and Lagardère, J. P. (1990). Feeding rhythms and food of *Penaeus japonicus* Bate (*Crustacea Penaeidae*) in salt marsh ponds. *Aquaculture* 84, 125–143. doi: 10.1016/0044-8486(90)90343-L

Riisgård, H. U. (1991). Filtration rate and growth in the blue mussel, *Mytilus edulis* Linneaus, 1758: dependence on algal concentration. *J. Shellfish Res.* 10, 29–35.

Rong, Y. J., Zhang, L., Chi, Z. M., and Wang, X. H. (2015). A carboxymethyl cellulase from a marine yeast (*Aureobasidium pullulans* 98): its purification, characterization, gene cloning and carboxymethyl cellulose digestion. *J. Ocean Univ. China.* 14, 913–921. doi: 10.1007/s11802-015-2574-4

Rønnestad, I., Yúfera, M., Ribeiro, L., and Boglione, C. (2013). Feeding behaviour and digestive physiology in larval fish: current knowledge, and gaps and bottlenecks in research. *Rev. in Aquac.* 5(Suppl. S1), S59–S98. doi: 10.1111/raq.12010

Sanchezvazquez, E. J. (1995). Light-dark and food restriction cycles in sea bass: effect of conflicting zeitgebers on demand-feeding rhythms. *Physiol. Behav.* 58:705. doi: 10.1016/0031-9384(95)00116-Z

Shen, H. D., Liu, G., Fang, L., and Li, J. (2013). Effect of microalgae and temperature on absorption efficiency of razor clam (*Sinonovacula constricta* Lamark, 1818). *Aquac. Res.* 44, 1524–1530. doi: 10.1111/j.1365-2109.2012.03159.x

Supannapong, P., Pimsalee, T., Komol, T. A., Engkagul, A., Kovitvadhi, U., and Kovitvadhi, S. (2008). Digestive enzymes and *in-vitro* digestibility of different species of phytoplankton for culture of the freshwater pearl mussel, *Hyriopsis bialatus*. *Aquac. Int.* 16, 437–453. doi: 10.1007/s10499-007-9156-4

Tengjaroenku, L. B., Smith, B., Caceci, J., and Smith, S. A. (2000). Distribution of intestinal enzyme activities along the intestinal tract of cultured Nile tilapia, *Oreochromis niloticus* L. *Aquaculture* 182, 317–327. doi: 10.1016/S0044-8486(99)00270-7

Thongsaiklaing, T., Sehawong, W., Kubera, A., and Ngernsiri, L. (2014). Analysis of the α-amylase gene sequence and the enzyme activity of indian rock oyster *Saccostrea forskali*. *Fish. Sci.* 80, 589–601. doi: 10.1007/s12562-014-0708-z

Tizon, R. U., Serrano, A. E., and Traifalgar, R. F. (2013). Effect of unialgal diets on digestive enzyme activity inthe angelwing clam (*Pholas orientalis*). *Isr. J. Aquac. Bamid.* 890, 1–6. doi: 10.1071/MF12240

Wang, J. Y. (2004). Aquaculture on the control measures of ecological environment pollution. *J. Beijing Fish.* 4, 4–6.

Williams, B. G., and Pilditch, C. A. (1997). The entrainment of persistent tidal rhythmicity in a filter-feeding bivalve using cycles of food availability. *J. Biol. Rhythms* 12, 173–181. doi: 10.1177/074873049701200208

Wu, G., Chen, P., Hang, R., Yang, S. Y., and Shen, J. L. (2002). Influence of salinity and day and night rhythm on feeding rate(FR) of *Philippinarum ruditapes*. *J. Oceanogr. Tanwan Strait*. 21, 73–77. doi: 10.1007/s11769-002-0041-9

Wu, Y., Liu, W. B., Li, H. Y., Xu, W. N., He, J. X., and Li, X. F. (2013). Effects of dietary supplementation of fructooligosaccharide on growth performance, body composition, intestinal enzymes activities and histology of blunt snout bream (*Megalobrama amblycephala*) fingerlings. *Aquac. Nutr.* 19, 886–894. doi: 10.1111/anu.12033

Yúfera, M., Moyano, F. J., and Martínez-Rodríguez, G. (2018). "The digestive function in developing fish larvae and fry. From molecular gene expression to enzymatic activity", in *Emerging Issues in Fish Larvae Research* ed. M. Yúfera (Cham: Springer International Publishing), 51–86. doi: 10.1007/978-3-319-73244-2_3

Conflict of Interest: The authors declare that the research was conducted in the absence of any commercial or financial relationships that could be construed as a potential conflict of interest.

Publisher's Note: All claims expressed in this article are solely those of the authors and do not necessarily represent those of their affiliated organizations, or those of the publisher, the editors and the reviewers. Any product that may be evaluated in this article, or claim that may be made by its manufacturer, is not guaranteed or endorsed by the publisher.

frontiers in Marine Science

ORIGINAL RESEARCH
published: 28 October 2021
doi: 10.3389/fmars.2021.725628

Comprehensive Analysis of Differentially Expressed mRNA, Non-coding RNA, and Their Competitive Endogenous RNA Network of Pacific Oyster *Crassostrea gigas* With Different Glycogen Content Between Different Environments

Xue Wang[1], Weijun Wang[1], Zan Li[1], Guohua Sun[1], Tao Xu[2], Xiaohui Xu[1], Yanwei Feng[1], Qihao Luo[1], Bin Li[1,3] and Jianmin Yang[1,3]**

[1] School of Agriculture, Ludong University, Yantai, China, [2] General Station of Fishery Development and Resource Conservation in Shandong Province, Jinan, China, [3] Yantai Haiyu Marine Science and Technology Co., Ltd., Yantai, China

Glycogen content is a quantitative trait, its phenotype differences are found between individual oysters due to genetic effects and environmental factors which were including food, water temperature, salinity, and so on. In this study, a full sibling family of Pacific oyster *Crassostrea gigas* showed different phenotypes with high and low glycogen content between South Huanghai Sea (Rizhao offshore area, RZ) and North Huanghai Sea (Kongtong Dao area, KTD), respectively. At the same time, the content of 11 glucogenic amino acids and 13 fatty acids were also significant differences between RZ and KTD. RNA-seq and small RNA-seq technologies were used for transcriptome sequencing and functional enrichment analysis of differentially expressed RNA were used by Gene Ontology (GO) and Kyoto Encyclopedia of Genes and Genomes (KEGG) pathway. A total of 2,084 mRNAs, 1,080 long non-coding RNAs (lncRNAs), 34 circular RNAs (circRNAs), and 7 microRNAs (miRNAs) were differentially expressed. Based on these differentially expressed genes (DEGs), miRNA target interactions (lncRNA/circRNA–miRNA pairs and miRNA–mRNA pairs) were predicted using the miRanda software. The differentially expressed mRNAs in this network were mainly shown to be involved in calcium signaling pathway and insulin signaling pathway. These findings could help to speculate that environmental factors may be epigenetically regulated by non-coding RNA in *C. gigas*, thereby further affecting glycogen content.

Keywords: *Crassostrea gigas*, glycogen, ncRNA, ceRNA, epigenetic regulation

OPEN ACCESS

Edited by:
Yuehuan Zhang,
South China Sea Institute of Oceanology, Chinese Academy of Sciences (CAS), China

Reviewed by:
Ryan Spengler,
University of Wisconsin–Madison, United States
Xiaoting Huang,
Ocean University of China, China
Yinghui Dong,
Zhejiang Wanli University, China

***Correspondence:**
Weijun Wang
wwj2530616@163.com
Jianmin Yang
ladderup@126.com

Specialty section:
This article was submitted to Marine Fisheries, Aquaculture and Living Resources, a section of the journal Frontiers in Marine Science

Received: *15 June 2021*
Accepted: *06 October 2021*
Published: *28 October 2021*

Citation:
Wang X, Wang W, Li Z, Sun G, Xu T, Xu X, Feng Y, Luo Q, Li B and Yang J (2021) Comprehensive Analysis of Differentially Expressed mRNA, Non-coding RNA, and Their Competitive Endogenous RNA Network of Pacific Oyster Crassostrea gigas With Different Glycogen Content Between Different Environments. Front. Mar. Sci. 8:725628. doi: 10.3389/fmars.2021.725628

INTRODUCTION

Pacific oyster (*Crassostrea gigas*) has the characteristics of strong adaptability to the external environment, fast growth, high yield, rich nutrition, and delicious flavor. Therefore, it is widely cultivated worldwide as a high-economic value aquatic product. At present, the improvement of oyster meat quality is one of the important research topics for its industrial development, because the quality of meat is often measured by people's basic sensory evaluation of taste. Glycogen content accounts for 20–40% of the dry weight of oysters, which directly affects the taste of oysters and is an important quality trait. Previous studies have found that on the one hand, the content of glycogen metabolism-related enzymes directly affects the changes in glycogen content (Hata et al., 1993), on the other hand, the metabolic level of amino acids and fatty acids also affects glycogen metabolism (Randle et al., 1963; Fromentin et al., 2011). Therefore, genetic and environmental factors (temperature, nutrition, salinity, etc.) may affect the glycogen content (Li et al., 2017b). At present, several key genes that have been cloned in the oyster glycogen metabolism pathway, such as: glycogen phosphorylase (Hata et al., 1993), phosphoglucomutase (Tanguy et al., 2006), glycogen synthase kinase (Zeng et al., 2013), glycogenin (Li et al., 2017a), protein phosphatase 1 regulatory subunit 3B (Liu et al., 2019), etc. Glycogen content fluctuates seasonally with gonad development, and glycogen-related genes express differences in different seasons and tissues (Bacca et al., 2005). And the increase of free fatty acid content could lead to reduce the consumption of glycogen. Similarly, high amino acid content also might increase glycogen content, because some amino acids could guide glycogen synthesis (Li et al., 2017b).

With the development of sequencing technology and the continuous improvement of the genome project, the human genome sequencing revealed that there are only about 20,000 protein-coding genes, and the proportion of the total genome sequence is <2%, and the remaining about 98% belong to non-coding RNA (ncRNA) (Chan and Tay, 2018). At present, ncRNA is divided into two types: housekeeping ncRNA and regulatory ncRNA. The common regulatory ncRNAs include microRNA (miRNA), long non-coding RNA (lncRNA), and circular RNA (circRNA). Studies have found that regulatory ncRNA is involved in the larval metamorphosis, shell pigmentation, and immune-related mechanisms (Yu et al., 2016; Feng et al., 2018). However, whether ncRNA mediates the genetic mechanism that causes changes in glycogen content due to environmental factors is still unknown.

Therefore, in order to increase our understanding of the regulation of glycogen content, we performed ncRNA transcriptome analysis. During the research process, we placed a full sibling family of *C. gigas* in two offshore areas and produced two different phenotypes: high glycogen content and low glycogen content. The gonads of individuals with high and low glycogen content were selected for analysis. These findings may help us to further understand the regulatory effects of ncRNA on glycogen content in different environments, and provide new information for future genetic breeding of *C. gigas* in aquaculture.

MATERIALS AND METHODS

Ethics Statement

In this study, all experiments were performed according to local and central government regulations. No endangered species were used in the study. No special permission was required to collect oysters or to perform the described experiments.

Experimental Animals and Sample Collection

In this study, we used a near-infrared (NIR) model (Wang et al., 2015) which constructed in our laboratory to determine the phenotypic value of the glycogen content of *C. gigas*. The families with high breeding value were selected through EBV calculation, and comprehensively consider the genetic relationship between families (the genetic relationship is less than 0.2) which could prevent the occurrence of inbreeding decline. During the oyster breeding season, the phenotypic value of glycogen content of the parents of each candidate family was determined by a NIR spectrometer (MicroNIR 1700 JDSU, United States) on site, and the male and female individuals with high glycogen content between each family were selected. Through mating between families, male and female parents from different families were fertilized to construct a full-sib family. Later, a full sibling family of *C. gigas* was farmed in the South Huanghai Sea (Rizhao offshore area, RZ) and North Huanghai Sea (Kongtong Dao area, KTD). In March 2018, we collected nine two-year-old oysters from RZ and KTD areas, and measured the glycogen content. In the RZ group and KTD group, three samples with similar growth characteristics were selected for follow-up experiments. We calculated the average glycogen content of RZ and KTD oysters, and each group selected three oyster individuals whose glycogen content was close to the average glycogen content of each group, and collected the gonadal tissues of these samples for RNA-seq and small RNA-seq, and determine its fatty acid content and amino acid composition. All samples were quick-frozen in liquid nitrogen and stored at −80°C.

Determination of Amino Acid Concentration

According to the Chinese National Standard GB 5009.124-2016, the amino acid analysis of the gonadal tissue was performed at the SGS-CSTC Standards Technical Services Co., Ltd. (Qingdao, China). The main steps were as follows. First, 15 mL of 6 mol/L HCl solution was hydrolyzed for 100 mg of sample at 110 ± 1°C for 22 h. Second, filter the acid hydrolysate with filter paper, and then used a tubular concentrator to evaporate under reduced pressure at 50°C. Third, 1.0 mL of sodium citrate buffer (pH = 2.2) was added to the dried hydrolysate, and the resulting solution was passed through a 0.22 μm filter. The external standard method is used in the amino acid analyzer to calculate the amino acid concentration in the sample solution from the peak area.

Determination of Fatty Acid Composition

According to the Chinese National Standard GB 5009.168-2016, the fatty acid composition of the gonadal tissue was measured

by gas chromatography (GC). Simply, 2 ml methanol solution of hydrochloric acid, 1 mL n-hexanewere added into 100 mg powder sample and then hydrolyzed at 80°C for 2 h. After cooling down, 3 mL 6% K_2CO_3 was added to the samples. After filtered using a 0.22−μm membrane, the samples were analyzed on a high performance gas chromatography analyzer (GC-2010, Shimadzu, Japan), each injection volume was 1 μL. The types and relative contents of fatty acids were calculated according to the standard peak time screening and the corrected area normalization method.

Total RNA Isolation and Illumina Sequencing

RNA-seq and small RNA-seq were completed by Novogene Bioinformatics Technology Co., Ltd. (Beijing, China). The total RNA from gonadal tissue was isolated using TRIzol reagent (Invitrogen, CA, United States) according to the manufacturer's instructions. The RNA degradation and contamination was monitored on 1% agarose gels, purity was checked using the NanoPhotometer Spectrophotometer® (IMPLEN, CA, United States), concentration was measured using Qubit® RNA Assay Kit in Qubit® 2.0 Flurometer (Life Technologies, CA, United States), integrity was assessed using the Agilent Bioanalyzer 2100 system (Agilent Technologies, CA, United States).

According to the manufacturer's instructions, a total amount of 3 μg RNA per sample was used as input material for the RNA sample preparations. Firstly, ribosomal RNA was removed by Epicentre Ribo-zero™ rRNA Removal Kit (Epicentre, United States), and rRNA free residue was cleaned up by ethanol precipitation. Subsequently, sequencing libraries were generated using the rRNA depleted RNA by NEBNext® Ultra™ Directional RNA Library Prep Kit for Illumina® (NEB, United States) following manufacturer's recommendations, products were purified (AMPure XP system) and library quality was assessed on the Agilent Bioanalyzer 2100 system. The clustering of the index-coded samples was performed on a cBot Cluster GenerationSystem using TruSeq PE Cluster Kit v3-cBot-HS (Illumia). After cluster generation, the libraries were sequenced on an Illumina Hiseq 4000 platform and 150 bp paired-end reads were generated.

A total amount of 3 μg total RNA per sample was used as input material for the small RNA library. Sequencing libraries were generated using NEBNext® Multiplex Small RNA Library Prep Set for Illumina® (NEB, United States), library quality was assessed on the Agilent Bioanalyzer 2100 system using DNA High Sensitivity Chips. The clustering using TruSeq SR Cluster Kit v3-cBot-HS (Illumia) After cluster generation, the library preparations were sequenced on an Illumina Hiseq 2500/2000 platform and 50 bp single-end reads were generated.

Sequencing Results

In RNA-seq, raw data were obtained by removing reads containing adapter, reads on containing ploy-N and low quality reads. At the same time, Q20, Q30, and GC contents of the clean data were calculated. Raw sequencing reads were submitted to Sequence Read Archive in NCBI; the SRA accession numbers were SRR15293269, SRR15293270, SRR15293271, SRR15293272, SRR15293273, and SRR15293274[1].

The reference genome and gene model annotation files are downloaded from the genome website.[2] Index of the reference genome was built using bowtie2 v2.2.8 and paired-end clean reads were aligned to the reference genome using HISAT2 (Langmead et al., 2009) v2.0.4. HISAT2 was run with "–rna-strandness RF," other parameters were setas default. The mapped reads of each sample were assembled by StringTie (v1.3.1) (Pertea et al., 2016) in a reference-based approach.

In small RNA-seq, raw data were obtained by removing reads containing ploy-N, with 5′ adapter contaminants, without 3′ adapter or the insert tag, containing ploy A or T or G or C and low quality reads. At the same time, Q20, Q30, and GC contents of the clean data were calculated. Raw sequencing reads were submitted to Sequence Read Archive in NCBI; the SRA accession numbers were SRR15293267 and SRR15293268 (see text footnote 1).

The reference genome and gene model annotation files are downloaded from the genome website (see text footnote 2). The small RNA tags were mapped to reference sequence by Langmead et al. (2009) without mismatch to analyze their expression and distribution on the reference.

Identification of Long Non-coding RNA and Circular RNA

The spliced transcripts were screened for lncRNA according to the following steps: first, selected transcripts with exon number ≥2 and length >200 bp; second, Cuffcompare software was used to screen annotation lncRNA (Trapnell et al., 2010); third, selected the transcripts with FPKM ≥0.5; finally, CPC (Coding Potential Calculator) and PfamScan were used to screen for coding potential (Kong et al., 2007; Mistry et al., 2007). CircRNA was screened and identified in the constructed lncRNA library. Because of the high false positives in circRNA identification, circRNA was screened using find_circ and CIRI2 (Gao et al., 2018), the results were merged and the intersection of the two was taken.

Identification of MicroRNA

The mapped small RNA tags were compared with the *Danio rerio* sequence in miRBase 20.0 to find known miRNAs. The modified software mirdeep2 (Friedlander et al., 2012) and srna-tools-cli[3] were used to obtain potential miRNAs and draw secondary structures. To remove tags originating from protein-coding genes, repeat sequences, rRNA, tRNA, snRNA, and snoRNA, small RNA tags were mapped to RepeatMasker, Rfam database. The software miREvo (Wen et al., 2012) and mirdeep2 were integrated to predict novel miRNA. To make every unique small RNA mapped to only one annotation, we follow the following priority rule: known

[1]https://www.ncbi.nlm.nih.gov/Traces/study/?acc=SRP330386&o=acc_s%3Aa

[2]https://www.ncbi.nlm.nih.gov/datasets/genomes/?txid=29159&source_db=RefSeq

[3]http://srna-workbench.cmp.uea.ac.uk/

miRNA > rRNA > tRNA > snRNA > snoRNA > repeat > gene > NAT-siRNA > gene > novel miRNA > ta-siRNA.

Target Gene Prediction

The lncRNA *cis*-acting target genes were screened for protein coding genes within 100 kb upstream and downstream; the lncRNA *trans*-acting target genes were screened for the Pearson correlation coefficient between lncRNA and mRNA than 0.95. Used miRanda (Enright et al., 2003) to predict the target gene of miRNA. The prediction was based on the miRNA binding site in the 3′UTR region of the gene. If the gene was uncertain or there was no 3′UTR region, then the miRNA binding site was determined according to the gene's stop codon within 1,000 bp downstream point.

Quantification of Gene Expression Level

Cuffdiff (v2.1.1) was used to calculate FPKMs of both lncRNAs and coding genes in each sample (Trapnell et al., 2010). Gene FPKMs were computed by summing the FPKMs of transcripts in each gene group. MiRNA expression levels were estimated by TPM (transcript per million) through the following criteria (Zhou et al., 2010).

Differentially Expressed RNA Gene Ontology and Kyoto Encyclopedia of Genes and Genomes Pathway Analysis

During the analysis, Ballgown was used for differential expression of lncRNA and mRNA analysis (Pertea et al., 2016), DESeq R package (1.10.1) was used for differential expression circRNA analysis, and DESeq R package (1.8.3) was used for differential expression miRNA analysis. The $p < 0.05$ and $|\log_2\text{FoldChange}| > 1$ as the threshold for differential screening to identify differential genes.

The GOseq R software package (Young et al., 2010) and KOBAS software (Mao et al., 2005) were used to perform Gene Ontology (GO) enrichment analysis and Kyoto Encyclopedia of Genes and Genomes (KEGG) pathway enrichment analysis on differentially expressed genes (DEGs) or ncRNA target genes, respectively.

Construction of the Long Non-coding RNA/Circular RNA–MicroRNA–mRNA Network

Used miRanda to predict the interaction between DEMis and DEG, DELs and DECs (Friedlander et al., 2012) and Cytoscape V3.2 software to visualize it, and choosed to express the trend as "up-down-up" or "down-up-down" network for further research (Saito et al., 2012).

Quantitative Real-Time PCR Validation

To verify the results of RNA-seq and small RNA-seq, quantitative real-time PCR (qRT-PCR) was performed. The sample used for qRT-PCR was the same as the sequencing sample. The verification primers involved were designed using Primer Premier 5 software (**Table 1**), and were specifically compared by NCBI Primer Blast, synthesized by Sangon Biotech Co., Ltd. (Shanghai, China). First, total RNA was used as the initial template, using PrimeScript™ RT reagent Kit with gDNA Eraser (TaKaRa, Beijing, China) (for mRNA and lncRNA), and Evo M-MLV RT Kit for qPCR (Accurate Biotechnology, Hunan, China) (for circRNA), Mir-X miRNA First-Strand Synthesis Kit (TaKaRa, Beijing, China) (for miRNA), convert total RNA into cDNA, with Oligo dT (for mRNA and lncRNA), random hexamer (For circRNA), poly-A RT primer (for miRNA). Second, qPCR used TB Green® Premix Ex Taq™ (TaKaRa, Dalian, China) for mRNAs, lncRNAs, and circRNAs, TB Green® Premix Ex Taq™ II (Tli RNaseH Plus) (TaKaRa, Dalian, China) for miRNAs. Extension factor 1 Genes (EF-1, used for mRNA, lncRNA, and circRNA) and U6 (used for miRNA) were used as endogenous controls (Renault et al., 2011). Finally, the Light Cycler 480 real-time PCR instrument (Roche Diagnostics, Burgess Hill, United Kingdom) was used for amplification, and $2^{-\Delta\Delta ct}$ method was used to calculate relative gene expression levels (Ballester et al., 2013).

TABLE 1 | The primers for qRT-PCR analysis.

Type	Gene name	Sequences (5′-3′)
mRNA	PPP1R3B	Forward: TCCCGGAGACAGCAGCAGAAG Reverse: ACTCCCGCCCTGATGAACATCC
	INSR	Forward: CCCAACGACCACTGCCCATTG Reverse: GCGATGAACCACACTCCGATGAC
	CAM	Forward: ACTTGGACGAGGAAGACCACGAG Reverse: TTCATCATACACAGGCGGAGTTCG
	IP3KB	Forward: TGCTCAGACCTCACTGCTGGAC Reverse: GCAAGACGGCGGTGGAATGG
LncRNA	XLOC-003125	Forward: CGGTGCGGCGCTACATTAGTC Reverse: GGCAGTATGTCCCACAGTCATCAG
	XLOC-097516	Forward: CGCTCGGCTGTCTCTGTAAATCTC Reverse: CCCTCGTTCAACCAGACTCTTAGC
	XLOC-020486	Forward: TCCCACACAGTCCACAAGATTTGC Reverse: GTAGCGATTGCGGCAGGTCAG
MiRNA	novel-miR-154	Forward: TTGAAGTCGTTGCTGGGGACATG
	novel-miR-225	Forward: CCGAGGATGTGAAGAAAGACAAAGACGT
	novel-miR-78	Forward: CGCGACCTGATTTTGTACTACAGTCTGT
	novel-miR-34	Forward: ACGTCTGTCTGAGGGTCGG
CircRNA	novel-circ-0000916	Forward: GCTGGTGGTGGATGAACAGA Reverse: TACGGGAGTGGAATGTTGGC
Reference gene	EF-1	Forward: CAAGAACGGAGATGCTGGTATGG Reverse: TTTCACTCTTTCCACCGGCTTT
	U6	Forward: GGAACGATACAGAGAAGATTAGC Reverse: TGGAACGCTTCACGAATTTGCG

Statistical Analyses

The Student's *t*-test analysis in SPSS statistical software v.22 (SPSS, Inc., Chicago, IL, United States) was used to analyze the data of glycogen content, fatty acid content and amino acid content. Quantitative data were expressed as means ± standard deviation (SD), and comparisons between different groups were completed using *t*-tests. The significance level for the statistical analyses was $p < 0.05$.

RESULTS

Phenotypic Statistics

The average glycogen content of the selected samples (fresh samples) in the RZ group and the KTD group were 7.173 ± 0.165

and 2.973 ± 0.055 mg/g, respectively. The differences in glycogen content between the two comparison groups were significantly different ($p < 0.001$). Therefore, in the follow-up analysis, we divided the two groups of oysters into high glycogen content of RZ (RZGH) group and low glycogen content of KTD (KTDGL) group.

As shown in **Table 2**, a total of 16 amino acid compositions were measured. 11 glucogenic amino acids were identified that were more abundant in KTDGL oysters ($p < 0.05$), such as aspartic acid, threonine, serine, glycine, alanine, valine, methionine, isoleucine, tyrosine, phenylalanine, and arginine. As shown in **Table 3**, there are differences in the content of 13 fatty acids in the RZGH and KTDGL groups ($p < 0.05$), and the content of 9 fatty acids in the RZGH group was significantly higher than that in the KTDGL group.

Expressional Differences in mRNAs, Long Non-coding RNAs, and MicroRNAs Between High Glycogen Content of Rizhao and Low Glycogen Content of Kongtong Dao Oysters

Compared with KTDGL oysters, there were 2,084 mRNAs (including 844 up- and 1,240 down-regulated), 1,080 lncRNAs (including 923 up- and 157 down-regulated), 34 circRNAs (including 26 up- and 8 down-regulated), and 7 miRNAs (including 4 up- and 3 down-regulated) that were differentially expressed in RZGH oysters (**Figures 1A–D**).

Functional Analysis of Differentially Expressed mRNAs, Long Non-coding RNAs, and Circular RNAs Gene Ontology Enrichment Analysis on Differentially Expressed Genes

It mainly includes three categories: biological process (BP) category, cellular component (CC) category, and molecular function (MF) category. GO enrichment analysis found that 120 GO terms were significantly enriched ($p < 0.05$). Among the three categories, microtubule-based movement, proteinaceous extracellular matrix and intramolecular oxidoreductase activity, and interconverting aldoses and ketoses were the most significant ones, which were selected separately the top 10 terms of significance are displayed (**Figure 2A**). KEGG enrichment analysis was performed on these DEGs to further determine the metabolic process pathway. The results showed that DEGs were significantly enriched in 13 pathways, such as calcium signaling pathway, ECM–receptor interaction, and insulin signaling pathway, among which 29 genes were enriched into the calcium signaling pathway, and 17 genes were enriched into the insulin signaling pathway (**Figure 2B**). Including protein phosphatase 1 regulatory subunit 3B (LOC105340237, PPP1R3B), calmodulin (LOC105327344, CAM), protein tyrosine phosphatase (LOC105329458, PTP), insulin-like peptide receptor (LOC105348544, INSR), acetyl coenzyme A carboxylase (LOC105343342, ACCA), inositol Triphosphate 3-kinase B (LOC105336889, IP3KB), and so on.

TABLE 2 | Amino acid composition of RZGH and KTDGL oysters.

Amino acids	RZGH (g/100 g)	KTDGL (g/100 g)	*p*-value
Aspartic acid	0.583 ± 0.015	0.983 ± 0.225	**0.037**
Threonine	0.360 ± 0.017	0.460 ± 0.082	**0.004**
Serine	0.287 ± 0.021	0.433 ± 0.090	**0.003**
Glutamic acid	1.153 ± 0.115	1.570 ± 0.453	0.198
Glycine	0.433 ± 0.023	0.623 ± 0.097	**0.005**
Alanine	0.517 ± 0.012	0.613 ± 0.165	**0.011**
Valine	0.340 ± 0.010	0.457 ± 0.095	**0.008**
Methionine	0.157 ± 0.006	0.267 ± 0.055	**0.001**
Isoleucine	0.290 ± 0.000	0.433 ± 0.115	**0.005**
Leucine	0.427 ± 0.006	0.717 ± 0.216	0.003
Tyrosine	0.133 ± 0.107	0.340 ± 0.066	**0.021**
Phenylalanine	0.237 ± 0.006	0.377 ± 0.055	**0.012**
Lysine	0.520 ± 0.020	0.787 ± 0.236	0.004
Histidine	0.190 ± 0.017	0.230 ± 0.020	0.059
Arginine	0.437 ± 0.015	0.697 ± 0.208	**0.001**
Proline	0.593 ± 0.023	0.563 ± 0.095	0.384
Sum of 16 amino acids	6.657 ± 0.099	9.550 ± 2.184	0.005

Bold fonts were differentially expressed of glycogenic amino acids.

TABLE 3 | Fatty acid content of RZGH and KTDGL oysters.

Fatty acid	RZGH (g/100 g)	KTDGL (g/100 g)	*p*-value
C14:0	3.302	4.206	**0.042**
C15:0	0.506	0.447	**0.042**
C16:0	0.429	0.230	0.1347
C17:0	3.409	3.003	0.617
C18:0	3.409	2.709	**0.027**
C20:0	0.102	0.143	0.198
C21:0	0.405	0.276	0.666
C22:0	0.045	0.061	0.424
C14:1	0.044	0.051	0.600
C15:1	18.412	18.105	0.655
C16:1	3.073	6.145	**0.003**
C17:1	0.434	0.149	0.187
C18:1n-9c	5.669	6.864	**0.024**
C18:1n-7	0.062	0.067	0.800
C20:1	4.575	3.699	**0.014**
C22:1n-9	0.172	0.078	**0.009**
C24:1	0.063	0.097	0.110
C18:2n-6c	1.258	1.758	0.060
C18:3n-6	0.127	0.100	**0.031**
C20:2	2.575	2.318	0.509
C20:3n-3	2.738	0.074	**0.003**
C20:3n-6	0.152	2.793	**0.021**
C22-2	0.601	0.471	0.160
C22:5n-3	0.323	0.257	**0.023**
ARA	2.030	1.758	0.414
EPA	20.166	23.097	**0.048**
DHA	10.991	8.447	**0.027**

Bold fonts were differentially expressed of fatty acids.

The *Cis* and *Trans* Role of Long Non-coding RNAs in Target Genes

To investigate the possible functions of lncRNAs, the *cis* and *trans* roles of DELs in target genes were identified, and the filtered mRNAs were analyzed in combination with DEGs. A total of 471 lncRNA–mRNA interactions were found to have *cis* roles and 1,327 lncRNA–mRNA interactions were found to

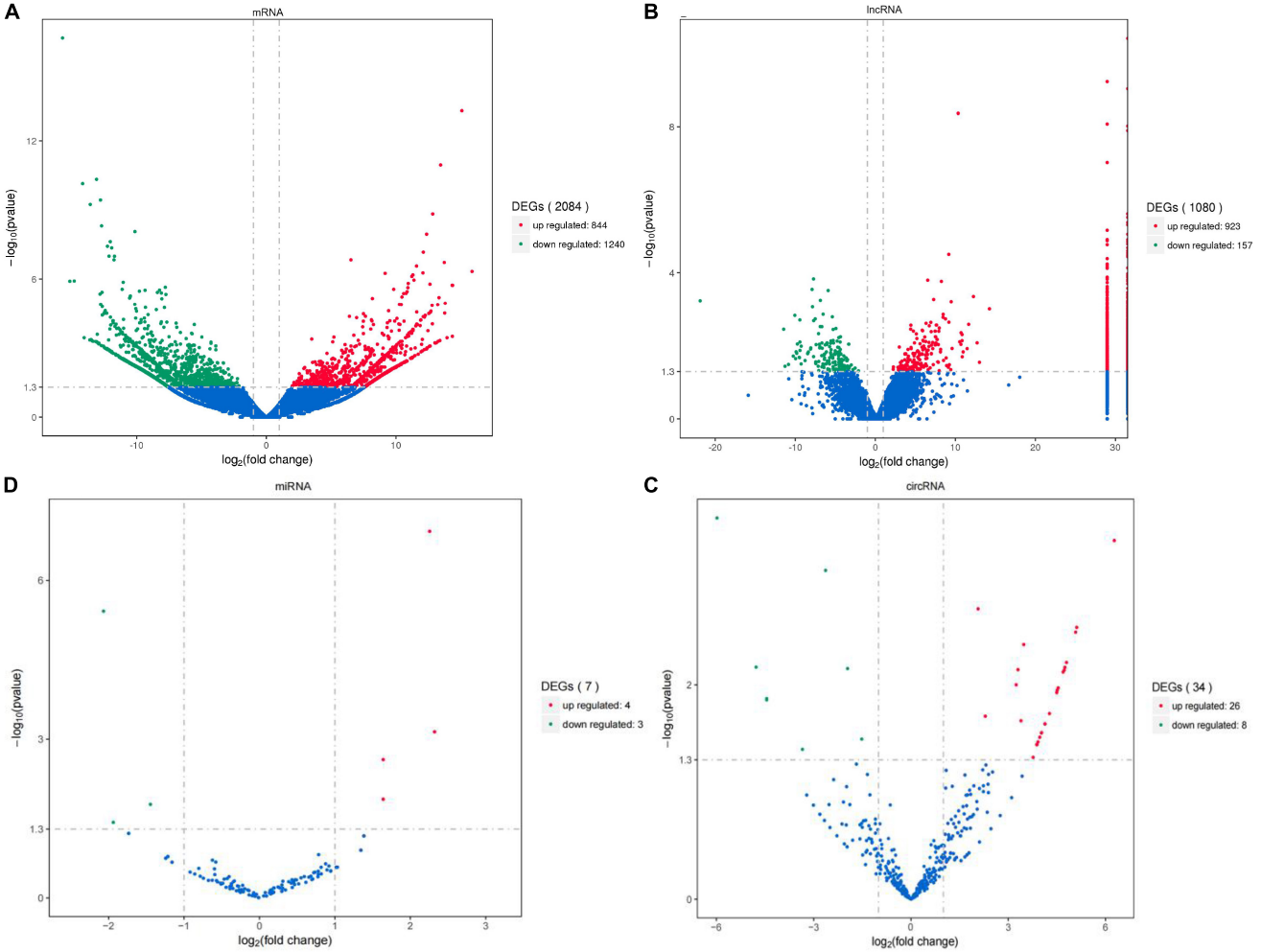

FIGURE 1 | The mRNAs **(A)**, lncRNAs **(B)**, circRNA **(C)**, and miRNAs **(D)** differentially expressed in RZGH and KTDGL groups. The red points showed the up-regulated, the green points showed the down-regulated, and the blue points showed the equally expressed ($p < 0.05$ and $|\log_2\text{FoldChange}| > 1$). The vertical dotted lines indicate $|\log_2\text{FC}| = 1$, and the horizontal dotted lines indicate $p = 0.05$.

have *trans* roles. The target genes were analyzed by GO and KEGG pathway enrichment. In the results of GO enrichment analysis, it was found that fucose metabolic process, mRNA cap binding complex, and L-fucose isomerase activity were the most significant among the three categories, respectively. The top 10 terms of significance were selected for display (**Figure 3A**). KEGG path analysis of lncRNA target genes to explore its function. Similar to the KEGG pathway of DEGs, it was found that 22 genes were enriched in the calcium signaling pathway, and 14 genes were enriched in the insulin signaling pathway, including PPP1R3B, CAM, PTP, INSR, DDO, etc. (**Figure 3B**).

Function Analysis of Differentially Expressed Circular RNAs

The functional enrichment of circRNA host genes was explored, 33 GO terms were significantly enriched ($p < 0.05$). KEGG pathway analysis was performed on the host genes of DECs to explore its function. The two pathways were significantly enriched ($p < 0.05$), other glycan degradation and propanoate metabolism. And it was found that novel-circ-0004211 were transcribed from acetyl-CoA synthase 2 (LOC105319828, ACAS2).

Construction of a Potential Long Non-coding RNA/Circular RNA–MicroRNA–mRNA Regulatory Network

A total of seven DEMis (four up- and three down regulated) were screened out with small RNA-seq. By analyzing the predicted target genes and DEGs, a total of 1,077 target genes were found. Analysis found that three down-regulated DEMis, novel-miR-34, novel-miR-78, and novel-miR-13 target a total of 283 up-regulated DELs; four up-regulated DEMis, novel-miR-154, novel-miR-44, novel-miR-225, and novel-miR-263 target a total

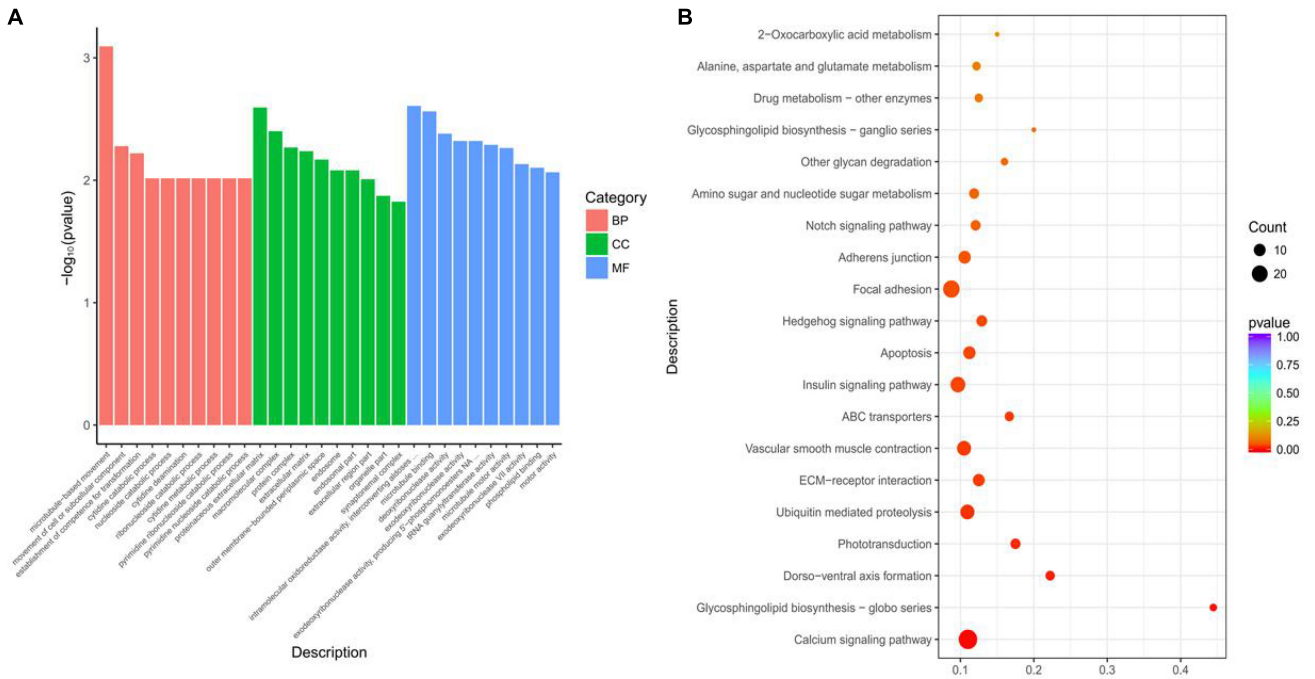

FIGURE 2 | Functional enrichment analysis of differentially expressed mRNAs between RZGH and KTDGL groups. **(A)** Gene Ontology (GO) terms and **(B)** KEGG pathways enriched.

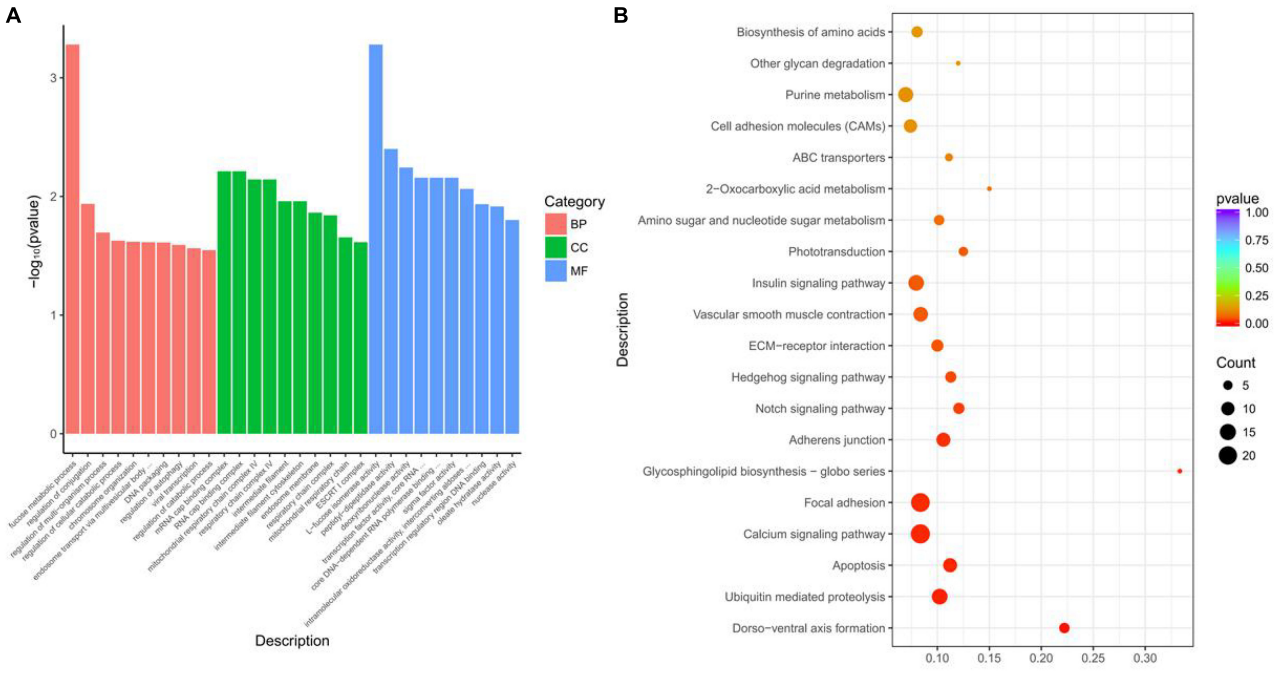

FIGURE 3 | Functional enrichment analysis of differentially expressed lncRNA target genes between RZGH and KTDGL groups. **(A)** Gene Ontology (GO) terms and **(B)** KEGG pathways enriched.

of 286 down-regulated DELs. In the interacting network, INSR gene and lncRNAs XLOC-116536, XLOC-104062, etc., were all negatively regulated by novel-miR-13 and novel-miR-34, PTP gene and 172 lncRNAs were all negatively regulated by novel-miR-154 and novel-miR-225. Some lncRNA–miRNA–mRNA network interactions are shown in **Figure 4A**.

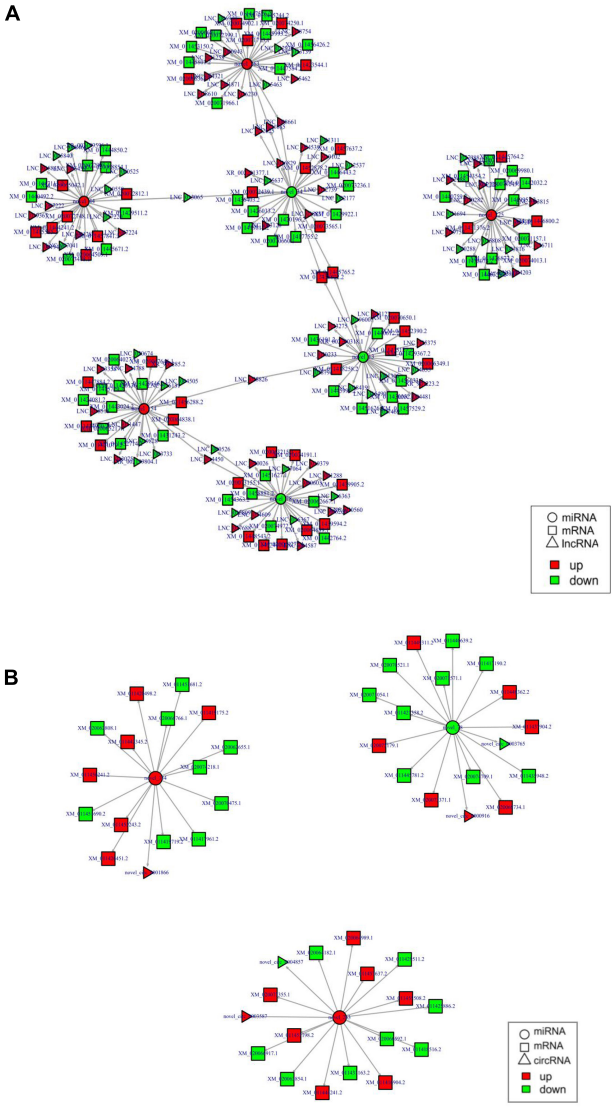

FIGURE 4 | (A) Partial lncRNA–miRNA–mRNA regulatory networks. **(B)** Partial circRNA–miRNA–mRNA regulatory networks.

In addition, two up-regulated DEMis were found, novel-miR-154 targeted novel-circ-0001866; novel-miR-263 targeted novel-circ-0004857 and novel-circ-0003587. One down-regulated DEMi, novel-miR-78 targets novel-circ-0003765 and novel-circ-0000916. In the interacting network, the other novel-circ-0000916 and INSR gene were all negatively regulated by novel-miR-78. Some circRNA–miRNA–mRNA network interactions were shown in **Figure 4B**.

Gene Ontology and KEGG pathway analyses of the functions of DEGs were included in the network. A total of 106 GO terms were significantly enriched ($p < 0.05$), and the top 10 terms of significance in the three categories were selected to display, as shown in **Figure 5A**. The BP mainly involves the response of microtubule-based motion, fucose metabolism, etc. The MFs mainly involved in deoxyribonuclease activity, mercury ion transmembrane transport protein activity, and intramolecular involvement of aldose, etc. A total of 14 pathways were significantly enriched ($p < 0.05$), of which 25 genes were enriched into calcium signaling pathway, and 15 genes were enriched into insulin signaling pathway (**Figure 5B**).

Quantitative Real-Time PCR Validation

The expression of twelve different genes was selected to confirm the utility of RNA-seq in qPCR analysis. The results showed that these transcripts were differentially expressed in oysters with different glycogen contents and were generally consistent with RNA sequencing data (**Figure 6**).

DISCUSSION

Oyster glycogen content is a quantitative trait, which varies greatly among individuals (Bacca et al., 2005; Aagesen and Haese, 2014). It is a complex and important trait that is affected by genetic and environmental factors, including seasons, nutrients, salinity, and temperature (Bacca et al., 2005; Varis et al., 2016). Liu's (2019) previous research showed that March is the proliferation period of oyster gonads, and the glycogen content of oysters is higher than the mature period of oyster gonads. Therefore, in this study, oysters of a full sibling family in two different sea areas RZ and KTD were farmed, to eliminate any potential genetic influence. In March 2018, we collected samples separately and found that the oyster glycogen in the RZ area was significantly higher than that of oysters in the KTD area. Since carbohydrates such as glycogen, amino acids, and fatty acids are the three major nutrients in organisms, their metabolic pathways are interrelated. An increase in free fatty acid levels may lead to an increase in glycogen content by reducing glycogen consumption (Randle et al., 1963). Similarly, a high-protein diet can increase glycogen content, because a large part of dietary amino acids are directed to glycogen synthesis (Fromentin et al., 2011). Therefore, we also measured the amino acid composition and fatty acid composition of the oysters in the RZGH and KTDGL groups, and the results found that there were significant differences in the amino acid composition and fatty acid composition of the oyster gonads between the two groups.

In this study, in order to get insight into the molecular regulation mechanism of glycogen content changes in oysters under different environments, we compared the differences in the expression profiles of mRNA, miRNA, lncRNA, and circRNA in the oyster gonads in the RZGH and KTDGL groups of a full sibling family. To determine the key factors involved in the regulation of glycogen content. Functional analysis of 2,084 differentially expressed genes showed that the insulin-like family genes were significantly enriched. Previous studies had shown that insulin could promote glycogen synthesis in mammals (Li et al., 2019). *Lymnaea stagnalis* was the first shellfish to discover insulin-like family genes, and for invertebrates, the insulin-like family was widespread and highly conserved (Li et al., 1992). It was mainly involved in growth, development, and metabolism (Brogiolo et al., 2001). However, whether insulin-like in *C. gigas* was related to glycogen content had not been

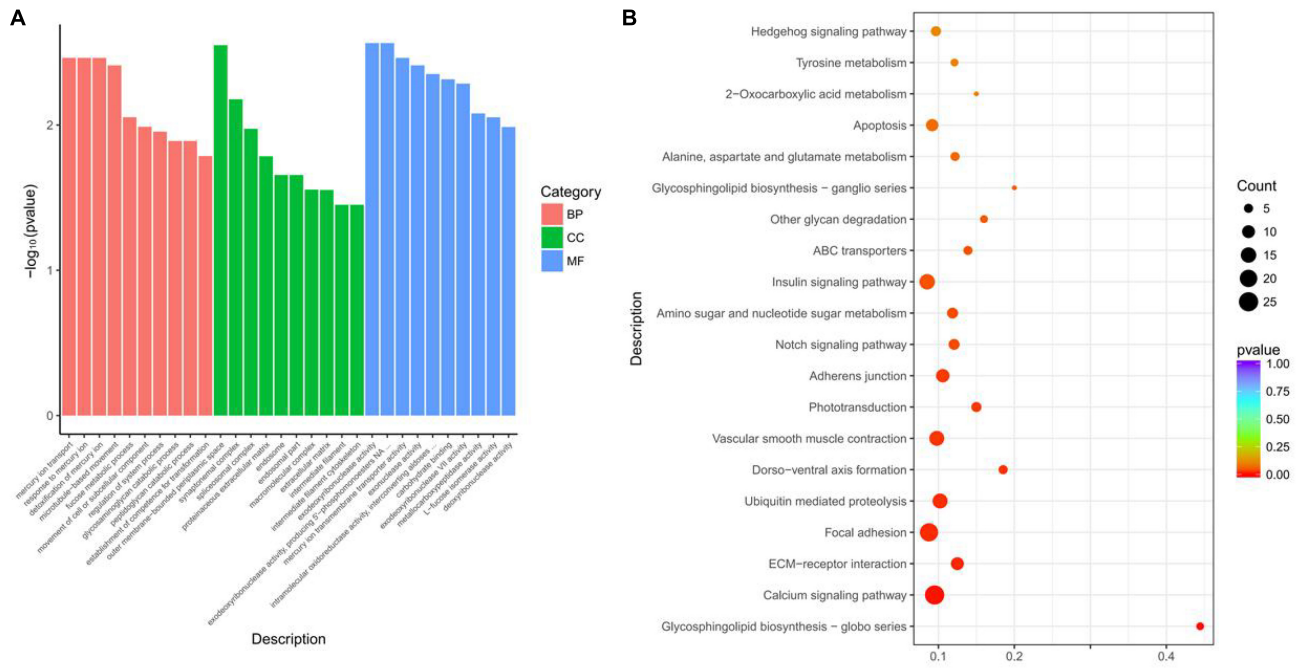

FIGURE 5 | Gene Ontology (GO) and KEGG analyses of the DEGs in the lncRNA/circRNA–miRNA–mRNA network. **(A)** GO analysis for DEGs in the lncRNA/circRNA–miRNA–mRNA network. **(B)** Statistics of pathways enrichment of DEGs in the lncRNA/circRNA–miRNA–mRNA network.

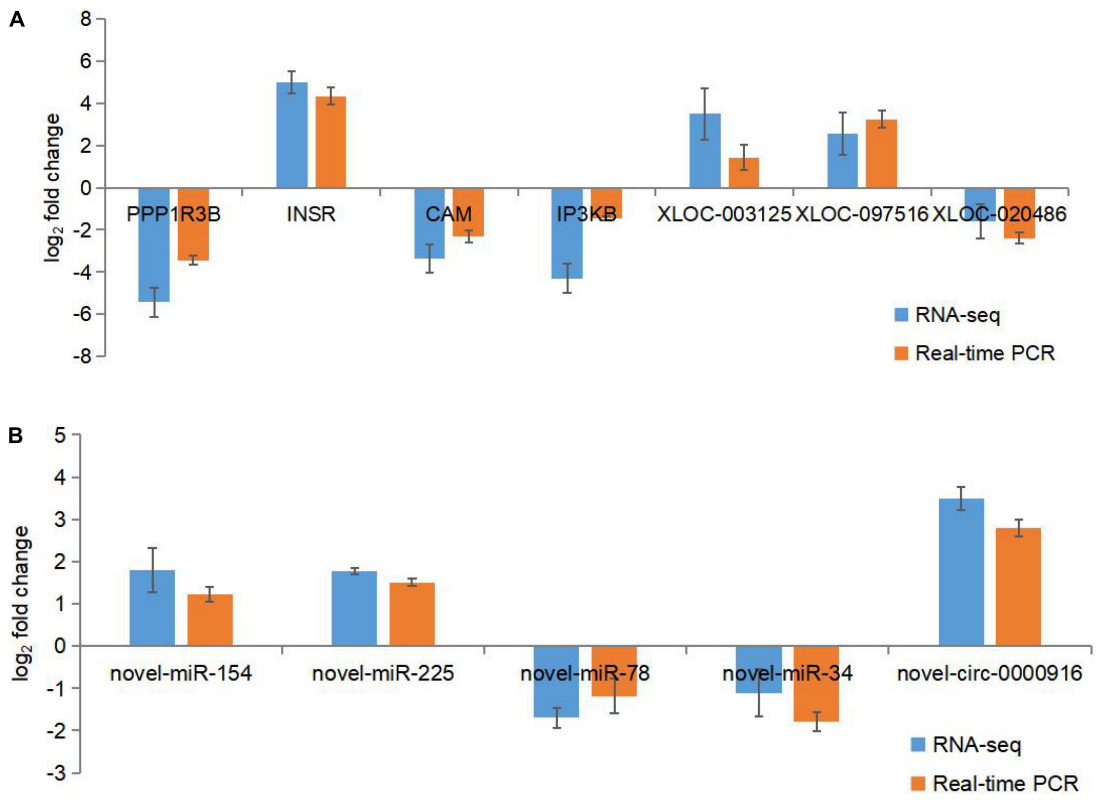

FIGURE 6 | RNA sequence data was verified using qPCR. **(A)** RNA-seq and q-PCR data for DEGs and DELs expression levels. **(B)** RNA-seq and q-PCR data of DECs and DEMis expression levels. Using eEF-1 and U6 as reference genes, the data represent the mean ± SD of three biological replicates, and each measurement was repeated three times. The fold change from the qPCR was calculated using the $2^{-\Delta\Delta ct}$ method.

reported. INSR is an insulin-like receptor protein tyrosine kinase substrate (Payankaulam et al., 2019), PTP dephosphorylates the tyrosine residues on the insulin receptor or its substrate, which prevents the insulin receptor from binding to insulin and negatively regulates insulin signal transduction (Haeusler et al., 2018). During the research, it was found that PTP was lowly expressed in RZGH oyster gonads, and INSR was highly expressed in RZGH oyster gonads. Therefore, it is speculated that the low expression of PTP in RZGH oyster gonads reduces the negative regulation of insulin-like signal transduction and further promotes glycogen synthesis. There are several genes related to glycogen synthesis in the insulin signaling pathway. For example, PPP1R3B was highly expressed in RZGH oyster gonad, it could cause glycogen synthase dephosphorylation, promote glycogen synthase activity, and further promote glycogen synthesis (Liu et al., 2019). LncRNA performs its function mainly by regulating mRNA, and analysis of the potential function of lncRNA is mainly predicted by analyzing their protein-coding target genes (Zhang et al., 2016). In the RZGH vs KTDGL group, it was found that lncRNA *cis* targets 471 mRNAs and *trans* targets 1,327 mRNAs. Functional enrichment analysis found that it was similar to differentially expressed mRNA and was related to insulin-like synthesis. For example, some of differentially expressed lncRNAs, XLOC-019254, XLOC-003125, XLOC-097516, and XLOC-020486 regulate CAM, PTP, INSR, IP3KB, etc., respectively. Therefore, lncRNA may play a certain regulatory role in insulin-like metabolism.

In eukaryotes, miRNAs have been reported to affect a variety of BPs, including glycogen metabolism (Dou et al., 2015), and their role in regulation is very important. With the development of high-throughput sequencing technology, studies on the miRNA transcriptome profiles of various mollusks have been reported (Xu et al., 2014; Zhou et al., 2014), and a new theory competitive endogenous RNA (ceRNA) has been proposed. However, in oysters, there is no report about miRNAs targeting glycogen metabolism in different environments. In this study, functional analysis of the seven differentially expressed miRNA target genes revealed that the differentially expressed miRNA might also be related to the insulin signaling pathway. The analysis found that in the network interaction analysis, INSR genes and lncRNAs XLOC-116536, XLOC-104062, etc., were all negatively regulated by novel-miR-13, novel-miR-34, and novel-circ-0000916 and INSR gene were all negatively regulated by novel-miR-78. These reports and our research results indicate that the ceRNA network formed by the interaction of lncRNA–miRNA–mRNA and circRNA–miRNA–mRNA related to the insulin-like signaling pathway may play a role in the regulation of glycogen content in different environments, but the specific function needs further study.

CONCLUSION

In summary, we compared the expression characteristics of mRNA and ncRNA in the same high-glycogen content sibling family produced two different phenotypes of *C. gigas* with high and low glycogen content. The results show that there are a large number of ncRNAs in gonadal tissues, and bioinformatics analysis shows that ncRNAs are involved in insulin-like metabolism. These include novel-miR-78, novel-miR-154, novel-miR-225, and novel-circ-0000916 and XLOC-116536, XLOC-105344, and XLOC-104062, etc. These findings may help us to further understand the regulatory effects of ncRNA on glycogen content in different environments, and provide new information for selective breeding of *C. gigas* in future.

DATA AVAILABILITY STATEMENT

The original contributions presented in the study are publicly available. This data can be found here: https://www.ncbi.nlm.nih.gov/Traces/study/?acc=SRP330386&o=acc_s%3Aa.

AUTHOR CONTRIBUTIONS

WW and JY contributed to the conception and design of the study. WW, XW, ZL, QL, and BL completed the material preparation, and data collection and analysis. GS, TX, XX, and YF supervised the data collection and analysis. WW and XW wrote the first draft. All authors read and approved the final manuscript.

FUNDING

This work was supported by the National Nature Science Foundation of China, No. 31402298, the Earmarked Fund for Agriculture Seed Improvement Project of Shandong Province, China, No. 2020LZGC016, and Innovation and Entrepreneurship Program of Jiangsu Province, China.

REFERENCES

Aagesen, A. M., and Haese, C. C. (2014). Seasonal effects of heat shock on bacterial populations, including artificial vibrio parahaemolyticus exposure, in the pacific oyster, *crassostrea gigas*. *Food Microbiol.* 38, 93–103. doi: 10.1016/j.fm.2013.08.008

Bacca, H., Huvet, A., Fabioux, C., Daniel, J.-Y., Delaporte, M., Pouvreau, S., et al. (2005). Molecular cloning and seasonal expression of oyster glycogen phosphorylase and glycogen synthase genes. *Comp. Biochem. Physiol. B Biochem. Mol. Biol.* 140, 635–646. doi: 10.1016/j.cbpc.2005.01.005

Ballester, M., Cordon, R., and Folch, J. M. (2013). DAG expression: high-throughput gene expression analysis of real-time PCR data using standard curves for relative quantification. *PLoS One* 8:e80385. doi: 10.1371/journal.pone.0080385

Brogiolo, W., Stocker, H., Ikeya, T., Rintelen, F., Fernandez, R., and Hafen, E. (2001). An evolutionarily conserved function of the *Drosophila* insulin receptor and insulin-like peptides in growth

control. *Curr. Biol.* 11, 213–221. doi: 10.1016/S0960-9822(01)00068-9

Chan, J. J., and Tay, Y. (2018). Noncoding RNA:RNA Regulatory Networks in Cancer. *Int J Mol Sci*. 19, 1310. doi: 10.3390/ijms19051310

Dou, L., Meng, X., Sui, X., Wang, S., Shen, T., and Huang, X. (2015). MiR-19a regulates PTEN expression to mediate glycogen synthesis in hepatocytes. *Sci. Rep.* 5:11602. doi: 10.1038/srep11602

Enright, A., John, B., Gaul, U., Tuschl, T., Sander, C., Marks, D., et al. (2003). MicroRNA targets in *Drosophila*. *Genome Biol.* 4, 1–27. doi: 10.1186/gb-2003-4-11-p8

Feng, D., Li, Q., Yu, H., Kong, L., and Du, S. (2018). Transcriptional profiling of long non-coding RNAs in mantle of *Crassostrea gigas* and their association with shell pigmentation. *Sci. Rep*. 8:1436. doi: 10.1038/s41598-018-19950-6

Friedlander, M. R., Mackowiak, S. D., Li, N., Chen, W., and Rajewsky, N. (2012). miRDeep2 accurately identifies known and hundreds of novel microRNA genes in seven animal clades. *Nucleic Acids Res*. 40, 37–52. doi: 10.1093/nar/gkr688

Fromentin, C., Azzout-Marniche, D., Tomé, D., Even, P., Luengo, C., Piedcoq, J., et al. (2011). The postprandial use of dietary amino acids as an energy substrate is delayed after the deamination process in rats adapted for 2 weeks to a high protein diet. *Amino Acids* 40, 1461–1472. doi: 10.1007/s00726-010-0756-3

Gao, Y., Zhang, J., and Zhao, F. (2018). Circular RNA identification based on multiple seed matching. *Brief Bioinform*. 19, 803–810. doi: 10.1093/bib/bbx014

Haeusler, R. A., McGraw, T. E., and Accili, D. (2018). Biochemical and cellular properties of insulin receptor signalling. *Nat. Rev. Mol. Cell Biol.* 19, 31–44. doi: 10.1038/nrm.2017.89

Hata, K., Hata, M., and Matsuda, K. (1993). Purification and properties of glycogen phosphorylase from the adductor muscle of the oyster, *Crassostrea gigas*. *Comp. Biochem. Physiol. B* 105, 481–486. doi: 10.1016/0305-0491(93)90077-I

Kong, L., Zhang, Y., Ye, Z. Q., Liu, X. Q., Zhao, S. Q., Wei, L., et al. (2007). CPC: assess the protein-coding potential of transcripts using sequence features and support vector machine. *Nucleic Acids Res*. 35, W345–W349. doi: 10.1093/nar/gkm391

Langmead, B., Trapnell, C., Pop, M., and Salzberg, S. L. (2009). Ultrafast and memory-efficient alignment of short DNA sequences to the human genome. *Genome Biol*. 10:R25. doi: 10.1186/gb-2009-10-3-r25

Li, B., Meng, J., Li, L., Liu, S., Wang, T., and Zhang, G. (2017a). Identification and functional characterization of the glycogen synthesis related gene glycogenin in pacific oysters *(Crassostrea gigas)*. *J. Agric. Food Chem*. 65, 7764–7773. doi: 10.1021/acs.jafc.7b02720

Li, B., Song, K., Meng, J., Li, L., and Zhang, G. (2017b). Integrated application of transcriptomics and metabolomics provides insights into glycogen content regulation in the Pacific oyster *Crassostrea gigas*. *BMC Genomics* 18:713. doi: 10.1186/s12864-017-4069-8

Li, K. W., Geraerts, W. P., and Joosse, J. (1992). Purification and sequencing of molluscan insulin-related peptide II from the neuroendocrine light green cells in *Lymnaea stagnalis*. *Endocrinol* 130, 3427–3432. doi: 10.1210/en.130.6.3427

Li, Q., Zhao, Q., Zhang, J., Zhou, L., Zhang, W., Chua, B., et al. (2019). The protein phosphatase 1 complex is a direct target of AKT that links insulin signaling to hepatic glycogen deposition. *Cell Rep.* 28, 3406–3422. doi: 10.1016/j.celrep.2019.08.066

Liu, P. (2019). *Study on Nutrition Quality, Flavor and Plankton Correlation of Crassostrea gigas*. Ph.D. thesis. Shanghai: Shanghai Ocean University.

Liu, S., Li, L., Meng, J., Song, K., Huang, B., Wang, W., et al. (2019). Association and functional analyses revealed that PPP1R3B plays an important role in the regulation of glycogen content in the pacific oyster *Crassostrea gigas*. *Front. Genet*. 10:106. doi: 10.3389/fgene.2019.00106

Mao, X., Cai, T., Olyarchuk, J. G., and Wei, L. (2005). Automated genome annotation and pathway identification using the KEGG Orthology (KO) as a controlled vocabulary. *Bioinformatics* 21, 3787–3793. doi: 10.1093/bioinformatics/bti430

Mistry, J., Bateman, A., and Finn, R. D. (2007). Predicting active site residue annotations in the Pfam database. *BMC Bioinformatics* 8:298. doi: 10.1186/1471-2105-8-298

Payankaulam, S., Raicu, A. M., and Arnosti, D. N. (2019). Transcriptional regulation of INSR, the insulin receptor gene. *Genes* 10:984. doi: 10.3390/genes10120984

Pertea, M., Kim, D., Pertea, G. M., Leek, J. T., and Salzberg, S. L. (2016). Transcript-level expression analysis of rna-seq experiments with hisat, stringtie and ballgown. *Nat. Protoc.* 11, 1650–1667. doi: 10.1038/nprot.2016.095

Randle, P. J., Garland, P. B., Hales, C. N., and Newsholme, E. A. (1963). The glucose fatty-acid cycle. its role in insulin sensitivity and the metabolic disturbances of diabetes mellitus. *Lancet* 281, 785–789. doi: 10.1016/S0140-6736(63)91500-9

Renault, T., Faury, N., Barbosa-Solomieu, V., and Moreau, K. (2011). Suppression substractive hybridisation (SSH) and real time PCR reveal differential gene expression in the Pacific cupped oyster, *Crassostrea gigas*, challenged with ostreid herpesvirus 1. *Dev. Comp. Immunol.* 35, 725–735. doi: 10.1016/j.dci.2011.02.004

Saito, R., Smoot, M. E., Ono, K., Ruscheinski, J., Wang, P. L., Lotia, S., et al. (2012). A travel guide to cytoscape plugins. *Nat. Methods* 9, 1069–1076. doi: 10.1038/nmeth.2212

Tanguy, A., Boutet, I., Boudry, P., Degremont, L., Laroche, J., and Moraga, D. (2006). Molecular identification and expression of the phosphoglucomutase (PGM) gene from the Pacific oyster *Crassostrea gigas*. *Gene* 382, 20–27. doi: 10.1016/j.gene.2006.06.005

Trapnell, C., Williams, B. A., Pertea, G., Mortazavi, A., Kwan, G., van Baren, M. J., et al. (2010). Transcript assembly and quantification by RNA-Seq reveals unannotated transcripts and isoform switching during cell differentiation. *Nat. Biotechnol*. 28, 511–515.doi: 10.1038/nbt.1621

Varis, J., Haverinen, J., and Vornanen, M. (2016). Lowering temperature is the trigger for glycogen build-up and winter fasting in crucian carp (*Carassius Carassius*). *Zool Sci* 33, 83–91. doi: 10.2108/zs150072

Wang, W. J., Yang, J. M., Li, Q., Ji, R., Gong, X. H., and Li, L. (2015). Development of calibration models for rapid determination of chemical composition of pacific oyster (*Crassostrea gigas*) by near infrared reflectance spectroscopy. *J. Shellfish Res*. 34, 303–309. doi: 10.2983/035.034.0212

Wen, M., Shen, Y., Shi, S., and Tang, T. (2012). miREvo: an integrative microRNA evolutionary analysis platform for next-generation sequencing experiments. *BMC Bioinformatics* 13:140. doi: 10.1186/1471-2105-13-140

Xu, F., Wang, X., Feng, Y., Huang, W., Wang, W., Li, L., et al. (2014). Identification of conserved and novel microRNAs in the Pacific oyster *Crassostrea gigas* by deep sequencing. *PLoS One* 9:e104371. doi: 10.1371/journal.pone.0104371

Young, M. D., Wakefield, M. J., Smyth, G. K., and Oshlack, A. (2010). Gene ontology analysis for RNA-seq: accounting for selection bias. *Genome Biol.* 11:R14. doi: 10.1186/gb-2010-11-2-r14

Yu, H., Zhao, X., and Li, Q. (2016). Genome-wide identification and characterization of long intergenic noncoding RNAs and their potential association with larval development in the Pacific oyster. *Sci. Rep.* 6:20796. doi: 10.1038/srep20796

Zeng, Z., Ni, J., and Ke, C. (2013). Expression of glycogen synthase (GYS) and glycogen synthase kinase 3beta (GSK3beta) of the Fujian oyster, *Crassostrea angulata*, in relation to glycogen content in gonad development. *Comp. Biochem. Physiol. B Biochem. Mol. Biol.* 166, 203–214. doi: 10.1016/j.cbpb.2013.09.003

Zhang, S., Qin, C., Cao, G., Xin, W., Feng, C., and Zhang, W. (2016). Systematic analysis of long noncoding RNAs in the senescence-accelerated mouse prone 8 brain using RNA sequencing. *Mol. Ther. Nucleic Acids* 5:e343. doi: 10.1038/mtna.2016.57

Zhou, L., Chen, J., Li, Z., Li, X., Hu, X., Yi, H., et al. (2010). Integrated profiling of micrornas and mrnas: micrornas located on xq27.3 associate with

clear cell renal cell carcinoma. *PLoS One* 5:e15224. doi: 10.1371/journal.pone.0015224

Zhou, Z., Wang, L., Song, L., Liu, R., Zhang, H., Huang, M., et al. (2014). The identification and characteristics of immune-related microRNAs in haemocytes of oyster *Crassostrea gigas*. *PLoS One* 9:e88397. doi: 10.1371/journal.pone.0088397

Conflict of Interest: BL and JY were employed by the company Yantai Haiyu Marine Science and Technology Co., Ltd.

The remaining authors declare that the research was conducted in the absence of any commercial or financial relationships that could be construed as a potential conflict of interest.

Publisher's Note: All claims expressed in this article are solely those of the authors and do not necessarily represent those of their affiliated organizations, or those of the publisher, the editors and the reviewers. Any product that may be evaluated in this article, or claim that may be made by its manufacturer, is not guaranteed or endorsed by the publisher.

frontiers in Marine Science

ORIGINAL RESEARCH
published: 08 November 2021
doi: 10.3389/fmars.2021.763269

Effects of Flow Velocity on the Growth and Survival of *Haliotis discus hannai* Larvae in the Recirculating Upflow System From the Point of Energy Metabolism

Mo Zhang[1,2,3], Xiaolong Gao[1,2,3], Mingxin Lyu[1,2,3], Shihui Lin[1,2,3], Ying Su[2], Xuan Luo[1,2,3], Weiwei You[1,2,3] and Caihuan Ke[1,2,3]*

[1] State Key Laboratory of Marine Environmental Science, Xiamen University, Xiamen, China, [2] College of Ocean and Earth Sciences, Xiamen University, Xiamen, China, [3] Fujian Key Laboratory of Genetics and Breeding of Marine Organisms, Xiamen University, Xiamen, China

OPEN ACCESS

Edited by:
Liping Liu,
Shanghai Ocean University, China

Reviewed by:
Yinghui Dong,
Zhejiang Wanli University, China
Zhiguo Dong,
Jiangsu Ocean University, China
Zhaoqun Liu,
Dalian Ocean University, China

***Correspondence:**
Weiwei You
wwyou@xmu.edu.cn

Specialty section:
This article was submitted to Marine Fisheries, Aquaculture and Living Resources, a section of the journal Frontiers in Marine Science

Received: 23 August 2021
Accepted: 19 October 2021
Published: 08 November 2021

Citation:
Zhang M, Gao X, Lyu M, Lin S, Su Y, Luo X, You W and Ke C (2021) Effects of Flow Velocity on the Growth and Survival of Haliotis discus hannai Larvae in the Recirculating Upflow System From the Point of Energy Metabolism. Front. Mar. Sci. 8:763269. doi: 10.3389/fmars.2021.763269

For the abalone *Haliotis discus hannai*, attachment and metamorphosis are crucial stages in the transition from planktonic to benthic life. Increasing the larval metamorphosis rate by artificially controlling the external environment and simulating natural seawater flow is vital to enhance the hatchery efficiency of *H. discus hannai*. Thus, in the current study, an upflow recirculating aquaculture unit was designed for the rearing of larval abalone, and the larval hatching rate, survival rate, mode of energy metabolism, and expression levels of metamorphosis-related genes at different flow velocities (0, 5, 10, 20, and 40 L/h) were compared and analyzed. At flow velocities less than 20 L/h, no significant differences occurred in larval hatching, survival, and metamorphosis rates, whereas significant differences were recorded at flow rates of 20 and 40 L/h. Differences were also observed in the activity of enzymes, such as hexokinase (HK), pyruvate kinase (PK), lactate dehydrogenase (LDH), succinate dehydrogenase (SDH), and malate dehydrogenase (MDH), as well as glycogen levels, at the higher flow rates. These results suggested that velocity in excess of a certain limit leads to a higher glycolysis rate and transition of energy utilization from aerobic to anaerobic metabolism for the abalone larvae. Compared with conventional still-water aquacultural systems, the flow velocity at 5–10 L/h could maintain the water environment stability, and avoid both fertilized eggs from being densely deposited before hatching and the consumption of energy needed to resist high flow velocities. Thus, these results are useful references to enhance the hatchery efficiency, and to conduct large-scale rearing, of abalone larvae.

Keywords: *Haliotis discus hannai*, flow velocity, larval rearing, energy metabolism, gene expression

INTRODUCTION

Haliotis discus hannai is one of the most important mariculture shellfish species in China. In 2019, abalone aquaculture production reached 180,300 tons, accounting for 90% of the total production worldwide (China Bureau of Fisheries, 2021). However, there are still many concerns and problems associated with abalone farming and artificial reproduction. For example, the low larval metamorphosis rate constrains the efficient and large-scale development of the abalone-rearing industry. Generally, the sperm and eggs are collected and placed directly in a small container (5 L) for artificial fertilization. Fertilized eggs are then directly transferred to the rearing pond for subsequent rearing. However, this rearing method is likely to lead to high-density accumulation and adhesion of fertilized eggs in a specific part of the pond, while dead eggs and decomposition products pollute the water and affect the larval survival rate. Thus, the postlarval metamorphosis rate is often less than 5% under this rearing mode in southern China, which is less than the flow-through rearing system used in northern China (Wu and Zhang, 2016). Therefore, it is necessary to develop a new system to improve the survival and metamorphosis rate of larvae.

Energy storage and release are essential activities in all organisms, and enzymes catalyze the metabolic reactions involved in these processes (Natalia et al., 2004). Such enzymes can, to a certain extent, regulate energy production in invertebrates. The activity of key energy metabolism enzymes in this pathway is crucial to the amount of energy generated (Friedrich, 1998). Respiratory metabolism is a crucial part of bioenergy metabolism, which can reflect the metabolic characteristics, physiological conditions, and nutritional status of the animal and its adaptability to its external environment. It is also considered an important field in aquatic bioenergetics and nutritional physiology research (Bao et al., 2018). Under anoxic conditions, aerobic metabolism of the fish *Astronotus crassipinnis* is inhibited and the activity of lactate dehydrogenase (LDH) continuously increases with the extension of anoxia (Heinrichs-Caldas et al., 2019). Similarly, when the shrimp *Litopenaeus vannamei* was exposed to hypoxic (1.57 ± 0.2 mg/L) conditions, the expression levels of LDH in glycolysis and phosphoenolpyruvate carboxylase in the gluconeogenic pathway increased (Reyes-Ramos et al., 2018); whereas, after 4 h of chasing prey, the activity of pyruvate kinase in the liver of rainbow trout was decreased (López-Patiño et al., 2014). Ivanina et al. (2011) found that the eastern oyster *Crassostrea virginica* had a higher free glycogen content and significantly enhanced hexokinase activity under hypoxic stress compared with control animals. Gao et al. (2017) considered that a decrease in salinity would lead to the enhanced activity of energy-metabolizing enzymes (i.e., hexokinase and pyruvate kinase) in the liver of the abalone *H. discus hannai*, suggesting that an increase in glycolysis rate would increase the energy needs of the body in a response to drastic changes in salinity. For marine invertebrates, energy reserves in the embryonic and larval stages are generally not enough to fulfill the total energy metabolism needs during metamorphism (Shilling and Manahan, 1990). Especially for lecithotrophic larval abalone, which depend on egg yolk nutrients, a longer planktonic period will exhaust the nutrients in the egg yolk, reducing the survival and growth rates of the juveniles (Maldonado and Young, 1999; Marshall et al., 2003; Thiyagarajan et al., 2007). The metabolic rate of *Balanus balanoides* increased during metamorphosis, but the protein and lipids as energy storage substances significantly reduced (Lucas et al., 1979). When metamorphosing, bivalve mollusks can directly absorb amino acids dissolved in seawater (Manahan and Crisp, 1983). The energy needs of *Haliotis rufescens* during larval metamorphosis are met by nutrients from its surroundings (e.g., dissolved organic material), but the oxygen consumption rate and glucose and alanine contents of larvae significantly increase during this process (Shilling et al., 1996). Thus, detection of the variation in energy metabolism enzyme activity can indicate the ability of the body to adapt to environmental change.

Larval metamorphosis of most marine invertebrate, which is an irreversible process and accompanied by high mortality, is triggered by external factors (Williamson et al., 2000). If environmental factors (e.g., temperature or salinity) change, the regulatory mechanism of the invertebrate neuroendocrine system would secrete hormones triggered by the stress response, leading to a series of physiological and biochemical reactions, including metabolism of principal energy substances, immunity, and respiration (Dong et al., 2017). In the short-wavelength blue/green light and dark environments, larval hatching rate and survival rate of *H. discus hannai* were significantly higher than in the long-wavelength red/orange group, suggesting that more energy accumulated during metamorphosis in blue/green light and dark environments (Gao et al., 2017). Wang et al. (2016) found that the expression levels of *IGFBP7* began to rise rapidly during the early trochophore stage and peaked during the metamorphosis stage. Given that *IGFBP7* was subject to RNA interference (RNAi), the larval metamorphosis rate in the group subject to RNAi was significantly reduced by 31.81% compared with the untreated group, suggesting that *IGFBP7* has a role in larval metamorphosis in *H. diversicolor*. The addition of adrenaline (AD) and noradrenaline (NA) within a concentration range of 10–100 μM significantly increased the larval metamorphosis rate of *Meretrix meretrix*; thus, the change in hormone and gene expression level could be used as an indicator to anticipate the initiation of metamorphosis (Wang et al., 2006).

In the current study, a new abalone larval upflow recirculating aquaculture system was constructed. The running seawater flow conditions for larval development were simulated by different velocities, during which water quality, energy metabolic enzyme activity, the concentration of energy-related substances (i.e., protein, glycogen, and triglyceride) and the expression levels of metamorphosis-related genes were evaluated to screen out appropriate velocities facilitating the hatching, survival and attachment metamorphosis of abalone larvae. The study provides a reference for enriching our basic biological understanding of abalone larval development and for improving the rearing efficiency of the abalone industry.

MATERIALS AND METHODS

Source and Acclimation of Experimental Abalones

The experiment was carried out at Fuda Abalone Farming Company (Jinjiang, Fujian). For adult abalones used in the experiment, the shell length was 75.15 ± 6.17 mm, shell width was 50.33 ± 5.85 mm, and body weight was 63.22 ± 5.01 g. Female and male abalones selected for the study had intact shells and feet, with gonadal development at Stage III (Ebert and Houk, 1984). During their acclimation, the water temperature was 19°C, salinity was 31 ± 1, pH was 7.9, and dissolved oxygen concentration was >6 mg/L, under a natural light/dark cycle. The abalones were fed with *Gracilaria lemaneiformis* daily at 17:00 h, at an amount that was 3% of the wet weight of the abalones.

Induced Egg-Laying

The female:male ratio of the abalones for induced egg-laying was 10:4. In the evening, the brood stocks were selected, dried in the shade for 1 h, and then male and female abalones were separately put in ultraviolet (UV)-radiated seawater (220 V, 40 W, 500 mWh^{-1}). Once the parent abalones laid sperm and eggs, artificial insemination was then performed. To shield the developing embryos from any adverse effect from the overly high concentration of sperm, eggs were washed repeatedly to remove excessive sperm, resulting in eight to ten sperm around one egg, as viewed under a field microscope.

Experimental Unit

Four sets of conical recirculating aquaculture systems were used as the experimental unit (**Figure 1**). Each unit comprised the aquaculture system and the water treatment system. Water flowed in at the bottom of each system, which comprised five transparent conical aquaculture containers (7.5 L), flowmeters, inlet pipes, venturis, one-way valves, valves, filter drums, and drain pipes; the water treatment system comprised a filter tank, filter partition, water pump, UV disinfection lamp, aeration disk, thermostat, and air pump. At the bottom of the filter partition, a layer of ceramic rings and pelelith formed the first layer of filtering material, on which a layer of biochemical cottons with different pore diameters were laid. The aeration disk and thermostat were placed at the bottom of the filter tank. The water for rearing was first passed through the filters, exposed to a UV disinfection lamp, and then returned to each conical container from the base. Before the pump was turned on, all water valves and drain valves on the bottom of the containers were closed and then opened once the pump started running. The flow velocity was controlled by a flowmeter, 1 water outlet (φ 2 cm, 10 cm from the tip of the cylinder) was placed on the cylindrical side wall of each conical container, a circular filter drum (φ 13 cm, thickness: 3 cm, with a 100-mesh screen adhered to each side) was joined to the outlet pipe so that larvae would not flow out with the water. An outfall was further placed at the bottom of the container. After the experiment, the valves were opened and the larvae that were about to enter the metamorphosis stage were collected with screens.

Experimental Design

Four velocity treatment groups (5, 10, 20, and 40 L/h) were designed for the experiment, whereas a still-water group (0 L/h) in the same recirculating water aquaculture system was used as the control. Once the experiment started, fertilized eggs were taken and transferred to the different velocity groups at a set density of 10 ind/ml; each group had four replicates. In the still-water group, no aeration was provided until larvae developed to the trochophore stage, at which point slight aeration was provided. Before the fertilized eggs developed into trochophores, the larval hatching rate, abnormality rate, and density were recorded in each group. Any larvae found with incomplete cilia, egg-shell damage, mulberry cells bulging into irregular shapes, or developmental retardation were considered to be deformed (Zhou et al., 2011). The development of embryos and larvae was observed under a microscope (Olympus CX22, Japan). When the larvae had developed into the secondary shell stage, their sizes were measured using a stage micrometer. Before each random sampling, the water was stirred lightly with a glass rod so that the larvae were evenly distributed. Then, 30 larvae were sampled from each group for measurement. If the fourth tubule on cephalic tentacles was observed, this indicated that the larva was about to enter the metamorphose stage. Water samples were randomly taken four times in each container, and the density of larvae in each group was counted for calculation of the survival rate; all larvae in each group were then collected using a filtering screen.

Throughout the experiment, the water temperature, salinity, pH, and dissolved oxygen concentration in each group was measured by using a YSI-556MPS portable multiparameter water quality measuring instrument (Yellow Springs Instruments Inc., OH, United States). After larvae were collected, the water was sampled to determine the TAN, NO_2-N, and NO_3-N concentrations. Each group was sampled three times and the concentrations were determined by SEAL Analytical-AA3 (Germany SEAL Analytical GmbH, Norderstedt, Germany). In the 0 L/h group, trochophores were collected with screens once they floated. The screens were used to remove all dead eggs and exchange water, with fresh water replenished into the rearing container. Before larval metamorphosis, aeration was provided continuously, but no water was exchanged.

Subsequently, the larvae collected from each group were transferred to glass containers of the same size (φ 15 cm, height: 8 cm) at a set density of 1 ind/ml, and polythene membranes (80 mm × 80 mm) with benthic diatoms were fixed to the bottom of each container. In the absence of planktonic larvae from the water, a section of polythene membranes (20 mm × 20 mm) was randomly cut, and the settlement and metamorphosis rate of larvae were determined. Before larval metamorphosis, a low level of aeration was applied, to the extent that the dissolved oxygen concentration was not less than 6 mg/L. The cut section was then fixed in a 4% formaldehyde solution and placed under a 4 × 10 magnification microscope; 30 larvae were measured with reference to a stage micrometer, and the metamorphosis rate, size of settlement and metamorphosis, and the time required for completion of metamorphosis were determined. Successful

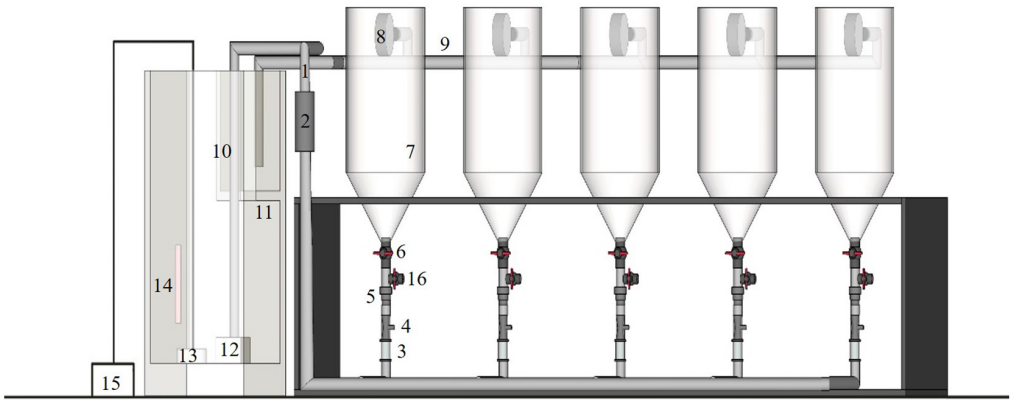

FIGURE 1 | Experimental RAS configuration: (1) inlet pipe; (2) ultraviolet disinfection lamp; (3) flow meter; (4) venturis; (5) one-way valves; (6) valves; (7) transparent cone container; (8) filter drums; (9) drain pipe; (10) filter tank; (11) filter partition; (12) water pump; (13) aeration disk; (14) thermostat; (15) air pump; (16) outfall.

metamorphosis of larvae was identified with reference to Vicose et al. (2007). The remaining larvae collected were transferred to a centrifuge tube, immediately stored in liquid nitrogen, until being used to assess larval biochemical composition, metabolic enzyme activity, and metamorphosis-related gene expression levels. The water used during the experiment was also subject to precipitation and sand filtration and had the same salinity and pH as during the acclimation period; the TAN concentration was no higher than 0.1 mg/L. During the experiment, the surrounding air temperature was maintained at 20°C using an air conditioner.

Assessing the Biochemical Composition of Larvae

The biochemical components of larvae were determined using a test kit supplied by the Jiancheng Institute of Bioengineering. Briefly, 0.1 g of larvae were placed in a test tube, to which 1 mL 0.86% normal saline was added; the tube was then transferred to an ice bath for grinding. After dipping with Coomassie Brilliant Blue, the solution turned blue, and the protein concentration of the specimen was calculated by detecting the absorbance at 595 nm. The method proposed by Gao et al. (2016) was used to determine the lactic acid content of the larvae. Briefly, with NAD^+ as the hydrogen acceptor, LDH catalyzes the dehydrogenation of lactate to produce pyruvate, turning NAD^+ into NADH. PMS transferred hydrogen to reduce NBT to a purple color, and the absorbance of the color material was linearly related to the lactic acid content at 530 nm; the lactic acid content was calculated by detecting the absorbance with ELISA.

To determine the triglyceride (TG) content, a homogenate was prepared with isotonic buffer solution at a ratio of 1:9 (weight: volume) using the GPO-PAP method and centrifuged at 2500 × *g* for 10 min. Then, 10% homogenate was taken as the supernatant and the TG content was calculated by detecting the absorbance at 510 nm with ELISA.

Creatine kinase catalyzes ATP and creatine to generate creatine phosphate. The ATP content was determined using phosphomolybdic acid colorimetry, and calculated by detecting the absorbance at 636 nm with ELISA.

Glycogen can be dehydrated under the action of concentrated sulfuric acid to produce aldehyde derivatives, and then reacted with anthrone to form a blue compound; thus, colorimetry was performed with the standard glucose solution treated in the same manner as described earlier. The larvae were taken at a specimen weight (mg): hydrolyzate volume (μL) of 1:3, added to a test tube, then boiled in a water bath for 20 min. The sample was then cooled, a Color-substrate solution was added and the test tube then was further boiled for 5 min. After cooling, the glycogen content was calculated by detecting the absorbance at 620 nm.

Assay of Larval Metabolic Enzyme Activity

The HK, PK, SDH, MDH, and LDH content was also determined using a test kit supplied by Jiancheng Institute of Bioengineering. To do so, 0.1 g larvae were placed in test tube and 1 mL homogenous medium (pH 7.4, 0.01 mol/L Tris–HCl, 1 mmol/L EDTA-2Na, 0.01 mol/L sucrose, 0.8% sodium chloride solution) was added; the tube was then centrifuged at 10,000 × *g* for 30 s.

HK catalyzes glucose to synthesize glucose-6-phosphate, the dehydrogenation of which is further catalyzed by glucose 6-phosphate dehydrogenase to NADPH. The activity of HK was calculated by detecting the special absorption peak of NADPH at 340 nm using a UV spectrophotometer. At 37°C and pH 7.6, an enzyme activity unit was defined as 1 μmol PEP converted by 1 g tissue protein into pyruvate per minute; the activity of PK was then calculated by detecting the absorbance at 340 nm using a UV spectrophotometer. The activity of SDH was defined as 1 specific activity unit that reduced the absorbance of the reaction system by 0.01 per mg protein per minute. The activity of SDH was calculated by detecting the reducing rate of 2,6-DPIP at 600 nm using a visible light spectrophotometer. The MDH-catalyzed redox reaction was accompanied by reduced absorbance at 340 nm. The activity of MDH was calculated by detecting the change in absorbance per minute using a UV spectrophotometer. After LDH catalyzes the conversion of lactic acid to pyruvate, pyruvate reacts with 2,4-dinitrophenylhydrazin to produce pyruvate dinitrophenylhydrazone (which appears

brownish red in alkaline solution); the activity of LDH can then be calculated by detecting the absorbance at 440 nm (Gao et al., 2016).

Gene Expression Analysis

The larvae that settled and metamorphosed were collected using a screen and then ground in a mortar with liquid nitrogen. RNA was extracted with TRIzol (Invitrogen, United States) and reverse transcription was performed by using the PrimeScript^{TM} RT Reagent Kit with gDNA Eraser (Takara, Japan). Three replicates samples were mixed and diluted five times, and then used as the template for real-time fluorescent quantitative PCR using the following reaction system: 5 × gDNA Eraser Buffer 5 μL; gDNA Eraser 1 μL; total RNA 500 ng; RNase Free dH_2O added up to 10 μL; at 42°C for 2 min; PrimeScriptRT Enzyme Mix I 1 μL, RT Primer Mix 4 μL, 5 × PrimeScript Buffer 4 μL, RNase Free dH_2O 1 μL were then added to the above reaction liquid at 37°C for 15 min, 85°C at 5 s, and then kept at 4°C and diluted five times before use.

The primers for fluorescence quantification were designed according to the ORF region of insulin-like growth factor binding protein 7 (*IGFBP7*) and α2- Adrenoceptor (*a2ADR*); the sequence of each primer is given in **Table 1**. The reaction system had a volume of 20 μL, comprising 2 × TB Green TM Premix Ex Taq TM (Takara, Japan) 10 μL; forward primer (10 μM) 0.6 μL, reverse primer (10 μM) 0.6 μL, cDNA template 1.6 μL, and dH_2O 7.2 μL. The samples were mixed in a PCR tube for amplification, under the following reaction conditions: initial denaturation at 94°C for 30 s; under the cycling conditions: 94°C for 5 s, 60°C for 30 s, with 40 cycles in total; the dissolution curve was analyzed at the end of the experiment. For individual RNA samples and genes, all PCR analyses were set with three replicates. The target gene mRNA level was calibrated by using the real-time PCR Ct ($2^{-\Delta\ \Delta\ Ct}$) relative quantitative method, with the reference gene β-actin treated as the quantitative standard.

Outcome Calculations

Outcomes were calculated as follows:

Hatching rate = (number of trochophore larvae within the field of view/total number of fertilized eggs within the field of view) × 100%.

Abnormality rate = (number of deformed embryos within the field of view/total number of fertilized eggs within the field of view) × 100%.

TABLE 1 | Oligonucleotide primers used in qRT-PCR.

Gene	Sequence (5′-3′)	Efficiency (%)	Size (bp)	References
IGFBP7	F: CCCTTGCACCAGGCTTAGCCT R: GAACTCCTCCCAATTCCCG	99.26	173	MT345605.1
α2ADR	F: CCGCTTTCTTAGTCCCGCA R: GAACCGGTAACCGTCTTCCGTTA	101.75	193	MZ359214
β-*Actin*	F: CCACTTGGTCCATTTCG R: GGACTGGATTTCCGGCCA	100.46	162	MW387000

IGFBP7, insulin-like growth factor binding protein 7; α2ADR, α2- Adrenoceptor; F, Forward primer; R, Reverse primer.

Survival rate = (total number of trochophores/number of larvae about to enter the metamorphosis stage).

Settlement and metamorphosis rate = (number of juvenile abalones on polythene membranes/number of planktonic larvae) × 100%.

Statistical Analysis

Data were expressed as the mean ± standard deviation. Logarithmic transformation was performed on data relating to hatching rate, abnormality rate, metamorphosis rate, and survival rate, to the extent that the homogeneity test of variance and the standard normal distribution were satisfied. Comparative analysis of the effects of flow velocity on the larval hatching rate, survival, biochemical composition, and metamorphosis-related gene expression levels was performed using SPSS18.0 coupled with one-way ANOVA and Tukey multiple comparisons, with $P < 0.05$ being significant.

RESULTS

Water Quality Monitoring

Under different flow velocities, there was no significant difference in the temperature, dissolved oxygen concentration, salinity, pH, and NO_3-N concentration of the water body (**Table 2**). In the control group, the TAN-N and NO_2-N concentrations were significantly higher than in any other velocity group ($P < 0.05$). By contrast, there was no significant difference in the concentrations of TAN-N and NO_2-N among the velocity groups ($P > 0.05$).

Hatching and Abnormality Rates

The larval hatching rate varied significantly under different velocities. No significant difference was identified in larval hatching rate between the 0, 5, and 10 L/h groups, but each was significantly higher than that in the 40 L/h group (**Figure 2A**, $P < 0.05$). The larval abnormality rate tended to increase as the flow velocity increased (**Figure 2B**). At 20 L/h, even though the larval abnormality rate was significantly higher than that in the 0, 5, or 10 L/h groups, it was significantly lower than that in the 40 L/h group ($P < 0.05$).

Survival Rate and Metamorphosis Rate

Velocity had significant effects on the larval survival and metamorphosis rates. When the flow velocity increased to 40 L/h, the larval survival rate and metamorphosis rate were significantly lower than in the 0, 5 and 10 L/h groups (**Figures 2C,D**, $P < 0.05$). Even though no significant difference was identified in the larval survival rate and metamorphosis rate between the 0, 5 and 10 L/h groups, each was significantly higher than that in the 20 L/h group ($P < 0.05$).

Larval Size

No significant difference was identified in larval sizes at the formation of the secondary shell stage among the 0, 5, 10, and 20 L/h groups, whereas larval sizes in 5, 10 L/h group

TABLE 2 | Effects of flow velocity on water quality parameters based on one-way ANOVA.

Flow velocity (L/h)	Water quality parameters						
	Temperature (°C)	Salinity	pH	DO (mg/L)	TAN-N (mg/L)	NO_2-N (mg/L)	NO_3-N (mg/L)
0	18.08 ± 0.12	31.28 ± 1.98	7.81 ± 0.17	6.51 ± 0.38	0.037 ± 0.016[a]	0.005 ± 0.001[a]	0.982 ± 0.064
5	17.98 ± 0.10	30.71 ± 2.03	7.75 ± 0.12	6.58 ± 0.49	0.025 ± 0.009[b]	0.003 ± 0.001[b]	0.965 ± 0.082
10	17.84 ± 0.31	30.09 ± 1.64	7.79 ± 0.25	6.54 ± 0.57	0.022 ± 0.015[b]	0.002 ± 0.002[b]	0.953 ± 0.051
20	18.02 ± 0.27	31.25 ± 1.47	7.75 ± 0.20	6.61 ± 0.44	0.020 ± 0.013[b]	0.002 ± 0.001[b]	0.965 ± 0.068
40	18.05 ± 0.22	31.16 ± 2.15	7.80 ± 0.24	6.68 ± 0.27	0.019 ± 0.011[b]	0.002 ± 0.001[b]	0.977 ± 0.032

Data are represented as mean ± SD (n = 4). Different superscripted lowercase letters within the same column indicate significant differences between flow velocities ($P < 0.05$).
DO, dissolved oxygen; TAN-N, total nitrogen; NO_2-N, nitrite nitrogen; NO_3-N, nitrate nitrogen.

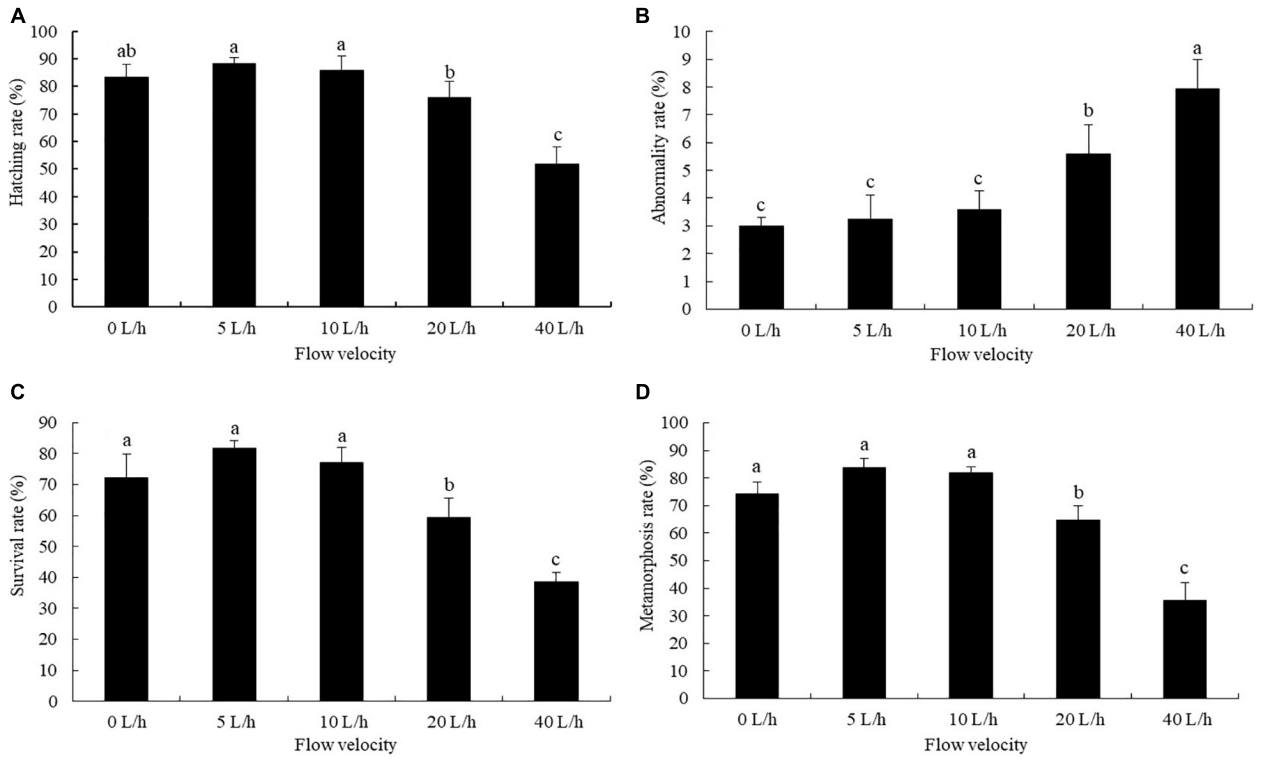

FIGURE 2 | Effects of flow velocity on the hatching rate **(A)**, abnormality rate **(B)**, survival rate **(C)**, and metamorphosis rate **(D)** of Pacific abalone *H. discus hannai* larvae. Values are means and standard deviation of four replicates (means ± SD; $n = 4$). Significant variations were found by one-way analysis of variance, $P < 0.05$, followed by Tukey test. Different letters denote significant differences between flow velocities.

were significantly smaller than in the 40 L/h group (**Table 3**, $P < 0.05$). The size at metamorphosis varied significantly at different velocities. Larval size in the 20 and 40 L/h groups was significantly higher than in any other group ($P < 0.05$). The time required for the larval metamorphosis in the 5 and 10 L/h groups was significantly shorter than in any other flow velocity group ($P < 0.05$). The time required for larval metamorphosis was longest in the 40 L/h group, but was not significantly different from that in the 20 L/h group ($P > 0.05$).

Biochemical Composition

No significant differences were identified in larval protein content among the velocity groups (**Table 4**, $P > 0.05$). The larval TG content in the 5 and 10 L/h groups was significantly higher than in any other group ($P < 0.05$), being lowest in the 20 L/h group. Velocity had significant effects on the larval lactic acid content. No significant difference was identified in larval lactic acid content among the 0, 5, and 10 L/h groups, but each was significantly lower than in the 40 L/h group ($P < 0.05$). The larval ATP content also increased with flow velocity, with the 5 L/h group having the lowest ATP content, whereas the ATP content in the 40 L/h group was significantly higher than in the 0, 5, and 10 L/h groups ($P < 0.05$). No significant difference was identified in larval glycogen content in the 0, 5, 10, or 20 L/h groups, but was significantly reduced when the velocity increased to 40 L/h ($P < 0.05$).

TABLE 3 | Performance of *H. discus hannai* larvae from completion of larvae shell to metamorphosis according to flow velocities.

Flow velocity (L/h)	Completion of larvae shell (shell length × shell width, μm)	Metamorphosis size (shell length × shell width, μm)	Metamorphosis time (h)
0	$261.11 \pm 4.34 \times 206.65 \pm 5.98^{ab}$	$381.49 \pm 4.86 \times 269.57 \pm 6.43^{b}$	28.57 ± 0.73^{b}
5	$255.33 \pm 4.92 \times 203.75 \pm 6.67^{b}$	$372.51 \pm 6.61 \times 260.54 \pm 7.79^{b}$	10.92 ± 0.41^{c}
10	$251.69 \pm 6.05 \times 201.67 \pm 5.01^{b}$	$375.30 \pm 8.97 \times 262.13 \pm 4.39^{b}$	22.46 ± 0.33^{c}
20	$266.75 \pm 7.36 \times 208.77 \pm 7.59^{ab}$	$405.41 \pm 5.55 \times 287.17 \pm 8.39^{a}$	33.79 ± 0.29^{a}
40	$272.58 \pm 4.98 \times 214.02 \pm 6.15^{a}$	$410.56 \pm 8.02 \times 291.05 \pm 5.08^{a}$	36.85 ± 0.62^{a}

Data are represented as mean ± SD (n = 4). Different superscripted lowercase letters within the same column indicate significant differences between flow velocities ($P < 0.05$).

TABLE 4 | Biochemical content of *H. discus hannai* larvae, reared under different flow velocities.

Variable	Flow velocity				
	0 L/h	5 L/h	10 L/h	20 L/h	40 L/h
Protein content (g/L)	0.98 ± 0.05^{a}	1.06 ± 0.05^{a}	1.01 ± 0.08^{a}	0.97 ± 0.07^{a}	1.04 ± 0.07^{a}
Lactic acid content (mmol/g prot)	0.076 ± 0.008^{b}	0.072 ± 0.006^{b}	0.078 ± 0.006^{b}	0.089 ± 0.007^{ab}	0.107 ± 0.010^{a}
Triglyceride (mmol/g prot)	0.83 ± 0.04^{b}	0.90 ± 0.07^{a}	0.88 ± 0.05^{a}	0.69 ± 0.07^{c}	0.80 ± 0.02^{b}
ATP (μmol/g prot)	229.38 ± 9.62^{b}	192.07 ± 7.33^{c}	199.44 ± 7.06^{c}	263.56 ± 8.65^{a}	277.05 ± 5.93^{a}
Glycogen (mg/g)	1.22 ± 0.04^{a}	1.13 ± 0.08^{a}	1.25 ± 0.02^{a}	1.17 ± 0.04^{a}	0.83 ± 0.06^{b}

Data are represented as mean ± SD (n = 4). Different superscripted lowercase letters within the same row indicate significant differences between flow velocities ($P < 0.05$).

Metabolic Enzyme Activity

Larval HK activity varied significantly at different velocities, gradually increasing with increasing flow velocity (**Table 5**). Larval HK activity in the 40 L/h group was significantly higher than in any other group ($P < 0.05$). The PK activity also followed a similar pattern, peaking in the 40 L/h group but not being significantly different across any other group. At 20 L/h, the larval SDH and MDH activities peaked, and then dropped significantly when the velocity increased to 40 L/h ($P < 0.05$). By contrast, the larval SDH activity in the 40 L/h group was significantly higher than in the 0, 5, and 10 L/h groups ($P < 0.05$). Flow velocity also had significant effects on larval LDH activity, which was significantly higher in the 40 L/h group compared with any other group ($P < 0.05$), although no significant differences were identified among the other velocity groups.

Gene Expression

The expression levels of *IGFBP7* varied significantly at different flow velocities, being significantly higher in the 10 L/h group than in the 40 L/h group, with no significant differences identified compared with any other velocity group (**Figure 3**, $P > 0.05$). No significant difference was identified in the expression levels of *a2ADR* between the 5, 10, and 20 L/h groups, although its expression levels in all three groups were significantly higher than in either the 0 or 40 L/h groups ($P < 0.05$).

DISCUSSION

Most marine invertebrates have a planktonic life-history stage, which can persist for an extended period of time until the most suitable substrate is found; thus, settlement by invertebrate larvae is seen as a passive delivery process to the surface (Abelson and Denny, 1997) with an active behavioral component once at the surface and possible active components in the water column (Harvey and Bourget, 1997; Walters et al., 1999). Thus, hydrodynamic force is also considered to be an external factor impacting larval settlement (Welch et al., 1999). Abalones reside on the bottom of coral reefs or in rock cracks. Their larvae usually adhere to the uneven sand surface, where the sedimentation process will be always affected by the flow of seawater (Boxshall, 2000; Wassnig et al., 2010). During aquacultural rearing, stable water flows avoid fertilized eggs from densely accumulating in particular areas of the rearing pond (Wu and Zhang, 2013). Thus, in the current study, five sets of recirculating water systems suitable for dense rearing of larvae were designed that not only simulated various water flow states, but also maintained a stable water temperature and salinity level. The larval hatching and survival rate in the recirculating water system were higher than in traditional still water rearing systems. With water quality indicators monitored, no significant differences in dissolved oxygen, NO_2-N, and NO_3-N concentrations under the recirculating water systems were found among the groups. The concentration of TAN-N and NO_2-N in the control group was significantly higher than in each velocity group. In still water aquaculture systems, some dead eggs and larvae are likely to accumulate, which could provide a natural medium for the growth of bacteria; and dead larvae would also lead to a higher concentration of TAN-N and NO_2-N in still water as a result of bacterial decomposition. In the recirculating aquaculture system, the measures taken to clean the filter cotton and add a UV disinfection lamp not only removed water contaminants to prevent the water quality from deterioration, but also suppressed the proliferation of harmful

TABLE 5 | Effect of flow velocity on the activity of metabolic enzymes of *H. discus hannai* larvae.

Variable	Flow velocity				
	0 L/h	5 L/h	10 L/h	20 L/h	40 L/h
Hexokinase (HK) (U/g prot)	12.17 ± 0.51^{c}	11.11 ± 0.37^{c}	10.08 ± 0.48^{c}	14.89 ± 0.26^{b}	18.89 ± 0.64^{a}
Pyruvate kinase (PK) (U/g prot)	7.15 ± 0.42^{b}	7.24 ± 0.22^{b}	6.99 ± 0.41^{b}	7.07 ± 0.53^{b}	9.93 ± 0.32^{a}
Succinate dehydrogenase (SDH) (U/mg prot)	3.38 ± 0.21^{c}	4.02 ± 0.34^{c}	3.79 ± 0.27^{c}	6.81 ± 0.19^{a}	5.07 ± 0.24^{b}
Malate dehydrogenase (MDH) (U/mg prot)	8.02 ± 0.73^{b}	7.62 ± 0.55^{b}	7.27 ± 0.40^{b}	9.15 ± 0.37^{a}	7.94 ± 0.53^{b}
Lactate dehydrogenase (LDH) (U/g prot)	2.45 ± 0.19^{b}	2.92 ± 0.28^{b}	2.07 ± 0.15^{b}	3.15 ± 0.18^{b}	5.47 ± 0.14^{a}

Data are represented as mean ± SD (n = 4). Different superscripted lowercase letters within the same row indicate significant differences between flow velocities (P < 0.05).

bacteria to maintain a stable aquaculture water quality. In water, NO_2-N is an intermediate product of ammonia nitrification resulting from the breakdown of aquatic organisms. Its ongoing accumulation in water impacts the physiological conditions of rearing organisms and can suppress their growth, resulting in higher mortality (Harris et al., 1998). The concentration of NO_2-N in each group did not exceed 0.1 mg/L, a level within the normal safe concentration tolerance of abalone (Kim et al., 2000); however, the decomposition products from dead larvae could not be readily removed, even though the cyclic accumulation in water is one of the crucial factors resulting in higher concentrations of NO_2-N and lower larval hatching and survival rates in the control group.

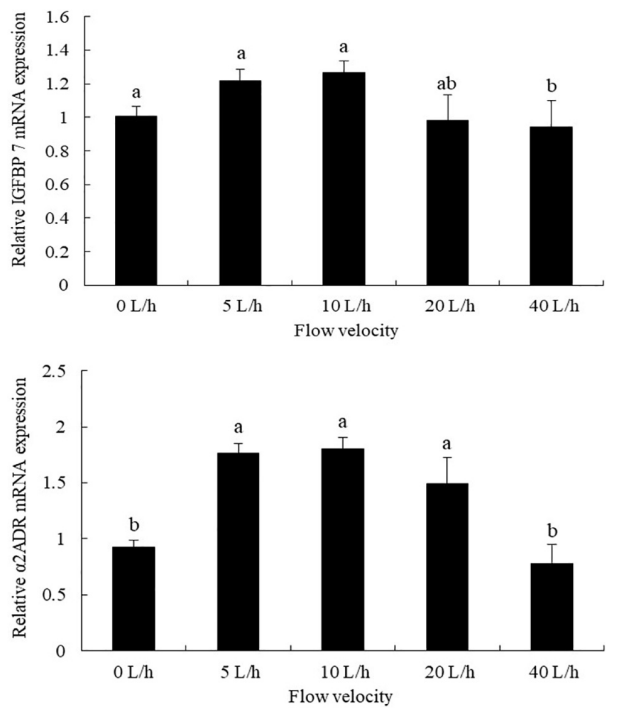

FIGURE 3 | Effects of flow velocity on the relative expression of *IGFBP7* (insulin-like growth factor binding protein 7) and *α2ADR* (α2-Adrenoceptor) in Pacific abalone *H. discus hannai* larvae. Values are means and standard deviation of four replicates (means ± SD; *n* = 4). Significant variations were found by one-way analysis of variance, $P < 0.05$, followed by Tukey test. Different letters denote significant differences between flow velocities.

The size upon completion of larval shell development and at metamorphosis in the 20 and 40 L/h groups were significantly higher than in any other group, but the metamorphosis and survival rates were decreased. Such an extended planktonic period could cause larvae to use more yolk nutrition for their growth, resulting in a greater size at larval metamorphosis. The energy available for larvae would reduce during metamorphosis, resulting in a decline of metamorphosis rate. In addition, the flow velocity at 20 L/h and 40 L/h might also cause stress to larvae. Thus, some energy would be used to resist such an unfavorable environment, further reducing the energy available for metamorphosis. Previous research showed that an extended planktonic stage leads to adverse effects on the survival and growth of juvenile mollusks (Pechenik and Rice, 2001; Huchette et al., 2003). Especially for larval abalone, which rely on yolk nutrition, an extended planktonic stage would deplete yolk nutrients, resulting in declining survival and growth rates of juvenile abalone (Marshall, 2008; Dineshram et al., 2013). Given that the culture water was not subject to disturbance before larval hatching in the control group, a lack of water flow could lead to a higher likelihood of mutual adhesion of fertilized eggs. Under the microscope, normally developed eggs adhering to dead eggs were observed in the control group. During adhesion, the increased mucus secretions will also impact normally developed fertilized eggs nearby, causing the larval hatching and survival rates in the control group to be significantly lower than in the recirculating water groups. It was also noted that the higher velocity was accompanied by a lower larval hatching rate and higher deformity rate. A possible reason is that the rapid water flow interferes with the normal development of fertilized eggs, impeding the formation of the ciliary band and increasing the deformity rate. Overly high velocity might also impact the formation of veliger larvae and cilia movement. Once the autonomous movement of larvae is completely altered as a response to the impact from high velocity, the energy stored in larvae would be gradually consumed, eventually leading to higher mortality. Thus, the flow velocity should be selected so that fertilized eggs would be evenly distributed as possible; larvae would then be able to move autonomously with the lowest-possible energy expenditure through the water, enabling more energy to be derived from the yolk nutrition for metamorphosis.

Although animals can acquire energy from the decomposition of various energy substances, most energy sources come from the consumption of protein, fat, and carbohydrates (Lauff and Wood, 1997; Kieffer et al., 1998; Weber, 2011). Larval attachment and metamorphosis both require abundant energy, most of which comes from the yolk nutrients (Roberts et al., 2001). The content of TG in larvae in the 20 L/h group was significantly lower than that in any other velocity group, suggesting that this higher velocity leads to higher energy demands of larvae. However, no significant difference was identified in the TG content between the control and 40 L/h groups, although the glycogen content in the latter was significantly lower than in the former, suggesting that energy sources delivered to larvae came from the conversion of TG to glycogen after the flow velocity increased. No significant difference was found in the protein content among the groups, suggesting that larvae had not utilized energy in the form of protein metabolism. Previous work revealed that shrimps make use of carbohydrates and TGs in different amounts. Li et al. (2019) found that at 3 cm/s, *Fenneropenaeus chinensis* depends on energy delivered from the decomposition of TG in muscles; at a velocity over 3 cm/s, the glycogen in muscles begins to be used as the primary substance for energy delivery, which is associated with the oxygen supply. Compared with glycogen, TG has a higher calorific value and can release more energy after following complete oxidation and decomposition (Livesey and Elia, 1988). In the current study, no significant difference was found in the dissolved oxygen concentration among the velocity groups. However, when the velocity increased to 40 L/h, the water flow impact might deprive the larvae from having control of their own movement. While resisting the water flow, a drastic increase in oxygen consumption might be a limiting factor to their growth. Compared with fat, glycogen would consume less oxygen for the production of ATP with the same molecular weight (Li et al., 2015). Thus, the energy available to larvae in the 40 L/h group is likely to have come from the conversion of TG to glycogen. At this velocity, the content of glycogen was significantly reduced compared with the 20 L/h group. Despite an increase in ATP content, the energy from the decomposition of glycogen might not satisfy the energy needs of larvae to cope with the impact of the increased water flow.

The energy metabolism balance of aquatic organisms can be negatively affected by the external and nutritional environment, given that they might require extra energy to relieve such stress (Boeck et al., 2006; Xu et al., 2015, 2016). Intensified sugar metabolism is a regular response to stress. Hexokinase and pyruvate kinase are the key rate-limiting enzymes in glycolysis, and variation in their activity has a significant role in regulating sugar metabolism, indicating the level of glycolysis (Van Aardt and Wolmarans, 1987). In the 40 L/h group, the HK and PK activity was significantly higher than in any other group, with the activity of HK gradually increasing with the flow velocity, suggesting that larvae produced more energy by increasing glycolysis. A higher rate of glycolysis facilitates the production of ATP and improves tolerance against stress (Laiz-Carrión et al., 2002). Gao et al. (2017) found that, as salinity decreased from 30 to 20‰, the activity of HK and PK in the liver of *H. discus hannai* increased; under a low salinity level, the liver accelerated the phosphorylation of glucose to promote glucose transformation and speed up glycolysis, thereby delivering energy to the tissues. SDH is the only enzyme embedded in the inner membrane of mitochondria in the TCA cycle. Oxaloacetate, as the product catalyzed by malate dehydrogenase, is one of the initiators of the TCA cycle. To a certain extent, two kinds of enzyme can represent the rate of the TCA cycle and the level of aerobic metabolism (Lussey-Lepoutre et al., 2015; Akila et al., 2016). Panepucci et al. (2000) reported that MDH acts as a carbon source and provides oxaloacetate for the TCA cycle, resulting in an additional 32 ATP molecules per glucose molecule oxidized. In the current study, the activity of SDH and MDH in the 20 L/h group was significantly higher than in any other group, whereas the ATP content in this group was also significantly higher than in the 0, 5, and 10 L/h groups. When the velocity increased to 40 L/h, the activity of SDH and MDH decreased significantly, suggesting that the activity of the TCA cycle was also reduced and aerobic metabolism suppressed. At this point, the activity of LDH significantly increase and the lactic acid content also peaked, implying that the energy delivery began to switch from aerobic to anaerobic metabolism, with the latter becoming the primary energy source for the larvae. Exposure of *Litopenaeus vannamei* to moderate hypoxia resulted in the accumulation of lactic acid and higher glucose content in hemolymph and muscle tissues, suggesting that anaerobic metabolism was increased (Soñanez-Organis et al., 2010). As a crucial glycolytic enzyme, lactate dehydrogenase appears to be more important when larvae need extra energy under stress (Gao et al., 2018). Especially in the 40 L/h group, an increase in the activity of lactate dehydrogenase caused the ATP content of larvae to peak. At this point, the content of glycogen further decreased, suggesting that the energy demand had increased in response to the high velocity; larvae began to utilize anaerobic metabolism to release more energy to satisfy the increased energy demand. As the direct supplier of biological energy, ATP is the main indicator of biological activity. When the salinity dropped suddenly from 56 to 52‰ and 48‰, the ATP content increased significantly in *L. vannamei*, suggesting that an extra energy supply was needed under the sudden change in salinity, thereby releasing a large amount of ATP (Shen et al., 2020). Once excessively accumulated, lactic acid as the by-product of anaerobic glycolysis would not only maintain the activity of glycolytic enzymes at a lower level, but also damage organs and tissues (Brizel et al., 2001; Zenteno-Savín et al., 2006). In the current study, as lactic acid increased, the larval survival rate in 40 L/h was significantly lower than that any other group, suggesting the accumulation of lactic acid adversely impacted the survival of the larvae.

Insulin-like growth factor binding protein 7 (IGFBP7) is a member of the IGFBP family. Overexpression of IGFBP7 in the MDA-MB-468 cell line significantly suppressed cell growth. IGFBP7 can also prevent the phosphorylation of mitogen-activated protein kinase (MAPK) ERK-1/2, resulting in weakening of the pathway signal, suggesting that IGFBP7 regulates cell growth by affecting this signaling pathway (Amemiya et al., 2011). IGFBP7 has biological functions and expression patterns that depend upon the diversity of cell types, which regulate cell growth and proliferation both positively and

negatively (Hwa et al., 1999). During the metamorphosis of *Haliotis diversicolor*, larvae shed the velum, the gills and feet gradually grow in size, and peristomal shell formation begins (Bishop et al., 2006; Heyland and Moroz, 2006). During the early larval period, *saIGFBP7* can promote the transition of larvae from a planktonic state to benthic life by upregulating the expression of growth-related genes and hormones (Wang et al., 2015). Wang et al. (2016) found that *IGFBP7* was engaged in the proliferation and differentiation of the mantle and foot cells of *H. diversicolor*. When the expression levels of *IGFBP7* were altered, the larval mortality rate significantly increased, whereas the settlement rate significantly dropped over 4 h. In the current study, the expression levels of *IGFBP7* in the 40 L/h group decreased significantly, as did the larval metamorphosis rate, suggesting that larval development can be predicted based on changes in the expression levels of *IGFBP7*; a longer planktonic duration would reduce the nutrients available from the yolk, and the energy ultimately required for the completion of metamorphosis. Thus, an appropriate of flow velocity range would be essential for the synchronous and rapid completion of larval metamorphosis in this species.

Numerous neurotransmitters are involved in the metamorphosis of larval shellfish. For example, Coon and Bonar (1987) found that alpha 1-adrenoceptor is involved in the metamorphosis of *Crassostrea gigas*. Epinephrine has been proven to induce the larval metamorphosis of *Venerupis pullastra* and *Ruditapes philippinarum* (García-Lavandeira et al., 2005). In research related to *Crassostrea angulate*, epinephrine was found to induce metamorphosis and alpha 1-adrenoceptor had higher expression levels (Yang et al., 2012). In the current study, the expression levels of *α2ADR* in the 0 and 40 L/h groups were significantly lower than in any other group, suggesting that flow velocity had significant effects on larval metamorphosis; the larval metamorphosis rate was higher at more appropriate velocities (5 and 10 L/h), whereas the expression levels of *a2ADR* in the 5 and 10 L/h group were also significantly higher than in the 0 and 40 L/h groups, suggesting that the expression levels of *a2ADR* are closely associated with larval metamorphosis. In the 5 and 10 L/h groups, the time required for larval metamorphosis shortened significantly, suggesting that the larvae would be less likely to consume all the yolk nutrients and would also face a reduced risk from any abrupt changes in the environment that might occur during metamorphosis, compared with if the period of metamorphosis was extended.

In the current study, the larval hatching rate, survival rate, and metamorphosis rate increased when the flow velocity was kept to 5–10 L/h. In the control group, a lack of water flow before larvae developed to the trochophore stage led to the mutual adhesion of fertilized eggs and their local accumulation; when dead eggs were recorded, the water quality also deteriorated, and the higher concentration of TAN and NO_2-N might be the main reason for the lower survival rate of the larvae. Larval density can be reduced to avoid their accumulation, but the presence of unfertilized eggs and dead larvae consistently impacts the stability of the aquaculture water environment, in that no water is exchanged before larval metamorphosis in conventional aquaculture systems. When the flow velocity increased to 40 L/h, despite the increase in the dissolved oxygen concentration and the decrease in TAN concentration, the impact of this rapid flow switched the mode of larval energy metabolism from aerobic to anaerobic metabolism, and the primary source of energy also shifted from TG to glycogen. Under these circumstances, the planktonic stage of larvae was prolonged and more energy was consumed, eventually reducing the amount of energy available for completion of metamorphosis and, thus, the larval metamorphosis rate. Therefore, future upflow larval rearing systems could be designed for *H. discus hannai* that maintain the quality of the rearing water and the velocity range at 5–10 L/h, which would not only reduce the adhesion of fertilized eggs and dead eggs and the energy consumption of larvae during metamorphosis, but also increase the larval metamorphosis rate and synchronization of metamorphosis, improving the aquaculture of this species as well as our understanding of its larval development.

DATA AVAILABILITY STATEMENT

All data generated or analyzed in this study are included in this published article.

ETHICS STATEMENT

This animal study was reviewed and approved by the Animal Welfare Committee of the College of Ocean & Earth Sciences, Xiamen University (permit no. COES-0001).

AUTHOR CONTRIBUTIONS

WY and XG conceptualized the study. MZ, ML, and SL conducted research and collected the data. XL and WY provided the materials and interpreted the data. MZ and XG wrote the manuscript. WY and CK had primary responsibility for the final content. All authors read and approved the final manuscript.

FUNDING

This research was supported by grants from the Chinese Ministry of Science and Technology through the Fujian Key S&T Project (No. 2020NZ08003 and 2019N0001), the Fujian Marine Economic Development Fund Project (FJHJF-L-2020-7), and Earmarked fund for the Modern Agro-industry Technology Research System (CARS-49).

ACKNOWLEDGMENTS

We would like to thank Chengyun Li and Jianxiong Li for their assistance with abalone collection and rearing.

REFERENCES

Abelson, A., and Denny, M. (1997). Settlement of marine organisms in flow. *Annu. Rev. Ecol. Evol. Syst*. 28, 317–339. doi: 10.1146/ANNUREV.ECOLSYS.28.1.317

Akila, P., Asaikumar, L., and Vennila, L. (2016). Chlorogenic acid ameliorates isoproterenol-induced myocardial injury in rats by stabilizing mitochondrial and lysosomal enzymes. *Biomed. Pharmacother*. 85, 582–591. doi: 10.1016/j.biopha.2016.11.067

Amemiya, Y., Yang, W., Benatar, T., Nofech-Mozes, S., Yee, A., Kahn, H., et al. (2011). Insulin like growth factor binding protein-7 reduces growth of human breast cancer cells and xenografted tumors. *Breast Cancer Res. Treat*. 126, 373–384. doi: 10.1007/s10549-010-0921-0

Bao, J., Li, X., Yu, H., and Jiang, H. (2018). Respiratory metabolism responses of Chinese mitten crab, *Eriocheir sinensis* and Chinese grass shrimp, *Palaemonetes sinensis*, subjected to environmental hypoxia stress. *Front. Physiol*. 9:1559. doi: 10.3389/fphys.2018.01559

Bishop, C. D., Erezyilmaz, D. F., Flatt, T., Georgiou, C. D., Hadfield, M. G., Heyland, A., et al. (2006). What is metamorphosis? *Integr. Comp. Biol*. 46, 655–661. doi: 10.1093/icb/icl004

Boeck, G. D., Ven, K. V. D., Hattink, J., and Blust, R. (2006). Swimming performance and energy metabolism of rainbow trout, common carp and gibel carp respond differently to sublethal copper exposure. *Aquat. Toxicol*. 80, 92–100. doi: 10.1016/j.aquatox.2006.07.017

Boxshall, A. J. (2000). The importance of flow and settlement cues to larvae of the abalone, *Haliotis rufescens Swainson*. *J. Exp. Mar. Biol. Ecol*. 254, 143–167. doi: 10.1016/S0022-0981(00)00274-4

Brizel, D. M., Schroeder, T., Scher, R. L., Walenta, S., Clough, R. W., Dewhirst, M. W., et al. (2001). Elevated tumor lactate concentrations predict for an increased risk of metastases in head-and-neck cancer. *Int. J. Radiat. Oncol*. 51, 349–353. doi: 10.1016/s0360-3016(01)01630-3

China Bureau of Fisheries (2021). *China Fisheries Yearbook in 2020*. Beijing: Agricultural Press of China.

Coon, S. L., and Bonar, D. B. (1987). Pharmacological evidence that alpha$_1$-adrenoceptors mediate metamorphosis of the Pacific oyster, *Crassostrea gigas*. *Neurosciece* 23, 1169–1174. doi: 10.1016/0306-4522(87)90190-4

Dineshram, R., Thiyagarajan, V., Lane, A., Yu, Z., Shu, X., and Leung, P. T. Y. (2013). Elevated CO_2 alters larval proteome and its phosphorylation status in the commercial oyster, *Crassostrea hongkongensis*. *Mar. Biol*. 160, 2189–2205. doi: 10.1007/s00227-013-2176-x

Dong, W., Liu, Z., Qiu, L., Wang, W., Song, X., Wang, X., et al. (2017). The modulation role of serotonin in Pacific oyster *Crassostrea gigas* in response to air exposure. *Fish Shellfish Immun*. 62, 341–348. doi: 10.1016/j.fsi.2017.01.043

Ebert, E. E., and Houk, J. L. (1984). Elements and innovations in the cultivation of red abalone *Haliotis rufescens*. *Aquaculture* 39, 375–392. doi: 10.1016/0044-8486(84)90279-5

Friedrich, C. G. (1998). Physiology and genetics of sulfur-oxidizing bacteria. *Adv. Microb. Physiol*. 39, 235–289. doi: 10.1016/s0065-2911(08)60018-1

Gao, X., Li, X., Shi, C., Wu, F., Song, C., and Liu, Y. (2018). Effects of stocking density on growth, metabolism, and energy budget of *Haliotis discus hannai* Ino. *Aquaculture* 483, 84–95. doi: 10.1016/j.aquaculture.2017.09.045

Gao, X., Li, Y., Li, X., Wu, F., Song, C., and Liu, Y. (2017). The response and osmotic pressure regulation mechanism of *Haliotis discus hannai* (*Mollusca. Gastropoda*) to sudden salinity changes. *Hydrobiologia* 795, 181–198. doi: 10.1007/s10750-017-3129-z

Gao, X., Zhang, M., Li, X., Song, C., and Liu, Y. (2016). Effects of light quality and intensity on the growth, survival and metamorphosis of *Haliotis discus hannai* Ino larvae. *Aquac. Res*. 48, 1–14. doi: 10.1111/are.13164

García-Lavandeira, M., Silva, A., Abad, M., Pazos, A. J., Sánchez, J. L., and Pérez-Parallé, M. L. (2005). Effects of GABA and epinephrine on the settlement and metamorphosis of the larvae of four species of bivalve molluscs. *J. Exp. Mar. Biol. Ecol*. 316, 149–156. doi: 10.1016/j.jembe.2004.10.011

Harris, J. O., Maguire, G. B., Edwards, S., and Hindrum, S. M. (1998). Effect of ammonia on growth rate and oxygen consumption of juvenile greenlip abalone, *Haliotis laevigata* donovan. *Aquaculture* 160, 259–272. doi: 10.1016/S0044-8486(97)00249-4

Harvey, M., and Bourget, E. (1997). Recruitment of marine invertebrates onto arborescent epibenthic structures: active and passive processes acting at different spatial scales. *Mar. Ecol. Prog. Ser*. 153, 203–215. doi: 10.3354/meps153203

Heinrichs-Caldas, W., Campos, D. F., Paula-Silva, M. N., and Almeida-Val, V. M. F. (2019). Oxygen-dependent distinct expression of *hif-1α* gene in aerobic and anaerobic tissues of the Amazon Oscar, *Astronotus crassipinnis*. *Comp. Biochem. Phys. B* 227, 31–38. doi: 10.1016/j.cbpb.2018.08.011

Heyland, A., and Moroz, L. L. (2006). Signaling mechanisms underlying metamorphic transitions in animals. *Integr. Comp. Biol*. 46, 743–759. doi: 10.1093/icb/icl023

Huchette, S. M. H., Koh, C. S., and Day, R. W. (2003). The effects of density on the behaviour and growth of juvenile blacklip abalone (*Haliotis rubra*). *Aquacult. Int*. 11, 411–428. doi: 10.1023/B:AQUI.0000004194.85299.38

Hwa, V., Oh, Y., and Rosenfeld, R. G. (1999). The insulin-like growth factor-binding protein (IGFBP) superfamily. *Endocr. Rev*. 20, 761–787. doi: 10.1210/edrv.20.6.0382

Ivanina, A. V., Froelich, B., Williams, T., Sokolov, E. P., Oliver, J. D., and Sokolova, I. M. (2011). Interactive effects of cadmium and hypoxia on metabolic responses and bacterial loads of eastern oysters C*rassostrea virginica* Gmelin. *Chemosphere* 82, 377–389. doi: 10.1016/j.chemosphere.2010.09.075

Kieffer, J. D., Alsop, D., and Wood, C. M. (1998). A respirometric analysis of fuel use during aerobic swimming at different temperatures in rainbow trout (*Oncorhynchus mykiss*). *J. Exp. Biol*. 201, 3123–3133. doi: 10.1242/jeb.201.22.3123

Kim, S. K., Kong, I., Lee, B. H., Kang, L., Lee, M. G., and Suh, K. H. (2000). Removal of ammonium-N from a recirculation aquacultural system using an immobilized nitrifier. *Aquacult. Eng*. 21, 139–150. doi: 10.1016/S0144-8609(99)00026-6

Laiz-Carrión, R., Sangiao-Alvarellos, S., Guzmán, J. M., Martín del Río, M. P., Míguez, J. M., Soengas, J. L., et al. (2002). Energy metabolism in fish tissues related to osmoregulation and cortisol action. *Fish Physiol. Biochem*. 27, 179–188. doi: 10.1023/B:FISH.0000032725.96481.b8

Lauff, R. F., and Wood, C. M. (1997). Effects of training on respiratory gas exchange, nitrogenous waste excretion, and fuel usage during aerobic swimming in juvenile rainbow trout (*Oncorhynchus mykiss*). *Can. J. Fish Aquat. Sci*. 54, 566–571. doi: 10.1139/cjfas-54-3-566

Li, D., Wei, X., Lin, X., Xu, Z., and Mu, X. (2015). Effects of exercise training on carbohydrate and lipid catabolism in the swimming muscles of Nile tilapia (*Oreochromis niloticus*). *J. Anim. Physiol. Anim. Nutr*. 99, 893–898. doi: 10.1111/jpn.12300

Li, J., Xu, X., Li, W., and Zhang, X. (2019). Behavioural and physiological responses to low-and high-intensity locomotion in Chinese shrimp *Fenneropenaeus chinensis*. *J. Comp. Physiol. A Neuroethol. Sens. Neural Behav. Physiol*. 205, 87–102. doi: 10.1007/s00359-018-1306-9

Livesey, G., and Elia, M. (1988). Estimation of energy expenditure, net carbohydrate utilization, and net fat oxidation and synthesis by indirect calorimetry: evaluation of errors with special reference to the detailed composition of fuels. *Am. J. Clin. Nutr*. 47, 608–628. doi: 10.1093/ajcn/47.4.608

López-Patiño, M. A., Hernández-Pérez, J., Gesto, M., Librán-Pérez, M., Míguez, J. M., and Soengas, J. L. (2014). Short-term time course of liver metabolic response to acute handling stress in rainbow trout, *Oncorhynchus mykiss*. *Comp. Biochem. Phys. A Mol. Integr. Physiol*. 168, 40–49. doi: 10.1016/j.cbpa.2013.10.027

Lucas, M. I., Walker, G., Holland, D. L., and Crisp, D. J. (1979). An energy budget for the free-swimming and metamorphosing larvae of *Balanus balanoides* (*Crustacea: Cirripedia*). *Mar. Biol*. 55, 221–229. doi: 10.1007/BF00396822

Lussey-Lepoutre, C., Bellucci, A., Morin, A., Buffet, A., Amar, L., Janin, M., et al. (2015). In vivo detection of succinate by magnetic resonance spectroscopy as a hallmark of *SDH*x mutations in paraganglioma. *Clin. Cancer Res*. 22, 1120–1129. doi: 10.1158/1078-0432.CCR-15-1576

Maldonado, M., and Young, C. M. (1999). Effects of the duration of larval life on postlarval stages of the demosponge *Sigmadocia caerulea*. *J. Exp. Mar. Biol. Ecol*. 232, 9–21. doi: 10.1016/S0022-0981(98)00076-8

Manahan, D. T., and Crisp, D. J. (1983). Autoradiographic studies on the uptake of dissolved amino acids from sea water by bivalve larvae. *J. Mar. Biol. Assoc. U.K*. 63, 673–682. doi: 10.1017/S0025315400070983

Marshall, D. J. (2008). Transgenerational plasticity in the sea: context-dependent maternal effects across the life history. *Ecology* 89, 418–427. doi: 10.1890/07-0449.1

Marshall, D. J., Pechenik, J. A., and Keough, M. J. (2003). Larval activity levels and delayed metamorphosis affect post-larval performance in the colonial, ascidian *Diplosoma listerianum*. *Mar. Ecol. Prog. Ser.* 246, 153–162. doi: 10.3354/meps246153

Natalia, Y., Hashim, R., Ali, A., and Chong, A. (2004). Characterization of digestive enzymes in a carnivorous ornamental fish, the Asian bony tongue *Scleropages formosus* (Osteoglossidae). *Aquaculture* 233, 305–320. doi: 10.1016/j.aquaculture.2003.08.012

Panepucci, L., Fernandes, M. N., Sanches, J. R., and Rantin, F. T. (2000). Changes in lactate dehydrogenase and malate dehydrogenase activities during hypoxia and after temperature acclimation in the armored fish, *Rhinelepis strigose* (siluriformes, loricariidae). *Rev. Brasil. Biol.* 60, 353–360. doi: 10.1590/S003471082000000200021

Pechenik, J. A., and Rice, M. E. (2001). Influence of delayed metamorphosis on post settlement survival and growth in the sipunculan *Apionsoma misakianum*. *Invertebr. Biol.* 120, 50–57. doi: 10.2307/3227225

Reyes-Ramos, C. A., Peregrino-Uriarte, A. B., Cota-Ruiz, K., Valenzuela-Soto, E. M., Leyva-Carrillo, L. L., and Yepiz-Plascencia, G. (2018). Phosphoenolpyruvate carboxykinase cytosolic and mitochondrial isoforms are expressed and active during hypoxia in the white shrimp *Litopenaeus vannamei*. *Comp. Biochem. Phys. B Biochem. Mol. Biol.* 226, 1–9. doi: 10.1016/j.cbpb.2018.08.001

Roberts, R. D., Lapworth, C., and Barker, R. J. (2001). Effect of starvation on the growth and survival of post-larval abalone (*Haliotis iris*). *Aquaculture* 200, 323–338. doi: 10.1016/S0044-8486(01)00531-2

Shen, M., Cui, Y., Wang, R., Dong, T., Ye, H., Wang, S., et al. (2020). Acute response of Pacific white shrimp *Litopenaeus vannamei* to high-salinity reductions in osmosis-, metabolism-, and immune-related enzyme activities. *Aquacult. Int.* 28, 31–39. doi: 10.1007/s10499-019-00441-y

Shilling, F. M., and Manahan, D. T. (1990). Energetics of early development for the sea urchins *Strongylocentrotus purpuratus* and *Lytechinus pictus* and the crustacean *Artemia* sp. *Mar. Biol.* 106, 119–127. doi: 10.1007/BF02114682

Shilling, F. M., Hoegh-Guldberg, O., and Manahan, D. T. (1996). Sources of energy for increased metabolic demand during metamorphosis of the abalone *Haliotis rufescens* (mollusca). *Biol. Bull U.S.* 191, 402–412. doi: 10.2307/1543013

Soñanez-Organis, J. G., Racotta, I. S., and Yepiz-Plascencia, G. (2010). Silencing of the hypoxia inducible factor 1-HIF-1-obliterates the effects of hypoxia on glucose and lactate concentrations in a tissue-specific manner in the shrimp *Litopenaeus vannamei*. *J. Exp. Mar. Biol. Ecol.* 393, 51–58. doi: 10.1016/j.jembe.2010.06.031

Thiyagarajan, V., Pechenik, J. A., Gosselin, L. A., and Qian, P. Y. (2007). Juvenile growth in barnacles: combined effect of delayed metamorphosis and sub-lethal exposure of cyprids to low-salinity stress. *Mar. Ecol. Prog. Ser.* 344, 173–184. doi: 10.3354/meps06931

Van Aardt, W. J., and Wolmarans, C. T. (1987). Effects of anoxia on the haemolymph physiology and lactate concentrations in the freshwater crab *Potamon warreni* calman. *Comp. Biochem. Physiol.* 88, 671–675. doi: 10.1016/0300-9629(87)90681-5

Vicose, G. C. D., Viera, M. P., Bilbao, A., and Izquierdo, M. S. (2007). Embryonic and larval development of *Haliotis tuberculate coccinea* Reeve: an indexed micro-photographic sequence. *J. Shellfish Res.* 26, 847–854.

Walters, L. J., Miron, G., and Bourget, E. (1999). Endoscopic observations of invertebrate larval substratum exploration and settlement. *Mar. Ecol. Prog. Ser.* 182, 95–108. doi: 10.3354/meps182095

Wang, G., Li, N., Zhang, L., Zhang, L., Zhang, Z., and Wang, Y. (2016). IGFBP7 is involved in abalone metamorphosis. *Aquaculture* 415, 377–384. doi: 10.1016/j.aquaculture.2015.09.031

Wang, G., Li, N., Zhang, L., Zhang, L., Zhang, Z., and Wang, Y. (2015). IGFBP7 promotes hemocyte proliferation in small abalone *Haliotis diversicolor*, proved by dsRNA and cap mRNA exposure. *Gene* 571, 65–70. doi: 10.1016/j.gene.2015.06.051

Wang, G., Liu, B., Tang, B., Zhang, T., and Xiang, J. (2006). Pharmacological and immunocytochemical investigation of the role of catecholamines on larval metamorphosis by β-adrenergic-like receptor in the bivalve *Meretrix meretrix*. *Aquaculture* 258, 611–618. doi: 10.1016/j.aquaculture.2006.04.031

Wassnig, M., Roberts, R. D., Krsinich, A., and Day, R. W. (2010). Effects of water flow rate on growth rate, mortality and biomass return of abalone in slab tanks. *Aquac. Res.* 41, 839–846. doi: 10.1111/j.1365-2109.2009.02361.x

Weber, J. M. (2011). Metabolic fuels: regulating fluxes to select mix. *J. Exp. Biol.* 214, 286–294. doi: 10.1242/jeb.047050

Welch, J. M., Forward, R. B., and Howd, P. A. (1999). Behavioral responses of blue crab *Callinectes sapidus* postlarvae to turbulence: implications for selective tidal stream transport. *Mar. Ecol. Prog. Ser.* 179, 135–143. doi: 10.3354/meps179135

Williamson, J. E., Nys, R. D., Kumar, N., Carson, D. G., and Steinberg, P. D. (2000). Induction of metamorphosis in the sea urchin *Holopneustes purpurascens* by a metabolite complex from the algal host *Delisea pulchra*. *Biol. Bull.* 198, 332–345. doi: 10.2307/1542689

Wu, F., and Zhang, G. (2013). Suitability of cage culture for Pacific abalone *Haliotis discus hannai* Ino production in China. *Aquac. Res.* 44, 485–494. doi: 10.1111/j.1365-2109.2012.03185.x

Wu, F., and Zhang, G. (2016). Pacific abalone farming in china: recent innovations and challenges. *J. Shellfish Res.* 35, 703–710. doi: 10.2983/035.035.0317

Xu, Z., Gan, L., Li, T., Xu, C., Chen, K., Wang, X., et al. (2015). Transcriptome profiling and molecular pathway analysis of genes in association with salinity adaptation in Nile tilapia *Oreochromis niloticus*. *PLoS One* 10:e0136506. doi: 10.1371/journal.pone.0136506

Xu, Z., Li, T., Li, E., Chen, K., Ding, Z., Qin, J., et al. (2016). Comparative transcriptome analysis reveals molecular strategies of oriental river prawn *Macrobrachium nipponense* in response to acute and chronic nitrite stress. *Fish Shellfish Immun.* 48, 254–265. doi: 10.1016/j.fsi.2015.12.005

Yang, B., Qin, J., Shi, B., Han, G., Chen, J., Huang, H., et al. (2012). Molecular characterization and functional analysis of adrenergic like receptor during larval metamorphosis in *Crassostrea angulata*. *Aquaculture* 36, 54–61. doi: 10.1016/j.aquaculture.2012.08.040

Zenteno-Savín, T., Saldierna, R., and Ahuejote-Sandoval, M. (2006). Superoxide radical production in response to environmental hypoxia in cultured shrimp. *Comp. Biochem. Phys. C. Toxicol. Pharmacol.* 142, 301–308. doi: 10.1016/j.cbpc.2005.11.001

Zhou, J., Zhu, X., and Cai, Z. (2011). The impacts of bisphenol A (BPA) on abalone (*Haliotis diversicolor supertexta*) embryonic development. *Chemosphere* 82, 443–450. doi: 10.1016/j.chemosphere.2010.09.056

Conflict of Interest: The authors declare that the research was conducted in the absence of any commercial or financial relationships that could be construed as a potential conflict of interest.

Publisher's Note: All claims expressed in this article are solely those of the authors and do not necessarily represent those of their affiliated organizations, or those of the publisher, the editors and the reviewers. Any product that may be evaluated in this article, or claim that may be made by its manufacturer, is not guaranteed or endorsed by the publisher.

frontiers in Marine Science

ORIGINAL RESEARCH
published: 11 November 2021
doi: 10.3389/fmars.2021.774925

Diversity of Three Small Type's Giant Clams and Their Associated Endosymbiotic Symbiodiniaceae at Hainan and Xisha Islands, South China Sea

Qiqi Chao[1,2], Zhifeng Gu[1,2], Aimin Wang[1,2], Chunsheng Liu[1,2] and Yi Yang[1,2]**

[1] State Key Laboratory of Marine Resource Utilization in South China Sea, Hainan University, Haikou, China, [2] College of Marine Science, Hainan University, Haikou, China

Giant clams are found in a mutualistic association with Symbiodiniaceae dinoflagellates, however, the diversity of the giant clams, as well as the diversity and distribution of Symbiodiniaceae in different Tridacnine species remain relatively poorly studied in the South China Sea. In this study, a total of 100 giant clams belonging to small type's giant clams, *Tridacna maxima*, *T. crocea*, and *T. noae*, were collected from Hainan and Xisha Islands. Based on mtDNA cytochrome c oxidase subunit 1 gene (COI) and 16S rRNA fragments, *T. maxima* and *T. crocea* showed a closer phylogenetic relationship than *T. noae*. All the three species of giant clams hosted Symbiodiniaceae including genera *Symbiodinium* (formerly Clade A) and *Cladocopium* (formerly Clade C). Geographically, symbionts in *Cladocopium* are restricted to Xisha Islands, probably because *Cladocopium* prefers to inhabit in waters with higher mean temperatures. The endosymbiont specificity among the three giant clam species was also detected. *T. noae* and *T. crocea* are found to harbor *Symbiodinium* preferentially, compared with *Cladocopium*. These results could provide important information to understand various endosymbionts occurring in giant clams in the South China Sea.

Keywords: Tridacna, Symbiodiniaceae, symbiont, COI, 16S rRNA, ITS1

OPEN ACCESS

Edited by:
Liqiang Zhao,
Guangdong Ocean University, China

Reviewed by:
Gang Ni,
Ocean University of China, China
Yuehuan Zhang,
South China Sea Institute of Oceanology, Chinese Academy of Sciences (CAS), China

****Correspondence:***
Chunsheng Liu
lcs5113@163.com
Yi Yang
yiyangouc@outlook.com

Specialty section:
This article was submitted to Marine Fisheries, Aquaculture and Living Resources, a section of the journal Frontiers in Marine Science

Received: *13 September 2021*
Accepted: *12 October 2021*
Published: *11 November 2021*

Citation:
Chao Q, Gu Z, Wang A, Liu C and Yang Y (2021) Diversity of Three Small Type's Giant Clams and Their Associated Endosymbiotic Symbiodiniaceae at Hainan and Xisha Islands, South China Sea. Front. Mar. Sci. 8:774925. doi: 10.3389/fmars.2021.774925

INTRODUCTION

Giant clams (Tridacninae) inhabit tropical coral reefs throughout the Indo-Pacific oceans (Lucas, 2014). In the world, the Tridacninae subfamily includes two extant genera, Hippopus (two species) and Tridacna (10 extant species), and all these species host symbiotic zooxanthellae in the mantle tissues that plays important ecological roles in the coral reef ecosystem (Liu et al., 2021b). Recently, the natural resources of giant clams sharply decreased in many countries, including Australia, Indonesia, Singapore, Philippines, and Japan because of overfishing, habitat destruction, and global climate change (Copland and Lucas, 1988; Pringgenies et al., 1995; Neo and Todd, 2012; Neo et al., 2019). Therefore, all the giant clam species are listed in Appendix II of the Convention on International Trade in Endangered Species [United Nations Environment Programme-World Conservation Monitoring Center (UNEP-WCMC), 2007] and International Union for Conservation of Nature (IUCN) Red List of Threatened Species (Wells, 1997).

In China, giant clams are distributed mainly in the South China Sea, which can be divided into five geographical populations, Hainan Islands, Xisha Islands, Zhongsha Islands, Dongsha Islands, and Nansha Islands (Zhang et al., 2020). Eight giant clams have been reported in the South China Sea, including two large species *Tridacna gigas* and *T. derasa*; three middle species *T. squamosa*, *H. hippopus*, and *H. porcellanus*; and three small species *T. maxima*, *T. crocea*, and *T. noae* (Neo et al., 2017; Liu J. et al., 2020). Recent surveys found that large and middle type's giant clams were in extremely low numbers, and small type's giant clams became the dominant giant clam species (Liu et al., 2021a). However, the genetic and phenotypic variation in several giant clam species has been reported in many geographical locations (Nuryanto and Kochzius, 2009; Hui et al., 2016; Pappas et al., 2017), while there were only a few reports on the diversity of giant clams in the South China Sea (Lim et al., 2019; Liu J. et al., 2020).

Symbiodinium is found in endosymbiosis with marine invertebrates such as giant clams, corals, Porifera, and Foraminifera, which could provide their hosts with up to 100% of energy requirements (Stat et al., 2006; Venn et al., 2008; Reich et al., 2017). Since pediveliger larva stage, the symbiont between the giant clam and Symbiodinium is established (Liu C. et al., 2020; Zhang et al., 2020; Wang et al., 2021). The diversity and community structure of Symbiodiniaceae in the giant clam could hence likely affect the growth, reproduction, and photosynthetic efficiency of the host (DeBoer et al., 2012). According to the previous molecular taxonomic research, nine distinctive Symbiodinium clades (A to I) have been identified (Pochon and Gates, 2010). Each major clade could be further resolved into diverse genetic subclades through the use of highly variable DNA markers such as the nuclear ribosomal internal transcribed spacer (ITS) (Arif et al., 2014; Ikeda et al., 2017). Previous studies have shown that the diversity of endosymbiontic Symbiodiniaceae in host is influenced by numerous factors, such as host species, physiology of the hosts, and environmental factors (LaJeunesse et al., 2010, 2018; Hume et al., 2016; Pappas et al., 2017; Lim et al., 2019).

The aim of this study is to illustrate the diversity of three small type's giant clams (*T. maxima*, *T. crocea*, and *T. noae*) using the mtDNA cytochrome c oxidase subunit 1 gene (CO1) and 16S rRNA gene in Hainan and Xisha Islands. Furthermore, the diversity of their endosymbiontic Symbiodiniaceae is also identified using DNA barcoding based on ITS1 region of rDNA.

MATERIALS AND METHODS

Ethics Statement

All giant clams and experimental protocols used in this study were reviewed and approved by the committee and laboratory animal department of the Hainan University.

Samples and DNA Extraction

The small type's giant clam samples (*T. maxima*, *T. crocea*, and *T. noae*) were collected from the two different sites, the lagoon of Zhaoshu, Xisha (112° 12′–112° 19′ E, 16° 57′–16° 59′ N) and the coastal waters of Sanya, Hainan (including Dongmao-Ximao Island, Luhuitou Peninsula, Yalong Bay and Wuzhizhou Island, 109° 21′–109°46′ E, 18° 11′–18°19′ N) in the South China Sea in June and July, and coded as Xisha01-Xisha77 and Sanya01-Sanya23, respectively. Briefly, about 1 cm^2 mantle tissue was removed from each individual using sterile disposable razors and stored in 100% ethanol at 4°C.

A subsample of mantle tissue of size about 2 mm^2 was used for the DNA extraction that was conducted using Tiangen DNA kit (Tiangen Biotech, Beijing, China) according to the instructions of the manufacturer.

PCR Amplification and Sequencing

The COI, 16S, and ITS1 fragments of the giant clams and Symbiodiniaceae, respectively, were amplified by PCR, which were carried out in a total volume of 20 μl with 10 μl of 2 × Rapid Taq Master Mix (with Taq DNA polymerase, dNTP mix, $MgCl_2$, and PCR buffer), 0.6 μl each of forward and reverse primers (10 μM), 1 μl of DNA diluted 1:5, and 7.8 μl of water. The primers were shown in **Table 1**. PCR conditions were set as follows: an initial denaturing step at 94°C for 5 min; 40 cycles of denaturing at 94°C for 30 s, annealing at 43–53°C for 30 s, and extension at 72°C for 90 s; and a final extension step at 72°C for 10 min. PCR products were sequenced at BGI (China).

Sequence Alignment and Phylogenetic Analyses

The three fragments (COI, 16S, and ITS1) were aligned separately using Clustal W in MEGA X (Kumar et al., 2018). Sequences were converted into NEXUS format for phylogenetic analysis using DAMBE5 (Xia, 2013). Phylogenetic trees were reconstructed using Bayesian inference (BI; Huelsenbeck and Ronquist, 2001) in the CIPRES gateway (Miller et al., 2010). BI analyses were performed with MrBayes v.3.2.7 (Ronquist and Huelsenbeck, 2003), running four simultaneous Monte Carlo Markov chains (MCMC) for 10,000,000 generations, sampling every 1,000 generations and discarding the first 25% generations as burn-in. Two independent runs were performed to increase the chance of adequate mixing of the Markov chains and to increase the chance of detecting failure to converge, as determined by using Tracer v1.6. The effective sample size (ESS) of all the parameters was higher than 200. The resulting phylogenetic trees were visualized in FigTree v1.4.4.

Genetic Diversity and Population Structure

Population genetic analyses were conducted based on the COI and 16S fragments of three giant clams. Genetic diversity indices, including haplotype diversity (Hd) and nucleotide diversity (π), were calculated in DNASP 5 (Librado and Rozas, 2009). To investigate the genetic relationships among haplotypes, a median-joining network was generated with PopART 1.7 (Clement et al., 2000). To infer if the three giant clams have experienced population expansion, Tajima's D (Tajima, 1989) and Fu's Fs statistics (Fu, 1997) of COI sequences were calculated in Arlequin

TABLE 1 | Information of primers used in this study.

Gene	Primer	Sequences (5′–3′)	Length (bp)	Annealing Temperature (°C)	References
Giant clams					
COI	COI(F)	GGGTGATAATTCGAACAGAA	500	43	Nuryanto et al., 2007
	COI(R)	TAGTTAAAGCCCCAGCTAAA			
16S	16SarF	CGCCTGTTTATCAAAAACAT	500	53	Marco et al., 2014
	16SbrR	CCGGTCTGAACTCAGATCACGT			
Zooxanthellae					
ITS1	ITSF	CCGGTGAATTATTCGGACTGACGCAGT	750	51	Satoe et al., 2012
	ITS4R	TCCTCCGCTTATTGATATGC			

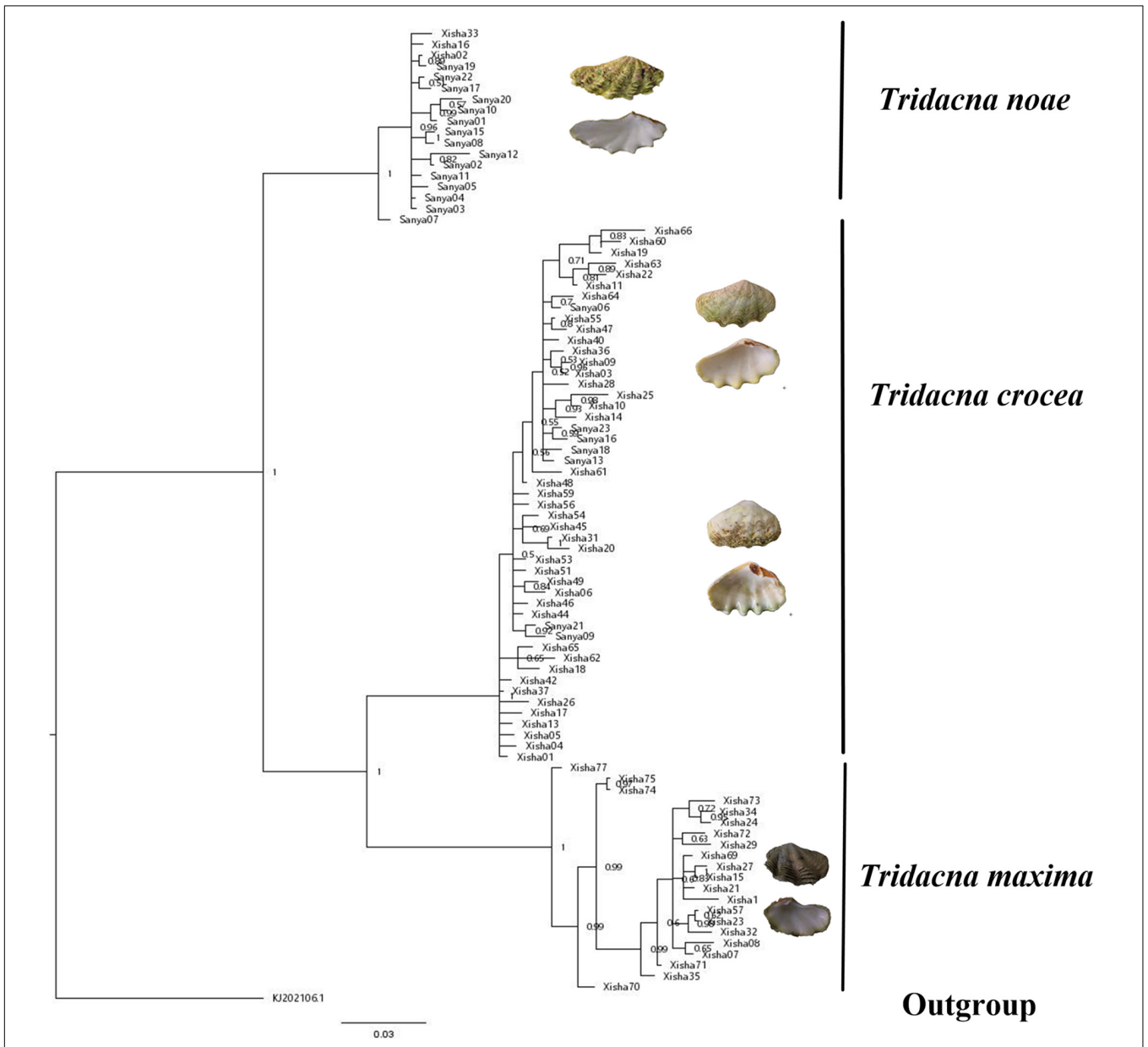

FIGURE 1 | Binary indexed tree of the three giant clams based on the COI fragment. *Hippopus hippopus* (KJ202106) was used as outgroup. Numbers at nodes are posterior probabilities.

3.5 (Excoffier and Lischer, 2010). The significance levels were evaluated under 10,000 permutations.

RESULTS

Phylogenetic Analyses of Giant Clams

A total of 88 COI and 89 16S sequences were obtained and submitted to Genbank (**Supplementary Table 1**). The phylogenetic relationships of three giant clams were reconstructed based on the aligned nucleotide sequences of COI (681 bp) and 16S (518 bp) fragments, respectively. Both BI analyses arrived at the identical topologies (**Figures 1**, **2**).

According to the reconstructed phylogeny, *T. maxima* was recovered closer to *T. crocea* than to *T. noae*. Although the sister relationship between *T. maxima* and *T. crocea* was not highly supported in the 16S analysis (**Figure 2**), it arrived at a maximum support value in the COI phylogeny (**Figure 1**). Both the COI and 16S sequences supported the monophyly of *T. crocea*, however, high-intraspecific morphological diversity was found within this group, such as the values of shell width/shell length, byssal opening length/shell length, byssal opening width/shell length and number of hinge tooth (**Supplementary Table 2**).

Genetic Diversity and Gene Genealogy

The Hd and nucleotide diversity (π) across two sampling sites were presented in **Table 2**. The genetic diversity indices derived

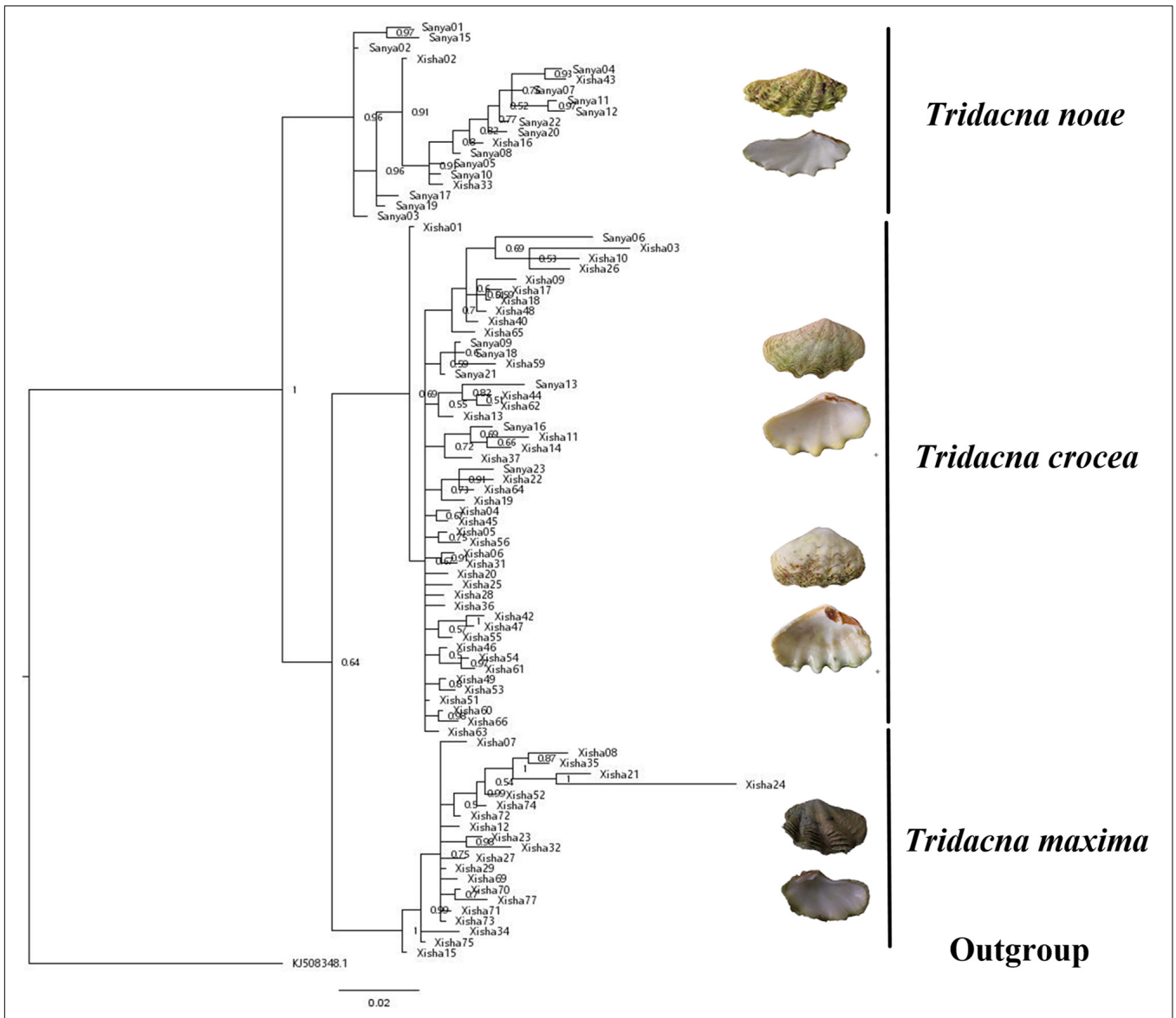

FIGURE 2 | BI tree of three giant clams based on 16S fragment. *Hippopus hippopus* (KJ508348) was used as outgroup. Numbers at nodes are posterior probabilities.

TABLE 2 | Genetic diversity of the COI and 16S among different species and sites, and COI neutrality tests.

Species	Sites	COI						16S			
		N	h	Hd	π	Tajima's D	Fu's Fs	*N*	h	Hd	π
T. crocea	Xisha	42	29	0.9779	0.00917	−1.56699*	−24.14330**	42	7	0.5854	0.00178
	Sanya	7	3	0.6667	0.00475	0.13210	1.41593	7	4	0.7143	0.00335
	Total	49	31	0.9677	0.00882	—	—	49	9	0.5961	0.00200
T. maxima	Xisha	21	15	0.9429	0.01000	−1.67280*	−6.90257*	21	6	0.4286	0.00539
	Sanya	0	—	—	—	—	—	0	—	—	—
	Total	21	15	0.9429	0.01000	—	—	21	6	0.4286	0.00539
T. noae	Xisha	3	2	0.6667	0.00151	—	—	4	1	0.0000	0.00000
	Sanya	15	9	0.8762	0.00637	−1.86906*	−3.06649*	15	4	0.4667	0.00230
	Total	18	10	0.8431	0.00560	—	—	19	4	0.3801	0.00185

Significant values ($P < 0.05$) are marked with an asterisk, while those of great significant values ($P < 0.01$) are indicated with two asterisks.

from COI were higher than those from 16S sequences. Compared with *T. noae*, *T. crocea*, and *T. maxima* showed relatively higher COI Hd and nucleotide diversity. Estimates of neutral tests for *T. crocea* and *T. maxima* of Xisha and *T. noae* of Sanya indicated population expansion by significant negative values of Fu's Fs and Tajima's D statistics (**Table 2**). The median-joining network analysis based on COI and 16S sequences revealed a star-like haplotype network (**Figure 3**).

Endosymbiont Genera and Species Diversity and Distribution

A total of 59 ITS1 sequences were amplified and submitted to GenBank (**Supplementary Table 1**). The final 814 bp length alignment was used for phylogenetic reconstruction by BI inference (**Figure 4**). The phylogenetic tree was successfully separated into two clades (namely, Clade I and Clade II; **Figure 4A**) that were identified by blasting in NCBI. The results (not shown here) indicated that they corresponded to *Symbiodinium* and *Cladocopium*, respectively. Since considerable sequence divergence could impede accurate alignments between distantly related lineages (LaJeunesse, 2001), two phylogenetic analyses of Clade I and Clade II were further conducted, respectively. Clade I was not separated while Clade II could be divided into two subclades when they were considered individually (**Figures 4B,C**).

The abundance of endosymbiont genus distribution, and their association to the three giant clam host species are shown in **Table 3**.

DISCUSSION

The COI and 16S sequences generated identical topologies, supporting the separation of three major clades corresponding to three individual species *T. crocea*, *T. maxima*, and *T. noae* (**Figures 1**, **2**). The latter two species are similar in general appearance, and they were even considered the same species (Rosewater, 1965). However, previous studies found that they could be distinguished by several morphological and ecological characteristics. For example, *T. maxima* was mainly distributed at the edges and crests of reefs, while *T. noae* was often found in the reef flat (Kubo and Iwai, 2007). In addition, *T. noae* has well-spaced rib scales, particularly on the upper third of the shell, while the ribs in *T. maxima* were closely crowded together (Su et al., 2014). Our phylogeny derived from COI and 16S fragments indicated a distant relationship between *T. noae* and *T. maxima*, shown as *T. noae* + (*T. maxima* and *T. crocea*), and therefore supported the validity of *T. noae* (Su et al., 2014). Although *T. maxima* has a short planktonic larvae duration (9 days; Lucas, 1988), it is widely distributed from the Red Sea to the central Pacific (Nuryanto and Kochzius, 2009). In our study, however, *T. maxima* was only found in Xisha, and this may probably be due to the low sample size of Sanya. High intraspecific morphological diversity was found within *T. crocea*, even though both the COI and 16S sequences supported the genetic monophyly of this species. Special attention should be paid during *T. crocea* identification since it shows high intraspecific diversity. Geographically, the sampling locations of *T. crocea* (Sanya and Xisha) in our study were restricted to the South China Sea, and corresponded to the western Pacific OTU (Liu J. et al., 2020).

A total of two clades (namely, Clade I and Clade II) were separated based on the ITS1 marker (**Figure 4A**), and they corresponded to *Symbiodinium* (formerly Clade A) and *Cladocopium* (formerly clade C; LaJeunesse et al., 2018), respectively. Until now, giant clam species have been reported to be associated with 30 Symbiodiniaceae phylotypes, all belonging to genera *Symbiodinium*, *Cladocopium*, and *Durusdinium* (not detected here) (Mies, 2019). In this study, Clade II could be further divided into two closely related lineages (**Figure 4B**), indicating the diversity of *Cladocopium*. Previous studies have also revealed that the diversity of *Cladocopium* was higher than *Symbiodinium* or *Durusdinium* in Dongsha Atoll (Lim et al., 2019), and this could be explained as the abundance of *Cladocopium* that is also species-rich among hosts in the South China Sea (Wong et al., 2016). Symbionts in *Symbiodinium* are widely distributed in the world (Baker, 2003; Tonk et al., 2013), and most members have been accustomed even to extreme conditions (Venn et al., 2008). For example, only *Symbiodinium* symbionts were found in the giant clams (*Tridacna* spp.; Pappas et al., 2017) in the Red Sea, which

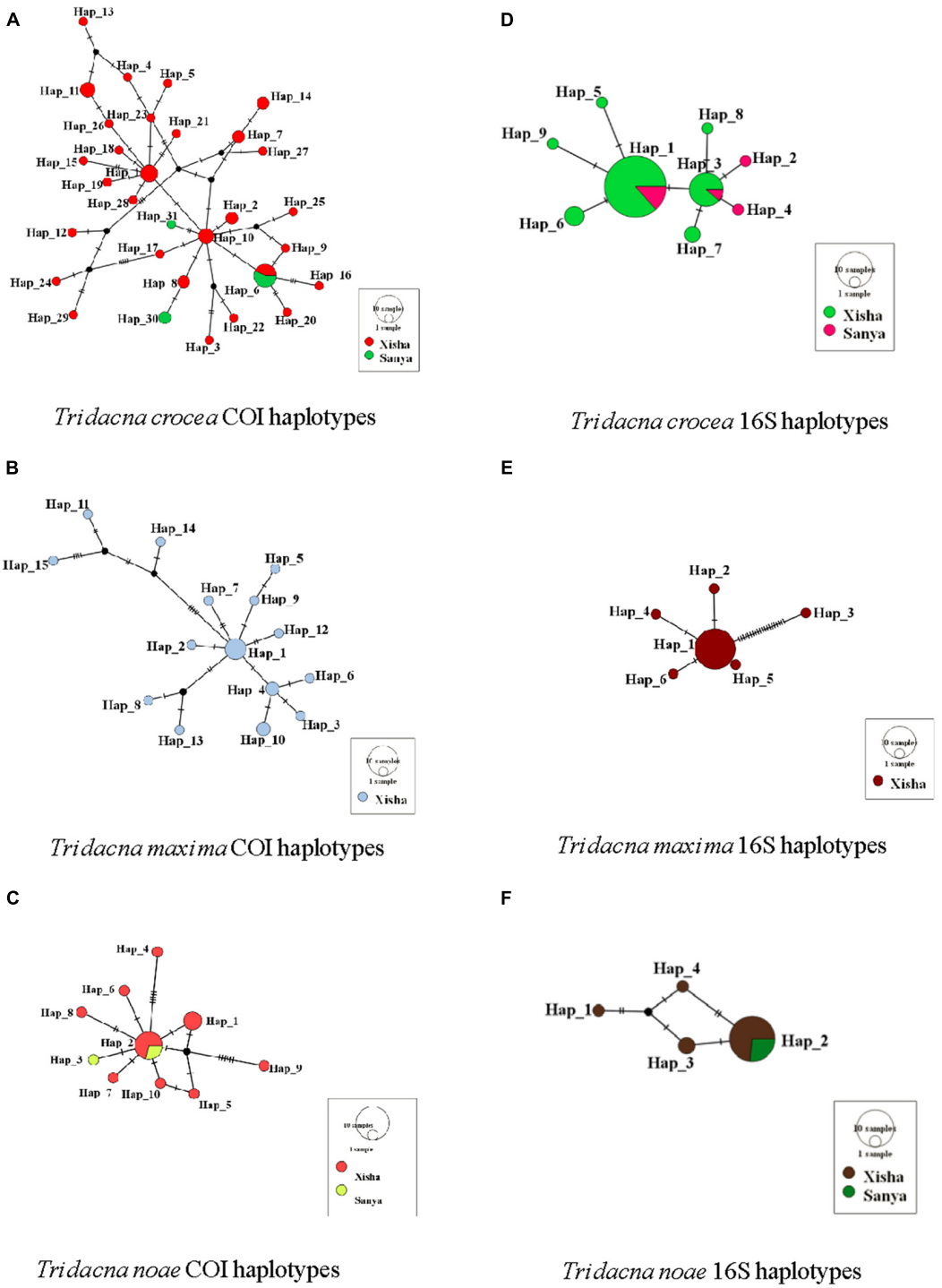

FIGURE 3 | Network of three giant clams for COI and 16S data. **(A)** *Tridacna crocea* COI haplotypes; **(B)** *Tridacna maxima* COI haplotypes; **(C)** *Tridacna noae* COI haplotypes; **(D)** *Tridacna crocea* 16S haplotypes; **(E)** *Tridacna maxima* 16S haplotypes; **(F)** *Tridacna noae* 16S haplotypes. The color of the circle indicates the geographic region, and the size of the circle indicates the haplotype frequency.

is characteristic of high heat and irradiance conditions. This could also be supported in our study, since the symbionts in *Symbiodinium* were found in both Xisha and Sanya, whereas most of the symbionts in *Cladocopium* were restricted to Xisha (**Figure 4A**), indicating that the former could be better adapted to the various conditions. This result may also be explained as that the clams with *Cladocopium* (formerly clade C) and *Durusdinium* (formerly clade D) were usually located in areas

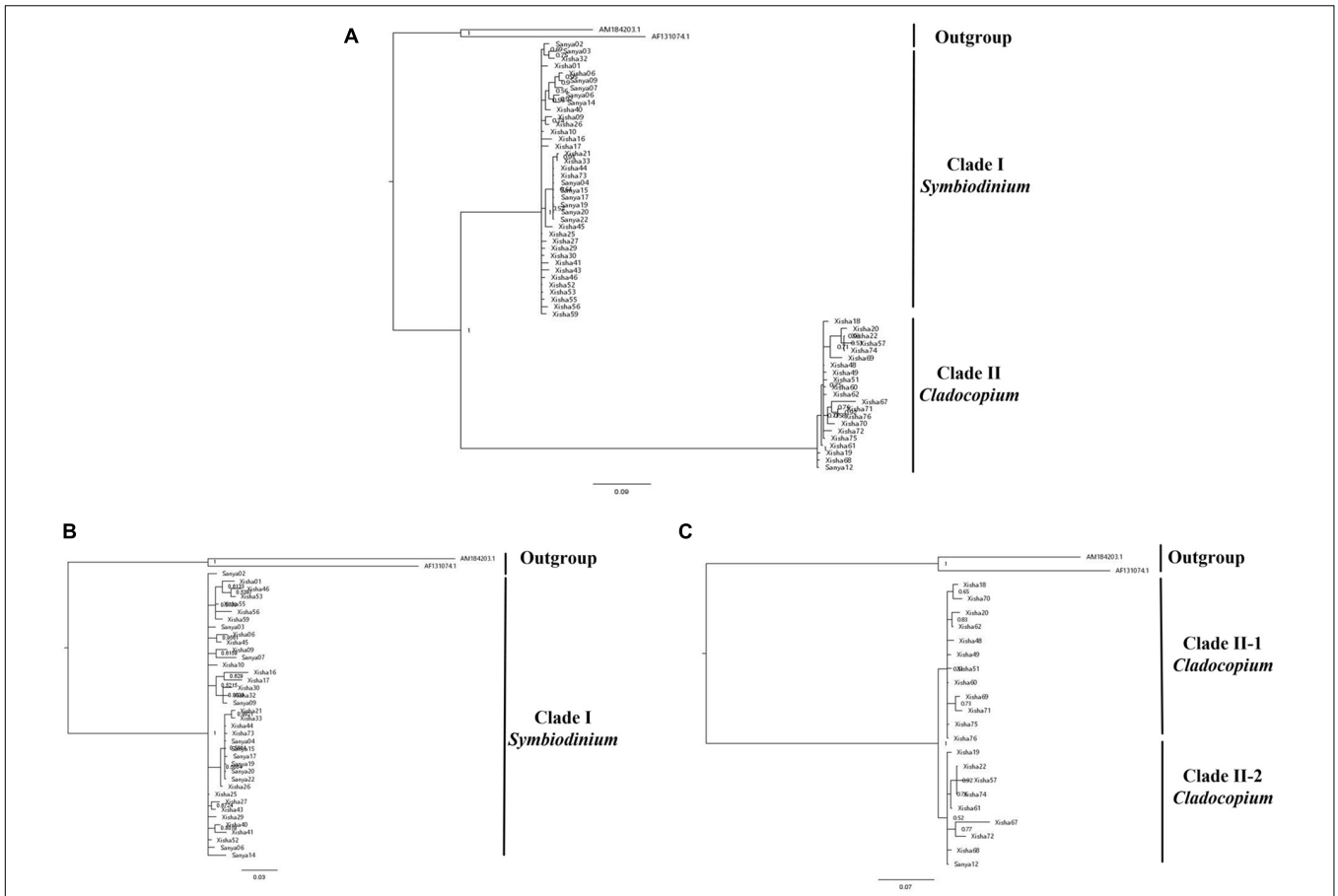

FIGURE 4 | BI tree of zooxanthellae based on ITS1 fragment. Numbers at nodes are posterior probabilities. **(A)** Phylogenetic tree of all the zooxanthellae individuals using *Gymnodinium* (AM184203) and *Gyrodinium* (AF131074) as outgroup and **(B)** Phylogenetic tree of Clade I, and **(C)** Phylogenetic tree of Clade II, derived from the phylogeny of all zooxanthellae individuals, using the same outgroup.

with higher mean temperatures as previous studies have revealed (DeBoer et al., 2012) since the climate of Xisha is warmer than Sanya at the same time.

This study reveals the endosymbiont specificity among the three giant clam species. At first, *T. maxima* associates slightly with *Cladocopium* (n = 7) over *Symbiodinium* (n = 5), but sample sizes are low. In the previous studies, both *T. maxima* host associations with *Cladocopium* and *Symbiodinium* endosymbionts have been reported. For example, in Dongsha (Lim et al., 2019), *T. maxima* associated preferentially with *Cladocopium*. In the Red Sea (Rossbach et al., 2021), however, strong *T. maxima* host associations with *Symbiodinium* endosymbionts were suggested. In French Polynesia, both *Symbiodinium* and *Cladocopium* were the dominant genera in *T. maxima* (Pochon et al., 2019). In order to better clarify *T. maxima* host associations in the South China Sea, future studies with broad sampling sites around this area are still needed. Different from *T. maxima*, the giant clams *T. noae* and *T. crocea* were found to associate with *Symbiodinium* over *Cladocopium*, and this host-endosymbiont specificity appears more obvious on *T. noae*. This result is supported by the study of Ikeda et al. (2017) showing that *T. crocea* had an apparent dominance of *Symbiodinium* (Clade A), although it is inconsistent with some previous studies which revealed *T. noae* and *T. crocea* host associations with *Durusdinium* (Lim et al., 2019) and *Cladocopium* (DeBoer et al., 2012), respectively. Within the stony coral *Stylophora pistillata*, *Symbiodinium* (Clade A) have been observed to be more related to individuals that inhabited shallow waters, whereas individuals in deeper waters were more associated with *Cladocopium* (Clade C) (Winters et al., 2009). In addition, *Symbiodinium* (Clade A) was found

TABLE 3 | Abundance of *Tridacna* clams with respective endosymbiont genus according to host species and sampling sites.

	T. maxima		*T. noae*		*T. crocea*	
	Hainan	**Xisha**	**Hainan**	**Xisha**	**Hainan**	**Xisha**
Symbiodinium	0	5	9	2	2	15
Cladocopium	0	7	1	0	0	10

in other coral species inhabiting shallow waters (Rowan et al., 1997), and therefore, it is inferred that *Symbiodinium* (Clade A) tends to be more insensitive to the high irradiance and high temperature stresses of shallow waters (Ikeda et al., 2017). The habits of *Symbiodinium* (Clade A) may attribute to *T. noae* and *T. crocea* that inhabit shallow waters, associating preferentially with *Symbiodinium*.

CONCLUSION

In this study, the reconstructed phylogeny using the COI and 16S fragments indicated a relationship shown as *T. noae* + (*T. maxima* and *T. crocea*) and supported the validity of *T. noae*. A total of two clades of Symbiodiniaceae symbionts that corresponded to *Symbiodinium* (formerly Clade A) and *Cladocopium* (formerly clade C) were separated based on the ITS1 marker. The wide distribution of *Symbiodinium* may indicate that it could be better adapted to various conditions, while the restriction of *Cladocopium* may be explained as a temperature preference. This study also reveals the endosymbiont specificity that is related to the shared living habits between giant clams and dinoflagellates.

DATA AVAILABILITY STATEMENT

The datasets presented in this study can be found in online repositories. The names of the repository/repositories and accession number(s) can be found in the article/ **Supplementary Material**.

ETHICS STATEMENT

The animal study was reviewed and approved by The Committee and Laboratory Animal Department of Hainan University.

AUTHOR CONTRIBUTIONS

QC was involved with the data curation, investigation, and writing the original draft. ZG worked with the software and supervision. AW was involved in the supervision and funding acquisition. CL was helped in the conceptualization, writing review and editing, supervision, and funding the acquisition. YY was helped in the data curation, formal analysis, methodology, and writing the original draft. All authors contributed to the article and approved the submitted version.

FUNDING

This research was supported financially by the National Key Research and Development Program of China (2019YFD0901301), the Key Research and Development Project of Hainan Province (ZDYF2019153), and the Starting Research Fund from the Hainan University (RZ2100003081).

SUPPLEMENTARY MATERIAL

The Supplementary Material for this article can be found online at: https://www.frontiersin.org/articles/10.3389/fmars.2021.774925/full#supplementary-material

REFERENCES

Arif, C., Daniels, C., Bayer, T., Banguera-Hinestroza, E., Barbrook, A., Howe, C. J., et al. (2014). Assessing *Symbiodinium* diversity in scleractinian corals via nextgeneration sequencing-based genotyping of the ITS2 rDNA region. *Mol. Ecol.* 23, 4418–4433. doi: 10.1111/mec.12869

Baker, A. C. (2003). Flexibility and specificity in coral-algal symbiosis: diversity, ecology, and biogeography of *Symbiodinium*. *Annu. Rev. Ecol. Evol. Syst.* 34, 661–689. doi: 10.1146/annurev.ecolsys.34.011802.132417

Clement, M., Posada, D., and Crandall, K. A. (2000). TCS: a computer program to estimate gene genealogies. *Mol. Ecol.* 9, 1657–1659. doi: 10.1046/j.1365-294x.2000.01020.x

Copland, J. W. E., and Lucas, J. S. E. (1988). Canberra Australia Australian Centre for International Agricultural Research. Giant clams in Asia and the pacific. *Monographs* 9:274.

DeBoer, T. S., Baker, A. C., Erdmann, M. V., Jones, P. R., and Barber, P. H. (2012). Patterns of *Symbiodinium* distribution in three giant clam species across the biodiverse Bird's Head region of Indonesia. *Mar. Ecol. Prog. Ser.* 444, 117–132. doi: 10.3354/meps09413

Excoffier, L., and Lischer, H. E. L. (2010). Arlequin suite ver 3.5: a new series of programs to perform population genetics analyses under Linux and Windows. *Mol. Ecol. Resour.* 10, 564–567. doi: 10.1111/j.1755-0998.2010.02847.x

Fu, Y. (1997). Statistical tests of neutrality of mutations against population growth, hitchhiking and background selection. *Genetics* 147, 915–925. doi: 10.1093/genetics/147.2.915

Huelsenbeck, J. P., and Ronquist, F. (2001). MRBAYES: bayesian inference of phylogenetic trees. *Bioinformatics* 17, 754–755.

Hui, M., Agus, N., and Marc, K. (2016). Concordance of microsatellite and mitochondrial DNA markers in detecting genetic population structure in the boring giant clam *Tridacna crocea* across the Indo-Malay Archipelago. *Mar. Ecol.* 38:e12389.

Hume, B., Voolstra, C. R., Arif, C., D' Angelo, C., Burt, J. A., Eyal, G., et al. (2016). Ancestral genetic diversity associated with the rapid spread of stress-tolerant coral symbionts in response to Holocene climate change. *Proc. Natl. Acad. Sci. U. S. A.* 113, 4416–4421. doi: 10.1073/pnas.1601910113

Ikeda, S., Yamashita, H., Kondo, S. N., Inoue, K., Morishima, S. Y., and Koike, K. (2017). Zooxanthellal genetic varieties in giant clams are partially determined by species-intrinsic and growth-related characteristics. *PLoS One* 12:e0172285. doi: 10.1371/journal.pone.0172285

Kubo, H., and Iwai, K. (2007). On sympatric two species within *Tridacna* "*maxima*". *Annu. Rep. Okinawa Fish. Ocean Res. Cent.* 68, 205–210.

Kumar, S., Stecher, G., Li, M., Knyaz, C., and Tamura, K. (2018). MEGA X: molecular evolutionary genetics analysis across computing platforms. *Mol. Biol. Evol.* 35:1547. doi: 10.1093/molbev/msy096

LaJeunesse, T. C. (2001). Investigating the biodiversity, ecology, and phylogeny of endosymbiotic dinoflagellates in the genus *Symbiodinium* using the ITS region: in search of a "species" level marker. *J. Phycol.* 37, 866–880. doi: 10.1046/j.1529-8817.2001.01031.x

LaJeunesse, T. C., Parkinson, J. E., Gabrielson, P. W., Jeong, H. J., Reimer, J. D., Voolstra, C. R., et al. (2018). Systematic revision of Symbiodiniaceae highlights the antiquity and diversity of coral endosymbionts. *Curr. Biol.* 28, 2570–2580. doi: 10.1016/j.cub.2018.07.008

LaJeunesse, T. C., Pettay, D. T., Sampayo, E. M., Phongsuwan, N., Brown, B., Obura, D. O., et al. (2010). Long-standing environmental conditions, geographic isolation and host-symbiont specificity influence the relative

ecological dominance and genetic diversification of coral endosymbionts in the genus *Symbiodinium*. *J. Biogeogr.* 37, 785–800.

Librado, P., and Rozas, J. (2009). DnaSP v5: a software for comprehensive analysis of DNA polymorphism data. *Bioinformatics* 25, 1451–1452. doi: 10.1093/bioinformatics/btp187

Lim, S. S. Q., Huang, D., Soong, K., and Neo, M. L. (2019). Diversity of endosymbiotic Symbiodiniaceae in giant clams at Dongsha Atoll, northern South China Sea. *Symbiosis* 78, 251–262.

Liu, C., Li, X., Wu, C., Wang, A., and Gu, Z. (2020). Effects of three light intensities on the survival, growth performance and biochemical composition of two size giant clams *Tridacna crocea* in the Southern China Sea. *Aquaculture* 528:735548.

Liu, C., Wu, C., Li, X., Liu, C., Wang, A., Gu, Z., et al. (2021a). Distribution and the influence of substrate on its mantle color of giant clam *Tridacna noae* in coastal waters of Sanya. *Acta Hydrobiol. Sinica* 45, 645–651.

Liu, C., Yang, X., Sun, Y., Yang, Y., Wang, A., He, L., et al. (2021b). Effects of the daily light/dark cycle on photosynthetic performance, oxidative stress and illumination-related genes in boring giant clam *Tridacna crocea*. *Mar. Biol.* 168:71.

Liu, J., Cui, D., Wang, H., Chen, J., Liu, H., and Zhang, H. (2020). Extensive cryptic diversity of giant clams (Cardiidae: Tridacninae) revealed by DNA-sequence-based species delimitation approaches with new data from Hainan Island, South China Sea. *J. Mollus. Stud.* 86, 56–63. doi: 10.1093/mollus/eyz033

Lucas, J. S. (1988). Giant clams: description, distribution and life history. Giant clams in Asia and the Pacific. *ACIAR Monogr.* 9, 21–33.

Lucas, J. S. (2014). Giant clams. *Curr. Biol.* 24, 183–184.

Marco, A., Lizano, D., and Santos, M. D. (2014). ARTICLE Updates on the status of giant clams *Tridacna* spp. and *Hippopus hippopus* in the Philippines using mitochondrial CO1 and 16S rRNA genes. *Philipp. Sci. Lett.* 7, 187–200.

Mies, M. (2019). Evolution, diversity, distribution and the endangered future of the giant clam–Symbiodiniaceae association. *Coral Reefs* 38, 1067–1084.

Miller, M. A., Pfeiffer, W., and Schwartz, T. (2010). "Creating the CIPRES Science Gateway for inference of large phylogenetic trees," in *2010 Gateway Computing Environments Workshop (GCE)*, (New Orleans: IEEE).

Neo, M. L., Lim, K. K., Yang, S., Soong, G. Y., Masucci, G. D., Biondi, P., et al. (2019). Status of giant clam resources around Okinawa-jima Island, Ryukyu Archipelago, Japan. *Aquat. Conserv.* 29, 1002–1011. doi: 10.1002/aqc.3033

Neo, M. L., and Todd, P. A. (2012). Giant clams (Mollusca: Bivalvia: Tridacninae) in Singapore: history, research and conservation. *Raffles Bull. Zool.* 25, 67–78.

Neo, M. L., Wabnitz, C. C., Braley, R. D., Heslinga, G. A., Fauvelot, C., Van Wynsberge, S., et al. (2017). Giant clams (Bivalvia: Cardiidae: Tridacninae): a comprehensive update of species and their distribution, current threats and conservation status. *Oceanogr. Mar. Biol.* 55, 87–388. doi: 10.1201/b21944-5

Nuryanto, A., Duryadi, D., Soedharma, D., and Blohm, D. (2007). Molecular phylogeny of giant clams based on mitochondrial DNA cytochrome coxidase I gene. *Hayati* 14, 162–166. doi: 10.11646/zootaxa.4007.2.1

Nuryanto, A., and Kochzius, M. (2009). Highly restricted gene flow and deep evolutionary lineages in the giant clam *Tridacna maxima*. *Coral Reefs* 28, 607–619.

Pappas, M. K., He, S., Hardenstine, R. S., Kanee, H., and Berumen, M. L. (2017). Genetic diversity of giant clams (*Tridacna* spp.) and their associated *Symbiodinium* in the central Red Sea. *Mar. Biodivers.* 47, 1209–1222. doi: 10.1007/s12526-017-0715-2

Pochon, X., and Gates, R. D. (2010). A new *Symbiodinium* clade (Dinophyceae) from soritid foraminifera in Hawaii. *Mol. Phylogenet. Evol.* 56, 492–497. doi: 10.1016/j.ympev.2010.03.040

Pochon, X., Wecker, P., Stat, M., Berteaux-Lecellier, V., and Lecellier, G. (2019). Towards an in-depth characterization of Symbiodiniaceae in tropical giant clams via metabarcoding of pooled multi-gene amplicons. *PeerJ* 7:e6898. doi: 10.7717/peerj.6898

Pringgenies, D., Suprihatin, J., and Lazo, L. (1995). Spatial and size distribution of giant clams in the Karimunjawa Islands, Indonesia. *Phuket Mar. Biol. Cent. Spec. Publ.* 15, 133–135.

Reich, H. G., Robertson, D. L., and Goodbody-Gringley, G. (2017). Do the shuffle: changes in *Symbiodinium* consortia throughout juvenile coral development. *PLoS One* 12:e0171768. doi: 10.1371/journal.pone.0171768

Ronquist, F., and Huelsenbeck, J. P. (2003). MrBayes 3: bayesian phylogenetic inference under mixed models. *Bioinformatics* 19, 1572–1574. doi: 10.1093/bioinformatics/btg180

Rosewater, J. (1965). The family Tridacnidae in the Indo-Pacific. *Molluscan Res.* 1, 347–396.

Rossbach, S., Hume, B. C., Cárdenas, A., Perna, G., Voolstra, C. R., and Duarte, C. M. (2021). Flexibility in Red Sea *Tridacna maxima*-Symbiodiniaceae associations supports environmental niche adaptation. *Ecol. Evol.* 11, 3393–3406.

Rowan, R., Knowlton, N., Baker, A., and Jara, J. (1997). Landscape ecology of algal symbionts creates variation in episodes of coral bleaching. *Nature* 388, 265–269. doi: 10.1038/40843

Satoe, A., Tomura, T., Saitoh, S., Yokokura, R., Kawanishi, Y., Shinjo, R., et al. (2012). Soft Coral Sarcophyton (Cnidaria: Anthozoa: Octocorallia) Species Diversity and Chemotypes. *PLoS One* 7:e30410. doi: 10.1371/journal.pone.0030410

Stat, M., Carter, D., and Hoegh-Guldberg, O. (2006). The evolutionary history of *Symbiodinium* and scleractinian hosts-Symbiosis, diversity, and the effect of climate change. *Perspect. Plant Ecol.* 8, 23–43. doi: 10.1016/j.ppees.2006.04.001

Su, Y., Hung, J. H., Kubo, H., and Liu, L. L. (2014). *Tridacna noae* (Röding, 1798)–a valid giant clam species separated from *T. maxima* (Röding, 1798) by morphological and genetic data. *Raffles Bull. Zool.* 62, 124–135.

Tajima, F. (1989). Statistical method for testing the neutral mutation hypothesis by DNA polymorphism. *Genetics* 123, 585–595. doi: 10.1093/genetics/123.3.585

Tonk, L., Sampayo, E. M., Weeks, S., Magno-Canto, M., and Hoegh-Guldberg, O. (2013). Host-specific interactions with environmental factors shape the distribution of *Symbiodinium* across the Great Barrier Reef. *PLoS One* 8:e68533. doi: 10.1371/journal.pone.0068533

United Nations Environment Programme-World Conservation Monitoring Center (UNEP-WCMC) (2007). *UNEP-WCMC Species Database: CITES-listed Species*. Cambridge: UNEP.

Venn, A. A., Loram, J. E., and Douglas, A. E. (2008). Photosynthetic symbioses in animals. *J. Exp. Bot.* 59, 1069–1080. doi: 10.1093/jxb/erm328

Wang, J., Zhou, Z., Ma, H., Li, J., Qin, Y., Wei, J., et al. (2021). Genetic Recombination of the Mantle Color Pattern of Two Boring Giant Clam (*Tridacna crocea*) Strains. *Front. Mar. Sci.* 8:657762. doi: 10.3389/fmars.2021.657762

Wells, S. (1997). *Giant Clams: Status, Trade and Mariculture, and the Role of CITES Management*. Gland: IUCN.

Winters, G., Beer, S., Zvi, B. B., Brickner, I., and Loya, Y. (2009). Spatial and temporal photoacclimation of Stylophora pistillata: zooxanthella size, pigmentation, location and clade. *Mar. Ecol. Prog. Ser.* 384, 107–119. doi: 10.3354/meps08036

Wong, J. C., Thompson, P., Xie, J. Y., Qiu, J. W., and Baker, D. M. (2016). *Symbiodinium* clade C generality among common scleractinian corals in subtropical Hong Kong. *Reg. Stud. Mar. Sci.* 8, 439–444. doi: 10.1016/j.rsma.2016.02.005

Xia, X. (2013). DAMBE5: a comprehensive software package for data analysis in molecular biology and evolution. *Mol. Biol. Evol.* 30, 1720–1728. doi: 10.1093/molbev/mst064

Zhang, Y., Zhou, Z., Qin, Y., Li, X., Ma, H., Wei, J., et al. (2020). Phenotypic traits of two boring giant clam (*Tridacna crocea*) populations and their reciprocal hybrids in the South China Sea. *Aquaculture* 519:734890. doi: 10.1016/j.aquaculture.2019.734890

Conflict of Interest: The authors declare that the research was conducted in the absence of any commercial or financial relationships that could be construed as a potential conflict of interest.

Publisher's Note: All claims expressed in this article are solely those of the authors and do not necessarily represent those of their affiliated organizations, or those of the publisher, the editors and the reviewers. Any product that may be evaluated in this article, or claim that may be made by its manufacturer, is not guaranteed or endorsed by the publisher.

frontiers in Marine Science

ORIGINAL RESEARCH
published: 30 November 2021
doi: 10.3389/fmars.2021.770702

Comparison in Growth, Feeding, and Metabolism Between a Fast-Growing Selective Strain and a Cultured Population of Pearl Oyster (*Pinctada fucata martensii*)

Xingzhi Zhang[1,2†], *Bingcong Ye*[1†], *Zhifeng Gu*[1], *Meng Li*[1], *Shouguo Yang*[1], *Aimin Wang*[1*] *and Chunsheng Liu*[1*]

[1] State Key Laboratory of Marine Resource Utilization in South China Sea, Hainan University, Haikou, China, [2] Guangxi Key Laboratory of Aquatic Genetic Breeding and Healthy Aquaculture, Guangxi Academy of Fisheries Sciences, Nanning, China

OPEN ACCESS

Edited by:
Liqiang Zhao,
Guangdong Ocean University, China

Reviewed by:
Pengzhi Qi,
Zhejiang Ocean University, China
Chuangye Yang,
Guangdong Ocean University, China
Linda Adzigbli,
University of Rostock, Germany

***Correspondence:**
Aimin Wang
aimwang@163.com
Chunsheng Liu
lcs5113@163.com

[†] These authors have contributed equally to this work

Specialty section:
This article was submitted to Marine Fisheries, Aquaculture and Living Resources, a section of the journal Frontiers in Marine Science

Received: 04 September 2021
Accepted: 12 October 2021
Published: 30 November 2021

Citation:
Zhang X, Ye B, Gu Z, Li M, Yang S, Wang A and Liu C (2021) Comparison in Growth, Feeding, and Metabolism Between a Fast-Growing Selective Strain and a Cultured Population of Pearl Oyster (Pinctada fucata martensii). Front. Mar. Sci. 8:770702. doi: 10.3389/fmars.2021.770702

Pearl oyster (*Pinctada fucata martensii*) is the main species cultured for marine pearls in the world. A breeding program was carried out for desirable production traits, including high growth rate, and a fast-growing selective strain of pearl oysters was established. In the current study, we compared the growth characteristics between a selective strain and a cultured population of *P. f. martensii* in Beihai, Guangxi Province, China. Large size (SL) and small size (SS) individuals of the selective strain were selected, and the differences of physiological and metabolic indexes, such as feeding, respiration, excretion, and enzyme activities between SL and SS and cultured population (CL), were also compared. The results showed that at the age of 6 months, pearl oysters of the selective strain were 14.61% larger than CL, and the proportion of SL (30–40 mm) was 59%, which was two times higher than CL (28%). SL with a rapid growth rate had a high clearance rate (CR), and the CR of SL was about 1.8 times higher than that of CL and 5 times higher than that of SS. In addition, the activities of digestive enzymes (amylase, pepsin, and lipase) and growth-related carbonic anhydrase enzymes in SL were higher than those in the other two groups ($p < 0.05$). SS with a slow growth rate had higher oxygen consumption (OCR) and ammonia excretion (AER) rates than SL and CL ($p < 0.05$). Our results suggest that the rapid growth of the selective strain *P. f. martensii* can be attributed to increased energy intake and reduced energy consumption.

Keywords: pearl oyster, selective strain, physiological, feeding, metabolism

INTRODUCTION

The pearl oyster, *Pinctada fucata martensii*, belonging to the family Pteriidae (Pterioida, Bivalvia), is naturally distributed in countries along the west coast of the Pacific Ocean, such as China, Japan, Australia, and the Philippines (Wang et al., 2004). *P. f. martensii* is the primary species cultured for marine pearls in China and Japan (Wang et al., 2011a). The pearl oyster industry has become one of the most important mariculture industries in several southern provinces of China, including Guangdong, Guangxi, and Hainan (Wang et al., 2004; Deng et al., 2009a, 2011; He et al., 2021; Xu et al., 2021). However, the conditions are changing due to the slow growth and mass mortalities

of oysters (Deng et al., 2011; Gu et al., 2011). Pearl production dropped sharply in recent years, and the cultivate industry was dealt a huge blow. A selective breeding program toward *P. f. martensii* was carried out in 2000. A rapid growth selective strain was obtained through hybrid breeding with the Indian population as the male parent and the Chinese Sanya population as the female parent (Wang et al., 2000, 2004). After seven generations of selection, remarkable genetic gains for growth rate and a high proportion of high-quality pearls were achieved in the selected strain (Wang et al., 2011b).

Specific mechanisms associated with fast growth rate in bivalves include the efficacies of processes of food acquisition and metabolic rates in resting or active states (Bayne, 1999, 2000; Bayne et al., 1999; Tamayo et al., 2011, 2014, 2015). Physiological processes related to these mechanisms include clearance rate (CR), oxygen consumption rate (OCR), ammonia excretion rate (AER), and enzyme activities. Therefore, ingestion and energy metabolism of some commercial bivalve species have received considerable attention (Ibarrola et al., 2017; Zhang et al., 2018). Individuals might exhibit faster growth due to increased energy acquisition and maintenance or growth costs (Bayne et al., 1999; Meyer and Manahan, 2010; Tamayo et al., 2011), and this explanation is applicable for other bivalve larval stages (Pace et al., 2006; Tamayo et al., 2014). Furthermore, in bivalves, the process of biological mineralization is closely related to shell growth. Carbonic anhydrase is one of the most important indicators of biological mineralization (Medaković, 2000; Cardoso et al., 2019).

Processes related to energy utilization and growth efficiency of mollusks are largely controlled by genetics, such as in oysters (Bayne et al., 1999; Parker et al., 2010; Zhao et al., 2019b), abalone (Gonzalez et al., 2010), and green-lipped mussels (Ibarrola et al., 2017). These theories provide a feasible scheme for improving the growth characteristics of bivalves (Newkirk, 1980; Evans and Langdon, 2006; Schöne et al., 2021). Numerous studies have confirmed effective improvement in commercial traits of bivalve species through selective experiments (Deng et al., 2009b; Gu et al., 2011; Li et al., 2011; Zhang et al., 2018). Physiological differences between improved selected and non-selected groups were explored (Bayne et al., 1999; Zhang et al., 2018). However, the relationship between fast-growth and physiological factors of *P. f. martensii* has not been documented. Therefore, the study aimed to figure out the physiological processes related to fast-growth, including CR (energy acquisition), OCR and AER (metabolic rate), and digestive enzyme and carbonic anhydrase activities in *P. f. martensii*, determine the physiological parameters leading to the existence of differences in the growth potential of the selective strain, and explore the mechanism of selected strain of fast-growing *P. f. martensii* from a physiological point of view.

MATERIALS AND METHODS

Pearl Oyster Collection

On June 10, 2020, two different stocks, A and B, of *P. f. martensii* were selected to conduct mass selection experiments at a shellfish hatchery in Beihai, Guangxi Province, China. Stock A descended from the fast-growing selective strain. Stock B was a cultured population without artificial selection. For the two stocks, 50 individuals were selected as parents in each group, and the two groups were inseminated to obtain progeny. Larval rearing was similar to the process previously described by Zheng et al. (2004) and Deng et al. (2011). After 30 d, juveniles from each group were taken from the polyethylene bags and raised in coastal areas suspended on a raft. The two groups were cultured in the same area located at Beihai, China (21°26′-21°55′ N, 108°50′-109°47′ E).

The polyethylene bags were cleaned periodically, and the oyster shell height was measured monthly. On November 10, 2020, a total of 270 randomly selected individuals from each group were taken to the laboratory and used in a physiological experiment. Pearl oysters of the selected strain were divided into two groups (SL, shell height 37.56 ± 9.01 mm; SS, shell height 10.01 ± 0.31 mm) based on shell height. Large-sized individuals from the cultured population (CL, shell height 36.76 ± 9.88 mm) were selected to compare the physiological differences between the populations (inter-population) (**Table 1**).

From December 10, 2020, the oyster shell height was measured for 6 months. A total of 100 oysters of the selective strain and cultured population were randomly selected to determine the size-frequency distribution (**Figure 1**).

TABLE 1 | Biological data of *P. f. martensii* in the experiments.

Experimental group	Shell height/mm	Shell length/mm	Wet weight/g	Dry weight/g
SL	37.56 ± 9.01^{a}	40.56 ± 9.01^{a}	3.20 ± 0.12^{a}	0.18^{a}
CL	36.76 ± 9.88^{a}	39.76 ± 9.88^{a}	3.16 ± 0.09^{a}	0.17^{a}
SS	10.01 ± 0.31^{b}	11.01 ± 0.31^{b}	0.82 ± 0.11^{b}	0.06^{b}

SL, selective strain pearl oyster with large size; CL, cultured population pearl oyster; SS, selective strain of pearl oyster with small size.
Values sharing different superscripted letters are significantly different ($p < 0.05$).

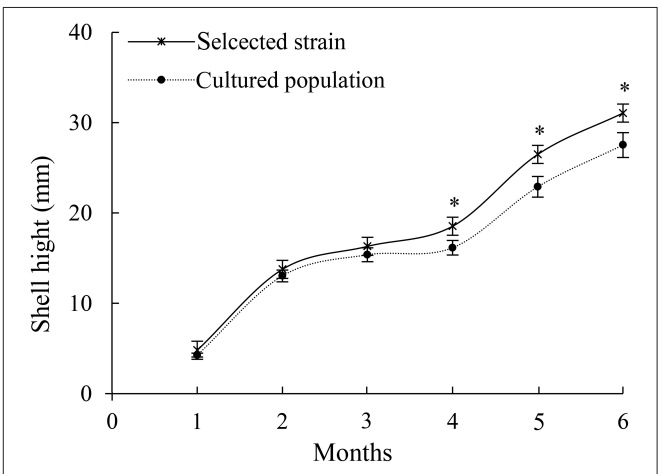

FIGURE 1 | Growth of shell height of selective strain and cultured population pearl oysters. *$p < 0.05$.

Experimental Design

After 24 h of starvation, the SL, SS, and CL oysters were placed in 100 L buckets, with 30 individuals per bucket. Each group was replicated thrice and domesticated in the laboratory for 7 d. Pearl oysters were fed twice a day with a microalgae diet of *Isochrysis galbana* (3×10^4 cells/mL). Water temperature and salinity were maintained at $19 \pm 0.5^{\circ}$C and 30 ± 0.5‰, respectively. Seawater was stored and aerated after precipitation and sand filtration before each experiment.

Physiological Parameters Determination

CR

After a week of acclimation, 10 pearl oysters from each of the three groups (SL, SS, and CL) were randomly collected and placed in 1 L beakers. Each treatment was replicated thrice. One blank beaker with no pearl oysters was set as the control group for each treatment. Pearl oysters were fed with *I. galbana* (6×10^4 cells mL^{-1}). The experiment lasted for 3 h, and the concentration of algae was calculated under a microscope by a hemocytometer.

CR (clearance rate) is defined as the volume of water cleared of algal cells per hour. The value of CR (L/h) was estimated following the equation (Zhang et al., 2018):

$$CR = \frac{V \times \ln\left[\left(C_t - C_0 \times Sd\right)\right]}{W \times t} \quad (1)$$

where V = volume (L) of beaker, t = duration of the measurement (h), C_0 = concentration of unicellular algae at initial time, and C_t = concentration of unicellular algae at t time. Cell concentrations were measured by direct counting with a haemocytometer. Sd = variable coefficient of the control group unicellular algae. W = dry weight of the pearl oyster soft tissues.

Metabolism Measurements

Closed-chamber respiration methods were employed to determine oxygen consumption rate (OCR) and ammonia excretion rate (AER). Six pearl oysters were placed in 3 L glass respiration chamber at test SL, SS, and CL, which was aerated for at least 1 h to reach oxygen saturation before the measurement. Each group was replicated thrice and one blank chamber with no oysters was used as the control. The experiment lasted for 3 h. Water samples were collected by siphoning, and dissolved oxygen (DO) was measured at the start and end of the experiment. DO was measured by the YSI (5331) polarographic electrode coupled with a micro-oxymeter (Yellow Springs, OH, USA). Ammonia determination was done by the sodium hypobromite method (Gu et al., 2020). The DO and ammonia of blank seawater were carried out and then subtracted from the experimental units to correct for autogenic trends. DO was not <4.2 mg/L (more than 70% of total DO) in test vessels at the end of the experiment. Ammonia accumulation did not exceed the maximum values of ammonium concentration (0.04 mg/L).

OCR (mg/h) was calculated using the following equation:

$$OCR = \frac{V \times (DO_0 - DO_t)}{W \times t} \quad (2)$$

The initial and final concentrations of DO are expressed as DO_0 and DO_t, t = duration of measurement (h), V = volume of the chamber (L), and W= dry weight of soft tissues.

AER (mg/L) was measured using the following equation:

$$AER = \frac{V \times (N_t - N_0)}{W \times t} \quad (3)$$

The initial and final concentrations of AER are expressed as N_0 and N_t, t = duration of measurement (h), V = volume of the chamber (L), and W = dry weight of the soft tissues.

The oxygen: nitrogen (O/N) atomic ratio was used to estimate the proportion of protein in relation to lipids or carbohydrates for metabolism, which was calculated as follows:

$$O/N = \frac{OCR/16}{AER/14} \quad (4)$$

Digestive Enzyme and Carbonic Anhydrase Activities

Before the experiment, three groups of pearl oysters were starved for 1 d. Ten oysters were randomly selected from each group. The visceral mass was removed from each oyster by vivisection on a liquid nitrogen cold plate, rapidly frozen, and stored at −80°C. The visceral mass was shredded with a tissue mashing instrument, and then the analytical balance was used to weigh visceral mass (0.01 g), diluted 10 times with sterilized normal saline, and centrifuged at 5,000 rpm for 10 min. Then, each supernatant was collected in an Eppendorf tube and stored at 4°C. Amylase, lipase, pepsin, and carbon acid anhydride enzyme activities were determined using commercial assay kits (Nanjing Jian-cheng Institute, Nanjing, China).

Amylase activity was determined by the method described by Vega-Villasante et al. (1993), using starch as a substrate. The samples were read spectrophotometrically at 540 nm, and results were expressed in units per milligram of protein (U/mg protein). Lipase activity was determined by the method described by Li et al. (2020), using β-naphthyl-caprylate as a substrate. The activity was evaluated spectrophotometrically at 540 nm, and the specific activity was expressed in units per milligram of protein (U/mg protein). Pepsin activity was determined by the method described by Li et al. (2020), using hydrolyzed proteins to produce amino acids containing phenols as a substrate. The samples were read spectrophotometrically at 660 nm, and results were expressed in units per milligram of protein (U/mg protein). Carbon acid anhydride enzyme activities were measured using the classical phenol red method (Roy et al., 2012). The samples were read spectrophotometrically at 450 nm, and results were expressed in units per milligram of protein (U/g protein).

Statistical Analysis

The results are presented as mean ± standard deviation (S.D.). The differences in physiological measurements among different categories were analyzed with one-way analysis of variance (ANOVA) to determine the significant differences among the treatments at $p < 0.05$. If the main effects were significant, Tukey's multiple range test was used to compare the mean values ($p < 0.05$) between individual treatments. Analysis was conducted using SPSS statistics 20.0 software (IBM, Armonk, NY, USA).

RESULTS

Growth Rate Comparisons

In 6 months, selective breeding pearl oysters had a higher phenotypic (shell height) mean than the cultured population (**Figure 1**). At the age of 6 months, the average shell height was 3.9 mm (14.61%), which was higher than the cultured population ($p < 0.05$). The cultured population had a higher value of phenotypic variation (CV) (**Table 2**). In the selective strain (**Figure 1**), the proportion of large size (30–40 mm) individuals was higher (59%) than the control group (28%). The proportion of 20–30 mm pearl oysters was the highest among the cultured population, accounting for 60% (**Figure 2**).

Differences in Physiological Performance

CR

CRs of pearl oysters of three groups are shown in **Figure 3A**. SL had a higher CR than the other two groups ($p < 0.05$) (**Table 3**). The value was about 1.8 times higher than CL and 5 times higher than SS.

OCR and AER

There were significant differences in OCR and AER between the SL and SS and CL (**Figures 3B,C**). ANOVA test showed that weight traits were significantly correlated with the changes of AER and OCR ($p < 0.05$) (**Table 3**). The AER and OCR decreased as the dry weight of soft tissues increased, and there was a negative correlation between them. The AER and OCR of SS were significantly higher than that in SL ($p < 0.05$). Under the same specifications, the AER and OCR in SL were significantly higher than that in CL ($p < 0.05$).

TABLE 2 | Statistical description of shell height of two groups of 6-month old pearl oysters.

Groups	Max/mm	Min/mm	Mean/mm	Median/mm	SD/mm	CV/%	*N*
Selective strain	37.51	10.11	30.64	31.52	5.12	17	100
Cultured population	37.12	10.43	26.71	27.10	5.60	21	100

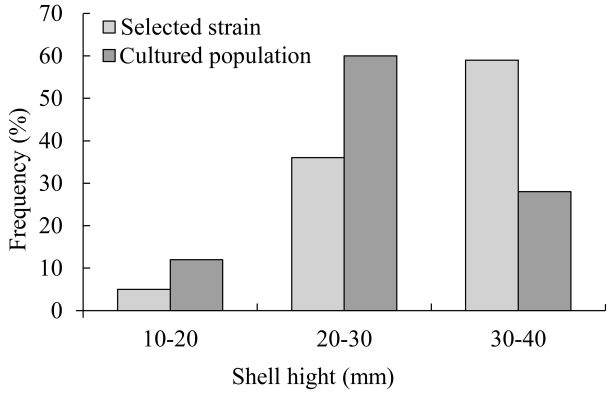

FIGURE 2 | Size distribution of selective strain and cultured population pearl oysters at 6-month-old.

Comparison of Enzyme Activities

Enzyme activities of the three groups are presented in **Figure 4**. For the three digestive enzymes, the activities of SL were significantly higher than those of SS and CL ($p < 0.05$). Amylase activity of SL was about 10 times higher than that of SS and 1.7 times higher than that of CL (**Figure 4A**). Although the specifications of CL and SS differ greatly, there was no significant difference in lipase activity between them (**Figure 4B**). When comparing the pepsin activity, significant differences were observed among three groups, and the activity in SL was about 3 times higher than that of SS (**Figure 4C**). For carbonic anhydrase, the enzyme activity in SL and CL was significantly higher than that in SS ($p < 0.05$) (**Figure 4D**).

DISCUSSION

In the present study, we compared the growth differences between the selective strain of *P. f. martensii* and the control group, and results showed that the growth rate of selective strain was significantly improved (14.61%) ($p < 0.05$), which was consistent with the previous study on 1-year-old selective strain pearl oyster (15.31%) (Wang et al., 2011a). The proportion of large-size (30–40 mm) oysters in the selected strain was two times higher than the cultured population. In addition, the median of shell height of the selected strain was larger, and the coefficient of variation was smaller, indicating that the cumulative multi-generation selection breeding improved the growth rate and reduced the phenotypic differences of the young generations (Wang et al., 2011b).

The differences of growth rate or survival were mainly caused by physiological variety, such as feeding, respiration, or enzyme activities (Bayne, 2000; Tamayo et al., 2014; Zhang et al., 2018; Zhao et al., 2019a, 2020). Feeding, respiration, and excretion are the most important basic forms of metabolism in organisms. In this study, we examined the difference of feeding and metabolism between the selected strain and cultured population of *P. f. martensii* and identified the mechanism responsible for the improved growth performance in the selective breeding of pearl oysters.

In this study, mean CR values in *P. f. martensii* ranged from 0.4 to 1.6 (L/g*h), which were close to the values of *Tapes decussatus* and banded carpet-shell clams *Paphia rhomboïdes* (Savina and Pouvreau, 2004), but comparatively lower than the values of the Indo-Pacific mytilid *Brachidontes pharaonis* (Sara et al., 2008) and clams *Ruditapes decussatus* (Sobral and Widdows, 1997). Inter-tidal species living in highly variable habitats should seize an immediate advantage from every profitable environmental situation allowing them to acquire energy to be allocated to growth and reproduction (Wang et al., 2015a). Pearl oysters showed a relatively low food acquisition speed, which explained that the species lived in an invariable condition. This hypothesis was proven by a study, which reported that ribbed mussel (*Geukensia demissa*) under subtidal zone conditions exhibited

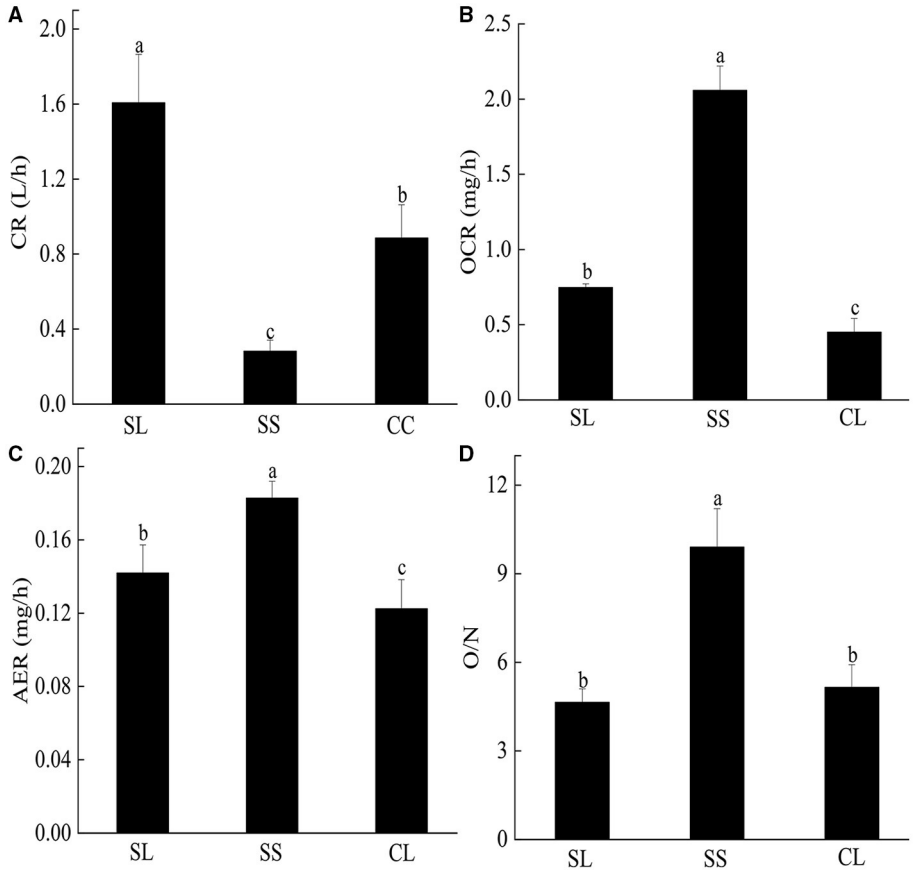

FIGURE 3 | (A–D) The clearance rate, oxygen consumption rate, ammonia excretion rate, and O/N rate of *P. f. martensii* in SL, CL, and SS groups. Means ± S.D. are presented. $n = 3$ replicate per treatment. Different letters represent significant differences ($p < 0.05$).

lower CR than intertidal conspecific (Charles and Newell, 1997). *P. f. martensii* is a species distributed in the subtidal zone (Wang et al., 2004). CR of the selected strain pearl oysters with a highly homologous genetic basis was significantly different, indicating that feeding rates were highly correlated with growth within species (Vladimirova et al., 2003). In the comparison between the selective strain and cultured population, CR values of the same size were also significantly different, which showed a reduced ecological footprint of the selective strain oysters (Hall et al., 2020). The results were similar to Tamayo et al. (2012), who found that the rapid growth of *R. philippinarum* showed a significantly higher CR than slow-growing ones, irrespective of temperature. Correlations between growth and CR have been published in several marine bivalves (Sousa et al., 2011; Tamayo et al., 2015; Zhang et al., 2018). The individuals with rapid growth had relatively higher clearance rate and absorption rate and lower metabolic cost (Hall et al., 2020). Bivalves may maximize energy for growth through rapid feeding. This hypothesis was supported by Bayne et al. (1999), who reported that rapid growth in Sydney rock oysters (*Saccostrea commercialism*) was positively related to increased food acquisition.

OCR is a crucial physiological parameter that reflects the energy metabolism level of aerobic respiration (Zhang et al., 2018). AER is considered an index to evaluate the tolerance of bivalves to environmental stress (Nie et al., 2017). In this study, OCR values ranged from 0.45 to 2.30 (mg/g*h), and AER values ranged from 0.07 to 0.19 (mg/g*h), which were different from the results reported by Wang et al. (2009). These differences may be caused by different temperatures, as temperature is a fundamental factor influencing energy metabolism in marine bivalves (Tamayo et al., 2015). Wang et al. (2009) also confirmed that OCR and AER of *P. f. martensii* were positively associated with temperature. The fast-growing selective strain of pearl oysters was obtained through generations of intensive mass selection. Therefore, the genetic basis was highly homologous (Wang et al., 2011a). According to the current study (showed in **Figure 3**), OCR and AER of SS pearl oysters were comparatively higher than SL. Such metabolic behavior was previously reported in *R. philippinarum* (Tamayo et al., 2011, 2012) and oyster (*C. gigas*) (Zhang et al., 2018), indicating that the size of an organism was closely associated with the metabolic rate (Kang et al., 2010). Generally, metabolic rate of the small specification was significantly faster than large

TABLE 3 | Analysis of variance (ANOVA) test of clearance rate, oxygen consumption rate, ammonia excretion rate, and O/N rate of *P. f. martensii* in the three groups.

Factor	DF	SS	MS	*F*	*P*
CR	2	3.52	1.76	42.14	0.001
OCR	2	5.549	2.73	318.43	0.001
AER	2	0.008	0.004	21.89	0.001
O/N	2	67.26	33.63	43.63	0.001

ones, including the larval stage (Beiras and Camacho, 1994; Kang et al., 2010; Xu et al., 2020). Higher metabolic rate in SS was associated with a smaller deficiency in heterozygote frequencies, a genetic condition imposing raised metabolic costs associated with elevated protein turnover rates (Hawkins et al., 1989; Hawkins, 1995; Tremblay et al., 1998; Myrand et al., 2002). As shown in **Figure 3**, both OCR and AER of metabolism were significantly higher in SL and SS than CL ($p < 0.05$). A similar metabolism behavior was reported in the hard clam (*Mercenaria mercenaria*), where the selective bred of hard clam showed a 33% increment in their standard OCR compared to the wild individuals (Pernet et al., 2006). It suggests that the differences in growth and metabolism of *P. f. martensii* are caused by genetic variation, and the genes that control growth are pleiotropic or closely linked to the genes determining physiological traits (Wang et al., 2009; Zhang et al., 2018).

O/N represents the ratio of protein to fat and carbohydrate catabolism in organism (Mayzaud, 1976). If the energy is completely supplied by protein, the O/N value is 7. If the energy is supplied by protein and fat, the ratio is 24. If the energy is completely supplied by fat or carbohydrate, the ratio will become infinite (Mayzaud, 1976). For SL and CL, the main energy supply was protein, followed by fat and carbohydrate, while the proportion of protein oxidation energy supply decreased for SS in this study. The results were consistent with *R. philippinarum* (Nie et al., 2017).

For energy utilization during the metabolic process, various complex organic compounds are hydrolyzed to monomeric subunits, including glucose, fatty acid, and amino acids (Boetius and Felbeck, 1995). Marine molluscs obtain multiple nutritional requirements by utilizing various digestive enzymes, such as amylase, lipase, trypsin, pepsin, and lysozyme, to catalyze and decompose different types of substrates (Weel, 1961; Wang et al., 2015b; Martínez-Montaño et al., 2018; Kong et al., 2019). In this study, we observed three typical digestive enzymes (amylase, lipase, and pepsin) in *P. f. martensii*. The types and activities of enzymes were different from those reported by Wang et al. (2010), for example, the value of amylase activity was comparatively lower than in their studies. The difference in the type and level of digestive enzymatic activity may be due to differences in diet (Fernández-Reiriz et al., 2001; Labarta et al., 2002; Alberto et al., 2020). In the experiment, we found no cellulase activity in any of the test tubes. During the experiment, the enzyme activity was examined to reduce the types of error in the feed. All groups were fed *I. galbana* for domestication, which was considered common feed for bivalves (Cheng et al., 2020). *I. galbana* has a naked cell without cell walls, but cellulase is related to the digestion of cell walls (Cheng et al., 2020), indicating the absence of cellulase in pearl oysters (*P. f. martensii*). In addition, digestive enzyme activity was strongly correlated with body size. A study on *Aulacomya ater* showed that increasing body-size increased specific amylase activity (Ibarrola et al., 2012). However, increasing body-size promoted a significant reduction in protease activity in *M. chilensis*, chorus mussel (*Choromytilus chorus*), and *A. ater* (Ibarrola et al., 2012). In the current study, the activities of three digestive enzymes were higher in large individuals (SL and CL) than SS, indicating a relatively higher food processing capacity in the gut of fast-growing pearl oysters (Tamayo et al., 2012). Metabonomics and transcriptome studies have showed that fast-growing pearl oysters (*P. f. martensii*) exhibited higher digestion, anabolic ability, and osmotic regulation ability than the slow-growing group (Hao et al., 2019).

The successive selection of fast-growing bivalves may have positive effects on hydrolytic activities of gland tissues and enzyme activities in digestive glands, which are closely correlated with the digestive capacities of bivalves (Ibarrola et al., 2000; Tamayo et al., 2015; Zhang et al., 2018). Studies on bivalves had confirmed that a significant degree of genetic control was exerted over parameters influencing energy utilization and growth efficiency, including oysters (Bayne et al., 1999; Parker et al., 2010) and green-lipped mussels (Ibarrola et al., 2017). By comparing first-generation yellow shell color and cultivated stocks of *P. f. martensii*, the digestive enzyme activity was effectively increased through breeding (Wang et al., 2010). We also obtained similar results for digestive enzyme activity.

Carbonic anhydrase, one of the major biocatalysts for carbon capture and storage, is involved in shell formation processes in bivalves. The activity of carbonic anhydrase in the mantle tissue of European abalone (*Haliotis tuberculate*) was closely related to the formation of shell structure (prismatic and nacreous layers) (Roy et al., 2012). Carbonic anhydrase plays a key role in regulating mineralized structures through calcium carbonate crystal formation (Cardoso et al., 2019). In the internal selected strain, SL had a higher carbonic anhydrase activity than SS, indicating that larger pearl oysters had a higher calcium carbonate formation and shell mineralization. Studies on blue mussels (*M. edulis*) have confirmed that carbonic anhydrase activity is essential for rapid shell development (Medaković, 2000). Wilbur and Anderson (1950) also reported that enzyme content might increase with the development of shellfish.

CONCLUSION

In summary, pearl oysters (*P. f. martensii*) from the fast-growing selective strain had more efficient food ingestion, food digestion, and energy absorption compared to the cultured population. In the inter selective strain, the OCR of SS was nearly 3 times higher than that of SL, and the

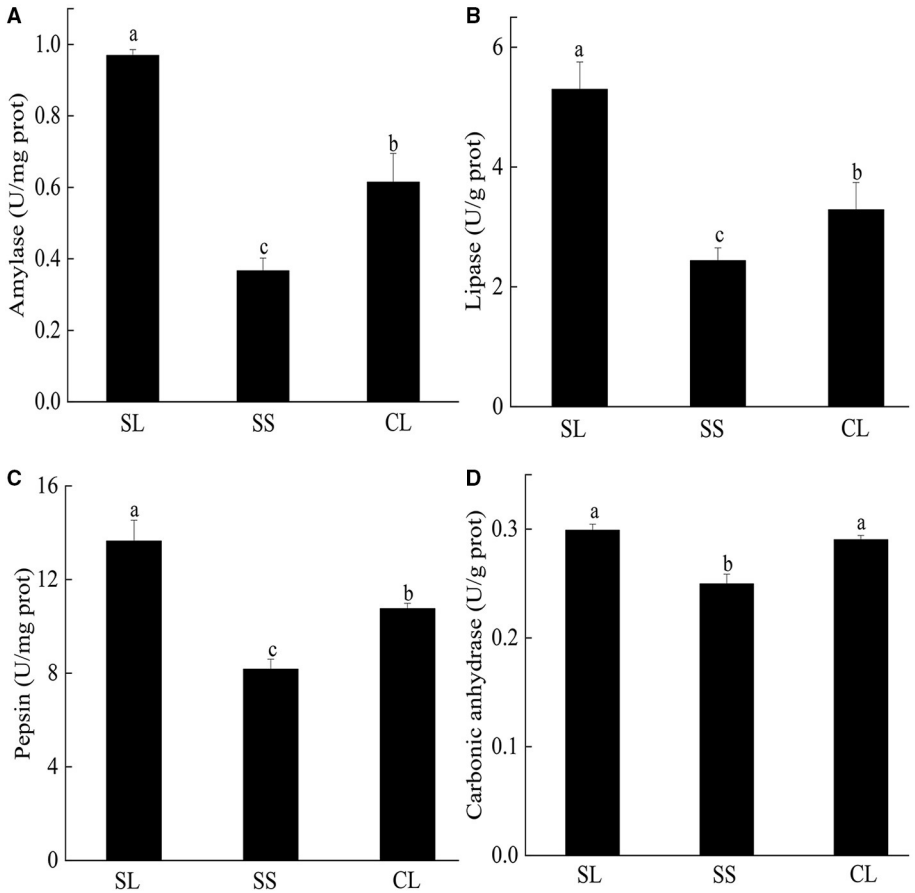

FIGURE 4 | (A–D) Specific activities of amylase, pepsin, lipase, and carbonic anhydrase activities in the visceral mass of *P. f. martensii*. Means ± S.D. are presented. $n = 3$ replicate per treatment. Different letters represent significant differences ($p < 0.05$).

AER of SS was 1.5 times higher than that of SL, which proved that a combination of fast feeding and reduced metabolic costs would enable SL to increase their growth rate. In order to identify growth-related regulatory genes, further investigation is required to compare gene expression in contrasting physiological phenotypes.

DATA AVAILABILITY STATEMENT

The original contributions presented in the study are included in the article/**Supplementary Material**, further inquiries can be directed to the corresponding author/s.

ETHICS STATEMENT

The animal study was reviewed and approved by the Committee and Laboratory Animal Department of Hainan University. Written informed consent was obtained from the owners for the participation of their animals in this study.

AUTHOR CONTRIBUTIONS

AW and CL designed the experiment. BY and ML performed the experiment. ZG analyzed the experimental data and draw diagrams. XZ wrote the paper. SY revised the paper. All authors contributed to the article and approved the submitted version.

FUNDING

This research was supported financially by the National Key Research and Development Program of China (2018YFD0900704), the National Natural Science Foundation of China (1772847), and the Talent Development Program of Hainan Province (HD-YSZX-202011).

SUPPLEMENTARY MATERIAL

The Supplementary Material for this article can be found online at: https://www.frontiersin.org/articles/10.3389/fmars.2021.770702/full#supplementary-material

REFERENCES

Alberto, P. R., Gabriela, M. A., Regina, E. G., Gabriela, M. C., Dariel, T. R., and Cristina, E. F. (2020). Seaweed single cell detritus effects on the digestive enzymes activity and microbiota of the oyster *Crassostrea gigas*. *J. Appl. Phycol.* 32, 3481–3493. doi: 10.1007/s10811-020-02167-4

Bayne, B. L. (1999). Physiological components of growth differences between individual oysters (*Crassostrea gigas*) and a comparison with *Saccostrea commercialis*. *Physiol. Biochem. Zool.* 72:705. doi: 10.1086/316714

Bayne, B. L. (2000). Relations between variable rates of growth, metabolic costs and growth efficiencies in individual Sydney rock oysters (*Saccostrea commercialis*). *J. Exp. Mar. Bio. Ecol.* 251, 185–203. doi: 10.1016/S0022-0981(00)00211-2

Bayne, B. L., Svensson, S., and Nell, J. A. (1999). The physiological basis for faster growth in the sydney rock oyster, *Saccostrea commercialis*. *Biol. Bull–US.* 197, 377–387. doi: 10.2307/1542792

Beiras, R., and Camacho, A. P. (1994). Influence of food concentration on the physiological energetics and growth of *Ostrea edulis* larvae. *Mar. Biol.* 120, 427–435. doi: 10.1007/bf00680217

Boetius, A., and Felbeck, H. (1995). Digestive enzymes in marine invertebrates from hydrothermal vents and other reducing environments. *Mar. Biol.* 122, 105–113. doi: 10.1007/BF00349283

Cardoso, J. C. R., Ferreira, V., Zhang, X., Anjos, L., Félix, R. C., Batista, F. M., et al. (2019). Evolution and diversity of alpha-carbonic anhydrases in the mantle of the Mediterranean mussel (*Mytilus galloprovincialis*). *Sci. Rep.* 9:10400. doi: 10.1038/s41598-019-46913-2

Charles, F., and Newell, R. (1997). Digestive physiology of the ribbed mussel *Geukensia demissa* (Dillwyn) held at different tidal heights. *J. Exp. Mar. Biol. Ecol.* 209, 201–213. doi: 10.1016/S0022-0981(96)02694-9

Cheng, P., Zhou, C., Chu, R., Chang, T., Xu, J., Ruan, R., et al. (2020). Effect of microalgae diet and culture system on the rearing of bivalve mollusks: Nutritional properties and potential cost improvements. *Algal. Research.* 51:102076. doi: 10.1016/j.algal.2020.102076

Deng, Y., Du, X., and Wang, Q. (2009a). Selection for fast growth in the chinese pearl oyster, pinctada martensii: response of the first generation line. *J. World. Aquacult. Soc.* 40, 843–847. doi: 10.1111/j.1749-7345.2009.00307.x

Deng, Y., Fu, S., Du, X., and Wang, Q. (2009b). Realized heritability and genetic gain estimates of larval shell length in the chinese pearl oyster *pinctada martensii* at three different salinities. *N. Am. J. Aquacult.* 71, 302–306. doi: 10.1577/A08-024.1

Deng, Y., Yu, Z., Du, X., Wang, Q., and Fu, S. (2011). Growth performance and physiological parameters of the second generation selected and control groups of *pinctada martensii*. *Acta. Oceanol. Sin.* 30, 120–125. doi: 10.1007/s13131-011-0112-9

Evans, S., and Langdon, C. (2006). Direct and indirect responses to selection on individual body weight in the Pacific oyster (*Crassostrea gigas*). *Aquaculture* 261, 546–555. doi: 10.1016/j.aquaculture.2006.07.037

Fernández-Reiriz, M., Labarta, U., Navarro, J., and Velasco, A. (2001). Enzymatic digestive activity in *Mytilus chilensis* (Hupé 1854) in response to food regimes and past feeding history. *J. Comp. Physiol. B.* 171, 449–456. doi: 10.1007/s003600100194

Gonzalez, G. G., Brokordt, K. B., and Winkler, F. E. (2010). Repeatability of physiological traits in juvenile Pacific abalone, *Haliotis discus* hannai. *Mar. Biol.* 157, 2195–2203. doi: 10.1007/s00227-010-1485-6

Gu, Z., Shi, Y., Wang, Y., and Wang, A. (2011). Heritable characteristics in the pearl oyster Pinctada martensii: comparisons of growth and shell morphology of Chinese and Indian populations, and reciprocal crosses. *J. Shellfish Res.* 30, 241–246. doi: 10.2983/035.030.0207

Gu, Z., Wei, H., Cheng, F., Wang, A., and Liu, C. (2020). Effects of air exposure time and temperature on physiological energetics and oxidative stress of winged pearl oyster (*Pteria penguin*). *Aquacult. Rep.* 17:100384. doi: 10.1016/j.aqrep.2020.100384

Hall, S. A., Méthé, D., Stewart-Clark, S. E., Clark, K. F., and Tremblay, R. (2020). Comparison of absorption efficiency and metabolic rate between wild and aquaculture oysters (*Crassostrea virginica*). *Aquaculture. Rep.* 16:100263. doi: 10.1016/j.aqrep.2019.100263

Hao, R., Du, X., Yang, C., Deng, Y., Zheng, Z., and Wang, Q. (2019). Integrated application of transcriptomics and metabolomics provides insights into unsynchronized growth in pearl oyster *Pinctada fucata martensii*. *Sci. Total Environ.* 666, 46–56. doi: 10.1016/j.scitotenv.2019.02.221

Hawkins, A. J. S. (1995). Effects of temperature change on ectotherm metabolism and evolution: Metabolic and physiological interrelations underlying the superiority of multi-locus heterozygotes in heterogeneous environments. *J. Therm. Biol.* 20, 23–33. doi: 10.1016/0306-4565(94)00023-C

Hawkins, A. J. S., Widdows, J., and Bayne, B. L. (1989). The relevance of whole-body protein metabolism to measured costs of maintenance and growth in *Mytilus edulis*. *Physiol. Zool.* 62, 745–763. doi: 10.1086/physzool.62.3.30157925

He, G., Liu, X., Xu, Y., Liang, J., Deng, Y., Zhang, Y., et al. (2021). Repeated exposure to simulated marine heatwaves enhances the thermal tolerance in pearl oysters. *Aquat. Toxicol.* 239:105959. doi: 10.1016/j.aquatox.2021.105959

Ibarrola, I., Arambalza, U., Navarro, J. M., Urrutia, M. B., and Navarro, E. (2012). Allometric relationships in feeding and digestion in the Chilean mytilids *Mytilus chilensis* (Hupé), *Choromytilus chorus* (Molina) and *Aulacomya ater* (Molina): A comparative study. *J. Exp. Mar. Biol. Ecol.* 426–427, 18–27. doi: 10.1016/j.jembe.2012.05.012

Ibarrola, I., Etxeberria, M., Iglesias, J. I. P., Urrutia, M. B., and Angulo, E. (2000). Acute and acclimated digestive responses of the cockle *Cerastoderma edule* (L.) to changes in the food quality and quantity II. Enzymatic, cellular and tissular responses of the digestive gland. *J. Exp. Mar. Biol. Ecol.* 21, 181–198. doi: 10.1016/s0022-0981(00)00233-1

Ibarrola, I., Hilton, Z., and Ragg, N. L. C. (2017). Physiological basis of inter-population, inter-familiar and intra-familiar differences in growth rate in the green-lipped mussel *Perna canaliculus*. *Aquaculture* 479, 544–555. doi: 10.1016/j.aquaculture.2017.06.031

Kang, K. H., Haemgoong, P., Kim, Y. H., Seon, S. C., and Zhou, B. (2010). Filtration and oxygen consumption rates on various growth stages of Scapharca broughtonii spat. *Aquaculture. Res.* 39, 195–199. doi: 10.1111/j.1365-2109.2007.01879.x

Kong, H., Wu, F., Jiang, X., Wang, T., Hu, M., Chen, J., et al. (2019). Nano-TiO_2 impairs digestive enzyme activities of marine mussels under ocean acidification. *Chemosphere* 237:124561. doi: 10.1016/j.chemosphere.2019.124561

Labarta, U., Fernández-Reiriz, M. J., Navarro, J. M., and Velasco, A. (2002). Enzymatic digestive activity in epifaunal (Mytilus chilensis) and infaunal (Mulinia edulis) bivalves in response to changes in food regimes in a natural environment. *Marine Biol.* 140, 669–676. doi: 10.1007/s00227-001-0742-0

Li, C., Liu, E., Li, T., Wang, A., Liu, C., and Gu, Z. (2020). Suitability of three seaweeds as feed in culturing strawberry conch *Strombus luhuanus*. *Aquaculture* 519:734761. doi: 10.1016/j.aquaculture.2019.734761

Li, Q., Wang, Q., Liu, S., and Kong, L. (2011). Selection response and realized heritability for growth in three stocks of the Pacific oyster *Crassostrea gigas*. *Fisheries. Sci.* 77, 643–648. doi: 10.1007/s12562-011-0369-0

Martínez-Montaño, E., Uriarte, I., Rosas, C., Amthauer, R., Romero, A., and Farías, A. (2018). Replacing live feed with formulated diets in juvenile Patagonian red octopus (*Enteroctopus megalocyathus*). *Aquacult. Nutr.* 24, 633–643. doi: 10.1111/anu.12589

Mayzaud, P. (1976). Respiration and nitrogen excretion of zooplankton. IV. The influence of starvation on the metabolism and the biochemical composition of some species. *Mar. Biol.* 37, 47–58. doi: 10.1007/BF00386778

Medaković, D. (2000). Carbonic anhydrase activity and biomineralization process in embryos, larvae and adult blue mussels *Mytilus edulis* L. *Helgol. Mar. Res.* 54, 1–6. doi: 10.1007/s101520050030

Meyer, E., and Manahan, D. T. (2010). Gene expression profiling of genetically determined growth variation in bivalve larvae (*Crassostrea gigas*). *J. Exp. Biol.* 213:749. doi: 10.1242/jeb.037242

Myrand, B., Tremblay, R., and Sévigny, J. M. (2002). Selection against blue mussels (*Mytilus edulis* L.) homozygotes under various stressful conditions. *J. Hered.* 93, 238–248. doi: 10.1093/jhered/93.4.238

Newkirk, G. F. (1980). Review of the genetics and the potential for selective breeding of commercially important bivalves. *Aquaculture* 19, 209–228. doi: 10.1016/0044-8486(80)90045-9

Nie, H. T., Huo, Z. M., Hou, X. L., Chen, Y., Yang, F., Yan, X. W., et al. (2017). Comparison study on the effect of temperature and salinity on oxygen consumption and ammonia excretion in zebra strain and wild *ruditapes philippinarum*. *Acta. Hydrobiol. Sinica* 41, 121–126.

Pace, D. A., Marsh, A. G., Leong, P. K., Green, A. J., D., Hedgecock, and Manahan, D. T. (2006). Physiological bases of genetically determined variation in growth of marine invertebrate larvae: A study of growth heterosis in the bivalve *Crassostrea gigas*. *J. Exp. Mar. Biol. Ecol.* 335, 188–209. doi: 10.1016/j.jembe.2006.03.005

Parker, L. M., Ross, P. M., and O'Connor, W. A. (2010). Comparing the effect of elevated pCO^2 and temperature on the fertilization and early development of two species of oysters. *Mar. Biol.* 157, 2435–2452. doi: 10.1007/s00227-010-1508-3

Pernet, F., Tremblay, R., Gionet, C., and Landry, T. (2006). Lipid remodeling in wild and selectively bred hard clams at low temperatures in relation to genetic and physiological parameters. *J. Exp. Biol.* 209, 4663–4675. doi: 10.1242/jeb.02581

Roy, N. L., Marie, B., Gaume, B., Guichard, N., Delgado, S., Zanella-Cléon, I., et al. (2012). Identification of two carbonic anhydrases in the mantle of the european abalone *Haliotis tuberculata* (Gastropoda, Haliotidae): Phylogenetic Implications. *J. Exp. Zool. Part. B.* 318, 353–367. doi: 10.1002/jez.b.22452

Sara, G., Romano, C., Widdows, J., and Staff, F. J. (2008). Effect of salinity and temperature on feeding physiology and scope for growth of an invasive species (*Brachidontes pharaonis*-mollusca: bivalvia) within the Mediterranean sea. *J. Exp. Mar. Biol. Ecol.* 363, 130–136. doi: 10.1016/j.jembe.2008.06.030

Savina, M., and Pouvreau, S. (2004). A comparative ecophysiological study of two infaunal filter-feeding bivalves: *Paphia rhombodes* and *Glycymeris glycymeris*. *Aquaculture* 239, 289–306. doi: 10.1016/j.aquaculture.2004.05.029

Schöne, B. R., Huang, X., Zettler, M. L., Zhao, L., Mertz-Kraus, R., Jochum, K. P., et al. (2021). Mn/Ca in shells of Arctica islandica (Baltic Sea) – A potential proxy for ocean hypoxia? Estuar. *Coast Shelf S* 251:107257. doi: 10.1016/j.ecss.2021.107257

Sobral, P., and Widdows, J. (1997). Effects of elevated temperatures on the scope for growth and resistance to air exposure of the clam *Ruditapes decussatus* (L.), from southern Portugal. *Sci. Mar.* 61:1128. doi: 10.1023/A:1018435711128

Sousa, J., Matias, D., Joaquim, S., Ben-Hamadou, R., and Leitão, A. (2011). Growth variation in bivalves: New insights into growth, physiology and somatic aneuploidy in the carpet shell *Ruditapes decussatus*. *J. Exp. Mar. Biol. Ecol.* 406, 46–53. doi: 10.1016/j.jembe.2011.06.001

Tamayo, D., Ibarrola, I., Cigarria, J., and Navarro, E. (2015). The effect of food conditioning on feeding and growth responses to variable rations in fast and slow growing spat of the Manila clam (*Ruditapes philippinarum*). *J. Exp. Mar. Biol. Ecol.* 471, 92–103. doi: 10.1016/j.jembe.2015.05.017

Tamayo, D., Ibarrola, I., and Navarro, E. (2012). Thermal dependency of clearance and metabolic rates in slow and fast growing spat of Manila clam *Ruditapes philippinarum*. *Comp. Biochem. Physiol. A. Mol. Integr. Physiol.* 163, 893–904. doi: 10.1007/s00360-013-0764-1

Tamayo, D., Ibarrola, I., Urrutia, M. B., and Navarro, E. (2011). The physiological basis for inter-individual growth variability in the spat of clams (*Ruditapes philippinarum*). *Aquaculture* 321, 113–120. doi: 10.1016/j.aquaculture.2011.08.024

Tamayo, D., Ibarrola, I., Urrutxurtu, I., and Navarro, E. (2014). Physiological basis of extreme growth rate differences in the spat of oyster (*Crassostrea gigas*). *Mar. Biol.* 161, 1627–1637. doi: 10.1007/s00227-014-2447-1

Tremblay, R., Myrand, B., Sevigny, J. M., Blier, P., and Guderley, H. (1998). Bioenergetic and genetic parameters in relation to susceptibility of blue mussels, *Mytilus edulis* (L.) to summer mortality. *J. Exp. Mar. Biol. Ecol.* 221, 27–58. doi: 10.1016/S0022-0981(97)00114-7

Vega-Villasante, F., Nolasco, H., and Civera, R. (1993). The digestive enzymes of the pacific brown shrimp *penaeus californiensis*.: I—properties of amylase activity in the digestive tract. *Comp. Biochem. Phys. B.* 106, 547–550. doi: 10.1016/0305-0491(93)90130-W

Vladimirova, I. G., Kleimenov, S. Y., and Radzinskaya, L. I. (2003). The relation of energy metabolism and body weight in bivalves (Mollusca: Bivalvia). *Biol. Bull. Russ. Acad. Sci.* 30, 392–399. doi: 10.1023/A:1024822225406

Wang, A., Deng, F., Zhang, X., Yan, B., and Zhang, M. (2000). RAPD Analysis on genetic diversity of *Pinctada martensii* Dunker. *Wuhan University J.* 46, 467–470.

Wang, A., Shi, Y., and Zhou, Z. (2004). Morphological trait parameters and their correlations of the first generation from matings and crosses of geographical populations of *Pinctada martensii* (Dunker). *Mar. Fish. Res.* 25, 39–45.

Wang, A., Wang, Y., Gu, Z., Li, S., Shi, Y., Guo, X., et al. (2011a). Development of expressed sequence tags from the pearl oyster, *Pinctada martensii* Dunker. *Mar. Biotechnol.* 13, 275–283. doi: 10.1007/s10126-010-9296-9

Wang, J., Zhao, L., Liu, J., Wang, H., and Xiao, S. (2015a). Effect of potential probiotic Rhodotorula benthica D30 on the growth performance, digestive enzyme activity and immunity in juvenile sea cucumber *Apostichopus japonicus*. *Fish. Shellfish. Immun.* 43, 330–336. doi: 10.1016/j.fsi.2014.12.028

Wang, Q., Deng, Y., Du, X., Fu, S., and Lu, Y. (2011b). Realized heritability and genetic gains of three generations for superior growth in the pearl oyster *Pinctada martensii*. *Acta Ecol. Sinica* 31, 108–111. doi: 10.1016/j.chnaes.2010.12.001

Wang, Q., Zhang, S., Du, X., Deng, Y., and Huang, R. (2009). Comparison of oxygen consumption rate and NH^3 excretion rate of the first-generation yellow shell color and control groups at different temperatures and salinities. *J. Fish. China* 33, 790–796.

Wang, Q., Zhang, S., Du, X., Deng, Y., and Huang, R. (2010). A comparative analysis of digestive enzyme activities of first generation yellow shell color and cultivated stocks of *Pinctada martensii* at suitable growth temperatures. *J. Fish. Sci. China*. 6, 1351–1356. doi: 10.3724/SP.J.1011.2010.01351

Wang, Y., Li, L., Hu, M., and Lu, W. (2015b). Physiological energetics of the thick shell mussel *Mytilus coruscus* exposed to seawater acidification and thermal stress. *Sci. Total. Environ.* 514, 261–272. doi: 10.1016/j.scitotenv.2015.01.092

Weel, P. B. V. (1961). The comparative physiology of digestion in molluscs. *Am. Zool.* 1, 245–252. doi: 10.1093/icb/1.2.245

Wilbur, K. M., and Anderson, N. G. (1950). Carbonic anhydrase and growth in the oyster and busycon. *Biol. Bull.* 98, 19–24. doi: 10.2307/1538594

Xu, C., Li, Q., and Chong, J. (2020). Combined effect of temperature, salinity, and rearing density on the larval growth of the black shell strain and wild population of the Pacific oyster *Crassostrea gigas*. *Aquacult. Int.* 28, 1–13. doi: 10.1007/s10499-019-00465-4

Xu, Y., Zhang, Y., Liang, J., He, G., Liu, X., Zheng, Z., et al. (2021). Impacts of marine heatwaves on pearl oysters are alleviated following repeated exposure. *Mar. Pollut. Bull.* 173:112932. doi: 10.1016/j.marpolbul.2021.112932

Zhang, J., Li, Q., Liu, S., and Yu, H. (2018). The effect of temperature on physiological energetics of a fast-growing selective strain and a hatchery population of the Pacific oyster (*Crassostrea gigas*). *Aquac. Res.* 49, 2844–2851. doi: 10.1111/are.13747

Zhao, L., Liu, L., Liu, B., Liang, J., Lu, Y., and Yang, F., (2019a). Antioxidant responses to seawater acidification in an invasive fouling mussel are alleviated by transgenerational acclimation. *Aquat. Toxicol.* 217:105331. doi: 10.1016/j.aquatox.2019.105331

Zhao, L., Shirai, K., Tanaka, K., Milano, S., Higuchi, T., Murakami-Sugihara, N., et al. (2020). A review of transgenerational effects of ocean acidification on marine bivalves and their implications for sclerochronology. *Estuar. Coast Shelf S* 235:106620. doi: 10.1016/j.ecss.2020.106620

Zhao, L., Zuykov, M., Tanaka, K., Shirai, K., Anderson, J., McKindsey, C. W., et al. (2019b). New insight into ligh-enhanced calcification in mytilid mussels, *Mytilus* sp., infected with photosynthetic algae *Coccomyxa* sp.: $\delta^{13}C$ value and metabolic carbon record in shells. *J. Exp. Mar. Biol. Ecol.* 520:151211. doi: 10.1016/j.jembe.2019.151211

Zheng, H., Zhang, G., Liu, X., Zhang, F., and Guo, X. (2004). Different responses to selection in two stocks of the bay scallop, *Argopecten irradians irradians* Lamarck (1819). *J. Exp. Mar. Biol. Ecol.* 313, 213–223. doi: 10.1016/j.jembe.2004.04.015

Conflict of Interest: The authors declare that the research was conducted in the absence of any commercial or financial relationships that could be construed as a potential conflict of interest.

Publisher's Note: All claims expressed in this article are solely those of the authors and do not necessarily represent those of their affiliated organizations, or those of the publisher, the editors and the reviewers. Any product that may be evaluated in this article, or claim that may be made by its manufacturer, is not guaranteed or endorsed by the publisher.

frontiers in Marine Science

ORIGINAL RESEARCH
published: 06 December 2021
doi: 10.3389/fmars.2021.793118

Characterizing the Role of *Glutamine synthetase* Gene on Ammonia Nitrogen Detoxification Metabolism of the Razor Clam *Sinonovacula constricta*

Gaigai Sun[1,2], Changsen Sun[3], Jing He[1,3], Hanhan Yao[1], Wenfang Dai[3], Zhihua Lin[1,3] and Yinghui Dong[1,3]**

[1] Key Laboratory of Aquatic Germplasm Resources of Zhejiang, College of Biological and Environmental Sciences, Zhejiang Wanli University, Ningbo, China, [2] College of Fisheries, Henan Normal University, Xinxiang, China, [3] Ninghai Institute of Mariculture Breeding and Seed Industry, Zhejiang Wanli University, Ningbo, China

OPEN ACCESS

Edited by:
Yuehuan Zhang,
South China Sea Institute of Oceanology, Chinese Academy of Sciences (CAS), China

Reviewed by:
Shoubao Yang,
Shaoxing University, China
Xiujun Sun,
Chinese Academy of Fishery Sciences (CAFS), China

***Correspondence:**
Jing He
hejing226@126.com
Yinghui Dong
dongyinghui118@126.com

Specialty section:
This article was submitted to Marine Fisheries, Aquaculture and Living Resources, a section of the journal Frontiers in Marine Science

Received: 11 October 2021
Accepted: 28 October 2021
Published: 06 December 2021

Citation:
Sun G, Sun C, He J, Yao H, Dai W, Lin Z and Dong Y (2021) Characterizing the Role of Glutamine synthetase Gene on Ammonia Nitrogen Detoxification Metabolism of the Razor Clam Sinonovacula constricta. Front. Mar. Sci. 8:793118. doi: 10.3389/fmars.2021.793118

Ammonia nitrogen is a common toxic substance in the aquatic system, which seriously threatens the survival and growth of clams. However, less is known about the ammonia metabolism and detoxification strategy in razor clam. In this study, the polymorphism of the *Glutamine synthetase* gene from *Sinonovacula constricta* (*Sc-GS*) was found to be related to ammonia tolerance. By comparing the coding sequence (CDS) region of *Sc-GS* from two geographical populations, a total of 14 and 12 single nucleotide polymorphisms (SNPs) were identified, respectively, of which 10 loci were shared between the two populations. Among them, the locus c.1133T > G exhibited an extremely significant and strong association with ammonia tolerance in both populations ($P < 0.01$), and it was missense mutation, which led to the amino acid change from leucine (Leu) to arginine (Arg). Furthermore, the results about H&E staining and immunohistochemistry of Sc-GS protein in gills and hepatopancreas revealed that it was specifically localized in the lateral cilia of gill filaments and the endothelial cells of hepatocytes. After inhibiting the *Sc-GS* expression by RNA interference (RNAi) technology, the transcript levels of *Sc-GS* were extremely significantly downregulated at 24, 48, 72, and 96 h ($P < 0.01$) in the hepatopancreas. Taken together, these results indicated that the *Sc-GS* gene may participate in ammonia metabolism. In addition, these results will help to demonstrate the role of *Sc-GS* in ammonia nitrogen metabolism and provide markers related to ammonia nitrogen tolerance for molecular marker-assisted selection (MAS) of the razor clam.

Keywords: ***Sinonovacula constricta*, ammonia tolerance, *Glutamine synthetase*, SNP, immunohistochemistry, RNAi**

INTRODUCTION

As we all know, the bivalve aquaculture industry is one of the fastest-growing global food sectors, and 89% of bivalves produced all over the world are from aquaculture (FAO, 2020). At present, mollusk aquaculture has accounted for 70% (20 million tons) of the total production of aquatic animals (FAO, 2020). The razor clam *Sinonovacula constricta*, which is an economically and

ecologically important marine bivalve, with an annual output of 860,265 tons in 2020 (The Ministry of Agriculture and Fishery of the People's Republic of China, 2021), was mainly polycultured with shrimps, crabs, and fish in Zhejiang and Fujian provinces of China (Li et al., 2015). Under a high-intensive cultivation situation, clams were threatened by various complex contaminants, such as nitrite and ammonia, which were typically important toxicity effectors in aquaculture systems (Cheng et al., 2019). *S. constricta*, as a benthic bivalve, often lives in mudflats or under 30 ∼ 40 cm of mud in ponds (Frankic and Hershner, 2003), they tend to experience more severe ammonia stress than other aquatic organisms (Zhang et al., 2020). Although it has been demonstrated that mollusks have a high tolerance to ammonia nitrogen (Widman et al., 2008), there are few reports on their detoxification mechanism of ammonia.

Ammonia exists in seawater with two different forms: NH_4^+ (ionized form) and NH_3 (unionized form) (Francis-Floyd et al., 2009), of which NH_3 (ammonia nitrogen) is toxic to the health of aquatic organisms because it can easily diffuse across the cell membrane (Randall and Tsui, 2002). In addition, ammonia is a primary environmental factor that can rapidly increase the mortality rate in the aquaculture industry and often brings serious economic losses to the aquatic cultivation industry (Schock et al., 2013). The high-concentration ammonia can reach a lethal effect on most aquatic animals, especially for invertebrates such as Manila clam *Ruditapes philippinarum* (Cong et al., 2017), Pacific white shrimp *Litopenaeus vannamei* (Zhang L. et al., 2018), and giant river prawn *Macrobrachium rosenbergii* (Dong et al., 2020). In addition, the different tissues from the same species differently respond to ammonia stress. For instance, it has been reported that ammonia level was higher in the hepatopancreases and gills than hemolymph and muscle when black tiger prawn *Penaeus monodon* was exposed to 0.718 mM ammonia (Chen and Chen, 2000). Similarly, the ammonia contents in the liver of swamp eel (*Monopterus albus*) had the highest levels under the 0.75 mM ammonia exposure (Ip et al., 2004). Furthermore, accumulating evidence has shown that their gills suffered significant physiological and histological damage when mollusk was exposed to toxic substances (e.g., the concentration of pH or ammonia exceeds the normal level) (Saravana and Geraldine, 2000; Henry et al., 2012). Accordingly, the lesion degree of the liver and gill is often used to assess the toxicity degree of harmful substances of aquatic animals (Mishra and Mohanty, 2008). In recent years, it has been reported the protein localization of genes related to ammonia-nitrogen excretion (Bucking et al., 2013; Boo et al., 2018; Sunga et al., 2020). However, at present, less is known about the protein localization of genes related to ammonia metabolism in the gill and hepatopancreas of benthic mollusk exposed to high ammonia.

Previous studies found that the synthesis of glutamine (Gln) was one of the most critical strategies to defend against ammonia toxicity, which was adopted by many invertebrates and vertebrate organisms, such as yellow catfish *Pelteobagrus fulvidraco* (Li et al., 2016), sea cucumber *Apostichopus japonicus* (Wang et al., 2014), swimming crab *Portunus trituberculatus* (Si et al., 2018), and *L. vannamei* (Qiu et al., 2018). Non-toxic Gln can be stored in the body and is used for other anabolic processes (Zhang et al., 2020). Gln was composed of glutamate (Glu) and ammonium (NH_4^+), which was catalyzed by Glutamine synthetase (GS) (Tok et al., 2011). GS was a multifunctional enzyme in nitrogen metabolism, which was a gateway to the conversion of inorganic nitrogen into organic nitrogen (Ding et al., 2018). However, few studies focus on the role of the *GS* gene on ammonia detoxification metabolism in mollusks. Zhang et al. (2020) found that the mRNA and protein expression levels of the *GS* gene from *S. constricta* (*Sc-GS*) were significantly increased under ammonia challenge ($P < 0.05$), which were higher in gills and hepatopancreases than foot, mantle, adductor muscle and haemocytes. Therefore, the *Sc-GS* gene was considered as the main object of the study, and its correlation with ammonia tolerance was analyzed by probing its gene polymorphism in two typical geographical populations of *S. constricta*. In addition, we tried to explore the histocellular localization and function of Sc-GS protein in response to ammonia nitrogen stress. Then, we identified the mRNA expression levels of *Sc-GS* at different times after RNA interference (RNAi) technology. These results provide a basis for screening the candidate genes of ammonia-nitrogen tolerance and for studying the molecular mechanism of ammonia-nitrogen metabolism regulation.

MATERIALS AND METHODS

Ethics Statement

The razor clams used in this study were from the Genetic Breeding Research Center of Zhejiang Wanli University, China, and all experimental procedures were approved by the Institutional Animal Care and Use Committee (IACUC) of Zhejiang Wanli University, China.

Sample Collection and Challenge Experiments

Two geographical populations of the razor clam *S. constricta* (shell length = 51.49 ± 4.32 mm, wet weight = 7.58 ± 1.45 g), consisting of 3,000 individuals at the age of 1 year, were sampled from Zhejiang (ZJ) and Fujian (FJ) provinces in China, respectively. Then, these clams were used for single nucleotide polymorphism (SNP) analysis, H&E, and immunohistochemistry test of the *Sc-GS* gene. All the clams were maintained in a 500-L recirculating seawater tank with a temperature of 23.5°C and a salinity of 20 with aeration for 3 days before experimentation and were fed with golden-brown algae two times per day. Before the ammonia stress experiment, 6 healthy clams were selected from the ZJ population for histological morphology study. During the ammonia challenge experiment, 2,400 clams from each population were randomly divided into 6 tanks (500 L), 3 control groups (CGs), and 3 ammonia stress groups (AGs). The CGs were filled with natural seawater, and the stress concentrations of ammonia in AGs were 180 mg/L (actual concentration = 174.00 ± 5.81 mg/L, the corresponding NH_3 concentrations was 7.23 ± 0.17 mg/L, according to the 96-h LC50 values of the study by Zhang et al., 2020). The ammonia concentration was adjusted by diluting 1,000 mg/L total ammonia

stock solution that is disposed of NH_4Cl (Sangon, Shanghai, China). All the clams were monitored at intervals of 2 h for the removal of dead individuals in time, and at the same time, the pH of AGs and CGs were detected to maintain at about 8 for ammonia exposure for 120 h.

The surviving clams from the 6 AGs (i.e., 3 AGs in each population) throughout the ammonia challenge experiment were divided into an ammonia tolerant group (TG). Then, the hepatopancreases of individuals in the TGs were dissected for RNA extraction. At the same time, gills and hepatopancreases of five clams were collected from AG and CG of the FJ population for the histocellular localization study.

RNA Interference Experiment

Live and healthy clams (1-year old, shell length = 52.15 ± 4.12 mm, and wet weight = 7.73 ± 1.38 g) were collected at the Ningbo Marine and Fishery Science and Technology Innovation Base (Zhejiang province, China) for RNAi assays. The control conditions of these clams acclimatized in seawater were the same as mentioned earlier.

For the *Sc-GS* RNAi assay, 300 healthy clams were selected and divided into 6 groups, in which three groups were treated as AGs and the remaining three groups as the CGs (the treatments of AGs and CGs were the same as mentioned earlier) for 120 h. The siRNA-negative control (NC, **Table 1**) and diethyl pyrocarbonate (DEPC)-treated water (DEPC-W) were used as a CG. *Sc-GS* small interfering RNA (siRNA-*GS*, Sangon, Shanghai, China, **Table 1**) was diluted to 5,000 ng/μl with DEPC-W and injected into the adductor muscle of clams in one group of AGs, and the remaining two groups were injected into NC and DEPC-W, respectively. The same treatment was used for the CGs. Then, the hepatopancreases of six clams from each group were collected at 0, 24, 48, 72, 96, and 120 h postinjection. These selected hepatopancreases were cut into pieces for RNA extraction.

RNA Extraction and cDNA Synthesis

The quality and quantity of RNA samples extracted using TRIzol Reagent (Omega, R6830-02, United States) were evaluated by 1% agarose gel electrophoresis and were quantified with UV spectrophotometers. For each sample, 2 μg DNase I-treated RNA was reverse-transcribed using the RT-PCR Kit (Takara, Dalian, China). The thermal cycles were conducted in a PCR machine (Bio-Rad, California, United States).

Primers and PCR Amplification

We designed the gene-specific primers using Primer 5 software based on the sequence of *Sc-GS* gene (GenBank accession No. MK451701). The PCR conditions and purification methods were same as those reported by Sun et al. (2021).

Association Analysis Between Polymorphisms and Ammonia Tolerance

The nucleotide sequences of the *Sc-GS* gene in different individuals were aligned using MEGA 7 and Mutation Surveyor software. The base locus with two peaks at the nearly same height was defined as a heterozygous locus. The genotype frequencies and their associations with ammonia tolerance were analyzed by SPSS version 22. The information of these SNPs between two populations was calculated by PopGen32.

Paraffin Section, H&E, and Immunofluorescence Staining

The gills and hepatopancreases of clams were first fixed in 4% paraformaldehyde at 4°C, then dehydrated, and finally embedded in paraffin sections. The paraffin sections (5 μm) were dewaxed with xylene and rehydrated with gradient ethanol, then stained with hematoxylin (10 min) and eosin (30 s), respectively. Additionally, immunofluorescence staining was carried out to analyze the expression changes of Sc-GS. The dewaxed paraffin sections were sealed with 5% skimmed milk powder solution at room temperature for 1.5 h after the antigen retrieval by ethylenediaminetetraacetic acid (EDTA), and then, the sections were added with primary antibody (Sc-GS, 1:250) overnight at 4°C, washing three times [0.01 M phosphate-buffered saline (PBS), 10 min per time]. Fluorescein isothiocyanate (FITC)-labeled murine anti-rabbit IgG as a secondary antibody (1:150, containing 4',6-diamidino-2-phenylindole (DAPI)) was added in a dark room and protected from light for 1 h at room temperature and washed three times (0.01 M PBS, 10 min per time). Finally, a fluorescence microscope (Nikon 80i, Japan) was used to take photographs.

Quantitative Real-Time PCR

The expression profiles of *Sc-GS* were analyzed by using triplicate quantitative real-time PCR (qRT-PCR). Primers *Sc-GS*-F1/R1 (**Table 1**) were designed by Primer 5, and the Ribosomal protein S9 (*RS9*, **Table 1**) gene was selected as an internal reference gene (Zhao et al., 2018). A 7500 Fast Real-Time PCR Machine (ABI, United States) was used for PCR, and the relative value of $2^{-\Delta\Delta Ct}$ was adopted for data processing (Montresor et al., 2013). SPSS version 22 was used to analyze the quantitative differences of fluorescence results. One-way ANOVA was used to compare the difference between groups.

RESULTS

Single Nucleotide Polymorphism Identification and Association Analysis of *Glutamine Synthetase* Gene From *Sinonovacula constricta* Gene Exons

In the ammonia challenge experiment, the first dead clam was observed at 22 h in the FJ population. The clams in both populations who survived after 120 h ammonia stress were contemplated as the TG, overall, 130 and 116 surviving clams were collected from ZJ and FJ populations, respectively. During the entire experimental period, no dead clam was found in the CG.

In this study, 14 and 12 SNPs were genotyped successfully in FJ and ZJ populations, respectively. Then, the genotyping results

TABLE 1 | Primers and sequences of the experiments.

Primers	Sequences (5′–3′)	Applications
siRNA-GS-F	GCCUCAAGCACAUCGAGAATT	RNAi
siRNA-GS-R	UUCUCGAUGUGCUUGAGGCTT	
NC-F	UUCUCCGAACGUGUCACGUTT	RNAi
NC-R	ACGUGACACGUUCGGAGAATT	
Sc-GS-F1	TTTATGAACGACCCAAAGTCCA	qRT-PCR
Sc-GS-R1	TTCACTGTTTGATAATAACGGCTG	
RS9-F	TGAAGTCTGGCGTGTCAAGT	qRT-PCR for the reference gene
RS9-R	CGTCTCAAAAGGGCATTACC	
Sc-GS-F2	GGAGAAGGACTCAGAAGCAAG	SNP
Sc-GS-R2	AATAACCTCCGTGACTGTGTAA	

of TG and CG individuals were used for the statistics of genotype frequencies. It was worth noting that only SNP c.1133T > G was strongly and significantly associated with the ammonia tolerance in both two populations ($P < 0.01$) (**Table 2**). Notably, 6 out of the 12 SNPs in the ZJ population were transitions, while there were 7 transitions out of the 14 SNPs in the FJ population (**Table 2**). It was noteworthy that c.1133T > G was a non-synonymous mutation, resulting in an amino acid exchange from leucine (Leu) to arginine (Arg).

Histological Structure and Histocellular Localization of *Glutamine Synthetase* Gene From *Sinonovacula constricta* Protein

The histological structure, expression level and histocellular localization of *Sc-GS* in the gills and hepatopancreas were determined by paraffin section, HE staining and immunohistochemistry assay. The gills were made up of two gill flaps on the left and right sides. A pair of gill flaps in the middle of both sides of the mantle cavity was inner gill flaps, while a pair on both sides was outer gill flaps. Each gill flap was composed of ascending and descending gill lamellae, which was composed of numerous gill filaments in dense clusters perpendicular to the longitudinal axis of the body. These gill filaments could be subdivided into flat cells and columnar cells of frontal cilia and lateral cilia according to their different positions (**Figure 1A**). Then, the FITC-labeled antibody selected in this study could specifically bind to Sc-GS protein, which led to the protein expression region showing green fluorescence. In view of this, we found that the columnar cells of lateral cilia of gills in the AG showed stronger positive signals than those in CG (**Figure 2**).

The hepatopancreas surrounded the sides of the stomach and was made up of individual hepatocyte cells. The hepatic sinusoid formed between hepatocytes cells was composed of endothelial cells (**Figure 1B**). On this basis, the endothelial cells of a hepatic sinusoid in the AG were showed a positive signal in relation to CG (**Figure 3**). Furthermore, the combination of green and blue signals showed that the two colors were not coincident, indicating that Sc-GS protein was not expressed in the nucleus (**Figures 2**, **3**).

Expression of *Glutamine Synthetase* Gene From *Sinonovacula constricta* After RNA Interference Silencing

The function of *Sc-GS* in hepatopancreas was further investigated by RNAi. In AGs, the mRNA expression level of *Sc-GS* in hepatopancreas was extremely significantly ($P < 0.01$) lower at 24, 48, 72, and 96 h in siRNA-*GS* than that in NC, which downregulated to approximately 86.44, 89.10, 91.17, and 84.45%, respectively (**Figure 4A**). Similarly, the mRNA expression level of *Sc-GS* in CGs was extremely significantly ($P < 0.01$) lower at 24, 48, 72, and 96 h in siRNA-*GS* compared to that in NC, which downregulated to approximately 71.69, 74.44, 80.44, and 80.03%, respectively (**Figure 4B**). In addition, the variation trend of the mRNA expression level of *Sc-GS* genes in DEPC-W and NC in each group (AG or CG) was roughly the same.

DISCUSSION

Ammonia was a major toxicant in the aquatic system, which led to adverse effects such as growth reduction (Sinha et al., 2012), oxidative stress and damage (Zhang M. et al., 2018), immune suppression (Li et al., 2016), histological changes (Cheng et al., 2019), and mortality. However, it is still quite limited to the understanding of the molecular mechanism of ammonia tolerance in aquatic animals. It is well known that GS can catalyze the synthesis of Gln from NH_4^+ and Glu, which in turn provides a substrate for the synthesis of urea-related formula phosphate synthetase III (i.e., it plays a central role in the urea cycle) (Wang and Walsh, 2000). So far, the research on the *GS* genes in aquatic organisms has mainly focused on fish and crustaceans (Ip et al., 2005; Qiu et al., 2018; Dong et al., 2020). On the contrary, research on the ammonia nitrogen detoxification metabolism of *Sc-GS* is very scarce. In this study, our objective was to identify the polymorphisms in the *Sc-GS* gene and to investigate the association between its polymorphisms and tolerance to ammonia. In addition, we explored the histocellular localization and function of the *Sc-GS* gene in response to ammonia tolerance using H&E staining, immunohistochemistry, and RNAi technology.

Studies on *L. vannamei* (Qiu et al., 2018) and pharaoh cuttlefish *Sepia pharaonis* (Peng et al., 2017) have shown that the mRNA and protein expression level of *GS* in some tissues (i.e., liver, muscle, intestine, and gills) was increased significantly when exposed to ammonia. Our previous studies showed that *Sc-GS* could be involved in ammonia detoxification (Zhang et al., 2020). In this study, 12 SNPs were detected in the *Sc-GS* gene (1 per 87 bp) of the ZJ population, while 14 SNPs (1 per 74 bp) were found in the FJ population. The difference in the numbers of SNPs between the ZJ and FJ populations may be due to the population genetic divergence or the deviation of sequencing. To our knowledge, the highest levels of DNA polymorphism were reported in the animal kingdom such as nematode *Caenorhabditis remanei* (Cutter et al., 2006) and ascidian *Ciona savignyi* (Small et al., 2007) with 1 per 20 bp. In addition to that, the density of SNPs in insect species was often highly

TABLE 2 | Genotype, variation type, and gene frequency of single nucleotide polymorphisms (SNPs) in *Glutamine synthetase* gene from *Sinonovacula constricta* (*Sc-GS*).

Position/Variation type	Genotype	ZJ			FJ		
		TG/CG		χ^2/*P*-value	TG/CG		χ^2/*P*-value
		Number	Genotype frequency		Number	Genotype frequency	
c.363C > T/Transition	CC	107/87	82.3/80.55	0.534/0.766	86/84	74.14/89.36	7.907/0.019
	CT	18/18	13.85/16.67		16/6	13.79/6.38	
	TT	5/3	3.85/2.78		14/4	12.07/4.26	
c.420T > C/Transition	TT	63/52	48.46/48.15	0.115/0.944	48/47	41.38/50	1.641/0.44
	TC	45/36	34.62/33.33		46/33	39.66/35.11	
	CC	22/20	16.92/18.52		22/14	18.96/14.89	
c.446C > T/Transition	CC	130/108	100/100	–	101/88	87.07/93.62	1.8/0.18
	CT	0/0	0/0		15/6	12.93/6.38	
c.465T > G/Transversion	TT	117/96	90/88.89	0.439/0.803	98/86	84.48/91.49	2.563/0.278
	TG	11/9	8.46/8.33		15/6	12.93/6.38	
	GG	2/3	1.54/2.78		3/2	2.59/2.13	
c.477G > A/Transition	GG	87/74	66.92/68.52	3.804/0.149	74/61	63.79/64.89	0.159/0.924
	GA	37/23	28.46/21.29		25/21	21.55/22.34	
	AA	6/11	4.62/10.19		17/12	14.86/12.77	
c.504C > T/Transition	CC	115/95	88.46/87.96	0.251/0.882	116/94	100/100	–
	CT	13/12	10/11.11		0/0	0/0	
	TT	2/1	1.54/0.93		0/0	0/0	
c.600T > A/Transversion	TT	109/89	83.85/82.41	0.217/0.897	94/84	81.04/89.36	2.788/0.248
	TA	18/17	13.85/15.74		11/5	9.48/5.32	
	AA	3/2	2.3/1.85		11/5	9.48/5.32	
c.673T > C/Transition	TT	116/97	89.23/89.82	0.069/0.966	99/78	85.34/82.98	0.734/0.693
	TC	12/9	9.23/8.33		12/13	10.35/13.83	
	CC	2/2	1.54/1.85		5/3	4.31/3.19	
c.804A > T/Transversion	AA	110/91	84.62/84.26	1.569/0.456	102/82	87.93/87.23	0.118/0.943
	AT	19/14	14.61/12.96		11/10	9.48/10.64	
	TT	1/3	0.77/2.78		3/2	2.59/2.13	
c.813G > A/Transition	GG	114/95	87.69/87.96	1.569/0.456	98/77	84.48/81.92	1.261/0.532
	GA	14/11	10.77/10.19		15/16	12.93/17.02	
	AA	2/2	1.54/1.85		3/1	2.59/1.06	
c.822C > T/Transition	CC	130/108	100/100	–	96/86	82.76/91.49	2.711/0.1
	CT	0/0	0/0		20/8	17.24/8.51	
c.898C > A/Transversion	CC	130/108	100/100	–	101/84	87.07/89.36	0.088/0.767
	CA	0/0	0/0		15/10	12.93/10.64	
c.981T > C/Transition	TT	105/82	80.77/75.93	2.219/0.33	86/62	74.14/65.96	6.382/0.041
	TC	23/21	17.69/19.44		18/27	15.52/28.72	
	CC	2/5	1.54/4.63		12/5	10.34/5.3	
c.987C > T/Transition	CC	118/92	90.77/85.18	1.809/0.405	116/94	100/100	–
	CT	11/15	8.46/13.89		0/0	0/0	
	TT	1/1	0.77/0.93		0/0	0/0	
c.1073C > T/Transition	CC	130/108	100/100	–	100/82	86.20/87.23	0.047/0.989
	CT	0/0	0/0		16/12	13.80/12.77	
c.1133T > G/Transversion	TT	82/87	63.08/80.56	**8.964/0.005**	105/70	90.52/74.47	**8.509/0.004**
	TG	48/21	36.92/19.44		11/24	9.48/25.53	

The loci in bold were those that showed significant differences between the two populations.

polymorphic, e.g., 1 per 50 bp in fruit fly *Drosophila* (Shapiro et al., 2007) and 1 per 125 bp in mosquitoes *Aedes aegypti* (Morlais and Severson, 2003). Similarly, accumulating evidence has shown that a high density of DNA polymorphism was detected in mollusks (Saavedra and Bachère, 2006). This study reached the same conclusion as mentioned earlier, indicating that bivalves have abundant genetic variation. Notably, we found two types of mutation, namely, transversion and transition in two populations. In this study, the frequency of the transition of C-T was much higher than that of A-G, which can be explained by the

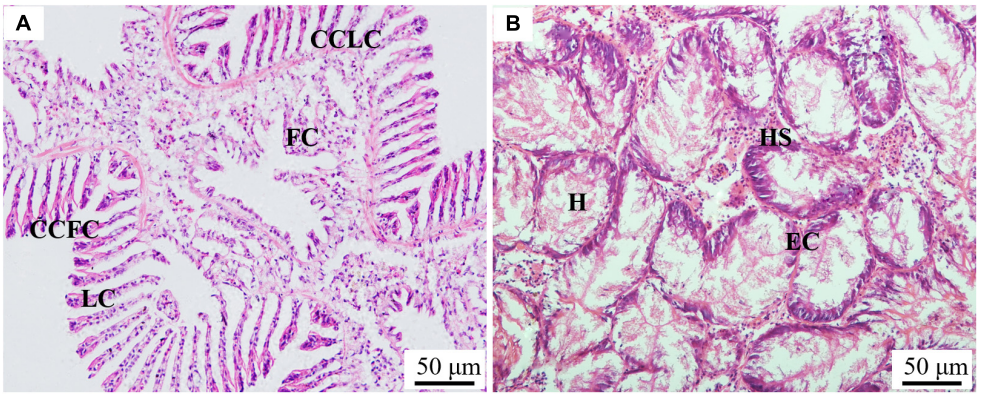

FIGURE 1 | Paraffin section observation of gills **(A)** and the hepatopancreas **(B)** in the *Sinonovacula constricta*. CCFC, columnar cells of frontal cilia; CCLC, columnar cells of lateral cilia; FC, flat cells; HS, hepatic sinusoid; EC, endothelial cells; H, hepatocytes. Scale bars were 50 μm.

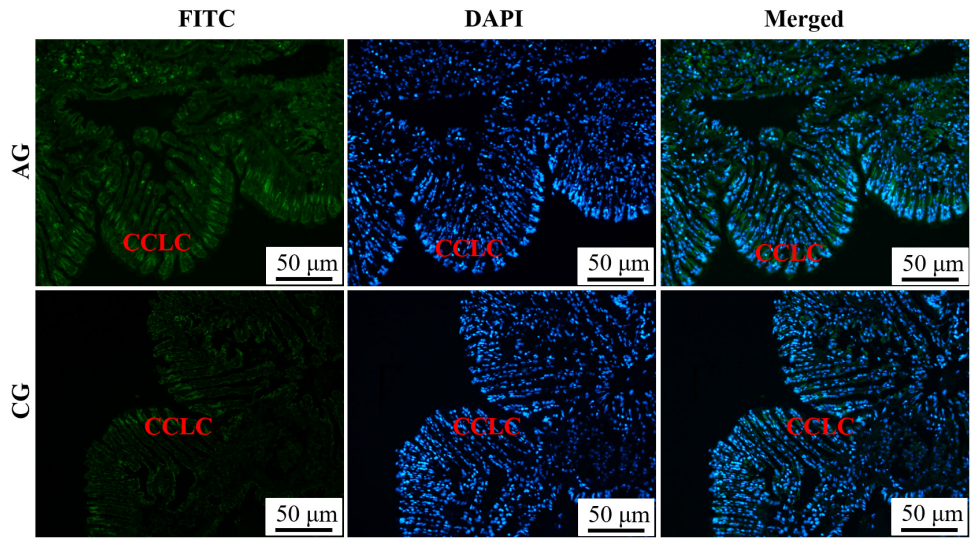

FIGURE 2 | Immunofluorescence of *Glutamine synthetase* gene from *Sinonovacula constricta* (*Sc-GS*) in the gills. Sc-GS protein was stained with the anti-GS antibody in green, and nuclei were stained with DAPI in blue. The merged images were colocalized with Sc-GS protein (green) and DAPI (blue) in the columnar cells of lateral cilia of gills. Scale bars were 50 μm.

fact that C in the C&G sequence has been often methylated and can be spontaneously deaminated to form T (Yoon et al., 2001).

The discovery of SNPs with missense mutation provides a new possibility for molecular marker-assisted selection (MAS) of aquatic animal varieties with economic traits to relieve environmental stress (Syvänen, 2001; Wang et al., 2013). It has been shown that three SNPs about factor inhibiting HIF-1 (Fih-1) found in Wuchang bream *Megalobrama amblycephala* were significantly associated with hypoxia traits (Zhang et al., 2016). A study on the association between candidate gene and heat tolerance in bay scallop *Argopecten irradians* showed that SNP all-53308-760T/C may be related to heat (Du et al., 2014). Similarly, SNPs in other candidate genes for related heat tolerance, such as metallothionein 1 and heat shock protein 90, have been reported in bay scallops (Yang et al., 2013, 2015). Notably, high-concentration ammonia is a harmful environmental factor in the survival, development, and growth of aquatic animals. In this regard, it is significant to explore the molecular markers associated with ammonia tolerance. It has been reported that one SNP (C > T545) of hemocyanin may be served as a marker for selecting high growth performance in ammonia-tolerant *L. vannamei* (Janpoom et al., 2020). Another study on *L. vannamei* showed that 12 SNP loci related to ammonia resistance may be significantly associated with disease resistance, which can provide the critical potential for genetic selection to increase the production of shrimp (Lu et al., 2018). These findings highlight the usefulness of missense mutation SNP in environmental resistance-related MAS. In this study, one missense mutation (c.1133T > G) was identified in the *Sc-GS* gene, which mutated from Leu to Arg between two populations. Furthermore, the protein homology analysis showed that c.1133T > G had high homology in mollusk, suggesting that

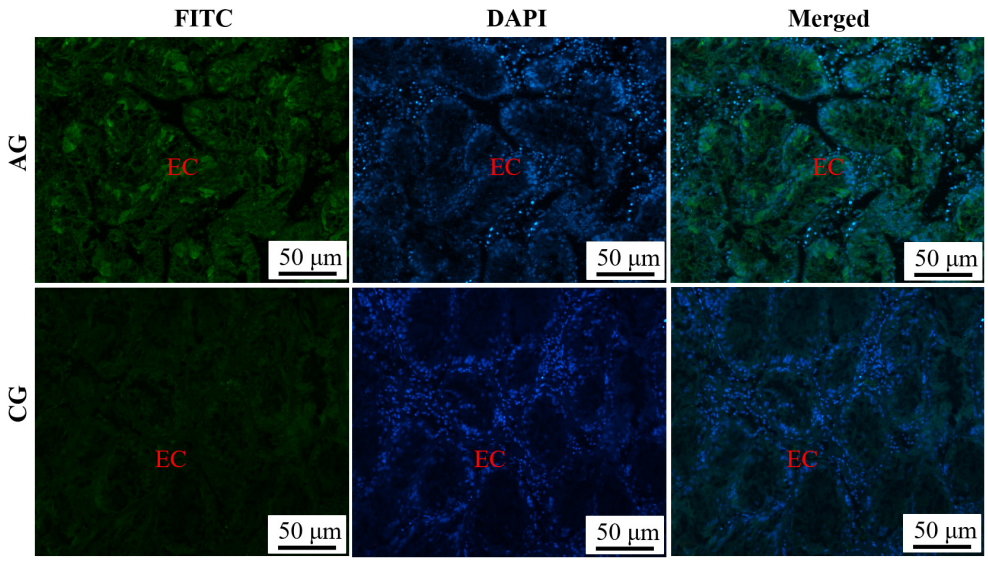

FIGURE 3 | Immunofluorescence of Sc-GS in hepatopancreas. Sc-GS protein was stained with the anti-GS antibody in green, and nuclei were stained with DAPI in blue. The merged images were colocalized with Sc-GS protein (green) and DAPI (blue) in the endothelial cells of hepatic sinusoid. Scale bars were 50 μm.

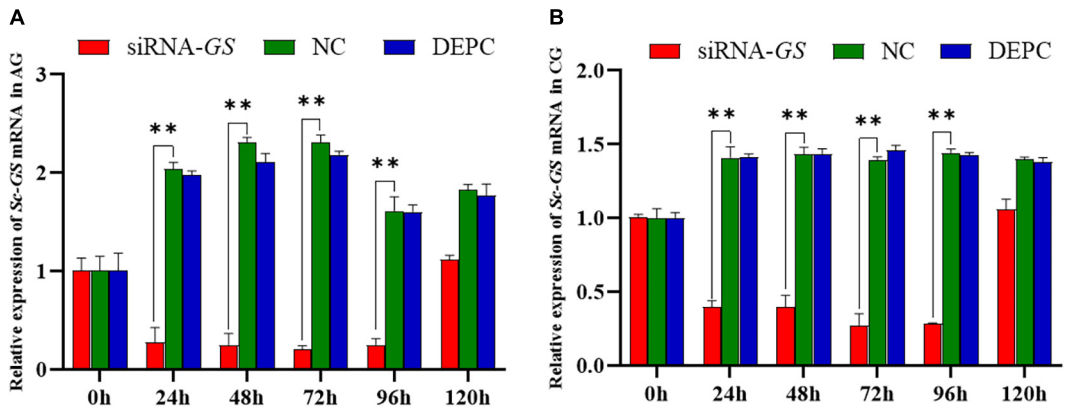

FIGURE 4 | Relative expression of *Sc-GS* genes in the hepatopancreas after RNA interference (RNAi) Time-course expression of *Sc-GS* genes in ammonia stress group (AG) after RNAi **(A)**. Time-course expression of *Sc-GS* genes in the control group (CG) after RNAi **(B)**. Vertical bars represent the mean ± SD ($n = 4$).
** Denotes an extremely significant difference between *Sc-GS* small interfering RNA (siRNA-*GS*) and negative control (NC) ($P < 0.01$).

this locus plays an important role in the normal structure and function of *Sc-GS* (Zhang et al., 2020). As we all know, Leu was a non-polar hydrophobic amino acid (Madeira et al., 2013), and Arg was a polar hydrophilic amino acid with side chain charged (Harms et al., 2011), which changes the conformation of proteins. It has been shown that heterozygous variant c.35G > T (i.e., a substitution of Arg to Leu) identified in exon 1 of *CRYAA* gene was closely related to the human congenital cataract and microphthalmia (Song et al., 2018). Therefore, we speculate that the mutation c.1133T > G may affect the secondary structure of the mutant protein, leading to changes in its folded conformation and stability, eventually resulting in changes in the function of the *GS* gene. At present, the genetic selection program for *S. constricta* with high ammonia tolerance is still in its infancy. Our findings suggest that c.1133T > G, which was found associated with ammonia tolerance in both populations, can be used as a universal marker for further breeding in *S. constricta*.

Immunohistochemistry has become the most effective method for protein expression localization due to its advantages of visualization of target proteins (Lugos et al., 2020). Hepatopancreas was known to be the essential digestion and detoxification organ (Wu et al., 2013). At high levels of ammonia, the hepatopancreases of aquatic animals are injured in different degrees and even cause death (Mishra and Mohanty, 2008). Similarly, in this study, the distribution of Sc-GS protein was changed after the ammonia challenge, which was highly expressed in the cytoplasm of endothelial cells, and the same conclusions were found in the livers of vertebrates such as chicken (Smith and Campbell, 1988; Ueberham et al., 2004). Thus, it can be concluded that Sc-GS protein in hepatopancreas

from razor clam may play a key role in the detoxification process of dealing with high ammonia concentration in the organism.

The RNA interference was first discovered in the nematode worm *Caenorhabditis elegans* as a response to double-stranded RNA (dsRNA), which leads to the silencing of homologous genes (Fire et al., 1998). Fabioux et al. (2009) successfully induced Pacific oyster *Crassostrea gigas* sterility by injecting dsRNA of the *Oyvlg* gene into an oyster, which was the first report that RNAi induced homologous gene silencing in mollusk. In addition, dsRNA of *PfN23* gene was injected into the adult pearl oyster (*Pinctada fucata*), resulting in a disordered of nacre surface, suggesting that *PfN23* gene may be a key accelerator in the control of crystal growth in nacre (Fang et al., 2012). Similarly, the expression of the *BMP7* gene was successfully suppressed by injecting dsRNA into the razor clam, indicating that the *BMP7* gene plays a vital role in repairing shell damage (Zhao et al., 2020). Moreover, in our previous study, the silencing of *Glutamate dehydrogenase*, a gene related to ammonia nitrogen detoxification, was induced by the injection of specific siRNA into the razor clam (Sun et al., 2021). Beyond that, a study in *GS* RNAi transgenic rice showed that *GS* contributed an important role in the amelioration of NH_4^+ toxicity (Le et al., 2018). In addition, the extended developmental duration and pupal weight losses in fruit fly could be associated with a disruption in ammonia metabolism after *GS* gene silence (Hazel et al., 2003; Zhang M. Y. et al., 2018). In this study, the mRNA expression of *Sc-GS* genes in the hepatopancreas was successfully inhibited by injecting specific siRNA into *S. constricta*, thus providing a practical method to characterize the function of *Sc-GS* in response to ammonia stress.

CONCLUSION

The genetic improvement for stress tolerance is extremely beneficial for the sustainable development of the clam aquaculture industry. In this study, a significant difference in the SNP with the missense mutation (c.1133T > G) in *Sc-GS* was detected between the two geographical populations. Further results of H&E staining, immunohistochemistry, and RNAi indicated that the *Sc-GS* gene plays a vital role in the detoxification of ammonia in razor clam. Collectively, these findings could provide candidate markers for the molecular selective breeding of ammonia-tolerant clams in the future and could provide a basis for the detoxification metabolism of bivalves under ammonia stress.

DATA AVAILABILITY STATEMENT

The original contributions presented in the study are included in the article/supplementary material, further inquiries can be directed to the corresponding author/s.

ETHICS STATEMENT

The animal study was reviewed and approved by the Institutional Animal Care and Use Committee (IACUC) of Zhejiang Wanli University.

AUTHOR CONTRIBUTIONS

YD and JH conceived and designed the experiments. GS performed the experiments under the support of HY and CS. GS and YD analyzed the data and plot. GS, YD, WD, and ZL wrote and revised the manuscript. All authors read and approved the final manuscript.

FUNDING

This study was supported by the National Key Research and Development Program of China (2018YFD0901405), the Zhejiang Major Program of Science and Technology (2021C02069-7), the Ningbo Major Project of Science and Technology (2019B10005), and the National Marine Genetic Resource Center Program.

REFERENCES

Boo, M. V., Hiong, K. C., Goh, E. J. K., Choo, C. Y. L., Wong, W. P., Chew, S. F., et al. (2018). The ctenidium of the giant clam, *Tridacna squamosa*, expresses an ammonium transporter 1 that displays light-suppressed gene and protein expression and may be involved in ammonia excretion. *J. Comp. Physiol. B Biochem. Syst. Environ. Physiol.* 185, 765–777. doi: 10.1007/s00360-018-1161-6

Bucking, C., Edwards, S. L., Tickle, P., Smith, C. P., McDonald, M. D., and Walsh, P. J. (2013). Immunohistochemical localization of urea and ammonia transporters in two confamilial fish species, the ureotelic gulf toadfish (*Opsanus beta*) and the ammoniotelic plainfin midshipman (*Porichthys notatus*). *Cell Tissue Res.* 352, 623–637. doi: 10.1007/s00441-013-1591-0

Chen, J. M., and Chen, J. C. (2000). Study on the free amino acid levels in the hemolymph, gill, hepatopancreas and muscle of *Penaeus monodon* exposed to elevated ambient ammonia. *Aquat. Toxicol.* 50, 27–37. doi: 10.1016/s0166-445x(99)00095-8

Cheng, C. H., Ma, H. L., Su, Y. L., Deng, Y. Q., Feng, J., Xie, J. W., et al. (2019). Ammonia toxicity in the mud crab (*Scylla paramamosain*): the mechanistic insight from physiology to transcriptome analysis. *Ecotoxicol. Environ. Saf.* 179, 9–16. doi: 10.1016/j.ecoenv.2019.04.033

Cong, M., Wu, H., Yang, H., Zhao, J., and Lv, J. (2017). Gill damage and neurotoxicity of ammonia nitrogen on the clam *Ruditapes philippinarum*. *Ecotoxicology* 26, 459–469. doi: 10.1007/s10646-017-1777-4

Cutter, A. D., Baird, S. E., and Charlesworth, D. (2006). High nucleotide polymorphism and rapid decay of linkage disequilibrium in wild populations of *Caenorhabditis remanei*. *Genetics* 174, 901–913. doi: 10.1534/genetics.106.061879

Ding, Y., Zang, X., Shi, J., Hou, L., He, B., Dong, M., et al. (2018). cDNA cloning of *gs*, *gogat*, and *gdh* from *Haematococcus pluvialis* and transcription and enzyme level analysis in different nitrogen concentration. *J. Appl. Phycol.* 31, 183–190. doi: 10.1007/s10811-018-1564-5

Dong, X., Liu, Q., Kan, D., Zhao, W., Guo, H., and Lv, L. (2020). Effects of ammonia-N exposure on the growth, metabolizing enzymes, and metabolome of *Macrobrachium rosenbergii*. *Ecotoxicol. Environ. Saf.* 189:110046. doi: 10.1016/j.ecoenv.2019.110046

Du, X., Li, L., Zhang, S., Meng, F., and Zhang, G. (2014). SNP identification by transcriptome sequencing and candidate gene-based association analysis for heat tolerance in the bay scallop *Argopecten irradians*. *PLoS One* 9:e104960. doi: 10.1371/journal.pone.0104960

Fabioux, C., Corporeau, C., Quillien, V., Favrel, P., and Huvet, A. (2009). In vivo RNA interference in oyster -vasa silencing inhibits germ cell development. *FEBS J.* 276, 2566–2573. doi: 10.1111/j.1742-4658.2009.06982.x

Fang, D., Pan, C., Lin, H., Lin, Y., Zhang, G., Wang, H., et al. (2012). Novel basic protein, PfN23, functions as key macromolecule during nacre formation. *J. Biol. Chem.* 287, 15776–15785. doi: 10.1074/jbc.M112.341594

FAO (2020). *The State of World Fisheries and Aquaculture (2020). Sustainability in Action*. Rome: FAO.

Fire, A., Xu, S., Montgomery, M. K., Kostas, S. A., Driver, S. E., and Mello, C. C. (1998). Potent and specific genetic interference by double-stranded RNA in *Caenorhabditis elegans*. *Nature* 391, 806–811. doi: 10.1038/35888

Francis-Floyd, R., Watson, C., Petty, D., and Pouder, D. (2009). Ammonia in aquatic systems. *Univ. Fla. Inst. Food Agric. Sci.* 16, 1–5.

Frankic, A., and Hershner, C. (2003). Sustainable aquaculture: developing the promise of aquaculture. *Aquac. Int.* 11, 517–530. doi: 10.1023/B:AQUI.0000013264.38692.91

Harms, M. J., Schlessman, J. L., Sue, G. R., and García-Moreno, B. (2011). Arginine residues at internal positions in a protein are always charged. *Proc. Natl. Acad. Sci. U.S.A.* 108, 18954–18959. doi: 10.1073/pnas.1104808108

Hazel, M. H., Christensen, R. J., and O'Donnell, M. J. (2003). Inhibition of the SAPK/JNK pathway blocks the stimulatory effects of glutamine on fluid secretion by the Malpighian tubules of *Rhodnius prolixus*. *J. Insect Physiol.* 49, 897–906. doi: 10.1016/s0022-1910(03)00138-0

Henry, R. P., Lucu, C., Onken, H., and Weihrauch, D. (2012). Multiple functions of the crustacean gill: osmotic/ionic regulation, acid-base balance, ammonia excretion, and bioaccumulation of toxic metals. *Front. Physiol.* 3:431. doi: 10.3389/fphys.2012.00431

Ip, Y. K., Leong, M. W. F., Sim, M. Y., Goh, G. S., Wong, W. P., and Chew, S. F. (2005). Chronic and acute ammonia toxicity in mudskippers, *Periophthalmodon schlosseri* and *Boleophthalmus boddaerti*: brain ammonia and glutamine contents, and effects of methionine sulfoximine and MK801. *J. Exp. Biol.* 208, 1993–2004. doi: 10.1242/jeb.01586

Ip, Y. K., Tay, A. S. L., Lee, K. H., and Chew, S. F. (2004). Strategies for surviving high concentrations of environmental ammonia in the swamp eel *Monopterus albus*. *Physiol. Biochem. Zool.* 77, 390–405. doi: 10.1086/383510

Janpoom, S., Kaewduang, B., Prasertlux, S., Rongmung, P., Ratdee, O., Lirdwitayaprasit, T., et al. (2020). A SNP of the hemocyanin gene (LvHc) is a marker for high growth and ammonia-tolerance in Pacific white shrimp *Litopenaeus vannamei*. *Fish Shellfish Immunol.* 106, 491–501. doi: 10.1016/j.fsi.2020.07.058

Le, T. N., Lee, B. B., Kyoungwhan, K., Young, S., and Cheong, H. (2018). Coordinated expression of cytosolic and chloroplastic *glutamine synthetase* during reproductive stage and its impact in GS1 RNAi transgenic rice. *Rice Sci.* 25, 250–260. doi: 10.1016/j.rsci.2018.08.001

Li, L., Yan, B., Li, S., Xu, J., and An, X. (2015). A comparison of bacterial community structure in seawater pond with shrimp, crab, and shellfish cultures and in non-cultured pond in Ganyu, Eastern China. *Ann. Microbiol.* 66, 317–328. doi: 10.1007/s13213-015-1111-4

Li, M., Gong, S., Li, Q., Yuan, L., Meng, F., and Wang, R. (2016). Ammonia toxicity induces glutamine accumulation, oxidative stress and immunosuppression in juvenile yellow catfish *Pelteobagrus fulvidraco*. *Comp. Biochem. Physiol. C* 183–184, 1–6. doi: 10.1016/j.cbpc.2016.01.005

Lu, X., Kong, J., Meng, X., Cao, B., Luo, K., Dai, P., et al. (2018). Identification of SNP markers associated with tolerance to ammonia toxicity by selective genotyping from de novo assembled transcriptome in *Litopenaeus vannamei*. *Fish Shellfish Immunol.* 73, 158–166. doi: 10.1016/j.fsi.2017.12.005

Lugos, M. D., Davou, G. I., Choji, T. P. P., Jugu, K. P., Ashi, R. R., Oyero, S. K., et al. (2020). Using immunohistochemistry without linkers to determine the optimum concentrations of primary antibodies for immunofluorescence staining of formalin-fixed paraffin-embedded tissue sections. *Appl. Immunohistochem. Mol. Morphol.* 28, 249–257. doi: 10.1097/PAI.0000000000000718

Madeira, P. P., Bessa, A., Álvares-Ribeiro, L., Aires-Barros, M. R., Rodrigues, A. E., and Zaslavsky, B. Y. (2013). Analysis of amino acid-water interactions by partitioning in aqueous two-phase systems. I–amino acids with non-polar side-chains. *J. Chromatogr. A* 1274, 82–86. doi: 10.1016/j.chroma.2012.11.080

Mishra, A. K., and Mohanty, B. (2008). Acute toxicity impacts of hexavalent chromium on behavior and histopathology of gill, kidney and liver of the freshwater fish, *Channa punctatus* (Bloch). *Environ. Toxicol. Pharmacol.* 26, 136–141. doi: 10.1016/j.etap.2008.02.010

Montresor, L. C., Miranda-Filho, K. C., Paglia, A., Luz, D. M. R., Araújo, J. M., Silva, M. J. D. S., et al. (2013). Short-term toxicity of ammonia, sodium hydroxide and a commercial biocide to golden mussel *Limnoperna fortune* (Dunker, 1857). *Ecotoxicol. Environ. Saf.* 92, 150–154. doi: 10.1016/j.ecoenv.2013.03.016

Morlais, I., and Severson, D. W. (2003). Intraspecific DNA variation in nuclear genes of the mosquito *Aedes aegypti*. *Insect Mol. Biol.* 12, 631–639. doi: 10.1046/j.1365-2583.2003.00449.x

Peng, R. B., Le, K. X., Wang, P. S., Wang, Y., Han, Q. X., and Jiang, X. M. (2017). Detoxification pathways in response to environmental ammonia exposure of the cuttlefish, *Sepia pharaonis*: glutamine and urea formation. *J. World Aquac. Soc.* 48, 342–352. doi: 10.1111/jwas.12341

Qiu, L., Shi, X., Yu, S., Han, Q., Diao, X., and Zhou, H. (2018). Changes of ammonia-metabolizing enzyme activity and gene expression of two strains in shrimp *Litopenaeus vannamei* under ammonia stress. *Front. Physiol.* 9:211. doi: 10.3389/fphys.2018.00211

Randall, D. J., and Tsui, T. K. N. (2002). Ammonia toxicity in fish. *Mar. Pollut. Bull.* 45, 17–23. doi: 10.1016/s0025-326x(02)00227-8

Saavedra, C., and Bachère, E. (2006). Bivalve genomics. *Aquaculture* 256, 1–14. doi: 10.1016/j.aquaculture.2006.02.023

Saravana, B. P., and Geraldine, P. (2000). Histopathology of the hepatopancreas and gills of the prawn *Macrobrachium malcolmsonii* exposed to endosulfan. *Aquat. Toxicol.* 50, 331–339. doi: 10.1016/s0166-445x(00)00096-5

Schock, T. B., Duke, J., Goodson, A., Weldon, D., Brunson, J., Leffler, J. W., et al. (2013). Evaluation of Pacific white shrimp (*Litopenaeus vannamei*) health during a super intensive aquaculture growout using NMR-based metabolomics. *PLoS One* 8:e59521. doi: 10.1371/journal.pone.0059521

Shapiro, J. A., Huang, W., Zhang, C., Hubisz, M. J., Lu, J., Turissini, D. A., et al. (2007). Adaptive genic evolution in the *Drosophila* genomes. *Proc. Natl. Acad. Sci. U.S.A.* 104, 2271–2276. doi: 10.1073/pnas.0610385104

Si, L., Pan, L., Wang, H., and Zhang, X. (2018). Identification of the role of Rh protein in ammonia excretion of swimming crab *Portunus trituberculatus*. *J. Exp. Biol.* 221:184655. doi: 10.1242/jeb.184655

Sinha, A. K., Diricx, M., Chan, L. P., Liew, H. J., Kumar, V., Blust, R., et al. (2012). Expression pattern of potential biomarker genes related to growth, ion regulation and stress in response to ammonia exposure, food deprivation and exercise in common carp (*Cyprinus carpio*). *Aquat. Toxicol.* 122–123, 93–105. doi: 10.1016/j.aquatox.2012.05.013

Small, K. S., Brudno, M., Hill, M. M., and Sidow, A. (2007). Extreme genomic variation in a natural population. *Proc. Natl. Acad. Sci. U.S.A.* 104, 5698–5703. doi: 10.1073/pnas.0700890104

Smith, D. D. Jr., and Campbell, J. W. (1988). Distribution of glutamine synthetase and carbamoyl-phosphate synthetase I in vertebrate liver. *Proc. Natl. Acad. Sci. U.S.A.* 85, 160–164. doi: 10.1073/pnas.85.1.160

Song, Z., Si, N., and Xiao, W. (2018). A novel mutation in the CRYAA gene associated with congenital cataract and microphthalmia in a Chinese family. *BMC Med. Genet.* 19:190. doi: 10.1186/s12881-018-0695-5

Sun, G., Dong, Y., Sun, C., Yao, H., and Lin, Z. (2021). Vital role of *Glutamate dehydrogenase* gene in ammonia detoxification and the association between its SNPs and ammonia tolerance in *Sinonovacula constricta*. *Front. Physiol.* 12:664804. doi: 10.3389/fphys.2021.664804

Sunga, J., Wilson, J. M., and Wilkie, M. P. (2020). Functional re-organization of the gills of metamorphosing sea lamprey (*Petromyzon marinus*): preparation for a blood diet and the freshwater to seawater transition. *J. Comp. Physiol. B* 190, 701–715. doi: 10.1007/s00360-020-01305-1

Syvänen, A. C. (2001). Accessing genetic variation: genotyping single nucleotide polymorphisms. *Nat. Rev. Genet.* 2, 930–942. doi: 10.1038/35103535

The Ministry of Agriculture and Fishery of the People's Republic of China. (2021). *Chinese Fishery Statistical Yearbook 2021*. Beijing: China Agriculture Press.

Tok, C. Y., Chew, S. F., and Ip, Y. K. (2011). Gene cloning and mRNA expression of glutamate dehydrogenase in the liver, brain, and intestine of the swamp

eel, *Monopterus albus* (Zuiew), exposed to freshwater, terrestrial conditions, environmental ammonia, or salinity stress. *Front. Physiol.* 2:100. doi: 10.3389/fphys.2011.00100

Ueberham, E., Arendt, E., Starke, M., Bittner, R., and Gebhardt, R. (2004). Reduction and expansion of the glutamine synthetase expressing zone in livers from tetracycline controlled TGF-beta1 transgenic mice and multiple starved mice. *J. Hepatol.* 41, 75–81. doi: 10.1016/j.jhep.2004.03.024

Wang, G., Li, X., and Li, J. (2013). Association between SNPs in interferon regulatory factor 2 (IRF-2) gene and resistance to *Aeromonas hydrophila* in freshwater mussel *Hyriopsis cumingii*. *Fish Shellfish Immunol.* 34, 1366–1371. doi: 10.1016/j.fsi.2013.02.006

Wang, G., Pan, L., and Ding, Y. (2014). Defensive strategies in response to environmental ammonia exposure of the sea cucumber *Apostichopus japonicus*: glutamine and urea formation. *Aquaculture* 432, 278–285. doi: 10.1016/j.aquaculture

Wang, Y., and Walsh, P. J. (2000). High ammonia tolerance in fishes of the family Batrachoididae (Toadfish and Midshipmen). *Aquat. Toxicol.* 50, 205–219. doi: 10.1016/s0166-445x(99)00101-0

Widman, J. C., Meseck, S. L., Sennefelder, G., and Veilleux, D. J. (2008). Toxicity of un-ionized ammonia, nitrite, and nitrate to juvenile bay scallops, *Argopecten irradians* irradians. *Arch. Environ. Contam. Toxicol.* 54, 460–465. doi: 10.1007/s00244-007-9051-z

Wu, H., Ji, C., Wei, L., Zhao, J., and Lu, H. (2013). Proteomic and metabolomic responses in hepatopancreas of *Mytilus galloprovincialis* challenged by *Micrococcus luteus* and *Vibrio anguillarum*. *J. Proteomics* 94, 54–67. doi: 10.1016/j.jprot.2013.09.001

Yang, C., Wang, L., Jiang, Q., Wang, J., Yue, F., Zhang, H., et al. (2013). The polymorphism in the promoter region of metallothionein 1 is associated with heat tolerance of scallop *Argopecten irradians*. *Gene* 526, 429–436. doi: 10.1016/j.gene.2013.05.033

Yang, C., Wang, L., Liu, C., Zhou, Z., Zhao, X., and Song, L. (2015). The polymorphisms in the promoter of *HSP*90 gene and their association with heat tolerance of bay scallop. *Cell Stress Chaperones* 20, 297–308. doi: 10.1007/s12192-014-0546-z

Yoon, J. H., Smith, L. E., Feng, Z. H., Tang, M. S., Lee, C. S., and Pfeifer, G. P. (2001). Methylated CpG dinucleotides are the preferential targets for G-to-T transversion mutations induced by benzo[a]pyrene diol epoxide in mammalian cells: similarities with the p53 mutation spectrum in smoking-associated lung cancers. *Cancer Res.* 61, 7110–7117. doi: 10.1097/00002820-200110000-00014

Zhang, B., Chen, N., Huang, C., Huang, C., Chen, B., Liu, H., et al. (2016). Molecular response and association analysis of *Megalobrama amblycephala* fih-1 with hypoxia. *Mol. Genet. Genomics* 291, 1615–1624. doi: 10.1007/s00438-016-1208-x

Zhang, H., Sun, G., Lin, Z., Yao, H., and Dong, Y. (2020). The razor clam *Sinonovacula constricta* uses the strategy of conversion of toxic ammonia to glutamine in response to high environmental ammonia exposure. *Mol. Biol. Rep.* 47, 9579–9593. doi: 10.1007/s11033-020-06018-w

Zhang, L., Pan, Q., Xu, L., and Si, L. (2018). Effects of ammonia-N exposure on the concentrations of neurotransmitters, hemocyte intracellular signaling pathways and immune responses in white shrimp *Litopenaeus vannamei*. *Fish Shellfish Immunol.* 75, 48–57. doi: 10.1016/j.fsi.2018.01.046

Zhang, M., Li, M., Wang, R., and Qian, Y. (2018). Effects of acute ammonia toxicity on oxidative stress, immune response and apoptosis of juvenile yellow catfish *Pelteobagrus fulvidraco* and the mitigation of exogenous taurine. *Fish Shellfish Immunol.* 79, 313–320. doi: 10.1016/j.fsi.2018.05.036

Zhang, M. Y., Wei, D., Li, R., Jia, H. T., Liu, Y. W., Taning, C. N. T., et al. (2018). Cytoplasmic glutamine synthetase gene expression regulates larval development in *Bactrocera dorsalis* (Hendel). *Arch. Insect Biochem. Physiol.* 97:e21447. doi: 10.1002/arch.21447

Zhao, J., Cui, B., Yao, H., Lin, Z., and Dong, Y. (2020). A potential role of bone morphogenetic protein 7 in shell formation and growth in the razor clam *Sinonovacula constricta*. *Front. Physiol.* 11:1059. doi: 10.3389/fphys.2020.01059

Zhao, X. L., Fu, J. P., Jiang, L. T., Zhang, W. W., Shao, Y. N., Jin, C. H., et al. (2018). Transcriptome-based identification of the optimal reference genes as internal controls for quantitative RT-PCR in razor clam (*Sinonovacula constricta*). *Genes Genomics* 40, 603–613. doi: 10.1007/s13258-018-0661-9

Conflict of Interest: The authors declare that the research was conducted in the absence of any commercial or financial relationships that could be construed as a potential conflict of interest.

Publisher's Note: All claims expressed in this article are solely those of the authors and do not necessarily represent those of their affiliated organizations, or those of the publisher, the editors and the reviewers. Any product that may be evaluated in this article, or claim that may be made by its manufacturer, is not guaranteed or endorsed by the publisher.

frontiers in Marine Science

ORIGINAL RESEARCH
published: 21 January 2022
doi: 10.3389/fmars.2021.800627

Comparative Profiling of Survival, Growth, and Intestinal Microbial Community of Pearl Oyster *Pinctada maxima* Juvenile in the Industrial Farming: The Feasibility of Using Spray-Dried Microalgae Powder

Shouguo Yang[1,2,3†], Xi Li[1†], Hebert Ely Vasquez[1,2], Aimin Wang[1,2], Yaohua Shi[2], Jiaoni Li[1], Xingzhi Zhang[1,4], Xing Zheng[1,2] and Zhifeng Gu[1,2*]*

[1] Ocean College, Hainan University, Haikou, China, [2] State Key Laboratory of Marine Resource Utilization in South China Sea, Hainan University, Haikou, China, [3] Hainan Academy of Ocean and Fisheries Sciences, Haikou, China, [4] Guangxi Academy of Fisheries Sciences, Nanning, China

OPEN ACCESS

Edited by:
Liqiang Zhao,
Guangdong Ocean University, China

Reviewed by:
Liang Junping,
Henan Normal University, China
Xiangdong Bi,
Tianjin Agricultural University, China

***Correspondence:**
Xing Zheng
zhengxing_edu@163.com
Zhifeng Gu
hnugu@163.com

† These authors have contributed equally to this work and share first authorship

Specialty section:
This article was submitted to Marine Fisheries, Aquaculture and Living Resources, a section of the journal Frontiers in Marine Science

Received: *23 October 2021*
Accepted: *06 December 2021*
Published: *21 January 2022*

Citation:
Yang S, Li X, Vasquez HE, Wang A, Shi Y, Li J, Zhang X, Zheng X and Gu Z (2022) Comparative Profiling of Survival, Growth, and Intestinal Microbial Community of Pearl Oyster Pinctada maxima Juvenile in the Industrial Farming: The Feasibility of Using Spray-Dried Microalgae Powder. Front. Mar. Sci. 8:800627. doi: 10.3389/fmars.2021.800627

Industrial farming is an alternative mode for *Pinctada maxima* juvenile cultivation to avoid mass mortality caused by natural disasters. Suitable and enough food is crucial for successful industrial bivalve farming. To investigate the feasibility of live microalga instead of spray-dried microalgal powder in *P. maxima* juvenile industrial farming, this study replaces a positive control live microalgal diet [*Isochrysis zhanjiangensis* (L-iso) and *Platymonas subcordiformis* (L-pla)] with spray-dried *I. zhanjiangensis* powder (P-iso) and *P. subcordiformis* powder (P-pla). Continuous feeding trials (30 days) were conducted on the *P. maxima* juvenile (1.2008 ± 0.0009 g initial weight and 30.12 ± 0.05 mm initial shell length), under laboratory conditions. Survival, growth performance, and intestinal microbial community were studied and compared across the groups. Results showed that survival rate (SR) did not differ significantly across the groups (ranged from 84 to 86%, $P > 0.05$). The growth performance in spray-dried microalgal groups, including total weight (TW), shell height (SH), absolute growth rate (AGR), and relative growth rate (RGR) for SH and TW, was slightly lower than that in live microalgal groups, while the activities of pepsin (PES), amylase (AMS), and lipase (LPS) were significantly higher ($P < 0.05$). The best growth performance was observed in the L-iso group, followed by the L-pla group. A 16S rRNA-based sequencing revealed that Proteobacteria was the dominant phylum in *P. maxima* juvenile intestinal bacterial community under controlled conditions, which accounted for 62–82% across groups. The intestinal bacteria at the genus level were more sensitive to diets, whereas *Burkholderia* was the dominant genus in both L-iso (66.52 ± 6.43%) and L-pla groups (54.00 ± 5.66%), while *Mycoplasma*, *Alphaproteobacteria*, and *Oxyphotobacteria* were in both P-iso and P-pla groups. The P-pla group got higher ACE, Chao1, and Simpson and Shannon indices ($P < 0.05$). The

above results suggested that the spray-dried P-iso and P-pla can serve as substitutes for live microalga in *P. maxima* juvenile industrial farming under controlled conditions. The finding in this study provides basic data to optimize industrial farming technology and healthy management for *P. maxima* juvenile.

Keywords: *Pinctada maxima*, juvenile, industrial farming, microalga substitution, spray-dried microalga powder

INTRODUCTION

The mollusks are the second-largest animal phylum with almost 100,000 species, of which 15,000 are bivalves (Barnes et al., 1993), and bivalves culturing is considered a sustainable maricultural practice as most bivalves obtain nutrition from natural seawater without artificial food input (Zhou et al., 2006; Zheng et al., 2020). Pearl oyster *Pinctada maxima* is known for producing large-sized nucleated pearls, which are among the most expensive pearls worldwide (Zhao et al., 2003). The species is naturally distributed in the central Indo-Pacific region from Myanmar to the Solomon Islands, including the Philippines, China, Australia, Papua New Guinea, Indonesia, Polynesia, Micronesia, and Southern Japan (Liang et al., 2016; He et al., 2021). In China, *P. maxima* exists naturally along with the coastal areas of southern provinces, such as Hainan, Guangxi, and Guangdong provinces. In addition, researchers have studied the protocols for seed production and pearl culturing of *P. maxima* since the early 1970s, while pearl production in this species was experimentally successful in the 1980s. However, the *P. maxima* pearl production industry has developed at a slow pace over the past decades, for overfished wild populations and mass mortality at juvenile stages. Aiming to solve this problem, researchers improved the survival rates (SRs) by developing rearing protocols for larvae, spat, and adults, as well as introducing wild populations (Liang et al., 2016).

Raft and pile farming offshore are the dominant farming modes of bivalves that are susceptible to natural disasters and pollution of the sea area. In contrast, the industrial farming mode can effectively reduce or avoid the above disadvantages, involving a combination of culture engineering and water treatment protocols (Wang et al., 2015). Under the industrial farming mode, the animals can be fed on high-quality diets to improve survival and growth rates. Pearl oyster *P. maxima* cultivation in China generally occurs in inshore or nearshore estuarine areas, where salinity fluctuates due to heavy rains and runoff in the summer months. The changes in environmental factors are bad for *P. maxima* juvenile survival and growth, even causing mass mortality (Deng et al., 2013). Thus, the industrial farming mode is an alternative and appropriate mode for *P. maxima* farming. In general, the industrial farming mode involves high stocking and requires a large demand for food diets. Phytoplankton, bacteria, organic debris, and microzooplankton from the sea are the food sources for bivalves, and phytoplankton is the dominant (Wang et al., 2010). However, diets that solely comprise microalgae can hardly meet the demand in bivalve industrial farming, and large-scale microalgal culture is often susceptible to changes in water temperature and salinity. Therefore, choosing suitable food instead of live microalga, without affecting growth, physiology, and meeting nutritional requirements from bivalves, is crucial for the industrial bivalve farming mode development.

The partial or total replacement of microalgal foods by a cheap, easily handled substitute with the same nutritive qualities has been attempted by hatcheries, while studies on the nutritional requirements and artificial feed of bivalve are relatively more laggard than those on other aquatic animals. A few studies of artificial diets in bivalve species have been reported, such as bacterial proteins (Philippe and Christopher, 1994), yeasts (Nell et al., 1996), microalgal concentrates (Brown and Robert, 2002), spray-dried microalgae (Arney et al., 2015), and so on. Substituting 50% of the traditional microalgae with single-cell detritus produced from seaweed (*Porphyra haitanensis*) can be used as a partial microalgal substitute for the nursery culture of the tropical oyster (*Crassostrea belcheri*) juvenile (Tanyaros and Chuseingjaw, 2016). Palatable artificial diets have good potential for replacement of costly natural diets of the green-lipped mussel *Perna canaliculus* post-settlement juveniles (Gui et al., 2016a). *Chlorella* sp. powder, *Spirulina platensis* powder, yeast powder, and soybean meal are suitable protein sources in diets for pearl oyster *Pinctada fucata martensii* (Yang et al., 2017a). Microalgae are still the main nutrient sources for pipi clam, *Paphies australis*, particularly for spat and juveniles, while corn flour should be considered in the formulation of diets for laboratory grown (Mamat and Alfaro, 2014).

However, information regarding artificial feed, reliable to substitute for live microalgal feed for pearl oyster *P. maxima*, is rare. In this study, we have attempted to explore the feasibility of using spray-dried microalgae as daily food in *P. maxima* juvenile industrial farming and developed industrial farming methods and technology for *P. maxima* juvenile. The growth, digestive enzyme activity, and intestinal microbial community were characterized under laboratory-controlled conditions in this study. To our knowledge, this study provides the first insights into the impacts of diets on intestinal bacteria of *P. maxima*, where the findings can provide some information on rearing protocols and management of industrial farming mode.

MATERIALS AND METHODS

Experimental Animal and Management

The *P. maxima* juveniles were obtained from Sanya Maifeng Industrial Co., Ltd. (Hainan, China). Before the experiment, the juveniles were kept in an aerated cement tank (28 ± 2°C, 30.0 ± 2 psu, pH 8.0 ± 0.2) for 7 days, fed daily with a mixture of *Isochrysis zhanjiangensis* and *Platymonas subcordiformis*. A total of 30% water exchange were taken every day to promise that the water quality is good enough for *P. maxima*

TABLE 1 | The survival and growth performance of *Pinctada maxima* juvenile after 30-day industrial farming.

	L-iso	P-iso	L-pla	P-pla
SR (%)	84.13 ± 1.37^{ab}	85.71 ± 2.38^{a}	84.54 ± 1.37^{a}	86.51 ± 1.37^{a}
TW (g)	2.6503 ± 0.1702^{a}	2.3701 ± 0.0302^{bc}	2.5002 ± 0.0201^{ab}	2.2601 ± 0.0301^{c}
SH (mm)	32.3747 ± 0.7783^{a}	25.8183 ± 0.9737^{b}	30.5350 ± 2.2149^{a}	25.8000 ± 0.3885^{b}
AGR of TW (g/d)	0.0469 ± 0.0060^{a}	0.0372 ± 0.0010^{bc}	0.0415 ± 0.0008^{ab}	0.0340 ± 0.0010^{c}
AGR of SH (mm/d)	0.2525 ± 0.026^{a}	0.0339 ± 0.0325^{c}	0.1912 ± 0.0738^{b}	0.0330 ± 0.0129^{c}
RGR of TW (%/d)	0.0391 ± 0.0050^{a}	0.0310 ± 0.0008^{bc}	0.0346 ± 0.0006^{ab}	0.0280 ± 0.0009^{c}
RGR of SH (%/d)	1.0345 ± 0.1063^{a}	0.1391 ± 0.1330^{b}	0.7832 ± 0.3025^{b}	0.1366 ± 0.00531^{b}

The significance level of $P < 0.05$ was used for all statistical tests. Different lower-case letters indicate significant differences.
SR, survival rate; TW, total weight; SH, shell height; AGR, absolute growth rate; RGR, relative growth rate.

juveniles, where total ammonia-nitrogen <0.05 mg/L and DO (dissolved oxygen) ≥7 mg/L. Then, *P. maxima* juveniles were divided into four rearing groups in triplicates for experiments, according to different feeding strategies. Triplicate tanks (500 L) containing 300 juveniles were used for each rearing group. A total of 3,600 *P. maxima* juveniles were used in this study, with 1.2008 ± 0.0009 g initial weight and 30.12 ± 0.05 mm initial shell length.

Feeding Diets and Experimental Design

The trials of 30 days were carried out. Two species of live microalgae (*Isochrysis zhanjiangensis* and *Platymonas subcordiformis*) were used in the experimental groups, respectively, the live *I. zhanjiangensis* group (L-iso group) and *P. subcordiformis* group (L-pla group). However, spray-dried microalgal powders (*I. zhanjiangensis* powder and *P. subcordiformis* powder) were used for the other two groups, namely, powder *I. zhanjiangensis* group (P-iso group) and powder *P. subcordiformis* group (P-pla group).

Microalgal stock cultures were obtained from the Microalgae Laboratories of Ocean College in Hainan University. These microalgae were cultured in 5 and 45 L glass buckets and grown at 25.0–27.0°C in Ningbo 3# nutrient medium. The photoperiod was 24:0 h (light/dark), and illumination was provided by 2-day light (40-W) fluorescent tubes. Filtered (0.45 mm) and UV-treated seawater (salinity, 30.2 psu) was used. Continuous aeration was provided to enhance growth and prevent the algae from settling. The microalgae were harvested during an exponential phase for feeding. The spray-dried microalgal powder was provided by SDIC Biotech Investment Co., Ltd. (Beijing, China).

To control the final concentration of microalgae in the experimental tanks, the feeding quantity was determined by measuring the original concentration of the different microalgal diets precisely. Prior to daily feeding, 2 g of each spray-dried diet was suspended in 1,000 ml of filtered seawater and pulsed in a commercial blender (JS39D-250, Supor, China). The liquefied mixture was filtered through a 50-μm mesh to eliminate foam and larger particles and then diluted to 15 L with filtered seawater. The diluted suspension was used in feeding. All diets were fed in culture media at a concentration of 150,000 cells/ml once every 12 h. The cell counts were made using a hemocytometer.

Survival and Growth Parameters

After the end of the experiment, the surviving pearl oyster, *P. maxima*, in each group was counted to calculate the SR. SR was calculated using the following equation: Survival rate = (the number of surviving individuals at the end of the experiment/the number of individuals at the beginning of the experiment) × 100%.

The shell height (SH) was measured using a Vernier caliper (an accuracy of 0.01 mm). In addition, the total weight (TW) was weighed using an electronic balance (an accuracy of 0.0001 g). The absolute growth rate (AGR) and relative growth rate (RGR) were calculated for SH and TW using the following formulas: $AGR = (X_2 - X_1)/t$, $RGR = 100\% \times (X_2 - X_1)/(t \times X_1)$, where "$X_1$" and "$X_2$" are the average of SH (or TW) at the beginning and the end of the experiment, respectively, and "t" is the experimental days.

Sample Collection

All experiments were complied with the standards of the Guidance of the Care and Use of Laboratory Animals in China. After the end of the culture, the intestinal tissue of each pearl oyster was dissected in a sterile environment and stored in liquid nitrogen for further bacterial community analysis, while soft tissues except the intestinal tissue and gill were used for digestive enzyme activity assay.

Assays for Digestive Enzyme Activity

The frozen soft tissues were homogenized on ice in 0.2 M (w/v) of ice-cold physiological saline (Gawlicka et al., 2000), and homogenates were centrifuged at 13,000 *g* for 10 min at 2°C. The supernatant was separated for enzyme analysis in triplicate. The activities of pepsin (PES, E.C.3.4.23.1), amylase (AMS, E.C.3.2.1.1), and lipase (LPS, E.C.3.1.1.3) were used as biochemical indicators and assayed by the commercial kits from Nanjing Jiancheng Bioengineering Institute (Nanjing, China).

DNA Extraction of Microbial Samples

Microbial DNA was extracted from intestinal contents using the EZNA Stool DNA Kit (Omega Bio-tek, Norcross GA, United States). The final DNA concentration was quantified by using Qubit 3.0 Fluorometer (Invitrogen, United States) and agarose gel electrophoresis (Zheng et al., 2019).

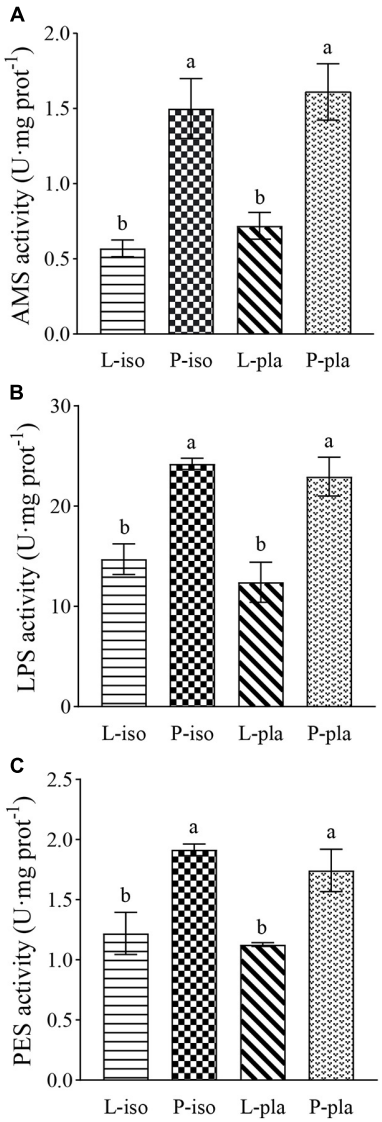

FIGURE 1 | The digestive enzyme activity of *Pinctada maxima* juvenile after 30-day industrial farming. The significance level of $P < 0.05$ was used for all statistical tests. Different lower-case letters indicate significant differences. **(A)** AMS activity, AMS = amylase; **(B)** LPS activity, LPS = lipase; **(C)** PES activity, PES = pepsin.

Amplicon Generation and Sequencing of Bacteria 16S rRNA Gene

A total of 50 ng DNA were used to generate amplicons. The V3–V4 region of the bacteria 16S ribosomal RNA gene was amplified by PCR, using the forward primers containing the sequence 341F (5′-CCTACGGGNGGCWGCAG-3′) and reverse primers containing the sequence 805R (5′-GACTACHVGGGTATCTAATCC-3′). The marker region of bacteria was amplified by PCR (thermal cycling program: 98°C for 30 s, 98°C for 10 s, followed by 35 cycles at 54°C for 30 s, 72°C for 45 s, and a final extension at 72°C for 10 min). The PCR reactions were performed in triplicate in a 12.5 μl mixture, containing 2.5 μl forward primer, 2.5 μl reverse primer, 25 μl dd H_2O, and 50 ng template DNA. Amplicons were extracted from 2% agarose gel and purified using the QIAquick Gel Extraction Kit (Qiagen, Hilden, Germany) according to the instructions of the manufacturer. Purified products were subjected to Illumina MiSeq Sequencing platform (Hangzhou, Lianchuan Gene Technology Company., Ltd., China), generating paired-end reads.

Bioinformatics Analysis

Raw fasta files were demultiplexed, quality filtered, and analyzed using QIIME 2.0 (Bolyen et al., 2019). The 250 bp reads were truncated at any site of more than three sequential bases receiving a Phred quality score of <Q20. Any reads containing ambiguous base calls or barcode/primer errors were discarded. Operational taxonomic units (OTUs) were clustered with 97% similarity cutoff using UPARSE (version 7.1) (Edgar, 2013)[1]. Chimeric sequences were identified and removed using UCHIME. The phylogenetic affiliation of each 16S rRNA gene sequence was analyzed by SILVA Classifier (release 132) (Quast et al., 2013) against Silva 16S rRNA database using the confidence threshold of 70%. According to the SILVA (release 132) classifier, the characteristic abundance was performed with normalization by the relative abundance of each sample, and then, five indexes (ACE, Chao1, Shannon, Simpson, and Goods coverage) were calculated using QIIME2 for alpha diversity analysis. Rarefaction analysis was also performed using the Mothur program. The structures of the microbial community in different samples were compared through column diagrams and principal component analysis (PCA).

Statistical Analysis

The data in this study were expressed as mean ± SE. For all statistical tests, *P*-values <0.05 were considered to be significant. Significant differences of each variable were first detected using the *t*-test in enzyme activities among groups. The least significant difference multiple-range test was used to determine the significance of differences in growth, alpha diversity metrics, and the relative abundance of phylum or genus in the intestinal microbial community. Prior to analysis, data were tested for normality using Kolmogorov-Smirnov's test and for homogeneity of variance using Cochran's C test. Data that did not meet the ANOVA assumptions were log-transformed before analysis, and percentage data were arcsine square-root-transformed. All statistical analyses were performed using DPS14.5 software (Hangzhou Rui Feng Information Technology Co., Ltd., Hangzhou, China).

RESULTS

Effect of Different Diets on Survival and Growth Performance

The SR was not affected by different diets used in this study ($P > 0.05$, **Table 1**). After 30-day industrial farming, the SR

[1]http://drive5.com/uparse/

in all groups ranged from 84 to 86%, without significant difference. The growth performances in L-iso, P-iso, L-pla, and P-pla were different ($P > 0.05$, **Table 1**). The best growth performance was observed in the L-iso group, followed by the L-pla group. The TW in the L-iso group was 2.6503 ± 0.1702 g, significantly higher than P-iso and P-pla groups ($P < 0.05$), and TM for the L-pla group (2.5002 ± 0.0201 g) significantly higher than the P-pla group (2.2601 ± 0.0301, $P < 0.05$). The characteristics of the difference for AGR and RGR of TW in groups were found the same as TW. The largest SH was gained in L-iso and L-pla groups (32.3747 ± 0.7783 and 30.5350 ± 2.2149 mm, respectively), significantly higher than P-iso and P-pla groups (25.8183 ± 0.9737 and 25.8000 ± 0.3885 mm, respectively). The best AGR and RGR of SH was observed in the L-iso group (0.2525 ± 0.026 mm/day and 1.0345 ± 0.1063%/day respectively), followed by the L-pla group (0.1912 ± 0.0738 mm/day, 0.7832 ± 0.3025%/day, respectively). The significant difference for AGR and RGR of SH was not existed between P-iso and P-pla groups ($P < 0.05$).

Effect of Different Diets on Digestive Enzyme Activity

Oyster filtered out all the diets fed in the experimental groups, without exception. The microalgal species, used as a daily food in this study, did not cause a significant difference in digestive enzyme activity of *P. maxima* juvenile after 30-day industrial farming ($P > 0.05$), while the microalgal types (live or spray-dried powder) did ($P < 0.05$, **Figure 1**). The PES and LPS activities in the P-iso group were observed highest (1.81 ± 0.20 and 24.22 ± 0.57 U/mg prot, respectively), followed by the P-pla group (1.74 ± 0.17 and 22.95 ± 1.95 U/mg prot, respectively), significantly higher than L-iso and L-pla groups ($P < 0.05$). In addition, the highest AMS activity (1.61 ± 0.29 U/mg prot) was found in the P-pla group, followed by the P-iso group (1.51 ± 0.20 U/mg prot), significantly higher than L-iso and L-pla groups (0.57 ± 0.05 and 0.72 ± 0.07 U/mg prot, respectively, $P < 0.05$).

Statistical Analysis of Sequences

Through the detection of intestinal microbiota, a total of 1,134,712 high-quality sequences from nine samples were obtained, with an average of 75,647 sequences per sample-based. A total of 4,872 OTUs at 97% sequence similarity were obtained, with an average of 353 OTUs in each sample. In addition, rarefaction curves indicated that the obtained sequence could reflect the majority of bacteria diversity in each sample (**Figure 2**).

In this study, results from the analysis of alpha diversity metrics showed that the diversity and richness of the intestinal microbial community had a significant difference in different diet groups ($P < 0.05$, **Table 2**). The ACE and Chao 1 were used as estimators of community richness, and Shannon and Simpson were used as estimators of community diversity. The ACE and Chao1 ranged from 331.92 ± 20.25 to 386.40 ± 20.42 and 331.37 ± 12.48 to 382.16 ± 19.19, respectively, where Chao1 in the P-iso group was significantly lower than other groups ($P < 0.05$). The Simpson in P-iso and P-pla groups was 0.73 ± 0.05, 0.77 ± 0.06, respectively, significantly higher than L-iso and L-iso groups (0.56 ± 0.03 and 0.77 ± 0.06, respectively, $P < 0.05$).

Taxonomic Composition

Different diets could significantly affect the relative abundance of phylum or genus in the intestinal microbial community of *P. maxima* juvenile. A total of 31 phyla and 413 genera were detected in all groups (**Figure 3**, $P < 0.05$).

Proteobacteria was the most abundant phylum in all groups, relative abundance ranged from 62.31 ± 6.17% to 82.37 ± 9.33% (**Figure 3A**). In addition, Tenericutes was the core phylum both in L-pla and P-pla groups (10.19 ± 1.1% and 20.50 ± 2.05%, respectively). Furthermore, Chlamydiae (7.79 ± 0.67%) and Firmicutes (5.43 ± 0.66%) were the abundant phyla in the L-iso group, while Actinobacteria (3.28 ± 0.13%), Planctomycetes (6.40 ± 0.58%), and Chloroflexi (1.79 ± 0.11%) in the P-iso group and Cyanobacteria (10.52 ± 1.10%) in the P-pla group.

Burkholderia was the dominant genus in both L-iso (66.52 ± 6.43%) and L-pla groups (54.00 ± 5.66%), while *Mycoplasma*, *Alphaproteobacteria*, and *Oxyphotobacteria* were in both P-iso and P-pla groups. Furthermore, *Simkaniaceae* and *Variovorax* were the dominant genera in the L-iso group, and hence relative abundance was significantly higher than the other groups ($P < 0.05$). *Amphritea*, *Cohaesibacter*, and *Kiloniella* were the dominant genera in both P-iso and L-pla groups (**Figure 3B**).

In addition, the principal component analysis (PCA) indicated that the bacteria community in L-iso and L-pla groups clustered together, while P-iso and P-pla groups clustered together. The bacteria community in L-iso and L-pla groups widely differs from that in P-iso and P-pla groups (**Figure 3C**).

DISCUSSION

Survival and growth performances are the most important factors in the pearl oyster industry (Liao et al., 2020). In this study, we initially attempted to investigate the feasibility of spray-dried microalgae instead of live microalgae in *P. maxima* juvenile industrial farming. After an interview with the technician on the farm, we confirmed that the growth performance of *P. maxima* juveniles from industrial farming in this study was not good as that cultured in sea area, maybe due to the limited food availability, and is considered as the bottleneck for developing the culture mode for bivalves (Yang et al., 2017a,b). Similar results have been reported previously in species of some bivalves. For example, the absolute and RGRs of shell length and TW of the pearl oyster *Pinctada martensii* spat were lower than those cultured in the sea (Yang et al., 2015). Even so, the results in this study showed that *P. maxima* juvenile cultured indoor can promise the SR (ranged from 84 to 86%, no significant difference was observed) and significantly higher than those cultured in the natural sea (10%, unpublished data form farm). This is because culturing pearl oyster indoor can avoid the influence of extreme weather factors effectively, such as typhoons (usually happen in Hainan from August to October), temperature and salinity change caused by rain, and so on.

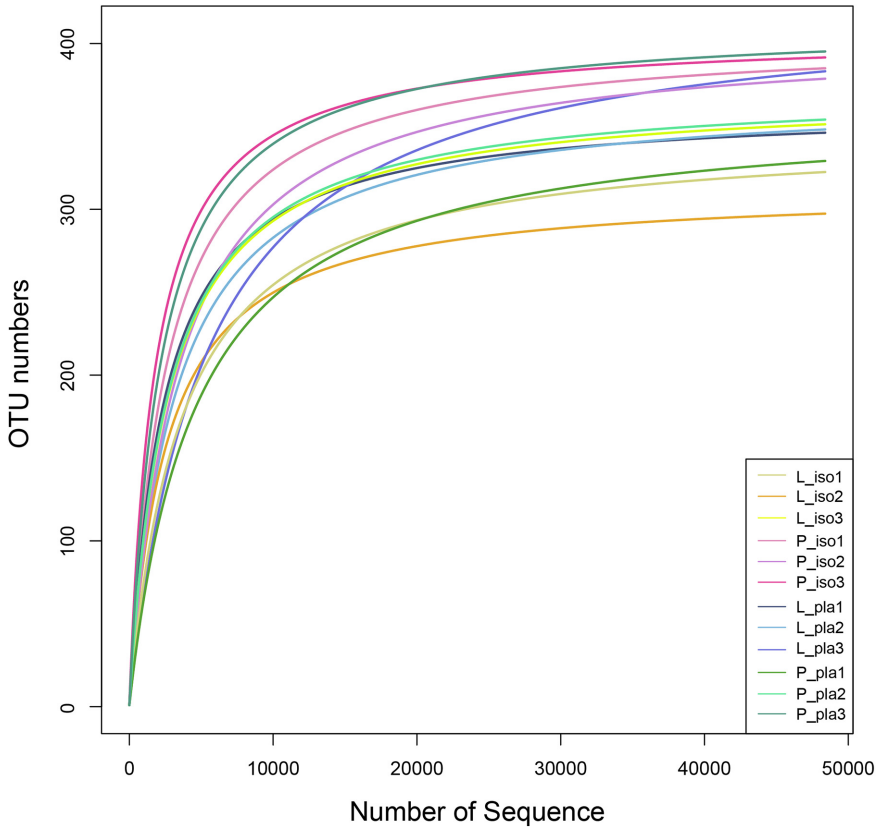

FIGURE 2 | Rarefaction analyses of all samples. Rarefaction curves represented the number of OUT detected in the L-iso group (L-iso 1, L-iso 2, and L-iso 3), P-iso group (P-iso 1, P-iso 2, and P-iso 3), L-pla group (L-pla 1, L-pla 2, and L-pla 3), and P-pla group (P-pla 1, P-pla 2, and P-pla 3). Sequences were clustered at 97% sequence similarity. OTU, operational taxonomic unit.

TABLE 2 | OTUs, ACE, Chao 1, Simpson, Shannon, and Good's coverage for 16s rRNA libraries of all samples.

	L-iso	P-iso	L-pla	P-pla
OTUs	327.33 ± 32.01^{a}	377.67 ± 12.66^{a}	349.67 ± 29.40^{a}	359.00 ± 29.61^{a}
ACE	331.92 ± 20.25^{a}	340.33 ± 14.56^{a}	362.75 ± 21.16^{a}	366.40 ± 20.42^{a}
Chao1	331.37 ± 12.48^{b}	335.38 ± 15.46^{b}	373.28 ± 11.32^{a}	382.16 ± 19.19^{a}
Simpson	0.56 ± 0.03^{b}	0.73 ± 0.05^{a}	0.59 ± 0.04^{b}	0.77 ± 0.06^{a}
Shannon	2.54 ± 0.54^{a}	2.89 ± 0.22^{a}	3.15 ± 0.65^{a}	3.19 ± 0.33^{a}
Goods coverage	1.00 ± 0.00^{a}	1.00 ± 0.00^{a}	1.00 ± 0.00^{a}	1.00 ± 0.00^{a}

The significance level of $P < 0.05$ was used for all statistical tests. Different lower-case letters indicate significant differences.
OTU, operational taxonomic unit; ACE, abundance-based coverage estimator.

Filter-feeding bivalves usually take phytoplankton as a part of the natural diet. *Isochrysis zhanjiangensis* and *Platymonas subcordiformis* are the main microalgal species widely used in the fodder industry as good bait for aquaculture activity (Zheng et al., 2011; An et al., 2015; Cheng et al., 2020). But an operation to culture live microalgae requires dedicated staff and facilities that represent 30–50% of the costs (Gui et al., 2016b), and live microalgal growth is easily affected by environmental factors. Therefore, replacing live microalgae with a substitute and the same nutritive quality food is important and necessary in filter-feeding bivalve industrial farming. In this study, we used the spray-dried microalgal powder instead of live microalga. The results indicated that spray-dried microalgal powder can promise the *P. maxima* juvenile SR as live microalgae in industrial farming, improving pearl oyster production. However, the growth performance was slower than that in the live microalgal group. The difference may be caused by the spray-dried microalgal powder that was insufficient in other essential nutrients for the growth of pearl oyster juveniles, such as carbohydrate and protein, or not easy to digest as live microalga (Numaguchi, 2002; Cheng et al., 2020).

Digestive enzyme activity is often used as an indicator of digestive processes and nutritional condition of fish, including AMS, PES, and LPS, and reflects growth performance

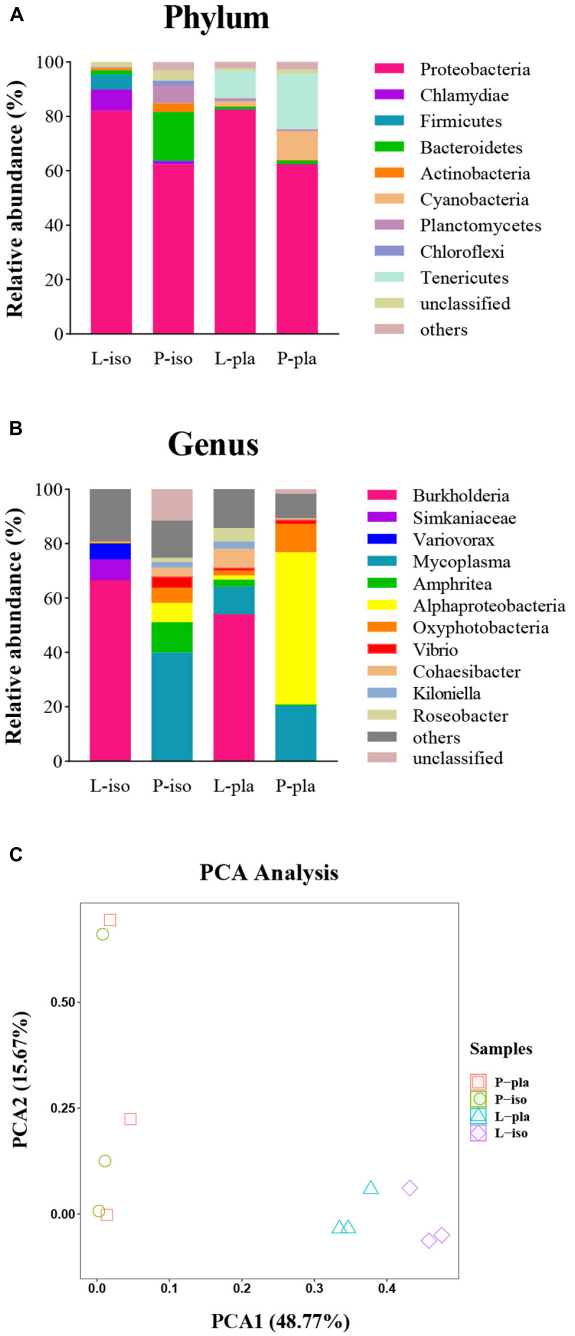

FIGURE 3 | Composition of intestinal microflora of *P. maxima* fed with different diets. **(A)** Microbiota composition at the phylum level with relative abundance. **(B)** Microbiota composition at the genus level with relative abundance. "Others" meant the means of the sum of phylum or genus with relative abundance < 2% in L-iso, P-iso, L-pla, P-pla groups, respectively. **(C)** PCA analisys of bacteria community in different diet groups. The colored plot represents the bacteria from L-iso, P-iso, L-pla, and P-pla groups.

(Cahu et al., 1998). Various digestive enzymes are involved in digestive and absorptive processes and are important indicators of the growth performance of aquatic animals (Abolfathi et al., 2012). In this study, *P. maxima* juveniles fed with spray-dried microalgal powder displayed higher PES, AMS, and LPS activities than those with live microalgae. The phenomenon due to spray-dried microalgal powder needs more energy to digest and absorb nutrients. Thus, the growth performance is slightly lower, compared with the live microalgal group.

Intestinal microbiota, composed of a diverse and vast population of microorganisms, interacting with each other to form a complex ecological network through various types of interactions, plays key functions in host growth, physiology, and development (Nayak, 2010; Deng et al., 2012; Tremaroli and Bäckhed, 2012). In addition, intestinal microbiota activity is reported to be related to host longevity (Nayak, 2010). A disturbance in the intestinal microbial community can lead to changes in the microbial diversity and abundance of certain bacteria, resulting in beneficial or harmful effects in the aquatic animal (Gómez and Balcázar, 2008). An altered microbiota in the intestine can lead to altered immune functions of hosts and increase the risk of disease (Morgan et al., 2012). Thus, maintaining a functional and steady intestinal microbiota is important to the host. The composition of the intestinal bacterial community varies with a unique core microbiome in each specific host species. In comparison to mammals, the intestinal microbial composition in aquatic animals is susceptible to diet (De Filippo et al., 2010; Ringø et al., 2016), drugs (Zwolinska-Wcislo et al., 2011), stresses (Galley et al., 2014), and so on. The results in this study indicated that the Proteobacteria was the dominant bacteria in pearl oysters at the phylum level, consistent with the findings on oysters (Fernandez-Piquer et al., 2012; Trabal Fernández et al., 2014). Proteobacteria is the largest, most phenotypically diverse, and abundant phylum throughout all the life stages of animals (Qin et al., 2010; Sevellec et al., 2014; Zhou et al., 2018; Liao et al., 2020). Proteobacteria could catabolize feedstuff components (Jumpertz et al., 2011) and may play an important role in degrading cellulose and agar, the major components of food consumed by bivalve mollusks, as well as fixing nitrogen in the gastrointestinal tract of bivalves (Prieur et al., 1990; Harris, 1993; Newell, 2004; Liao et al., 2020). The relative abundance of Proteobacteria in spray-dried microalgal powder groups was significantly lower than that in live microalgal groups in this study, and this phenomenon may consequently result in slower growth performance of *P. maxima* juveniles in spray-dried microalgal powder groups.

Microbial identification is meaningful only when microbiota can be classified at the level of genus or species in relation to animal husbandry (Petrosino et al., 2009). *Burkholderia* was found as the main genus of *P. maxima* juvenile intestinal microbial community that from live microalgal groups, while *Mycoplasma*, *Alphaproteobacteria*, and *Oxyphotobacteria* in spray-dried microalgal powder groups. This phenomenon indicated the intestinal bacteria of *P. maxima* juvenile at genus were more sensitive to diets. Additionally, the top 10 representative genera mainly comprised of facultative anaerobes and anaerobes. Both Gram-positive and negative bacteria can produce phosphatases, helping in nutrient absorption (Ramirez and Dixon, 2003; Rasheeda et al., 2017). Although the genus

observed in this study is reported to contain opportunistic pathogens, such as *Burkholderia* and *Vibrio*, all the *P. maxima* juvenile examined were healthy. The presence of pathogenic microbes in the intestinal of aquatic animals can be seen as a common phenomenon, playing a vital role in the internal metabolism and immune, rather than playing the role of a pathogen (Grimes et al., 1985; Pujalte et al., 2003; Valdenegro-Vega et al., 2013; Wu et al., 2013; Rasheeda et al., 2017). *Alphaproteobacteria* was the dominant Proteobacteria, widely distributed in marine environments (Wagner-Döbler and Biebl, 2006). *Mycoplasma* is the abundant member of gut microbiota in numerous vertebrate hosts and has been found to dominate in the gut of Atlantic salmon (Holben et al., 2002), farmed rainbow trout *Oncorhynchus mykiss* (Lyons et al., 2017), Trinidadian guppies (Sullam et al., 2015), and the long-jawed mudsucker *Gillichtythys mirabilis* (Bano et al., 2007).

The intestinal microbiome revealed rich biodiversity that predictably reacts to changing gut conditions, and diet components played a key role in regulating the intestinal bacterial community (Hennersdorf et al., 2016; Huyben et al., 2017). The overall intestinal bacterial diversity increased in pearl oysters *P. maxima* juvenile fed with spray-dried microalgal powder in this study. Therefore, the spray-dried microalgal powder leads to a high biodiversity level, benefit to maintain the intestinal micro ecological balance. The antioxidant capacity and immunity may be related to the biodiversity level of intestinal bacteria (Nie et al., 2017; Wang et al., 2017). Thus, the change of antioxidant capacity and immunity in *P. maxima* juveniles that feed with spray-dried microalgal powder need to be established and investigated in the future, as well as the underlying mechanisms.

CONCLUSION

In summary, this study is the first to analyze the feasibility of spray-dried microalgal powder instead of live microalga in *P. maxima* juvenile industrial farming. The survival, growth, and intestinal microbial community were used as an indicator for comparative profiling. The results indicated that the spray-dried microalgal powder used in this study (*Isochrysis zhanjiangensis* and *Platymonas subcordiformis* powder) can promise the SR as live microalgae, even though the growth performance is slightly lower. The characterization of the intestinal bacterial community of *P. maxima* juveniles under controlled conditions was first presented in this study, with Proteobacteria as the dominant phylum, and intestinal bacteria at the genus level were more sensitive to diets. However, the relationship between intestinal bacteria of *P. maxima* juveniles and diet needs further research. The results in this study suggested that the spray-dried *I. zhanjiangensis* powder and *P. subcordiformis* powder can serve as substitutes for live microalgae in *P. maxima* juvenile industrial farming under controlled conditions. The findings in this study will be helpful to develop the industrial farming mode for *P. maxima* juvenile, to avoid mass mortality caused by increasing pollution offshore or unexpected natural disasters. Furthermore, this study provides basic data to optimize industrial farming technology and healthy management for *P. maxima* juvenile.

DATA AVAILABILITY STATEMENT

Raw sequence data of samples in this study are available in the Sequence Read Archive database of NCBI under the SRA Accession: PRJNA790867.

ETHICS STATEMENT

The animal study was reviewed and approved by the Animal Care and Use Committee of Hainan University. Written informed consent was obtained from the owners for the participation of their animals in this study.

AUTHOR CONTRIBUTIONS

XZ and ZG conceptualized the study. SY and XL were responsible for the experimental operation, and prepared and wrote the original draft. HV and XZZ conducted the sample determination. XZ, ZG, AW, JL, and YS reviewed, edited, and wrote the manuscript. All authors read and approved the final manuscript.

FUNDING

This project was supported by the National Key Research and Development Program of China (Grant No. 2018YFD0900704) and the National Science Foundation of China (Grant No. 31772847).

REFERENCES

Abolfathi, M., Hajimoradloo, A., Ghorbani, R., and Zamani, A. (2012). Effect of starvation and refeeding on digestive enzyme activities in juvenile roach, *Rutilus rutilus* caspicus. *Comp. Biochem. Physiol. A* 161, 166–173. doi: 10.1016/j.cbpa.2011.10.020

An, X., Li, X., Li, Z., and Zhang, Y. (2015). Growth characteristics of platymonas subcordiformis and oxyrrhis marina in their co-culture systems. *Nat. Environ. Pollut. Technol.* 14:967.

Arney, B., Liu, W., Forster, I. P., Mckinley, R. S., and Pearce, C. M. (2015). Feasibility of dietary substitution of live microalgae with spray-dried *Schizochytrium*, sp. or spirulina, in the hatchery culture of juveniles of the pacific geoduck clam (*Panopea generosa*). *Aquaculture* 444, 117–133. doi: 10.1016/j.aquaculture.2015.02.014

Bano, N., Smith, A. D., Bennett, W., Vasquez, L., and Hollibaugh, J. T. (2007). Dominance of mycoplasma in the guts of the long-jawed mudsucker, *Gillichthys mirabilis*, from five California salt marshes. *Environ. Microbiol.* 9, 2636–2641. doi: 10.1111/j.1462-2920.2007.01381.x

Barnes, R., Calow, P., Olive, P., and Golding, D. (1993). *The Invertebrates: A Synthesis*. Cambridge: Blackwell Science Lyd.

Bolyen, E., Rideout, J. R., Dillon, M. R., Bokulich, N. A., Abnet C. C., Al-Ghalith, G. A., et al. (2019). Reproducible, interactive, scalable and extensible microbiome data science using QIIME 2. *Nat. Biotechnol.* 37, 852–857. doi: 10.1038/s41587-019-0209-9

Brown, M., and Robert, R. (2002). Preparation and assessment of microalgal concentrates as feeds for larval and juvenile pacific oyster (*Crassostrea gigas*). *Aquaculture* 207, 289–309. doi: 10.1016/s0044-8486(01)00742-6

Cahu, C., Zambonino Infante, J., Peres, A., Quazuguel, P., and Gall, M. (1998). Algal addition in sea bass (*Dicentrarchus labrax*) larvae rearing: effect on digestive enzymes. *Aquaculture* 161, 479–489. doi: 10.1016/s0044-8486(97)00295-0

Cheng, P., Zhou, C., Chu, R., Chang, T., Xu, J., Ruan, R., et al. (2020). Effect of microalgae diet and culture system on the rearing of bivalve mollusks: nutritional properties and potential cost improvements. *Algal Res.* 51:102076. doi: 10.1016/j.algal.2020.102076

De Filippo, C., Cavalieri, D., Di Paola, M., Ramazzotti, M., Poullet, J. B., Massart, S., et al. (2010). Impact of diet in shaping gut microbiota revealed by a comparative study in children from Europe and rural Africa. *Proc. Natl. Acad. Sci. U.S.A.* 107, 14691–14696. doi: 10.1073/pnas.1005963107

Deng, Y., Fu, S., Liang, F., Du, X., and Xie, S. (2013). Growth and survival of pearl oyster pinctada maxima spat reared under different environmental conditions. *J. Shellfish Res.* 32, 675–679.

Deng, Y., Jiang, Y. H., Yang, Y., He, Z., Luo, F., and Zhou, J. (2012). Molecular ecological network analyses. *BMC Bioinformatics* 13:113. doi: 10.1186/1471-2105-13-113

Edgar, R. C. (2013). UPARSE: Highly accurate OTU sequences from microbial amplicon reads. *Nat. Methods* 10, 996–998. doi: 10.1038/nmeth.2604

Fernandez-Piquer, J., Bowman, J. P., Ross, T., and Tamplin, M. L. (2012). Molecular analysis of the bacterial communities in the live Pacific oyster (*Crassostrea gigas*) and the influence of postharvest temperature on its structure. *J. Appl. Microbiol.* 112, 1134–1143. doi: 10.1111/j.1365-2672.2012.05287.x

Galley, J. D., Nelson, M. C., Yu, Z., Dowd, S. E., and Bailey, M. T. (2014). Exposure to a social stressor disrupts the community structure of the colonic mucosa-associated microbiota. *BMC Microbiol.* 14:189. doi: 10.1186/1471-2180-14-189

Gawlicka, A., Parent, B., Horn, M. H., Ross, N., Opstad, I., and Torrissen, O. J. (2000). Activity of digestive enzymes in yolk-sac larvae of Atlantichalibut (*Hippoglossus hippoglossus*): indication of readiness for first feeding. *Aquaculture* 184, 303–314. doi: 10.1016/s0044-8486(99)00322-1

Gómez, G. D., and Balcázar, J. L. (2008). A review on the interactions between gutmicrobiota and innate immunity of fish. *Pathog. Dis.* 52, 145–154. doi: 10.1111/j.1574-695x.2007.00343.x

Grimes, D. J., Brayton, P., Colwell, R. R., and Gruber, S. H. (1985). Vibrios as autochthonous flora of neritic sharks. *Syst. Appl. Microbiol.* 6, 221–226.

Gui, Y., Kaspar, H. F., Zamora, L. N., Dunphy, B. J., and Jeffs, A. G. (2016a). Capture efficiency of artificial food particles of post-settlement juveniles of the greenshellTM mussel, *Perna canaliculus*. *Aquaculture* 464, 1–7. doi: 10.1016/j.aquaculture.2016.06.011

Gui, Y., Zamora, L., Dunphy, B. J., and Jeffs, A. G. (2016b). Evaluation of the formulated diet MySpat for feeding hatchery-reared spat of the green-lipped mussel, *Perna canaliculus* (Gmelin, 1791). *Aquac. Res.* 42, 3907–3912. doi: 10.1111/are.12841

Harris, J. (1993). The presence, nature, and role of gut microflora in aquatic invertebrates: a synthesis. *Microb. Ecol.* 25, 195–231. doi: 10.1007/BF00171889

He, G., Liu, X., Xu, Y., Liang, J., Deng, Y., Zhang, Y., et al. (2021). Repeated exposure to simulated marine heatwaves enhances the thermal tolerance in pearl oysters. *Aquat. Toxicol.* 239:105959. doi: 10.1016/j.aquatox.2021.105959

Hennersdorf, P., Kleinertz, S., Theisen, S., Abdul-Aziz, M. A., Mrotzek, G., Palm, H. W., et al. (2016). Microbial diversity and parasitic load in tropical fish of different environmental conditions. *PLoS One* 11:e151594. doi: 10.1371/journal.pone.0151594

Holben, W. E., Williams, P., Saarinen, M., Sarkilahti, L. K., and Apajalahti, J. H. A. (2002). Phylogenetic analysis of intestinal microflora indicates a novel mycoplasma phylotype in farmed and wild salmon. *Microb. Ecol.* 44, 175–185. doi: 10.1007/s00248-002-1011-6

Huyben, D., Nyman, A., Vidakoviæ, A., Passoth, V., Moccia, R., Kiessling, A., et al. (2017). Effects of dietary inclusion of the yeasts *Saccharomyces cerevisiae* and *Wickerhamomyces anomalus* on gut microbiota of rainbow trout. *Aquaculture* 473, 528–537.

Jumpertz, R., Le, D. S., Turnbaugh, P. J., Trinidad, C., Bogardus, C., Gordon, J. I., et al. (2011). Energy-balance studies reveal associations between gut microbes, caloric load, and nutrient absorption in humans. *Am. J. Clin. Nutr.* 94, 58–65. doi: 10.3945/ajcn.110.010132

Liang, F., Xie, S., Fu, S., Li, J., and Deng, Y. (2016). Growth pattern and biometric relationship of pearl oyster *Pinctada maxima* cultured in Beibu Bay, China. *J. Appl. Aquac.* 28, 110–118. doi: 10.1080/10454438.2016.1172535

Liao, Y., Cai, C., Yang, C., Zheng, Z., Wang, Q., Du, X., et al. (2020). Effect of protein sources in formulated diets on the growth, immune response, and intestinal microflora of pearl oyster *Pinctada fucata martensii*. *Aquac. Rep.* 16:100253. doi: 10.1016/j.aqrep.2019.100253

Lyons, P. P., Turnbull, J. F., Dawson, K. A., and Crumlish, M. (2017). Effects of low-level dietary microalgae supplementation on the distal intestinal microbiome of farmed rainbow trout *Oncorhynchus mykiss* (Walbaum). *Aquac. Res.* 48, 2438–2452. doi: 10.1111/are.13080

Mamat, N. Z., and Alfaro, A. C. (2014). Evaluation of microalgal and formulated diets for the culture of the New Zealand pipi clam *Paphies australis*. *Int. Aquat. Res.* 6, 1–13.

Morgan, X., Tickle, T., Sokol, H., Gevers, D., Devaney, K., Ward, D., et al. (2012). Dysfunction of the intestinal microbiome in inflammatory bowel disease and treatment. *Genome Biol.* 13:R79. doi: 10.1186/gb-2012-13-9-r79

Nayak, S. K. (2010). Role of gastrointestinal microbiota in fish. *Aquac. Res.* 41, 1553–1573. doi: 10.1111/j.1365-2109.2010.02546.x

Nell, J. A., Diemar, J. A., and Heasman, M. P. (1996). Food value of live yeasts and dry yeast-based diets fed to Sydney rock oyster *Saccostrea commercialis*, spat. *Aquaculture* 145, 235–243. doi: 10.1016/s0044-8486(96)01337-3

Newell, R. I. R. (2004). Ecosystem influences of natural and cultivated populations of suspension-feeding bivalve molluscs: a review. *J. Shellfish Res.* 23, 51–61.

Nie, L., Zhou, Q. J., Qiao, Y., and Chen, J. (2017). Interplay between the gut microbiota and immune responses of ayu (*Plecoglossus altivelis*) during *Vibrio anguillarum* infection. *Fish Shellfish Immunol.* 68, 479–487. doi: 10.1016/j.fsi.2017.07.054

Numaguchi, K. (2002). Effect of an artificial diet on early spat growth of the Japanese pearl oyster *Pinctada fucata martensii*. *Fisheries* 68, 694–696. doi: 10.1046/j.1444-2906.2002.00446.x

Petrosino, J., Highlander, S., Luna, R., Gibbs, R., and Versalovic, J. (2009). Metagenomic pyrosequencing and microbial identification. *Clin. Chem.* 55, 856–866. doi: 10.1373/clinchem.2008.107565

Philippe, A. D., and Christopher, J. L. (1994). Use of a probiotic for the culture of larvae of the pacific oyster (*Crassostrea gigas*, thunberg). *Aquaculture* 119, 25–40. doi: 10.1016/0044-8486(94)90441-3

Prieur, D., Mevel, G., Nicolas, J. L., Plusquellec, A., and Vigneulle, M. (1990). Interactions between bivalve molluscs and bacteria in the marine environment. *Oceanogr. Mar. Biol. Annu. Rev.* 28, 277–352.

Pujalte, M. J., Sitjā-Bobadilla, A., Ā-Lvarez-Pellitero, P., and Garay, E. (2003). Carriage of potentially fish-pathogenic bacteria in *Sparus aurata* cultured in Mediterranean fish farms. *Dis. Aquat. Organ.* 54, 119–126. doi: 10.3354/dao054119

Qin, J., Li, R., Raes, J., Arumugam, M., Burgdorf, K. S., Manichanh, C., et al. (2010). A human gut microbial gene catalogue established by metagenomic sequencing. *Nature* 464, 59–65. doi: 10.1038/nature08821

Quast, C., Pruesse, E., Yilmaz, P., Gerken, J., Schweer, T., Yarza, P., et al. (2013). The SILVA ribosomal RNA gene database project: improved data processing and web-based tools. *Nucl. Acids Res.* 41, D590–D596. doi: 10.1093/nar/gks1219

Ramirez, R. F., and Dixon, B. A. (2003). Enzyme production by obligate intestinal anaerobic bacteria isolated from oscars (*Astronotus ocellatus*), angelfish (*Pterophyllum scalare*) and southern flounder (*Paralichthys lethostigma*). *Aquaculture* 227, 417–426. doi: 10.1016/s0044-8486(03)00520-9

Rasheeda, M. K., Rangamaran, V. R., Srinivasan, S., Ramaiah, S. K., Gunasekaran, R., Jaypal, S., et al. (2017). Comparative profiling of microbial community of three economically important fishes reared in sea cages under tropical offshore environment. *Mar. Genom.* 34, 57–65. doi: 10.1016/j.margen.2017.04.003

Ringø, E. Z. Z. V., Dimitroglou, A., Foey, A., Davies, S., Owen, M., Lauzon, H. L., et al. (2016). Effect of dietary components on the gut microbiota of aquatic animals. A never-ending story? *Aquac. Nutr.* 22, 219–282.

Sevellec, M., Pavey, S. A., Boutin, S., Filteau, M., Derome, N., and Bernatchez, L. (2014). Microbiome investigation in the ecological speciation context of lake whitefish (*Coregonus clupeaformis*) using next-generation sequencing. *J. Evol. Biol.* 27, 1029–1046. doi: 10.1111/jeb.12374

Sullam, K. E., Rubin, B. E. R., Dalton, C. M., Kilham, S. S., Flecker, A. S., and Russell, J. A. (2015). Divergence across diet, time and populations rules out parallel evolution in the gut microbiomes of Trinidadian guppies. *ISME J.* 9, 1508–1522. doi: 10.1038/ismej.2014.231

Tanyaros, S., and Chuseingjaw, S. (2016). A partial substitution of microalgae with single cell detritus produced from seaweed (*Porphyra haitanensis*) for the nursery culture of tropical oyster (*Crassostrea belcheri*). *Aquac. Res.* 47, 2080–2088.

Trabal Fernández, N., Mazón-Suástegui, J. M., Vázquez-Juárez, R., Ascencio-Valle, F., and Romero, J. (2014). Changes in the composition and diversity of the bacterial microbiota associated with oysters (*Crassostrea corteziensis*, *Crassostrea gigas* and *Crassostrea sikamea*) during commercial production. *FEMS Microbiol. Ecol.* 88, 69–83. doi: 10.1111/1574-6941.12270

Tremaroli, V., and Bäckhed, F. (2012). Functional interactions between the gut microbiota and host metabolism. *Nature* 489, 242–249. doi: 10.1038/nature11552

Valdenegro-Vega, V., Naeem, S., Carson, J., Bowman, J., Tejedor Del Real, J., and Nowak, B. (2013). Culturable microbiota of ranched southern bluefin tuna (*Thunnus maccoyii* Castelnau). *J. Appl. Microbiol.* 115, 923–932. doi: 10.1111/jam.12286

Wagner-Döbler, I., and Biebl, H. (2006). Environmental biology of the marine Roseobacter lineage. *Annnu. Rev. Microbiol.* 60, 255–280. doi: 10.1146/annurev.micro.60.080805.142115

Wang, A., Shi, Y., Wang, Y., and Gu, Z. (2010). *The Biology and Breeding of New Technologies of Pinctada Martensii*. Beijing: Chinese Agricultural Science and Technology Press.

Wang, Q., Yang, C., Du, X., Liu, X., Sun, R., and Deng, Y. (2015). Growth performance and biochemical composition of juvenile pearl oyster *Pinctada martensii* fed on artificial diets. *Aquac. Int.* 24, 995–1005. doi: 10.1007/s10499-015-9966-8

Wang, X., Sun, Y., Wang, L., Li, X., Qu, K., and Xu, Y. (2017). Synbiotic dietary supplement affects growth, immune responses and intestinal microbiota of *Apostichopus japonicus*. *Fish Shellfish Immunol.* 68, 232–242. doi: 10.1016/j.fsi.2017.07.027

Wu, S. G., Tian, J. Y., Gatesoupe, F. J., Li, W. X., Zou, H., Yang, B. J., et al. (2013). Intestinal microbiota of gibel carp (*Carassius auratus gibelio*) and its origin as revealed by 454 pyrosequencing. *World J. Microbiol. Biotechnol.* 29, 1585–1595. doi: 10.1007/s11274-013-1322-4

Yang, C., Hao, R., Deng, Y., Liao, Y., Wang, Q., Sun, R., et al. (2017a). Effects of protein sources on growth, immunity and antioxidant capacity of juvenile pearl oyster *Pinctada fucata martensii*. *Fish Shellfish Immunol.* 67, 411–418. doi: 10.1016/j.fsi.2017.06.037

Yang, C., Luo, S., Wang, Q., Deng, Y., and Du, X. (2015). Evaluation of the applicability of a microencapsulated diet developed for the pearl oyster, *Pinctada martensii*. *J. Fish. Sci. China* 22, 442–449.

Yang, C., Wang, Q., Hao, R., Liao, Y., Du, X., and Deng, Y. (2017b). Effects of replacing microalgae with an artificial diet on pearl production traits and mineralization-related gene expression in pearl oyster *Pinctada fucata martensii*. *Aquac. Res.* 48, 5331–5337.

Zhao, B., Zhang, S., and Qian, P. Y. (2003). Larval settlement of the silver- or goldlip pearl oyster *Pinctada maxima* (Jameson) in response to natural biofilms and chemicalcues. *Aquaculture* 220, 883–901. doi: 10.1016/s0044-8486(02)00567-7

Zheng, J., Hao, J., and Wang, B. (2011). Bioremediation of aquiculture wastewater by microalgae *Isochrysis zhanjiangensis* and production of the biomass material. *Key Eng. Mater.* 460–461, 491–495. doi: 10.4028/www.scientific.net/kem.460-461.491

Zheng, X., Fu, Z., Lin, S., Yang, R., Wang, A., Gu, Z., et al. (2020). Which is the major trigger in aquatic environment for pearl oyster *Pinctada fucata martensii* sperm from gonad: ammonia ion or pH ? *Aquaculture* 520:734673. doi: 10.1016/j.aquaculture.2019.734673

Zheng, X., Yang, R., Hu, J., Lin, S. Q., Gu, Z. F., and Ma, Z. H. (2019). The gut microbiota community and antioxidant enzymes activity of barramundi reared at seawater and freshwater. *Fish Shellfish Immunol.* 89, 127–131. doi: 10.1016/j.fsi.2019.03.054

Zhou, M., Liang, R., Mo, J., Yang, S., Gu, N., Wu, Z., et al. (2018). Effects of brewer's yeast hydrolysate on the growth performance and the intestinal bacterial diversity of largemouth bass (*Micropterus salmoides*). *Aquaculture* 484, 139–144. doi: 10.1016/j.aquaculture.2017.11.006

Zhou, Y., Yang, H. S., Zhang, T., Liu, S. L., Zhang, S. M., Liu, Q., et al. (2006). Influence of filtering and biodeposition by the cultured scallop *Chlamys farreri* on benthic-pelagic coupling in a eutrophic bay in China. *Mar. Ecol. Prog. Ser.* 317, 127–141. doi: 10.3354/meps317127

Zwolinska-Wcislo, M. K. G. P., Sliwowski, Z., Urbanczyk, K., Drozdowicz, D., Konturek, S. J., Pawlik, W. W., et al. (2011). Antibiotic treatment with ampicillin accelerates the healing of colonic damage impaired by aspirin and coxib in the experimental colitis. Importance of intestinal bacteria, colonic microcirculation and proinflammatory cytokines. *J. Physiol. Pharmacol.* 62, 357–368.

Conflict of Interest: The authors declare that the research was conducted in the absence of any commercial or financial relationships that could be construed as a potential conflict of interest.

Publisher's Note: All claims expressed in this article are solely those of the authors and do not necessarily represent those of their affiliated organizations, or those of the publisher, the editors and the reviewers. Any product that may be evaluated in this article, or claim that may be made by its manufacturer, is not guaranteed or endorsed by the publisher.

frontiers in Marine Science

ORIGINAL RESEARCH
published: 10 February 2022
doi: 10.3389/fmars.2022.832494

Transcriptomic Analysis of Gill and Hepatopancreas in Razor Clam (*Sinonovacula constricta*) Exposed to Acute Ammonia

Liyuan Lv[1], Jianfeng Ren[2], Huan Zhang[3], Changsen Sun[1], Yinghui Dong[3] and Zhihua Lin[1,3]**

[1] Ninghai Institute of Mariculture Breeding and Seed Industry, Zhejiang Wanli University, Ninghai, China, [2] Key Laboratory of Exploration and Utilization of Aquatic Genetic Resources, Ministry of Education, Shanghai Ocean University, Shanghai, China, [3] Key Laboratory of Aquatic Germplasm Resource of Zhejiang, College of Biological and Environmental Sciences, Zhejiang Wanli University, Ningbo, China

OPEN ACCESS

Edited by:
Liqiang Zhao,
Guangdong Ocean University, China

Reviewed by:
Jun Li,
Key Laboratory of Marginal Sea Geology, South China Sea Institute of Oceanology, Chinese Academy of Sciences (CAS), China
Xing Zheng,
Hainan University, China

***Correspondence:**
Jianfeng Ren
jfren@shou.edu.cn
Zhihua Lin
zhihua9988@126.com

Specialty section:
This article was submitted to Marine Fisheries, Aquaculture and Living Resources, a section of the journal Frontiers in Marine Science

Received: *09 December 2021*
Accepted: *07 January 2022*
Published: *10 February 2022*

Citation:
Lv L, Ren J, Zhang H, Sun C, Dong Y and Lin Z (2022) Transcriptomic Analysis of Gill and Hepatopancreas in Razor Clam (Sinonovacula constricta) Exposed to Acute Ammonia. Front. Mar. Sci. 9:832494. doi: 10.3389/fmars.2022.832494

Accumulation of excessive ammonia is a big threat to aquatic animals, which causes adverse effects on the health, production reduction, and even high mortality. The razor clam *Sinonovacula constricta*, a bivalve living in intertidal mudflat with a deep-burrowing lifestyle, often faces a high concentration of ambient ammonia. However, there is less available information concerning the toxic effects of ammonia on razor clam and its molecular mechanisms of adaptation to ammonia stress. The aim of this study was to investigate the effects of ammonia exposure on the gill and hepatopancreas of razor clam by transcriptome sequencing. The results showed that the median lethal concentration of ammonia was 244.55 mg/L for 96 h. A total of 1,415 and 306 differentially expressed genes (DEGs) were identified in the gill and hepatopancreas, respectively. The functional annotation showed that DEGs of the gill were mainly involved in the regulation of nitrogen compound metabolic process, nitrogen compound transport, and amide transport. The DEGs of the hepatopancreas were mostly enriched in oxidation-reduction process, response to stress, and amine metabolic process. The expression levels of NH_3/NH_4^+ transporting channels and H^+ excreting-related genes, including *Rhesus glycoproteins* (*Rh*), *Na^+/K^+-ATPase (NKA)*, *Na^+/H^+ exchanger*, *V-ATPase* (*VHA*), and *carbonic anhydrase* (*CA*), were upregulated significantly in the gill ($p < 0.05$). In addition, the expression levels of glutamine and urea synthesis-related genes that played vital roles in ammonia detoxification, such as *glutamine synthetase* (*GS*), *arginase* (*ARG*), and *argininosuccinate synthetase* (*ASS*), were also increased obviously in the hepatopancreas ($p < 0.05$). Taken together, our results indicate that the synergistic action of ammonia excretion in the gill and ammonia metabolism in the hepatopancreas might be the mechanism through which the clams tolerate to environmental ammonia. This study provides a molecular basis for the better evaluation of the responding mechanism of ammonia tolerance.

Keywords: ammonia tolerance, transcriptomic analysis, NH_3/NH_4^+ transporter, ammonia excretion and metabolism, gene expression, *Sinonovacula constricta*

INTRODUCTION

With the development of intensive aquaculture and high feed inputs, ammonia has become a particularly harmful stress factor to aquatic animals. Generally, there are mainly two chemical forms of ammonia in water, namely, ionized (NH_4^+) and unionized (NH_3) form. The latter is more toxic as the NH_3 diffuse more easily across the cell membrane for its lipid solubility and non-polarity (Cong et al., 2018). Meantime, other environmental factors also affect the ratio of two forms of ammonia. Higher pH and temperature (Miron et al., 2008; Kir et al., 2015) can lead to higher ratio of NH_3, as well as lower salinity (Kir et al., 2019). Previous studies have shown that excessive ammonia causes physiological dysfunctions, such as decreased growth rate (Harris et al., 1998; Hu et al., 2018), changed histological structure in gill (Cong et al., 2017), disturbed energy and amino acid metabolism (Miranda-Filho et al., 2009), and suppressed immunity response (Cui et al., 2017). It also resulted in massive mortality (Chen et al., 2019). Therefore, clarifying the strategies of ammonia detoxification would provide reliable data for practical guidance of reducing ammonia toxicological effects and protecting aquaculture environment.

The detoxification mechanisms have been explored more thoroughly in fishes and crustaceans than in molluscs. Researchers pointed out that ammonotelism was one of the primary strategies for detoxification in most teleosts, including Nile tilapia (*Oreochromis niloticus*) (Zhu et al., 2019), large-scale loach (*Paramisgurnus dabryanus*) (Shang et al., 2021), and mudskipper (*Boleophthalmus pectinirostris*) (Chew and Ip, 2014). You et al. (2018) found that NH_4^+/NH_3 transporting channels and H^+ excreting-related genes were involved in ammonia excretion in the gill of mudskippers. Meanwhile, non/less-toxic glutamine synthesis by glutamine synthetase (GS) has been noted as another traditional strategy to cope with high level of ammonia in teleosts (Ip et al., 2004). In addition, an unnegligible pathway of detoxifying ammonia into urea, which had been commonly found in the liver of ureogenic animals, maintained low concentration of ammonia. It occurs principally through ornithine-urea cycle involving catalysis of crucial enzymes, including arginase (ARG), argininosuccinate synthetase (ASS), and GS (Mommsen and Walsh, 1989; You et al., 2018; Sun et al., 2021). Although the study on molecular mechanism underlying regulation expose to ammonia in molluscs is still at its infancy, preliminary studies have been reported. The ammonia detoxification metabolism in triangle sail mussel (*Hyriopsis cumingii*) may transfer ammonia into glutamine, alanine, and aspartate (Zhao et al., 2021). In razor clam *Sinonovacula constricta*, the potential protective strategies of glutamine formation, which are mediated by glutamine dehydrogenase (GDH) and GS, convert ammonia into non/less-toxic nitrogenous compounds under ammonia stress (Zhang H. et al., 2020). Taken together, more attention should be paid to the comprehensive study on molecular response mechanism of ammonia stress in mollusks, especially in terms of ammonia excretion.

RNA sequencing is a well-established comprehensive subject to explore molecular mechanisms in responding to abiotic stresses, especially effective for blank areas of studies (Gao et al., 2018; Stark et al., 2019). Recently, more and more studies have investigated the complex interplay among cellular pathways when exposed to ammonia (Yu et al., 2019; Xue et al., 2021). However, only limited works have been reported in bivalves. In Manila clam *Ruditapes philippinarum*, short- and long-tern exposure to ammonia displayed the different responding patterns in the gill *via* digital gene expression analysis. It induced pathways of notch signaling and protein processing in endoplasmic reticulum in short-term exposure and pathways of gap junction, immunity, and key substance metabolism in long-term exposure (Cong et al., 2018). Digestive gland transcriptome analysis of response mechanism to ammonia in Asian clam *Corbicula fluminea* revealed that the immunity and apoptotic signaling pathways play important roles during stress (Zhang et al., 2019). Although abovementioned studies revealed a mass of important genes responding to ammonia stress in a few species, the potential molecular mechanisms were not fully elucidated for most economic molluscs.

The razor clam *S. constricta* is one of the most economically important marine bivalves, which is widely distributed in the intertidal zones and estuarine areas of China, Japan, Korea, and Vietnam along the western Pacific Ocean with a deep-burrowing lifestyle (Dong et al., 2020). According to the statistical data from U.S. Environmental Protection Agency (USEPA), shellfish are more sensitive to ammonia nitrogen. Of the top 10 sensitive genera, eight genera belong to molluscs (USEPA, 2013). However, the clam-fish/shrimps polyculture makes razor clam to face to high concentration of ambient ammonia (Sun et al., 2021). Therefore, *S. constricta* is a suitable model species to explore the molecular mechanism of higher tolerance to ammonia in molluscs. To date, the molecular mechanism of ammonia toxicity has not been understood comprehensively in razor clam. In this study, the influence of high concentration ammonia stress was systematically evaluated by profiling the gill and hepatopancreas transcriptomes of *S. constricta*, which were subjected to acute challenge of 180 mg/L ammonia for 72 h. This study provides insights into the molecular regulatory mechanism of ammonia tolerance in bivalve.

MATERIALS AND METHODS

Clam Culture

The healthy razor clams (wet weight 9.43 ± 1.60 g, shell length 63.42 ± 1.57 mm) were collected from aquafarm in Xiangshan (Ningbo, China). Before the experiment, the clams were acclimated for 1 week in 1,000 L tanks containing filtered seawater (salinity 22) with aeration at the temperature (14–16°C). During the acclimatization and ammonia exposure periods, the clams were fed twice per day at 8:00 and 18:00 on a diet of microalgae *Chlorella vulgaris* and *Chaeroeeros moelleri*. All the seawater was renewed two times daily. The whole experiment was maintained under a photoperiod of 12 h light and 12 h dark.

Toxicity and Exposure Experiments of Ammonia

The total ammonia nitrogen (TAN) concentrations were designed by equal space between logarithm with the gradients of 0, 120, 164, 225, 309, 423, and 579 mg/L. The stock solution of 1,000 mg/L TAN (stock solution was disposed of ammonium chloride NH_4Cl; CNW, Shanghai, China, ACS reagent grade >99%) was used for producing the desired final concentrations of TAN. A total of 420 clams were randomly divided into seven groups with three replicates in each different ammonia concentration and cultured in plastic tanks with 30 L of filtered seawater (20 individuals in each replicate). Water quality parameters were tested daily throughout the experiment. The pH and dissolved oxygen were measured using HACH HQ30d pH meter (Hach Company, CO, United States). The salinity and temperature were tested by AZ8371 Salinometer (Hengxing, Taiwan, China) and fish tank thermometer, respectively. During 96 h duration of ammonia exposure, observation was performed every 12 h. To calculate the median lethal concentrations (LC_{50}), the mortality rates were measured every 24 h until it reached 100%.

Based on the median lethal concentrations (LC_{50}-96 h) of ammonia established in the toxicity tests, the clams were subjected to a 96 h ammonia exposure at three concentrations of 100, 140, and 180 mg/L comparing with 0 mg/L with three replicate tanks for each treatment (100 clams per tank). Daily acclimation was performed referred from Zhang H. et al. (2020). Six individuals were randomly sampled from each treatment at 0, 1, 3, 6, 9, 12, 24, 48, 72, and 96 h time points, respectively. For each sampled clam, hemolymph was immediately collected from adductor using a 2 mL disposable sterilized syringe for pH value and ammonia content analysis. The pH value was measured using HACH HQ30d Portable Dissolved Oxygen Tester Conductivity Meter pH meter (Hach Company). The ammonia content was measured with the commercial kits (no. A086-1-1) of Nanjing Jiancheng Bioengineering Co. (Nanjing, China) according to the instructions of the manufacturer. Meanwhile, the gill and hepatopancreas were dissected separately and frozen in liquid nitrogen immediately for RNA extraction. Finally, the tissues obtained at 72-h exposure to 180 mg/L group were considered for RNA-seq analysis.

RNA Extraction and Transcriptome Sequencing

Total RNA was extracted from the gill and hepatopancreas at each time point using TRIzol reagent (Omega, Norcross, GA, United States) according to the instructions of the manufacturer. Then RNA concentration and integrity was assessed using NanoDrop 2000 (Thermo Scientific, Waltham, MA, United States). The cDNA libraries were constructed by a NEBNext® Ultra™ RNA Library Prep Kit for Illumina® (NEB, Ipswich, MA, United States) and then assessed on the Agilent Bioanalyzer 2100 system. After quality assessment, the sequencing was performed on Illumina Hiseq 2000 platform.

Transcriptome Assembly and Gene Expression Quantification

Clean data were filtered out as reads containing adapter, poly-N, and low-quality reads. The sequence quality was assessed by Q20, Q30, and GC content. Trinity was used for clean reads assembly (Grabherr et al., 2013). Subsequently, the clean reads were aligned to the *S. constricta* reference genome (Dong et al., 2020) using Tophat (Trapnell et al., 2009).

The gene expression levels were estimated using RSEM (Dewey and Li, 2011). Then, gene expression was normalized using the reads per kilobase per million mapped reads (RPKM). Genes with low read counts (<10 reads) were filtered out before gene expression analysis by using featureCounts software (Liao et al., 2014). Differential expression analysis between ammonia-N group (TG) and control group (CG) was performed using the DESeq2. Differentially expressed genes (DEGs) were defined with a fold change >2 and a cutoff false discovery rate (FDR) of 0.05.

Functional Annotation and Enrichment of Differentially Expressed Genes

Gene function was annotated based on the following databases including NR (NCBI non-redundant protein sequences)[1], Pfam (Protein family),[2] KOG/COG (Clusters of Orthologous Groups of proteins),[3] Swiss-Prot[4], KEGG (Kyoto Encyclopedia of Genes and Genomes),[5] and GO (Gene Ontology).[6]

To identify GO terms and KEGG pathways among the DEGs under ammonia stress, enrichment analyses were implemented by the software GOseq (Young et al., 2010) and KOBAS (Chen et al., 2011), respectively, with a cutoff *q*-value of 0.05. The significantly enriched DEGs were subject to further scrutiny to identify genes potentially involved in ammonia stress response.

Validation of RNA-Seq Data by Quantitative Real-Time PCR

To confirm the gene expression profiles from RNA-seq analysis, six DEGs were selected to perform quantitative real-time PCR (qRT-PCR) for tissues of gill and hepatopancreas, respectively. Specific primers for candidate genes and the housekeeping gene (*Rs9*) were designed based on the unigene sequences using Primer Premier 5.0 software (**Table 1**).

Total RNA was extracted from the gill and hepatopancreas tissues using the Omega RNA-Solv Reagent and was visualized with agarose gel electrophoresis. The qRT-PCR was performed using the SYBR® PremixEXTaq™II (Takara, Dalian, China) kit

[1]http://www.ncbi.nlm.nih.gov/
[2]http://pfam.xfam.org/
[3]http://www.ncbi.nlm.nih.gov/COG/
[4]http://www.ebi.ac.uk/uniprot/
[5]http://www.genome.jp/kegg/
[6]http://www.geneontology.org/

TABLE 1 | Primers used for qRT-PCR validation of differentially expressed genes.

Genes	Forward primer (5′–3′)	Reverse primer (5′–3′)
Sc-Rh	GGGCTGTTGACATCGGTGAA	CAGTTGAGAGAAAGCGAAGGC
Sc-NKA	CAGGTTGAATACCGACCCTAATG	GGCACCAATCCAAAGCAGC
Sc-NHE	TCCCCTCTCAACTCTCACACT	GAGCAATCACTGGTTCATCG
Sc-V-ATP	GCAAGAGTGTGATGGACGA	GCCAAGTTCAGGAAGAGAC
Sc-ASS	GCGAAGGTGAACGGCATT	GGTGTTAGGGTCCTCCAAAATAC
Sc-ARG	AAAACTCCCTGTGATGGC	GGGGAAGGTCCACAAATA
Sc-Rs9	TGAAGTCTGGCGTGTCAAGT	CGTCTCAAAAGGGCATTACC

on the Roche LightCycler® 480 System (Roche Diagnostics, Basel, Switzerland). The PCR reaction was carried out in a total volume of 20 μl, containing 10.0 μl of 2 × SYBR Green Master Mix (Applied Biosystems), 2.0 μl 500 ng of first-strand cDNA, 1.0 μl of each primer (10 μmol/L), and 6.0 μl of PCR-grade DEPC water. Then, the amplification parameters were set as follows: initial denaturation at 95°C for 10 min, followed by 40 cycles of 95°C for 10 s, 60°C for 60 s, and 40°C for 5 s in 96-well optical reaction plates (Roche, Basel, Switzerland). All reactions were performed in quadruplicate. The gene expression levels were quantitatively analyzed and converted to fold differences by the comparative CT method ($2^{-\Delta\Delta CT}$ method).

Statistical Analyses

The median lethal concentrations (LC_{50}-96 h) of ammonia were calculated by the probit method (Denham, 2016). The relationship between concentration of ammonia and mortality was subjected to linear regression analysis. All data were expressed as means ± SD. The gene expression levels were subjected to one-way ANOVA followed by least significant difference (LSD) analysis. Statistical significance was defined at $p \leq 0.05$. All statistical analyses were performed using the SPSS version 13.0.

RESULTS

Median Lethal Concentration (LC_{50}) of Total Ammonia–Nitrogen and NH_3–N

To calculate LC_{50} of TAN, we recorded the mortality per 24 h for a total of 96 h ammonia exposure till all clams died. As expected, the mortality rate was increased with the increased concentration of TAN and exposure time (**Table 2**). No death occurred in the CGs as well as the groups treated with 120 mg/L of TAN for 24 h. All clams died after 96 h of exposure in 579 mg/L of TAN. According to the statistical method, the corresponding LC_{50} of unionized ammonia (NH_3–N) was calculated (**Table 3**). The LC_{50} value of TAN determined at 96 h was 244.55 mg/L and the corresponding LC_{50} value of NH_3–N was 9.69 mg/L.

TABLE 2 | Mortality of *S. constricta* exposed to total ammonia nitrogen during 96 h exposures.

Total ammonia nitrogen (mg/L)	No. of clams	Mortality rate (%)			
		24 h	48 h	72 h	96 h
Control	60	0	0	0	0
120	60	0	5	5	15
164	60	5	10	15	25
225	60	5	15	30	45
309	60	5	20	50	75
423	60	10	30	80	90
579	60	20	45	95	100

Effects of Ammonia Content and pH in Hemolymph

The ammonia content in the hemolymph of *S. constricta* increased dramatically under ammonia exposure. After 1 h of exposure, the ammonia content increased sharply and then the level reached a plateau occurred after 24 h exposure in all treatment groups. Finally, the highest value was up to 3,331.2 μmol/L at 96 h in 100 mg/L group. It is worthy to note that ammonia contents showed an opposite decrease trend with increased ammonia concentration during 12–96 h (**Figure 1A**). Moreover, the pH of hemolymph showed significant decreases in all treatment groups (**Figure 1B**).

Characterization of Transcriptome Data

The details on the transcriptome data for each sample are summarized in **Supplementary Table 1** and the raw sequence data were deposited at the NCBI Sequence Read Archive (SRA) with the accession numbers of SRR9943679–SRR9943690. After data filtering, approximately 28.44 and 28.51 million high-quality clean reads were obtained from the gill and hepatopancreas, respectively. In total of 12 libraries, the Q20 and Q30 were >97.07% and >92.83%. And the GC content ranged from 40.10 to 43.13%. Among the samples from the gill, 66.99–71.71% of the clean reads could be mapped onto the reference genome, and the mapping rates to the reference genome for hepatopancreas reads were 67.10–69.90%.

Analysis of Differentially Expressed Genes in Gill and Hepatopancreas

With the criteria of a FDR ≤ 0.05, and |fold change of expression level > 2, we identified 1,415 DEGs in the gill after 72 h ammonia exposure, which included 1,029 upregulated and 386 downregulated genes. Meanwhile, there were 306 DEGs in the hepatopancreas, which included 248 upregulated and 58 downregulated genes (**Figure 2A**). In

TABLE 3 | Median lethal concentration (LC_{50}) of total ammonia-N (TAN) and unionized ammonia-N (NH_3–N) exposed to *S. constricta*.

Exposure time (h)	TAN (95% CI) (mg/L)		NH_3–N (95% CI) (mg/L)	
24	876.50	(642.97–2248.29)	34.71	(21.42–74.91)
48	589.73	(399.21–850.06)	23.36	(13.30–28.32)
72	314.29	(235.29–374.69)	12.45	(7.84–12.48)
96	244.55	(162.89–300.74)	9.69	(5.43–10.02)

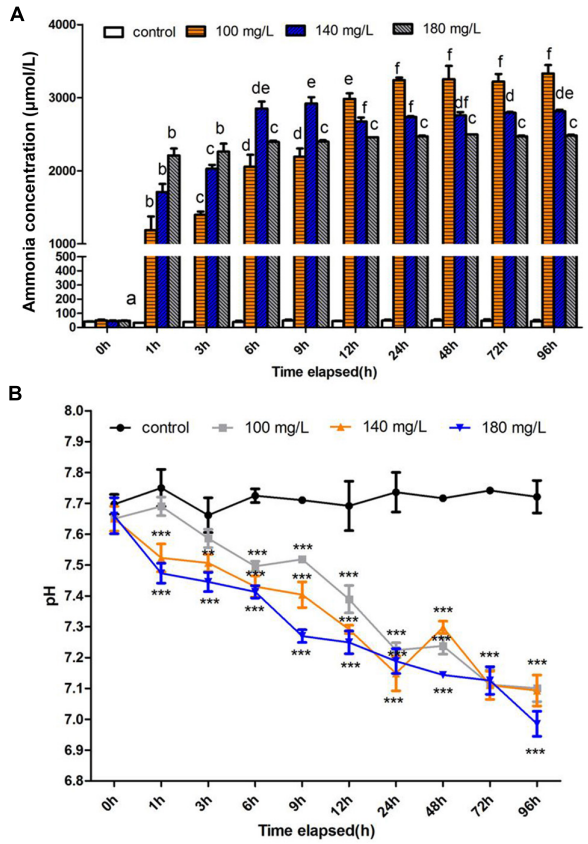

FIGURE 1 | Effects of ammonia concentration and pH in *Sinonovacula constricta* hemolymph under ammonia stress. **(A)** Ammonia concentration is mean ± SD ($n = 3$). Data with different letters are significantly different in the same concentration group ($p < 0.05$). **(B)** pH value is mean ± SD ($n = 3$). Asterisk (*) indicates a significant difference between the exposed group and its respective control (*$p < 0.05$; **$p < 0.01$; ***$p < 0.001$).

addition, overlapping analysis of data sets from both two tissues revealed 85 common DEGs in response to ammonia-N stress, of which 79 genes were upregulated and four genes were downregulated in both the gill and the hepatopancreas. The remaining two genes were downregulated in the gill but were upregulated in the hepatopancreas (**Figure 2B** and **Supplementary Table 2**).

Gene Ontology and Kyoto Encyclopedia of Genes and Genomes Pathway Enrichment of Differentially Expressed Genes

Gene ontology analysis was conducted to profile the functional annotation of DEGs in the gill and hepatopancreas. The DEGs were assigned into three GO terms including biological process (BP), molecular function (MF), and cellular component (CC), and the significantly enriched items were illustrated (**Figure 2C** and **Supplementary Figures 1, 2**). In the gill, DEGs primarily enriched in BP, including regulation of cellular metabolic process (GO:0031323), regulation of biosynthetic process (GO:0009889), regulation of nitrogen compound metabolic process (GO:0051171), organic substance transport (GO:0071702), nitrogen compound transport (GO:0071705), organic anion transport (GO:0015711), and amide transport (GO:0042886) (**Figure 2C**). In the hepatopancreas, DEGs were mainly enriched in oxidation-reduction process (GO:0055114), response to oxidative stress (GO:0006979), response to stress (GO:0006950), amine metabolic process (GO:0009308), copper ion binding (GO:0005507), enzyme inhibitor activity (GO:0004857), and antioxidant activity (GO:0016209) (**Figure 2D**).

The results of KEGG enrichment analyses are summarized in **Table 4**. Specifically, the upregulated DEGs in the gill were related to protein processing in endoplasmic reticulum and endocytosis (spu04141), autophagy/mitophagy (spu04140 and spu04137), and aminoacyl-tRNA biosynthesis (spu00970). The downregulated DEGs in the gill were related to nucleotide/base excision repair (spu03420 and spu03410) and lysine degradation (spu00310). At the same time, DEGs in the hepatopancreas were assigned to Wnt signaling pathway (spu04310) and amino acid metabolism, including arginine, proline, tyrosine, and phenylalanine biosynthesis and metabolism (i.e., spu00220, spu00330, spu00350, and spu00360). Despite no KEGG pathways were significantly enriched, the DEGs were also analyzed according to their KEGG pathways to describe the toxic effect and response mechanism of ammonia in *S. constricta*, which are summarized in **Table 5**. Ammonia exposure obviously induced significant expressed changes of genes that were related to nitrogen compounds-related metabolism and excretion, pH regulation, immune, and apoptosis in both tissues. In aforementioned pathways, DEGs involved in glutamine-arginine-urea cycle such as *ARG*, *ASS*, and *GS* were mostly upregulated in both the hepatopancreas and the gill, while glutathione *S*-transferase (*GST*) related to antioxidant activity was significantly downregulated. In addition, the RNA-seq data showed that ammonium transporter (*AMT*) responsibility for ammonia excretion was significantly downregulated after 72 h ammonia exposure in gill, which is the primary organ for ammonia excretion. In contrast, carbonic anhydrase (*CA*) related to nitrogen metabolism showed upregulation in the gill. The abundant expression of immune response- and apoptosis-related genes suggested that their corresponding pathways were activated during ammonia stress.

Validation of Differentially Expressed Genes by Quantitative Real-Time PCR

Four genes related to ammonia excretion (i.e., *Rh*, *NKA*, *V-ATP*, and *NHE*) in the gills and two genes related to ammonia metabolism (i.e., *ARG* and *ASS*) in the hepatopancreas were selected to verify the accuracy of RNA-seq data by qRT-PCR. *Rs9* were chosen as reference genes. As shown in **Figure 3**, four genes in the gill (i.e., *Rh*, *NKA*, *V-ATP*, and *NHE*), as well as *ARG* in the hepatopancreas, all presented the same trend with earlier increase and later decrease when exposed to 180 mg/L ammonia. Unlike the abovementioned genes, the expression of *ASS* was increased along whole time points and reached the

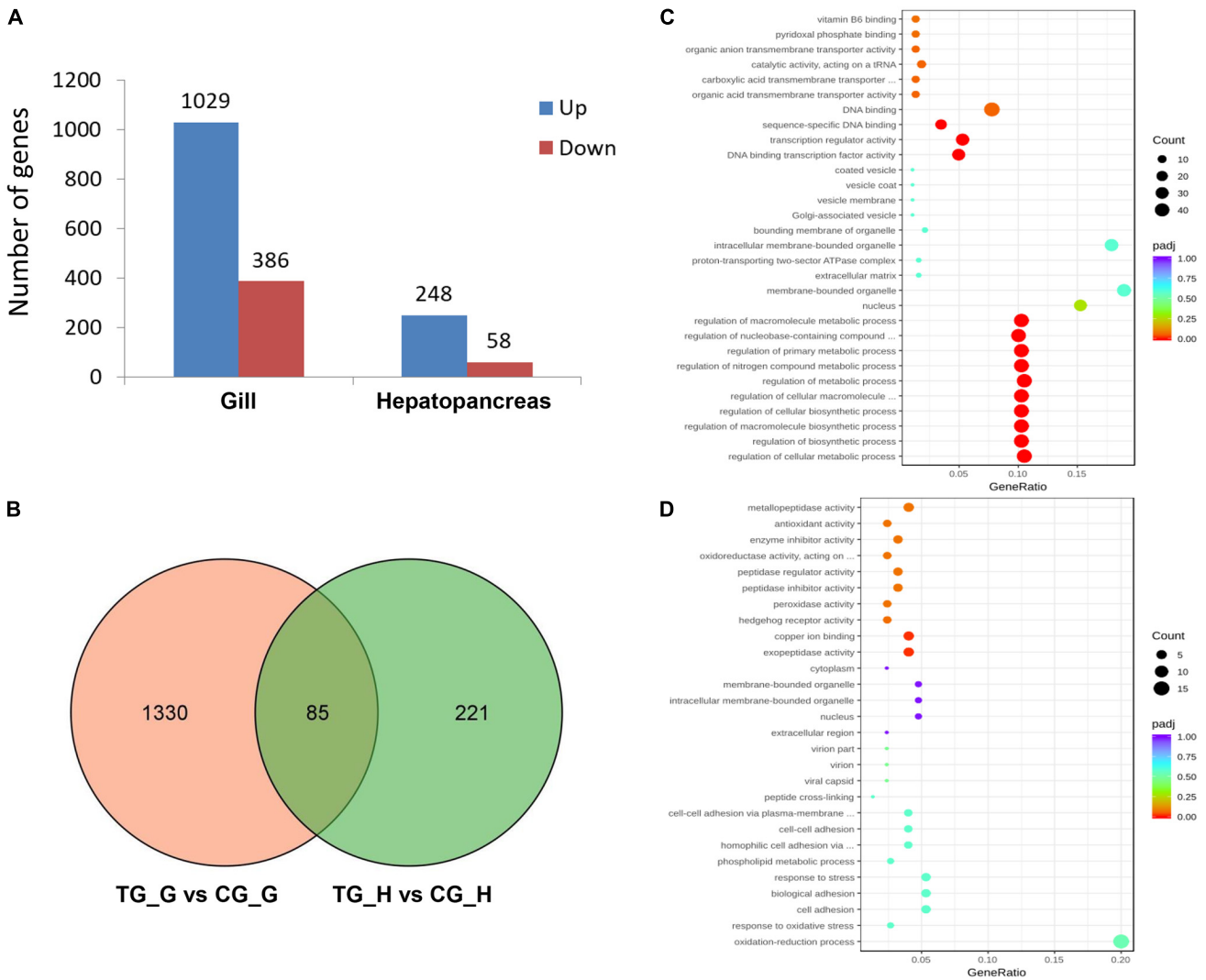

FIGURE 2 | A summary of differentially expressed genes (DEGs) of the gill and hepatopancreas in *S. constricta* exposure to acute ammonia. **(A)** The numbers of DEGs in the gill and hepatopancreas. **(B)** Venn diagram of DEGs shared between gill and hepatopancreas. G represents gill and H represents hepatopancreas. **(C)** Enriched gene ontology (GOs) in the gill. **(D)** Enriched GOs in the hepatopancreas.

TABLE 4 | Kyoto Encyclopedia of Genes and Genomes (KEGG) enrichment of differentially expressed genes (DEGs) in the gill and hepatopancreas of *S. constricta* under ammonia exposure.

Tissue	KEGG pathway enrichment	Gene number (up)	Gene number (down)	KEGG pathway enrichment
Gill	RNA transport	14	5	DNA replication
	Protein processing in endoplasmic reticulum	13	4	Base excision repair
	Endocytosis	13	3	Lysine degradation
	Autophagy - animal	10	3	Other glycan degradation
	Mitophagy - animal	7	5	Nucleotide excision repair
	Aminoacyl-tRNA biosynthesis	6	2	Starch and sucrose metabolism
	SNARE interactions in vesicular transport	3	2	Mismatch repair
Hepatopancreas	AGE-RAGE signaling pathway in diabetic complications	3	1	Phenylalanine metabolism
	Wnt signaling pathway	2	1	Tyrosine metabolism
	Arginine biosynthesis	1	1	Arginine and proline metabolism

maximum at 96 h. It should be noted that the expression of *Rh* in the treatment group was significantly decreased at 96 h when compared with CG.

DISCUSSION

Tolerate Capacity to Ammonia Adapt to the Deep-Burrowing Habit

Ammonia is one of major contaminants in aquaculture environment. Its excessive accumulation would limit animal health and production in aquaculture (Shang et al., 2021; Shen et al., 2021). Therefore, it is necessary to know the tolerance and lethal concentrations of ammonia nitrogen for aquatic animals and controlling the ammonia nitrogen to safe concentration in water environment.

In fact, the USEPA has accomplished the comparison of available toxicity data for 69 genera and concluded that shellfish may be more sensitive to ammonia than other aquatic animals (USEPA, 2013; Zhang et al., 2019). However, only freshwater molluscs, but no saltwater ones, were collected in their report. Recently, many tests about the sublethal effects of ammonia

TABLE 5 | List of DEGs of the gill and hepatopancreas involved in responding to ammonia stress in *S. constricta*.

Gene ID	Gill log_2FoldChange	Hepatopancreas log_2FoldChange	Symbol	Gene description	Function
evm.TU.ctg235.6	1.92	3.67	*ARG*	Arginase-1	Arginine metabolism
evm.TU.ctg413.46	1.67	−0.50	*ASS*	Argininosuccinate synthetase	Urea cycle
evm.TU.ctg154.24	−2.44	−4.00	*GST*	Glutathione *S*-transferase	Antioxidant activity
evm.TU.ctg103.20	−1.04	−1.17	*CAT*	Catalase	Antioxidant activity
evm.TU.ctg295.3	–	4.75	*GS*	Glutamine synthetase 1, mitochondrial	Glutamine metabolism
evm.TU.ctg646.10	4.07	−0.45	*GS*	Glutamine synthetase	Glutamine metabolism
evm.TU.ctg528.25	1.91	−0.45	*VHA*	V-type H^+-transporting ATPase subunit a	Oxidative phosphorylation
evm.TU.ctg6.79	2.83	–	*Rh*	Ammonium transporter 3	Ammonia excretion
evm.TU.ctg365.7	−4.28	−2.57	*Rh*	Ammonium transporter	Ammonia excretion
evm.TU.ctg271.27	−1.55	−0.50	*Rh*	Ammonium transporter Rh type B	Ammonia excretion
evm.TU.ctg271.28	−1.58	−0.63	*Rh*	Ammonium transporter Rh type C	Ammonia excretion
evm.TU.ctg8590.1	−1.86	1.56	*Rh*	Ammonium transporter Rh type B	Ammonia excretion
evm.TU.ctg8590.2	−2.83	−0.32	*Rh*	Ammonium transporter Rh type B	Ammonia excretion
evm.TU.ctg1123.4.1	2.00	−0.69	*NHE*	Sodium/hydrogen exchanger 2	pH regulation
evm.TU.ctg359.3	−1.36	0.21	*NHE*	Sodium/hydrogen exchanger 9	pH regulation
evm.TU.ctg524.7	−1.21	0.79	*NHE*	Sodium/hydrogen exchanger 3-like	pH regulation
evm.TU.ctg670.8	−0.18	−2.09	*NHE*	Sodium/hydrogen exchanger 3	pH regulation
evm.TU.ctg1.112	2.39	−0.71	*CA*	Carbonic anhydrase 2	Nitrogen metabolism
evm.TU.ctg187.10	2.72	0.35	*CA*	Carbonic anhydrase 2	Nitrogen metabolism
evm.TU.ctg208.45	0.33	−1.64	*CA*	Carbonic anhydrase 1	Nitrogen metabolism
evm.TU.ctg109.5	−0.26	−1.76	*CA*	Carbonic anhydrase 1	Nitrogen metabolism
evm.TU.ctg155.36	1.12	–	*CA*	Carbonic anhydrase 13	Nitrogen metabolism
evm.TU.ctg162.3	2.24	–	*CA*	Carbonic anhydrase 14	Nitrogen metabolism
evm.TU.ctg943.3	1.75	4.10	*CA*	Carbonic anhydrase 12	Nitrogen metabolism
evm.TU.ctg943.6	1.72	4.12	*CA*	Carbonic anhydrase	Nitrogen metabolism
evm.TU.ctg391.1	1.71	–	*CA*	Carbonic anhydrase-related protein 10	Nitrogen metabolism
evm.TU.ctg602.15	2.47	–	*CA*	Carbonic anhydrase-related protein 10	Nitrogen metabolism
evm.TU.ctg593.2	4.81	–	*CA*	Carbonic anhydrase-related protein 10	Nitrogen metabolism
evm.TU.ctg41.49	−0.74	−6.82	*OGG1*	*N*-Glycosylase/DNA lyase	Base excision repair
evm.TU.ctg449.31	1.61	2.64	*DIS3L*	DIS3-like exonuclease 1	RNA degradation
evm.TU.ctg11.67	−0.24	−4.15	*LIG1*	DNA ligase 1-like	DNA replication
evm.TU.ctg631.9	6.00	7.03	*HSP70*	Heat shock protein 70 B2 protein	Protein processing in endoplasmic reticulum
evm.TU.ctg184.25	2.01	0.26	*HSP90*	Heat shock protein 90	Protein processing in endoplasmic reticulum
evm.TU.ctg642.1	2.58	2.15	*TNFR16*	Tumor necrosis factor receptor superfamily member 16-like	Apoptosis
evm.TU.ctg406.9	1.56	1.18	*Bcl-xl*	Apoptosis regulator Bcl-X	Apoptosis
evm.TU.ctg30.30	2.51	−0.85	*CTSB*	Cathepsin B	Apoptosis
evm.TU.ctg131.15	2.31	1.67	*AP-1*	AP-1	Autophagy
evm.TU.ctg885.9	3.10	−0.65	*CTSL*	Cathepsin L	Immunity
evm.TU.ctg255.18	1.87	1.96	*TLR*	Toll-like receptor 2	Immunity

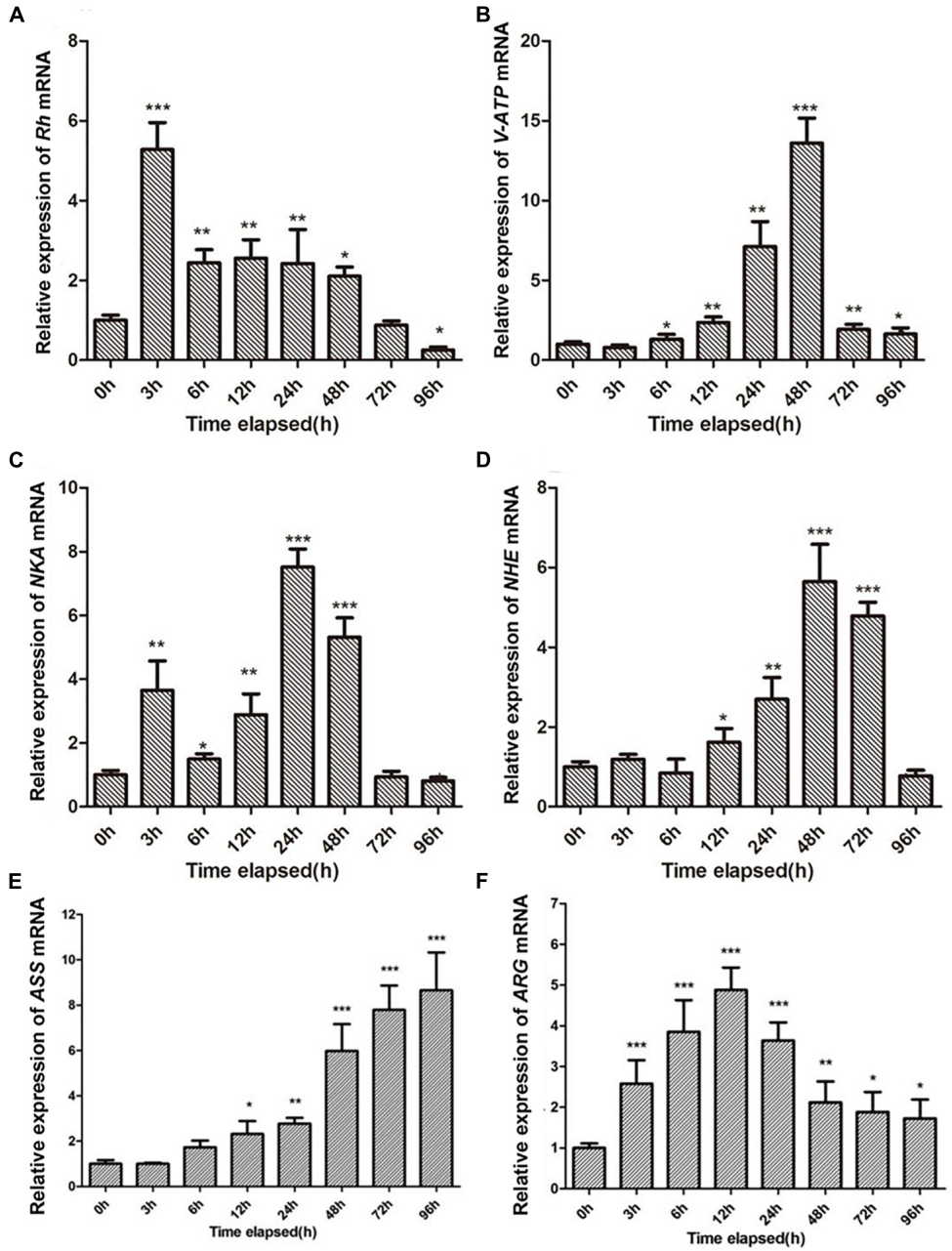

FIGURE 3 | Validation of RNA-seq profiles by qRT-PCR. **(A–D)** Represent the expression patterns of *Rh*, *NKA*, *V-ATP*, and *NHE* genes in the gill of *S. constricta* after exposure to 180 mg/L ammonia for 96 h, respectively. **(E,F)** Panels represent the expression patterns of the *ARG* and *ASS* genes in the hepatopancreas after exposure to 180 mg/L ammonia for 96 h, respectively. Vertical bars represent the mean ± SD ($n = 4$). Asterisk (*) indicates a significant difference between the exposed shellfish and its respective control (*$p < 0.05$; **$p < 0.01$; ***$p < 0.001$).

have been performed on saltwater animals, including the shellfish. The available data are presented in **Table 6**. The ammonia tolerance displayed a distinct difference among species. Particularly, excellent ammonia tolerance had been found in marine bivalves such as clam *Estellarca olivacea* (Zhang et al., 2009), blood clam *Tegillarca granosa* (Lv et al., 2012), *R. philippinarum* (Wang et al., 2007), and *S. constricta* (this study, 96-h LC_{50}: 244.55 mg/L). Notably, these four species are all benthic bivalves. Weihrauch et al. (2004) had confirmed that benthic animals (crabs and bivalves) faced to higher ambient ammonia compared with those living free in the water. The razor clam is one of typical deep-burrowing bivalves living in intertidal zones, where the ammonia concentration is high in water (Newton and Bartsch, 2010). Therefore, we speculated that the deep-burrowing habitat possibly promoted the acquisition of greater capacity to tolerate higher ambient ammonia in razor

TABLE 6 | Range of the median lethal concentration LC_{50} values of TAN among aquatic animals.

Species	Life stage/size (mm)	Temperature (°)	pH	Duration (h)	LC_{50} (mg/L)	References
Fish						
Oncorhynchus mykiss	94	13.2	7.82	96	32.9	Thurston et al., 1981
Pimephales promelas	52	12.0	7.82	96	67.0	Thurston et al., 1981
Crustaceans						
Macrobrachium amazonicum	92.6 ± 7.0	24.9–27.2	7.6–7.9	96	36.59	Dutra et al., 2016
Freshwater mussels						
Villosa iris	Age 5 days	20 ± 1	7.41	96	11.4	Mummert et al., 2003
Lampsilis fasciola	Age 5 days	20 ± 1	7.96	96	7.74	Mummert et al., 2003
Lampsilis cardium	Juveniles, 104–108	21.3 ± 0.1	7.2 ± 0.1	96	19.4	Newton and Bartsch, 2010
Limnoperna fortunei	Juveniles, 21–26	20.03 ± 2.98	7.7 ± 0.39	96	11.53	Montresor et al., 2013
Marine bivalves						
Crassostrea virginica	Adult, 48–62	20 ± 2	7.70–8.23	96	17.79	Epifanio and Srna, 1975
Estellarca olivacea	Juveniles, 2.72 ± 0.25	25 ± 0.5	8.3 ± 0.2	96	50.0	Zhang et al., 2009
	Adult, 16.08 ± 1.34				556.9	
Tegillarca granosa	Adult, 11.82 ± 0.75	24 ± 0.5	8.1	96	348.40 ± 9.74	Lv et al., 2012
Ruditapes philippinarum	Adult, 40.0 ± 2.8	18 ± 0.5	7.6	24	239.88	Wang et al., 2007
Sinonovacula constricta	Adult, 63.42 ± 1.57	14–16	8.17 ± 0.43	96	244.55	This study

clam. Hence, it is considered to be a suitable model to explore the response mechanism of ammonia toxicity. In this study, the molecular mechanism on response to high ammonia tolerance was investigated through transcriptomic analysis.

Response to Ammonia Toxicity in *Sinonovacula constricta*

Previous studies have shown that ammonia stress caused a variety of adverse effects, such as energy metabolism disturbance, induced oxidative stress and immune defense, increased sensitivity of the animal to pathogens, and even death (Cheng et al., 2015; Shang et al., 2021; Shen et al., 2021). In this study, our results also demonstrated that ammonia exposure induced the change of metabolic process, oxidative stress, immune response, and apoptosis-related signaling pathways in *S. constricta*.

Oxidative stress, one of the toxicity mechanisms of environmental stress on aquatic organisms, is usually coupled with DNA damage (Wang et al., 2016). In this study, the genes encoding antioxidant enzymes, i.e., GST and catalase (CAT), were significantly downregulated, suggesting a weakness in compensatory mechanism due to excessive reactive oxygen species (ROS). The excessive ROS might destruct cell membranes with the formation of lipid peroxides and oxidized proteins (Liang et al., 2016). In contrast, the accumulation of free radicals resulted in the ischemia and hypoxia in cells, which further aggravated the metabolic disorders and tissue damage (Zhang et al., 2016). In addition, the gene encoding *N*-glycosylase/DNA lyase, which was involved in base excision repair (Wyatt, 2009), was also significantly downregulated after ammonia exposure ($\log_2$FoldChange $= -6.82$). The altered expressions of DIS3-like exonuclease and DNA ligase 1 involved in RNA degradation and DNA replication indicated the disorder of genetic information processing (Staals et al., 2010), which might produce "protein-oaf" causing metabolic impairments (Hasenbein et al., 2014). Besides, previous study has been demonstrated that ammonia has severe impacts on the immune system (Lu et al., 2016), and functioned as predisposing factors, which accompanied with low levels of pathogen infections, could lead to high mortalities (Hasenbein et al., 2014). The DEGs related to immune defense, including heat shock protein, toll-like receptor, and cathepsin L, presented significant upregulation exposure to ammonia in *S. constricta*. The similar findings have been reported in some invertebrates, such as abalone *Haliotis discus hannai* (Shen et al., 2015), Pacific white shrimp *Litopenaeus vannamei* (Liu et al., 2020), and freshwater shrimp *Macrobrachium nipponense* (Yu et al., 2019).

Ammonia Excretion in Gill of *Sinonovacula constricta*

Most teleost fishes excrete ammonia across branchial and/or epithelial surfaces to maintain appropriate internal ammonia concentration, which is an effective way to protect against ammonia toxicity under ammonia stress (You et al., 2018). The bulk of ammonia excretion mainly occurred in the gill is thought to depend on the cooperation of various transport proteins, including Rh glycoproteins, Na^+/K^+-ATPase, and so on (Sinha et al., 2015). As is well known, NH_3 diffusion across the gills of ammoniotelic fish is facilitated by Rh glycoproteins (Wood et al., 2013), such as Pacific hagfish *Eptatretus stoutii* (Clifford et al., 2015), *P. dabryanus* (Shang et al., 2021), and gulf toadfish *Opsanus beta* (Rodela et al., 2011). In addition, ammonia has also been excreted as NH_4^+ (Ip et al., 2001). NH_4^+ possesses similar ionic characteristics, hydration shell sizes, and water mobility rates compared with K^+, which allows it to compete against K^+ to be transported through the K^+-associated channels like NKA (Sinha et al., 2015). We found that mRNA expressions of *Rh* glycoproteins and *NKA* were increased significantly in the gill during ammonia stress, suggesting that ammonia excretion *in vivo* was activated together by $NH_3/NH4^+$

transport proteins in *S. constricta*. However, *Rh* was dramatically decreased after 96-h ammonia excretion. It is reported that the expression of *Rh* and *NKA*, together with activities of related enzymes in the gill tissue, decreased significantly with increased ammonia concentration (Yang et al., 2010; Ren et al., 2015). The reason leading to a decrease in the transcription and activity of related enzymes may be the gradual changes occurring in the gill morphology culminated in drastic lesions when long-term exposure to high concentrations of ammonia (Schram et al., 2010). Although the morphological change of gill was not investigated in this study, a large number of DEGs were enriched into the apoptosis-related signaling pathways, suggesting the occurrence of gill injury after ammonia exposure. The microstructure damage of gill tissue has been observed in the gill of *R. philippinarum* after subacute exposure of ammonia, which reinforces our assumption (Cong et al., 2017).

Ammonia excretion is augmented by acidic conditions in the water because any NH_3 excreted into the water is rapidly converted to and trapped as NH_4^+ (Ip et al., 2001). There are two potential mechanisms for this acidification, namely, the hydration of CO_2 (also crossing the membrane as CO_2 gas) to form H^+ and HCO_3^- and the active transport of protons *via* H^+ transport like V-type-H^+-ATPase (VHA) and Na^+/H^+ exchanges (NHE) (Clifford et al., 2015; Tresguerres et al., 2020). CA catalyzes the HCO_3^- and H^+ reaction on the gill surface, which contributes to the secretion of acid and traps the excretion of NH_4^+ actively (Tresguerres et al., 2020). The significant upregulation of *CA* genes was found in both the tissues of TGs (**Table 5**). The expressions of *VHA* and *NHE* were significantly upregulated in the gill. These results confirmed that *S. constricta* could augment ammonia excretion by excreting acid through H^+ pump, also like mudskipper *Periophthalmus magnuspinnatus* (You et al., 2018). In summary, the upregulated mRNA expression of *Rh* together with upregulated *NKA*, *NHE*, and *V-ATP* suggested that the coordinated protective response of ammonia excretion by NH_3/NH_4^+ transport proteins and acid-trapping of ammonia by H^+ transport contributed to maintain a relatively low ammonia concentration in the body fluids during ambient ammonia exposure in razor clam.

Detoxification of Endogenous Ammonia *via* Glutamine Synthesis and Urea Formation in Hepatopancreas

It has been reported that some fish convert excess ammonia into low toxic compound glutamine to avoid ammonia toxicity (Ip et al., 2001). The key enzymes in the pathway of glutamine synthesis are GS and GDH. Glutamine is produced from glutamate and NH_4^+, which was catalyzed by GS. The GDH catalyzes α-ketoglutarate and NH_4^+ to synthesize glutamate (Ip et al., 2001). Hence, one mole of glutamine synthesis is needed to consume two moles of NH_4^+, which is a highly efficient choice for the detoxification of ammonia. Previous study has shown that exposure to sublethal concentration of NH_3 could induce high activities of GS and GDH enzymes in mudskipper *Periophthalmodon schlosseri* and *Boleophthalmus boddaerti* (Peng et al., 1998). Exposure to ammonia also results in significant increases in enzyme activity, protein content, and mRNA levels of GS in liver, intestine, and muscle to detoxify ammonia in the Chinese black sleeper *Bostrichthys sinensis* (Anderson et al., 2002). In accordance with previous results, the significant increased expressions of *GS* in both the hepatopancreas and the gill in our results suggested that the clam could also reduce the toxicity of ammonia by converting ammonia into glutamine, although the mRNA level of GDH showed no significant change in treatment group compared with CG. However, a recent study showed a dramatic increase in glutamate concentration in the hemocytes of *S. constricta* exposure to ammonia coupled with an increment of relative mRNA and protein expression of both GS and GDH (Zhang H. et al., 2020). Combined these results together, we believe that it is an important protective strategy for razor clam to convert ammonia into non- or less-toxic nitrogenous compounds such as glutamate formation when faced high ambient ammonia concentration (Zhang H. et al., 2020).

Accumulated ammonia could also be converted into urea to reduce ammonia toxicity, while only a few species could synthesize urea *via* the ornithine-urea cycle (Peng et al., 1998). The urea production from ornithine cycle has usually been suppressed in all freshwater teleosts, except for some airbreathers, such as the tilapia fish *Oreochromis alcalicus graham*, which is the only fish that can live in the high alkaline soda lake with pH 9.6–10 (Randall et al., 1989). Besides, urea biosynthesis increases in the estivating African lungfish *Protopterus aethiopicus* living in shallow waters and burrowing beneath the substratum to survive in estivation, as well as in *Xenopus laevis* under water-shortage condition (Janssens and Cohen, 1968). Interestingly, there was a significant increase in the urea content in the liver of *P. schlosseri* after 48 h of aerial exposure, but no changes were observed in *B. boddaerti* (Lim et al., 2001). Hence, these different results from different fishes indicate that ammonia detoxification through urea cycle is not a universal mechanism, but a unique adaptation to some special environmental circumstances (Ip et al., 2001). In this study, the significantly higher expression of *ARG* and *ASS* in the hepatopancreas indicated that the pathway of urea synthesis might have been activated in *S. constricta* when exposed to high environmental ammonia. As we known, the razor clam lives in intertidal mudflat amount of high ammonia, which place to undergo overlying seawater changing gradually to overlying air during low tide, particularly in summer with increased temperature (Zhang W. Y. et al., 2020). Therefore, it is supported that the retention of urea synthesis pathway contributes to the survival of *S. constricta* under high ammonia stress during low tide with the condition of extreme dry or heat. Since urea content has not detected in this study, further investigation of this issue is warranted.

CONCLUSION

This study carried out a preliminary analysis of the responding mechanisms under ammonia stress in *S. constricta*. The higher capacity of tolerance to ammonia was observed and the 96 h sublethal concentration of ammonia was 244.55 mg/L.

A total of 1,415 and 306 DEGs were identified in the gill and hepatopancreas subjected to 180 mg/L TAN for up to 72 h. The DEGs in the gill were majorly enriched in metabolic processes, including regulation of nitrogen compound metabolic process, nitrogen compound transport, and amide transport. Most of DEGs in the hepatopancreas were enriched in oxidation-reduction process, response to stress, and amine metabolic process. In addition, the expressions of ammonia transport-related genes (e.g., *Rh*, *VHA*, *NHE*, and *NKA*) in the gill were significantly changed under ammonia stress ($p < 0.05$), indicating that the ammonia excretion by NH_3/NH_4^+ transport and H^+ transport proteins synergistically contributed to maintain ammonia at a relative low level during ammonia exposure. Besides, ammonia metabolism-related genes such as *GS*, *ARG*, and *ASS* were upregulated in the hepatopancreas. These results provided preliminary evidence for detoxification of endogenous ammonia *via* glutamine synthesis and urea formation in *S. constricta*. Furthermore, the pathways and genes identified in this study would facilitate further studies on the more detailed molecular mechanisms of the ammonia detoxification in molluscs and promote molecular selective breeding for ammonia-tolerance varieties.

DATA AVAILABILITY STATEMENT

The datasets presented in this study can be found in online repositories. The names of the repository/repositories and accession number(s) can be found at: NCBI (accession: SRR9943679-SRR9943690).

ETHICS STATEMENT

The animal study was reviewed and approved by Institutional Animal Care and Use Committee (IACUC) of Zhejiang Wanli University.

AUTHOR CONTRIBUTIONS

JR and ZL designed the experiments. LL and HZ performed the experiments. LL, JR, and HZ analyzed the data. LL, JR, YD, and CS wrote and revised the manuscript. All authors read and approved the final manuscript.

FUNDING

This work was supported by the National Key Research and Development Program of China (2018YFD0901405), Zhejiang Major Program of Science and Technology (2021C02069-7), Ningbo Major Project of Science and Technology (2019B10005 and 2019C10046), and the Project of "3315" Innovative Team of Ningbo City.

SUPPLEMENTARY MATERIAL

The Supplementary Material for this article can be found online at: https://www.frontiersin.org/articles/10.3389/fmars.2022.832494/full#supplementary-material

REFERENCES

Anderson, P. M., Broderius, M. A., Fong, K. C., Tsui, K. N. T., Chew, S. F., and Ip, Y. K. (2002). *Glutamine synthetase* expression in liver, muscle, stomach and intestine of *Bostrichthys sinensis* in response to exposure to a high exogenous ammonia concentration. *J. Exp. Biol.* 205, 2053–2065.

Chen, S., Yu, Y., Gao, Y., Yin, P., and Tian, L. (2019). Exposure to acute ammonia stress influences survival, immune response and antioxidant status of pacific white shrimp (*Litopenaeus vannamei*) pretreated with diverse levels of inositol. *Fish Shellfish Immunol.* 89, 248–256. doi: 10.1016/j.fsi.2019.03.072

Chen, X., Mao, X., Huang, J., Yang, D., Wu, J., Dong, S., et al. (2011). KOBAS 2.0: a web server for annotation and identification of enriched pathways and diseases. *Nucleic Acids Res.* 39, 316–322. doi: 10.1093/nar/gkr483

Cheng, C. H., Yang, F. F., Ling, R. Z., Liao, S. A., Miao, Y. T., Ye, C. X., et al. (2015). Effects of ammonia exposure on apoptosis, oxidative stress and immune response in pufferfish (*Takifugu obscurus*). *Aquatic Toxicology*. 164, 61–71. doi: 10.1016/j.aquatox.2015.04.004

Chew, S. F., and Ip, Y. K. (2014). Excretory nitrogen metabolism and defence against ammonia toxicity in air-breathing fishes. *J. Fish Biol.* 84, 603–638. doi: 10.1111/jfb.12279

Clifford, A. M., Goss, G. G., and Wilkie, M. P. (2015). Adaptations of a deep sea scavenger: high ammonia tolerance and active NH4? excretion by the Pacific hagfish (*Eptatretus stoutii*). *Comp. Biochem. Physiol. A Mol. Integr. Physiol.* 182, 64–74. doi: 10.1016/j.cbpa.2014.12.010

Cong, M., Wu, H., Cao, T., Lv, J., Wang, Q., Ji, C., et al. (2018). Digital gene expression analysis in the gills of *Ruditapes philippinarum* exposed to short- and long-term exposures of ammonia nitrogen. *Aquat. Toxicol.* 194, 121–131. doi: 10.1016/j.aquatox.2017.11.012

Cong, M., Wu, H., Yang, H., Zhao, J., and Lv, J. (2017). Gill damage and neurotoxicity of ammonia nitrogen on the clam *Ruditapes philippinarum*. *Ecotoxicology* 26, 1–11. doi: 10.1007/s10646-017-1777-4

Cui, Y., Ren, X., Li, J., Zhai, Q., Feng, Y., Xu, Y., et al. (2017). Effects of ammonia-N stress on metabolic and immune function via the neuroendocrine system in *Litopenaeus vannamei*. *Fish Shellfish Immunol.* 64, 270. doi: 10.1016/j.fsi.2017.03.028

Denham, B. E. (2016). *Categorical Statistics for Communication Research*. Hoboken: Blackwell Publishing Ltd, 255–258. doi: 10.1002/9781119407201.ch12

Dewey, C. N., and Li, B. (2011). RSEM: accurate transcript quantification from RNA-Seq data with or without a reference genome. *BMC Bioinformatics* 12:323. doi: 10.1186/1471-2105-12-323

Dong, Y., Zeng, Q., Ren, J., Yao, H., Lv, L., He, L., et al. (2020). The chromosome-level genome assembly and comprehensive transcriptomes of the razor clam (*Sinonovacula constricta*). *Front. Genet.* 11:664. doi: 10.3389/fgene.2020.00664

Dutra, F. M., Freire, C. A., Santos, A., Forneck, S. C., Brazão, C. C., and Ballester, E. L. C. (2016). Acute toxicity of ammonia to various life stages of the Amazon river prawn, *Macrobrachium amazonicum*, Heller, 1862. *Aquaculture* 453, 104–109. doi: 10.1007/s00128-016-1932-2

Epifanio, C. E., and Srna, R. F. (1975). Toxicity of ammonia, nitriteion, nitrateion, and orthophosphate to *Mercenaria mercenaria* and *Crassostrea virginica*. *Mar. Biol.* 33, 241–246. doi: 10.1007/BF00390928

Gao, M., Lv, M., Liu, Y., and Song, Z. (2018). Transcriptome analysis of the effects of Cd and nanomaterial-loaded Cd on the liver in zebrafish. *Ecotoxicol. Environ. Saf.* 164, 530–539. doi: 10.1016/j.ecoenv.2018.08.068

Grabherr, M. G., Haas, B. J., Yassour, M., Levin, J. Z., and Amit, I. (2013). Trinity: reconstructing a full-length transcriptome without a genome from RNA-Seq data. *Nat. Biotechnol.* 29, 644–652. doi: 10.1038/nbt.1883

Harris, J. O., Maguire, G. B., Edwards, S., and Hindrum, S. M. (1998). Effect of ammonia on the growth rate and oxygen consumption of juvenile greenlip

abalone, *Haliotis laevigata* Donovan. *Aquaculture* 160, 259–272. doi: 10.1016/S0044-8486(97)00249-4

Hasenbein, M., Werner, I., Deanovic, L. A., Geist, J., Fritsch, E. B., Javidmehr, A., et al. (2014). Transcriptomic profiling permits the identification of pollutant sources and effects in ambient water samples. *Sci. Total Environ.* 468-469, 688–698. doi: 10.1016/j.scitotenv.2013.08.081

Hu, W., Zhao, B., Li, C., Han, S., and Zhang, S. (2018). Effects of chronic ammonia nitrogen stress on the feeding and digestive enzyme activities of sea cucumber (*Apostichopus japonicas* Selenka). *J. Fish. Sci. China* 25, 137–146. doi: 10.3724/SP.J.1118.2018.17117

Ip, Y. K., Chew, S. F., and Randall, D. J. (2001). Ammonia toxicity, tolerance, and excretion. *Fish Physiol.* 20, 109–148. doi: 10.1016/S1546-5098(01)20005-3

Ip, Y. K., Chew, S. F., Wilson, J. M., and Randall, D. J. (2004). Defences against ammonia toxicity in tropical air-breathing fishes exposed to high concentrations of environmental ammonia: a review. *J. Comp. Physiol. B Biochem. Syst. Environ. Physiol.* 174, 565–575. doi: 10.1007/s00360-004-0445-1

Janssens, P. A., and Cohen, P. P. (1968). Biosynthesis of urea in the estivating African lungfish and in *Xenopus laevis* under conditions of water-shortage. *Comp. Biochem. Physiol.* 24, 887–898. doi: 10.1016/0010-406x(68)90800-1

Kir, M., Sunar, M. C., and Gök, M. (2019). Acute ammonia toxicity and the interactive effects of ammonia and salinity on the standard metabolism of European sea bass (*Dicentrarchus labrax*). *Aquaculture* 511:734273. doi: 10.1016/j.aquaculture.2019.734273

Kir, M., Topuz, M., Sunar, M. C., and Topuz, H. (2015). Acute toxicity of ammonia in Meagre (*Argyrosomus regius* Asso, 1801) at different temperatures. *Aquac. Res.* 47, 3593–3598. doi: 10.1111/are.12811

Liang, Z., Liu, R., Zhao, D., Wang, L., and Sun, M. (2016). Ammonia exposure induces oxidative stress, endoplasmic reticulum stress and apoptosis in hepatopancreas of pacific white shrimp (*Litopenaeus vannamei*). *Fish Shellfish Immunol.* 54, 523–528. doi: 10.1016/j.fsi.2016.05.009

Liao, Y., Smyth, G. K., and Shi, W. (2014). featureCounts: an efficient general purpose program for assigning sequence reads to genomic features. *Bioinformatics* 30, 923–930. doi: 10.1093/bioinformatics/btt656

Lim, C. B., Chew, S. F., Anderson, P. M., and Ip, Y. K. (2001). Reduction in the rates of protein and amino acid catabolism to slow down the accumulation of endogenous ammonia: a strategy potentially adopted by mudskippers (*Periophthalmodon schlosseri* and *Boleophthalmus boddaerti*) during aerial exposure in constant darkness. *J. Exp. Biol.* 204, 1605–1614.

Liu, F., Li, S., Yu, Y., Sun, M., and Li, F. (2020). Effects of ammonia stress on the hemocytes of the Pacific white shrimp *Litopenaeus vannamei*. *Chemosphere* 239:124759. doi: 10.1016/j.chemosphere.2019.124759

Lu, X., Kong, J., Luan, S., Dai, P., Meng, X., Cao, B., et al. (2016). Transcriptome analysis of the hepatopancreas in the Pacific white shrimp (*Litopenaeus vannamei*) under acute ammonia stress. *PLoS One* 11:0164396. doi: 10.1371/journal.pone.0164396

Lv, Y. L., Zhang, Y. P., and Shan, S. S. (2012). Acute toxic effects of ammonia-N to *Tegillarca granosa* at different temperatures. *J. Zhejiang Ocean Univ.* 31, 54–58.

Miranda-Filho, K. C., Pinho, G. L. L., Wasielesky, W., and Bianchini, A. (2009). Long-term ammonia toxicity to the pink-shrimp *Farfantepenaeus paulensis*. *Comp. Biochem. Physiol. Toxicol. Pharmacol.* 150, 377–382. doi: 10.1016/j.cbpc.2009.06.001

Miron, D., Moraes, B., Becker, A. G., Crestani, M., Spanevello, R., Loro, V. L., et al. (2008). Ammonia and pH effects on some metabolic parameters and gill histology of silver catfish, *Rhamdia quelen* (Heptapteridae). *Aquaculture* 277, 192–196. doi: 10.1016/j.aquaculture.2008.02.023

Mommsen, T., and Walsh, P. (1989). Evolution of urea synthesis in vertebrates: the piscine connection. *Science* 243, 72–75. doi: 10.1126/science.2563172

Montresor, L. C., Miranda-Filho, K. C., Paglia, A., Luz, D., Araújo, J., Silva, M., et al. (2013). Short-term toxicity of ammonia, sodium Hydroxide and a commercial biocide to golden mussel *Limnoperna fortunei* (Dunker, 1857). *Ecotoxicol. Environ. Saf.* 92, 150–154. doi: 10.1016/j.ecoenv.2013.03.016

Mummert, A. K., Neves, R. J., Newcomb, T. J., and Cherry, D. S. (2003). Sensitivity of juvenile freshwater mussels (*Lampsilis fasciola*, *Villosa iris*) to total and un-ionized ammonia. *Environ. Toxicol. Chem.* 22, 2545–2553. doi: 10.1897/02-341

Newton, T. J., and Bartsch, M. R. (2010). Lethal and sublethal effects of ammonia to juvenile *Lampsilis* mussels (Unionidae) in sediment and water-only exposures. *Environ. Toxicol. Chem.* 26, 2057–2065. doi: 10.1897/06-245R.1

Peng, K. W., Chew, S. F., Lim, C. B., Kuah, S., Kok, W. K., and Ip, Y. K. (1998). The mudskippers *Periophthalmodon schlosseri* and *Boleophthalmus boddaerti* can tolerate environmental NH_3 concentrations of 446 and 36μM, respectively. *Fish Physiol. Biochem.* 19, 59–69. doi: 10.1023/A:1007745003948

Randall, D. J., Wood, C. M., Perry, S. F., Bergman, H. L., and Wright, P. A. (1989). Urea excretion as a strategy for survival in a fish living in a very alkaline environment. *Nature* 337, 165–166. doi: 10.1038/337165a0

Ren, Q., Pan, L., Zhao, Q., and Si, L. (2015). Ammonia and urea excretion in the swimming crab *Portunus trituberculatus* exposed to elevated ambient ammonia-N. *Comp. Biochem. Physiol. A Mol. Integr. Physiol.* 187, 48–54. doi: 10.1016/j.cbpa.2015.04.013

Rodela, T. M., Esbaugh, A. J., McDonald, M. D., Gilmour, K. M., and Walsh, P. J. (2011). Evidence for transcriptional regulation of the urea transporter in the gill of the Gulf toadfish, *Opsanus beta*. *Comp. Biochem. Physiol. B Biochem. Mol. Biol.* 160, 72–80. doi: 10.1016/j.cbpb.2011.06.004

Schram, E., Roques, J., Abbink, W., Spanings, T., de Vries, P., Bierman, S., et al. (2010). The impact of elevated water ammonia concentration on physiology, growth and feed intake of African catfish (*Clarias gariepinus*). *Aquaculture* 306, 108–115. doi: 10.1016/j.aquaculture.2010.06.005

Shang, Z. H., Huang, M., Wu, M. X., Mi, D., You, K., and Zhang, Y. L. (2021). Transcriptomic analyses of the acute aerial and ammonia stress response in the gill and liver of large-scale loach (*Paramisgurnus dabryanus*). *Comp. Biochem. Physiol. C Toxicol. Pharmacol.* 250:109185. doi: 10.1016/j.cbpc.2021.109185

Shen, C., Tang, D., Bai, Y., Luo, Y., and Wang, Z. (2021). Comparative transcriptome analysis of the gills of *Procambarus clarkii* provide novel insights into the response mechanism of ammonia stress tolerance. *Mol. Biol. Rep.* 48, 2611–2618. doi: 10.1007/s11033-021-06315-y

Shen, J. D., Cai, Q. F., Yan, L. J., Du, C. H., Liu, G. M., Su, W. J., et al. (2015). Cathepsin L is an immune-related protein in Pacific abalone (*Haliotis discus hannai*)–Purification and characterization. *Fish Shellfish Immunol.* 47, 986–995. doi: 10.1016/j.fsi.2015.11.004

Sinha, A. K., Zinta, G., AbdElgawad, H., Asard, H., Blust, R., and De Boeck, G. (2015). High environmental ammonia elicits differential oxidative stress and antioxidant responses in five different organs of a model estuarine teleost (*Dicentrarchus labrax*). *Comp. Biochem. Physiol. C Toxicol. Pharmacol.* 174-175, 21–31. doi: 10.1016/j.cbpc.2015.06.002

Staals, R. H. J., Bronkhorst, A. W., Schilders, G., Slomovic, S., and Pruijn, G. J. M. (2010). Dis3-like 1: a novel exoribonuclease associated with the human exosome. *EMBO J.* 29, 2358–2367. doi: 10.1038/emboj.2010.122

Stark, R., Grzelak, M., and Hadfield, J. (2019). RNA sequencing: the teenage years. *Nat. Rev. Genet.* 20, 631–656. doi: 10.1038/s41576-019-0150-2

Sun, G., Sun, C., He, J., Yao, H., Dai, W., Lin, Z., et al. (2021). Characterizing the role of *glutamine synthetase* gene on ammonia nitrogen detoxification metabolism of the razor clam *Sinonovacula constricta*. *Front. Mar. Sci.* 8:793118. doi: 10.3389/fmars.2021.793118

Thurston, R. V., Russo, R. C., and Vinogradov, G. A. (1981). Ammonia toxicity to fishes. Effect of pH on the toxicity of the unionized ammonia species. *Environ. Sci. Technol.* 15, 837–840. doi: 10.1021/es00089a012

Trapnell, C., Pachter, L., and Salzberg, S. L. (2009). TopHat: discovering splice junctions with RNA-Seq. *Bioinformatics* 25, 1105–1111. doi: 10.1093/bioinformatics/btp120

Tresguerres, M., Clifford, A. M., Harter, T. S., Roa, J. N., and Brauner, C. J. (2020). Evolutionary links between intra- and extracellular acid-base regulation in fish and other aquatic animals. *J. Exp. Zool. A Ecol. Integr. Physiol.* 333, 1–17. doi: 10.1002/jez.2367

USEPA (2013). *Final Aquatic Life Ambient Water Quality Criteria for Ammonia-Freshwater. EPA-822-R-13-001*. Washington: United States Environmental Protection Agency.

Wang, W. N., Zhou, J., Wang, P., Tian, T. T., Zheng, Y., Liu, Y., et al. (2016). Oxidative stress, DNA damage and antioxidant enzyme gene expression in the Pacific white shrimp, *Litopenaeus vannamei* when exposed to acute pH stress. *Comp. Biochem. Physiol. C Toxicol. Pharmacol.* 150, 428–435. doi: 10.1016/j.cbpc.2009.06.010

Wang, W. Q., Jiang, L. X., Yang, N., Jian, L. I., and Wang, R. J. (2007). The effect of ammonia-N on immune activity of *Ruditapes philippinarum*. *Mar. Sci.* 31, 23–27.

Weihrauch, D., Morris, S., and Towle, D. W. (2004). Ammonia excretion in aquatic and terrestrial crabs. *J. Exp. Biol.* 207, 4491–4504. doi: 10.1242/jeb.01308

Wood, C. M., Nawata, C. M., Wilson, J. M., Laurent, P., Chevalier, C., Bergman, H. L., et al. (2013). Rh proteins and NH4(+)-activated Na^+-ATPase in the Magadi tilapia (*Alcolapia grahami*), a 100% ureotelic teleost fish. *J. Exp. Biol.* 216, 2998–3007. doi: 10.1242/jeb.078634

Wyatt, M. (2009). Differential effects of reactive nitrogen species on DNA base excision repair initiated by the alkyladenine DNA glycosylase. *Carcinogenesis* 30, 2123–2129. doi: 10.1093/carcin/bgp256

Xue, S., Lin, J., Zhou, Q., Wang, H., and Han, Y. (2021). Effect of ammonia stress on transcriptome and endoplasmic reticulum stress pathway for common carp (*Cyprinus carpio*) hepatopancreas. *Aquac. Rep.* 20:100694. doi: 10.1016/j.aqrep.2021.100694

Yang, W., Xiang, F., Sun, H., Chen, Y., Minter, E., and Yang, Z. (2010). Changes in the selected hematological parameters and gill Na(+)/K(+) ATPase activity of juvenile crucian carp *Carassius auratus* during elevated ammonia exposure and the post-exposure recovery. *Biochem. Syst. Ecol.* 38, 557–562. doi: 10.1016/j.bse.2010.06.005

You, X., Chen, J., Bian, C., Yi, Y., Ruan, Z., Li, J., et al. (2018). Transcriptomic evidence of adaptive tolerance to high environmental ammonia in mudskippers. *Genomics* 110, 404–413. doi: 10.1016/j.ygeno.2018.09.001

Young, M. D., Wakefield, M. J., Smyth, G. K., and Oshlack, A. (2010). Gene ontology analysis for RNA-seq: accounting for selection bias. *Genome Biol.* 11:R14. doi: 10.1186/gb-2010-11-2-r14

Yu, J., Sun, J., Zhao, S., Wang, H., and Zeng, Q. (2019). Transcriptome analysis of oriental river prawn (*Macrobrachium nipponense*) hepatopancreas in response to ammonia exposure. *Fish Shellfish Immunol.* 93, 223–231. doi: 10.1016/j.fsi.2019.07.036

Zhang, H., Sun, G., Lin, Z., Yao, H., and Dong, Y. (2020). The razor clam *Sinonovacula constricta* uses the strategy of conversion of toxic ammonia to glutamine in response to high environmental ammonia exposure. *Mol. Biol. Rep.* 47, 1–15. doi: 10.1007/s11033-020-06018-w

Zhang, W. Y., Storey, K., and Dong, Y.-W. (2020). Adaptations to the mudflat: insights from physiological and transcriptional responses to thermal stress in a burrowing bivalve *Sinonovacula constricta*. *Sci. Total Environ.* 710:136280. doi: 10.1016/j.scitotenv.2019.136280

Zhang, L., Zhao, Z., and Fan, Q. (2016). Effects of ammonia on growth, digestion and antioxidant capacity in juvenile yellow catfish *Pelteobagrus fulvidraco* (Richardson, 1846). *J. Appl. Ichthyol.* 32, 1205–1212. doi: 10.1111/jai.13203

Zhang, T., Yan, Z., Zheng, X., Fan, J., and Guo, S. (2019). Transcriptome analysis of response mechanism to ammonia stress in Asian clam (*Corbicula fluminea*). *Aquat. Toxicol.* 214:105235. doi: 10.1016/j.aquatox.2019.105235

Zhang, Y. P., Xiao, G. Q., Lin, L. Z., Zhang, J. M., and Chai, X. L. (2009). Effects of pH and ammonia-N on tolerance of *Estellarca olivacea*. *Sichuan J. Zool.* 28, 73–76. doi: 10.1360/972009-1142

Zhao, Q., Feng, K., Zhang, L., Bai, Y., and Yao, W. (2021). Effects of acute ammonia stress on antioxidant responses, histopathology and ammonia detoxification metabolism in triangle sail mussels (*Hyriopsis cumingii*). *Water* 13, 1–16. doi: 10.3390/w13040425

Zhu, Z. X., Jiang, D. L., Li, B. J., Qin, H., and Xia, J. H. (2019). Differential transcriptomic and metabolomic responses in the liver of Nile tilapia (*Oreochromis niloticus*) exposed to acute ammonia. *Mar. Biotechnol.* 21, 488–502. doi: 10.1007/s10126-019-09897-8

Conflict of Interest: The authors declare that the research was conducted in the absence of any commercial or financial relationships that could be construed as a potential conflict of interest.

Publisher's Note: All claims expressed in this article are solely those of the authors and do not necessarily represent those of their affiliated organizations, or those of the publisher, the editors and the reviewers. Any product that may be evaluated in this article, or claim that may be made by its manufacturer, is not guaranteed or endorsed by the publisher.

frontiers in Marine Science

ORIGINAL RESEARCH
published: 15 February 2022
doi: 10.3389/fmars.2022.851142

Study on the Effect of Mass Selection and Hybridization on Growth Performance of Chinese Pearl Oyster *Pinctada martensii*

Chao Fan[1†], Xuekai Zhang[1†], Liming Tang[1], Xingzhi Zhang[2], Jinlong Li[1], Yangchun Li[1], Qiongzhen Li[2] and Zhaoping Wang[1]*

[1] The Key Laboratory of Mariculture of Ministry of Education, Ocean University of China, Qingdao, China, [2] Guangxi Key Laboratory of Aquatic Genetic Breeding and Healthy Aquaculture, Guangxi Academy of Fisheries Sciences, Nanning, China

The pearl oyster *Pinctada martensii* is an important species for sea pearl production in China. To explore the influence of the combination of mass selection and hybridization on growth performance of *P. martensii*, we established four selected groups and four control groups (each with two within-family crosses and two reciprocal hybrid crosses) using 1-year-old offspring of two families (Family A and Family B) from Beihai, Guangxi Province, China. Generally, the growth of the selected group was greater than that of the control group for both within-family crosses and reciprocal hybrid crosses. Shell length and width were affected by genotype, environmental factors, and the interaction between the two on Days 210 and 360. The shell widths of the four reciprocal hybrid crosses all showed heterosis on Day 360. The four within-family crosses showed a certain degree of inbreeding depression during the growth period. On Day 360, the three genetic parameters for shell width of the selected group of ♀ Family B and ♂ Family A were the largest, with values of 0.70, 1.17, and 0.06 for realized heritability, standard response to selection, and current genetic gain, respectively. Overall, the growth performance of ♀ Family B × ♂ Family A in the selected group was the best. Therefore, the combination of mass selection and hybridization could be an effective way to improve the growth performance of *P. martensii*.

Keywords: *Pinctada martensii*, mass selection, hybridization, production performance, response to selection

OPEN ACCESS

Edited by:
Liqiang Zhao,
Guangdong Ocean University, China

Reviewed by:
Yanping Qin,
South China Sea Institute of Oceanology, Chinese Academy of Sciences (CAS), China
Zhe Zheng,
Guangdong Ocean University, China

***Correspondence:**
Zhaoping Wang
zpwang@ouc.edu.cn

[†] These authors have contributed equally to this work

Specialty section:
This article was submitted to Marine Fisheries, Aquaculture and Living Resources, a section of the journal Frontiers in Marine Science

Received: *09 January 2022*
Accepted: *24 January 2022*
Published: *15 February 2022*

Citation:
Fan C, Zhang X, Tang L, Zhang X, Li J, Li Y, Li Q and Wang Z (2022) Study on the Effect of Mass Selection and Hybridization on Growth Performance of Chinese Pearl Oyster Pinctada martensii. Front. Mar. Sci. 9:851142. doi: 10.3389/fmars.2022.851142

INTRODUCTION

Pinctada martensii is a dioecious pearl oyster native to Guangxi, Guangdong, and Hainan provinces in China. The pearls produced by *P. martensii* are called "South China Sea pearl." *P. martensii* is the most important seawater pearl-producing species in China, and it once enjoyed a worldwide reputation. However, in recent years, the output of pearls in China has decreased significantly, and the quality and price of pearls have continued to decline. The germplasm of *P. martensii* in China is degraded seriously, with growth rate, small size, and poor secretion ability (Gu et al., 2009; Liu et al., 2011; Li et al., 2017; He et al., 2021). One of the most important reasons for the problems above is the inability to provide high-quality seedlings for the industry. Therefore, the breeding program of *P. martensii* is imperative. Mass selection is a frequently used and effective

method in shellfish breeding. However, due to the destruction of the natural environment, the wild population resources of *P. martensii* are very scarce. Aquaculture currently mainly relies on hatchery production, while the shellfish in the hatchery can easily cause inbreeding depression due to the long-term inbreeding (Li et al., 2017). Hybridization is an effective method to reduce inbreeding depression. Therefore, the combination of mass selection and crossbreeding cannot only quickly achieve the purpose of breeding, but also reduce the decline of inbreeding.

Due to poorly developed selective breeding technology, the global output of aquatic products after selective breeding only accounted for 8.2% of the total aquaculture in 2010 (Gjedrem and Rye, 2018). The genetic gain of each generation of selected aquatic species can reach 12.5%, and the annual growth rate can reach 5.4%. If selective breeding is applied to all aquatic species, the world aquaculture production could be doubled in 13 years (Gjedrem et al., 2012). Effective selective breeding requires selection of parents with favorable phenotypes, such as fast growth and strong stress resistance (Gjedrem and Baranski, 2009). To date, many shellfish selective breeding programs initially selected parents from wild populations (Li et al., 2011; Zhao et al., 2012; Dégremont et al., 2015; Du et al., 2015; He, 2016; Barros et al., 2018), which have high genetic diversity and are easy to adapt to the environment due to natural selection (Zhao et al., 2020). However, some shellfish breeding programs have used advantageous breeding groups that are selected from laboratory strains as the basic populations (Li, 2012; Huo et al., 2015; Wang et al., 2020).

Mass selection and hybridization are common and effective approaches that have been widely used for genetic improvement of aquaculture animals. The advantage of mass selection for highly fertile aquatic animals is that strong selection pressures can be applied to them (Gjedrem and Baranski, 2010). Results from challenge test experiments on animals from family selection can be highly consistent with results from natural experiments, but the former are more expensive to conduct (Gjedrem and Rye, 2018). Mass selection is also a lower-cost alternative to family selection (Dégremont et al., 2015). Dégremont et al. (2015) reported that after four generations of mass selection for the Pacific oyster *Crassostrea gigas*, resistance to the ostreid herpesvirus 1 and the growth rate of each generation improved gradually. However, the growth rate of offspring selected from a suitable environment will not show a significant advantage compared with the control group in an unsuitable environment (Deng et al., 2009a; Zhao et al., 2019, 2020). Crossbreeding, which uses dominant parents to produce offspring with heterosis (Newkirk, 1980), is one method that may improve profitable traits. Crosses between inbred lines can also reduce the increased inbreeding coefficient of multiple generations of inbreeding and at the same time increase genetic diversity. Huo et al. (2015) selected two families with the fastest growth rate from 45 full-sib families of the clam *Ruditapes philippinarum* and applied a certain intensity of selection to self-crosses and crosses. The hybrid offspring showed obvious signs on growth at the age of 30–90 days. Thus, the growth advantage conferred by increasing the selection intensity of highly fertile species followed by hybridization may improve production performance. Researchers have carried out a series of breeding programs on *P. martensii*, including mass selection (Deng et al., 2009b; Wang et al., 2011), cross breeding (Gu et al., 2011), and molecular marker assisted breeding (Shi et al., 2009). Through these studies, new varieties of *P. martensii* with genetic advantages, such as "Haixuan No. 1" (Du et al., 2015), "Haiyou No. 1" (Li, 2012), and "Nanke No. 1" (He, 2016), have been cultivated. These new varieties have the characteristics of fast growth, large shell width, and a strong secreting ability.

In this study, we combined mass selection and hybridization to evaluate the growth parameters of the selected groups and the control groups, as well as the inbred and hybrid groups. We calculated the heterosis and inbreeding depression based on measurements of shell length and width and estimated values for several genetic parameters for shell width of the selected groups.

MATERIALS AND METHODS

Base Stock and Intensity of Selection

In March 2019, we established 27 families using three new varieties of *P. martensii* (Haiyou No. 1, Haixuan No. 1, and Nanke No. 1). In April 2020, the 1-year-old offspring of these 27 families were transported from the culture sites to Guangxi Comprehensive Test Station Hatchery of the National Shellfish Industry Technology System at Guangxi Academy of Fisheries Sciences. The shell width of specimens from the 27 families was measured using a vernier caliper (accuracy 0.01 mm), and the two families (named Family A and Family B) with the largest mean shell width were selected as the parent population for our experiment. The parents of Family A were ♀ Haixuan No. 1 and ♂ Nanke No. 1, and the parents of Family B were ♀ Nanke No. 1 and ♂ Haiyou No. 1. Seven bags of offspring were randomly selected for each family. After removing the dead individuals and those with irregularly shaped shells, there were 1,075 individuals in Family A and 1,025 individuals in Family B. We used a vernier caliper (accuracy 0.01 mm) to measure the shell width of all individuals from the two families, and then the top 12% of individuals with the largest shell width from each family were selected as the selected groups (named SA and SB, respectively). Additionally, 100 individuals were randomly taken from each family to serve as the control groups (named CA and CB, respectively) before selection. Due to different levels of gonadal development, we actually used 112 individuals from Family A and 120 individuals from family B during the experiment. **Figure 1** and **Table 1** show the shell width frequency distribution, selection cutoff points, and intensity of selection (*i*) of the two families.

Establishment of Crosses

Oocytes from females were obtained by dissecting gonads and gathering them into a 50 L bucket filled with filtered sea water. Impurities such as tissue fragments were filtered out with a 100 μm mesh screen. For each line, egg suspensions were mixed well and divided equally into six 10 L buckets. A few drops of ammonia (2–3 mM) (Ohta et al., 2007) were added and the

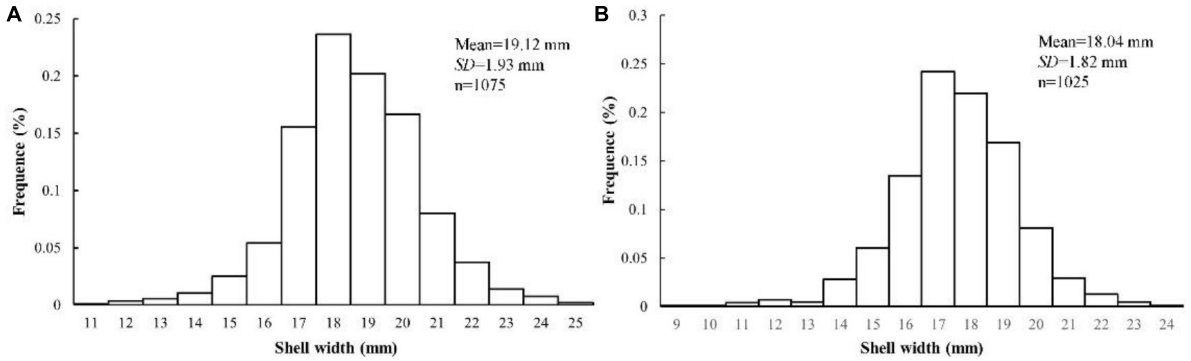

FIGURE 1 | Shell width frequency distribution of *P. martensii*: **(A)** Family A and **(B)** Family B.

TABLE 1 | Shell width (mean ± SD) of base populations and selected group parents, cutoff points, and selection intensity of *P. martensii.*

Items	Base population shell width (mm)	Cutoff point (mm)	Selected parents			Selection intensity
			Sire	Dam	Shell width (mm)	
Family A	19.12 ± 1.93	22.59	61	51	22.43 ± 1.01	1.72
Family B	18.04 ± 1.82	20.05	68	52	20.99 ± 0.91	1.62

TABLE 2 | Mating strategy of *P. martensii.*

Parents	♀ SA	♀ SB	♀ CA	♀ CB
♂SA	SAA	SBA	—	—
♂SB	SAB	SBB	—	—
♂CA	—	—	CAA	CBA
♂CB	—	—	CAB	CBB

buckets were set aside. Oocyte maturity was monitored during the process of oocytes soaking. Semen was extracted from the gonad of each male with a pipette and then divided equally into six 1 L beakers. According to Qin et al. (2018), after the germinal vesicle breakdown ratio of the oocytes reached 100%, a few drops of ammonia were added to the seminal fluid, and the sperm activity was observed immediately. Eggs were examined to rule out the occurrence of uncontrolled fertilization before formal fertilization. When we observed that most of the sperm were activated, an appropriate amount of seminal fluid was poured into the oocyte fluid for fertilization to produce two within-family crosses and two reciprocal hybrid crosses for both the selected groups and the control groups. **Table 2** shows the mating strategy, and the experiment was conducted in triplicate for each group. The fertilized eggs were pooled and placed in a 1 m^3 beaker for hatching at a density of 10–20 eggs mL^{-1}. The temperature of the hatching water was maintained at 28°C, and the salinity was kept at 30 ppt.

Larval Rearing, Spat Nursery, and Grow-Out

The fertilized eggs developed into D-veliger larvae in about 16 h. Larvae were collected after being passed through a 40 μm nylon screen, and the density of each group was adjusted to 3–5 individuals mL^{-1}. The density of each group was adjusted regularly during cultivation to eliminate the effect of density. The larvae were fed on *Isochrysis galbana* before they reached a size of 110–120 μm. As the spat grew, *Chaetoceros muelleri* and *Platymonas subcordiformis* were added to the diet. Feeding was gradually increased from 3,000 to 50,000 cells mL^{-1} day^{-1}. The proportion of the three phytoplankton species was 1:1:1. The water was completely exchanged with filtered seawater once a day.

The spat from each group were gathered into polyethylene mesh bags with a 2 mm aperture at a density of 120–150 individuals/bag when the shell length of juveniles was about 2–3 mm. They were then transferred to three culture sites in Beihai in Guangxi Zhuang Autonomous Region. The three culture sites were named Zhulin (Z), Huolu (H), and Qingshantou (Q) (**Figures 2a,b**). The mesh bags at Zhulin were hung on a floating raft in a large pond (**Figure 2c**). The mesh bags at Huolu and Qingshantou were suspended from off-bottom piles, which were located in the shoal offshore (**Figure 2d**). The biofouling on the mesh bags was removed regularly to prevent it from affecting the flow of seawater through the bags. The mesh bags were changed periodically as the oysters grew. The density of oysters in the mesh bags was adjusted to avoid the influence of density on the experiment.

Evaluation of Growth Performance

The shell length of oysters in each cross was measured on Days 9, 45, 210, and 360, and the shell width was measured on Days 210 and 400. The shell length on Day 9 was measured with a micrometer under a microscope (10×), and the other measurements were made using an electronic vernier caliper (accuracy 0.01 mm).

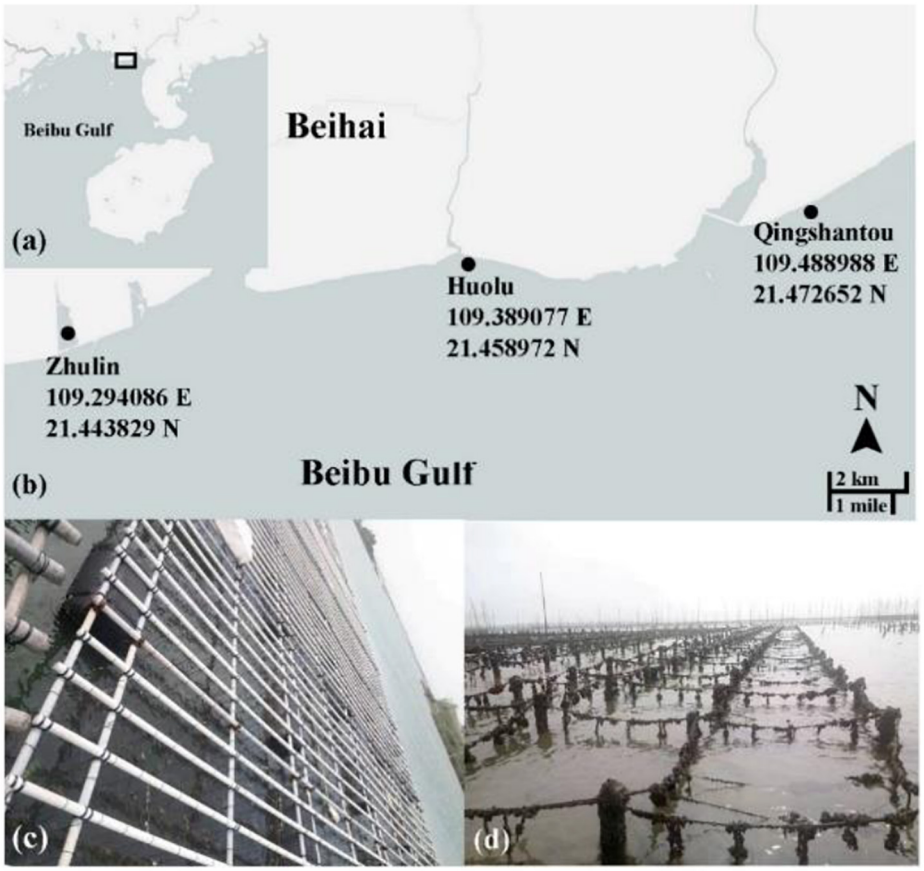

FIGURE 2 | Culture sites and methods. **(a,b)** The three culture sites used in this study; **(c)** oyster hanging culture at Zhulin; **(d)** oyster off-bottom cultures at Huolu and Qingshantou.

Statistical Analyses

Differences in the growth parameters on Days 9 and 45 among the different groups were analyzed by multiple comparisons using a one-way analysis of variance of the means. The growth parameters on Days 210 and 360 among the different groups were analyzed by multiple comparisons using a two-way analysis of variance of the means. The shell length and shell width were log transformed to ensure normality and homoscedasticity. All statistical analyses were performed using R software Version 3.6.3 for Windows. $P < 0.05$ was considered to be statistically significant.

To evaluate the effects of the genotype and environmental factors on the growth of *P. martensii*, a two-factor analysis of variance was used as Zhang et al. (2007):

$$Y_{ijk} = \mu + G_i + E_j + (G \times E)_{ij} + e_{ijk}$$

where Y_{ijk} is the mean shell length or shell width at Days 210 and 360 of the k replicates, i genotype, and j site; G_i is the genotype effect on the mean shell length or shell width at Days 210 and 360 ($i = 1, 2$); E_j is the environmental effect on the mean shell length or shell width at Days 150, 210, and 360 ($j = 1, 2, 3$); $(G \times E)_{ij}$ is the interaction effect between the genotype and the environmental factors; and e_{ijk} is the random observation error ($k = 1, 2, 3$).

Heterosis (H%) was calculated using the following formula (Eq. 1):

$$H\% = \frac{(F_1 - M_p)}{M_p} \times 100 \quad (1)$$

where F_1 is the mean shell length (shell width) of the reciprocal hybrid crosses, and M_P is the mean shell length (shell width) of within-family crosses.

According to Falconer and Mackay (1996), the intensity of selection was calculated as the difference in mean shell width between the selected parents and the base population divided by the standard deviation of the population. The realized heritability ($h^2{}_R$) was calculated following as Hadley et al. (1991):

$$h^2_{\mathrm{R}} = \frac{X_s - X_c}{i\sigma_c} \quad (2)$$

According to Wang (2017), Eq. 2 was adjusted to Eq. 3 to calculate the realized heritability of the reciprocal hybrid crosses for a selected group:

$$h^2_{\mathrm{R}} = \frac{X_s - X_c}{\frac{1}{2}(i_1 + i_2)\sigma_c} \quad (3)$$

where X_S and X_C are the mean shell width of offspring in selected and control groups, respectively; σ_c is the standard deviation of control offspring; and i is the intensity of selection (i_1 for Family A and i_2 for Family B). The standard response to selection (SR) was estimated as Zheng et al. (2006):

$$SR = \frac{X_s - X_c}{\sigma_c} \quad (4)$$

Current genetic gain (GG) was calculated following Zheng et al. (2006):

$$GG(\%) = \frac{X_s - X_c}{X_c} \times 100 \quad (5)$$

The magnitude of inbreeding depression (*ID*) was calculated using the following equation (Zhang et al., 2020):

$$\delta_X\% = \frac{(P_X - S_X)}{P_X} \times 100 \quad (6)$$

where δ_X is the estimate of *ID* for family X; S_X is the mean phenotypic value of offspring from within-family crosses; and P_X is the mean phenotypic value of offspring from reciprocal hybrid crosses.

RESULTS

Growth Parameters of Different Groups

Figure 3 show the growth of shell length and shell width, respectively, in the different groups. The growth rates of each group differed, and the differences began to appear during the larval stage (Day 9). On Day 9, the shell length of the SAB group was the largest at 103.41 ± 9.95 μm, which was significantly larger than that of the other groups ($P < 0.05$) (**Figure 3A**). On Day 45, the shell length of the SAA group was the largest, followed by that of the CAA group. The difference between these two groups was not statistically significant ($P > 0.05$), but their values were significantly higher than those of the other groups ($P < 0.05$) (**Figure 3B**).

During the grow-out stage, both shell length and width were significantly affected by genotype, environmental factors, and the interaction of genotype and environmental factors (**Table 3**). Among the three sites, the shell length of each group was smallest at Zhulin, and the shell lengths of the SBA group on Days 210 and 360 were the largest among the groups within a given site (**Figure 3C**). The shell width of each group was the smallest at Zhulin on Days 210 and 360. With the exception of the SAB group at Qingshantou on Day 210, which had a smaller shell width than that of the CAB group, shell widths were always larger in selected groups than in the control groups. On Day 210, the groups with the largest shell widths at Zhulin, Huolu, and Qingshantou were SBA (9.15 ± 1.69 μm), SAA (11.74 ± 2.03 μm), and SBB (12.71 μm), respectively. On Day 360, the shell width of the SBA group was the largest at all three sites (**Figure 3D**).

Heterosis

Table 4 shows the heterosis results of shell length and shell width for each cross. In general, from the larval stage to the grow-out stage, the heterosis of the selected groups first decreased and then increased, whereas the control groups decreased, increased, and then decreased again. Shell length did not show heterosis in the CAB group ($H\%$ = –0.26%), but all of the other crosses exhibited heterosis at the end of the experiment. The shell width of each cross showed heterosis on Day 360, and the SBA group had the largest value ($H\%$ = 26.12%).

Inbreeding Depression

Table 5 presents the results of *ID* analysis. During the entire growth period, the growth of the four within-family crosses showed varying degrees of *ID*. Values ranged from 6.01 to 7.18% in the larval stage (Day 9), but none of the four within-family crosses showed *ID* by the juvenile stage (Day 45). On Day 210, the shell lengths of the two selected groups exhibited *ID* values of 2.76% (SAA) and 5.16% (SBB). The shell widths of all but the SBB group showed *ID*. At the end of the experiment (Day 360), the *ID* rates for shell length (6.37%) and width (6.61%) were largest in the SBB group.

Shell Width Genetic Parameters

Table 6 shows the realized heritability, standard response to selection, and current genetic gain values for shell width for the four selected groups during the grow-out stage (Days 210 and 360). The three genetic parameters for the reciprocal hybrid crosses all increased, whereas they decreased for the within-family crosses. On Day 210, the values of the three genetic parameters were highest in the SAA group and lowest in the SAB group, whereas on Day 360 the values were highest in the SBA group and lowest in the SAA group.

DISCUSSION

According to New (1991), aquaculture production may have to increase to 63 million tons in 2025 to meet the expected demands. The future needs for aquatic products cannot be met without a substantial increase in aquaculture production because the harvest of many wild stocks has come close to or exceeded the limits of sustainable exploitation (Bentsen and Olesen, 2002). Genetic improvement and domestication are proven routes to increasing agricultural productivity (Hedgecock, 2011). The results of our study indicated that the shell length and width of almost all selected groups were greater than those of the corresponding control groups from the larval stage (Day 9) to the adult stage (Day 360), regardless of mating method or culture site, but the differences were not all statistically significant. The initial selective trait in this study was shell width, so the shell length advantage of the selected groups may be due to the strong correlation between shell length and width of *P. martensii*. Additionally, the operation methods were the same throughout the experiment at a given site, which suggests that the differences in growth between the selected groups and the control groups were caused by genetics (changes in gene frequency caused by selection).

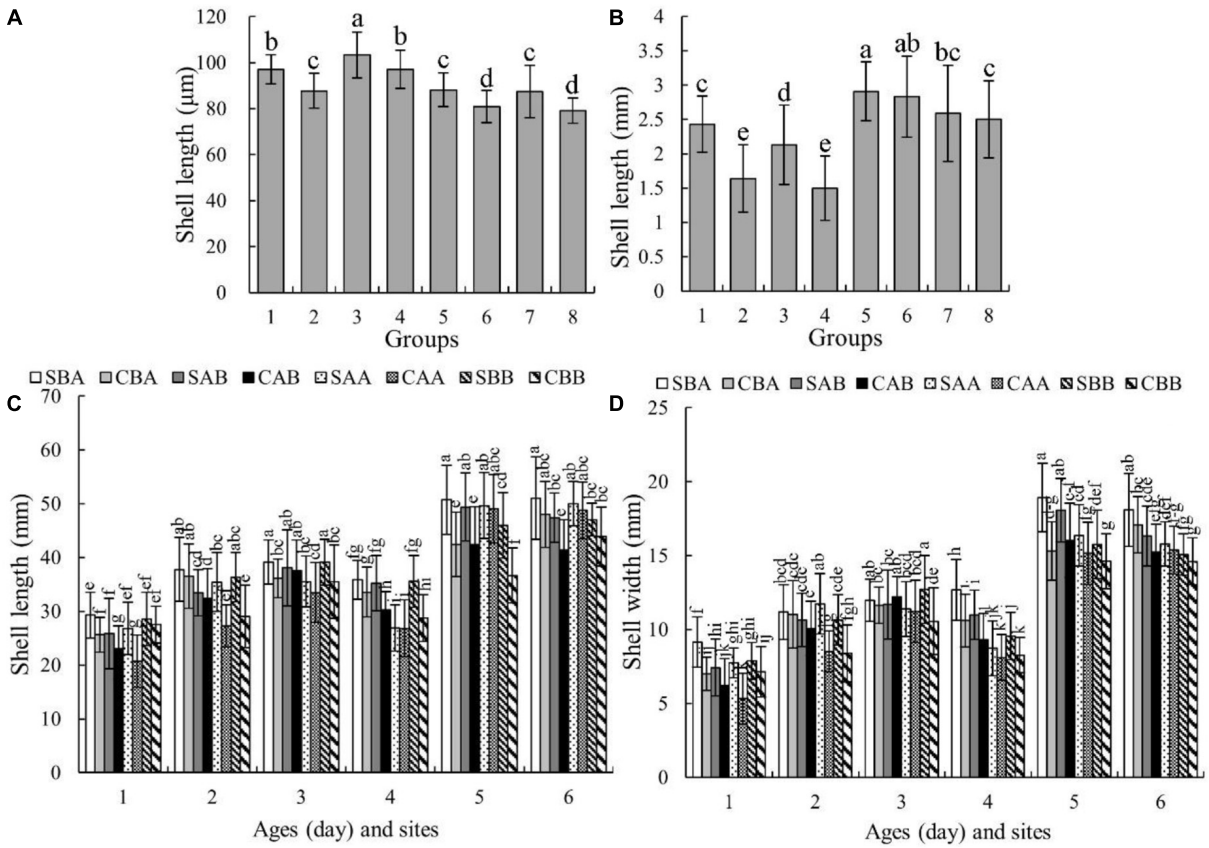

FIGURE 3 | The shell length and shell width of each group of *P. martensii* at different ages and sites. The different letters at each age indicate significant differences among groups ($P < 0.05$). **(A)** Shell length on Day 9, on the horizontal, 1 for SBA, 2 for CBA, 3 for SAB, 4 for CAB, 5 for SAA, 6 for CAA, 7 for SBB, 8 for CBB; **(B)** shell length on Day 45, on the horizontal, 1 for SBA, 2 for CBA, 3 for SAB, 4 for CAB, 5 for SAA, 6 for CAA, 7 for SBB, 8 for CBB; **(C)** shell length on Day 210 and 360, on the horizontal, 1 for Day 210 at Zhulin site, 2 for Day 210 at Huolu site, 3 for Day 210 at Qingshantou site, 4 for Day 360 at Zhulin site, 5 for Day 360 at Huolu site, 6 for Day 360 at Qingshantou site; **(D)** shell width on Day 210 and 360, on the horizontal, 1 for Day 210 at Zhulin site, 2 for Day 210 at Huolu site, 3 for Day 210 at Qingshantou site, 4 for Day 360 at Zhulin site, 5 for Day 360 at Huolu site, 6 for Day 360 at Qingshantou site.

TABLE 3 | One-way analysis of variance showing the differences in growth parameters among different groups (Days 9 and 45) of *P. martensii*.

Group	Sources	*df*	Shell length			Shell width		
			MS	*F*	*P*	*MS*	*F*	*P*
Day 9		7	2123.456	32.333	<0.001***			
Day 45		7	8.165	28.560	<0.001***			
Day 210	G	7	453.860	17.448	<0.001***	63.184	19.806	<0.001***
	E	2	7481.858	287.629	<0.001***	1231.346	385.980	<0.001***
	G × E	14	168.838	6.491	<0.001***	16.635	5.214	<0.001***
Day 360	G	7	696.755	23.802	<0.001***	155.362	43.328	<0.001***
	E	2	17802.111	608.132	<0.001***	3209.583	895.102	<0.001***
	G × E	14	389.451	13.304	<0.001***	11.977	3.340	<0.001***

*Two-way analysis of variance showing the effects of genotype (G) and environmental factors (E) on growth (Days 210 and 360). ***Indicates P < 0.001.*

When planning a selective breeding program, the genotype-environment interaction is one of the important factors that must be considered. The selection led to changes in gene frequency, which in turn led to changes in genotypes, and different genotypes had different sensitivity to the environment. Therefore, the interaction may be related to the sensitivity of different genotypes to the environment (Falconer and Mackay, 1996). Genotype-environment interactions are common in shellfish culture, which may reflect poor control of the environment by shellfish (Evans and Langdon, 2006). Thus, in future breeding projects, we can choose genotypes that are less sensitive to the environment and/or we can breed strains that adapt to

TABLE 4 | Heterosis values for growth of reciprocal hybrid crosses of *P. martensii* (SL: shell length; SW: shell width).

Group	Day 9 SL (%)	Day 45 SL (%)	Day 210 SL (%)	Day 360 SL (%)	Day 210 SW (%)	Day 360 SW (%)
SBA	10.96	−8.96	6.55	9.44	6.75	26.12
SAB	18.38	−20.20	−2.32	6.54	−3.17	16.59
CBA	21.69	−42.31	8.51	7.27	13.50	8.59
CAB	9.79	−36.68	15.68	−0.26	19.53	13.97

TABLE 5 | Inbreeding depression of growth for within-family crosses of *P. martensii* (SL: shell length; SW: shell width).

Group	Day 9 SL (%)	Day 45 SL (%)	Day 210 SL (%)	Day 360 SL (%)	Day 210 SW (%)	Day 360 SW (%)
SAA	6.01	−13.68	2.76	−0.54	0.47	1.20
SBB	6.42	−6.75	5.16	6.37	−0.01	6.61
CAA	6.22	−40.33	−8.77	−2.41	7.42	−1.69
CBB	7.18	−29.80	−2.39	3.94	3.97	2.54

specific environments. In this study, the shell length and width of *P. martensii* were significantly affected by genotype-environment interaction. We found that the growth of each group at the Zhulin site at each time point was the slowest. The Huolu site and Qingshantou site were more suitable for pearl oyster aquaculture than the Zhulin site. This may be due to the low frequency of seawater exchange and the deposition of harmful substances, which make this site unsuitable for the rapid growth of *P. martensii*.

Throughout the experimental period, only spat at the juvenile stage (Day 45) did not show heterosis, whereas other stages exhibited a certain degree of heterosis. On Day 360, all reciprocal hybrid crosses except for the CAB group showed heterosis for shell length. The emergence of heterosis indicated a difference in gene frequency between the two families (Zhang et al., 2017). Maintaining two or more populations with different genetic bases as parents for reciprocal crosses is considered to be a good choice for selective breeding, as it may produce heterosis (Goyard et al., 2008). The parents used in this study were the F_1 generation of two families that are characterized by rapid shell width growth. The parents of the two families were ♀ Haixuan No. 1 × ♂ Nanke No. 1 and ♀ Nanke No. 1 × ♂ Haiyou No. 1. These three new *P. martensii* varieties were generated through multiple generations of breeding. Although they are more suitable for artificial breeding than other populations and have the advantageous traits that aquaculturists expect, they may have lost most of the allelic variability available in the wild. Nevertheless, when multiple new varieties are used to generate crosses with each other, the F_1 generation is guaranteed to be hybrid because the parents are unrelated. We have already observed heterosis (unpublished data) during the growth of the offspring of these two families. However, because the offspring of each family were produced by a pair of parents, the simple use of the dominant family for mass selection may cause *ID*. Therefore, we first selected offspring from the two families and then used the selected population to cross and observe the growth of the hybrid offspring. Ultimately, the target traits of the two families were the same, and whether their offspring will show reduced diversity as a result remains to be determined.

TABLE 6 | Realized heritability (h^R_2), standardized response to selection (SR), and current genetic gain (GG) of selected groups of *P. martensii*.

Group	210			360		
	h^2_R	SR	GG (%)	h^2_R	SR	GG (%)
SBA	0.45	0.76	11.61	0.70	1.17	16.35
SAB	0.12	0.20	7.92	0.46	0.77	12.60
SAA	0.74	1.27	28.13	0.24	0.42	6.18
SBB	0.52	0.85	19.16	0.41	0.66	8.79

Inbreeding is harmful to most organisms and leads to a reduction in fitness (Falconer, 1989). According to Evans et al. (2004), any amount of inbreeding may cause phenotypic *ID*. In our study, the within-family crosses in both the selection and control groups showed *ID*. During the entire experimental period, most of reciprocal hybrid crosses performed better than all within-family crosses. This result showed that although we exerted great intensity of selection on pearl oysters, *ID* is likely to be one factor that affects the growth performance of within-family crosses. *ID* can be explained by the hypotheses of partial dominance and over dominance (Kristensen and Sørensen, 2005; Zheng et al., 2008, 2012). Deleterious recessive effects are also thought to be a major reason for *ID* (Charlesworth and Charlesworth, 1999). *ID* is often more obvious in the early stages of animal development and relatively weak in the later stages (Bierne et al., 1998; McCune et al., 2002; Escobar et al., 2008; Anderson and Hedgecock, 2010; Plough and Hedgecock, 2011). This may be because harmful genes are eliminated with the death of individuals in the early stages of development. This phenomenon is manifested in organisms with high fertility. In our study, all within-family crosses exhibited *ID* at the larval stage (Day 9), whereas the opposite was observed for the juvenile stage (Day 45). This may be because during development, slow-growing individuals were prone to death, while the surviving individuals grew faster, and therefore, showed obvious inbreeding advantages in the juvenile stage. Taris et al. (2007) reported similar results for Pacific oysters. As the offspring grew, *ID* did not disappear but the degree was different, which may also be related

to high mortality during the larval stage. For both the selected and control groups, the *ID* of the BB group was highest during the entire experimental period, which may be related to the degree of *ID* of the parents.

Several researchers have estimated genetic parameters for growth of adult *P. martensii* after mass selection. After Wada (1986) conducted three generations of mass selection on *P. martensii*, the realized heritability values of shell length and width were 0.47 and 0.35, respectively. He et al. (2006) reported that the shell length genetic gain of the first generation was 3.91%. He et al. (2008) conducted mass selection on *P. martensii*, and the genetic gain of shell height at harvest was 15.86% and the realized heritability was 1.065. Deng et al. (2009b) found that the 360-day-old shell length genetic gain of *P. martensii* was 16.6%. Wang et al. (2011) reported that the third generation breeding population of *P. martensii* had a genetic gain of 13.27 and 13.83% for shell length and height at 360 days, respectively. On Day 360 in our study, the shell width genetic gain of *P. martensii* was in the range of 6.18–16.35%. The genetic gain of the two reciprocal hybrid crosses was larger than that of the two within-family crosses. The reason for the lower genetic gain of the two within-family crosses may be related to *ID* because the offspring were all born from a pair of parents. When harvesting, the realized heritability of shell width ranged from 0.24 to 0.70. Like genetic gain, the realized heritability of reciprocal hybrid crosses was greater than that of within-family crosses. Only the realized heritability of the SAA groups was lower than the result reported by Wada (1986), which may be because we only carried out one generation of selection. From Days 210 to 360 in our study, the realized heritability of shell width for reciprocal hybrid crosses increased, indicating that the breeding program was effective because of the significant additive genetic variation (Dégremont et al., 2015). Newkirk (1980) predicted that the genetic improvement of shellfish will be between 10 and 20% per generation. Heritability values above 0.20 indicate that genetic improvement can be easily achieved through the application of selective breeding programs (Newkirk et al., 1977; Falconer and Mackay, 1996).

In summary, we found that using two families as the base populations for mass selection successfully improved the growth performance of *P. martensii*. Although the within-family crosses produced a certain degree of *ID*, growth was improved to a certain extent. In contrast, the growth performance of reciprocal hybrid crosses improved more significantly, resulting in greater responses to selection. Therefore, the method of combining cross-breeding and mass selection is effective. Therefore, the combination of crossbreeding and mass selection is an ideal breeding method. It can provide a large number of excellent seeds for pearl industry and alleviate the shrinking status of pearl shell industry. Of course, if we want to revitalize the pearl oyster industry in China, we still need a lot of follow-up work.

DATA AVAILABILITY STATEMENT

The raw data supporting the conclusions of this article will be made available by the authors, without undue reservation.

AUTHOR CONTRIBUTIONS

CF and XKZ designed the experiment, performed the experiments, analyzed the data, wrote the manuscript, and revised manuscript. LT designed the experiment and performed the experiments. XZZ, JL, and YL performed the experiments. QL supported site. ZW revised the manuscript. All authors contributed to the article and approved the submitted version.

FUNDING

This project was funded by the National Natural Science Foundation of China.

ACKNOWLEDGMENTS

We thank Beihai Xiaoyuzhou Cooperative and Guangxi Jinggong Marine Science and Technology Co., Ltd. for providing the experimental sites. We are also grateful to the reviewers for reviewing our manuscript.

REFERENCES

Anderson, D., and Hedgecock, D. (2010). Inbreeding depression and growth heterosis in larvae of the purple sea urchin *Stronglyocentrotus purpuratus* (Stimpson). *J. Exp. Mar. Biol. Ecol.* 384, 68–75. doi: 10.1016/j.jembe.2009.12.005

Barros, J., Velasco, L. A., and Winkler, F. M. (2018). Heritability, genetic correlations and genotype by environment interactions in productive traits of the Caribbean scallop, *Argopecten nucleus* (Mollusca: bivalvia). *Aquaculture* 488, 39–48. doi: 10.1016/j.aquaculture.2018.01.011

Bentsen, H. B., and Olesen, I. (2002). Designing aquaculture mass selection programs to avoid high inbreeding rates. *Aquaculture* 204, 349–359.

Bierne, N., Launey, S., Naciri-Graven, Y., and Bonhomme, F. (1998). Early effect of inbreeding as revealed by microsatellite analyses on *Ostrea edulis* larvae. *Genetics* 148, 1893–1906. doi: 10.1093/genetics/148.4.1893

Charlesworth, B., and Charlesworth, D. (1999). The genetic basis of inbreeding depression. *Genet. Res.* 74, 329–340.

Dégremont, L., Nourry, M., and Maurouard, E. (2015). Mass selection for survival and resistance to OsHV-1 infection in *Crassostrea gigas* spat in field conditions: response to selection after four generations. *Aquaculture* 446, 111–121. doi: 10.1016/j.aquaculture.2015.04.029

Deng, Y. W., Fu, S., Du, X. D., and Wang, Q. H. (2009a). Realized heritability and genetic gain estimates of larval shell length in the chinese pearl oyster *Pinctada martensii* at three different salinities. *North Am. J. Aquac.* 71, 302–306. doi: 10.1577/a08-024.1

Deng, Y. W., Du, X. D., and Wang, Q. H. (2009b). Selection for fast growth in the Chinese pearl oyster, *Pinctada martensii*: response of the first generation line. *J. World Aquac. Soc.* 40, 843–847. doi: 10.1111/j.1749-7345.2009.00307.x

Du, X. D., Deng, Y. W., Wang, Q. H., Xie, S. H., and Liu, D. (2015). Haixuan No 1 stock of pearl oyster *Pinctada martensii*. *China Fish* 10, 53–56.

Escobar, J. S., Nicot, A., and David, P. (2008). The different sources of variation in inbreeding depression, heterosis and outbreeding depression in a metapopulation of *Physa acuta*. *Genetics* 180, 1593–1608. doi: 10.1534/genetics.108.092718

Evans, F., Matson, S., Brake, J., and Langdon, C. (2004). The effects of inbreeding on performance traits of adult Pacific oysters (*Crassostrea gigas*). *Aquaculture* 230, 89–98. doi: 10.1016/j.aquaculture.2003.09.023

Evans, S., and Langdon, C. (2006). Effects of genotype×environment interactions on the selection of broadly adapted Pacific oysters (*Crassostrea gigas*). *Aquaculture* 261, 522–534.

Falconer, D. S. (1989). *Introduction to Quantitative Genetics*, 3rd Edn. New York, NY: Longman.

Falconer, D. S., and Mackay, T. F. C. (1996). *Introduction to Quantitative Genetics*, 4th Edn. London: Pearson Education Limited, Essex.

Gjedrem, T., and Baranski, M. (2009). *Selective Breeding in Aquaculture: An Introduction*. Dordrecht: Springer Netherlands.

Gjedrem, T., and Baranski, M. (2010). *Selective Breeding in Aquaculture: An Introduction*, Vol. 10. Berlin: Springer Science & Business Media.

Gjedrem, T., Robinson, N., and Rye, M. (2012). The importance of selective breeding in aquaculture to meet future demands for animal protein: a review. *Aquaculture* 350–353, 117–129. doi: 10.1016/j.aquaculture.2012.04.008

Gjedrem, T., and Rye, M. (2018). Selection response in fish and shellfish: a review. *Rev. Aquac.* 10, 168–179. doi: 10.1111/raq.12154

Goyard, E., Goarant, C., Ansquer, D., Brun, P., Decker, S., Dufour, R., et al. (2008). Cross breeding of different domesticated lines as a simple way for genetic improvement in small aquaculture industries: heterosis and inbreeding effects on growth and survival rates of the Pacific blue shrimp *Penaeus* (*Litopenaeus*) *stylirostris*. *Aquaculture* 278, 43–50. doi: 10.1016/j.aquaculture.2008.03.018

Gu, Z. F., Shi, Y. H., Wang, Y., and Wang, A. M. (2011). Heritable characteristics in the pearl oyster *Pinctada martensii*: comparisons of growth and shell morphology of Chinese and Indian populations, and reciprocal crosses. *J. Shellfish Res.* 30, 241–246. doi: 10.2983/035.030.0207

Gu, Z. F., Wang, Q. Y., Fang, J. G., Ye, N. H., Mao, Y. Z., Shi, Y. H., et al. (2009). Growth of cultured pearl oyster (*Pinctada martensii*) in Li'an Lagoon, Hainan Island, China. *J. Shellfish Res.* 28, 465–470. doi: 10.2983/035.028.0307

Hadley, N. H., Dillon, R. T., and Manzi, J. J. (1991). Realized heritability of growth rate in the hard clam *Mercenaria mercenaria*. *Aquaculture* 93, 109–119. doi: 10.1016/0044-8486(91)90210-x

He, G., Liu, X., Xu, Y., Liang, J., Deng, Y., Zhang, Y., et al. (2021). Repeated exposure to simulated marine heatwaves enhances the thermal tolerance in pearl oysters. *Aquatic. Toxicol.* 239:105959. doi: 10.1016/j.aquatox.2021.105959

He, M. X. (2016). Nanke No 1 stock of pearl oyster *Pinctada martensii*. *Mar. Fish.* 10:51.

He, M. X., Guan, Y. Y., Yuan, T., and Zhang, H. Y. (2008). Realized heritability and response to selection for shell height in the pearl oyster *Pinctada fucata* (Gould). *Aquac. Res.* 39, 801–805. doi: 10.1111/j.1365-2109.2008.01889.x

He, M. X., Shi, J. H., Lin, Y. G., and Jiang, Y. P. (2006). Studies on growth traits of first generation of selective line of Pinctada martensii Dunker. *J. Tropical Oceanogr.* 25, 19–22.

Hedgecock, D. (2011). *Genetics of Shellfish on a Human-Dominated Planet. Shellfish Aquaculture and the Environment Chichester, West Sussex, UK*. Hoboken, NJ: Wiley, 339–357.

Huo, Z. M., Yan, X. W., Zhao, L. Q., Liang, J., Yang, F., and Zhang, G. F. (2015). Larval and juvenile growth performance of Manila clam hybrids of two full-sib families. *J. Ocean Univ. China* 14, 564–568. doi: 10.1007/s11802-015-2354-1

Kristensen, T. N., and Sørensen, A. C. (2005). Inbreeding–lessons from animal breeding, evolutionary biology and conservation genetics. *Anim. Sci.* 80, 121–133. doi: 10.1079/asc41960121

Li, J. H., Luo, Y. Q., Zhong, Y. S., Huang, Y., Huang, R. L., Wang, Q. H., et al. (2017). Effects of inbreeding on growth traits, genetic diversity and biomineraliazation gene expression of *Pinctada fuctada martensii*. *J. Southern Agric.* 48, 132–138.

Li, Q., Wang, Q. H., Liu, S. K., and Kong, L. F. (2011). Selection response and realized heritability for growth in three stocks of the Pacific oyster *Crassostrea gigas*. *Fisheries Sci.* 77, 643–648.

Li, Z. L. (2012). Brief introduction to the varieties approved by the fourth meeting of the Fourth National Committee for the examination and approval of original and improved varieties of aquatic products. *China Fish.* 6, 54–55.

Liu, W. G., Lin, J. S., and He, M. X. (2011). Evaluation on mid-term growth of 9 families of pearl oyster Pinctada fucata. *South China Fish. Sci.* 7, 30–36.

McCune, A. R., Fuller, R. C., Aquilina, A. A., Dawley, R. M., Fadool, J. M., Houle, D., et al. (2002). A low genomic number of recessive lethals in natural populations of bluefin killifish and zebrafish. *Science* 296, 2398–2401. doi: 10.1126/science.1071757

New, M. (1991). Turn of the millennium aquaculture. *World Aquac.* 22, 28–49.

Newkirk, G. F. (1980). Review of the genetics and the potential for selective breeding of commercially important bivalves. *Aquaculture* 19, 209–228. doi: 10.1016/0044-8486(80)90045-9

Newkirk, G. F., Haley, L. E., Waugh, D. L., and Doyle, R. (1977). Genetics of larvae and spat growth rate in the oyster *Crassostrea virginica*. *Mar. Biol.* 41, 49–52. doi: 10.1007/bf00390580

Ohta, H., Kawamoto, T., Isowa, K., Aoki, H., Hayashi, M., Narita, T., et al. (2007). Motility of spermatozoa obtained from testes of Japanese pearl oyster *Pinctada fucata martensii*. *Fish. Sci.* 73, 107–111. doi: 10.1111/j.1444-2906.2007.01308.x

Plough, L. V., and Hedgecock, D. (2011). Quantitative trait locus analysis of stage-specific inbreeding depression in the pacific oyster *Crassostrea gigas*. *Genetics* 189, 1473–1486. doi: 10.1534/genetics.111.131854

Qin, Y. P., Xiao, S., Ma, H. T., Mo, R. G., Zhou, Z. H., Wu, X. W., et al. (2018). Effects of salinity and temperature on the timing of germinal vesicle breakdown and polar body release in diploid and triploid Hong Kong oysters, *Crassostrea hongkongensis*, in relation to tetraploid induction. *Aquac. Res.* 49, 3647–3657. doi: 10.1111/are.13833

Shi, Y. H., Kui, H., Guo, X. M., Gu, Z. F., Wang, Y., and Wang, A. M. (2009). Genetic linkage map of the pearl oyster, *Pinctada martensii* (Dunker): genetic map of *Pinctada martensii*. *Aquac. Res.* 41, 35–44. doi: 10.1111/j.1365-2109.2009.02299.x

Taris, N., Batista, F. M., and Boudry, P. (2007). Evidence of response to unintentional selection for faster development and inbreeding depression in *Crassostrea gigas* larvae. *Aquaculture* 272, S69–S79.

Wada, K. T. (1986). Genetic selection for shell traits in the Japanese pearl oyster, *Pinctada fucata martensii*. *Aquaculture* 57, 171–176. doi: 10.1016/0044-8486(86)90194-8

Wang, J. K. (2017). *Quantitative Genetics*, Vol. 1st edn. Beijing: Science Press.

Wang, Q. H., Deng, Y. W., Du, X. D., Fu, S., and Lu, Y. Z. (2011). Realized heritability and genetic gains of three generation for superior growth in the pearl oyster *Pinctada martensii*. *Acta Ecol. Sin.* 31, 108–111. doi: 10.1016/j.chnaes.2010.12.001

Wang, X. B., Ding, S. Q., Yin, D. D., Song, J., and Chang, Y. Q. (2020). Response to selection for growth in the second generation of two shell color lines of the bay scallop *Argopecten irradians*. *Aquaculture* 528:735536. doi: 10.1016/j.aquaculture.2020.735536

Zhang, H. B., Liu, X., Zhang, G. F., and Wang, C. D. (2007). Growth and survival of reciprocal crosses between two bay scallops, *Argopecten irradians concentricus* Say and *A. irradians irradians* Lamarck. *Aquaculture* 272, S88–S93.

Zhang, Y. H., Ma, H. T., Li, X. Y., Zhou, Z. H., Li, J., Wei, J. K., et al. (2020). Analysis of inbreeding depression on performance traits of three giant clams (*Tridacna derasa*, *T. squamosa*, and *T. crocea*) in the South China Sea. *Aquaculture* 521:735023. doi: 10.1016/j.aquaculture.2020.735023

Zhang, Y. H., Su, J. Q., Li, J., Zhang, Y., Xiao, S., and Yu, Z. N. (2017). Survival and growth of reciprocal crosses between two stocks of the Hong Kong oyster *Crassostrea hongkongensis* (Lam & Morton, 2003) in southern China. *Aquaculture Res.* 48, 2344–2354.

Zhao, L., Liu, L., Liu, B., Liang, J., Lu, Y., and Yang, F. (2019). Antioxidant responses to seawater acidification in an invasive fouling mussel are alleviated by transgenerational acclimation. *Aquatic Toxicol.* 217:105331. doi: 10.1016/j.aquatox.2019.105331

Zhao, L., Shirai, K., Tanaka, K., Milano, S., Higuchi, T., Murakami-Sugihara, N., et al. (2020). A review of transgenerational effects of ocean acidification on marine bivalves and their implications for sclerochronology. *Estuarine Coastal Shelf Sci.* 235:106620.

Zhao, L., Yan, X., Huo, Z., Yang, F., and Zhang, G. (2012). Divergent selection for shell length in the Manila clam, *Ruditapes philippinarum*. *J. World Aquaculture Soc.* 43, 878–884. doi: 10.1111/j.1749-7345.2012.00612.x

Zheng, H. P., Li, L., and Zhang, G. F. (2012). Inbreeding depression for fitness-related traits and purging the genetic load in the hermaphroditic bay scallop *Argopecten irradians irradians* (Mollusca: bivalvia). *Aquaculture* 366, 27–33.

Zheng, H. P., Zhang, G. F., Guo, X. M., and Liu, X. (2008). Inbreeding depression for various traits in two cultured populations of the American bay scallop, *Argopecten irradians irradians* Lamarck (1819) introduced into China. *J. Exp. Mar. Biol. Ecol.* 364, 42–47.

Zheng, H. P., Zhang, G. F., Liu, X., and Guo, X. M. (2006). Sustained response to selection in an introduced population of the hermaphroditic bay scallop *Argopecten irradians irradians* Lamarck (1819). *Aquaculture* 255, 579–585. doi: 10.1016/j.aquaculture.2005.11.037

Conflict of Interest: The authors declare that the research was conducted in the absence of any commercial or financial relationships that could be construed as a potential conflict of interest.

frontiers in Marine Science

BRIEF RESEARCH REPORT
published: 16 February 2022
doi: 10.3389/fmars.2022.841561

AquaGWAS: A Genome-Wide Association Study Pipeline for Aquatic Animals and Its Application to Reference-Required and Reference-Free Genome-Wide Association Study for Abalone

Chao Deng[1†], Wenzhu Peng[2,3,4†], Zhi Ma[1], Caihuan Ke[2,3,4], Weiwei You[2,3,4] and Ying Wang[1,5,3*]*

[1] Department of Automation, Xiamen University, Xiamen, China, [2] State Key Laboratory of Marine Environmental Science, Xiamen University, Xiamen, China, [3] Fujian Key Laboratory of Genetics and Breeding of Marine Organisms, Xiamen, China, [4] College of Ocean and Earth Sciences, Xiamen University, Xiamen, China, [5] Xiamen Key Laboratory of Big Data Intelligent Analysis and Decision, Xiamen, China

OPEN ACCESS

Edited by:
Yinghui Dong,
Zhejiang Wanli University, China

Reviewed by:
Xiaoting Huang,
Ocean University of China, China
Zhiyi Bai,
Shanghai Ocean University, China

***Correspondence:**
Weiwei You
wwyou@xmu.edu.cn
Ying Wang
wangying@xmu.edu.cn

[†]These authors share first authorship

Specialty section:
This article was submitted to Marine Fisheries, Aquaculture and Living Resources, a section of the journal Frontiers in Marine Science

Received: 22 December 2021
Accepted: 17 January 2022
Published: 16 February 2022

Citation:
Deng C, Peng W, Ma Z, Ke C, You W and Wang Y (2022) AquaGWAS: A Genome-Wide Association Study Pipeline for Aquatic Animals and Its Application to Reference-Required and Reference-Free Genome-Wide Association Study for Abalone. Front. Mar. Sci. 9:841561. doi: 10.3389/fmars.2022.841561

Aquaculture is a rapidly growing industry that brings huge economic benefits. Genome-wide association study (GWAS) is critical for aquaculture species' productivity, sustainability, and product quality. The current integrated GWAS pipeline either includes only specific limited steps or requires a complex prerequisite environment and configurations. In this study, we developed AquaGWAS, a highly user-friendly graphical user interface (GUI) GWAS pipeline, by integrating four well-known GWAS models. AquaGWAS is a complete GWAS pipeline from preprocessing, multiple choice of GWAS models, postprocessing to visualizations. AquaGWAS offers GUI easy running on Linux and automatically generates running command lines for high-performance computing (HPC) or non-GUI servers. AquaGWAS is free from installation, configurations, and complicated augment inputs. It offers whole packages of required reference files for 27 common aquatic species. Furthermore, aiming at the issue that the availability of genomic reference sequences limits single-nucleotide polymorphism (SNP) detection, we attempted to detect SNPs in Pacific abalone using classical alignment-based reference-required strategy and *k*-mer-based reference-free strategy combined with downstream AquaGWAS. On 222 resequencing data of Pacific abalone, two strategies detected 221,061 and 230,213 variants, respectively, with 180,161 common variants. The two strategies emphasized different variant situations: capturing variants missed by incomplete or inaccurate reference genomic sequence (*k*-mer-based) and capturing the indel variants having the baseline of genomic sequence (alignment-based). Combining the two strategies offers a complementary framework to obtain the accurate and complete GWAS analysis for non-model organism species. AquaGWAS is available at https://github.com/Ying-Lab/AquaGWAS.

Keywords: GWAS, aquatic animal, integrated pipeline, abalone, *k*-mer-based GWAS

INTRODUCTION

Genome-wide association study (GWAS) effectively identifies genotypic variants associated with particular phenotypic traits. Lots of related tools have been developed to improve the efficiency of GWAS analysis. However, many tools were designed using a specific model or for a certain processing step, which led to fussy file format conversions between various interfaces and frequent switches among different running environments (C/C++, Python, R, etc.). In contrast, the integrated pipeline, such as iPat (Chen and Zhang, 2018), HAPPI GWAS (Slaten et al., 2020), either prerequire a JAVA environment or includes only a single GWAS model, and the complicated augments and options in command lines limit the feasibility for non-computational researchers.

Aquaculture is a rapidly growing industry that brings huge economic benefits (FAO, 2017). GWAS, which is used for exploring molecular markers and mechanisms related to traits, is critical to improving aquaculture species' productivity, sustainability, and product quality. Meanwhile, species-specific single-nucleotide polymorphism (SNP) arrays are still not widely used for aquaculture species. In most cases, species were sequenced and aligned to reference genomic sequence and then genotyped using a *vcf* format file (Jiang et al., 2019; Wu et al., 2019). Three obstructions limit the feasibility of the GWAS study: (1) Most marine biologists have a limited background in modeling and bioinformatics. At the same time, it is hard for them to switch among different running environments, convert fussy file formats, and handle command lines with complex augments and different models. (2) Due to the diversity of aquaculture species, there is no common data format and there are a few available public databases. In that way, annotation and reference information requires extra manual operations. (3) A large amount of non-model aquaculture animals, novel species, or species are hard to detect SNPs because of lack of reference genomes or incomplete genome. Therefore, it is necessary to develop environment-friendly software to resolve these problems.

This study developed AquaGWAS, a highly integrated GWAS analysis pipeline with a full reference package, including 27 aquatic species. AquaGWAS offers an easy-to-use graphic user interface (GUI) for stand-alone Linux server running mode and an automatic command-generator on Windows for HPC job-submission running mode. Free from complex installation and configurations, AquaGWAS is compatible with various file formats and highly friendly to users with a non-computational background.

Furthermore, to implement GWAS analysis for aquaculture species without a reference genome or only with an incomplete genome, we attempted to detect SNPs for Pacific abalone *Haliotis discus hannai* using classical alignment-based reference-required strategy and *k*-mer-based reference-free strategy. The two strategies were implemented using AquaGWAS combined with upstream alignment-based [Bowtie2 (Langmead and Salzberg, 2012) SAMtools and BCFtools (Danecek et al., 2021)] and *k*-mer-based [DISCOSNP (Uricaru et al., 2015)] pipelines. Based on 222 genomic resequencing data of Pacific abalones, the two strategies detected 221,061 and 230,213 variants, respectively, with 180,161 common variants. The detected variants belonged to 2,048 and 2,068 genes, respectively, with 2,046 common gene resolutions. The two strategies were highly consistent in both gene and nucleotide resolutions. With MWR $\left(\frac{\text{Foot muscle weight}}{\text{Wet weight}}\right)$ and SLW $\left(\frac{\text{Shell length}}{\text{Shell width}}\right)$ as traits, the two strategies captured four and five common-associated SNPs using AquaGWAS. The two strategies have clear advantages and limitations due to their basic principle and have explicit complementation during the GWAS analysis.

MATERIALS AND METHODS

Data Acquisition of the Pacific Abalone

The Pacific abalone used in this study contained a total of 222 individuals randomly selected from 10 families (Peng et al., 2021). Two growth-related traits (the ratio of foot muscle weight divided by wet weight, MWR, and the ratio of shell length divided by shell width, SLW) were measured and calculated after 2.5 years of culture. The genotypic data were generated using whole-genome sequencing (WGS) technology. Sequence reads for each sample were quality controlled using an in-house Perl script with a total of 2,408.162 Gb clean data remaining. The average sequencing depth for each sample was 7.75×.

Framework of AquaGWAS

Currently, AquaGWAS integrates widely used GWAS tools within a GUI on Linux to perform a complete GWAS analysis pipeline for aquatic animals using various SNP files, *vcf*, *ped/map*, *tped/tfam,* and *bed/bim/fam* as inputs. AquaGWAS contains five functional modules: (1) GWAS; (2) linkage disequilibrium (LD) decay analysis; (3) visualization with principal component analysis (PCA), Manhattan plot, and quantile-quantile (Q-Q) plot; (4) gene structural annotation; and (5) gene functional annotation. After integrating the reference sequences, structural annotation, and function annotation information from 27 aquatic species, AquaGWAS can implement the complete GWAS analysis for these aquatic species without extra reference databases.

The framework of AquaGWAS is shown in **Figure 1**. The input to AquaGWAS was phenotype data and SNP information data. The SNP information data, generally containing *genotype* and *map*, were compatible with the following commonly used file formats: (1) *vcf*, (2) *ped/map*, (3) *tped/tfam*, and (4) *bed/bim/fam*. Quality control (QC) was performed for SNP input files. The optional files included covariate and kinship files, which would be the additional information for GWAS analysis models and postprocessing for gene structural or functional annotation, respectively. The output included *p*-values of SNPs, Manhattan plot, Q-Q plot, PCA plot, LD decay plot, and the following structural annotations and functional annotations.

Implementation of AquaGWAS

The GWAS of AquaGWAS offered a linear model and a regression model from PLINK (Purcell et al., 2007), a linear mixed model (LMM, also called MLM) from GEMMA (Zhou and Stephens, 2012), and an efficient mixed-model association (EMMA) from EMMAX (Kang et al., 2010). Meanwhile, QC

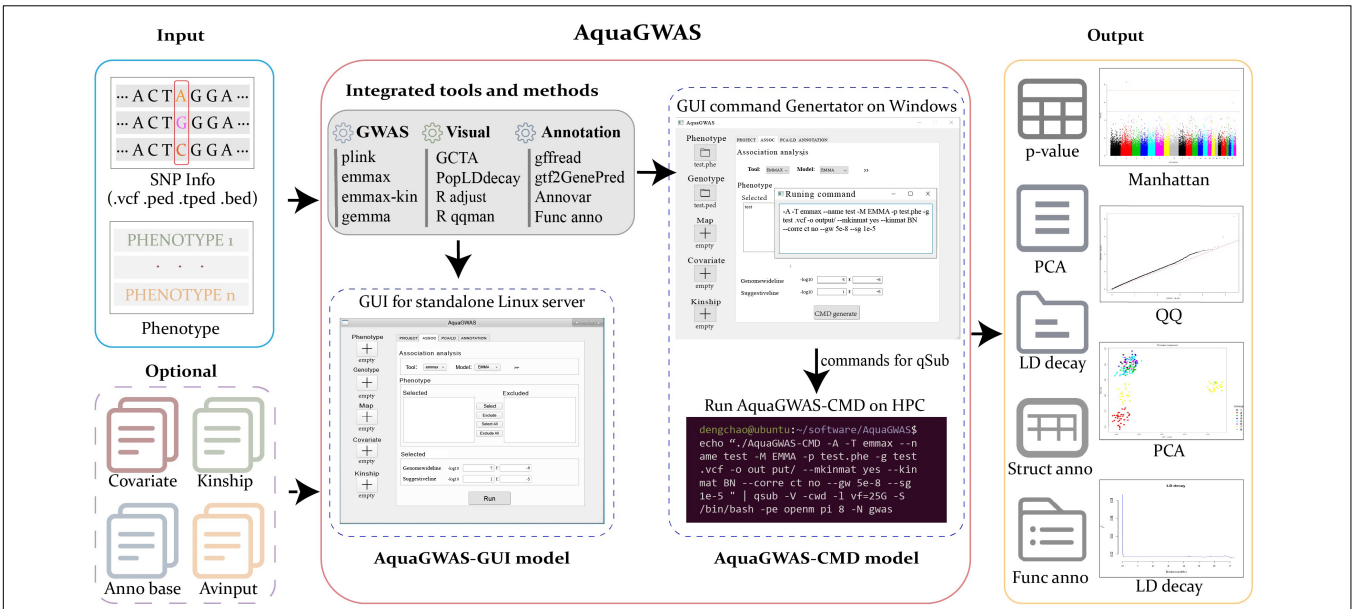

FIGURE 1 | The framework of AquaGWAS. AquaGWAS is compatible with several SNP information file formats, *vcf*, *ped/map*, *tped/tfam*, and *bed/bim/fam*. Several widely used GWAS tools, preprocessing and postprocessing, visualizations, and structural and functional annotations are integrated seamlessly, and output textual and visual analyzing results.

was achieved through PLINK. The PopLDdecay (Zhang et al., 2018) and GCTA (Yang et al., 2011) were used for LD decay analysis and PCA analysis of AquaGWAS, respectively. Regarding the structural annotation, it was achieved using Annovar (Wang et al., 2010). In addition, the gffread and gtfToGenePred (Pertea and Pertea, 2020) helped to automatically generate the input file of Annovar. Then, some custom functions were used for functional annotation to extract the response gene annotation information directly from the gene functional annotation database file by gene ID.

The tools integrated by AquaGWAS, such as PLINK and GEMMA, include multiple small functions. Additionally, some of them might not be required for GWAS analysis. In AquaGWAS, we only integrated the required function packages and offered the corresponding parameter options in GUI. The fixed parameters are predetermined in the code. For more flexible parameters and options, we welcome more voices, and we will always update and improve AquaGWAS according to the user's feedback.

Alignment-Based Reference-Required and *k*-mer-Based Reference-Free Genome-Wide Association Study

Different from the plant and livestock, many aquatic animals do not have genomic reference sequences or only have an incomplete genomic sequence, which limits the accurate and complete GWAS analysis for these species. Therefore, using Pacific abalone as an example, we implemented classical alignment-based reference-required GWAS (called alignment-based) and *k*-mer-based reference-free GWAS (called *k*-mer-based) and combined AquaGWAS with two different upstream strategies, as shown in **Figure 2**. The alignment-based strategy refers to the classical GWAS processing pipeline. It aligns the genomic sequencing reads to reference genomic sequences using sequence alignment tools, such as Bowtie (Langmead et al., 2009) or BWA (Li and Durbin, 2009). The alignment results were then sorted and filtered using SAMtools and BCFtools to call the candidate genetic variants. The *k*-mer-based strategy was implemented using DISCOSNP, which calls the candidate variants free from the genomic reference sequence. DISCOSNP detects SNPs with a *k*-mer comparison based on a *de Bruijn* graph. It is a directed graph that contains all the *k*-mers present in the read dataset as vertices, and all the possible $(k-1)$ overlaps between *k*-mers as edges. Then, for each such couple of *k*-mers starting with the same $k-1$ length prefix, if both paths cannot be right extended with the same nucleotide, the bubble was discarded, and only isolated SNPs can be detected. Then, the detected *k*-mers with SNPs were assembled into contigs, and the whole procedure was free from the genomic reference sequence. The detail of DISCOSNP can be found in the study by Uricaru et al. (2015). The variants calling files from the above two strategies were input into AquaGWAS for GWAS, with MWR and SLW as traits.

RESULTS

Functions of AquaGWAS

There are several functions for AquaGWAS. First, AquaGWAS offers the thresholds to exclude individuals with too much missing genotype data, SNPs with too small minor allele frequency (MAF), and SNPs with too large missing genotype rate. Users are free to select none/some/all these parameters, and the parameters (window size, step length, and r^2 threshold) for

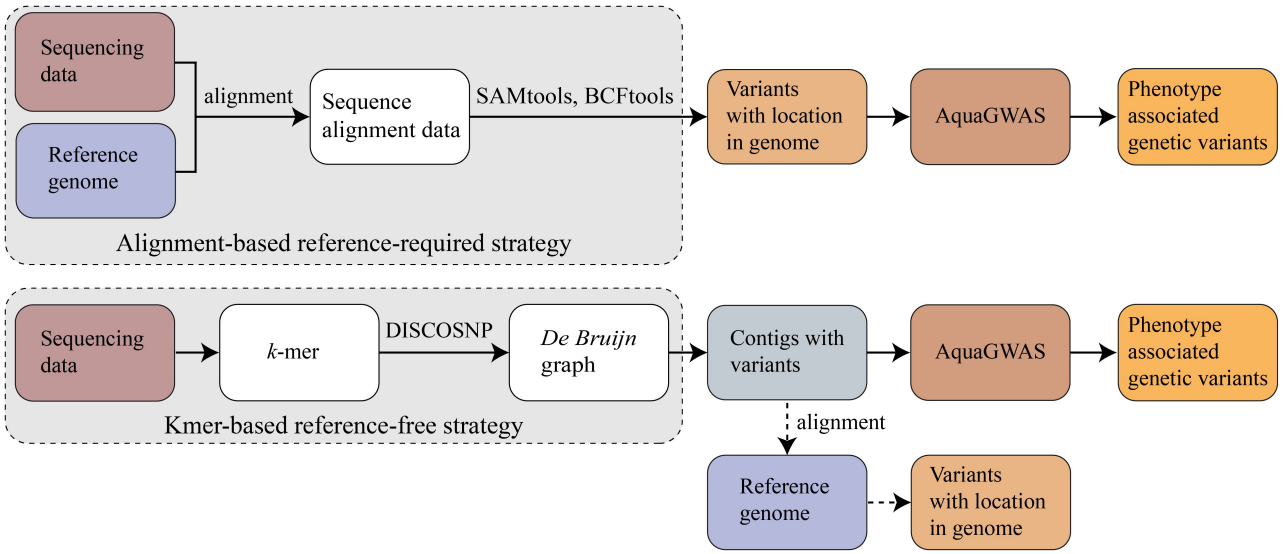

FIGURE 2 | The two different upstream strategies, namely, alignment-based reference-required and *k*-mer-based reference-free, combined AquaGWAS for genome-wide association study (GWAS). The alignment-based strategy aligns the genomic sequencing reads to reference genomic sequences and then calls the candidate genetic variants. Additionally, the *k*-mer-based strategy calls the candidate variants free from reference genomic sequence with a *k*-mer comparison based on a de *Bruijn* graph. The variants calling files from the above two strategies are input into AquaGWAS for GWAS.

data filtering using linkage disequilibrium are also allowed to be selected and set.

Second, PLINK, GEMMA, and EMMAX are integrated by AquaGWAS for GWAS. Users can input single phenotype or multiple phenotype files for association analysis, and the kinship and covariates can be used as optional inputs to control false positive analysis results. The analysis results are visualized using the Manhattan plot and Q-Q plot. Users can also get the results of population genetic diversity of samples and linkage disequilibrium decay analysis, which are subsequently implemented using GCTA and PopLDdecay, and then visualized using PCA and LD plots.

Third, the process of annotation was divided into two steps, structure annotation and function annotation. Among these, the first step abstracted information of SNPs above the threshold [–log (10–5) by default] from the *vcf* file and then converted it into the file needed for gene structural and functional annotation. Structural annotations offer exon regions such as variant functions, types, amino acid changes, and all the genes and positions of the mutations. Additionally, the functional annotation is realized on the gene functional annotation database of corresponding species.

Features of AquaGWAS

AquaGWAS is an easy and user-friendly software for analyzing aquatic animals with non-commonly used reference genome databases and rare information in public databases, which makes it difficult for analyses by regular software and pipeline. Several features of the AquaGWAS are as follows.

First, AquaGWAS is free from any installation and environmental configuration, which offers the executable file to be run directly.

Second, AquaGWAS offers a user-friendly GUI. To begin with, encapsulating the entire tedious process, AquaGWAS offers an intuitive parameter setting interface. Furthermore, in AquaGWAS, users can switch among various tools smoothly and seamlessly during the analysis process, free from complicated file format conversions between interfaces, complicated command lines with tedious running arguments, and file folder switching.

Third, AquaGWAS automatically generate a command line in HPC. For HPC users, jobs are required to submit with command lines, where the direct running on the graphic interface is not available. Therefore, AquaGWAS also offers GUI automatic command-line generator on Windows so that users can submit the job with the generated command line on Windows conveniently.

Finally, AquaGWAS is compatible with various file formats. Because different GWAS tools support various file formats, AquaGWAS automatically converts the input file according to the selected tool. For example, although EMMAX only supports *tped/tfam* files, users can choose *vcf*, *ped/map*, or *bed/bim/fam* in AquaGWAS for analysis using EMMAX through automatic file format conversion. AquaGWAS also supports the automatic loading of multiple files with the same prefix filename under the same folder. For example, if the input file is of *ped/map* or *tped/tfam* format, users can choose to input only *ped* or *tped* file. AquaGWAS will automatically load the associated *map* or *tfam* file under the same path with the same prefix of the filename.

Meanwhile, because the AquaGWAS is a pipeline that integrates the current widely used GWAS analyzing tools, the upper limit of the amount of running data is determined by the selected tool during the

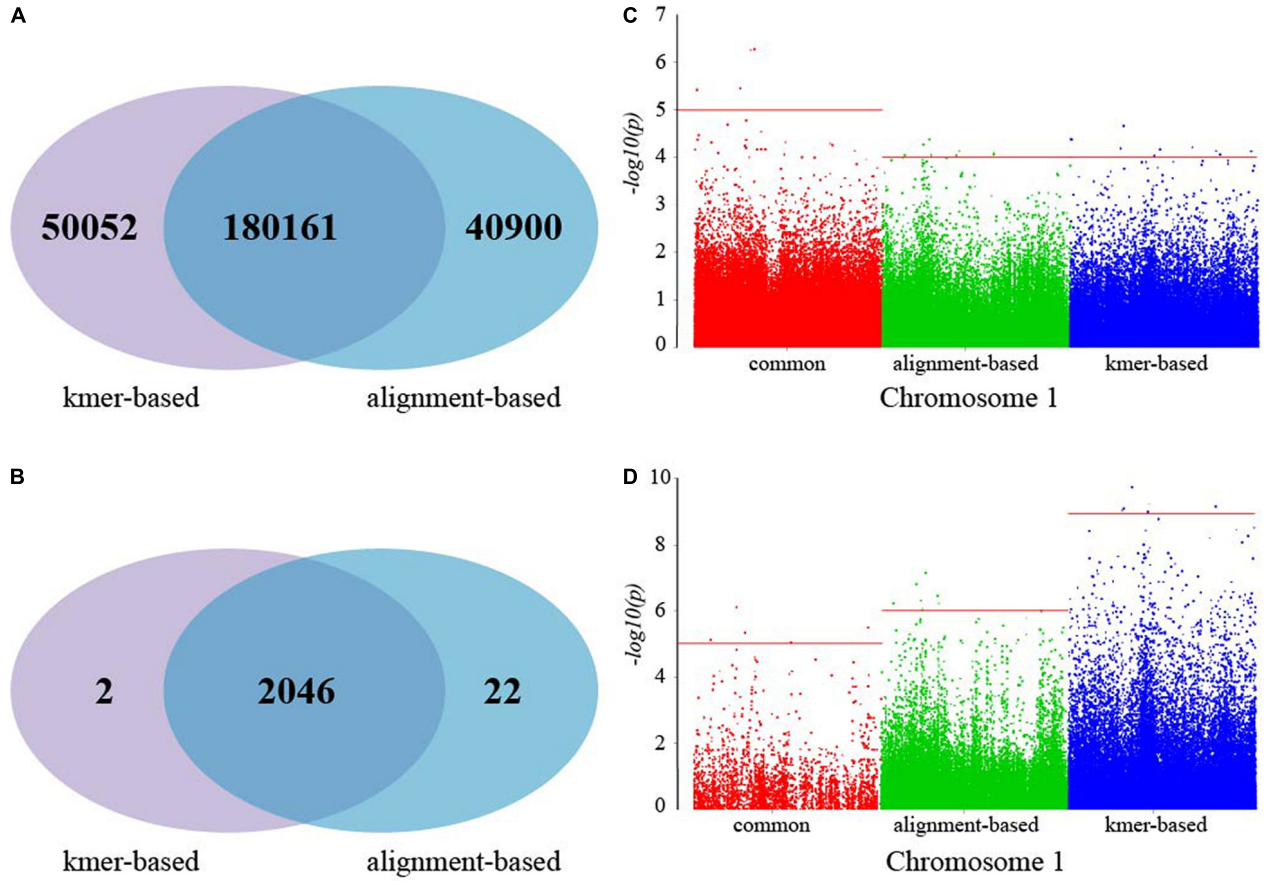

FIGURE 3 | The comparison of the results from the alignment-based and the *k*-mer-based strategies. **(A)** The Venn diagram of candidate variants from *k*-mer-based and alignment-based strategies; **(B)** the Venn diagram of genes including variants from *k*-mer-based and alignment-based strategies; **(C)** the Manhattan plots for MWR traits from common, alignment-based, and *k*-mer-based SNPs; **(D)** the Manhattan plots for SLW traits from common, alignment-based, and *k*-mer-based SNPs.

AquaGWAS running and the hardware of the running server.

Genome-Wide Association Study for Pacific Abalone

The alignment-based and *k*-mer-based strategies were applied for GWAS analysis of Pacific abalone using 222 genomic resequencing data. Using Chromosome 1 as an example, the alignment-based and *k*-mer-based methods detected 221,061 and 230,213 variants, respectively. To compare the results from the two strategies, the contigs from the *k*-mer-based strategy were aligned to the reference genome of the Pacific abalone, and the corresponding position in Chromosome 1 was obtained. Compared with the genetic variants from the alignment-based method, 180,161 common variants were detected by the two strategies, as shown in the Venn diagram in **Figure 3A**. The 50,052 variants detected by *k*-mer-based but missed from alignment-based were partly caused by incomplete or inaccurate genomic reference sequences. In contrast, the *k*-mer-based method also missed 40,900 variants found by the alignment-based method, which is probably caused by the structural insert and delete due to the *de Bruijn* assembly errors caused by low reads coverage, repeat sequences, and short overlaps. Considering the genes corresponding to SNP, the intersection number of genes detected by kmer-based (2048) and alignment-based (2068) is 2046, as shown in the Venn diagram in **Figure 3B**.

The variant calling files from the two strategies were input into AquaGWAS. The *k*-mer-based method used $p-\text{value} \leq 10^{-4}$ and $p-\text{value} \leq 10^{-9}$ to screen the significant SNPs of MWR and SLW and obtained 10 and 6 significant SNPs, respectively. For the alignment-based method, 11 and 8 significant SNPs were obtained by using a $p-\text{value} \leq 10^{-4}$ and $p-\text{value} \leq 10^{-5}$ of MWR and SLW. Using $p-\text{value} \leq 10^{-5}$, there are 4 and 5 common SNPs associated with MWR and SLW traits detected by both alignment-based and *k*-mer-based methods, which are shown in **Figures 3C,D**. The detailed analysis results are presented in **Supplementary Table 1**.

To compare the variants detected by two strategies elaborately, the contigs, including variants detected by alignment-based strategy and the *k*-mers detected by variants from the *k*-mer-based strategy, are aligned to the genomic sequences of Pacific

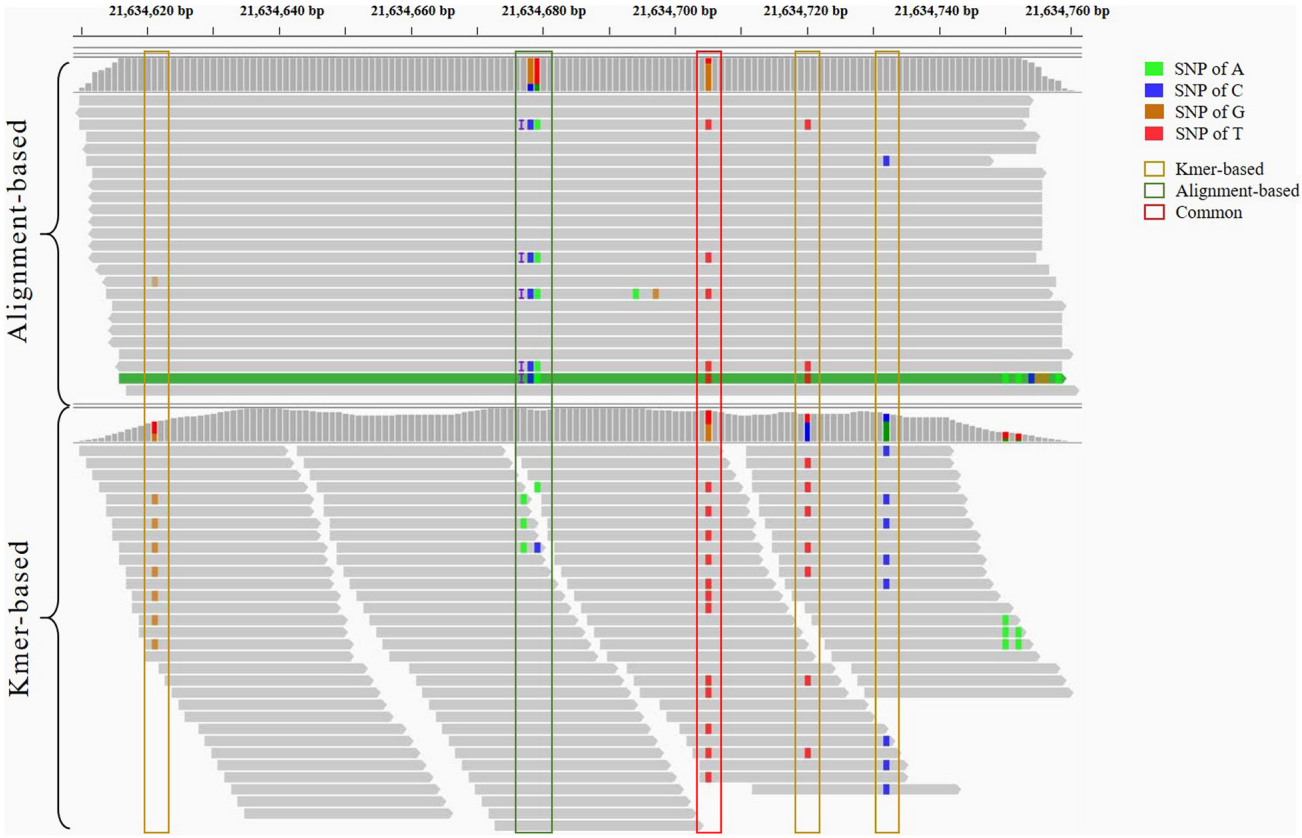

FIGURE 4 | The detailed comparison of genetic variants detected by the alignment-based and *k*-mer-based strategies. Both strategies detect the variant in the red border. Furthermore, the variants in yellow borders are detected only by *k*-mer-based strategy. The variant and insertion in the green border are detected only by alignment-based strategy.

abalone. Because a reference sequence is required, we only gave the situations that both the *k*-mers and reads can be aligned to the reference genomic sequences shown in **Figure 4**. The genomic region from *chromosome 1:21634620-21634760* is selected and viewed on Integrative Genomics Viewer (IGV) (Robinson et al., 2011). The variant in the red border is detected by both strategies. Additionally, the variants in yellow borders are detected only by *k*-mer-based strategy. The variant and insertion in the green border are detected only by alignment-based strategy. The two strategies emphasized different variant situations. After tracing back to the original variant detection process, we found *k*-mer-based method can capture variants missed by incomplete or inaccurate reference genomic sequences. In contrast, an alignment-based strategy can capture the insertion or deletion having the baseline of genomic sequence. Therefore, the two strategies have explicit complementation for GWAS analysis.

CONCLUSION AND DISCUSSION

The current integrated GWAS pipeline either includes only specific limited steps or requires a complex prerequisite environment and configurations. AquaGWAS offers GUI easy running for stand-alone Linux servers and an automatic command line generator for HPC or non-GUI servers. AquaGWAS integrated complete GWAS pipeline from preprocessing, multiple choice of GWAS models, postprocessing to visualizations. Furthermore, AquaGWAS is highly friendly to users of non-computational background, which is free from installation, configurations, and complicated augments input. AquaGWAS is compatible with various frequently used SNP file formats and can be applied to several species, especially aquatic animals. AquaGWAS offers whole packages of required reference files for 27 common aquatic species to implement the express aquaculture GWAS analysis without any extra reference inputs.

The experiment shows that the *k*-mer-based strategy can capture the variants, which are missed because of the incomplete or inaccurate reference genomic sequences. However, the *k*-mer-based reference-free strategy also missed SNPs, which are found by the classical reference-alignment strategy. The two strategies have clear advantages and limitations due to their basic principle and have explicit complementation during the GWAS analysis.

Our exploration not only offers an option to study the genetic variants for non-model organism species, novel species, or species without genomic reference sequence but also provides a complementary framework for accurate and complete GWAS analysis.

DATA AVAILABILITY STATEMENT

The data analyzed in this study is subject to the following licenses/restrictions: The dataset is on another ongoing manuscript, which will be public available after that manuscript is published. Requests to access these datasets should be directed to WY, 109852383@qq.com.

AUTHOR CONTRIBUTIONS

YW, WY, and CK planned the project. CD and ZM finished the programming. WP designed the processing steps of GWAS. WP, CD, and ZM tested the software. YW and CD designed the experiments. YW, CD, and WP wrote the main manuscript. All the authors read and approved the final manuscript.

FUNDING

This study was supported by the National Natural Science Foundation of China (62173282, U1605213, and 31872564), the National Key Research and Development Program of China (2018YFD0901401), Fujian Provincial S&T Project (2019N0001 and 2017FJSCZY02), Open Fund of Engineering Research Center for Medical Data Mining and Application of Fujian Province (MDM2018002), and Natural Science Foundation of Fujian (2018J01097).

ACKNOWLEDGMENTS

We thank W. He, S. Fang, and T. Wu from the Information and Network Center of Xiamen University for their help with GPU computing.

SUPPLEMENTARY MATERIAL

The Supplementary Material for this article can be found online at: https://www.frontiersin.org/articles/10.3389/fmars.2022.841561/full#supplementary-material

REFERENCES

Chen, C. J., and Zhang, Z. (2018). iPat: intelligent prediction and association tool for genomic research. *Bioinformatics* 34, 1925–1927. doi: 10.1093/bioinformatics/bty015

Danecek, P., Bonfield, J. K., Liddle, J., Marshall, J., Ohan, V., Pollard, M. O., et al. (2021). Twelve years of SAMtools and BCFtools. *GigaScience* 10:8. doi: 10.1093/gigascience/giab008

FAO (2017). *Genome-Based Biotechnologies in Aquaculture*. Rome: Food and Agriculture Organization of the United Nations, 2–3.

Jiang, D. L., Gu, X. H., Li, B. J., Zhu, Z. X., Qin, H., Meng, Z. N., et al. (2019). Identifying a long QTL cluster across chrLG18 associated with salt tolerance in tilapia using GWAS and QTL-seq. *Mar. Biotechnol.* 21, 250–261. doi: 10.1007/s10126-019-09877-y

Kang, H. M., Sul, J. H., Service, S. K., Zaitlen, N. A., Kong, S.-Y., Freimer, N. B., et al. (2010). Variance component model to account for sample structure in genome-wide association studies. *Nat. Genet.* 42, 348–354. doi: 10.1038/ng.548

Langmead, B., and Salzberg, S. L. (2012). Fast gapped-read alignment with Bowtie 2. *Nat. Methods* 9, 357–359. doi: 10.1038/nmeth.1923

Langmead, B., Trapnell, C., Pop, M., and Salzberg, S. L. (2009). Ultrafast and memory-efficient alignment of short DNA sequences to the human genome. *Genome Biol.* 10:R25. doi: 10.1186/gb-2009-10-3-r25

Li, H., and Durbin, R. (2009). Fast and accurate short read alignment with Burrows–Wheeler transform. *Bioinformatics* 25, 1754–1760. doi: 10.1093/bioinformatics/btp324

Peng, W., Yu, F., Wu, Y., Zhang, Y., Lu, C., Wang, Y., et al. (2021). Identification of growth-related SNPs and genes in the genome of the Pacific abalone (*Haliotis discus hannai*) using GWAS. *Aquaculture* 541:736820. doi: 10.1016/j.aquaculture.2021.736820

Pertea, G., and Pertea, M. (2020). GFF utilities: GffRead and GffCompare. *F1000Research* 9:23297. doi: 10.12688/f1000research.23297.1

Purcell, S., Neale, B., Todd-Brown, K., Thomas, L., Ferreira, M. A., Bender, D., et al. (2007). PLINK: a tool set for whole-genome association and population-based linkage analyses. *Am. J. Hum. Genet.* 81, 559–575. doi: 10.1086/519795

Robinson, J. T., Thorvaldsdóttir, H., Winckler, W., Guttman, M., Lander, E. S., Getz, G., et al. (2011). Integrative genomics viewer. *Nat. Biotechnol.* 29, 24–26. doi: 10.1038/nbt.1754

Slaten, M. L., Chan, Y. O., Shrestha, V., Lipka, A. E., and Angelovici, R. (2020). HAPPI GWAS: holistic analysis with Pre- and Post-integration GWAS. *Bioinformatics* 36, 4655–4657. doi: 10.1093/bioinformatics/btaa589

Uricaru, R., Rizk, G., Lacroix, V., Quillery, E., Plantard, O., Chikhi, R., et al. (2015). Reference-free detection of isolated SNPs. *Nucleic Acids Res.* 43:e11. doi: 10.1093/nar/gku1187

Wang, K., Li, M., and Hakonarson, H. (2010). ANNOVAR: functional annotation of genetic variants from high-throughput sequencing data. *Nucleic Acids Res.* 38:e164. doi: 10.1093/nar/gkq603

Wu, L., Yang, Y., Li, B., Huang, W., Wang, X., Liu, X., et al. (2019). First genome-wide association analysis for growth traits in the largest coral reef-dwelling bony fishes, the giant grouper (*Epinephelus lanceolatus*). *Mar. Biotechnol.* 21, 707–717. doi: 10.1007/s10126-019-09916-8

Yang, J., Lee, S. H., Goddard, M. E., and Visscher, P. M. (2011). GCTA: a tool for genome-wide complex trait analysis. *Am. J. Hum. Genet.* 88, 76–82. doi: 10.1016/j.ajhg.2010.11.011

Zhang, C., Dong, S., Xu, J., He, W., and Yang, T. (2018). PopLDdecay: a fast and effective tool for linkage disequilibrium decay analysis based on variant call format files. *Bioinformatics* 35, 1786–1788. doi: 10.1093/bioinformatics/bty875

Zhou, X., and Stephens, M. (2012). Genome-wide efficient mixed-model analysis for association studies. *Nat. Genet.* 44, 821–824. doi: 10.1038/ng.2310

Conflict of Interest: The authors declare that the research was conducted in the absence of any commercial or financial relationships that could be construed as a potential conflict of interest.

Publisher's Note: All claims expressed in this article are solely those of the authors and do not necessarily represent those of their affiliated organizations, or those of the publisher, the editors and the reviewers. Any product that may be evaluated in this article, or claim that may be made by its manufacturer, is not guaranteed or endorsed by the publisher.

frontiers in Marine Science

ORIGINAL RESEARCH
published: 23 February 2022
doi: 10.3389/fmars.2022.843312

SSR Marker-Based Genetic Resource Assessment of the Rainbow Clam *Moerella iridescens* Along the Coasts of China: Implications for Strategy of Conservation Management

*Xiaoying Li[1,2,3], Shan Gao[1,2,3], Manman Zhao[1,2,3] and Zhiguo Dong[1,2,3]**

[1] Jiangsu Key Laboratory of Marine Bioresources and Environment, Jiangsu Ocean University, Lianyungang, China, [2] Co-Innovation Center of Jiangsu Marine Bio-industry Technology, Jiangsu Ocean University, Lianyungang, China, [3] Jiangsu Key Laboratory of Marine Biotechnology, Jiangsu Ocean University, Lianyungang, China

OPEN ACCESS

Edited by:
Zhongming Huo,
Dalian Ocean University, China

Reviewed by:
Zulin Zhang,
The James Hutton Institute, United Kingdom
Zhiyi Bai,
Shanghai Ocean University, China

***Correspondence:**
Zhiguo Dong
dzg7712@163.com

Specialty section:
This article was submitted to Marine Fisheries, Aquaculture and Living Resources, a section of the journal Frontiers in Marine Science

Received: *25 December 2021*
Accepted: *24 January 2022*
Published: *23 February 2022*

Citation:
Li X, Gao S, Zhao M and Dong Z (2022) SSR Marker-Based Genetic Resource Assessment of the Rainbow Clam Moerella iridescens Along the Coasts of China: Implications for Strategy of Conservation Management. Front. Mar. Sci. 9:843312. doi: 10.3389/fmars.2022.843312

This study aims to determine the genetic structure of rainbow clam *Moerella iridescens* in different sea areas of China. Seventeen pairs of microsatellite primers (SSR) were used to amplify the SSRs of rainbow clam in Lianyungang of Haizhou Bay, Chongming of Shanghai, Ningde of Fujian, Daishan of Zhoushan, and Cixi and Wenzhou of Zhejiang. A total of 1,146 alleles were detected in 310 individuals from the 17 SSR loci. The average observed heterozygosity of six populations was 0.4381−0.6139, the average expected heterozygosity was 0.5897−0.7325, and the average Shannon diversity index was 1.2655−1.7998. The clams exhibited rich genetic diversity, and the F_{ST} of the genetic differentiation index of the six populations was 0.0470, indicating low genetic differentiation among the populations. The results indicated that rainbow clams along the coasts of China exhibited high diversity and low population differentiation.

Keywords: *Moerella iridescens*, SSR, genetic diversity, China coasts, conservation management

HIGHLIGHTS

- This study aims to determine the genetic structure and diversity of rainbow clam *Moerella iridescens* in different sea areas of China.
- The clams exhibited rich genetic diversity and the F_{ST} of the genetic differentiation index of the six populations was 0.0470, indicating low genetic differentiation amongst the populations.
- The results indicated that rainbow clam along China coasts exhibited high diversity and low population differentiation.

INTRODUCTION

The rainbow clam *Moerella iridescens* is an economically important small-sized marine clam due to its delicious taste and high nutritional value. The clam is mainly distributed on the West Pacific coast and northern Australia. In recent years, the rainbow clam has been increasingly used as high-valued seafood and is preferred by consumers of China, and the output of the rainbow

TABLE 1 | Sampling time, place, and sample size of rainbow clam.

Stock	LYG	CM	ND	ZS	CX	WZ
Sampling time	2012·10	2012·10	2012·10	2012·10	2012·10	2012·10
Number of samples	50	50	50	50	50	50
Sampling site	Sanyang harbor, Haizhou Bay	East beach, Chongming Island	Xiabaishi, Sansha Bay in Fu'an	Datian Bay, Daishan, Zhoushan	Cixi Sanbei shoal, Hangzhou Bay	Simon Island, Yueqing Bay
GPS	E119.2835 N34.7996	E122.0058 N31.5316	E119.6263 N26.7948	E122.2095 N30.2888	E121.4337 N30.2998	E121.2031 N28.3229

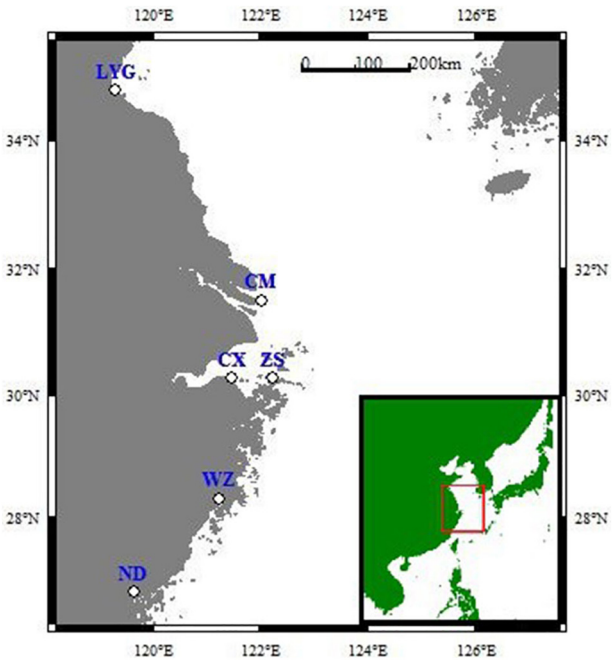

FIGURE 1 | Sample collection map of rainbow clams in coastal China.

clams mainly comes from marine fishing. However, in the past 2 years, the development of the shrimp and crab aquaculture industry and the overfishing of wild rainbow clams have exacerbated the destruction of the habitat of rainbow clams. Moreover, the status of genetic diversity of the germplasm resources of rainbow clams remains unclear. Thus, the protection of rainbow clam resources is of great importance. Several authors have explored the biological characteristics and morphological differences of rainbow clams (Ji et al., 2007; Lv et al., 2012). To date, however, reports on the genetic diversity and relationships among clam populations are limited (Xu et al., 2016).

Microsatellites, also known as simple repetitive sequences (SSRs), present the advantages of co-dominance, single locus, high polymorphism, and easy operation and can be screened from different populations to complete genetic diversity studies (Cui et al., 2011). Microsatellite marker technology has been widely used in the structural analysis of the population genetics of aquatic animals, e.g., the rainbow trout (Zhao et al., 2010), the scallop *Patinopecten yessoensis* (Chang et al., 2007), and the triangle pearl *Hyriopsis cummingii* (Bai et al., 2015). So far, few reports are available on the genetic diversity of the population of rainbow clams. In the present study, the genetic diversity of six populations of rainbow clams in Lianyungang, Chongming Island, Ningde, Zhoushan, Cixi, and Wenzhou was analyzed by using microsatellite markers. The results obtained can provide a scientific basis for assessing germplasm resources and genetic diversity protection of rainbow clams.

MATERIALS AND METHODS

Materials

Rainbow clams were collected from the six coastal mudflats, namely, Lianyungang Haizhou Bay (LYG), Chongming Island Dongtan (CM), Ningde Fu'an (ND), Zhoushan Daishan (ZS), Hangzhou Bay Cixi (CX), and Wenzhou Yueqing Bay (WZ). Fifty samples were randomly obtained from each population. Information on the samples collected is presented in **Table 1** and **Figure 1**. The sampled rainbow clams were stored at −70°C until analysis.

Microsatellite Primer

The M13 (−21) universal primer sequence of 5′-TGTAAAACGACGGCCAGT-3′ reported by Schuelke (2000) was adopted in this study to elongate short primers for economic consideration in genotyping. We used two fluorescent labels, FAM and HEX, for forwarding primes, which were abbreviated as FAM-M13 and HEX-M13. Nineteen SSRs were used for PCR, and the information of these primers is shown in **Table 2**.

Method

Total DNA was extracted with the sodium dodecyl sulphate (SDS) phenol-chloroform method and according to the detailed protocol for the DNA extraction as previously described by Li et al. (2020). The PCR system and program in this study was done as previously described by Zhang et al. (2019). Specifically, the used PCR system consisted of 1 μl of template DNA (about 30 ng), 2 μl of primer mix, 1 μl of universal fluorescent primers, 10 μl of 2 × Taq PCR Master Mix (TaKaRa, Dalian, China), and 6 μl of ddH_2O to form a total volume of 20 μl. The PCR program was as follows: pre-denaturation at 90°C for 5 min, 30 cycles, denaturation at 94°C for 3 min, annealing at 53°C for 1 min

TABLE 2 | Microsatellite primer information.

SSR	Repeat motif	Sequence (5′–3′)*	Size of original fragment/bp	(Tm)/°C
HGZ2	(AC)17(CA)11	F: TGAGGTGGAATGAGTTAC R: TAAGTTCGGATGACAAAG	124	45
HGZ3	(GT)22	F: ATGGGAGACAACTCGCTAC R: CTGTCACAACGGCAATCT	353	52
HGZ6	(TG)4	F: GGGCCAAATCAGGGAATG R: AGCAGGAAACGCAGCACA	103	58
HGZ9	(AC)9(AC)7(CA)7	F: CAGCCTGGGCAACATAGT R: TAGGACCACAGGTAAGCATC	116	53
HGZ10	(GT)6(GT)8(GT)6	F: AGGTAGGGCGTGAAGGAA R: GCAAAATCGACCCTACTACATA	193	55
HGZ14	(CA)6	F: ACTAGTACGTGAAGATTAGCCAA R: GAGGCGATACTCATAATGTTCA	338	55
HGZ17	(AC)26(CA)21	F: ATGAGAGAGCGACAGAATG R: TAGAGGCTCCCTAAATGG	150	50
HGZ22	(GA)19(AG)12	F: TTTCCACTTCGCACATTG R: CTCGCACAAACAAATGAAC	196	52
Mir8	(GT)15	F: GTAGGTTTGGCATGGCTTTGTAGC R: ACCATTGAGGGCTCGTCTGAATTAT	124	64
Mir12	(AG)16	F: TCACCAGAAAGGAGACCGTAAAAGT R: CTACGGATTTCGCAGTGAAAATGT	120	63
Mir13	(AC)15	F: GCAACACAACGAGAGTG R: ACAACAAACAACAAAGAAAT	116	47
Mir14	(CT)4	F: ATCGTTGGGGCATTCTAGTTTTCT R: GGGTATAATAATTTTGAAACGCAGC	83	62
MH19A	(TG)28	F: GTGAGCAGGAATCAAAGGTG R: CTCCGCTCTGTTTGCCTAT	105–145	55
Mi44A	(TG)61	F: CCTCGGAGACCATTCGCTAC R: TGCTTTTCTATGACAACCCT	85–101	52
MW33A	(TG)13TA(TG)5(CG)2TGCG	F: TTCCTATCCTTACCCTTG R: CTGACTGGAAACTCAACAC	111–171	48
MW15A	(CA)24	F: GATCAAAATTGACAAGGCT R: AAGACAAACACGGATGGT	88–150	46
MX39C	TGTT(TG)6(GG)4GT	F: CCCAACCAGAATAATACCA R: TCCAACAAAGGAATACGATA	200–220	48
MY36B	(TG)7(GG)3	F: CCGTTGGTAAAGACGATAT R: TGGTTGCGAGTTGGACAC	251–283	58
MZT46B	(TG)75	F: GACATAAAGGTTGTAGGGA R: ATGGTAGTGATGATGCTTG	151–283	46

**Primers of forward sequence tailed with universal M13 (–21) sequences (5′-TGTAAAACGACGGCCAGT-3′) at their 5′ ends.*

and at 72°C for 30 s, and a final extension at 72°C for 10 min at the end of the cycle. The PCR products were subjected to capillary electrophoresis, and the electrophoresis patterns were genotyped by GeneMapper 3.7 and Peak Scanner software.

Data Processing

Pop32 software was utilized to calculate the number of effective alleles (*Ne*), expected heterozygosity (*He*), observed heterozygosity (*Ho*), and gene flow ($Nm = 1- F_{ST}/4 F_{ST}$, where the F_{ST} represent genetic differentiation index), genetic distance (*Ds*), and Shannon diversity index (Raymond and Rousset, 1995). Population clustering was analyzed using the unweighted pair-population method with arithmetic means (UPGMA) of the MEGA 3.0 software. Analysis of molecular variance (AMOVA) was performed using Arlequin 3.11software, and the genetic diversity and genetic differentiation index (F_{ST}) were computationally analyzed.

RESULTS

Genetic Diversity of the Rainbow Clam

There were 1,146 alleles that were successfully detected from the genomes of rainbow clam population *via* 17 SSR loci scanning in the six populations. Despite this, the HGZ22 in the Wenzhou population failed to be amplified by PCR. Except for the alleles detected at the two loci of HGZ2 and HGZ14, the remaining alleles were highly polymorphic loci, which indicated that the 17 microsatellite loci could be used to study the population genetics of rainbow clam (**Table 3**).

The average number of alleles among the 17 loci in the six populations was 5.5000–22.5000 (17 loci average, 11.9039),

TABLE 3 | Genetic diversity of six populations of rainbow clams.

Pop	SSR	MH19A	Mi44A	MW15A	MX39C	MY36B	MZT46B	HGZ3	HGZ6	HGZ9	Mir8	Mir12	Mir14	HGZ10	HGZ17	HGZ22	Mir13	MW33A	Mean
ZS	Sample No.	96	100	100	98	84	96	100	100	100	96	96	94	96	92	10	14	34	83
	Na	17	7	20	18	27	6	19	3	10	10	21	21	5	7	5	9	13	12.8235
	Ne	7.5789	3.3003	4.1391	3.2035	17.9086	2.3226	8.7260	1.1064	5.6243	5.8701	7.1888	4.3829	1.6317	2.0564	3.8462	6.5333	9.6333	5.5913
	Ho	0.8542	0.9600	0.6200	0.8980	0.2619	0.8958	0.0400	0.0600	0.8800	0.8125	0.9583	0.8085	0.0000	0.2174	0.2000	0.4286	0.1765	0.5336
	He	0.8772	0.7040	0.7661	0.6949	0.9555	0.5754	0.8943	0.0972	0.8305	0.8384	0.8700	0.7801	0.3912	0.5194	0.8222	0.9121	0.9234	0.7325
	I	2.3251	1.3946	1.9772	1.8728	3.0815	1.0159	2.5069	0.2322	1.9486	1.9286	2.4370	2.0440	0.8046	1.0947	1.4708	2.0449	2.4172	1.7998
ND	Sample No.	78	92	96	98	78	86	98	98	98	100	96	94	100	96	54	50	50	86
	Na	18	8	30	10	15	24	8	14	2	8	9	10	21	5	5	7	7	9
	Ne	11.7000	2.9782	11.1036	2.7805	18.2156	2.3012	5.5514	1.0416	5.2082	3.6928	3.3932	3.8518	1.3951	1.4908	4.7032	4.4326	5.6306	5.2630
	Ho	0.7692	1.0000	0.8333	0.8163	0.4615	0.9767	0.0204	0.0408	1.0000	0.9800	0.9583	0.7447	0.0000	0.1042	0.0000	0.0000	0.0000	0.5121
	He	0.9264	0.6715	0.9195	0.6470	0.9574	0.5721	0.8283	0.0404	0.8163	0.7366	0.7127	0.7483	0.2861	0.3327	0.8022	0.7902	0.8392	0.6839
	I	2.6503	1.3328	2.8777	1.6638	3.0326	1.0217	2.0495	0.0996	1.7543	1.5876	1.4903	2.0490	0.6114	0.7219	1.7032	1.6550	1.9249	1.6603
CX	Sample No.	90	100	100	96	82	88	98	100	100	94	100	98	100	94	58	96	26	89
	Na	22	5	30	18	28	5	11	4	15	11	6	18	7	5	14	8	9	12.7059
	Ne	11.3764	4.0750	6.7843	5.2364	15.0089	1.9979	2.4984	1.3369	6.8871	7.1143	2.9656	3.0703	1.8997	2.0771	8.7604	2.7560	6.1455	5.2935
	Ho	0.9111	1.0000	0.9400	0.9167	0.6585	0.7045	0.7755	0.0000	0.9400	0.9362	0.9600	0.6735	0.0600	0.4255	0.1034	0.3542	0.0769	0.6139
	He	0.9223	0.7622	0.8612	0.8175	0.9449	0.5052	0.6059	0.2545	0.8634	0.8687	0.6695	0.6813	0.4784	0.5241	0.9014	0.6439	0.8708	0.7162
	I	2.7154	1.4715	2.5566	2.2264	2.9907	0.8671	1.3413	0.5388	2.2126	2.0765	1.2420	1.7969	0.9429	1.0515	2.3665	1.2693	2.0008	1.7451
CM	Sample No.	108	120	114	112	90	116	116	120	120	120	118	92	110	118	36	48	28	99
	Na	21	5	17	15	25	9	11	5	11	8	22	10	4	4	10	17	9	11.9412
	Ne	12.7615	2.3614	4.3995	2.1261	8.8621	2.3168	1.4771	1.4682	3.9067	5.1173	6.0592	1.6067	2.0481	1.6927	7.0435	14.0488	7.6863	4.9989
	Ho	0.9815	1.0000	0.3333	0.4464	0.4667	0.5690	0.1207	0.3500	0.9167	0.9500	0.7797	0.0870	0.0000	0.0678	0.1111	0.1250	0.1429	0.4381
	He	0.9303	0.5814	0.7795	0.5344	0.8971	0.5733	0.3258	0.3216	0.7503	0.8113	0.8421	0.3817	0.5164	0.4127	0.8825	0.9486	0.9021	0.6701
	I	2.7482	0.9969	1.9305	1.4246	2.6834	1.1756	0.8329	0.6585	1.6460	1.7885	2.3283	0.9337	0.9241	0.7746	2.1073	2.7358	2.1138	1.6355
WZ	Sample No.	100	98	96	56	82	76	96	100	100	100	100	56	96	94	–	12	12	85
	Na	23	12	18	10	9	8	2	5	8	9	10	3	4	2	–	5	5	12.3648
	Ne	11.5207	3.6051	7.1331	1.6049	1.4038	2.3442	1.6528	1.5494	4.3365	5.3022	3.1250	1.1979	2.0907	1.2605	–	4.5000	4.8000	3.8135
	Ho	1.0000	1.0000	0.8333	0.3214	0.1220	1.0000	0.0000	0.3200	0.9600	0.9000	0.9600	0.0357	0.0000	0.0638	–	0.0000	0.1667	0.5102
	He	0.9224	0.7301	0.8689	0.3838	0.2912	0.5811	0.3991	0.3582	0.7772	0.8196	0.6869	0.1682	0.5272	0.2089	–	0.8485	0.8636	0.6266
	I	2.7197	1.6343	2.2915	0.9778	0.7424	1.0546	0.5841	0.7232	1.6415	1.7577	1.3815	0.3456	0.8837	0.3609	–	1.5607	1.5890	1.6135
LYG	Sample No.	98	100	94	100	72	86	94	100	100	92	100	100	100	90	48	88	30	88
	Na	21	5	20	16	29	5	4	2	17	18	4	20	3	10	13	13	14	12.5882
	Ne	12.0957	3.9777	4.6456	2.0080	18.6475	1.9091	1.5314	1.0202	10.0402	10.2470	2.5316	2.7397	2.0358	3.1395	7.0675	2.7172	11.8421	5.7762
	Ho	0.8571	1.0000	0.8085	0.5200	0.8056	0.3488	0.3830	0.0200	0.7000	0.6957	0.9600	0.6600	0.0000	0.2000	0.0417	0.2727	0.1333	0.4945

(Continued)

TABLE 3 | (Continued)

Pop	SSR	MH19A	Mi44A	MW15A	MX39C	MY36B	MZT46B	HGZ3	HGZ6	HGZ9	Mir8	Mir12	Mir14	HGZ10	HGZ17	HGZ22	Mir13	MW33A	Mean
	He	0.9268	0.7562	0.7932	0.5071	0.9597	0.4818	0.3507	0.0200	0.9095	0.9123	0.6111	0.6414	0.5139	0.6891	0.8768	0.6392	0.9471	0.6786
	I	2.7247	1.4155	2.0706	1.3773	3.1140	0.9262	0.6279	0.0560	2.5136	2.5504	1.0406	1.7503	0.8030	1.4816	2.2518	1.5439	2.5520	1.6941
Mean	Sample No.	95	101.7	100.0	93.3	81.3	91.3	100.3	103.0	103.0	100.3	101.7	89.0	100.3	97.3	41.2	51.3	30.0	88.3
	Na	20.3333	7.0000	22.5000	14.5000	22.1667	9.5000	9.1667	5.5000	10.5000	10.6667	12.0000	13.6667	7.3333	5.5000	9.4000	9.8333	9.5000	11.9039
	Ne	11.1722	3.3830	6.3675	2.8266	13.3411	2.1986	3.5729	1.2538	6.0005	6.2240	4.2106	2.8082	1.8502	1.9528	6.2842	5.8313	7.6230	5.1287
	Ho	0.8955	0.9933	0.7281	0.6531	0.4627	0.7491	0.2233	0.1318	0.8995	0.8791	0.9294	0.5016	0.0100	0.1798	0.0912	0.1968	0.1161	0.5171
	He	0.9176	0.7009	0.8314	0.5975	0.8343	0.5482	0.5674	0.1820	0.8245	0.8312	0.7321	0.5668	0.4522	0.4478	0.8570	0.7971	0.8910	0.6847
	I	2.6472	1.3743	2.2840	1.5905	2.6074	1.0102	1.3238	0.3847	1.9528	1.9482	1.6533	1.4866	0.8283	0.9142	1.9799	1.8016	2.0996	1.6914

Ne, the number of effective alleles; Na, observed number of alleles; Ho, observed heterozygosity; He, expected heterozygosity; I, Shannon's Information index.

the *Ne* was 1.2538−13.3411 (average, 5.1287), the *Ho* was 0.0100−0.9933 (average, 0.5171), the *He* was 0.1820−0.9176 (average, 0.6847), and the Shannon diversity index was 0.3847−2.6472 (average, 1.6914).

The average number of alleles of the six populations was 8.3125−12.8235, the *Ne* was 3.8135−5.7762, and the *Ho* was 0.4381−0.6139 (average, 0.5121). Among the populations studied, the *Ho* of CX was the highest, whereas the *Ho* of CM was the lowest. The average *He* was 0.6266−0.7325 (average, 0.6847). The Zhoushan population was the highest, whereas the Wenzhou population was the lowest. The average Shannon diversity indices were 1.7998 (ZS), 1.7451 (CX), 1.6603 (ND), 1.6941 (LYG), 1.6355 (CM), and 1.2655 (WZ). These results showed that, although the genetic diversities of the six wild populations of rainbow clam were different, the overall genetic diversity was high (**Table 3**).

Phylogenetic Relationships of the Six Populations of Rainbow Clams

Analysis of Molecular Variance

Analysis of molecular variance (AMOVA) of the six different geographical populations of rainbow clams showed that 4.70% of their genetic variation could be derived from the population, while 95.30% of their variation was from within the population. The F_{ST} of the populations was 0.0470, indicating that the degree of genetic differentiation among the populations was low (**Table 4**).

Genetic Distance

The *Ds* among the six populations of rainbow clam was 0.0668−0.3020. The *Ds* between the Wenzhou and Zhoushan populations was the largest (0.3020), and their genetic relationship was far. In contrast, the *Ds* between the Lianyungang and Cixi populations was the smallest (0.0668), and their genetic relationship was relatively close (**Table 5**).

Genetic Differentiation Index and Gene Flow

Among those of the different populations, the F_{ST} between the Chongming and Zhoushan populations was the highest (0.0790), whereas that between the Cixi and Lianyungang populations was the lowest (0.0185). The *Nm* values between the Lianyungang and Cixi populations and those between the Ningde and Zhoushan populations were 13.2635 and 10.4019, respectively. The *Nm* between the Chongming and Zhoushan populations was 2.9146. The total F_{ST} between populations was 0.04702. $F_{ST} < 0.05$ indicates a low degree of genetic differentiation, which, in turn, reveals rich genetic diversity. The overall differentiation degree among populations was low (**Table 6**).

Cluster Analysis

Based on the genetic distances among the populations, a clustering map was constructed using the UPGMA method of the MEGA3.0 software. The six populations of rainbow clam could be divided into the following three branches: LYG and CX in the first branch, CM and WZ in the second branch, and ZS and ND in the third branch (**Figure 2**).

TABLE 4 | Analysis of molecular variance among six populations of rainbow clam.

Source of variation	d.f.	Sum of square	Variance component	Percentage of variation (%)
Among populations	5	100.815	0.16327 Va	4.70
Within populations	614	2031.833	3.30917 Vb	95.30
Total	619	2132.648	3.47245	
Fixation Index			F_{ST}: 0.04702 ($P < 0.05$)	

TABLE 5 | Nie's unbiased genetic distance of six populations of rainbow clams.

Populations	ZS	ND	CX	LYG	CM	WZ
ZS						
ND	0.1196					
CX	0.1680	0.1921				
LYG	0.2157	0.2540	0.0668			
CM	0.2297	0.1986	0.1160	0.1140		
WZ	0.3020	0.2292	0.2204	0.2185	0.1228	

TABLE 6 | Genetic similarity coefficient and gene flow between six populations of rainbow clams.

Populations	ZS	ND	CX	LYG	CM	WZ
ZS	****	10.4019	6.0283	3.7538	2.9146	3.4532
ND	0.0235	****	4.9507	3.3291	3.6003	6.2250
CX	0.0398	0.0481	****	13.2635	6.1635	7.1116
LYG	0.0624	0.0699	0.0185	****	5.4267	5.7052
CM	0.0790	0.0649	0.0390	0.0440	****	9.2629
WZ	0.0675	0.0386	0.0340	0.0420	0.0263	****

*Genetic similarity coefficient above the diagonal, gene flow below the diagonal. The symbol **** represents blank values.*

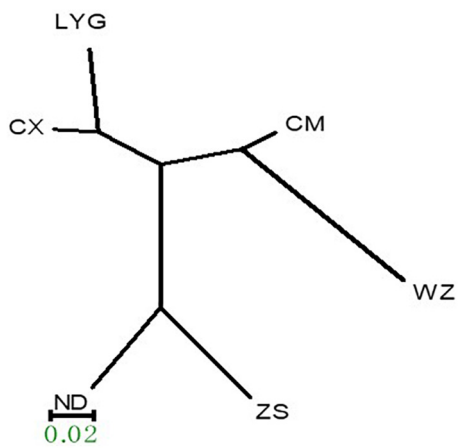

FIGURE 2 | Rainbow clam six populations of unweighted pair-population method with arithmetic means (UPGMA) trees.

DISCUSSION

Genetic differentiation index (F_{ST}) is an important parameter for measuring the degree of genetic differentiation in a population. A large F_{ST} value indicates a high degree of differentiation between populations. No differentiation exists when F_{ST} is 0−0.05, moderate differentiation is observed when F_{ST} is 0.05−0.15, high differentiation is obtained when F_{ST} is 0.15−0.25, and great differentiation is found when $F_{ST} > 0.25$ (Hartl and Clark, 1997). In this study, the F_{ST} of the six populations under study was 0.047 (<0.05). Overall, the differentiation between the populations was minimal at best. However, the F_{ST} values of the ZS−LYG, ZS−CM, ZS−WZ, LYG−ND, and CM−ND populations were in the range of 0.0624−0.0790 (0.05), which indicates that moderate genetic differentiation existed between the Zhoushan and each of the Lianyungang, Chongming, and Wenzhou populations and between the Ningde and each of the Lianyungang and Chongming populations of rainbow clams. *Nm* can indicate the degree of genetic differentiation in a population. If $Nm < 1$, genetic differentiation occurs among populations. If $Nm > 1$, genetic differentiation is relatively low. If $Nm > 4$, genetic differentiation is very low (Ratnaningrum et al., 2017). The results of AMOVA showed that the *Nm* values among the six populations of rainbow clams lay between 2.9146 and 13.2635, and the *Nm* values among the ZS−LYG, ZS−CM, ZS–WZ, LYG−ND, and CM−ND populations were greater than 1 and less than 4. These results indicate low genetic differentiation among these populations. In the present study, the sampling area of rainbow clams was distributed in the Yellow Sea and East China Seas. LYG and CM are in the Yellow Sea with a geographical distance (about 1,000 km coastline), and no differentiation between these populations was observed ($F_{ST} = 0.0040 < 0.05$). Although the geographical distance between the Chongming and Zhoushan populations is close, the Yangtze estuary is situated between them. The inflow of the Yangtze River lowers the salinity of the seawater and, hence, obstructs the passage of larvae and hinders gene communication to some extent (the *Nm* for CM−ZS is 2.9146). Therefore, moderate genetic differentiation occurs between the CM and ZS populations ($F_{ST} = 0.0790$). Xu et al. (2016) analyzed the population morphology and genetic diversity of rainbow clams from Zhejiang and revealed that the Zhoushan population has great variation from the Yueqing, Taizhou, and Wenling populations ($G_{ST} = 0.2479$). The present study also indicated that genetic differentiation occurred in the Zhoushan population ($F_{ST} = 0.2479$), which was consistent with Xu et al. (2016), who showed that the Zhoushan population of rainbow clams presents moderate genetic differentiation.

This study also found that the degree of genetic differentiation between rainbow clam populations is not related to the geographical distance. Although the geographical distance between LYG and CX was relatively far away, the F_{ST} value between the LYG and CX populations of the rainbow was

shallow, only 0.0180 (<0.05), which indicated a lack of genetic differentiation between the two populations. The gene exchange between the two populations occurred frequently (Nm = 13.2635 > 4). The inconsistency of the relationship between the degree of genetic differentiation and geographical distance has previously been observed in different populations of *Coelomactra antiquata*. Meng et al. (2013) showed that the population genetic differentiation between the *C. antiquata* from the Southeastern Sea and that from the Yellow Sea in Lianyungang and Rizhao is not apparent based on the results of ITS2 and 16S rRNA for six populations of *C. antiquata* in the coasts of China. By contrast, the difference between the Guangxi and Fujian populations, which have a relatively close geographical distance, reached the interspecies level. The real reason may be from human activity, such as artificial farming and introduction, but more detailed reasons remain unknown so far.

Genetic diversity, including the degree of genetic variation and the genetic structure of the population, is an important basis for evaluating the status of genetic resources. A higher genetic diversity of a population results in a stronger adaptability to the living environment and a greater potential for evolution (Tian et al., 2013). The genetic diversity of a population is mainly manifested in two aspects: heterozygosity and the number of alleles (Yu et al., 2012). Many reports have explored the genetic diversity of aquatic animals by using SSR markers. Li et al. (2011) studied the population genetics of *Portunus trituberculatus* by microsatellite markers and found an average *Ho* of 0.2222−1.0000 and an average *He* of 0.4367−0.9099. Li et al. (2009) used SSR technology to measure the average *Ho* (0.32−0.49) of wild and cultured populations of scallops and found an average *He* of 0.37−0.55. Chang et al. (2007) analyzed the genetic diversity of five populations of scallops *P. yessoensis* in China and abroad and found an average *Ho* of 0.2708−0.3292 and an average *He* of 0.3620−0.4595 for the five populations. Tian et al. (2013) determine the *Ho* and *He* of four populations of *Scapharca broughtonii* by using the 20 microsatellite markers, and the results showed that the ranges of *Ho* and *He* was 0.667–0.9667 and 0.6198–0.9318, respectively. An et al. (2012) studied the genetic structure of five wild-type populations of *Ruditapes philippinarum* in two sea areas of Korea by using seven SSR markers and noted high genetic diversity among the clams (total *He* = 0.813). The results of the present study revealed that the average *Ho* of the six populations of rainbow clam was between 0.4381 and 0.6139 and that the *He* was 0.6266−0.7325. Specifically, the value of *He* was as follows: ZS (0.7325), CX (0.7162), ND (0.6839), LYG (0.6786), CM (0.6701), and WZ (0.6266). The average number of alleles of the 17 loci in the six populations ranged from 5.5000 to 22.500, and the *Ne* was between 1.2538 and 13.3411. The genetic diversity of the rainbow clams was higher than those of bay scallop *Argopecten irradians* and scallop *P. yessoensis*. This particular genetic diversity is similar to the *He* of four populations of clams *T. quinquefasciatus* and is lower than that of five populations of clam *R. philippinarum*. Generally, the *He* (0.7325) of the present study and Shannon diversity index (1.7998) were the highest in the Zhoushan population, which indicated that the Zhoushan population has the richest genetic diversity among the clam populations studied.

The population differentiation of the existing rainbow clams is not obvious, and the genetic diversity of germplasm resources is relatively high, indicating that the effective population of rainbow clams in nature is large enough. At present, it is not very urgent to establish a germplasm resource reserve and its *ex situ* culture technology. In the future, the monitoring and evaluation of the germplasm resources of rainbow clams should be strengthened.

CONCLUSION

The six populations of rainbow clams all presented high genetic diversity, which reflect the good protection and development prospects of rainbow clam resources in China. These results would be helpful to genetic breeding practice and resources management.

DATA AVAILABILITY STATEMENT

The original contributions presented in the study are included in the article/supplementary material, further inquiries can be directed to the corresponding author.

ETHICS STATEMENT

All applicable International, National, and/or Institutional Guidelines for the Care and Use of Animals (invertebrates) were followed.

AUTHOR CONTRIBUTIONS

XL conceived and designed the experiments. SG performed the experiments. MZ analyzed the data. XL and ZD wrote the manuscript. All authors contributed to the article and approved the submitted version.

FUNDING

This study was supported in part by grants from the Modern Agricultural Industry Technology System of China (No. CAR49), National Natural Science Foundation of China (No. 31101900), and Priority Academic Program Development of Jiangsu Higher Education Institutions.

ACKNOWLEDGMENTS

We greatly acknowledge the following colleagues for their help and support in the process of investigation and sampling for rainbow clam: Feng Zhao from East China Sea Fisheries Institute of *CAFS* for the specimen in East Beach of Chongming Island, Binlun Yan from Huaihai Institute of Technology for the specimen in Sanyang harbor of Haizhou bay, Zehui Hu from Marine Fisheries Research Institute of Zhejiang of China for the

specimen in Datian Bay at Daishan of Zhoushan, Chen from Xiabaishi at Sansha bay in Fu'an for the specimen in the site, Meizheng Wang from Institute of Cixi Fisheries for the specimen in Cixi Sanbei shoal at Hangzhou Bay, and Weicheng Lui from Zhejiang Mariculture Research Institute for the specimen in Simon Island at Yueqing Bay.

REFERENCES

An, H. S., Kwang, K. J., Cho, K. C., Han, H. S., and Myeong, J. I. (2012). Genetic structure of Korean populations of the clam *Ruditapes philippinarum* inferred from microsatellite marker analysis. *Biochem. Syst. Ecol.* 44, 186–195.

Bai, Z., Han, X., Luo, M., Lin, J., Wang, J., and Li, J. (2015). Constructing a microsatellite-based linkage map and identifying QTL for pearl quality traits in triangle pearl mussel (*Hyriopsis cumingii*). *Aquaculture* 437, 102–110.

Chang, Y. Q., Chen, X. X., and Ding, J. (2007). Genetic diversity in five scallop populations of the Japanese scallop (*Patinopecten yessoensis*). *Ecol. J.* 27, 1145–1152.

Cui, H. Y., Ma, H. L., and Ma, C. Y. (2011). Genetic diversity among different families of mud crab *Scylla paramamosain* by microsatellite markers. *Mar. Fish.* 33, 274–281.

Hartl, D. L., and Clark, A. G. (1997). *Principles of population genetics*, 3rd Edn. Sunderland, MA: Sinauer Associates Inc.

Ji, Y. B., Li, T. W., and Su, X. R. (2007). Preliminary study on biological characteristics of rainbow clam in Zhejiang coast. *Fish. Sci.* 26, 494–496.

Li, H. J., Liu, X., Du, X. D., Song, R., Zhang, G. F., Hu, J. J., et al. (2009). Development and isolation of microsatellite markers in bay scallop. *Mar. Sci.* 33, 3–8.

Li, X., Liu, P., and Song, X. (2011). Construction on enriched microsatellite library and characterization of microsatellite markers from swimming crab. *J. Fish. Sci. China* 18, 194–201.

Li, X. Y., Zhang, M., Lu, G. Z., Mao, S., Wu, R. X., Ge, H. X., et al. (2020). Population genetic analysis of Rainbow Clam *Moerella iridescens* by Using rDNA [J]. *Isr. J. Aquacult-Bamid.* 72:1120903.

Lv, G. T., Zhang, X. M., and Zhao, J. (2012). The Effect of Phenotypic and Morphometric Traits on Body Weight of *Moerella iridescens*. *J. Zhejiang Ocean Univ*. Nat. Sci. Edit. 31, 487–491.

Meng, X. P., Shen, X., Zhao, N. N., Tian, M., Zeng, Y., Chen, J. A., et al. (2013). Microsatellite analysis of genetic diversity in four geographic populations of Sca parc brughtonii. *Prog. Fish. Sci.* 34, 59–67.

Ratnaningrum, Y. W. N., Indrioko, S., Faridah, E., and Syahbudin, A. (2017). Gene flow and selection evidence of sandalwood (*Santalum album*) under various population structures in gunung sewu (Java, Indonesia), and its effects on genetic differentiation. *Biodiversitas* 18, 1493–1505. doi: 10.13057/biodiv/d180427

Raymond, M., and Rousset, F. (1995). GENEPOP (version3.3) population genetics software for exact tests and ecumenicism. *J. Hered.* 86, 248–249. doi: 10.1093/oxfordjournals.jhered.a111573

Schuelke, M. (2000). An economic method for the fluorescent labeling of PCR fragments. *J. Nat. Biotechnol.* 18, 233–234. doi: 10.1038/72708

Tian, J. T., Liu, Z. H., Yang, A. G., Wu, B., and Zhou, L. Q. (2013). Microsatellite analysis of genetic diversity of 4 geographic populations of *Scapharca broughtonii*. *Prog. Fish. Sci.* 6, 59–67.

Xu, H., Hu, Y. L., Xu, Y. P., Jin, K., and Chen, P. (2016). The analysis of genetic diversity and morphology of *Moerella iridescens* in Zhejiang Province. *J. Shanghai Ocean Univ.* 4, 508–514.

Yu, Z. F., Yan, X. C., Zhang, Y. H., Yang, F., Yang, F., and Zhang, G. F. (2012). EST-SSR diversity of Philippines clam in different age groups in Dalian. *Acta Ecologica. Sinica.* 1, 4673–4681. doi: 10.5846/stxb201105150625

Zhang, M., Wei, M., Dong, Z., Duan, H., Mao, S., Feng, S., et al. (2019). Fecal DNA isolation and degradation in clam *Cyclina sinensis*: noninvasive DNA isolation for conservation and genetic assessment. *BMC. Biotechnol.* 19:99. doi: 10.1186/s12896-019-0595-6

Zhao, Y., Zhu, X., and Sun, X. (2010). Microsatellite diversity in cultured populations of rainbow trout *Oncorhynchus mykiss* in China. *J. Fish. Biol.* 73, 1249–1255.

Conflict of Interest: The authors declare that the research was conducted in the absence of any commercial or financial relationships that could be construed as a potential conflict of interest.

Publisher's Note: All claims expressed in this article are solely those of the authors and do not necessarily represent those of their affiliated organizations, or those of the publisher, the editors and the reviewers. Any product that may be evaluated in this article, or claim that may be made by its manufacturer, is not guaranteed or endorsed by the publisher.

frontiers in Marine Science

ORIGINAL RESEARCH
published: 01 March 2022
doi: 10.3389/fmars.2022.847585

Responses of Pearl Oysters to Marine Heatwaves as Indicated by HSP70

*Yang Xu[1], Jian Liang[1,2], Guixiang He[1], Xiaolong Liu[1], Ke Yang[1], Fortunatus Masanja[1], Yuewen Deng[1] and Liqiang Zhao[1]**

[1] Fisheries College, Guangdong Ocean University, Zhanjiang, China, [2] Department of Fisheries, Tianjin Agricultural University, Tianjin, China

Marine heatwaves (MHWs) can severely affect bivalves and ecosystems they support. Heat shock proteins (HSPs) are a group of molecular chaperones playing a critical role in the cellular protection and thermo tolerance and thereby constraining physiological responses of marine bivalves to MHWs. Here, we cloned the full-length of *HSP70* cDNA from the *Pinctada maximal* (*PmHSP70*) and evaluated the expression of *PmHSP70* in pearl oysters under acute and repeatedly occurring MHWs conditions. The full-length of *PmHSP70* is 2,474 bp, containing an ORF of 1,956 bp encoding 655 amino acids with a predicted molecular weight of 71.23 kDa and 5.26 theoretical isoelectric point. Under the scenario of acute MHWs, the expression of *PmHSP70* was significantly highly expressed at 32 and 36°C, and reached the highest at 12 and 72 h, respectively, indicating that pearl oysters rapidly up-regulated the expression of *HSP70* in response to MHWs. In the repeatedly occurring MHWs scenario, the thermal response of pearl oysters was alleviated, as best exemplified by significantly lowered expression levels of *PmHSP70*. Therefore, we speculate that long-term and repeated MHWs can alleviate the thermal stress of pearl oysters. This finding is encouraging and will provide us with meaningful insights into the acclimation of marine bivalves to extreme environments in the future.

Keywords: ***Pinctada maxima***, ***PmHSP70***, **extreme weather events, acclimation, climate change**

OPEN ACCESS

Edited by:
Hui Zhang,
Institute of Oceanology (CAS), China

Reviewed by:
Xing Zheng,
Hainan University, China
Yuan Wang,
Dalian Ocean University, China

***Correspondence:**
Liqiang Zhao
lzhao@gdou.edu.cn

Specialty section:
This article was submitted to Marine Fisheries, Aquaculture and Living Resources, a section of the journal Frontiers in Marine Science

Received: *03 January 2022*
Accepted: *25 January 2022*
Published: *01 March 2022*

Citation:
Xu Y, Liang J, He G, Liu X, Yang K, Masanja F, Deng Y and Zhao L (2022) Responses of Pearl Oysters to Marine Heatwaves as Indicated by HSP70. Front. Mar. Sci. 9:847585. doi: 10.3389/fmars.2022.847585

INTRODUCTION

Marine heatwaves (MHWs) are prolonged discrete anomalously climatic events that can last for days or longer (Hobday et al., 2016). Since 2011, MHWs have been retrospectively and contemporaneously observed in the world's oceans and now are recognized to become more frequent, intense and longer-lasting over a wide range of spatio-temporal scales (Holbrook et al., 2020). Although MHWs can be short-term and discrete events, they can have devastating impacts on marine ecosystems (Smale et al., 2019). Accumulating evidence indicates devastating impacts of MHWs on marine organisms, especially sessile species such as corals (Fordyce et al., 2019; Rendina et al., 2019) and mollusks (Caputi et al., 2016; Chandrapavan et al., 2019; Zhao et al., 2019; Amorim et al., 2020; Scanes et al., 2020) because they must endure anomalously high seawater temperatures during MHWs events. Stress responses caused by seawater temperature sudden changes due to MHWs can affect the innate immune system of marine bivalves (Nie et al., 2017;

Rahman and Rahman, 2021). Sessile marine bivalves are vulnerable to heatwaves because they cannot physically remove themselves and seek refuge (Pörtner, 2001; Somero, 2005), and several studies have demonstrated that MHWs causes the mass mortality events in mytilid mussels such as *Mytilus californianus* (Harley, 2008), *M. galloprovincialis* (Petes et al., 2007), and *M. edulis* (Seuront et al., 2019). In response to the challenges associated with temperature changes caused by MHWs, some aquatic organisms employ biochemical, physiological, and molecular mechanisms for self-protection at extreme temperatures (Dong et al., 2020), such as increasing the activity of enzymes and up-regulating the expression of HSPs genes (He et al., 2021; Xu et al., 2021, 2022).

Heat shock protein (HSP) expression is a key cellular mechanism of acclimation to environmental temperature fluctuations (Bedulina et al., 2013). Under thermal stress, HSPs perform critical protein-stabilizing functions (Tomanek and Somero, 2002) and thus play a crucial role in the development of thermotolerance (Clegg et al., 1998). HSP is a type of conservative family protein (Hu et al., 2012), playing an important role in protein folding and biosynthesis as a molecular chaperone (Zhang and Xie, 2019). Among HSPs, the proteins of molecular mass 70 kDa, termed heat shock protein 70 (HSP70), are the most abundant and highly conserved type of protein (Hassan et al., 2019). HSP70 is an important biomolecule for biological resistance, and is most sensitive to environmental degradation. When the cells of the organism are stressed by the external environment, it interacts with many key regulators of signal transduction pathways to control cell homeostasis, proliferation, differentiation, and cell death (Mayer and Bukau, 2005). In particular, HSP70 proteins play an important role in the adaptation of poikilothermic organisms to adverse environmental (Evgen'ev et al., 2007).

Pinctada maxima is an important economic species and is widely distributed in coastal areas such as Australia and the South China Sea (FAO, 2014; Xu et al., 2021). The "South China Sea" pearls cultivated from *P. maxima* are widely popular in the world because of the large diameter, thick nacre and beautiful (Jones et al., 2013). The Beibu Gulf is a hot spot for MHWs in the South China Sea (Zhang et al., 2020). However, in the context of global climate change and intensified human activities, the duration, frequency and intensity of MHWs have increased sharply in recent decades (Li et al., 2019; Yao et al., 2020; Liu et al., 2021). The coastal waters where pearl oysters live have undergone unprecedented changes, especially MHWs posing a great threat to the survival of *P. maxima*. Although studies have been conducted to evaluate the effects of temperature on the expression level of HSP genes in some marine invertebrates (Park et al., 2015; Chen et al., 2018; Liu et al., 2018; Zhao et al., 2020), little is known about thermal resistant gene expression responses of the *P. maxima* to MHWs. Therefore, it is particularly important to explore the molecular mechanism of pearl oysters' adaptability to MHWs.

In this study, we cloned the full-length of *HSP70* by RACE technology, and then evaluated the tissue expression specificity of *HSP70* and expression when exposed to acute and repeatedly occurring MHWs. We also attempted to discover the role of *HSP70* in thermal resistance ability and plasticity during the process of MHWs acclimation in *P. maxima*. To clarify the potential contributions of *HSP70* in *P. maxima* to against environmental stress. The results of this study provide useful information on the response of *P. maxima* to MHWs, and this information can be used to improve the ability of pearl oysters to withstand such adverse environments as MHWs in an aquaculture environment.

MATERIALS AND METHODS

Experiment Design and Sample Collection

The pearl oysters *P. maxima* (1-year-old; 34.69 ± 5.25 mm shell length, 3.33 ± 0.99 g wet weight) were collected from the Liusha Bay, Beibu Gulf, South China Sea. After arriving in the laboratory, they were carefully cleaned to remove epiphytes on the shell surface and then temporarily cultivate in the laboratory to acclimate to laboratory conditions. The gills (Gi), hepatopancreas (He), mantle (M), and adductor muscle (A) were selected from five healthy individuals for gene tissue distribution, and the tissues were quickly frozen in liquid nitrogen and then stored in a refrigerator at −80°C until RNA extraction.

In order to explore the impact of MHWs on HSPs, we adopted the definition of MHWs by Hobday et al. (2016), who defined the MHWs event is considered a long-term discrete abnormal warm water event, which can be described in terms of intensity, duration, spatial scope, and evolution speed. The specific experimental design is shown in Xu et al. (2022). Specifically, the temperature of 24°C represents contemporaneously annual average sea surface temperature in the Beibu Gulf as control group, and temperature regimes of 28, 32, 36°C correspond to instrumental data recorded during periods of MHWs (Yao et al., 2020; Zhang et al., 2020). In the MHWs experiment, the pearl oysters experienced two MHWs stimulation and two recovery scenarios (**Figure 1**). In the acute MHWs experiment, 5 gills in each group were carefully dissected at 6, 12, 24, and 72 h after the temperature stabilized. During repeatedly occurring MHWs experiments, the gills of 5 individuals were sampled at 3, 7, 10, and 14 days in repeatedly occurring MHWs experiments, and immediately placed in liquid nitrogen and stored at −80°C pending analysis.

Total RNA Extraction and First-Strand cDNA Synthesis

The total RNA was extracted from the tissues using the Trizol Reagent (Invitrogen, United States) according to the manufacturer's instructions. The RNA quantity, purity and integrity were verified by 1% agarose gel electrophoresis and Nano Drop ND1000 ultraviolet spectrophotometer. Preparing 5′RACE and 3′RACE templates according to the instructions of SMARTer^{TM} RACE cDNA Amplification kit follow the instructions of Reverse Transcriptase M-MLV (RNaseH) to synthesize cDNA templates for RT-qPCR.

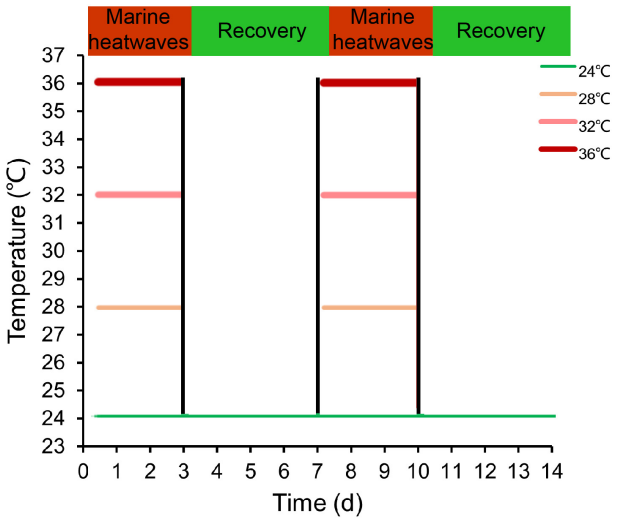

FIGURE 1 | Overview of the experimental design illustrating MHWs scenarios varying in frequency and intensity. Green line indicates the temperature regime designated in the control and color intensity of red lines represents the intensity of temperature regimes designated under MHWs conditions.

TABLE 1 | Primers used in the study of *PmHSP70*.

Primer	Primer sequence (5′–3′)	Function
HSP70-F	GGAGACTGCTGAGGCTTACTTAGG	Middle clone
HSP70-R	TTGCTAATACTCTGGACTACTC	Middle clone
5′-HSP70-outer	GCTTGTGTGCTGGATGACAGGGTT	5′RACE
5′-HSP70-inner	CGCCAACCTTCTTATCCAGACCGT	5′RACE
3′-HSP70-outer	ACACAGACCTTCACAACATACTCCGACA	3′RACE
3′-HSP70-inner	GCTGCCCCAGGAGGTGGAAGTGAT	3′RACE
UPM (long)	CTAATACGACTCACTATAGGGC AAGCAGTGGTATCAACGCAGAGT	RACE
UPM (short)	CTAATACGACTCACTATAGGGC	RACE
NUP	AAGCAGTGGTATCAACGCAGAGT	RACE
M13-47	CGCCAGGGTTTTCCCAGTCACGAC	PCR detection of colony PRC
M13-48	AGCGGATAACAATTTCACACAGGA	PCR detection of colony PRC
HSP70-qF	ACCCCAGATTGTGGTGACCTTCG	RT-PCR
HSP70-qR	TATTCCTGTTTGTATTTTTCGGC	RT-PCR
βactin-F	CGGTACCACCATGTTCTCAG	Reference gene
βactin-R	GACCGGATTCATCGTATTCC	Reference gene

The partial sequence of *HSP70* was obtained from the *P. maxima* transcriptome database (data of our research group), and we used Primer Premier 5 software to design specific primers (**Table 1**). Using RACE technology to obtain 3′- and 5′-ends sequences, polymerase chain reaction amplification was performed for intermediate fragment verification. The amplified products were detected by 1% agarose gel electrophoresis. The target gene fragments separated and purified by the purification and recovery kit were connected to the PMD19-T vector and transformed into DH5α competent cells. The positive cloned bacteria were selected by LA (containing ampicillin Apm +) and sequenced by Sangon (Sangon Biotech, Shanghai, China). Then the 3′- and 5′-RACE PCR fragment sequences were aligned to assemble the full nucleotide sequence of the pearl oysters putative HSP70 cDNA. The resulting sequences were verified by the amplification of the whole full length and further subjected to cluster analysis.

Bioinformatics Analysis

The full-length sequence of *PmHSP70* was spliced with DNAMAN. The ORF Finder[1] in the NCBI database was used to predict the open reading frame and amino acid sequence of the PmHSP70. The physical and chemical properties were determined by Expasy-ProtParam online tool[2] and ExPASy-ProtScale[3] for amino acid hydrophilicity analysis, use PSITE-Search for Prosite patterns with statistics[4] for predicting amino acid sub-basic functional sites. SignalP 4.1[5] predict amino acid sequence signal peptide and domains were identified with SMART[6] with the three-dimensional structure built with the SWISS-MODEL[7]. The similarity analysis of nucleotide and protein sequence was carried out using NCBI online BLAST,[8] and then Clustal W was used to compare multiple sequences of PmHSP70 protein. A phylogenetic tree was constructed using MEGA 6.0 software.

Relative Quantitative Real-Time PCR Analysis

Total RNA was extracted using Trizol reagent (Invitrogen, United States) in accordance with the manufacturer's instructions. cDNA was synthesized using PrimeScript RT Reagent Kit (TaKaRa, Dalian, China). RT-qPCR was conducted using a Roche LightCycler 480 RT-PCR system with SYBR(R) Premix Ex Taq^{TM} (TOYOBO, Japan) following the manufacturer's protocol. The reactions were carried out in a total volume of 10 μL containing 5 μL of SYBR mixture, 0.4 μL cDNA, 3.8 μL of ddH_2O, 0.4 μL of forwarding primer, and 0.4 μL of the reverse primer (Wang et al., 2019). The comparative Ct method ($2^{-\Delta Ct}$) was used to analyze the relative expression of these genes by taking β-actin as an endogenous control.

Statistical Analysis

All data were analyzed using the software SPSS 22.0. Shapiro-Wilk's test and Levene's *F*-test were, respectively, performed to examine the normal distribution and homogeneity of experimental data. Two-way analysis of variance (ANOVA) was applied to test whether and how various MHWs scenarios stimulated in duration, frequency and intensity significantly

[1]http://www.ncbi.nlm.nih.gov/orffinder/
[2]http://web.expasy.org/protparam/
[3]http://web.expasy.org/protscale/
[4]http://linux1.softberry.com/berry.phtml?topic=psite&group=programs&subgroup=proloc
[5]http://www.cbs.dtu.dk/services/SignalP/
[6]http://smart.embl-heidelberg.de/
[7]https://swissmodel.expasy.org/interactive
[8]https://blast.ncbi.nlm.nih.gov/Blast.cgi

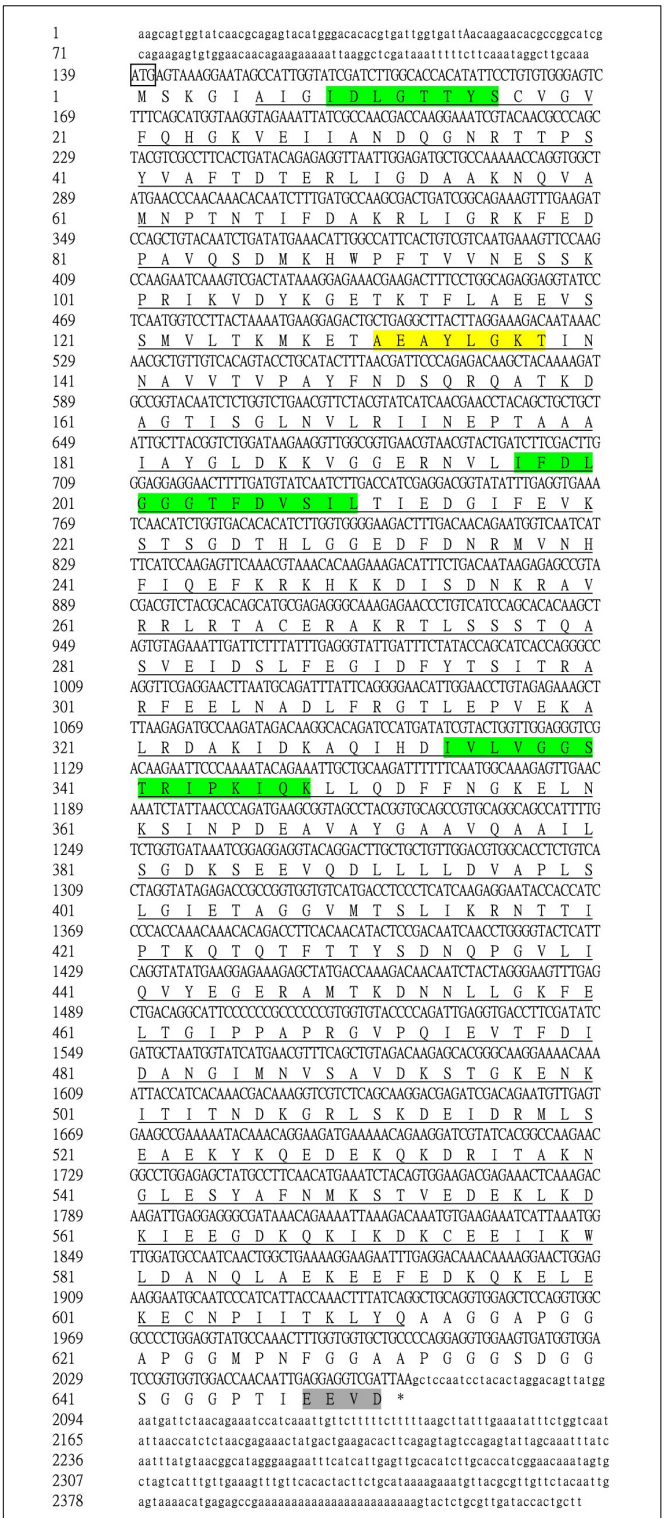

FIGURE 2 | The nucleotide sequence analysis of Pm-HSP70. 5′ UTR and 3′ UTR are indicated with small letters; The deduced amino acid sequences are indicated with capital letters; The start codon in the 5′-UTR was in a box and the stop codons (TAA) was indicated with an asterisk (*). Three signatures were green background; a putative ATP-GTP binding site was yellow background; the cytoplasmic characteristic motif was gray background and the underlined indicates the HSP70 domain.

affect the expression levels of genes. Statistical significance was set at $P < 0.05$.

RESULTS

Sequence Analysis of *PmHSP70*

The cDNA of *PmHSP70* gene was cloned by RACE technology with a full length of 2,474 bp, containing an open reading frame (ORF) of 1,956 bp, encoding 655 amino acids, a 138 bp 5′-terminal untranslated region (UTR) and a 363 bp 3′-UTR. *PmHSP70* had a predicted molecular weight of 71.23 kDa, a 5.26 theoretical isoelectric point. ExPASy-ProtParam analysis showed that the aliphatic index of PmHSP70 protein is 80.48, and the instability index is 34.69, indicating the stability of HSP70. Amino acid sub-basic functional sites predicted found PmHSP70 has an ATP/GTP-binding site (AEAYLGKT), three HSP70 family signature (IDLGTTYS, IFDLGGGTFDVSIL, IVLVGGSTRIPKIQK) and the cytoplasmic characteristic motif EEVD. The average coefficient of hydrophilicity (GRAVY) is −0.490, which is a hydrophilic protein. SMART analysis revealed that PmHSP70 has an HSP70 domain at positions 6–612 (**Figure 2**).

Structural and Homologous Analysis

The species information of multiple alignment and phylogenetic tree are shown in **Table 2**. The multiple sequence alignment based on the amino acid sequence alignment of PmHSP70 and other bivalves HSP70 shows that HSP70 has high homology among bivalves, and *Pinctada fucada martensii* HSP70 has the highest homology with PmHSP70, which is 95.70% (**Figure 3**). The phylogenetic tree shows that *PmHSP70* clusters with bivalves

TABLE 2 | Information of the sequences used in the multiple alignment and phylogenetic analysis.

Species	Style	Accession number
Pinctada fucata martensii	HSP70	BAL52328.1
Pteria penguin	HSP70	ABJ97377.1
Crassostrea ariakensis	HSP70	AAO41703.1
Mytilus coruscus	HSP70	AGY56119.1
Mytilisepta virgata	HSP70	BAS29644.1
Meretrix meretrix	HSP70	ADT78476.1
Ruditapes philippinarum	HSP70	AHY27547.1
Sinonovacula constricta	HSP70	AEP26350.1
Paratapes undulatus	HSP70	AFZ93094.1
Mylopharyngodon piceus	HSP70	AVO65116.1
Megalobrama amblycephala	HSP70	ACC93993.2
Ctenopharyngodon idella	HSP70	AZM69450.1
Hypophthalmichthys molitrix	HSP70	ACJ03595.1
Xiphophorus hellerii	HSP70	XP_032432933.1
Epinephelus coioides	HSP70	AGG55391.1
Danio rerio	HSP71	NP_001103873.1
Mus musculus	HSP71	NP_112442.2
Homo sapiens	HSP71	NP_006588.1

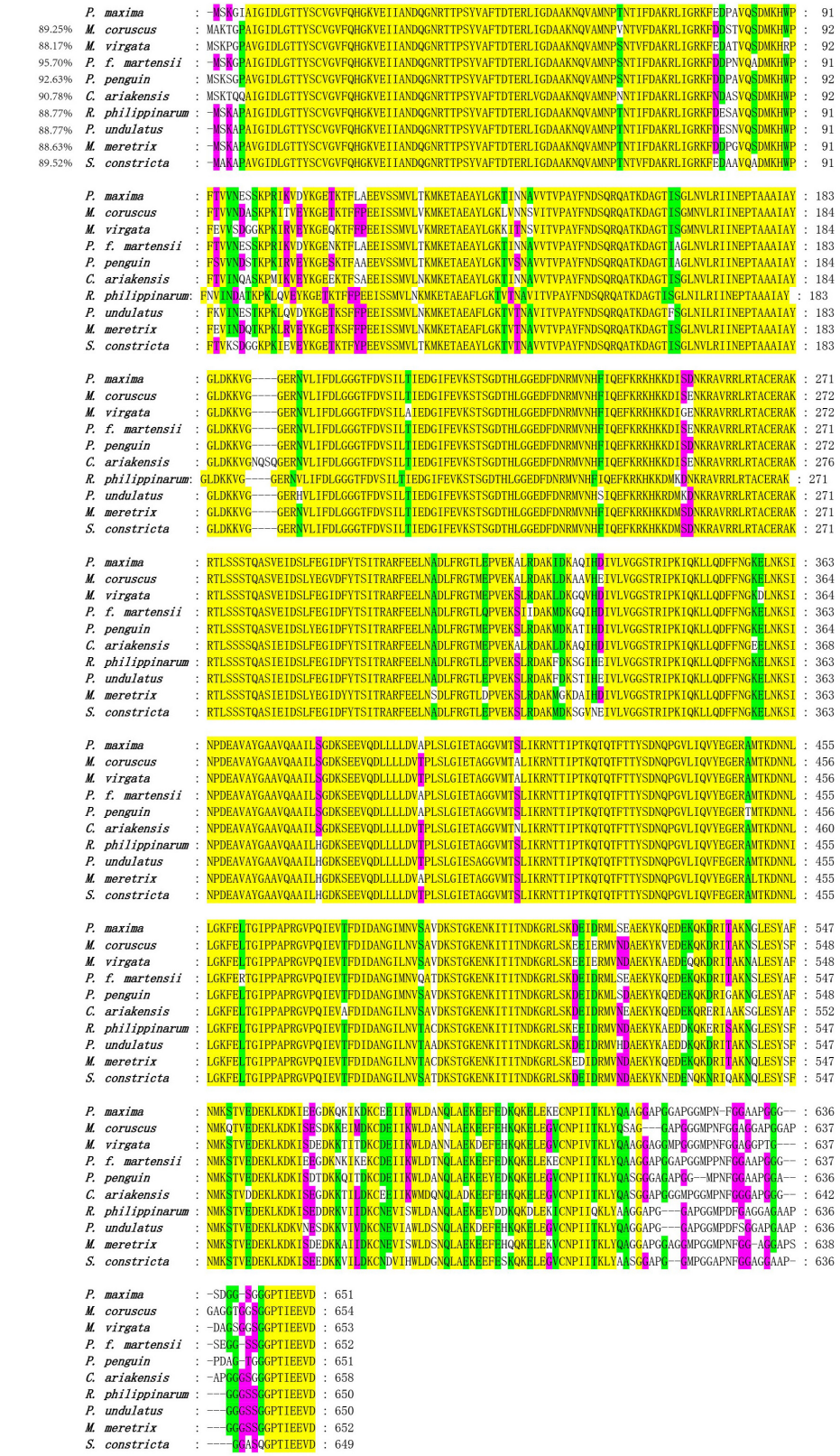

FIGURE 3 | Multiple alignment of the deduced amino acid sequences of HSP70 from *P. maxima* and other organisms. Yellow means 100% homology, green means homology greater than 90%, purple means homology greater than 80%.

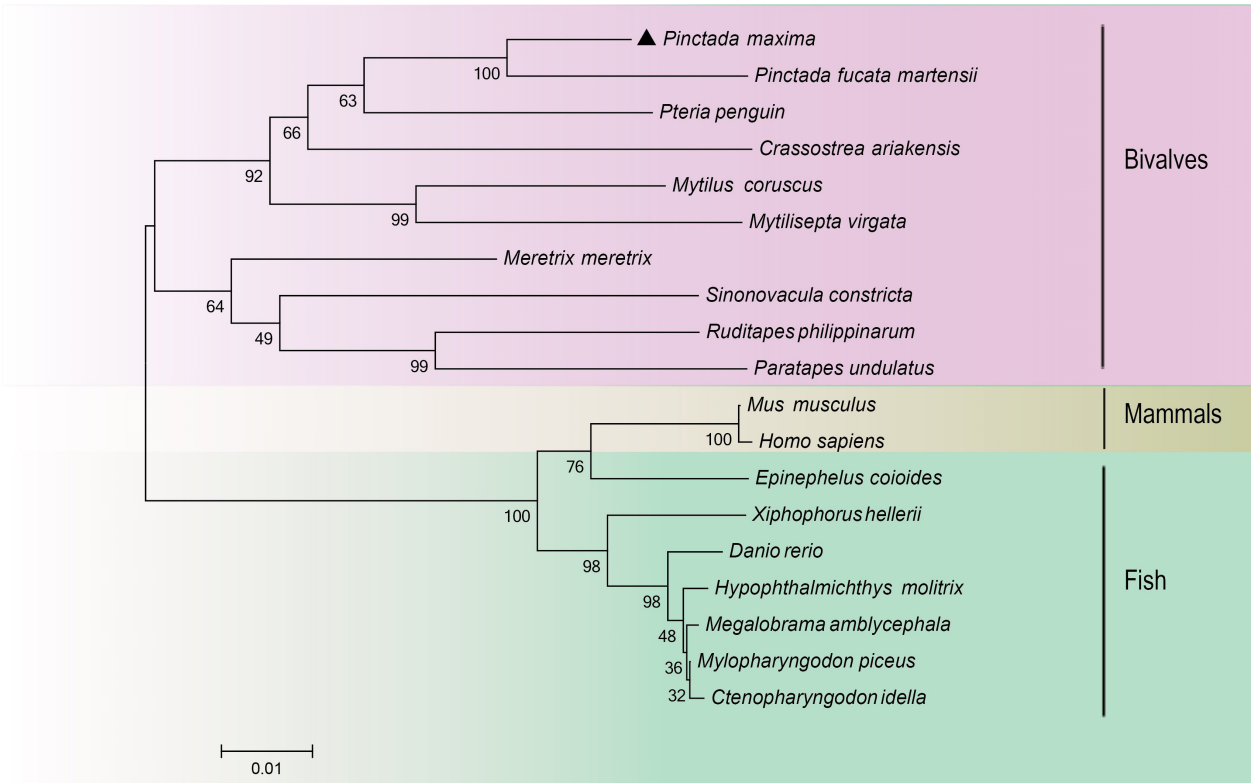

FIGURE 4 | A phylogenetic tree constructed using the neighbor-joining method based on amino acids sequence deduced from *HSP70* of *Pinctada maxima* and other species. *Pinctada maxima* was labeled with "▲". The GenBank accession numbers of all the HSP70 were shown in **Table 2**.

and is most closely related to *P. f. martensii* and *Pteria penguin*, and is farther from mammals and fish (**Figure 4**).

mRNA Expression in Different Tissues

The RT-qPCR was used to investigate the tissue distribution and expression level of *PmHSP70* under normal conditions. The results showed that the *PmHSP70* was expressed in the mantle, gills, hepatopancreas, and adductor muscle of *P. maxima*, with the highest expression level in the hepatopancreas and gills, and the lowest expression level in the adductor muscle (**Figure 5**).

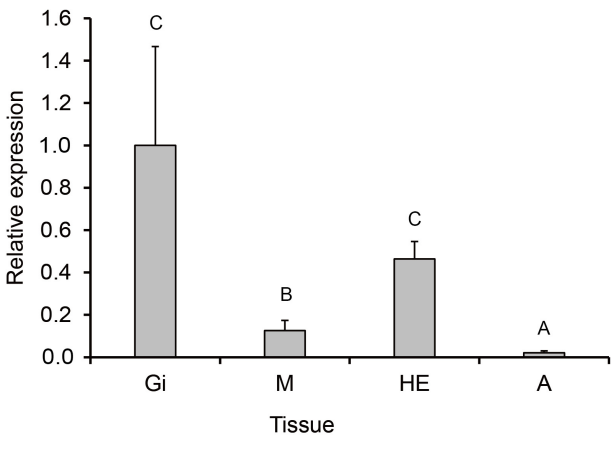

FIGURE 5 | Tissue distribution of *PmHSP70* mRNA expression. Different capital letters indicate significant differences ($P < 0.05$). The four tissues include gills (Gi), hepatopancreas (He), mantle (M), and adductor muscle (A).

mRNA Expression After Marine Heatwaves Stimulation

During the acute exposure, in gills, compared with the control groups, the expression level was significantly up-regulated in the experimental groups especially in the 36°C groups. After being stimulated by the MHWs, the expression level of *PmHSP70* in the 28°C groups reached the highest level at 72 h, while the expression level of the 32°C groups reached the highest level at 12 h (**Figure 6**). Analysis of variance shows that both temperature of MHWs and stress time made significant impact on the gene expression level ($P < 0.05$), and their interaction was significant ($P < 0.05$) (**Table 3**).

Following repeat exposure to MHWs, we found the expression level of *HSP70* in the second MHWs, the fold changes between the experimental groups and the control groups were lower than those in the first MHWs (**Figure 7**). Analysis of variance shows that both temperature of MHWs and stress time made significant impact on the gene expression level ($P < 0.05$), and their interaction was significant ($P < 0.05$) (**Table 3**).

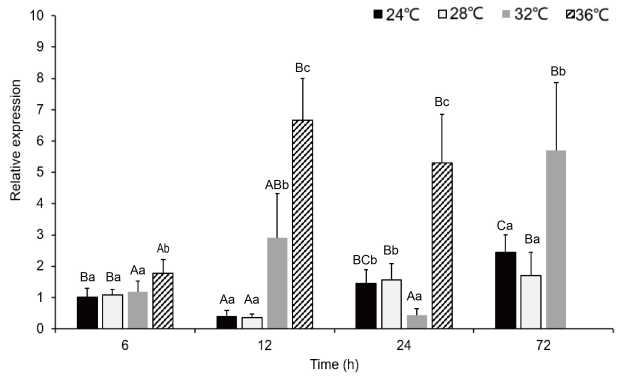

FIGURE 6 | The expression levels of *PmHSP70* mRNA in gill from *P. maxima* after acute MHWs stress. Small letters indicate significant differences between four temperature levels within each time, and capital letters indicate significant difference between four time within each temperature treatment ($P < 0.05$). As pearl oysters exposed to the temperature anomaly of 36°C suffered 100% mortality at 24 h, the experiment was terminated accordingly.

TABLE 3 | Two-way ANOVA results for relative expression of *HSP70* in pearl oysters exposed to acute and repeatedly occurring MHWs scenarios accounting for temperature and sampling time.

Scenarios	Factors/interactions	df	*F*	*P*
Acute MHWs	Temperature	3	51.901	0.000
	Time	3	27.002	0.000
	Temperature*time	8	17.494	0.000
Repeatedly occurring MHWs	Time	3	18.633	0.000
	Temperature	2	11.794	0.000
	Time*temperature	6	6.737	0.000

DISCUSSION

HSP70 genes in the pearl oyster P. maxima was characterized for the first time in present study. The *PmHSP70* has a typical domain HSP70 and three characteristic sequences (IDLGTTYS, IFDLGGGTFDVSIL, IVLVGGSTRIPKIQK) of the HSP70 family (Gupta and Singh, 1994), which are well conserved in the eukaryotic HSP70 family (Gupta and Singh, 1994). And we observed an ATP/GTP-binding site (AEAYLGKT) in *PmHSP70*, which demonstrates that the activity regulation of *PmHSP70* requires the participation of ATP (Sousa, 2012). The highly conserved intracellular specific motif EEVD ends in *PmHSP70*, indicating that *PmHSP70* belongs to cytoplasmic HSP70 family (Boutet et al., 2003; Liu et al., 2015). The results of multiple sequence alignments show that HSP70 in various bivalve species is highly conserved. The similarity of these sequence and structure suggest that PmHSP70 is functionally conserved. The construction of the phylogenetic tree found that *PmHSP70* and *HSP70* of bivalves such as *P. f. martensii* clustered together.

The distribution patterns of *PmHSP70* gene expression in different tissues indicate that *PmHSP70* was ubiquitously expressed in all tested tissues, including gills, hepatopancreas, adductor muscle and mantle, where the highest expression in gills. These results are consistent with previous findings of *Ruditapes philippinarum* (Nie et al., 2017) and *Chlamys nobilis*

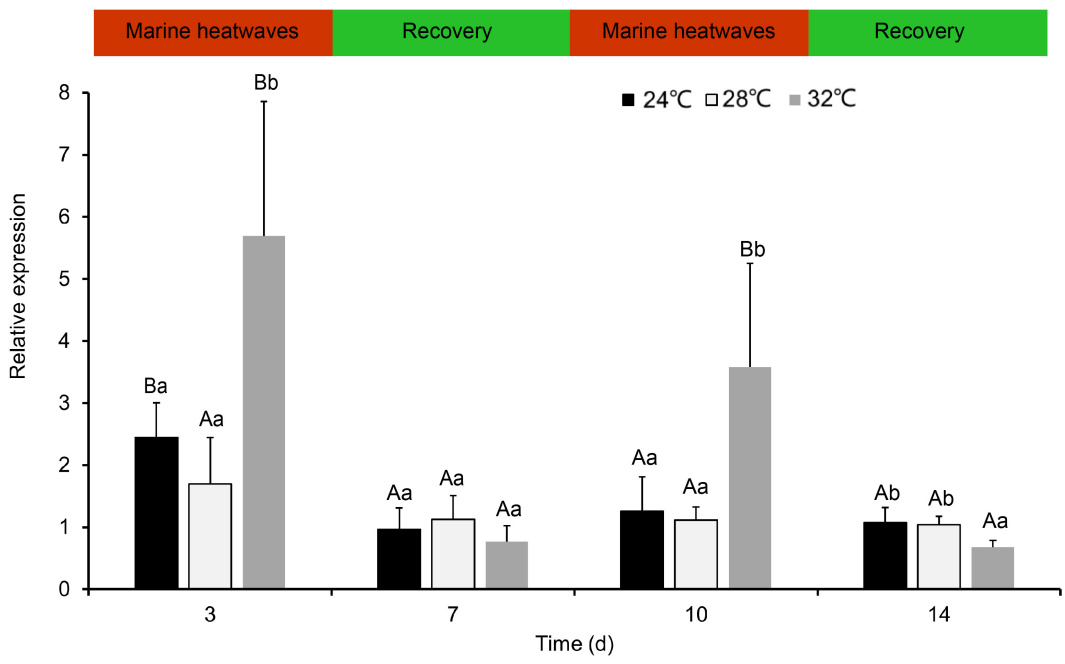

FIGURE 7 | The expression levels of *PmHSP70* mRNA in gill from *P. maxima* after exposed to repeatedly occurring MHWs scenarios. Small letters indicate significant differences between four temperature levels within each time, and capital letters indicate significant difference between different time within each temperature treatment ($P < 0.05$).

(Cheng et al., 2019). Studies have found that heat stress has the potential to destroy cell and tissue integrity, and impair the physiological functions of gills in marine bivalves (Rahman and Rahman, 2021). This is because bivalves are filter-feeding organisms, and the gills are both their respiratory and feeding organs which can directly sense environmental changes more than other tissues (Cheng et al., 2019), so in the face of MHWs, the expression of *HSP70* in the gills was significantly higher than that in other tissues.

In the present study, the expression of *PmHSP70* mRNA in gills of MHWs was measured at, 6, 12, 24, and 72 h after acute MHWs. As expected, *PmHSP70* is significantly up-regulated and correlated with temperature, and was highly expressed at 32 and 36°C groups, and the relative expression reached the highest at 72 and 12 h, respectively. These results are consistent with previous findings in *R. philippinarum, C. nobilis* and *Laternula elliptica* (Clark et al., 2008; Nie et al., 2017; Cheng et al., 2019). It is well known that when organisms are exposed to high temperatures, they produce amounts of reactive oxygen species (ROS) (Wang et al., 2018), which severely impairs normal cell functions. HSP70 is a universal molecular chaperone that participates in repairing or degrading damaged proteins (Feder and Hofmann, 1999), thereby protecting cells from environmental stress. The previous study showed that the HSPs of oysters is up-regulated under adverse environmental pressures and may be central to the oyster defense against all stresses (Zhang et al., 2012). We speculated that under the conditions of MHWs, the protein synthesis of pearl oysters was wrong, and too many harmful polymers were produced. The upregulation of *PmHSP70* expression in the pearl oysters corrects the misfolded peptide chain, promotes the degradation of harmful polymers in the cell, resists harsh environments and responds to changes in environmental temperature.

It is worth noting that the relative expression of *PmHSP70* in experimental groups was significantly lower than that at first MHWs, when pearl oysters are exposed to repeated MHWs. The expression level of *HSP70* has no significant difference between the second MHWs and the recovery period. These findings indicate that long-term and repeated occurring MHWs stimulate relieve the thermal stress of pearl oysters caused by MHWs. The previous study showed that in the *Crassostrea gigas* a moderate elevation of temperature promotes the induction of members of the HSP gene family, which makes cells more resistant to any further challenge with heat stress (Li and Werb, 1982; Hamdoun et al., 2003). Similar phenomena was found in our previous studies, where the activity of various antioxidant enzymes was significantly lower than that of the first MHWs during repeated MHWs, and the expression of some genes related to metabolism was also alleviated during the recurring MHWs (He et al., 2021; Xu et al., 2021, 2022).

In recent years, due to the unprecedented speed of MHWs, whether marine bivalves can keep up and adapt to rapid environmental changes has attracted widespread concern. Results in present study indicated *PmHSP70* expression in pearl oysters was inducible under MHWs stress. Plasticity of the heat-shock response is apparently a common feature in sessile intertidal invertebrates (Tomanek and Somero, 1999). In the laboratory, other bivalve species such as *Mytilus trossulus* and *C. gigas* exhibit significant plasticity in various features of the heat shock response (Buckley et al., 2001; Hamdoun et al., 2003). HSP family plays a critical role in rapid adaptation to novel thermal environments by preventing the degradation of intracellular proteins, and the high correlation between the induction of this gene family and the strong thermotolerance mechanism contributes to the environmental adaptation of aquatic animals (Kim et al., 2017). This adaptive plasticity will help marine bivalves adapt to changing marine environments and buffer the extinction of intertidal populations.

CONCLUSION

This study was the first report of full-length cloning, characterization and inducible expression of *HSP70* of *P. maxima*. The results of the phylogenetic tree and multiple sequence alignment showed that the sequence of the *PmHSP70* was relatively conserved among species and had high homology with the *HSP70* of other species. The tissue expression characteristics showed that the *PmHSP70* was expressed the highest in the gills. The expression level of *HSP70* in the acute MHWs scenario indicates that pearl oyster can respond to the adverse effects of MHWs by rapidly up-regulating the expression of *PmHSP70* under MHWs stimulation. It is worth noting that when faced with recurring MHWs, compared with the first MHWs period the expression of *PmHSP70* was significantly down-regulated and had no significant difference between the recovery period. We speculated that the pearl oysters have adaptation potential under the stress of long-term and repeatedly occurring. Our findings will provide reference materials for the adaptation of marine organisms to the extreme marine environment. But we have only done one generation of impact. Further investigations are needed to elucidate transmission of carryover effects of MHWs within and across generations.

DATA AVAILABILITY STATEMENT

The datasets presented in this study can be found in online repositories. The names of the repository/repositories and accession number(s) can be found in the article/supplementary material.

AUTHOR CONTRIBUTIONS

YX: methodology, investigation, and writing—original draft preparation. JL, GH, and FM: methodology. XL: methodology, formal analysis. KY: resources and formal analysis. YD: conceptualization. LZ: conceptualization, writing—original draft preparation, and project administration. All authors contributed to the article and approved the submitted version.

FUNDING

The present study has been made possible by the research grants from National Natural Science Foundation of China (42076121, M-0163), the Department of Education of Guangdong Province (2020KTSCX050) and the Starting Research Fund from Guangdong Ocean University (R20083) to LZ, and the Earmarked Fund for Modern Agro-industry Technology Research System (CARS-49) to YD.

REFERENCES

Amorim, V., Gonçalves, O., Capela, R., Fernández-Boo, S., Oliveira, M., Dolbeth, M., et al. (2020). Immunological and oxidative stress responses of the bivalve *Scrobicularia plana* to distinct patterns of heatwaves. *Fish Shellfish Immunol.* 106, 1067–1077. doi: 10.1016/j.fsi.2020.09.024

Bedulina, D., Evgen'Ev, M., Timofeyev, M., Protopopova, M., Garbuz, D., Pavlichenko, V., et al. (2013). Expression patterns and organization of the hsp70 genes correlate with thermotolerance in two congener endemic amphipod species (*Eulimnogammarus cyaneus* and *E. verrucosus*) from Lake Baikal. *Mol. Ecol.* 22, 1416–1430. doi: 10.1111/mec.12136

Boutet, I., Tanguy, A., Rousseau, S., Auffret, M., and Moraga, D. (2003). Molecular identification and expression of heat shock cognate 70 (hsc70) and heat shock protein 70 (hsp70) genes in the Pacific oyster *Crassostrea gigas*. *Cell Stress Chaperones* 8:76. doi: 10.1379/1466-1268(2003)8<76:miaeoh>2.0.co;2

Buckley, B. A., Owen, M.-E., and Hofmann, G. E. (2001). Adjusting the thermostat: the threshold induction temperature for the heat-shock response in intertidal mussels (genus Mytilus) changes as a function of thermal history. *J. Exp. Biol.* 204, 3571–3579. doi: 10.1242/jeb.204.20.3571

Caputi, N., Kangas, M., Denham, A., Feng, M., Pearce, A., Hetzel, Y., et al. (2016). Management adaptation of invertebrate fisheries to an extreme marine heat wave event at a global warming hot spot. *Ecol. Evol.* 6, 3583–3593. doi: 10.1002/ece3.2137

Chandrapavan, A., Caputi, N., and Kangas, M. I. (2019). The decline and recovery of a crab population from an extreme marine heatwave and a changing climate. *Front. Mar. Sci.* 6:510. doi: 10.3389/fmars.2019.00510

Chen, T., Lin, T., Li, H., Lu, T., Li, J., Huang, W., et al. (2018). Heat shock protein 40 (HSP40) in pacific white shrimp (*Litopenaeus vannamei*): molecular cloning, tissue distribution and ontogeny, response to temperature, acidity/alkalinity and salinity stresses, and potential role in ovarian development. *Front. Physiol.* 9:1784. doi: 10.3389/fphys.2018.01784

Cheng, D., Liu, H., Zhang, H., Soon, T. K., Ye, T., Li, S., et al. (2019). Differential expressions of HSP70 gene between golden and brown noble scallops *Chlamys nobilis* under heat stress and bacterial challenge. *Fish Shellfish Immunol.* 94, 924–933. doi: 10.1016/j.fsi.2019.10.018

Clark, M. S., Fraser, K. P., and Peck, L. S. (2008). Antarctic marine molluscs do have an HSP70 heat shock response. *Cell Stress Chaperones* 13, 39–49. doi: 10.1007/s12192-008-0014-8

Clegg, J., Uhlinger, K., Jackson, S., Cherr, G., Rifkin, E., and Friedman, C. (1998). Induced thermotolerance and the heat shock protein-70 family in the Pacific oyster *Crassostrea gigas*. *Mol. Mar. Biol. Biotechnol.* 7, 21–30.

Dong, S., Nie, H., Ye, J., Li, D., Huo, Z., and Yan, X. (2020). Physiological and gene expression analysis of the Manila clam *Ruditapes philippinarum* in response to cold acclimation. *Sci. Total Environ.* 742:140427. doi: 10.1016/j.scitotenv.2020.140427

Evgen'ev, M., Garbuz, D., Shilova, V., and Zatsepina, O. (2007). Molecular mechanisms underlying thermal adaptation of xeric animals. *J. Biosci.* 32, 489–499. doi: 10.1007/s12038-007-0048-6

FAO (2014). *Fishery and Aquaculture Statistics*. Rome: Food and Agriculture Organization.

Feder, M. E., and Hofmann, G. E. (1999). Heat-shock proteins, molecular chaperones, and the stress response: evolutionary and ecological physiology. *Ann. Rev. Physiol.* 61, 243–282.

Fordyce, A. J., Ainsworth, T. D., Heron, S. F., and Leggat, W. (2019). Marine heatwave hotspots in coral reef environments: physical drivers, ecophysiological outcomes, and impact upon structural complexity. *Front. Mar. Sci.* 6:498. doi: 10.3389/fmars.2019.00498

Gupta, R. S., and Singh, B. (1994). Phylogenetic analysis of 70 kD heat shock protein sequences suggests a chimeric origin for the eukaryotic cell nucleus. *Curr. Biol.* 4, 1104–1114. doi: 10.1016/s0960-9822(00)00249-9

Hamdoun, A. M., Cheney, D. P., and Cherr, G. N. (2003). Phenotypic plasticity of HSP70 and HSP70 gene expression in the Pacific oyster (*Crassostrea gigas*): implications for thermal limits and induction of thermal tolerance. *Biol. Bull.* 205, 160–169. doi: 10.2307/1543236

Harley, C. D. G. (2008). Tidal dynamics, topographic orientation, and temperature-mediated mass mortalities on rocky shores. *Mar. Ecol. Prog. Ser.* 371, 37–46.

Hassan, F. U., Nawaz, A., Srehman, M., Aali, M., Mrdilshad, S., and Yang, C. J. (2019). Prospects of HSP70 as a genetic marker for thermo-tolerance and immuno-modulation in animals under climate change scenario. *Anim. Nutr.* 5, 340–350. doi: 10.1016/j.aninu.2019.06.005

He, G., Liu, X., Xu, Y., Liang, J., Deng, Y., Zhang, Y., et al. (2021). Repeated exposure to simulated marine heatwaves enhances the thermal tolerance in pearl oysters. *Aquatic Toxicol.* 239:105959. doi: 10.1016/j.aquatox.2021.105959

Hobday, A. J., Alexander, L. V., Perkins, S. E., Smale, D. A., Straub, S. C., Oliver, E. C., et al. (2016). A hierarchical approach to defining marine heatwaves. *Prog. Oceanography* 141, 227–238. doi: 10.1016/j.pocean.2015.12.014

Holbrook, N. J., Gupta, A. S., Oliver, E. C., Hobday, A. J., Benthuysen, J. A., Scannell, H. A., et al. (2020). Keeping pace with marine heatwaves. *Nat. Rev. Earth Environ.* 1, 482–493.

Hu, M., Qiu, Z., Zhou, P., Xu, L., and Zhang, J. (2012). Proteomic analysis of 'Zaosu'pear (*Pyrus bretschneideri* Rehd.) and its red skin bud mutation. *Proteome Sci.* 10, 1–15. doi: 10.1186/1477-5956-10-51

Jones, D. B., Jerry, D. R., Khatkar, M. S., Raadsma, H. W., and Zenger, K. R. (2013). A high-density SNP genetic linkage map for the silver-lipped pearl oyster, *Pinctada maxima*: a valuable resource for gene localisation and marker-assisted selection. *BMC Genom.* 14:810. doi: 10.1186/1471-2164-14-810

Kim, B.-M., Kim, K., Choi, I.-Y., and Rhee, J.-S. (2017). Transcriptome response of the Pacific oyster, *Crassostrea gigas* susceptible to thermal stress: a comparison with the response of tolerant oyster. *Mol. Cell. Toxicol.* 13, 105–113.

Li, G. C., and Werb, Z. (1982). Correlation between synthesis of heat shock proteins and development of thermotolerance in Chinese hamster fibroblasts. *Proc. Natl. Acad. Sci. U S A.* 79, 3218–3222. doi: 10.1073/pnas.79.10.3218

Li, Y., Ren, G., Wang, Q., and You, Q. (2019). More extreme marine heatwaves in the China Seas during the global warming hiatus. *Environ. Res. Lett.* 14:104010.

Liu, K., Xu, K., Zhu, C., and Liu, B. (2021). Diversity of marine heatwaves in the South China Sea regulated by the ENSO phase. *J. Climate* 35, 877–893. doi: 10.1175/jcli-d-21-0309.1

Liu, T., Pan, L., Ca, I. Y., and Miao, J. (2015). Molecular cloning and sequence analysis of heat shock proteins 70 (HSP70) and 90 (HSP90) and their expression analysis when exposed to benzo(a)pyrene in the clam *Ruditapes philippinarum*. *Gene* 555, 108–118. doi: 10.1016/j.gene.2014.10.051

Liu, Z. M., Zhu, X. L., Lu, J., Cai, W. J., Ye, Y. P., and Lv, Y. P. (2018). Effect of high temperature stress on heat shock protein expression and antioxidant enzyme activity of two morphs of the mud crab *Scylla paramamosain*. *Comp. Biochem. Physiol. Part A Mol. Integrative Physiol.* 223, 10–17. doi: 10.1016/j.cbpa.2018.04.016

Mayer, M., and Bukau, B. (2005). Hsp70 chaperones: cellular functions and molecular mechanism. *Cell. Mol. Life Sci.* 62, 670–684. doi: 10.1007/s00018-004-4464-6

Nie, H., Liu, L., Huo, Z., Chen, P., Ding, J., Yang, F., et al. (2017). The HSP70 gene expression responses to thermal and salinity stress in wild and cultivated Manila clam *Ruditapes philippinarum*. *Aquaculture* 470, 149–156.

Park, K., Lee, J. S., Kang, J. C., Kim, J. W., and Kwak, I. S. (2015). Cascading effects from survival to physiological activities, and gene expression of heat shock protein 90 on the abalone Haliotis discus hannai responding to continuous thermal stress. *Fish Shellfish Immunol.* 42, 233–240. doi: 10.1016/j.fsi.2014.10.036

Petes, L. E., Menge, B. A., and Murphy, G. D. (2007). Environmental stress decreases survival, growth, and reproduction in New Zealand mussels. *J. Exp. Mar. Biol. Ecol.* 351, 83–91.

Pörtner, H. (2001). Climate change and temperature-dependent biogeography: oxygen limitation of thermal tolerance in animals. *Naturwissenschaften* 88, 137–146. doi: 10.1007/s001140100216

Rahman, M. S., and Rahman, M. S. (2021). Effects of elevated temperature on prooxidant-antioxidant homeostasis and redox status in the American oyster: signaling pathways of cellular apoptosis during heat stress. *Environ. Res.* 196:110428. doi: 10.1016/j.envres.2020.110428

Rendina, F., Bouchet, P. J., Appolloni, L., Russo, G. F., Sandulli, R., Kolzenburg, R., et al. (2019). Physiological response of the coralline alga *Corallina officinalis* L. to both predicted long-term increases in temperature and short-term heatwave events. *Mar. Environ. Res.* 150:104764. doi: 10.1016/j.marenvres.2019.104764

Scanes, E., Parker, L. M., O'Connor, W. A., Dove, M. C., and Ross, P. M. (2020). Heatwaves alter survival of the Sydney rock oyster, *Saccostrea glomerata*. *Mar. Pollution Bull.* 158:111389. doi: 10.1016/j.marpolbul.2020.111389

Seuront, L., Nicastro, K. R., Zardi, G. I., and Goberville, E. (2019). Decreased thermal tolerance under recurrent heat stress conditions explains summer mass mortality of the blue mussel *Mytilus edulis*. *Sci. Rep.* 9:17498. doi: 10.1038/s41598-019-53580-w

Smale, D. A., Wernberg, T., Oliver, E. C., Thomsen, M., Harvey, B. P., Straub, S. C., et al. (2019). Marine heatwaves threaten global biodiversity and the provision of ecosystem services. *Nat. Climate Change* 9, 306–312. doi: 10.1038/s41558-019-0412-1

Somero, G. N. (2005). Linking biogeography to physiology: evolutionary and acclimatory adjustments of thermal limits. *Front. Zool.* 2:1. doi: 10.1186/1742-9994-2-1

Sousa, R. (2012). A dancer caught midstep: the structure of ATP-bound Hsp70. *Mol. Cell* 48, 821–823. doi: 10.1016/j.molcel.2012.12.008

Tomanek, L., and Somero, G. N. (1999). Evolutionary and acclimation-induced variation in the heat-shock responses of congeneric marine snails (genus Tegula) from different thermal habitats: implications for limits of thermotolerance and biogeography. *J. Exp. Biol.* 202, 2925–2936. doi: 10.1242/jeb.202.21.2925

Tomanek, L., and Somero, G. N. (2002). Interspecific-and acclimation-induced variation in levels of heat-shock proteins 70 (hsp70) and 90 (hsp90) and heat-shock transcription factor-1 (HSF1) in congeneric marine snails (genus Tegula): implications for regulation of hsp gene expression. *J. Exp. Biol.* 205, 677–685. doi: 10.1242/jeb.205.5.677

Wang, J., Dong, B., Yu, Z.-X., and Yao, C.-L. (2018). The impact of acute thermal stress on green mussel *Perna viridis*: oxidative damage and responses. *Comp. Biochem. Physiol. Part A: Mol. Integrat. Physiol.* 222, 7–15. doi: 10.1016/j.cbpa.2018.04.001

Wang, Z., Liang, F., Huang, R., Deng, Y., and Li, J. (2019). Identification of the differentially expressed genes of *Pinctada maxima* individuals with different sizes through transcriptome analysis. *Regional Stud. Mar. Sci.* 26:100512. doi: 10.1016/j.rsma.2019.100512

Xu, Y., Wang, Z., Zhang, Y., Liang, J., He, G., Liu, X., et al. (2022). Transcriptome analysis reveals acclimation responses of pearl oysters to marine heatwaves. *Sci. Total Environ.* 810:151189. doi: 10.1016/j.scitotenv.2021.151189

Xu, Y., Zhang, Y., Liang, J., He, G., Liu, X., Zheng, Z., et al. (2021). Impacts of marine heatwaves on pearl oysters are alleviated following repeated exposure. *Mar. Pollution Bull.* 173:112932. doi: 10.1016/j.marpolbul.2021.112932

Yao, Y., Wang, J., Yin, J., and Zou, X. (2020). Marine heatwaves in china's marginal seas and adjacent offshore waters: Past, Present, and Future. *J. Geophys. Res.: Oceans* 125:e2019JC015801.

Zhang, G., Fang, X., Guo, X., Li, L., Luo, R., Xu, F., et al. (2012). The oyster genome reveals stress adaptation and complexity of shell formation. *Nature* 490, 49–54. doi: 10.1038/nature11413

Zhang, W., Zheng, Z., Zhang, T., and Chen, T. (2020). Strengthened marine heatwaves over the Beibu Gulf coral reef regions from 1960 to 2017. *Haiyang Xuebao* 42, 41–49.

Zhang, X., and Xie, J. (2019). Analysis of proteins associated with quality deterioration of grouper fillets based on TMT quantitative proteomics during refrigerated storage. *Molecules* 24:2641. doi: 10.3390/molecules24142641

Zhao, L., Liu, L., Liu, B., Liang, J., Lu, Y., and Yang, F. (2019). Antioxidant responses to seawater acidification in an invasive fouling mussel are alleviated by transgenerational acclimation. *Aquatic Toxicol.* 217:10533. doi: 10.1016/j.aquatox.2019.105331

Zhao, L., Shirai, K., Tanaka, K., Milano, S., Higuchi, T., Murakami-Sugihara, N., et al. (2020). A review of transgenerational effects of ocean acidification on marine bivalves and their implications for sclerochronology. *Estuarine Coastal Shelf Sci.* 235:106620. doi: 10.1016/j.ecss.2020.106620

Conflict of Interest: The authors declare that the research was conducted in the absence of any commercial or financial relationships that could be construed as a potential conflict of interest.

Publisher's Note: All claims expressed in this article are solely those of the authors and do not necessarily represent those of their affiliated organizations, or those of the publisher, the editors and the reviewers. Any product that may be evaluated in this article, or claim that may be made by its manufacturer, is not guaranteed or endorsed by the publisher.

frontiers in Marine Science

ORIGINAL RESEARCH
published: 14 March 2022
doi: 10.3389/fmars.2022.851098

Transcriptome Analysis of *Crassostrea sikamea* (♀) × *Crassostrea gigas* (♂) Hybrids Under Hypoxia in Occluded Water

*Xuekai Zhang[1], Chao Fan[1], Jinlong Li[1], Xingzhi Zhang[2], Qiongzhen Li[2] and Zhaoping Wang[1]**

[1] Key Laboratory of Mariculture of Ministry of Education, Ocean University of China, Qingdao, China, [2] Guangxi Key Laboratory of Aquatic Genetic Breeding and Healthy Aquaculture, Guangxi Academy of Fisheries Sciences, Nanning, China

OPEN ACCESS

Edited by:
Yuehuan Zhang, South China Sea Institute of Oceanology (CAS), China

Reviewed by:
Xizhi Huang, Johannes Gutenberg University Mainz, Germany
Zhenming Lv, Zhejiang Ocean University, China
Linlin Zhang, Key Laboratory of Experimental Marine Biology, Institute of Oceanology (CAS), China

***Correspondence:**
Zhaoping Wan
zpwang@ouc.edu.cn

Specialty section:
This article was submitted to Marine Fisheries, Aquaculture and Living Resources, a section of the journal Frontiers in Marine Science

Received: *09 January 2022*
Accepted: *31 January 2022*
Published: *14 March 2022*

Citation:
Zhang X, Fan C, Li J, Zhang X, Li Q and Wang Z (2022) Transcriptome Analysis of Crassostrea sikamea (♀) × Crassostrea gigas (♂) Hybrids Under Hypoxia in Occluded Water. Front. Mar. Sci. 9:851098. doi: 10.3389/fmars.2022.851098

Hypoxia is considered to be one of the key factors affecting the survival of ocean organisms, it is necessary to parse the molecular processes involved in response to hypoxia. As a potential breeding species, the hybrid of *Crassostrea sikamea* (♀) × *Crassostrea gigas* (♂) shows valuable heterosis in survival and growth traits. Thus, RNA *de novo* was deployed in this study to analyze the molecular processes in the hybrids under hypoxia stress. The hybrids were cultured in occluded water, then the dissolved oxygen was gradually consumed by oysters, and the gill tissue of hybrids was sampled at the very beginning and the lowest respiration point in the experiment. In the current study, 901 significant differentially expressed genes (DEGs) were identified under hypoxia compared to normoxia, among which 432 DEGs were downregulated, and the other 469 DEGs were upregulated. A total of 27 GO terms were significantly enriched, such as an integral component of membrane, extracellular region, immune response, tumor necrosis factor receptor binding, and neurotransmitter: sodium symporter activity. Besides, 19 KEGG pathways were significantly enriched, such as apoptosis, Th1 and Th2 cell differentiation, complement, and coagulation cascades, antigen processing and presentation, notch signaling pathway, and cytokine–cytokine receptor interaction. The current results showed that the *TRAIL* genes were downregulated, but the *HSP*70 and *LIGHT* genes were upregulated, which indicated the inhibition of Apoptosis, and the activity of innate immunity in oysters under hypoxia. This study provides preliminary insight into the molecular response to hypoxia in the gill of hybrids.

Keywords: oyster hybrids, gill, hypoxia, transcriptome, *de novo*

INTRODUCTION

Mollusks, including oysters, serve as indeed important aquaculture resources providing considerable economic value for the coastal areas. Hybridization could be a considerable way to enhance yield or survival due to better performance than the half-siblings, which is known as heterosis (Hedgecock and Davis, 2007). Recently, the studies on oyster interspecific crossbreeding have been well documented (Xu et al., 2011, 2019; Huo et al., 2014; Zhang et al., 2017), and some

of these hybrids have shown adaptabilities or better growth traits. Previous studies only focused on growth performance, while identifying the changes in physiological mechanisms that respond to environmental stress is critical to help determine the growth and survival of individuals and the yield potential in aquaculture (Furr et al., 2021).

In recent years, with the development of the oyster industry summer mortality has been one of the most severe questions in farming practice. Previous studies indicated that the two major reasons for bivalve mass mortality were temperature increasing and dissolved oxygen decreasing (Parthasarathy et al., 1992; Joos et al., 2003; Soon and Zheng, 2019; Zhao et al., 2019; He et al., 2021), and hypoxia is considered to be one of the key factors affecting the survival of ocean organisms (Gu et al., 2019; Andreyeva et al., 2021). Benthic intertidal communities have developed appropriate survival mechanisms due to daily exposure into the air during low tide (Larade and Storey, 2002; Zhao et al., 2020), but over-farming, sediment covering, or algae blooming (Wu, 2002) could also cause water hypoxia. Recent studies showed that the fluctuations of dissolved oxygen frequently influence physiological, metabolic, and cellular processes in organisms, and in this situation, oxidative stress becomes one of the reasons that cause cellular damage (Nogueira et al., 2017; Andreyeva et al., 2021).

The heterosis of survival and maternal comparable growth traits have been reported in *Crassostrea gigas* and *Crassostrea sikamea* hybrids (Xu et al., 2019). According to our previous study, the hybrids have lower mortality than both parents when they were cultured in southern China, particularly the sire-siblings, where the annual water temperature is high (Zhang et al., 2021). Therefore, hybrids could be a potential breeding species. Gills of bivalves are in direct contact with seawater and therefore are the first issue facing the damaging effect of hypoxia, besides, the gill is an important organ involved in the innate immunity of shellfish among a variety of organs (Seo et al., 2013; Guo et al., 2015; Wang et al., 2018). The antioxidant complex in the gills of bivalves has been fully characterized in several studies (Bo-Mi et al., 2018; Box et al., 2020), and the expressions of stress response-related adapting genes could also be triggered by environmental threats in oyster gills (Guo et al., 2015).

The purpose of this experiment was to explore the molecular mechanism of hypoxia tolerance in gills of *C. sikamea* × *C. gigas* hybrids. RNA *de novo* was used to analyze the transcriptome in gills under hypoxia stress. This study provides preliminary insight into the molecular response to hypoxia in the gill of hybrids.

MATERIALS AND METHODS

Experimental Design and Animal Sampling

The hybrids of *C. sikamea* (♀) × C. *gigas* (♂) that were 12 months old were used in the experiment with a shell length of 43.19 ± 6.71 mm and weight of 15.17 ± 3.71 g (mean ± SD). The hybrids were cultured in Beihai, China, in 2018, as described by Zhang et al. (2021). A total of 60 healthy non-injured hybrids were selected and reared in filtered, aerated water with the temperature of 26.00 ± 0.11°C, dissolved oxygen of 6.12 ± 0.11 mg/L, the salinity of 30.56 ± 0.02 ppt, and pH 8.18 ± 0.02 for 2 weeks of acclimatization, and fed with a mixture of *Isochrysis galbana* and *Chaetoceros muelleri*.

The experiment was performed in June 2019 and the oysters were placed in three 30 L tanks with filtered seawater. Three tanks were used for each control group and test group. About 20 oysters were placed in each tank in separate small cases. Control groups were 3 sealed tanks without oysters to test the changes of dissolved oxygen in the water itself. All groups were being aerated till the system was in a steady state, then stop aerating. To avoid the exchange of air, floating plastic membranes were placed on the surface of the water. Hypoxia condition occurred in the 3 test tanks due to dissolved oxygen consumed by oysters. Each tank was connected to a dissolved oxygen detector to monitor the water condition. The experiment lasted for 60 h and recorded the dissolved oxygen every 2 h. As dissolved oxygen decreases, the oxygen consumption rate of the oyster changes. It was observed that the dissolved oxygen in the occluded water was lower than 3.0 mg/L after 36 h, and decreased to less than 2.5 mg/L after 48 h, and then the oxygen consumption level of oysters was extremely low (**Figure 1**). This occluded water was chosen to mimic the hypoxia water conditions. According to the national standard of water quality, the ammonia–nitrogen in water was below 0.02 mg/L (minimum detection limit) before and after the experiment determined by gas-phase molecular absorption spectrometry (Standard No: HJ/T 195-2005).

Oysters were sampled under the steady state (normoxia) and DO less than 2.5 mg/L (hypoxia) in occluded water (around 54 h culturing), respectively. The gills of six oysters were sampled, pooled, and stored at −80°C until total RNA was extracted.

RNA Extraction, Library Construction, and Sequencing

Total RNA was extracted from the normoxia and hypoxia gills using TRIzol (Invitrogen, Carlsbad, CA, United States). RNA samples were qualified and quantified using a NanoDrop spectrophotometer (NanoDrop Technologies, Wilmington, DE, United States) and the Agilent Technologies 2100 Bioanalyzer (Thermo Fisher Scientific, Waltham, MA, United States).

The mRNA was purified by removing potential DNA pollution with DNase I, removing possible rRNA pollution with RNase H, and finally recovered with Oligo(dT)-attached magnetic beads (Illumina, San Diego, CA, United States). Purified mRNA was fragmented with a fragment buffer at an appropriate temperature. Then, first-/second-strand cDNA was generated by polymerase chain reaction. The A-Tailing Mix and RNA index adapters were added and incubated to carry out end-repair. The cDNA fragments with adapters were amplified, and the products were purified with Ampure XP beads. The library was validated on the Agilent Technologies 2100 Bioanalyzer for quality control. The final library was amplified with phi29 to create DNA nanoballs (DNB), containing more than 300 copies of the original template. The DNBs were loaded into the patterned nanoarray, and pair-end 100 base reads were generated on a BGISEQ500 platform (BGI, Shenzhen, China).

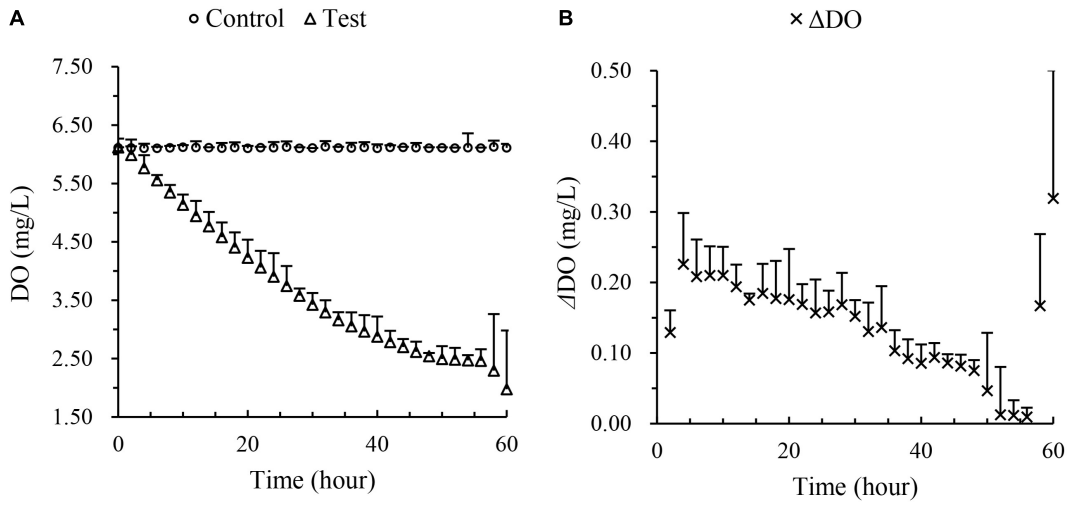

FIGURE 1 | Dissolved oxygen in occluded water with time: **(A)** The average DO of control groups and test groups; **(B)** the average Δ DO in the test groups between two successive recording points.

Transcriptome Assembly

The filtering software SOAPnuke v1.4.0 developed by BGI was used for statistical analysis and filtering. Raw reads with joint contamination and high numbers of unknown N bases were removed before the data analysis to ensure the reliability of the results. Then, the Q20/Q30 and GC-content of the clean data were measured. Clean reads were assembled with Trinity v2.0.6 software, and the transcripts were clustered with Tgicl v 2.1 to generate unigenes. The quality of the assembled transcripts was assessed using Benchmarking Universal Single-Copy Orthologs (BUSCO), a single-copy lineal homology database, and the integrity of the transcriptome assembly was demonstrated by comparison with conserved genes.

Functional Annotation of the Assembled Unigenes

The fragments per kilobase per million reads (FPKM) method was used to calculate the expression levels. Bowtie2 v2.2.5 software was used to compare clean reads with the reference gene sequence, and then RSEM was used to calculate the expression levels of the unigenes and transcripts. The prediction and annotation data of all unigenes were compared with protein databases, including NCBI non-redundant protein sequences and nucleotide sequences (Nr&Nt),[1] Gene Ontology (GO),[2] Kyoto Encyclopedia of Genes and Genomes (KEGG),[3] Clusters of Orthologous Groups of proteins/eukaryotic Orthologous Groups (COG/KOG),[4] Swiss-Prot,[5] and Protein family (Pfam).[6] Hmmscan v3.0, Blast v2.2.23, and Blast2GO software were used to obtain the annotation information for the unigenes. When the annotation of different databases conflicted, the priority order of alignments from the Nr, Nt, KEGG, Swiss-Prot, GO, COG, and Pfam databases were followed.

Analysis of Differentially Expressed Genes

In this study, the FPKM method was used to calculate the expression of unigenes so that to compare gene expression levels between samples. The FDR (false discovery rate) was applied to identify the threshold of the *p*-value in multiple tests (Mortazavi et al., 2008). The threshold of significantly expressed genes was set as FPKM $\geq$ 1, $|\log_2^{(\text{fold change})}| \geq 2$, FDR < 0.05. Then, GO and KEGG enrichment was performed to analyze the main biochemical and signal transduction pathways by using $p < 0.01$ as the threshold of significantly enriched differentially expressed genes (DEGs).

Quantitative Real-Time Polymerase Chain Reaction

Total RNA was reverse-transcribed into cDNA with the PrimeScript RT Reagent Kit (Takara, Beijing, China). Eight typical DEGs, tumor necrosis factor (*TNF*) superfamily member 10 (*TNFSF*10), meprin B (*MEP*1*B*), histone deacetylase 11 (*HDAC*11), Notch 1 (*NOTCH*1), caspase 7 (*CASP*7), mucin-2 (*MUC*2), plasminogen (*PLG*), interferon regulatory factor 2 (*IRF*2), and a reference gene (tubulin α, TUBG) were selected for verification by qRT-PCR.

Gene-specific primers were designed with Primer Premier 5.0 software. All real-time PCR experiments were carried out in 96-well PCR plates. Each 20 μL amplification reaction was conducted using the StepOne Plus system (ABI, Foster City, CA, United States) in triplicate. The PCR process included 95°C for 3 min; 45 cycles of 95°C for 5 s, and 60°C for 30 s; followed by a melting curve. The differentiation expression was calculated

[1] ftp://ftp.ncbi.nlm.nih.gov/blast/db
[2] http://www.geneontology.org/
[3] http://www.genome.jp/kegg/
[4] https://www.ncbi.nlm.nih.gov/COG/
[5] http://www.ebi.ac.uk/uniprot
[6] http://pfam.xfam.org

with the method by Livak and Schmittgen (2001). The expression fold change ($2^{-\Delta\Delta CT}$) of the qRT-PCR data and $Log_2^{(foldchange)}$ of the RNA-seq data were used, and correlation was calculated in Spearman analysis.

RESULTS

RNA Sequencing and *de novo* Assembly

The statistical information of sequencing data for the normoxia and hypoxia samples is given in **Table 1**. The average number of total raw reads generated from each library was 66.84 million, and the average clean reads were 64.03 million. The total mapping rate of the library was 81.11–83.21%, and the average Q30 value was 89.49. In total, 84,359 unigenes were assembled into six libraries with an average unigene number of 54,010, with a mean length of 932 bp. The average GC percentage of unigene was 39.67%, and the N50 was 1,640 bp.

According to the evaluation of transcript assembly, more than 85% of unigenes matched or partially matched into the BUSCO database, and only around 2.31% were unmatched (**Figure 2**). The results showed that transcription data could be used for annotation analysis. All raw reads were deposited in the NCBI Short Read Archive database with an Accession number of PRJNA587775.

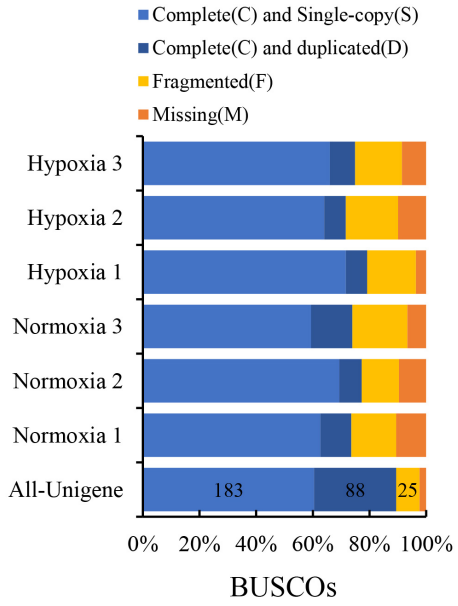

FIGURE 2 | Evaluation of transcript assembly by Benchmarking Universal Single-Copy Orthologs (BUSCO).

Functional Annotation and Classification

To identify the categories and functions of transcriptional sequences, all unigenes were blasted into seven functional databases. Among which 56,071 unigenes in the NR protein sequence database (66.47%), 67,797 unigenes in the NT database (80.37%), 32,377 unigenes in the Swiss-Prot (38.38%), 39,082 unigenes in the KEGG (46.33%), 29,614 unigenes in the KOG (35.10%), 38,026 unigenes in the Pfam (45.08%), and 29,415 unigenes in the GO (34.87%) were annotated. Overall, 72,724 (86.21%) unigenes matched to at least one database, and 15,016 (17.80%) unigenes were annotated into all seven databases (**Table 2**). There were five species in the NR annotations, including *C. gigas*, *Crassostrea virginica*, *Mizuhopecten yessoensis*, *Lottia gigantea*, and *Apostichopus japonicus*, with the annotation rates of 89.88% (50,396), 6.39% (3,581), 0.65% (365), 0.14% (81), and 0.11% (64), respectively (**Supplementary Table 1**).

The classification of 25 KOG gene homologs was identified, and the top three annotated terms were signal transduction mechanisms (5,451), general function prediction only (5,066), and post-translational modifications, protein turnover, and chaperones (3,088) (**Figure 3**).

Identification and Enrichment Analysis of the Differentially Expressed Genes

In total, 901 DEGs were identified in the analysis between the normoxia and hypoxia groups. Among these genes, 432 DEGs were downregulated and 469 were upregulated (**Figure 4**). The GO annotation assigns all DEGs into three major functional categories: molecular functions, cellular components, and biological processes. Overall, 325 genes were grouped into molecular functions, that is, catalytic activity (116 genes) and binding sectors (154 genes); 531 genes were grouped into cellular components, that is, membrane part (163 genes) and membrane (172 genes); 292 genes were grouped into biological processes, that is, metabolic process (56 genes) and cellular process (73 genes), respectively (**Figure 5**).

TABLE 1 | Sequencing data statistics for the normoxia and hypoxia samples.

Sample	Raw reads (M)	Clean reads (M)	Total mapping (%)	Clean reads Q30 (%)	Unigene number	Mean length (bp)	N50	GC (%)
Normoxia 1	67.68	64.75	82.80	90.42	53,835	995	1,736	39.54
Normoxia 2	67.68	64.59	83.21	89.48	54,007	912	1,551	39.73
Normoxia 3	65.17	62.51	82.10	89.88	54,799	985	1,726	39.32
Hypoxia 1	65.17	62.48	81.11	88.87	55,325	894	1,489	39.87
Hypoxia 2	67.68	64.81	83.04	88.84	53,199	902	1,512	39.89
Hypoxia 3	67.68	65.03	81.69	89.42	52,897	904	1,527	39.68
Average	66.84	64.03	82.33	89.49	54,010	932	1,590	39.67

TABLE 2 | The annotation number and proportion of unigenes in NR, NT, Swiss-prot, KEGG, KOG, Pfam, and GO databases.

Values	Total	NR	NT	Swiss-prot	KEGG	KOG	Pfam	GO	Intersection	Overall
Number	84,359	56,071	67,797	32,377	39,082	29,614	38,026	29,415	15,016	72,724
Percentage	100%	66.47%	80.37%	38.38%	46.33%	35.10%	45.08%	34.87%	17.80%	86.21%

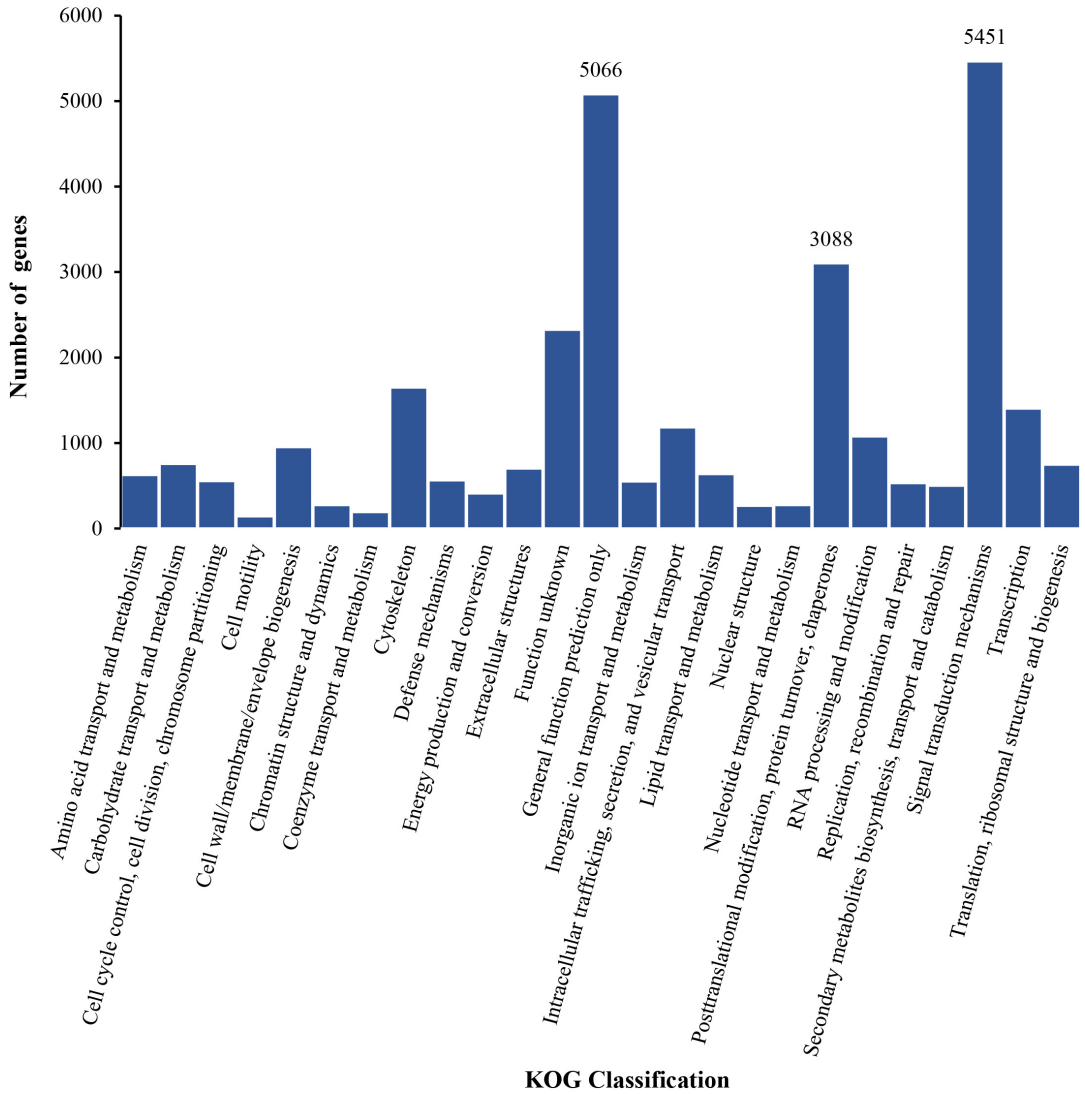

FIGURE 3 | The annotated classification information of unigene sequence on the gene homologs from the Eukaryotic Orthologous Groups (KOG) database.

The KEGG annotation assigns all DEGs into six major functional categories: organismal systems, metabolism, human diseases, genetic information processing, environmental information processing, and cellular processes. Overall, 317 genes were grouped into organismal systems, that is, endocrine system (72 genes) and immune system (108 genes); 136 genes were grouped into a metabolism, that is, global overview maps (51 genes); 444 genes were grouped into human diseases, that is, cancers: specific types (71 genes), cancers: overview (77 genes), and infectious diseases: viral (77 genes); 70 genes were grouped into genetic information processing, that is, folding, sorting, and degradation (31 genes); 147 genes were grouped into environmental information processing, that is, signal transduction (109 genes); 139 genes were grouped into cellular processes, that is, transport catabolism (46 genes), respectively (**Figure 6**).

The GO analysis was deployed to clarify the changes of the DEGs in the hybrids under hypoxia stress. Overall, 27 GO terms were significantly enriched, and the order of the GO term enriching number in the different categories was BP (13 terms) > MF (12 terms) > CC (2 terms). The primary enriched GO terms that included the GO:0016021_Integral

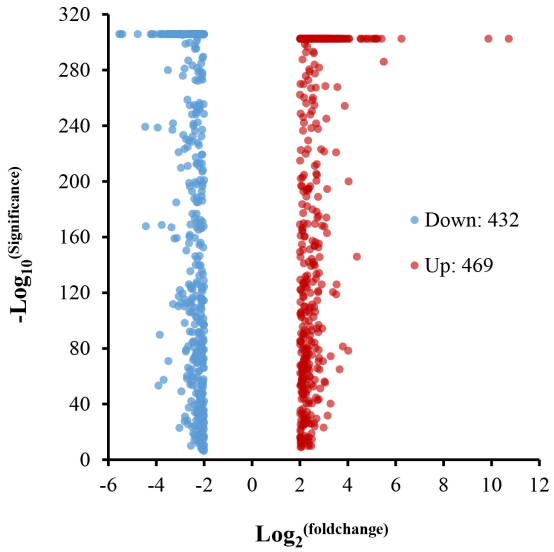

FIGURE 4 | Differentially expressed genes between the normoxia and hypoxia groups.

component of membrane (e.g., *GLYT*, *NCOR*2, and *SR*140), GO:0005576_Extracellular region (e.g., *TIMP*3, *MUC*2, and *FAT*4), GO:0006955_Immune response (e.g., *DPCD* and *TRAIL*), GO:0005164_Tumor necrosis factor receptor binding (e.g., *TNF* and *LIGHT*), GO:0005328_Neurotransmitter: sodium symporter activity (e.g., *PROT* and *SLC*6*A*5_9), and the enriched number of DEGs into the above GO terms counting for 157, 16, 7, 7, and 5 DEGs, respectively (**Figure 7**). The lists of these representative DEGs and their functional results are shown in **Supplementary Tables 3, 4**.

The KEGG analysis was deployed to investigate the predicted functional information of DEGs in the gills under hypoxia stress. The KEGG analysis mainly focused on cellular processes, environmental information processing, genetic information processing, human diseases, metabolism, and organismal systems in KEGG classification level 1. The analysis of the KEGG enrichment analysis provides an overview of the pathway regulation.

In this study, the DEGs were assigned to 19 KEGG pathways, among which 43, 40, 28, 26, 24, 16, 11, and 8 genes were grouped into signal transduction, immune system, endocrine system, development, cell growth and death, folding, sorting and degradation, aging, and signaling molecules and interaction, respectively, in KEGG classification level 2. The main enriched pathways included the ko04210_Apoptosis (e.g., *IAP*/*XIAP*, *CASP*7, and *PARP*), ko04658_Th1 and Th2 cell differentiation (e.g., *NOTCH*1/2/3), ko04610_Complement and coagulation cascades (e.g., *A2M, PLG, and C*1*QG*), ko04612_Antigen processing and presentation (e.g., *HSPA*1s, and *CTSL*), ko04330_Notch signaling pathway (e.g., *NUMBL*, *NOTCH*, and *SMRT*), ko04060_Cytokine–cytokine receptor interaction (e.g., *TNFSF*10/14, *XDEAR*, and *SF*19). Among the listed pathways above, the ko04330_Notch signaling pathway enriched the most number of genes as 25 (**Figure 8**). The lists of these representative DEGs and their functional results are shown in **Supplementary Tables 5, 6**.

Validation of Transcriptome Data by qRT-PCR

The comparison of the qRT-PCR gene and RNAseq expression is shown in **Figure 9**. The qRT-PCR expression pattern was consistent with RNA-seq ($r = 0.8095$, $p < 0.05$; **Figure 9** and **Supplementary Table 7**) that validated the reliability and accuracy of the transcriptome data.

DISCUSSION

Summer mortality has been of great concern in aquaculture all over the world. It has been observed in many countries since the 1970s, recently hypoxic stress was proved that played an important role in summer mortality events (Parache, 1989; Sussarellu et al., 2010). In our previous study, hybrids of *C. sikamea* (♀) × *C. gigas* (♂) had lower mortality in summer than the half-siblings (Zhang et al., 2021). Thus, we deployed an occluded water experiment to assess hybrids' transcriptome responses to hypoxia stress. In this study, 901 DEGs were found involved in the resistance to environmental hypoxia in hybrid oysters, in which there were 432 downregulated DEGs and 469 upregulated DEGs. According to GO annotation, the cellular component term grouped the most numbered DEGs, and the KEGG annotated 108 DEGs in the immune system and 109 DEGs in signal transduction, respectively. A previous study identified 616 DEGs in *C. gigas* gills, mantle, and digestive gland after 7–10 and 24 days of hypoxia stress with 30% O_2-saturation that was associated with 12 major cellular physiological functions, including protein synthesis and degradation, transcription, cell cycle regulation, and metabolism of nucleic acid components, cellular matrix, and cytoskeleton, immune system, membrane receptors, and so on (David et al., 2005). Our study partially matches their result, the cell cycle regulation, and metabolism of nucleic acid components, cellular matrix, and cytoskeleton-related processes have not been identified in this study which may be related to the duration of hypoxia.

The GO contains a set of terms to describe the activity and actions of gene products with three sectors: cellular component, molecular function, and biological process (Roncaglia et al., 2013; Ding et al., 2018). In our study, the integral component of membrane (GO:0016021) and extracellular region (GO:0005576) in the cellular component category enriched the most numbered DEGs, which indicated that the gill tissue is actively involved in the response to hypoxic stress. In a previous study, extracellular region term was also significantly enriched in oyster gills under aerial exposure (Zhang et al., 2015), which further supports our finding. In addition, another study has also shown that extracellular region term was involved in the osmotic pressure regulation of *C. virginica* (Eierman and Hare, 2014). Moreover, the integral component of the membrane term is more discussed in oyster larval development (Xu and Zhang, 2020; Durland et al., 2021), which needs a further comparative study between

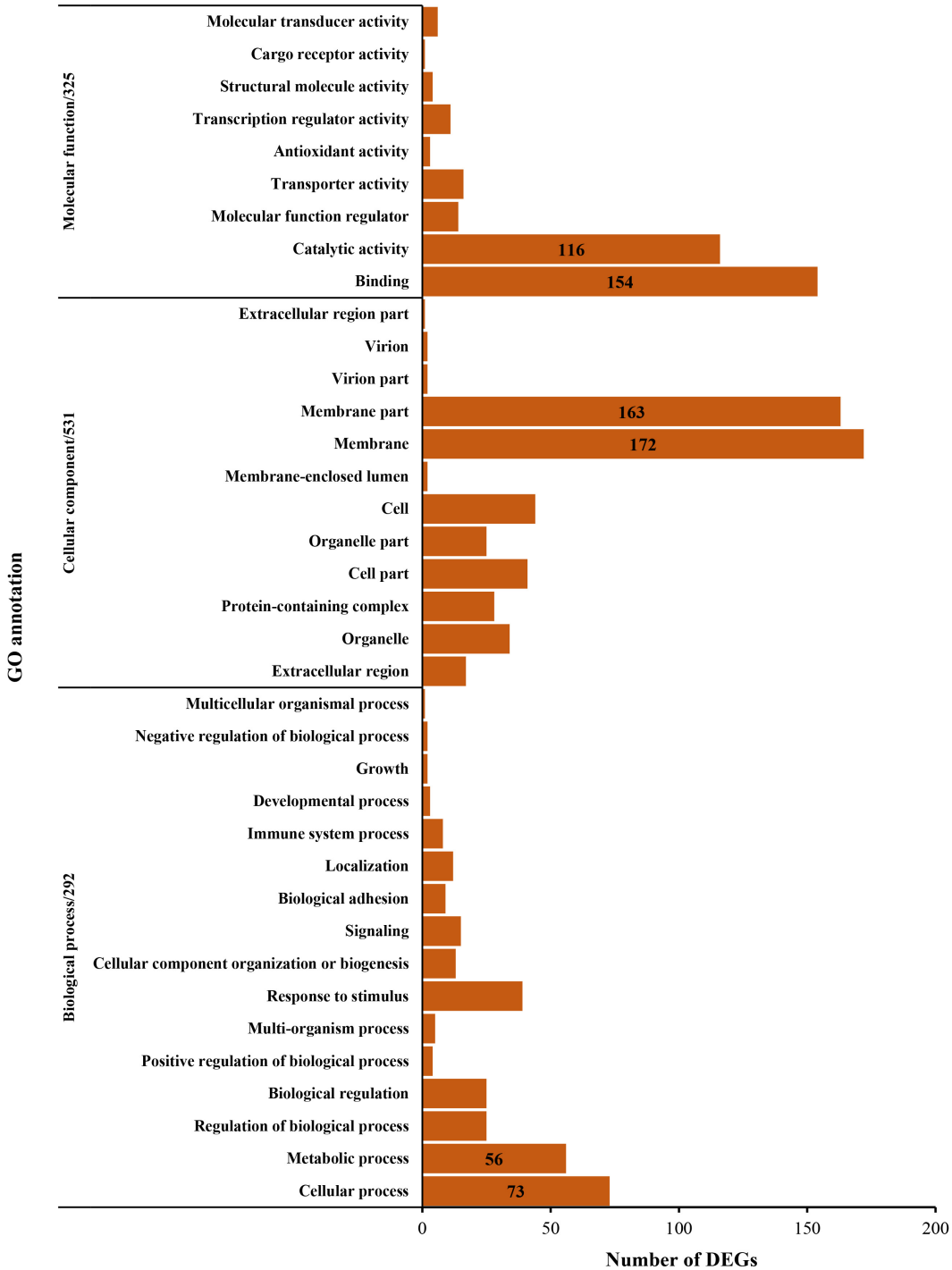

FIGURE 5 | Gene Ontology analysis of the differentially expressed genes between the normoxia and hypoxia groups.

larvae and adult oysters under hypoxia stress. The immune response (GO:0006955) is defined as an immune system process that functions in the calibrated response of an organism to a potential internal or invasive threat (Dunwoodie et al., 2018), which is the only significantly enriched GO term under the biological process category in hypoxia stress. In previous studies, it has been shown to also participate in *Saccostrea glomerata* threatened by environmental stressors (Ertl et al., 2016) and in *Ruditapes philippinarum* under lipopolysaccharide challenge (Zuo et al., 2020). Under the molecular function category, neurotransmitter:sodium symporter activity (GO:0005328) and tumor necrosis factor receptor binding (GO:0005614) were

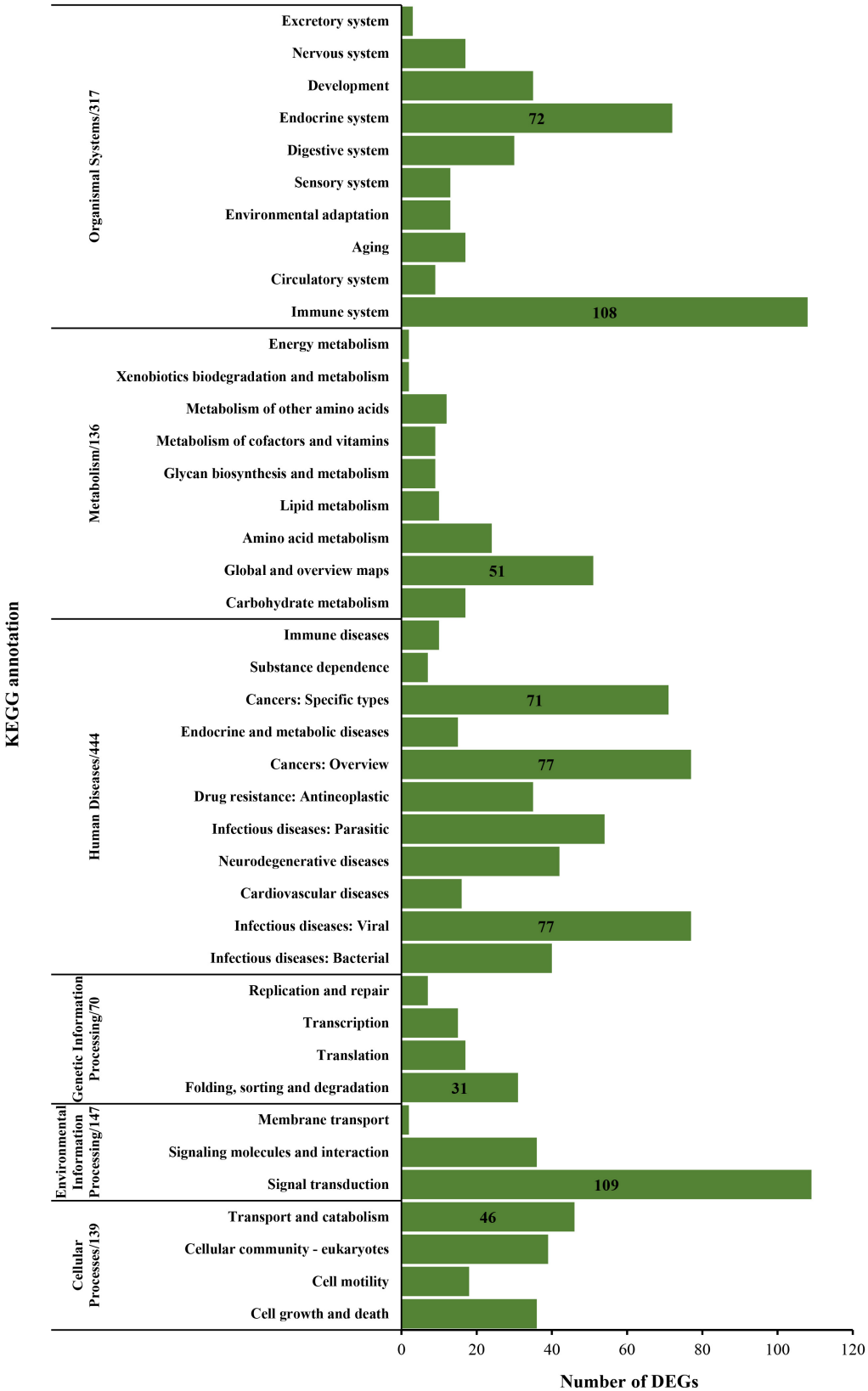

FIGURE 6 | KEGG annotation of the differentially expressed genes between the normoxia and hypoxia groups.

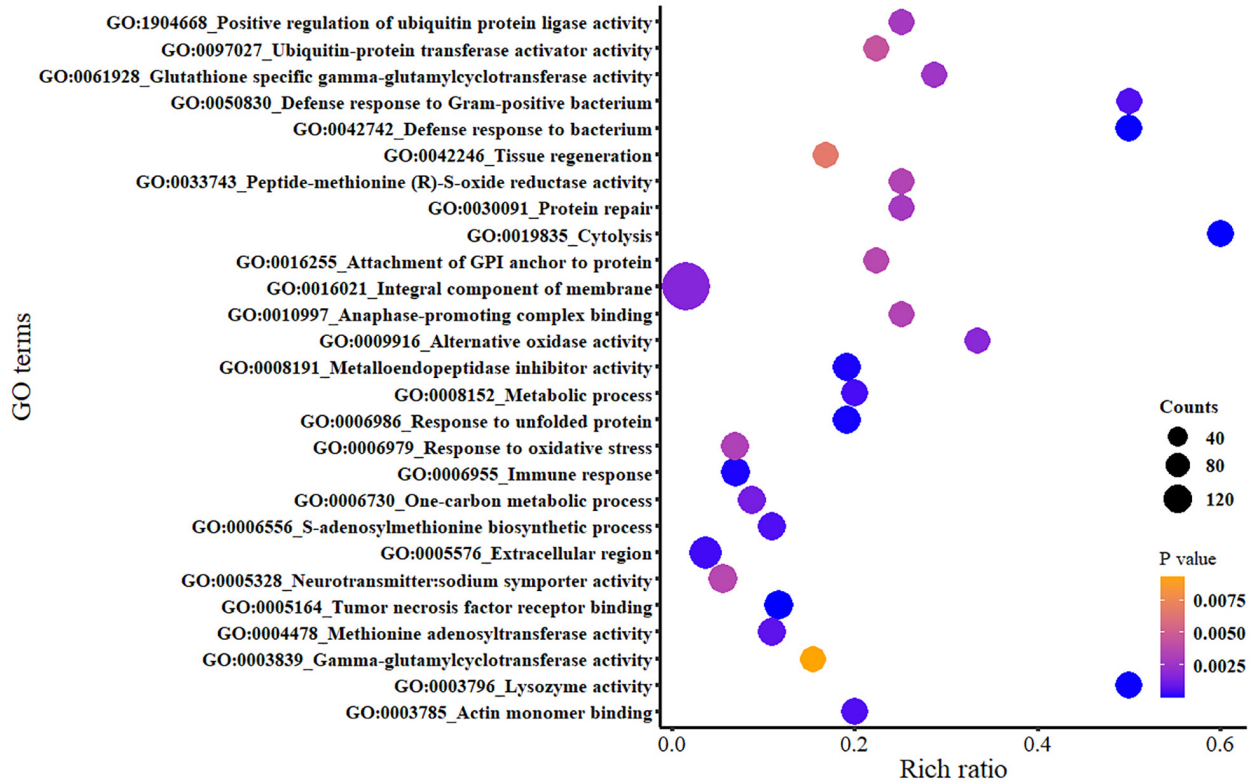

FIGURE 7 | The Gene Ontology enrichment of the differentially expressed genes (DEGs) between the normoxia group and hypoxia group. The color of the marker represents the significance; the square area represents the number of DEGs enriched in each pathway; the x coordinate represents the rich ratio (the ratio of the number of genes annotated to an item in the selected gene set to the number of genes annotated to the item by the species), similarly hereinafter.

both highly enriched that involved in membrane transport and receptor recognition binding, separately. The GO:0005328 term related to the transport function of sodium ions in the neural structure indicated that the information transmission function in the gill tissue of the hybrid oyster was more excited and activated under hypoxia stress, and the function of information collection and transmission was strengthened in response to stress (Adhikary et al., 2017), and this term was also enriched in the study of mechanisms of heat and hypoxia defense in hard clam (Hu et al., 2022). The GO:0005614 was also reported as highly enriched in the transcriptome analysis of *Aequipecten opercularis* exposure to *Pseudo-nitzschia* (Ventoso et al., 2019) that referred to a group of multifunctional inflammatory cytokines which indicates that hypoxia stress might cause various pathological and immune processes (Zheng et al., 2020).

The innate immune is a vital defensive system to protect oysters from the environment (Guo et al., 2015). The regulation of innate immunity relies on the pathways of the ko04610_complement and coagulation cascades (Bajic et al., 2015), ko04658_Th1 and Th2 cell differentiation (Dong and Flavell, 2000), and ko04612_antigen processing and presentation (Gaudino and Kumar, 2019). The complement system is a non-specific defense mechanism against pathogens, and the effector molecules of complement could be generated by enzymatic activity. In the present study, the immune system-related pathways, such as ko4610, ko4658, and ko4612, were highly enriched with DEGs, indicating that hybrid oysters rely heavily on innate immunity in coping with hypoxic stress. The fact that hypoxia stress could be a factor in activating the complement and coagulation cascades pathway has also been reported in Pacific abalone, which supports our findings (Shen et al., 2019). Organism immune to different microorganisms is regulated by separate lineages of effector T helper cells, that differentiate from primal CD4 + precursor cells in response to cues provided by antigen-presenting cells and include T helper type 1 and type 2 (Amsen et al., 2009; Knosp and Johnston, 2012), and also the transporter associated with antigen processing is essential for the adaptive immune system (Abele and Tampe, 2004). In the study of solid tumors, hypoxia was generally taken as a common biological determinant of immune exclusion (Doedens et al., 2013; Pietrobon and Marincola, 2021). Hypoxia enhances the immune response and leads to cellular stabilization of hypoxia-inducible factor 1α, resulting in a synergistic effect with the key inflammatory transcription factor nuclear factor of activated B cells (Saikumar et al., 1998; Kiers et al., 2016). Therefore, we hypothesized that cell damage caused by hypoxia could also be recognized in some forms by the antigen processing and presentation pathway in hybrid oyster gills involved in the immune response. Notch signaling is an evolutionarily conserved pathway, and it is a key intercellular signaling

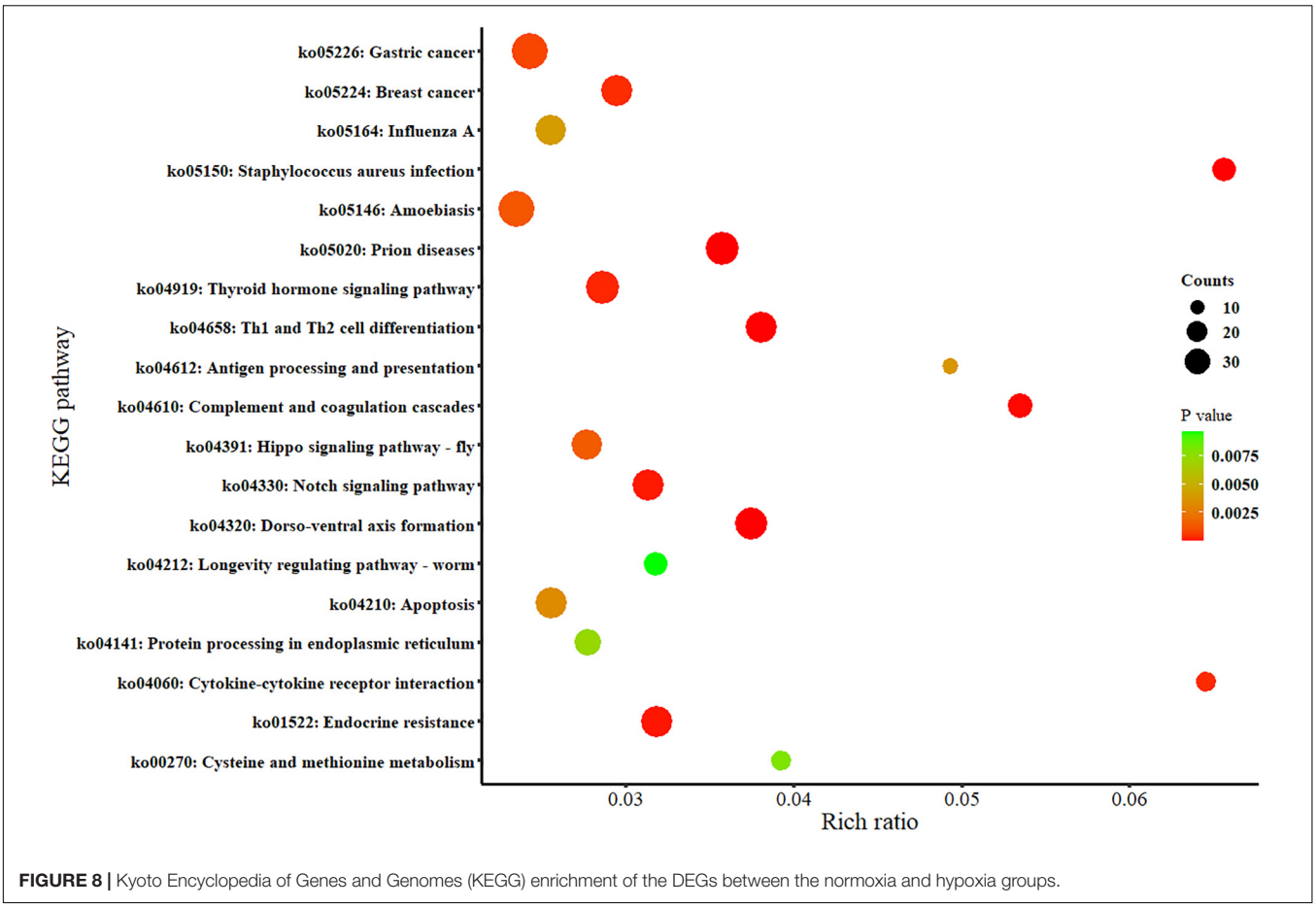

FIGURE 8 | Kyoto Encyclopedia of Genes and Genomes (KEGG) enrichment of the DEGs between the normoxia and hypoxia groups.

mechanism for embryonic development (Hansson et al., 2004). The notch signaling pathway also participates in environmental information processing. Jiao et al. (2019) reported that the notch signaling pathway participates in the recovery of pearl oysters after allograft and xenograft transplantations, and it was also actively involved in the regulation of *Crassostrea gigas* and *Crassostrea hongkongensis* under low osmotic stress (Zhao et al., 2014). In the present study, 25 DEGs were enriched into the notch signaling pathway, thus the environmental information processing function of the notch signaling pathway may be highly activated by hypoxia (Hiyama et al., 2011; Danza et al., 2012). Cytokines are soluble extracellular proteins or glycoproteins that are key modulators of inflammation, participating in cells engaged in innate immunity *via* a complex and sometimes seemingly contradictory network of interactions (Turner et al., 2014). The latest study on *Onchidium reevesii* revealed that cytokine–cytokine receptor interaction pathway involved in resisting the low-frequency noise stress (Tu et al., 2021), and Zhao et al. (2016) analyzed the gene expression profiles of oyster gills that have found that cytokine–cytokine receptor interaction pathway was also involved in salinity tolerance. The lack of available oxygen contributes to a bioenergetic crisis within cells, which in turn can lead to cellular necrosis-promoting inflammatory processes in a non-specific manner through the release of intracellular contents into the surrounding space (Nizet and Johnson, 2009; Taylor and Colgan, 2017). In this experiment, it was found that the hypoxia stress might induce adaptive inflammation in the gill tissue of hybrid oyster, thus activating the cytokine–cytokine receptor, which was consistent with the above conclusions.

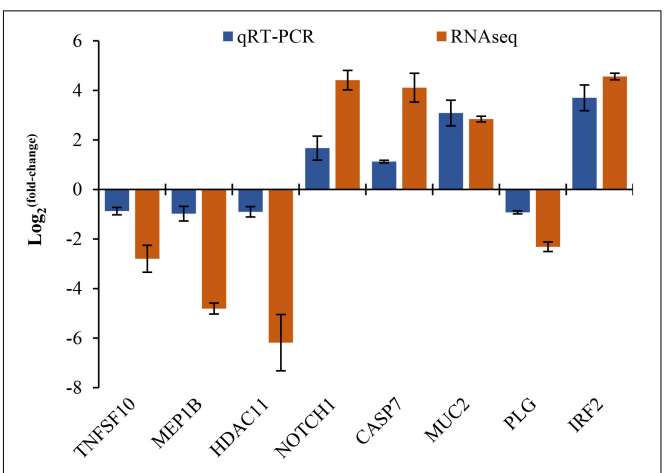

FIGURE 9 | The correlation analysis between the qRT-PCR and the RNA-seq data set.

The Notch family has four transmembrane receptors (Notch1–Notch4) and five ligands (Kadesch, 2004). In the previous studies, fibropellin-1, related to the Notch protein, drastically increased when post chronic hypoxia in the clam *Ruditapes philippinarum* (Nie et al., 2020) and the *NOTCH*s were upregulated in *Hermodice carunculata* under hypoxia (Grimes et al., 2021). Notch signaling was originally identified as a pleiotropic mediator of cell fate in invertebrates, which has recently emerged as an important regulator of immune cells (Radtke et al., 2013; Vanderbeck and Maillard, 2021). In the current study, several upregulated DEGs were annotated into the notch signaling pathway, which participates in the response to hypoxia stress by regulating the innate immunity in oyster gills.

Heat shock proteins (*HSP*s) are a group of molecular chaperones that can be induced by hypoxia (Wang et al., 2019), temperature (Zhang et al., 2021), and a variety of other stresses (Murphy, 2013; Cheng et al., 2016). *HSPA*1s contain the heat shock 70 kDa protein 1, 2, 6, and 8. Hsp70 proteins are central components of molecular chaperones and folding catalysts, and they assist a large variety of protein folding processes in the cell (Mayer and Bukau, 2005). The *HSP*70 gene was significantly upregulated in the study. Hypoxia could induce protein misfolding due to the lack of oxygen required for the formation of disulfide linkages, which leads to endoplasmic reticulum stress and the activation of unfolded protein response (Bartoszewska and Collawn, 2020; Díaz-Bulnes et al., 2020). As a chaperone protein, the hsp70 proteins facilitate the proper folding of proteins and DNA repair (Duan et al., 2014). In a previous study, *HSP*70 genes were also increased in *Anadara broughtonii* when exposed to sulfide and hypoxia (Wang et al., 2019), which further supports our finding. All findings suggest that the *HSP70* genes might play key roles in bivalves dealing with different stress factors.

Apoptosis is another evolution-conserved process in organisms, which is also an important process in the molluskan immune system (Zhang et al., 2021). The *TNF* family has been verified as a key inducer in apoptosis, both *LIGHT* and *TRAIL* are important members of it. *LIGHT* is also named *TNFSF*14 (tumor necrosis factor superfamily member 14) which has two spliced transcript variants encoding distinct isoforms (Locksley et al., 2001). *TRAIL* is a cytokine that is produced and secreted by most normal tissue cells, which induces apoptosis by binding the DR4 and DR5 receptors that result in trimerization of the receptor and clustering of the receptor's intracellular DD, leading to the formation of the death-inducing signaling (Wang and El-Deiry, 2003; Szliszka et al., 2009). In this study, both *TRAIL* and *CASP*7 were significantly downregulated, which indicated that the normal apoptosis might be inhibited due to hypoxia stress and the hypoxia has not caused cell damage that required the apoptotic process in this experiment. Previous studies have also verified that *TRAIL*/*LIGHT* could rapidly induce apoptosis in diverse origin cell lines, and *LIGHT* could be ligands for herpesvirus entry mediators (Wiley et al., 1995; Mauri et al., 1998; McGrath et al., 2011).

Gray et al. (2002) demonstrated that marine bivalves have the least sensitivity in the classified marine organisms according to their tolerance to hypoxia. Sussarellu et al. (2010) infer that the hypoxic effects appeared late in such a low oxygen-tolerant species, and their study indicated that all of the complexes of the electron transport chain were involved. In the current study, the typical genes of the respiratory chain, like NADH-ubiquinone oxidoreductase chains, succinate dehydrogenase, cytochromes b and c, and cytochrome c oxidase subunits weren't overexpressed, which echoes his point of view at some layer. The *LIGHT*s and *TRAIL*s play a part in apoptosis, and the downregulation of *TRAIL*s and *CASP*7 indicates the inhibiting of the apoptosis process. Therefore, in this experiment, the *LIGHT*s may only be involved in the adaptive inflammatory defenses through the cytokine–cytokine receptor interaction process, which was upregulated. *HSP*70 interacts with *NOTCH*s and contributes to the activity of Notch signaling, and the interaction represents a mechanism regulating Notch signaling (Juryńczyk et al., 2015). In our study, the typical immune genes, such as *NOTCH*1, *HSP*70s, and *LIGHT*s were all upregulated, were found to be involved in the immune response of oyster gills to hypoxia, by which the innate immune process is mediated. However, the *TRAIL*s, which also come from the *TNF* family with *LIGHT*s, were downregulated in this study, suggesting that the apoptosis was inhibited under hypoxia, and the downregulated *CASP*7 also confirmed this conclusion.

CONCLUSION

This study is the first transcriptome report of *C. sikamea* ♀ × *C. gigas* ♂hybrids under hypoxia stress. In total, 902 DEGs were identified in gill tissue of the hybrids under hypoxia stress, among which 432 downregulated and 469 upregulated DEGs were identified, respectively. In addition, several immune-related pathways were significantly enriched, such as Th1 and Th2 cell differentiation; complement and coagulation cascades, and antigen processing and presentation, which indicated that the innate immunity of oysters plays an important role in coping with hypoxic stress. Our findings demonstrated a gradually complicated immune pathway network in the gill tissue of hybrids under hypoxia stress. In conclusion, these results provide a basis for genetic breeding and transcriptome study of the hybrid oyster.

DATA AVAILABILITY STATEMENT

The datasets presented in this study can be found in online repositories. The names of the repository/repositories and accession number(s) can be found below: NCBI (accession: PRJNA587775).

AUTHOR CONTRIBUTIONS

XuZ, CF, and ZW gathered, analyzed, and interpreted data, discussed the results, and co-wrote the manuscript. JL, XiZ, and

QL contributed constructively ideas for the work. All authors contributed to the article and approved the submitted version.

FUNDING

This study was supported by the National Natural Science Foundation of China (Grant No. 31172403), and the Science and Technology Major Project of Guangxi (Grant/Award No. GuiAA17204094-3).

SUPPLEMENTARY MATERIAL

The Supplementary Material for this article can be found online at: https://www.frontiersin.org/articles/10.3389/fmars.2022.851098/full#supplementary-material

Supplementary Table 1 | The proportion of different species that are annotated onto the transcription.

Supplementary Table 2 | Total differentially expressed genes.

Supplementary Table 3 | Gene Ontology categorization of the unigenes in a cellular component, biological process, and molecular function from the transcriptome.

Supplementary Table 4 | DEGs that were assigned to the significantly enriched GO terms.

Supplementary Table 5 | Kyoto Encyclopedia of Genes and Genomes (KEGG) assignment of unigenes in transcriptome under hypoxia stress.

Supplementary Table 6 | DEGs that were assigned to the significantly enriched KEGG pathways.

Supplementary Table 7 | Primers designed and used in qRT-PCR validation of hypoxia-responsive genes identified by RNA-seq analysis.

REFERENCES

Abele, R., and Tampe, R. (2004). The ABCs of immunology: structure and function of TAP, the transporter associated with antigen processing. *Physiology*. 19, 216–224. doi: 10.1152/physiol.00002.2004

Adhikary, S., Deredge, D. J., Nagarajan, A., Forrest, L. R., Wintrode, P. L., and Singh, S. K. (2017). Conformational dynamics of a neurotransmitter: sodium symporter in a lipid bilayer. *Proc. Natl. Acad. Sci. U.S.A.* 114, E1786–E1795. doi: 10.1073/pnas.1613293114

Amsen, D., Spilianakis, C. G., and Flavell, R. A. (2009). How are TH1 and TH2 effector cells made? *Curr. Opin. Immunol.* 21, 153–160.

Andreyeva, A. Y., Gostyukhina, O., Kladchenko, E., Afonnikov, D., Rasskazov, D., Lantushenko, A., et al. (2021). Hypoxia exerts oxidative stress and changes in expression of antioxidant enzyme genes in gills of *Mytilus galloprovincialis* (Lamarck, 1819). *Mar. Biol. Res.* 17, 369–379.

Bajic, G., Degn, S. E., Thiel, S., and Andersen, G. R. (2015). Complement activation, regulation, and molecular basis for complement-related diseases. *EMBO J.* 34, 2735–2757. doi: 10.15252/embj.201591881

Bartoszewska, S., and Collawn, J. F. (2020). Unfolded protein response (UPR) integrated signaling networks determine cell fate during hypoxia. *Cell. Mol. Biol. Lett.* 25, 1–20. doi: 10.1186/s11658-020-00212-1

Bo-Mi, K., Haque, M. D. N., Do-Hee, L., Sang-Eun, N., and Jae-Sung, R. (2018). Comparative toxicokinetics and antioxidant response in the Microcystin-LR-Exposed gill of two marine bivalves, *Crassostrea gigas* and *Mytilus edulis*. *J. Shellfish Res.* 37, 497–506. doi: 10.2983/035.037.0305

Box, A., Capó, X., Tejada, S., Catanese, G., Grau, A., Deudero, S., et al. (2020). Reduced antioxidant response of the fan mussel *Pinna nobilis* related to the presence of *Haplosporidium pinnae*. *Pathogens* 9:932. doi: 10.3390/pathogens9110932

Cheng, J., Xun, X., Kong, Y., Wang, S., Yang, Z., Li, Y., et al. (2016). Hsp70 gene expansions in the scallop *Patinopecten yessoensis* and their expression regulation after exposure to the toxic dinoflagellate *Alexandrium catenella*. *Fish Shellfish Immunol.* 58, 266–273. doi: 10.1016/j.fsi.2016.09.009

Danza, G., Di Serio, C., Rosati, F., Lonetto, G., Sturli, N., Kacer, D., et al. (2012). Notch signaling modulates hypoxia-induced neuroendocrine differentiation of human prostate cancer cells. *Mol. Cancer Res.* 10, 230–238. doi: 10.1158/1541-7786.MCR-11-0296

David, E., Tanguy, A., Pichavant, K., and Moraga, D. (2005). Response of the Pacific oyster *Crassostrea gigas* to hypoxia exposure under experimental conditions. *FEBS J.* 272, 5635–5652. doi: 10.1111/j.1742-4658.2005.04960.x

Díaz-Bulnes, P., Saiz, M. L., López-Larrea, C., and Rodríguez, R. M. (2020). Crosstalk between hypoxia and ER stress response: a key regulator of macrophage polarization. *Front. Immunol.* 10:2951. doi: 10.3389/fimmu.2019.02951

Ding, R., Qu, Y., Wu, C. H., and Vijay-Shanker, K. (2018). Automatic gene annotation using GO terms from cellular component domain. *BMC Med. Inform. Decision Making* 18:119. doi: 10.1186/s12911-018-0694-7

Doedens, A. L., Phan, A. T., Stradner, M. H., Fujimoto, J. K., Nguyen, J. V., Yang, E., et al. (2013). Hypoxia-inducible factors enhance the effector responses of CD8+ T cells to persistent antigen. *Nat. Immunol.* 14, 1173–1182. doi: 10.1038/ni.2714

Dong, C., and Flavell, R. A. (2000). Cell fate decision: t-helper 1 and 2 subsets in immune responses. *Arthritis Res. Ther.* 2:179. doi: 10.1186/ar85

Duan, Y., Huang, S., Yang, J., Niu, P., Gong, Z., Liu, X., et al. (2014). HspA1A facilitates DNA repair in human bronchial epithelial cells exposed to Benzo[a]pyrene and interacts with casein kinase 2. *Cell Stress Chaperones* 19, 271–279. doi: 10.1007/s12192-013-0454-7

Dunwoodie, L. J., Poehlman, W. L., Ficklin, S. P., and Feltus, F. A. (2018). Discovery and validation of a glioblastoma co-expressed gene module. *Oncotarget* 9:10995. doi: 10.18632/oncotarget.24228

Durland, E., De Wit, P., Meyer, E., and Langdon, C. (2021). Larval development in the Pacific oyster and the impacts of ocean acidification: differential genetic effects in wild and domesticated stocks. *Evolution. Appl.* 14, 2258–2272. doi: 10.1111/eva.13289

Eierman, L. E., and Hare, M. P. (2014). Transcriptomic analysis of candidate osmoregulatory genes in the eastern oyster *Crassostrea virginica*. *BMC Genomics* 15:503. doi: 10.1186/1471-2164-15-503

Ertl, N. G., O'Connor, W. A., Papanicolaou, A., Wiegand, A. N., and Elizur, A. (2016). Transcriptome analysis of the sydney rock oyster, *Saccostrea glomerata*: insights into molluscan immunity. *PLoS One* 11:e0156649. doi: 10.1371/journal.pone.0156649

Furr, D., Ketchum, R. N., Phippen, B. L., Reitzel, A. M., and Ivanina, A. V. J. (2021). Physiological variation in response to vibrio and hypoxia by aquacultured eastern oysters in the Southeastern United States. *Integrat. Comparat. Biol.* 61, 1715–1729. doi: 10.1093/icb/icab176

Gaudino, S. J., and Kumar, P. (2019). Cross-talk between antigen presenting cells and T cells impacts intestinal homeostasis, bacterial infections, and tumorigenesis. *Front. Immunol.* 10:360. doi: 10.3389/fimmu.2019.00360

Gray, J. S., Wu, R. S.-S., and Or, Y. Y. (2002). Effects of hypoxia and organic enrichment on the coastal marine environment. *Mar. Ecol. Progr. Series* 238, 249–279.

Grimes, C. J., Petersen, L. H., and Schulze, A. (2021). Differential gene expression indicates modulated responses to chronic and intermittent hypoxia in corallivorous fireworms (*Hermodice carunculata*). *Sci. Rep.* 11:11110. doi: 10.1038/s41598-021-90540-9

Gu, H., Shang, Y., Clements, J., Dupont, S., Wang, T., Wei, S., et al. (2019). Hypoxia aggravates the effects of ocean acidification on the physiological energetics of the blue mussel *Mytilus edulis*. *Mar. Pollut. Bull.* 149:110538. doi: 10.1016/j.marpolbul.2019.110538

Guo, X., He, Y., Zhang, L., Lelong, C., and Jouaux, A. (2015). Immune and stress responses in oysters with insights on adaptation. *Fish Shellfish Immunol.* 46, 107–119. doi: 10.1016/j.fsi.2015.05.018

Hansson, E. M., Lendahl, U., and Chapman, G. (2004). Notch signaling in development and disease. *Semin. Cancer Biol.* 14, 320–328.

He, G., Liu, X., Xu, Y., Liang, J., Deng, Y., Zhang, Y., et al. (2021). Repeated exposure to simulated marine heatwaves enhances the thermal tolerance in pearl oysters. *Aquatic Toxicol.* 239:105959. doi: 10.1016/j.aquatox.2021.105959

Hedgecock, D., and Davis, J. P. (2007). Heterosis for yield and crossbreeding of the Pacific oyster *Crassostrea gigas*. *Aquaculture* 272, S17–S29.

Hiyama, A., Skubutyte, R., Markova, D., Anderson, D. G., Yadla, S., Sakai, D., et al. (2011). Hypoxia activates the notch signaling pathway in cells of the intervertebral disc: implications in degenerative disc disease. *Arthritis Rheumatism* 63, 1355–1364. doi: 10.1002/art.30246

Hu, Z., Feng, J., Song, H., Zhou, C., Yu, Z.-L., Yang, M.-J., et al. (2022). Mechanisms of heat and hypoxia defense in hard clam: insights from transcriptome analysis. *Aquaculture* 549:737792. doi: 10.1016/j.aquaculture.2021.737792

Huo, Z., Wang, Z., Yan, X., and Yu, R. (2014). Hybridization between *Crassostrea hongkongensis* and *Crassostrea ariakensis* at different salinities. *J. World Aquacult. Soc.* 45, 226–232.

Jiao, Y., Yang, S., Cao, Y., Zheng, Z., Deng, Y., Wang, Q., et al. (2019). Genome and transcriptome analyses providing insight into the immune response of pearl oysters after allograft and xenograft transplantations. *Fish Shellfish Immunol.* 90, 109–117. doi: 10.1016/j.fsi.2019.04.061

Joos, F., Plattner, G. K., Stocker, T. F., Körtzinger, A., and Wallace, D. W. (2003). Trends in marine dissolved oxygen: implications for ocean circulation changes and the carbon budget. *Eos Trans. Am. Geophys. Union* 84, 197–201.

Juryńczyk, M., Lewkowicz, P., Domowicz, M., Mycko, M. P., and Selmaj, K. W. (2015). Heat shock protein 70 (Hsp70) interacts with the Notch1 intracellular domain and contributes to the activity of Notch signaling in myelin-reactive CD4 T cells. *J. Neuroimmunol.* 287, 19–26. doi: 10.1016/j.jneuroim.2015.08.007

Kadesch, T. (2004). Notch signaling: the demise of elegant simplicity. *Curr. Opin. Genet. Dev.* 14, 506–512. doi: 10.1016/j.gde.2004.07.007

Kiers, H. D., Scheffer, G.-J., van der Hoeven, J. G., Eltzschig, H. K., Pickkers, P., and Kox, M. (2016). Immunologic consequences of hypoxia during critical illness. *Anesthesiology* 125, 237–249. doi: 10.1097/ALN.0000000000001163

Knosp, C. A., and Johnston, J. A. (2012). Regulation of CD4+ T-cell polarization by suppressor of cytokine signalling proteins. *Immunology* 135, 101–111. doi: 10.1111/j.1365-2567.2011.03520.x

Larade, K., and Storey, K. (2002). Chapter 3—a profile of the metabolic responses to anoxia in marine invertebrates. *Cell. Mol. Response Stress* 3, 27–46. doi: 10.1016/s1568-1254(02)80005-5

Livak, K. J., and Schmittgen, T. D. (2001). Analysis of relative gene expression data using real-time quantitative PCR and the $2^{-\Delta\Delta CT}$ method. *Methods* 25, 402–408.

Locksley, R. M., Killeen, N., and Lenardo, M. (2001). The TNF and TNF receptor superfamilies: integrating mammalian biology. *Cell* 104, 487–501. doi: 10.1016/s0092-8674(01)00237-9

Mauri, D. N., Ebner, R., Montgomery, R. I., Kochel, K. D., Cheung, T. C., Yu, G.-L., et al. (1998). *LIGHT*, a new member of the TNF superfamily, and lymphotoxin α are ligands for herpesvirus entry mediator. *Immunity* 8, 21–30. doi: 10.1016/s1074-7613(00)80455-0

Mayer, M. P., and Bukau, B. (2005). Hsp70 chaperones: cellular functions and molecular mechanism. *Cell. Mol. Life Sci.* 62:670. doi: 10.1007/s00018-004-4464-6

McGrath, E. E., Marriott, H. M., Lawrie, A., Francis, S. E., Sabroe, I., Renshaw, S. A., et al. (2011). TNF-related apoptosis-inducing ligand (TRAIL) regulates inflammatory neutrophil apoptosis and enhances resolution of inflammation. *J. Leukocyte Biol.* 90, 855–865. doi: 10.1189/jlb.0211062

Mortazavi, A., Williams, B. A., McCue, K., Schaeffer, L., and Wold, B. (2008). Mapping and quantifying mammalian transcriptomes by RNA-Seq. *Nat. Methods* 5, 621–628. doi: 10.1038/nmeth.1226

Murphy, M. E. (2013). The *HSP*70 family and cancer. *Carcinogenesis* 34, 1181–1188.

Nie, H., Wang, H., Jiang, K., and Yan, X. (2020). Transcriptome analysis reveals differential immune related genes expression in *Ruditapes philippinarum* under hypoxia stress: potential HIF and NF-κB crosstalk in immune responses in clam. *BMC Genomics* 21:318. doi: 10.1186/s12864-020-6734-6

Nizet, V., and Johnson, R. S. (2009). Interdependence of hypoxic and innate immune responses. *Nat. Rev. Immunol.* 9, 609–617. doi: 10.1038/nri2607

Nogueira, L., Mello, D. F., Trevisan, R., Garcia, D., da Silva Acosta, D., Dafre, A. L., et al. (2017). Hypoxia effects on oxidative stress and immunocompetence biomarkers in the mussel *Perna perna* (Mytilidae, Bivalvia). *Mar. Environ. Res.* 126, 109–115. doi: 10.1016/j.marenvres.2017.02.009

Parache, A. (1989). Growth performance of oyster *Crassostrea angulata* and *Crassostrea gigas* reared in Arcachon Bay between 1950 and 1986: first results. *Haliotis* 19, 227–236.

Parthasarathy, A., Srinivasan, S., Appleby, A. J., and Martin, C. R. (1992). Temperature dependence of the electrode kinetics of oxygen reduction at the platinum/Nafion® interface—a microelectrode investigation. *J. Electrochem. Soc.* 139:2530.

Pietrobon, V., and Marincola, F. M. (2021). Hypoxia and the phenomenon of immune exclusion. *J. Transl. Med.* 19:9. doi: 10.1186/s12967-020-02667-4

Radtke, F., MacDonald, H. R., and Tacchini-Cottier, F. (2013). Regulation of innate and adaptive immunity by Notch. *Nat. Rev. Immunol.* 13, 427–437. doi: 10.1038/nri3445

Roncaglia, P., Martone, M. E., Hill, D. P., Berardini, T. Z., Foulger, R. E., Imam, F. T., et al. (2013). The Gene Ontology (GO) cellular component ontology: integration with SAO (Subcellular Anatomy Ontology) and other recent developments. *J. Biomed. Semantics* 4, 20–20. doi: 10.1186/2041-1480-4-20

Saikumar, P., Dong, Z., Weinberg, J. M., and Venkatachalam, M. (1998). Mechanisms of cell death in hypoxia/reoxygenation injury. *Oncogene* 17, 3341–3349. doi: 10.1038/sj.onc.1202579

Seo, J.-K., Lee, M. J., Go, H.-J., Do Kim, G., Do Jeong, H., Nam, B.-H., et al. (2013). Purification and antimicrobial function of ubiquitin isolated from the gill of Pacific oyster, *Crassostrea gigas*. *Mol. Immunol.* 53, 88–98. doi: 10.1016/j.molimm.2012.07.003

Shen, Y., Huang, Z., Liu, G., Ke, C., and You, W. (2019). Hemolymph and transcriptome analysis to understand innate immune responses to hypoxia in Pacific abalone. *Comparat. Biochem. Physiol. Part D: Genomics Proteomics* 30, 102–112. doi: 10.1016/j.cbd.2019.02.001

Soon, T. K., and Zheng, H. (2019). Climate change and bivalve mass mortality in temperate regions. *Rev. Environ. Contamination Toxicol.* 251, 109–129. doi: 10.1007/398_2019_31

Sussarellu, R., Fabioux, C., Le Moullac, G., Fleury, E., and Moraga, D. (2010). Transcriptomic response of the Pacific oyster *Crassostrea gigas* to hypoxia. *Mar. Genomics* 3, 133–143.

Szliszka, E., Mazur, B., Zydowicz, G., Czuba, Z. P., and Król, W. (2009). TRAIL-induced apoptosis and expression of death receptor TRAIL-R1 and TRAIL-R2 in bladder cancer cells. *Folia Histochem. Cytobiol.* 47, 579–585. doi: 10.2478/v10042-009-0111-2

Taylor, C. T., and Colgan, S. P. (2017). Regulation of immunity and inflammation by hypoxia in immunological niches. *Nat. Rev. Immunol.* 17, 774–785. doi: 10.1038/nri.2017.103

Tu, Z., Tang, L., Zhang, X., Jia, J., and Shen, H. (2021). Transcriptome analysis of the central nervous system of sea slug (*Onchidium reevesii*) exposed to low-frequency noise. *Front. Mar. Sci.* 8:807489. doi: 10.3389/fmars.2021.807489

Turner, M. D., Nedjai, B., Hurst, T., and Pennington, D. J. (2014). Cytokines and chemokines: at the crossroads of cell signalling and inflammatory disease. *Biochim. Biophys. Acta (BBA) - Mol. Cell Res.* 1843, 2563–2582. doi: 10.1016/j.bbamcr.2014.05.014

Vanderbeck, A., and Maillard, I. (2021). Notch signaling at the crossroads of innate and adaptive immunity. *J. Leukocyte Biol.* 109, 535–548. doi: 10.1002/JLB.1RI0520-138R

Ventoso, P., Pazos, A. J., Pérez-Parallé, M. L., Blanco, J., Triviño, J. C., and Sánchez, J. L. (2019). RNA-Seq transcriptome profiling of the queen scallop (*Aequipecten opercularis*) digestive gland after exposure to domoic acid-producing *Pseudo-nitzschia*. *Toxins.* 11, 1–26. doi: 10.3390/toxins11020097

Wang, L., Song, X., and Song, L. (2018). The oyster immunity. *Dev. Comparat. Immunol.* 80, 99–118. doi: 10.1016/j.dci.2017.05.025

Wang, S., and El-Deiry, W. S. (2003). TRAIL and apoptosis induction by TNF-family death receptors. *Oncogene* 22, 8628–8633. doi: 10.1038/sj.onc.1207232

Wang, Y., Zhou, S., Liu, T., Chen, M., Li, W., and Zhang, X. (2019). The transcriptomic responses of the ark shell, *Anadara broughtonii*, to sulfide and hypoxia exposure. *Mol. Biol. Rep.* 46, 4245–4257. doi: 10.1007/s11033-019-04879-4

Wiley, S. R., Schooley, K., Smolak, P. J., Din, W. S., Huang, C.-P., Nicholl, J. K., et al. (1995). Identification and characterization of a new member of the *TNF* family that induces apoptosis. *Immunity* 3, 673–682. doi: 10.1016/1074-7613(95)90057-8

Wu, R. S. (2002). Hypoxia: from molecular responses to ecosystem responses. *Mar. Pollut. Bull.* 45, 35–45.

Xu, F., Guo, X., Li, L., and Zhang, G. (2011). Effects of salinity on larvae of the oysters *Crassostrea ariakensis*, *C. sikamea* and the hybrid cross. *Mar. Biol. Res.* 7, 796–803.

Xu, F., and Zhang, G. (2020). Transcriptomic and proteomic dynamics during metamorphosis of Pacific oyster *Crassostrea gigas*. *bioRxiv [preprint]* 2020.2003.2025.004614. doi: 10.1101/2020.03.25.004614

Xu, H., Li, Q., Kong, L., Yu, H., and Liu, S. (2019). Fertilization, survival and growth of hybrids between *Crassostrea gigas* and *Crassostrea sikamea*. *Fisheries Sci.* 85, 821–828.

Zhang, X., Fan, C., Zhang, X., Li, Q., Li, Y., Ma, P., et al. (2021). Transcriptome analysis of *Crassostrea sikamea* (♀)× *Crassostrea gigas* (♂) hybrids under and after thermal stress. *J. Ocean Univ. China* 21, 213–224.

Zhang, Y., Sun, J., Mu, H., Li, J., Zhang, Y., Xu, F., et al. (2015). Proteomic basis of stress responses in the gills of the pacific oyster *Crassostrea gigas*. *J. Proteome Res.* 14, 304–317.

Zhang, Y., Zhang, Y., Li, J., Wang, Z., Yan, X., and Yu, Z. (2017). Incomplete sterility of hybrids produced by *Crassostrea hongkongensis* female× *Crassostrea gigas* male crosses. *Aquaculture Res.* 48, 1351–1358.

Zhao, L., Liu, L., Liu, B., Liang, J., Lu, Y., and Yang, F. (2019). Antioxidant responses to seawater acidification in an invasive fouling mussel are alleviated by transgenerational acclimation. *Aquatic Toxicol.* 217:105331.

Zhao, L., Shirai, K., Tanaka, K., Milano, S., Higuchi, T., Murakami-Sugihara, N., et al. (2020). A review of transgenerational effects of ocean acidification on marine bivalves and their implications for sclerochronology. *Estuarine Coastal Shelf Sci.* 235:106620.

Zhao, X., Yu, H., Kong, L., and Li, Q. (2016). Gene co-expression network analysis reveals the correlation patterns among genes in euryhaline adaptation of *Crassostrea gigas*. *Mar. Biotechnol.* 18, 535–544.

Zhao, X., Yu, H., Kong, L., Liu, S., and Li, Q. (2014). Comparative transcriptome analysis of two oysters, *Crassostrea gigas* and *Crassostrea hongkongensis* provides insights into adaptation to hypo-osmotic conditions. *PLoS One* 9:e111915. doi: 10.1371/journal.pone.0111915

Zheng, Y., Liu, Z., Wang, L., Li, M., Zhang, Y., Zong, Y., et al. (2020). A novel tumor necrosis factor in the Pacific oyster *Crassostrea gigas* mediates the antibacterial response by triggering the synthesis of lysozyme and nitric oxide. *Fish Shellfish Immunol.* 98, 334–341.

Zuo, S., Jiang, K., Li, D., Yan, X., and Nie, H. (2020). Transcriptomic analysis of Manila clam *Ruditapes philippinarum* under lipopolysaccharide challenge provides molecular insights into immune response. *Fish Shellfish Immunol.* 106, 110–119.

Conflict of Interest: The authors declare that the research was conducted in the absence of any commercial or financial relationships that could be construed as a potential conflict of interest.

Publisher's Note: All claims expressed in this article are solely those of the authors and do not necessarily represent those of their affiliated organizations, or those of the publisher, the editors and the reviewers. Any product that may be evaluated in this article, or claim that may be made by its manufacturer, is not guaranteed or endorsed by the publisher.

frontiers in Marine Science

ORIGINAL RESEARCH
published: 23 March 2022
doi: 10.3389/fmars.2022.865736

Genetic Evaluation of Growth and Survival-Related Traits in Yesso Scallop *Patinopecten yessoensis* in Sea-Based Culture System

Fucun Wu[1,2,3]*, *Chao Liu*[1], *Jibiao Zhang*[1] and *Guofan Zhang*[1,2,3]

[1] Key Laboratory of Experimental Marine Biology, Institute of Oceanology, Chinese Academy of Sciences, Qingdao, China, [2] Laboratory for Marine Fisheries Science and Food Production Processes, Pilot National Laboratory for Marine Science and Technology, Qingdao, China, [3] National and Local Joint Engineering Laboratory of Ecological Mariculture, Qingdao, China

Worldwide, the bivalve aquaculture industry has realized or recognized the potential gains from selective breeding programs using phenotypic and pedigree data. Yesso scallop *Patinopecten yessoensis* are among the most important commercial shellfish in China. A family-based breeding program to investigate the genetic variations for growth and survival-related traits at suspended and bottom environments of sea-based culture systems was reported in this study. We proposed and conducted a novel phenotyping technique to longitudinally evaluate the shell heights in the yesso scallop. At harvest after rearing for 20 months, the individual shell heights at 6, 10, 16, and 20 months were simultaneously obtained by the growth rings in the outer shells of the animals. Meanwhile, the body weight (BW) of the survived individuals at harvest was also recorded. Variance components and genetic parameters for growth and survival-related traits were estimated using an animal and threshold model, respectively. In the suspended environment, the heritability estimates for BW and shell heights at specific ages ranged from moderate to high (0.328–0.853). The estimated correlations between shell heights at contiguous ages were consistently high, ranging from 0.890 to 0.958 but decreased with increasing intervals between ages (0.496–0.828). The estimated correlations between shell heights at contiguous ages and BW at harvest were similar, ranging from 0.535 to 0.983. The heritability estimates for individual survival at harvest were at a low level of 0.128 by the probit-threshold model. While at the bottom environment, estimates of heritability for growth and survival-related traits were similar but slightly lower than those at the suspended environment. Furthermore, the genetic correlation for BW between the two environments was very small, which probably indicates genotype-by-environment interaction effects for growth in the yesso scallop. The study can provide prior information, which might develop a new idea for selection in this species. The results are discussed concerning selection work with yesso scallop, and solutions for accurate estimation of genetic parameters and increasing genetic gain are also outlined.

Keywords: yesso scallop *Patinopecten yessoensis*, heritability, genetic correlation, shell growth, sea-based culture

OPEN ACCESS

Edited by:
Liqiang Zhao,
Guangdong Ocean University, China

Reviewed by:
Jitao Li,
Chinese Academy of Fishery Sciences (CAFS), China
Xingzhi Zhang,
Guangxi Academy of Fishery Sciences, China
Liang Jian,
Tianjin Agricultural University, China

***Correspondence:**
Fucun Wu
wufucun@qdio.ac.cn

Specialty section:
This article was submitted to Marine Fisheries, Aquaculture and Living Resources, a section of the journal Frontiers in Marine Science

Received: *30 January 2022*
Accepted: *17 February 2022*
Published: *23 March 2022*

Citation:
Wu F, Liu C, Zhang J and Zhang G (2022) Genetic Evaluation of Growth and Survival-Related Traits in Yesso Scallop Patinopecten yessoensis in Sea-Based Culture System. Front. Mar. Sci. 9:865736. doi: 10.3389/fmars.2022.865736

INTRODUCTION

Selective breeding, the benefits of which can be cumulative and permanent, is an attractive approach in genetic improvement in aquaculture species (Gjedrem, 2010). Estimates of genetic gain per generation for economically important traits such as growth rate are reported high of average 13%, as demonstrated for major farmed species like Atlantic salmon and Nile tilapia (Gjedrem, 2012). Although the molecular breeding method was reported in animals in the genomics era, the best linear unbiased prediction method traditionally based on pedigree records and phenotypic data still comprises one of the main approaches in selective breeding programs so far, especially in aquaculture species (Boudry et al., 2022). The prerequisite of the traditional family-based selection is the accurate estimates of the genetic parameters including heritability and genetic correlations for the target traits. Factually, the genetic parameter estimation is vital to breeders to make an effective breeding plan, predict the genetic gains, and conduct a cost-benefit analysis in the program. In molluscan species especially in bivalves, the genetic parameter estimations were relatively widely reported in oysters, scallops, clams, and mussels (Alcapán et al., 2007; de Melo et al., 2016; Barros et al., 2018; Tan et al., 2020).

Scallops are one of the most ecologically and economically important bivalve groups in the world (Shumway and Parsons, 2006). They are a high-value aquaculture group, with an annual farmed yield of about 2 million metric tons accounting for more than 10% of aquaculture production for the major molluscan species groups in 2018 worldwide (Food and Agriculture Organisation [FAO], 2020). Yesso or Japanese scallop, *Patinopecten yessoensis*, was introduced from Japan to Dalian areas, China in the 1980s (Liu, 1983). The aquaculture of yesso scallops has been growing rapidly since its introduction because of the larger sizes and higher market prices compared with the native scallop species in China. It has become a major aquaculture industry in northern China, mostly in Liaoning and northern Shandong Province. Two main culture forms in sea-based culture were suitable for yesso scallop farming in China. Lantern nets on suspended longlines, the dominant form of grow-out for native scallops, are also implemented for yesso scallop culture. The scallops can also be released for on-bottom culture without any protective gear. During the past decade, the on-bottom culture of yesso scallops has gained popularity and greatly expanded in China. Although several studies were conducted to compare the merits and demerits between the two culture modes in yesso scallop, there remains controversy in which mode is more productive in China.

However, in recent years, outbreaks of mass mortality and slow growth rate are major threats to sustainable production and future expansion of yesso scallop aquaculture since 2007 in China (Ren et al., 2013). Mortalities of farmed stocks in this species have continued to 2014, however, no specific pathogens have been found associated with the mortalities. Although several selective breeding programs were initiated by varying organizations or companies in China (Wang et al., 2014), it seems that no sufficient data of genetic evaluations were reported on target traits in this species.

Here, we present estimates of heritability for shell heights, BW, and survival after growing full-sib families under two grow-out conditions (environments). We also try to evaluate the genotype by environment interaction effects for BW between different environments. This study would provide a theoretical and practical context for developing selective breeding programs for yesso scallop farming in China.

MATERIALS AND METHODS

Population, Mating, and Production of Families

The materials used in the study were from a scallop hatchery, Zoneco Group Co., Ltd., China. The base population of the selection experiments was established by two yesso scallop stocks, A and B. According to the hatchery records from Zoneco Company, stock A was introduced from Aomori, Japan in 1982. After breeding for 14 generations every 2 years since introduction, individuals from stock A were randomly chosen as broodstock. While, stock B was produced for 2 generations after being introduced in 2009, recently. Scallop stocks A and B are both commercially cultured using suspended longline in Changhai County, Dalian, China before being selected as broodstock in the study. To our knowledge, no experimental or field trials were conducted to evaluate the production performance or features between the two stocks previously. We used the two stocks as the base population for broadening the genetic base and detecting possible heterosis for the target traits in the study. Full- and half-sib families were produced by a 2×2 factorial mating design, in which two dams were mated to the same sire, and two sires were mated to the same dam. After fertilization and hatching, successfully established full-sibs were carefully separately in each 100 L tank.

Fertilized eggs, embryos, and larvae were reared following the procedures described by Wang and Wang (1993). The D-shaped and umbo larvae in each full-sib were cultured in appropriate 15°C seawater with aeration in succession. The density of larvae and the concentrations of feeds were maintained and adjusted to a suitable level to keep the larvae growing comfortably. In brief, the density of larvae in the tanks was maintained at 8 larvae/ml and reduced to 1–2 larvae/ml with the development of the larvae to metamorphosis by adjusting the water volume. About 30 days after fertilization, the collectors adhered to juvenile scallops were transferred to the field in the sea from nursery to grow-out stage. As the animals developed in the nursery stage, stocking densities in each full-sibs were adjusted for consistent rearing environmental conditions. Density adjustment was made in all families three times in the nursery stage. This practice is essential to adjust for possible bias resulting from environmental differences in the subsequent genetic evaluation. Finally, only 43 full-sibs with sufficient sample numbers were established when juvenile scallops with shell heights of ∼3 cm got to the grow-out stage. The numbers of mating pairs, sires, and dams used to generate the full families are presented in **Table 1**.

TABLE 1 | Summary statistics of families, sample number, and phenotypic values of traits in yesso scallops in the study.

Samples/Traits[a]		Grow-out conditions (Environment)	
		Suspended	**Bottom**
Families		43	33
Sires		32	23
Dams		34	23
Samples with records		2,667	778
Survived samples at harvest		1,192	335
Traits	SH_1 (mm)	42.28 (7.72)	NA
	SH_2 (mm)	57.15 (7.73)	NA
	SH_3 (mm)	68.85 (7.76)	NA
	SH_4 (mm)	80.07 (8.90)	NA
	BW (g)	76.48 (21.74)	84.04 (30.13)

[a] *The data of traits in the table are shown in the format of value (SD). SH_1, shell height at 6 month; SH_2, shell height at 10 month; SH_3, shell height at 16 month; SH_4, shell height at 20 month; BW, body weight at harvest; Survival, Survival at harvest. Suspended and bottom are the two environments in the study.*

Growth and Survival Tests at Suspended and Bottom Environments

Scallops with a shell height of ∼2.5 cm were tagged with digital numbered tags tied by a hole drilled in the ear part of the animal (Katherine et al., 2001). After tagging and acclimating for no mortality occurred, the scallops in each of the full-sib families were transferred to two sites closely located in Zhangzi Island of the North Yellow Sea, where yesso scallop is widely cultured in China, for adult growth periods (Guo and Luo, 2016). The lantern net suspension in longlines culture mode in one site and an on-bottom culture mode in the other site were utilized as two environments to measure the growth and survival performance of the full-sibs at the grow-out stage were separately conducted.

At the suspended environment, a total of 2,667 randomly selected individuals from the 43 full-sib families were placed in 13 lantern nets with the same density (20 scallops were placed in each layer of the lantern nets) and placed in the same natural water to minimize the effects of culture conditions. While, at the on-bottom environment, we placed netting cages in the bottom of the sea on the other site in this study. Compared with the routine way in yesso scallop on-bottom culture in open areas, this is to guarantee the recapture of the experimental animals at harvest. The netting cage consisted of a 2 m × 1 m × 0.45 m ($L \times W \times D$) rectangular frame made of rebar (ϕ = 1 cm), we placed two nets around each cage with a mesh size of 2 cm for holding scallops. In this study, seven netting cages as scallop bottom culture equipment were anchored into the seabed at a water depth of 20 m. However, during the culture at the bottom environment, one netting cage was crashed by rocks and destroyed, while two netting cages occurred predators of starfish (*Asterias amurensis*), nearly all the scallops totally occurred mortality. Therefore, a total of only 780 scallop samples from the 33 full-sib families in four cages were included in data collection at the bottom culture environment.

At harvest after grow-out in the suspended environment, the numbers of live and dead scallops at each site for each full-sib family were counted to obtain the survival data (0/1). Final sizes (the shell heights SH_4) and weights of the scallops (BW) were determined by measuring all the survived individuals at the site. Besides, the three number of growth rings present in our survived samples allowed recognition of shell height growth chronologies (**Figure 1**). With the help of the growth rings which we inferred occurrence at the age of 6, 10, and 16 months, we finally obtained the data of SH_1, SH_2, and SH_3 together with SH_4, simultaneously (**Figure 1**). Scallop shell heights were defined as the maximum distance from the hinge line to the growth rings or shell edges and measured using electronic vernier calipers to an accuracy of 0.01 mm. BW was recorded using an electronic balance to an accuracy of 0.01 g. To guarantee the accuracy of shell height data obtained by the new method, preliminary measurements were conducted during the culture at 6 months. Measurements were carried out to obtain the shell heights of 100 randomly chosen scallops at 6 months, which are seen as "true values." While at harvest, shell height data indicated by the growth ring at 6 months were recorded again to the survived animals from the 100 randomly chosen scallops. The means of shell heights obtained at harvest and "true values" were compared using Tukey's test (Zar, 1984). Additionally, Tukey's test revealed no significant difference between data recorded by the growth ring method and "true values" ($P > 0.05$). It indicated that the accuracy of shell height data obtained by the growth ring method was guaranteed.

While, at harvest after grow-out at the bottom environment, all the number of live scallops in only four cages were collected and counted to obtain the survival data. The final individual BW of the scallops (BW) was determined by measuring all the survived individuals at the site. Gender information including male, female, or undistinguished of all survived samples at the two culture conditions was also recorded at harvest.

Data Analysis

Genetic analyses for growth-related traits including SH_1, SH_2, SH_3, SH_4, and BW in the suspended culture condition were performed using a multivariate animal model as follows:

$$y = X\beta + Z_1 a + Wc + e \quad (1)$$

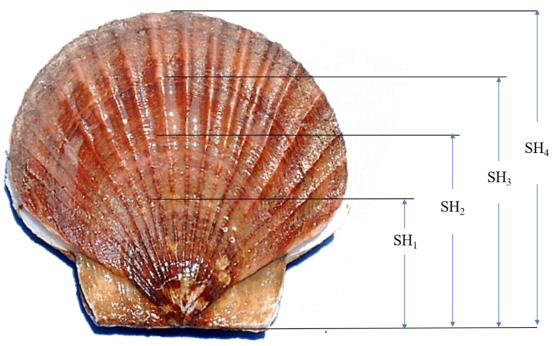

FIGURE 1 | Shell height growth was indicated by the rings in the outer shells of the yesso scallop in this study. SH_1, shell height at 6 months; SH_2, shell height at 10 months; SH_3, shell height at 16 months; SH_4, shell height at 20 months.

where $\boldsymbol{y}$ is the vector of phenotypes of each trait; β is the vector of fixed effects, including overall mean, crosses (AA, AB, BA, or BB), and sex (male, female, or undistinguished); $\boldsymbol{a}$ is the vector of random additive genetic effects, following a normal distribution of $N(\mathbf{0}, \mathbf{A}\sigma_a^2)$, where $\sigma^2 a$ is the additive genetic variance and **A** is the numerator relationship matrix based on pedigree information; $\boldsymbol{c}$ is the vector of common effects to full-sibs with the distribution of $N(0, \mathbf{I}\sigma_c^2)$, where $\mathbf{I}\sigma_c^2$ is the variance of common effects to full-sibs and **I** is the identity matrix; $\boldsymbol{e}$ is the vector of random residuals with the distribution of $N(0, \mathbf{I}\sigma_e^2)$, where σ_e^2 is the residual variance; **X**, **W**, and $\mathbf{Z}_1$ are incidence matrices linking β, $\boldsymbol{c}$, and $\boldsymbol{a}$ to $\boldsymbol{y}$, respectively. Ward-*F*-tests were conducted to detect the significance of the fixed effects, and the fixed effects should be removed if no significance was detected ($P < 0.05$). If the multivariate genetic analyses including all the traits cannot achieve convergence by the restricted maximum likelihood (REML) method, bivariate genetic analyses between any of two traits using an animal model were carried out.

Genetic analyses for growth-related traits including BW at the suspended and bottom environments were using a bivariate animal model to detect the genotype by environment interaction indicated by genetic correlation levels as Formula (1). Traits of BW at the two culture environments were seen as different variates as shown in G by E analysis proposed by Falconer and Mackay (1996).

Survival traits at each of the two environments were treated as a binary trait since survived and dead samples at harvest were assigned values of 1 and 0, respectively. Genetic analyses for survival traits in each of the two environments were using a threshold logit model to estimate the genetic components and narrow-sense heritability, respectively.

The assumed single-trait model for the underlying distribution of the liability (**If**) for analysis of each binary trait was

$$If = X\beta + Z_2 s + Z_3 d + e \quad (2)$$

where β is a vector of fixed effects as displayed in Formula (1); $\boldsymbol{s}$ and $\boldsymbol{d}$ is the vector of sire and dam genetic effects; $\boldsymbol{e}$ is a vector of residual effects, and $\mathbf{X}$, $\mathbf{Z_2}$, **and** $\mathbf{Z_3}$ are incidence matrices that link fixed and genetic effects to liabilities, respectively. The response in Formula (2) was modeled with a probit link function approach, thus, the $\sigma_e^2 = \pi^2/3$.

Heritabilities (h^2) in the animal model for growth-related traits including scallop SH and BW were calculated as $h^2 = \sigma_a^2/(\sigma_a^2 + \sigma_e^2)$, while heritabilities ($h^2$) in the sire-dam model for scallop survival-related traits using probit-link function were calculated $h^2 = 4\sigma_{sd}^2/(2\sigma_{sd}^2 + \pi^2/3)$.

The multivariate or bivariate animal models were used to estimate the genetic and phenotypic correlation between growth-related traits in suspended culture conditions, and between BW traits in the two culture conditions. The genetic correlation (r_g) formula is:

$$r_g = \sigma_{a12}/\sqrt{\sigma_{a1}^2\sigma_{a2}^2}$$

where σ_{a12} is the genetic covariance between trait 1 and trait 2, σ_{a1}^2 and σ_{a2}^2 are the additive genetic variance of traits 1 and 2, respectively. The phenotypic correlation (r_p) formula is:

$$r_p = (\sigma_{a12} + \sigma_{e12})/\sqrt{\left(\sigma_{a1}^2 + \sigma_{e1}^2\right)\left(\sigma_{a2}^2 + \sigma_{e2}^2\right)}$$

where σ_{e12} is the residual covariance between trait 1 and trait 2, σ_{e1}^2 and σ_{e2}^2 are the residual variance of traits 1 and 2, respectively.

RESULTS

Phenotype Statistics for Scallop Growth and Survival at Harvest

After 20-month rearing at the two environments in the sea-based culture system, the total number of survived scallops was 1,192 at the suspended environment, accounting for the survival rate of 44.69%. While, the total number of surviving scallops in the remaining four netting cages at the bottom environment was 335, accounting for the survival rate of 43.06%. The average BW of the yesso scallop was 76.48 g at the suspended environment and 84.04 g at the bottom environment, respectively. At harvest, according to the growth rings in the outer shells of yesso scallops, the shell heights at varying ages were also shown in **Table 1**. The mean and SD for shell heights increased while the coefficient of variation (proportion of SD to mean) decreased from 18 to 11% with advancing age.

At the family level, there were large variations in the average BW of yesso scallop cultured at both environments, respectively. Additionally, it seemed that large difference in average BW between the same families in the two environments (**Figure 2**). The phenotypic variations were similar in terms of survival rates of the animals at the suspended and bottom environments at the family level (**Figure 2**).

Genetic Parameter Estimates for Scallop Growth and Survival at Suspended and Bottom Environments

In the study, a cross between two populations, A and B, and scallop sex at harvest were treated as fixed effects in REML analysis. Wald-F statistical analysis was conducted and showed that these two factors had no significant effect on scallop growth and survival at harvest ($P > 0.05$). Therefore, the two factors were removed in the subsequent analysis using REML in the mixed linear model.

Estimated variance components from multivariate models including SH_1, SH_2, SH_3, SH_4, and BW traits could not obtain a converged result by the REML method. Therefore, we re-analyzed the longitudinal data of SH_1, SH_2, SH_3, and SH_4 from a multivariate model to get a reliable estimation of narrow-sense heritability and genetic correlation between any two of the traits. For the genetic correlation analysis between each one of the shell heights at varying ages and BW at harvest, a bivariate model using REML was conducted. Since the common effects to full-sib family indicated by the Z-ratio in components were very small, we

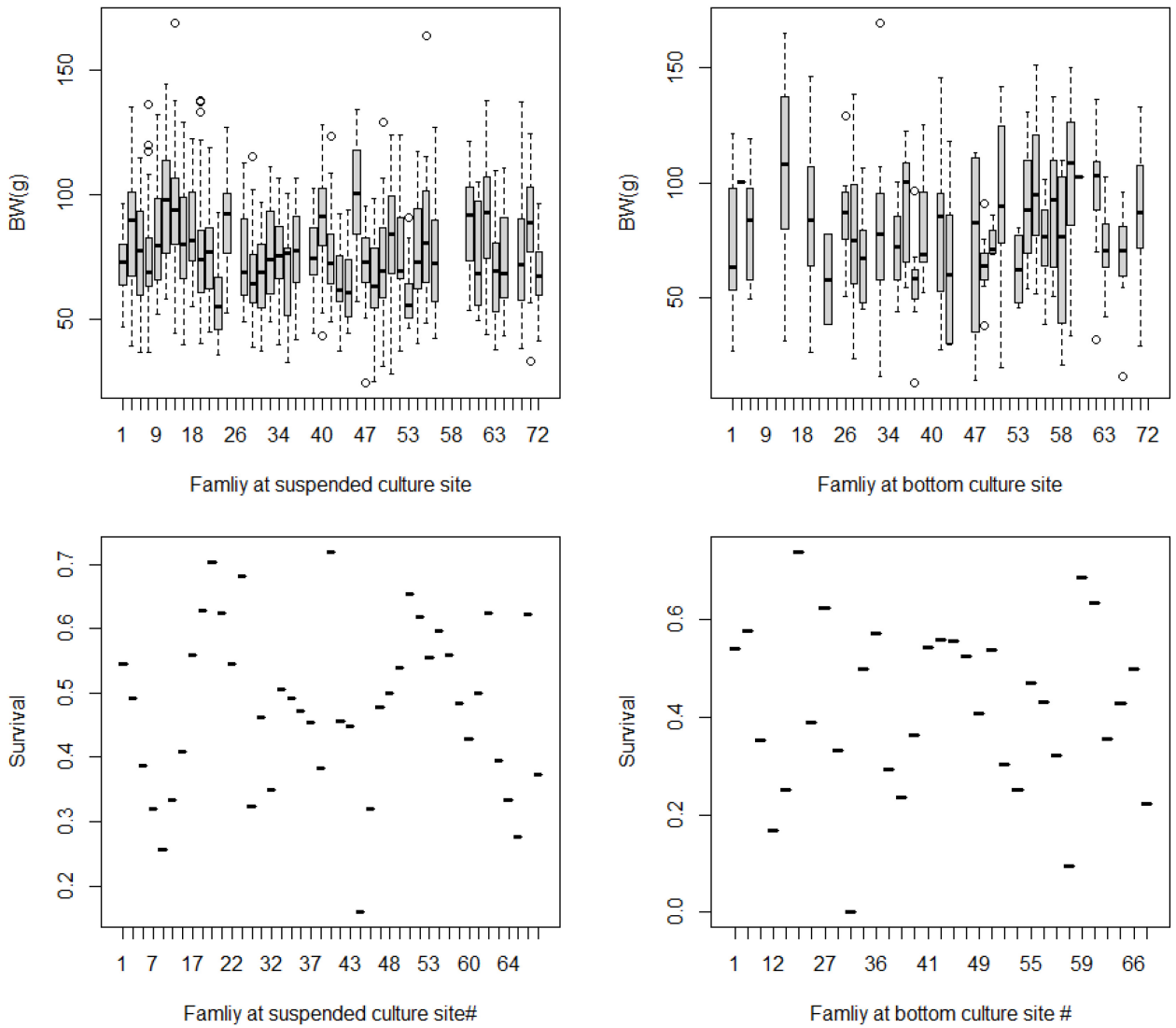

FIGURE 2 | Body weight (BW, g) and survival rate (Survival, × 100%) of yesso scallop full-sib families at suspended and bottom culture environments.

removed it in the model, and therefore, only additive and residue effects were treated as random effects in the mixed linear model.

At the suspended environment, the estimated heritability of scallop shell heights at varying ages was of the medium to the high level, ranging from 0.410 at 20 months to 0.853 at 6 months as shown in **Table 2**. Genetic correlations between SH from 6 to 20 months were significantly different from zero (**Table 2**, above the diagonal). Genetic correlations between contiguous ages were high ranging from 0.496 between 6 and 20 months to 0.958 between 6 and 10 months. As the length of the interval increased, genetic correlations tended to decrease. At harvest, the estimated heritability of scallop BW was of medium level (0.328, **Table 2**), while the estimated heritability of scallop survival was of low level (0.128, **Table 2**). Genetic correlations between BW at harvest to shell height at varying ages were also significantly different from zero (**Table 2**, above the diagonal). The genetic correlations between BW and shell height at varying ages were high, ranging from 0.535 between shell height at 6 months and BW at harvest to 0.983 between shell height at 20 months and BW at harvest. Similarly, as the length of the interval increased, genetic correlations between BW at harvest to shell height tended to decrease. The genetic correlation between BW and survival at harvest was of a low level (0.398) and was not significantly different from zero.

At the bottom culture environment, the estimated heritability of scallop BW was 0.198 (**Table 2**), while the estimated heritability of scallop survival was of low level (0.101, **Table 2**). Both estimates were significantly different from zero, however, lower than those at the suspended culture environment.

G × E interaction in terms of scallop BW at two culture environments was indicated by the estimate of genetic correlation for BW between the environments. The genetic correlation for

TABLE 2 | Estimates of heritabilities (the diagonal), genetic correlation (above the diagonal), and phenotypic correlation (below the diagonal) between varying traits in yesso scallop at two environments.

Environment/Trait[a]		Suspended						Bottom	
		SH1	SH2	SH3	SH4	BW	Survival	BW	Survival
Suspended	SH1	0.853 (0.126)	0.958 (0.017)	0.828 (0.060)	0.496 (0.142)	0.535 (0.138)			
	SH2	0.850 (0.015)	0.618 (0.114)	0.942 (0.022)	0.687 (0.101)	0.697 (0.102)			
	SH3	0.730 (0.026)	0.880 (0.011)	0.501 (0.103)	0.890 (0.041)	0.894 (0.043)			
	SH4	0.561 (0.042)	0.722 (0.026)	0.877 (0.011)	0.410 (0.091)	0.983 (0.012)			
	BW	0.525 (0.040)	0.656 (0.027)	0.775 (0.016)	0.863 (0.009)	0.328 (0.080)	0.339 (0.198)[b]	<0.001[b]	
	Survival					0.023 (0.042)[b]	0.128 (0.041)		
Bottom	BW					<0.001[b]		0.198 (0.098)	
	Survival								0.101 (0.038)

[a] *The data in the table are shown in the format of value (standard errors). SH1, shell height at 6 month; SH2, shell height at 10 month; SH3, shell height at 16 month; SH4, shell height at 20 month; BW, body weight at harvest; Survival, Survival at harvest. Suspended and bottom are the two environments in the study.*

[b] *All the data in the table were significantly different from 0 ($P < 0.01$, based on t-distribution) with the exceptions of genetic and phenotypic correlations between BW and survival at the suspended environment, and between BW at two environments.*

BW between the environments was very small (<0.001, **Table 2**), which indicates a considerable genotype by environment interaction for growth in yesso scallop.

DISCUSSION

Because of their high economic importance, genetic improvement in scallop species is continuously attracting attention in recent years (Zheng et al., 2004; Wang et al., 2017, 2018; Tan et al., 2020). Heritability reflects the genetic ability of traits, which is an important parameter for selective breeding (Song et al., 2022). In this study, animal or individual models by the REML method were used to estimate narrow-sense heritability for the growth-related traits of shell heights and BW, and the results showed that the heritability was at a moderate to a high level in yesso scallop in sea-based aquaculture system. Similar results were obtained by Barros et al. (2018), in the Caribbean scallop, *Argopecten nucleus*, with estimated heritability larger than 0.26 from growth traits. Wang et al. (2018) also reported that the single-nucleotide polymorphism-based heritability for shell length, shell height, shell width, and whole weight in Zhikong scallop, *Chlamys farreri*, was of high level, from 0.28 to 0.54, respectively. The moderate to high heritability for shell height, BW in this study indicates that the potential for genetic improvement of these traits is large, and it is necessary to perform selective breeding in yesso scallop in the environment of a sea-based aquaculture system. While the estimated heritabilities for survival trait in yesso scallop after rearing for 20 months were relatively low at both environments (suspended and bottom conditions). Generally, the additive genetic variation for survival or stress tolerance-related trait is reported low in aquaculture species, such as shrimp (Li et al., 2015) and oyster (de Melo et al., 2016). It might indicate the large confounded non-additive effects including environmental effects for survival-related traits and the difficulty to obtain considerable gains through selective breeding for survival traits in yesso scallop. Furthermore, at the bottom environment, estimates of heritability for growth and survival-related traits were similar but slightly lower than those at the suspended environment. Comparatively, the bottom environment seems to be harsher to scallops indicated by the destroyed cages and predating during the culture period than the suspended environment. The higher environmental variations at the bottom environment for the target traits probably might be the reason for the lower level of estimated heritability than that at the suspended environment.

A narrow genetic base or limited additive genetic variance of the foundation population will lead to a fast accumulation of inbreeding at a high level and decrease the genetic gain during selection. In this study, we used two stocks A and B as broodstock for the sake of broadening the genetic base. Intraspecies and interspecies crossbreeding were reported to be an effective means to improve the growth and survival traits in aquaculture species, such as salmon (Bryden et al., 2004), prawn (Thanh et al., 2010), oyster (Hedgecock and Davis, 2007), and scallop (Xing et al., 2022). However, the Wald-*F*-test from the mixed linear model showed that the crossing effects by the two stocks (A and B) were not significant for all the traits. This is maybe due, at least in part, to low genetic variation in the introduced yesso scallop stocks of A and B. Although there existed a difference in domesticated generations after being introduced into China, the lack of genetic variation due to small effective population size and poor genetic management after introduction might be responsible for the results.

Common environmental effects to full-sibs were reported important in a family-based selective breeding program (Gjedrem et al., 2012). Estimation of variance components including the additive variance and common environmental variance was vital to the selection accuracy for target traits. However, in this study, common environmental variances in both environments (suspended and bottom conditions) were estimated very small, which is different from published studies (Gjerde et al., 2004; Luan et al., 2012). This is maybe due to the absence of genetic ties between half-sib families from different sires (**Table 1**). In this study, there were 73 full-sib scallop families before metamorphosis, however, about 30

families were culled for parallel environmental control. Since no sufficient samples were partitioned from the same full-sib, this is the reason that the inconsistent number of families were used in the two environments. The lack or loss of genetic ties between families may have contributed to the fact that the common environmental effects for BW and survival could not be partitioned effectively in this study.

In the genetic breeding program in animals, growth and developmental traits at a specific age (in the day, month, or year), such as the time to market are the main targets of selection improvement. As such, genetic evaluation of the growth and developmental process can increase the efficiency of selection compared to that of traits measured at specific ages (Schaeffer, 2004; He et al., 2017). However, the repeated records of growth or body size on an individual in aquaculture animals are apparently a labor and time-cost task in genetic evaluation (Hollenbeck and Johnston, 2018). Besides, repeated measurements at specific ages can often cause stress to farmed animals, especially aquaculture animals (Boudry et al., 2022). In this study, we put forward and conducted a longitudinal evaluation of shell heights at harvest, obtaining four shell height data by the growth rings in the outer shells of the yesso scallop. The characteristics of the growth cycle of the yesso scallop were reported per the water temperature (Wang et al., 1986; Wang and Wang, 1993). It is reported that the suitable temperature range for yesso scallops is 5–20°C, and about 15°C is the most suitable growth temperature in China. The upper and lower limits of the water temperature are 23 and 0°C, respectively (Wang et al., 1986). Thereafter, two rapid growth periods for yesso scallop in northern China usually occur in late spring and early winter. Additionally, shell rings are usually shaped in a suspended culture environment when the animals stop growth during the high water temperature period (>23°C) in late August and low-temperature period (<0°C) in February (Wang et al., 1986). In this study, we conducted spawning of the broodstock at the hatchery in February and reared the animals for 20 months. Therefore, a total of three growth rings corresponds to the time when the scallop stopped growing. It is clear that the points of the growth rings are determined to be 6, 10, and 16 months, respectively, in the study. In fact, the fine periodic growth patterns on shell surfaces have been widely used for studies in the ecology and evolution of scallops (Xing et al., 2017). Due to seasonal changes in the physical and chemical properties of seawater in the environment, the rates of secretion and deposition of shell materials are varied, resulting in a periodic appearance of growth patterns on shells with different densities in the internal structure and chemical elements (Michio and Hiromichi, 2013). Apparently, the growth rings in the outer shells of the yesso scallop cannot change with time, which guarantees the accuracy of shell height data recorded by the growth ring method at harvest in this study.

There are merits and demerits of the shell growth ring method for longitudinally scallop shell height recording in this study. First, one merit of the method was easy to conduct and labor and time cost-effective. Furthermore, compared with the traditional measurements at each of the specific ages on scallops, many of which might occur mortality subsequently, the data collected at harvest were from the survived animals and more valuable. Finally, with the help of shell rings or other shell markers, more repeated records of shell growth data can be obtained by elaborately recording such as the computed tomography (CT) approach (Xing et al., 2017). In this situation, recent developments in mixed model theory and advances in computer software now allow for the implementation of random effects in the statistical model and the modeling of the covariance structure of the data (König et al., 2006), e.g., random regression model reported in aquaculture animals (He et al., 2017). However, the shortcoming of the method might be that heritability for shell height at an earlier age was overestimated (e.g., $h^2 \sim 0.853$ for SH_1 at 6 months). This estimate is expected to be biased upward due to possible effects that have not partitioned from additive genetic effect (Eknath et al., 2007). The possible effects might be the maternal or common environmental effect which is more important in the early days after fertilization.

Good environmental control is the key to the design of all selective breeding experiments. Selection is effective in non-stress environments because they are reproducible; selection is also successful in reproducible stress environments but not irreproducible ones (Hufstetler et al., 2007). According to the theory of quantitative genetics, heritability is relative and varies with the environment. In addition, when the environmental variance is large, it will increase the difficulty of estimating the genetic variance. Estimates of heritability depend on the environment, which is variable over time and space. The goal of environmental control is to minimize environmental variation and maximize the ratio of genetic variation in phenotypic variation, thereby increasing the accuracy of breeding selection and improving genetic gain. For marine mollusks including the yesso scallop, it is very hard to conduct good environmental control, especially in a sea-based culture system. The survival results in this study (∼ 40% at harvest) also indicated the difficult task to conduct good environmental control in a scallop selection program. Environmental control will likely be an important area of research in scallop selective breeding programs in the future.

In this study, a very low level of genetic correlation between scallop BW at the two environments (suspended vs. bottom) indicated the occurrence of G × E interaction for BW trait. Low genetic correlation between environments indicates significant G × E interaction according to the study of Falconer and Mackay (1996). It means that the potential different genes are responsible for the phenotypic variation of a target trait in different environments. According to Robertson (1959) and Sae-Lim et al. (2016), the genetic correlation between environments less than 0.8 indicates the occurrence of G × E interaction in aquaculture animals. Our results indicate that selecting yesso scallop individuals of greater genetic merit evaluated at suspended sea-based culture environment may reduce the accuracy of selection when transferred to the animals reared at the bottom-based environment. However, Sae-Lim et al. (2016) suggested at least 100 families per environment are required for target traits to G × E interaction study in aquaculture. In this study, only a limited number of 33–43 full-sib families were assessed in the two environments (suspended vs. bottom) for G × E interaction evaluation. It seems that no sufficient genetic ties existed between the environments. This is might

be one of the reasons for the low level (<0.01) of genetic correlation for the scallop growth between the two environments analyzed by the multitrait mixed model. Compared with the reported high levels of genetic correlation (>0.8) for growth at varying environments in aquaculture (refer to the review by Sae-Lim et al., 2016), the estimate in this study apparently biased downward. More data especially more full-sib families should be provided to get a more reliable G × E interaction evaluation in the future. Furthermore, the sample size in a specific full-sib was also reported as important to heritability and genetic correlation estimates, especially for survival traits in marine mollusks with vary large phenotypic variation within full-sib families (Kube et al., 2007). The differences in the survival rate among different families were shown in **Figure 2**. Large variation in terms of survival rate among different families within and between the environments was detected. However, we have not displayed the genetic correlation estimates for the scallop survival traits between the environments. Owing to the insufficient samples to each full-sib per environment with the only average number of 23–62 individuals per full-sibs, and the low level of heritability estimates for survival traits at both environments, it is reasonable that the estimate of G × E interaction effects analyzed by the multitrait mixed model will be of very low confidence.

Genomic selection has been found to outperform traditional selection in bivalve species, however, one of the major limitations of genomic selection is the cost, especially genotyping a large number of animals (Hollenbeck and Johnston, 2018). A family-based selection program is still an important approach in yesso scallop. Estimates of genetic parameters including heritability and genetic correlation for growth and survival traits are still important in the genomic selection era such as they can provide prior information to scallop selection program.

CONCLUSION

We found a considerable level of additive genetic variation for shell height and BW measured in yesso scallop at suspended and bottom sea-based culture environments, which indicated that the traits will show a favorable response to selection in this species. A longitudinal evaluation of shell heights was carried out and proved to be feasible in yesso scallop genetic evaluation. The G × E interaction effects between BW measured in suspended vs. bottom environments will decrease the accuracy of selection for growth in bottom culture, the major culture mode in China. In addition, good environmental control can be used to improve heritability and estimated breeding value accuracy and accelerate the rate of genetic gain in the yesso scallop.

DATA AVAILABILITY STATEMENT

The original contributions presented in the study are included in the article/supplementary material, further inquiries can be directed to the corresponding author/s.

AUTHOR CONTRIBUTIONS

FW conceived the study, conducted the data analysis, and drafted the manuscript. FW, CL, and JZ carried out the field and laboratory work. FW and GZ discussed the draft manuscript. All authors approved the manuscript for publication.

FUNDING

This study was supported by the National Key R&D Program of China (No. 2019YFD0900801), the National Science Foundation of China (No. 31972790), and the China Agriculture Research System of MOF and MARA (CARS-49).

ACKNOWLEDGMENTS

We thank all members of the Lab of Marine Mollusc Aquaculture and Biotechnology, IOCAS for valuable discussions. We are grateful to Zoneco Group Co., Ltd., for support during our study.

REFERENCES

Alcapán, A. C., Nespolo, R. F., and Toro, J. E. (2007). Heritability of body size in the Chilean blue mussel (*Mytilus chilensis* Hupé 1854): effects of environment and ageing. *Aquac. Res.* 38, 313–320. doi: 10.1111/j.1365-2109.2007.01678.x

Barros, J., Velasco, L. A., and Winkler, F. M. (2018). Heritability, genetic correlations and genotype by environment interactions in productive traits of the Caribbean scallop, *Argopecten nucleus* (Mollusca: Bivalvia). *Aquaculture* 488, 39–48. doi: 10.1016/j.aquaculture.2018.01.011

Boudry, P., Allal, F., Aslam, M. L., Bargelloni, L., Bean, T. P., Brard-Fudulea, S., et al. (2022). Current status and potential of genomic selection to improve selective breeding in the main aquaculture species of International Council for the exploration of the Sea (ICES) member countries. *Aquac. Rep.* 20:100700. doi: 10.1016/j.aqrep.2021.100700

Bryden, C. A., Heath, J. W., and Heath, D. D. (2004). Performance and heterosis in farmed and wild Chinook salmon (*Oncorhynchus tshawytscha*) hybrid and purebred crosses. *Aquaculture* 235, 249–261. doi: 10.1016/j.aquaculture.2004.01.027

de Melo, C. M. R., Durland, E., and Langdon, C. (2016). Improvements in desirable traits of the Pacific oyster, *Crassostrea gigas*, as a result of five generations of selection on the West Coast, USA. *Aquaculture* 460, 105–115. doi: 10.1016/j.aquaculture.2016.04.017

Eknath, A. E., Bentsen, H. B., Ponzoni, R. W., Rye, M., Nguyen, N. H., Thodesen, J., et al. (2007). Genetic improvement of farmed tilapias: composition and genetic parameters of a synthetic base population of *Oreochromis niloticus* for selective breeding. *Aquaculture* 273, 1–14. doi: 10.1016/j.aquaculture.2007.09.015

Falconer, D. S., and Mackay, T. F. C. (1996). *Introduction to Quantitative Genetics*, fourth Edn. Harlow: Prentice Hall, Longman Group Limited.

Food and Agriculture Organisation [FAO] (2020). *Fishery and Aquaculture Statistics. Global Production by Production Source 1950-2018 (FishstatJ)*. Rome: FAO Fisheries and Aquaculture Department.

Gjedrem, T. (2010). The first family-based breeding program in aquaculture. *Rev. Aquac.* 2, 2–15. doi: 10.1111/j.1753-5131.2010.01011.x

Gjedrem, T. (2012). Genetic improvement for the development of efficient global aquaculture: a personal opinion review. *Aquaculture* 344-349, 12–22. doi: 10.1016/j.aquaculture.2012.03.003

Gjedrem, T., Robinson, N., and Rye, M. (2012). The importance of selective breeding in aquaculture to meet future demand for animal protein: a review. *Aquaculture* 350-353, 117–129. doi: 10.1016/j.aquaculture.2012.04.008

Gjerde, B., Terjesen, B. F., Barr, Y., Lein, I., and Thorland, I. (2004). Genetic variation for juvenile growth and survival in Atlantic cod (*Gadus morhua*). *Aquaculture* 236, 167–177. doi: 10.1016/j.aquaculture.2004.03.004

Guo, X., and Luo, Y. (2016). Scallops and scallop aquaculture in China. *Dev. Aquac. Fish. Sci.* 40, 937–952.

He, J., Zhao, Y., Zhao, J., Gao, J., Han, D., Xu, P., et al. (2017). Multivariate random regression analysis for body weight and main morphological traits in genetically improved farmed tilapia (*Oreochromis niloticus*). *Genet. Sel. Evol.* 49:80.

Hedgecock, D., and Davis, J. P. (2007). Heterosis for yield and crossbreeding of the Pacific oyster *Crassostrea gigas*. *Aquaculture* 272(Suppl. 1), S17–S29. doi: 10.1016/j.aquaculture.2007.07.226

Hollenbeck, C. M., and Johnston, I. A. (2018). Genomic tools and selective breeding in molluscs. *Front. Genet.* 9:253. doi: 10.3389/fgene.2018.00253

Hufstetler, E. V., Boerma, H. R., Carter, T. E., and Earl, H. J. (2007). Genotypic variation for three physiological traits affecting drought tolerance in soybean. *Crop Sci.* 47, 25–35. doi: 10.2135/cropsci2006.04.0243

Katherine, A., Ross, K. A., Thorpe, J. P., Norton, T. A., and Brand, A. R. (2001). An assessment of some methods for tagging the great scallop, *Pecten maximus*. *J. Mar. Biol. Assoc. U. K.* 81, 975–977. doi: 10.1017/S0025315401004921

König, S., Köhn, F., Kuwan, K., Simianer, H., and Gauly, M. (2006). Use of repeated measures analysis for evaluation of genetic background of dairy cattle behavior in automatic milking systems. *J. Dairy Sci.* 89, 3636–3644. doi: 10.3168/jds.S0022-0302(06)72403-1

Kube, P. D., Appleyard, S. A., and Elliott, N. G. (2007). Selective breeding greenlip abalone (*Haliotis laevigata*): preliminary results and issues. *J. Shellfish Res.* 26, 821–824. doi: 10.2983/07308000

Li, W., Luan, S., Luo, K., Sui, J., Xu, X., Tan, J., et al. (2015). Genetic parameters and genotype by environment interaction for cold tolerance, body weight and survival of the Pacific white shrimp *Penaeus vannamei* at different temperatures. *Aquaculture* 441, 8–15. doi: 10.1016/j.aquaculture.2015.02.013

Liu, Y. (1983). Culture of Japanese scallops. *Fish. Sci. China* 1, 14–19. (in Chinese),

Luan, S., Yang, G., Wang, J., Luo, K., Zhang, Y., Gao, Q., et al. (2012). Genetic parameters and response to selection for harvest body weight of the giant freshwater prawn *Macrobrachium rosenbergii*. *Aquaculture* 362–363, 88–96. doi: 10.1016/j.aquaculture.2012.05.011

Michio, S., and Hiromichi, N. (2013). Mollusk shell structures and their formation mechanism. *Can. J. Zool.* 91, 529–531. doi: 10.1139/cjz-2012-0333

Ren, W., Chen, H., Renault, T., Cai, Y., Bai, C., Wang, C., et al. (2013). Complete genome sequence of acute viral necrosis virus associated with massive mortality outbreaks in the Chinese scallop, *Chlamys farreri*. *Virol. J.* 10, 110–116. doi: 10.1186/1743-422X-10-110

Robertson, A. (1959). The sampling variance of the genetic correlation coefficient. *Biometrics* 15, 469–485. doi: 10.1007/BF00285414

Sae-Lim, P., Gjerde, B., Nielsen, H. M., Mulder, H., and Kause, A. (2016). A review of genotype-by-environment interaction and micro-environmental sensitivity in aquaculture species. *Rev. Aquac.* 8, 369–393. doi: 10.1111/raq.12098

Schaeffer, L. R. (2004). Application of random regression models in animal breeding. *Livest. Prod. Sci.* 86, 35–45. doi: 10.1016/S0301-6226(03)00151-9

Shumway, S. E., and Parsons, G. J. (2006). Scallops: biology, ecology and aquaculture. *Dev. Aquac. Fish. Sci.* 164, 280–281.

Song, H., Xu, S., Luo, K., Hu, M., Luan, S., Shao, H., et al. (2022). Estimation of genetic parameters for growth and egg related traits in Russian sturgeon (*Acipenser gueldenstaedtii*). *Aquaculture* 546:737299. doi: 10.1016/j.aquaculture.2021.737299

Tan, K., Zhang, H., Lim, L., and Zheng, H. (2020). Selection breeding program of Nan'ao Golden Scallop *Chlamys nobilis* with higher nutritional values and less susceptible to stress. *Aquaculture* 517:734769. doi: 10.1016/j.aquaculture.2019.734769

Thanh, N. M., Nguyen, N. H., Ponzoni, R. W., Vu, N. H., Barnes, A. C., and Mather, P. B. (2010). Estimates of strain additive and non-additive genetic effects for growth traits in a diallel cross of three strains of giant freshwater prawn (*Macrobrachium rosenbergii*) in Vietnam. *Aquaculture* 299, 30–36. doi: 10.1016/j.aquaculture.2009.12.011

Wang, C., Liu, B., Liu, X., Ma, B., Zhao, Y., Zhao, X., et al. (2017). Selection of a new scallop strain, the Bohai Red, from the hybrid between the bay scallop and the Peruvian scallop. *Aquaculture* 479, 250–255. doi: 10.1016/j.aquaculture.2017.05.045

Wang, Q. Z., Li, S., Fu, C., Zhang, M., Teng, W., Liu, Z., et al. (2014). Establishment of high temperature resistance families and use of laboratory assays to predict subsequent survival in juvenile stage of the Japanese scallop (*Mizuhopecten yessoensis*). *J. Fish. China* 38, 371–377. (in Chinese), doi: 10.3724/SP.J.1231.2014.48971

Wang, Q., Kou, B., Liu, Y., and Li, W. (1986). A primary approach to the subject of rearing spats of Japanese scallop (*Pecten yessoensis*) at optimum temperature. *Mar. Sci. China* 10, 49–50. (in Chinese),

Wang, R., and Wang, Z. (1993). *Science of Marine Shellfish Culture*. Qingdao: China Ocean University Press.

Wang, Y., Sun, G., Zeng, Q., Chen, Z., Hu, X., Li, H., et al. (2018). Predicting growth traits with genomic selection methods in Zhikong Scallop (*Chlamys farreri*). *Mar. Biotechnol.* 20, 769–779. doi: 10.1007/s10126-018-9847-z

Xing, Q., Wei, T., Chen, Z., Wang, Y., Lu, Y., Wang, S., et al. (2017). Using a multiscale image processing method to characterize the periodic growth patterns on scallop shells. *Ecol. Evol.* 7, 1616–1626. doi: 10.1002/ece3.2789

Xing, Q., Yang, Z., Zhu, X., Liu, J., Huang, X., Hua, J., et al. (2022). Interspecific hybridization between *Patinopecten yessoensis* (♀) and *P. caurinus* (♂) with heterosis in growth and temperature tolerance. *Aquaculture* 547:737489. doi: 10.1016/j.aquaculture.2021.737489

Zar, J. H. (1984). *Biostatistical Analysis*, 2nd Edn. Englewood Cliffs, NJ: Prentice-Hall, 718.

Zheng, H., Zhang, G., Liu, X., Zhang, F., and Guo, X. (2004). Different responses to selection in two stocks of the bay scallop, *Argopecten irradians irradians* Lamarck (1819). *J. Exp. Mar. Biol. Ecol.* 313, 213–223. doi: 10.1016/j.jembe.2004.04.015

Conflict of Interest: The authors declare that the research was conducted in the absence of any commercial or financial relationships that could be construed as a potential conflict of interest.

Publisher's Note: All claims expressed in this article are solely those of the authors and do not necessarily represent those of their affiliated organizations, or those of the publisher, the editors and the reviewers. Any product that may be evaluated in this article, or claim that may be made by its manufacturer, is not guaranteed or endorsed by the publisher.

frontiers in Marine Science

ORIGINAL RESEARCH
published: 24 March 2022
doi: 10.3389/fmars.2022.864037

Functional Characterization of *Cfap206* for Bivalve Ciliogenesis by RNAi and CRISPR/Cas9 Technologies

Yinghui Wang[1†], *Xiaomei Zhu*[1†], *Shanshan Lian*[1,2*], *Yiran Li*[1], *Naina Hu*[1], *Xiaoli Hu*[1,3], *Zhenmin Bao*[1,3,4] *and Shi Wang*[1,2,4]

[1] *Sars-Fang Centre and Ministry of Education (MOE) Key Laboratory of Marine Genetics and Breeding, Ocean University of China, Qingdao, China,* [2] *Laboratory for Marine Biology and Biotechnology, Pilot Qingdao National Laboratory for Marine Science and Technology, Qingdao, China,* [3] *Laboratory for Marine Fisheries Science and Food Production Processes, Pilot Qingdao National Laboratory for Marine Science and Technology, Qingdao, China,* [4] *Key Laboratory of Tropical Aquatic Germplasm of Hainan Province, Sanya Oceanographic Institution, Ocean University of China, Sanya, China*

Cilia are organelles located on the surface of eukaryotic cells and play important roles in numerous physiological and developmental processes. Cilia- and flagella-associated proteins (CFAP family) are well known due to their close relation to the assembly and functionalization of both cilia and flagella. In vertebrates, *Cfap206* is reported to function during motile cilia assembly, and its abolished expression could lead to abnormal ciliary beating and decreased sperm motility. However, there is scarcely any information on the function of *Cfap206* in marine invertebrates. Here, through using an ideal shellfish research model, the dwarf surf calm *Mulinia lateralis*, we explored the role of *Cfap206* during embryonic ciliogenesis as well as during male gametogenesis. In trochophore larvae, effective knocking down or knocking out of *Cfap206* was detected respectively through RNAi and CRISPR/Cas9 technology, showing an obviously decreased number of cilia. During the period of gonadal maturation, we managed to deliver the dsRNA of *Cfap206* to male individuals for 14 days through carrier vector feeding. Significant suppression of *Cfap206* was observed, together with impaired sperm motility and aberrant sperm tail assembly. The present study provided valuable information on gene function exploration methods in *M. lateralis* and further enriched the understanding of *Cfap206* on ciliogenesis in marine invertebrates. Furthermore, by revealing the relationship between *Cfap206* and spermatozoa flagellum, it is possible to generate male sterile populations in hermaphroditic marine organisms to improve crossbreeding efficiency.

Keywords: ***Mulinia lateralis*, *Cfap206*, ciliogenesis, RNAi, CRISPR/Cas9, breeding**

OPEN ACCESS

Edited by:
Yuehuan Zhang,
South China Sea Institute of Oceanology (CAS), China

Reviewed by:
Xiaotong Wang,
Ludong University, China
Ernesto Maldonado,
National Autonomous University of Mexico, Mexico

***Correspondence:**
Shanshan Lian
lianshanshan@ouc.edu.cn

[†]*These authors share first authorship*

Specialty section:
This article was submitted to Marine Fisheries, Aquaculture and Living Resources, a section of the journal Frontiers in Marine Science

Received: *28 January 2022*
Accepted: *01 March 2022*
Published: *24 March 2022*

Citation:
Wang Y, Zhu X, Lian S, Li Y, Hu N, Hu X, Bao Z and Wang S (2022) Functional Characterization of Cfap206 for Bivalve Ciliogenesis by RNAi and CRISPR/Cas9 Technologies. Front. Mar. Sci. 9:864037. doi: 10.3389/fmars.2022.864037

INTRODUCTION

Cilia are membranous organelles that protrude from the surface of most eukaryotic cells, contributing to multiple functions such as movement, sensation, and signal transmission (Pazour and Witman, 2003; Jakobsen et al., 2006; Verhey et al., 2011; Bangs and Anderson, 2017). The basic structure of cilia is highly conserved, including four parts: matrix, transition zone, axoneme, and ciliary membrane (Elliott and Brugmann, 2019). According to the differential axoneme microtubule composition, cilia could be divided into motile cilia and nonmotile cilia (known as primary cilia) (Verhey et al., 2011). The axoneme of motile cilia usually possesses nine doublet microtubules surrounding a central pair of singlet microtubules (Satir and Christensen, 2007). The microtubule doublets are interconnected with ciliary dynein motors, the activity of which is regulated through radial spokes (RS1, RS2, and RS3) to produce fluid and pulsatile motion. Thus, motile cilia could mediate the movement of cells and extracellular fluid, such as the movement of eggs and sperm, as well as the removal of foreign bodies in the respiratory tract (Afzelius and Eliasson, 1983; Lyons et al., 2006; Orhon et al., 2015). The axoneme of primary cilia lack the central pair of singlet microtubules, and there are a number of surrounding sensory membrane proteins that can assist in performing sensory, signal transduction, and coordination functions (Hua and Ferland, 2018; Tao et al., 2020). Primary cilia are closely related to the transduction of Hedgehog (Hh) pathway (Danwei et al., 2003), Wnt pathway (Ross et al., 2005), platelet-derived growth factor (PDGF) pathway, and Ca^{2+} signaling cascade (Orhon et al., 2015).

The cilia- and flagella-associated protein (CFAP) family is proven to be associated with the normal assembly of cilia or flagella (Tang et al., 2017). *Cfap39* and *Cfap65*, for example, are required for the assembly of the dynein regulatory complex in the generation of motile cilia (Lin et al., 2012; Beckers et al., 2020) and deletion of *Cfap43*, *Cfap44*, *Cfap65*, *Cfap69*, and *Cfap251* will lead to abnormal sperm flagellum assembly in mice or humans, resulting in male infertility (Tang et al., 2017; Dong et al., 2018; He et al., 2020; Li et al., 2020). In particular, *Cfap206* has recently been identified as a downstream target gene of *Foxj1*, a key transcription factor that has been proven to be closely related to the occurrence of mobile cilia in vertebrates (Stubbs et al., 2008; Thomas et al., 2010; Alten et al., 2012; Vij et al., 2012). Any mutation or deletion of them may lead to severe cilia diseases, such as primary ciliary dysmotility (PCD), hydrocephalus, retinitis pigmentosa, polycystic kidney disease (PKD), and multiple morphological abnormalities of the sperm flagella (MMAF) (Pazour and Rosenbaum, 2002; Satir and Christensen, 2007; Sironen et al., 2020). Moreover, CFAP206 protein was found to be located in cilia, which was required for establishing the dynamin motor RS2 (Beckers et al., 2020). It was reported that the stable assembly of calmodulin- and spoke-associated complex (CSC), which is considered to mediate the specific connection of radial spokes with adjacent structures in cilia, was regulated by *Cfap206* in a dependent manner (Heuser et al., 2012; Vasudevan et al., 2015; Toure et al., 2021). Although *Cfap206* is a key gene for ciliogenesis, it has only been studied in several model organisms, such as *Tetrahymena* and *Mus musculus*. For example, when *Cfap206* was knocked out, the cilia of *Tetraphymena* cells were found to produce abnormal waveforms due to the abnormal RS2 assembly and showed reduced bending amplitude and weakened intertemporal coordination, but there was no significant difference in cilia number and length (Vasudevan et al., 2015). Interestingly, the loss of *Cfap206* also leads to abnormal patterns of bending or curling of sperm flagellum in mice; however, the *Cfap206*-KO mice did show sperm flagella shortening or loss (Shen et al., 2021). Bivalve mollusc is an ancient Lophotrochozoa group of marine invertebrates that possesses rich species diversity. Cilia play critical roles in important physiological activities of bivalve species, such as filter feeding, respiration, reproduction, as well as larval movement. However, knowledge of molecular modulation of ciliogenesis is quite limited in bivalves, and to the best of our knowledge, this is the first study on *Cfap206* to point to the regulation of both cilia and flagella. Notably, many bivalves, such as *Argopecten irradians* (Wei et al., 2021), are hermaphroditic, and a better understanding of the regulation of *Cfap206* on sperm flagellum may help to produce a male sterile population, thus improving artificially crossbreeding efficiency.

The dwarf surf clam (*Mulinia lateralis*) is a small, buried bivalve mollusc belonging to the family Mactridae, which is naturally distributed in estuaries and mudflats along the Atlantic coast from Canada to the Caribbean Sea (Walker and Tenore, 1984). They possess many appealing features for becoming a promising bivalve model, such as small adult size (15–20 mm), rapid development and early transparent shell, short generation time (~2 months), and convenient artificial cultivation (no attachment base) (Calabrese, 1970; Santos and Simon, 1980). In addition, *M. lateralis* represents the first bivalve with successful demonstration of transgene technology (Lu et al., 1996). At present, our team has established a standard laboratory artificial breeding system for *M. lateralis*, and we have successfully achieved gene knockdown through RNAi as well as gene knockout through CRISPR/Cas9 microinjection. Thus, we chose *M. lateralis* to explore the participation of *Cfap206* in both ciliogenesis and spermatogenesis in this study. Our study provides the functional characterization of bivalve *Cfap206* and assists in a better understanding of cilia/flagella regulation in marine invertebrates. Further investigation of the relationship between *Cfap206* and sperm flagellum formation may provide a possible method for the generation of male sterile individuals to improve the crossbreeding efficiency for hermaphroditic marine organisms.

MATERIALS AND METHODS

Identification, Phylogenetic and Spatiotemporal Expression Analysis of *Cfap206* in *M. lateralis*

The available CFAP206 protein sequence of 14 representative species were downloaded from NCBI and Uniprot databases (**Table 1** shows the accession numbers). These orthologous sequences were used as queries for whole-genome blast with the *E*-value threshold of 1*E*−05 in the *M. lateralis* proteome and genome database. To ensure the integrity and accuracy of *Cfap206*, its nucleic acid sequence was predicted using ORF

TABLE 1 | The accession numbers of CFAP206 proteins.

Species	Accession number
Homo sapiens	NP_001026913.1
Crassostrea gigas	XP_011442159.1
Xenopus tropicalis	XP_002938343.1
Macaca fascicularis	XP_005552462.1
Rattus norvegicus	XP_017449021.1
Mizuhopecten yessoensis	XP_021375351.1
Pomacea canaliculata	XP_025093619.1
Actinia tenebrosa	LOC116292837
Orbicella faveolata	XP_020624489.1
Exaiptasia diaphana	XP_020907483.1
Felis catus	XP_003986405.2
Ciona intestinalis	LOC100178966
Psetta maxima	F2P81_018558
Mus musculus	NP_001333991

Finder, and the amino acid sequence was submitted to the SMART database to verify the presence of the CFAP domain. The molecular weights and isoelectric points were calculated by using Compute PL/Mw tools. The genetic structure of *Cfap206* was mapped using the GSDS2.0 website. The Geneious Prime software and PHYRE2.0 website were used to predict the secondary structure and tertiary structure of CFAP206 protein.

CFAP206 protein sequences of 12 species were obtained from the NCBI and Uniprot databases, including *Homo sapiens, Mus musculus, Petromyzon marinus, Crassostrea gigas, Mizuhopecten yessoensis, Mulinia lateralis, Capitella teleta, Aplysia californica, Lingula anatina, Ciona intestinalis, Nematostella vectensis, and Lottia gigantea*. ClustalW (Larkin et al., 2007) and Genedoc Software (Nicholas, 1997) were used for multiple sequence alignment. The phylogenetic analysis of *Cfap206* was performed by MEGA7.0, and the establishment method of the tree was neighbor joining (NJ). The parameter was P-distance, and the value of bootstrap replications was set to 1,000. According to the transcriptome data of *M. lateralis* obtained in our laboratory, the expression level of *Cfap206* in fourteen embryonic stages and seven adult tissues were plotted.

RNAi Based on Electroporation

Based on unpublished genome and transcriptome information from our lab, the exon and intron of *Cfap206* gene were annotated by MAKER2 (Version 3.01.03) to obtain cDNA sequence information. Also, the interference sites (110–594 bp) were identified using SiDirect Version 2.0. *Cfap206*-dsRNA was synthesized by MEGA Script RNAi kit (Thermo Fisher Scientific, America) (RNAi primers were shown in **Table 2**). Male and female *M. lateralis* with well-developed gonads were selected, then the fresh sperm and eggs were obtained under standard laboratory conditions. After extrusion of the first polar body (around 15 min after mixing the sperm and eggs), each group collected 6,000–7,000 fertilized eggs for electroporation. Bio-Rad Gene Pulser Xcell (America) was selected as the electroporation instrument, and the electric transfer parameters were set according to **Table 3**. We chose filtered seawater as the electroporation buffer: blank control group was not processed; electroporation-control group was given electric shock without dsRNA; and experimental group was added with dsRNA (concentration maintained at 250 ng/μl) and was given electric shock. After 30 min on ice, all groups were cultured at room temperature in a 6-well plate to trochophore larvae stage.

Deletion of *Cfap206* Gene Using CRISPR-Cas9 System

The functional domain of *Cfap206* was predicted using the SMART website. Single-guided RNAs (sgRNAs) were designed on the exons of this domain, and sgRNAs containing SNPs were excluded (sgRNA sequences are shown in **Table 2**). sgRNAs were synthesized using MEGAscript™ T7 Transcription Kit (Thermo

TABLE 2 | Primers used for RNAi, qPCR, sgRNA synthesis, and PCR analyses.

Name	Sequence
Cfap206-RNAi-F	TAAAGGCAGTAGTGTTGGACCCATC
Cfap206-RNAi-R	ATTGAAGAGTCTAATTCCCGTCACA
Cfap206-sgRNA-F1	GAAATTAATACGACTCACTATAGTTATGTGTTGATCGATTGAgttttagagctagaaatagcaagttaa
Cfap206-sgRNA-F2	GAAATTAATACGACTCACTATAGGAATTAACAATGATTGTGAgttttagagctagaaatagcaagttaa
Cfap206-sgRNA-F3	GAAATTAATACGACTCACTATACATTCATGTCACTAACAAAGgttttagagctagaaatagcaagttaa
Cfap206-sgRNA-F4	GAAATTAATACGACTCACTATAGAGTGGATTTCAAGATGAGAgttttagagctagaaatagcaagttaa
Cfap206-sgRNA-F5	GAAATTAATACGACTCACTATATTGTAGTTGTTCCATACGAGgttttagagctagaaatagcaagttaa
Cfap206-sgRNA-F6	GAAATTAATACGACTCACTATACAGTAACATTTTAGCCAGTTgttttagagctagaaatagcaagttaa
sgRNA-R	AAAAAAAGCACCGACTCGGTGCCAC
Cfap206-verify-F1	AAATCTAGCAGAATTATGAGGTATG
Cfap206-verify-R1	CCAGACCTGAGGAGAACAGCGGA
Cfap206-verify-F2/3	TCGCTGTCGTGAGAGAGGCTA
Cfap206-verify-R2/3	ACATTCTGAGTTGTTGCAGGG
Cfap206-verify-F4/6	CCAATACCTGCCTACCTTGACTTA
Cfap206-verify-R4/6	AACACCACTTAAGAATGGAACCAA
Cfap206-verify-F5	GAGAAGATTCAGTCTGGAGATAGC
Cfap206-verify-F5	GTCAAGGTAGGCAGGTATTGGAAT
Cfap206-qPCR-F	AGATTCAGTCTGGAGATAG
Cfap206-qPCR-R	GTACAGTAGCTTGTAGTTG
RS23-qRCR-F	CCATCAAGATGGGTGAAAC
RS23-qRCR-R	CGAATCCAGCGACTAAGA

TABLE 3 | The electroporation parameters for *Cfap206*-dsRNA delivery.

Criteria	Parameter
Voltage (V)	100
Cuvette (mm)	4
Number of pulse	1
Pulse interval (s)	0
Pulse length (ms)	0.2

Fisher Scientific, America). The editing efficiency of sgRNAs was tested *in vitro* using the Guide-it sgRNA Screening Kit (Takara, Japan). sgRNAs and Cas9 protein in different concentrations were incubated at 37° C for 15 min (**Table 4**), and then, microinjection was performed using fertilized eggs of *M. lateralis*. The control and injected embryos were cultured in filtered seawater at 24°C. The injection volume of the Cas9 protein-sgRNAs mixture is about 0.1 nl. A single embryo was collected approximately 24 h after microinjection, and genomic DNA was extracted by the Chelex®-100 method (Li et al., 2021). The DNA fragment containing the target site was amplified using MightAmp™ DNA Polymerase Ver.3 (Takara, Janpan), and the corresponding verified primers are shown in **Table 2**. The PCR fragments were sequenced in Sangon Biotech.

Plasmid Construction and Induction of Interfering dsRNA

Following the relevant method developed in the Pacific oyster *Crassostrea gigas* (Feng et al., 2019), the interference fragment of *Cfap206* (110–594 bp) was inserted into the L4440 vector to construct the *Cfap206*-dsRNA-L4440 plasmid. The *Cfap206*-dsRNA-L4440 and L4440 plasmids were transfected into competent *Escherichia coli* cells HT115 for expression. The strain HT115 carrying the *Cfap206*-dsRNA-L4440 plasmid was inoculated in LB medium containing ampicillin (50 μg/ml) and tetracycline (12.5 μg/ml) at 37°C and 220 rpm to the logarithmic stage (OD: 0.4–0.6). In total, 0.8 Mm IPTG was added to a 40 ml bacterial solution and stirred at 37°C for 4 h to induce dsRNA. The bacteria of the induced group and the noninduced group were centrifuged at 5,500 rpm for 2 min. After the supernatant was removed, the total RNA was extracted by the Trizol method, and the presence of dsRNA was determined by 1.5% agarose gel.

RNAi by Ingested dsRNA-Expressing Bacteria

Three hundred male *M. lateralis* with healthy growth status, equal size, and immature gonads were selected and divided into three groups (blank-control group, L4440-control group, and *Cfap206*-dsRNA-L4440 group). Eight liters of filtered seawater was added to the glass tank, and each group was fed with a micropump. The water flow rate was controlled at 12 ml/min, and the water temperature was maintained at about 25°C. Each group was temporarily reared for 5 days without treatment to observe the mortality under natural growth state. During the interference process, *Chlorella pyrenoidesa* was fed twice a day from days 1 to 7, with 180 μl (1×10^{10}/ml) each time. In detail, normal algae were fed at 10 am, and normal algae or algae-bacteria were fed at 10 pm for different groups, and the sea water was changed once a day. From days 8 to 14, to speed up gonadal ripening to maturation, 180 μl of normal *C. pyrenoidesa* were fed at 10 am, and normal mixed algae (**Table 5**) or mixed algal-bacteria were fed at 10 pm, and egg yolk was fed continuously during these 2 weeks.

Quantitative RT-PCR

According to the phenol chloroform extraction method described by Hu et al. (2006), the total RNA of embryos was extracted. The Reverse Transcriptase M-MLV (Rnase H-) kit (Takara, Japan) was used to reverse transcription into cDNA, with a concentration of 20 ng/μl after inversion. Fluorescent real-time quantitative PCR was performed using the 2× ChamQ SYBR Color qPCR Master Mix (Vazyme, China). The $2^{-}\Delta\Delta t$ method is used to quantify the expression of *Cfap206*. Quantitative RT-PCR primers are shown in **Table 2**. All qPCR experiments were repeated twice, with two biological replicates and three technical parallels for each sample, using *RS23* as an internal control.

Immunofluorescence

Embryos were washed twice with 1×PBS to remove seawater and fixed overnight with 4%PFA at 4°C. The next day, after being centrifuged at 300 rcf at room temperature for 30 s, the embryos were washed with 1×PBS 3 times. After washing, the sample was dehydrated with 80% methanol and 20% DMSO at 4°C overnight. After washing with PBST (1×PBS+0.5%Triton X-100) 3 times, the sample was then added with 500 μl trypsin and incubated for 5 min. After repeated washing with PBST, the sample was incubated with 10% goat serum (NGS) at room temperature for 2 h. Rabbit antiacetylated tubulin antibody was then added to 10%NGS in a ratio of 1:1,000 and the samples were incubated overnight at 4°C. After washing with PBST three times, goat anti-rabbit FITC was added to 2%NGS/PBST at the ratio of 1:200, and the sample was incubated at room temperature for 2 h. Following washing with PBST, the sample

TABLE 4 | The editing efficiency and survival rate of trochophore larvae after injection.

Cas9 protein concentration (ng/μl)	sgRNA concentration (ng/μl)	Editing efficiency (%)		Survival rate (%)	
		sgRNA4	sgRNA6	sgRNA4	sgRNA6
0	0	0	0	90	90
800	0	0	0	23	20
800	800	43	60	20	18
800	1500	20	19	13	15
800	3000	25	43	5.6	8.3

TABLE 5 | Mixed algae used to ripen *M. lateralis*.

Species	Density (per/ml)	Dosage (μl/h)
Platymonas helgolandica	5×10^8	5
Isochrysis galbana	1×10^9	5
Chaetoceros muelleri	1×10^9	15

was added with phalloidin and DAPI in a ratio of 1:500 and stained for 30 min at room temperature. After being washed with PBS three times, the sample was mounted and the confocal images were taken.

Sperm Motility Test

After 14 days of feeding, sexually mature males were selected for artificial sperm stimulation for each group. Sperm motility was tracked using the CASAS-QH-III automatic sperm analyzer (Tsinghua Tongfang, China). The process was completed by the National Laboratory (Qingdao).

Microscopy

For confocal observation, the cellular morphology was observed with the A1R Ti-E confocal microscopy (Nikon, Japan). For SEM observation, the critical point-dried sample was coated in gold and the sample surface was observed through a Tescan™ Vega3 scanning electron microscope (Czechia).

RESULTS AND DISCUSSION

Identification of *Cfap206* in *M. lateralis* and Phylogenetic Analysis

We identified one *Cfap206* (*MlCfap206*) gene through whole-genome searching of *M. lateralis*, and its genomic structure showed 16 exons, 15 introns, a 5′UTR, and a 3′UTR (**Figure 1A**). The ORF length and protein length of *MlCfap206* were 1875bp and 624 amino acids, respectively. A similar protein structure was revealed for CFAP206 from various species. For example, in mice, *Cfap206* encodes 620-amino acids and possesses the conserved FAP206 domain (Shen et al., 2021) (**Figure 1B**). This may suggest the conservative function of *MlCfap206* related to cilia and flagella. The secondary structure of CFAP206 protein is shown in **Figure 1C**, which contained 27 α-helixes, 25 β-folds, 36 β-bends, and 35 random coils. Based on template d1mhyd (confidence: 87.5), the predicted tertiary ferritin-like structure within the CFAP206 domain (420aa-467aa) is shown in **Figure 1D**.

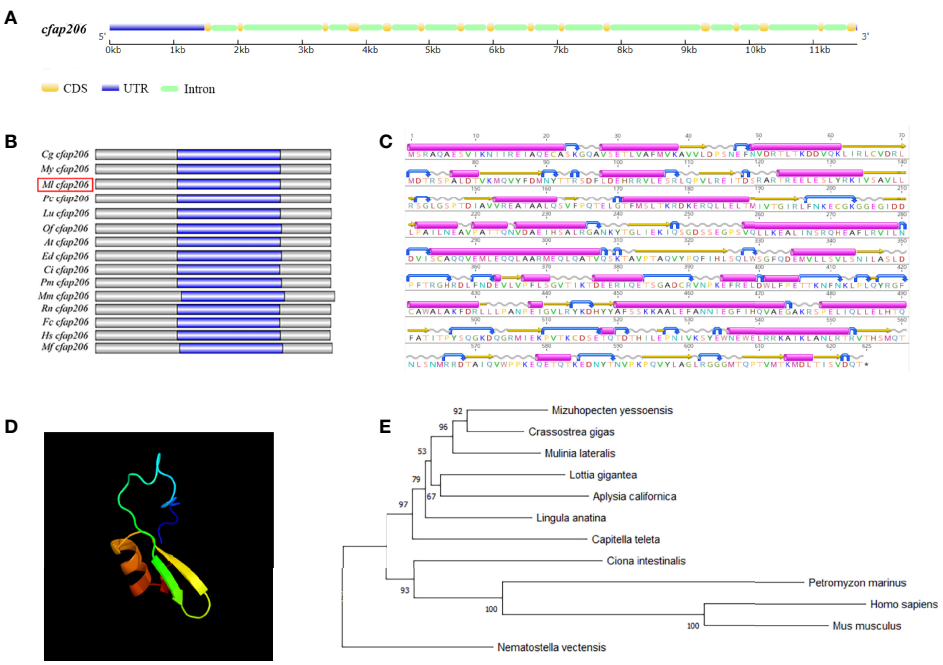

FIGURE 1 | Characterization of *Cfap206* in *M. lateralis* and phylogenetic analysis. **(A)** Genetic structure of *Cfap206*. CDS, coding sequence; UTR, untranslated region. **(B)** Protein structures of CFAP206s of fifteen representative species. Grey represents the whole protein region, and the magenta region represents the CFAP206 domain of each species. **(C)** Prediction of the secondary structure of CFAP206 protein. Magenta represents α-helixes, yellow represents β-folds, blue represents β-bends, and gray represents random coils. **(D)** Prediction of the tertiary ferritin-like structure within the CFAP206 domain (420aa-467aa). **(E)** Phylogenetic analysis of CFAP206 proteins.

Phylogenetic analysis of CFAP206 proteins was performed using the NJ method with 1,000 bootstrap pseudoreplicates (**Figure 1E**), from 12 selected animals spanning Cnidaria (including *N. vectensis*), Brachiopoda (*L. anatina*), Mollusca (including *C. gigas*, *M. yessoensis*, *M. lateralis*, *A. californica*, and *L.gigantea*), Annelida (including *C. teleta*), and Chordata (including *H. sapiens*, *M. musculus*, *C. intestinalis*, and *P. marinus*). Obviously, *Ml*CFAP206 was first grouped together with CFAP206 proteins from molluscs (such as *M. yessoensis* and *C. gigas*). These mollusc CFAP206s were then sequentially clustered with CFAP206s from brachiopods, annelids, and chordates. The clustering relationship of CFAP206 is consistent with the species' evolutionary relationship.

Spatiotemporal Expression Analysis

Spatiotemporal expression analysis of *MlCfap206* in the present study was performed based on our unpublished transcriptomic data. Transcripts per million (TPM) of *MlCfap206* in fourteen embryonic stages as well as in seven adult tissues was used to perform the expression level analysis (**Figure 2**). During development (**Figure 2A**; **Supplementary Table S1**), the high expression level of *Cfap206* is mainly observed in blastula, gastrula, and trochophore larvae, three key periods for embryonic motile cilia formation and development. A similar pattern could be observed in *M. yessoensis* based on the published transcriptome data (Hou et al., 2011), which suggests that *Cfap206* may be required for embryonic ciliogenesis regulation. Among the seven adult tissues of *M. lateralis*, the highest expression of *Cfap206* was found in the male gonad, followed by foot and gill (**Figure 2B**; **Supplementary Table S2**). Functionalization of these three organs needs specialized cilia for sperm tail formation, byssus attachment, as well as for respiration, food intake, or waste removal through gill filaments (Ward et al., 1993; Andrade et al., 2015; Shen et al., 2021). Lines of evidence showed that *Cfap206* plays important roles in ensuring the stability of RS and CSC, participating in cilia and flagella formation regulation (Dubruille et al., 2002; Vasudevan et al., 2015). Similar to our findings, previous studies have found that *Cfap206* is massively overexpressed in human testicles, and the sperm of mice without the *Cfap206* gene shows abnormalities in the morphology, number, and length of flagella (Shen et al., 2021). To date, cilia regulation of gill has only been reported in marine invertebrates including *Ciona intestinalis* and *C. gigas*, mainly focusing on *calaxin*, *Meichroacidin*, *Tektin A1*, and *Tektin B1* (Shimazaki et al., 2006; Wang et al., 2015), and the regulatory genes of foot cilia have not been reported yet. Our results suggested that *Cfap206* may be involved in these organs' cilia regulation in marine bivalves.

RNAi to Suppress *Cfap206* Expression Affected Embryonic Ciliogenesis

The trochophore larvae possess apical tuft and cilia band which are the typical ciliated features and are responsible for sensation, movement, and feeding (Arenas-Mena, 2010). Moreover, the

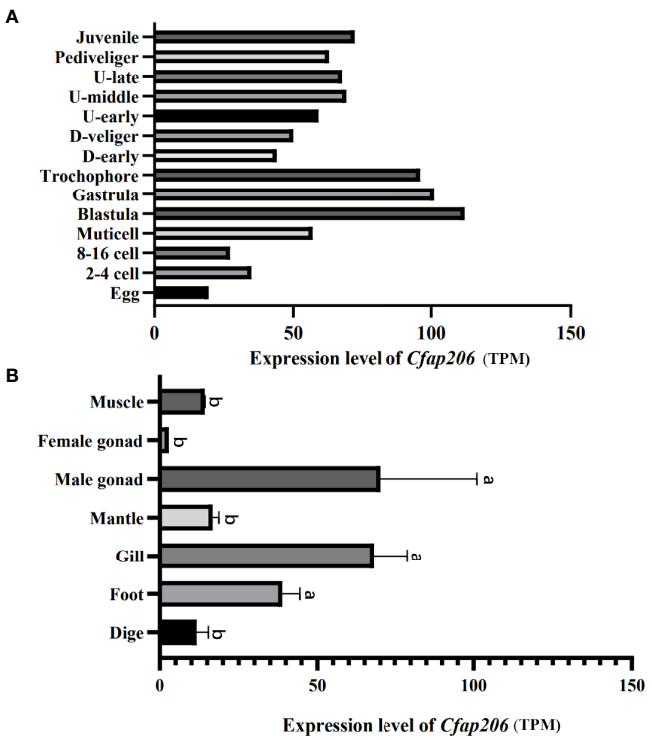

FIGURE 2 | Spatiotemporal expression of *Cfap206* in *M. lateralis*. **(A)** The expression of *Cfap206* in fourteen embryonic stages. **(B)** The expression of *Cfap206* in seven tissues. SPSS28.0 was used for one-way ANOVA analysis of the data, and Duncan method was used to test the significance of the difference between the values of each group.

ciliated trochophore larvae are considered to be the most conserved phylogenetic stage of marine Lophotrochozoans, and several pieces of evidence show they share an ancient and common origin (Paps et al., 2015; Xu et al., 2016; Wang et al., 2020). Thus, we chose trochophore larvae to explore whether or not *Cfap206* participate in bivalve embryonic ciliogenesis. Firstly, we generated the *Cfap206*-dsRNA through *in vitro* transcription and the target bands were correctly located (**Figure 3A**). With optimized electroporation conditions and reasonable dose of *Cfap206*-dsRNA (~250 ng/μl), we detected significant suppression of *Cfap206* ($p < 0.01$) in *M. lateralis* trochophore larvae by qPCR (**Figure 3B**). Compared with the control group, the electroporation-blank group showed normal gene expression level, excluding that there might be side effects of electroporation itself on gene expression. Morphological observations of each group of larvae were then made by confocal microscopy and scanning electron microscopy (**Figures 3C, D**). Similar size as well as spindle-shaped body were observed for the larvae from three groups, indicating the normal speed of embryo development. However, obvious cilia reduction/abolishment showed up in the larvae when *Cfap206* was significantly suppressed, demonstrating the irreplaceable requirement of *Cfap206* during embryonic ciliogenesis of *M. lateralis*. Previous studies in model animals such as *Xenopus laevis* and *Tetrahymena* revealed that *Cfap206* is mainly involved with the regulation of cilia motility (Vasudevan et al., 2015). In *X. laevis*, moderate ciliary defect occurred during larva development when *Cfap206* gene was knocked out, leading to abnormal ciliary movement waveform and decreased motor ability. Similarly, the axoneme of the cilia of *Tetrahymena* with *Cfap206* knocked out were compressed, which swam at only 30% of the speed of the wild type (Vasudevan et al., 2015). However, the relationship between *Cfap206* and ciliogenesis is not clear in bivalves. According to our results, it was obvious that the downregulation of *Cfap206* expression in *M. lateralis* led to a significant decrease in the number of cilia. This phenomenon reminded us that there might be function divergence of *Cfap206* on cilia regulation among different species, or *Cfap206* is effective at different hierarchies during signal transduction which is worthy of further in-depth study.

CRISPR/Cas9 Knockout of *Cfap206* Affected Embryonic Ciliogenesis

The efficiency of sgRNAs plays a key role in the editing effect (Li et al., 2021). Thus, to generate *Cfap206*-KO larvae of *M. lateralis*, we first performed the *Cfap206*-sgRNA screening to avoid the influence of SNP and to perform *in vitro* efficiency test. Six sgRNAs (sgRNA1-6) were chosen (**Figure 4A**). Among them, it was found that *Cfap206*-sgRNA-2, *Cfap206*-sgRNA-4, and *Cfap206*-sgRNA-6 could work and cut the target DNA fragment into two pieces *in vitro*, and *Cfap206*-sgRNA-4 seems to be the most effective one (**Figure 4B**). Next, through microinjection together with Cas9 protein (800 ng/μl), we performed the *in vivo* editing efficiency test of these three effective *Cfap206*-sgRNAs. A previous study revealed that the concentration ratio of sgRNA-Cas9 was a key factor in inducing effective gene mutation (Li et al., 2021). In the present study, three different concentrations of *Cfap206*-sgRNA (800/1,500/3,000 ng/μl) were tested and showed a different editing efficiency as well as survival rate. Unfortunately, after *Cfap206*-sgRNA-2/Cas9 microinjection, no positive editing results turned back. However, *Cfap206*-sgRNA-4 and *Cfap206*-sgRNA-6 still worked *in vivo* and 800 ng/μl was the optimal concentration for microinjection (**Table 4**). In comparison, under optimal concentration, the *in vivo* editing efficiency of *Cfap206*-sgRNA-6 (60%) was higher than *Cfap206*-sgRNA-4 (43%), and the corresponding positive editing results are shown in **Figure 4C**. In *M. lateralis*, the target gene mutations *in vivo* which were induced by *Cfap206*-sgRNA/Cas9 mainly included insertion or deletion mutations within 11 bp, similar to the editing results of other invertebrates (Lin and Su, 2016; Hiruta et al., 2018; Li et al., 2021). In addition, we noticed that the editing efficiency of different sgRNAs might be different *in vitro* or *in vivo*. This may be due to the influence of complex physicochemical factors in the internal environment on the sensitivity of sgRNA, leading to the difference in the efficiency of sgRNA *in vivo* and *in vitro*. Due to the limited number of positive-edited trochophore larvae, we performed bright field morphological observation (about 20–30 larvae were observed) which showed an obvious reduced cilia number after *Cfap206* knocked out (**Figure 4D**), consisting with the *Cfap206*-RNAi phenotype. It reinforced that *Cfap206* played a key role during embryonic ciliogenesis regulation in *M. lateralis*. In addition, CRISPR/Cas9 system has been widely used as a powerful gene editing tool in agriculture and animal breeding, so the CRISPR/Cas9 system we established in *M. lateralis* for mediating gene knockout may be beneficial for trait improvement in marine bivalves.

dsRNA-Expressing Bacteria Feeding Interfered With Adult Ciliogenesis

To further explore whether or not *Cfap206* also participates in the male gametogenesis, we managed to deliver the dsRNA of *Cfap206* to male individuals for 14 days feeding during the gonadal maturation period. We successfully induced *Cfap206*-dsRNA expression in competent HT115 *E. coli* cells with *Cfap206*-dsRNA-L4440 vector (**Figure 5A**). After feeding *Cfap206*-dsRNA-L4440 bacteria, the expression level of *Cfap206* in each group was detected on days 7 and 14. *Cfap206* was markedly suppressed (~70%) in male gonad compared with that of the control group, and no obvious expression change could be detected after L4440-blank feeding (**Figure 5B**). At each check point, the survival rate and body size were roughly equal between different groups, suggesting negligible side effects of this experimental approach. Thereafter, sexually mature individuals from each group were chosen to perform the sperm viability investigation (**Table 6**; **Supplementary Videos 1–3**). According to the sperm motility, the sperm viability could be rated as A–D four grades, respectively as fast forward movement (A), slow forward movement (B), nonforward movement (C), and extremely slow or inactive movement (D). The results showed that more than 80% of sperms from the control group or L4440-blank group could be rated as grade A/B, while more than 90% of

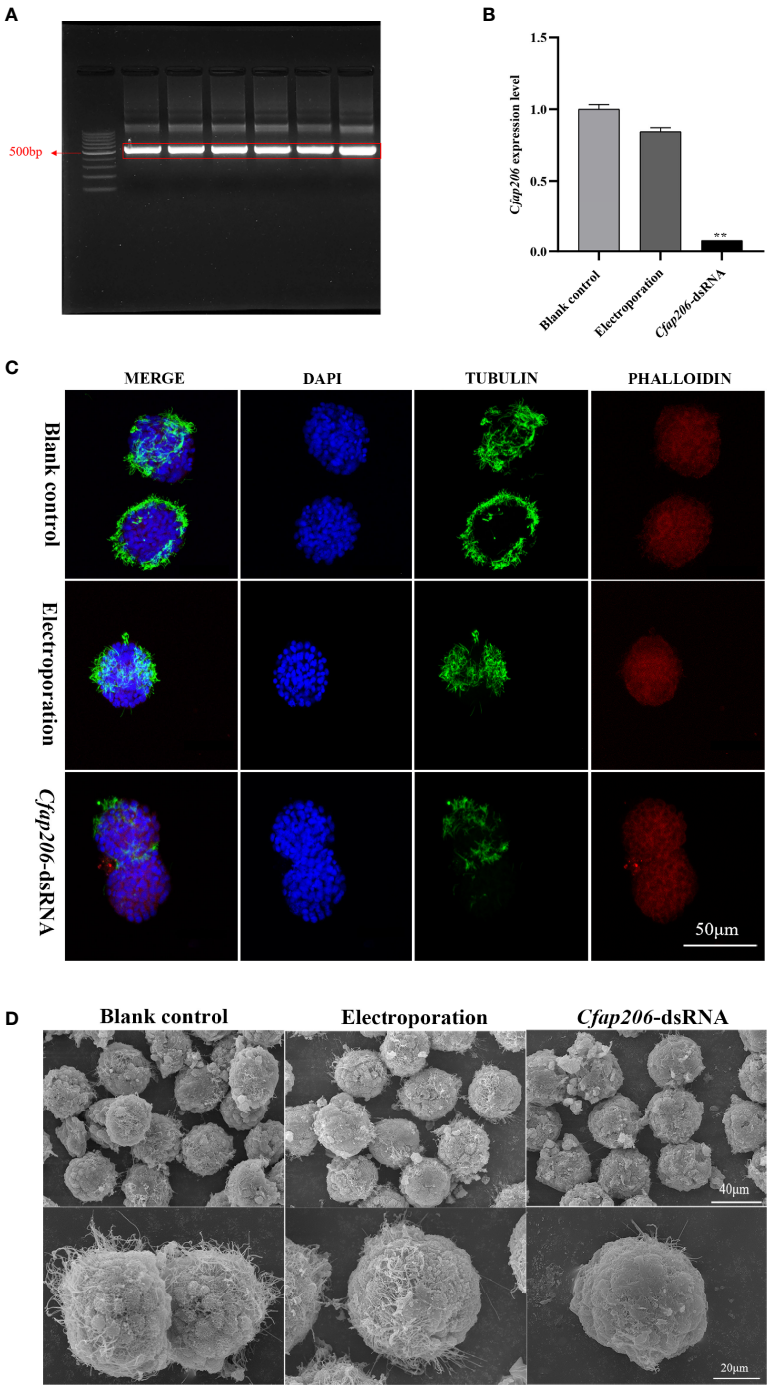

FIGURE 3 | Expression analysis of *Cfap206* and morphological observation of trochophore larvae after RNAi. **(A)** Electrophoresis result of *Cfap206* dsRNA. Lane 1, 100 bp DNA ladder. Lanes 2–7, bands of *Cfap206*-dsRNA (500 bp). **(B)** The expression of *Cfap206* after RNAi (detected by qPCR). $^{**}p < 0.01$. **(C)** Confocal observation of trochophore larvae after RNAi. Cytoskeleton was stained red by phalloidin, nucleus was stained blue by DAPI, and cilia were stained green by tubulin antibody. **(D)** SEM observation of trochophore larvae after RNAi.

sperms from the *Cfap206*-dsRNA-L4440 group was rated as grade D, demonstrating the severe defect of sperm motility after significant suppression of *Cfap206* (**Table 6**). Further morphological observation showed that although the head of sperm from the *Cfap206*-dsRNA-L4440 group was still normal shaped, the sperm tail appeared to be disintegrated (**Figure 5C**), which could be the obvious cause for their abolished motility. Similarly, it was found that sperm cells with short flagella or

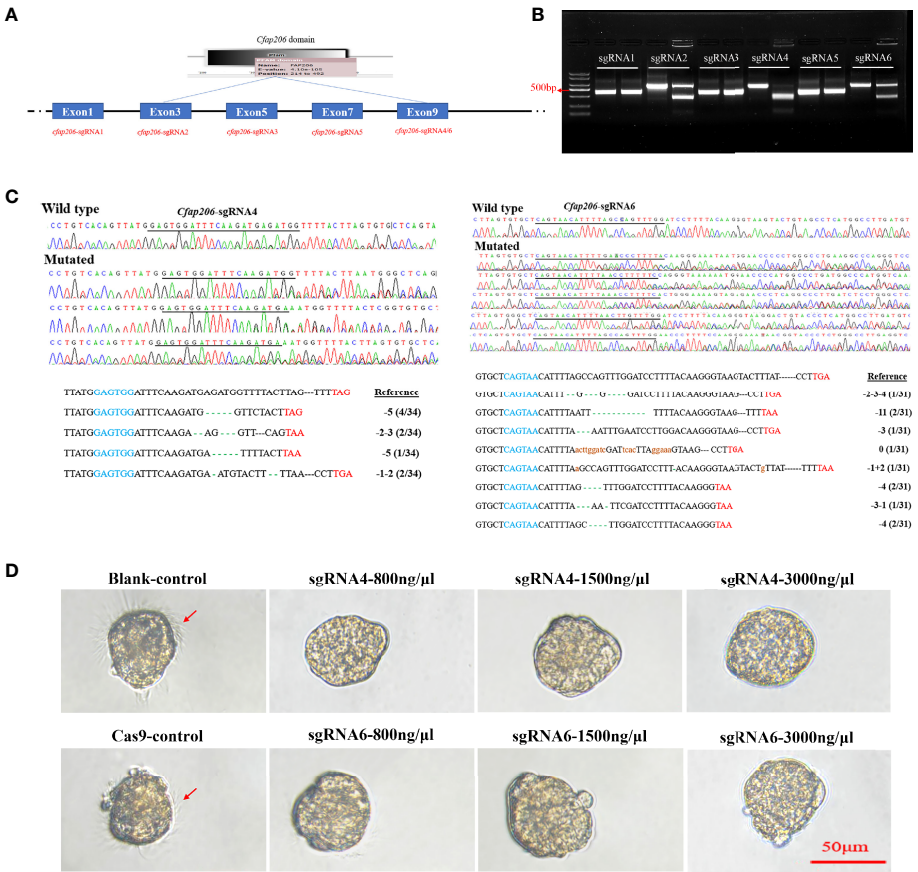

FIGURE 4 | *In vitro* and *in vivo* efficiency detection of *Cfap206*-sgRNAs. **(A)** sgRNA screening for *MlCfap206*. **(B)** *In vitro* cutting efficiency detection of sgRNA1-6. For each sgRNA, the left lane was the control group and the right lane was the experimental group. **(C)** Sanger sequencing of PCR products from injected embryos and the identification of mutations. In the left and right bottom panels, the blue sequence marks the start sequence of *Cfap206*-sgRNA and the red sequence is the stop codon. **(D)** Light microscope observation of trochophore larvae after *Cfap206* knockout.

without flagella were significantly increased in *Cfap206*-KO mice compared with wild-type mice (Shen et al., 2021). Previous studies have shown that the sperm flagellum without *Cfap206* showed severe axoneme disorganization and peri-axonemal defects, resulting in abnormal sperm morphology and decreased motility (Shen et al., 2021). This is because *Cfap206* is closely related to the assembly of the radial spoke RS2 in the axoneme, and the absence of *Cfap206* would result in the radial spoke RS2 either not being assembled or being assembled without the front fork (Shen et al., 2021). *Cfap206* is also a condition for the stable assembly of CSC elements, and CSC connects three major axonemal complexes involved in the dynein regulation of RS2 (Vasudevan et al., 2015). Taken together, our findings showed that *Cfap206* plays critical roles during spermatogenesis, and its participation in the sperm flagella assembly is presented not only in vertebrates but also in marine bivalves. It is worth mentioning that the sexual system of bivalves is diversified, including hermaphrodite, simultaneous hermaphrodite, and sequential hermaphrodite (Collin, 2013). Before the gametes are expelled from the body, hermaphrodite species cannot determine the sex of their gametes. Considering the important role of *Cfap206* in spermatogenesis, it may be possible to use gene editing technology to knockout *Cfap206* gene to obtain male sterile population, to effectively improve the crossbreeding efficiency of hermaphrodite bivalves.

CONCLUSION

In the present study, we explore the functional role of *Cfap206* during embryonic ciliogenesis as well as during male gametogenesis in a promising bivalve model *M. lateralis*. Through RNAi and CRISPR/Cas9 technologies, *MlCfap206* was effectively knocked down or knocked out in trochophore larvae, and an obvious decreased number of cilia were detected. Through the dsRNA carrier vector feeding, significant suppression of *Cfap206* was observed in the male gonad, together with impaired sperm motility and aberrant sperm tail assembly. Our results suggest that *Cfap206* is critical for the formation and functionalization of both embryonic cilia and

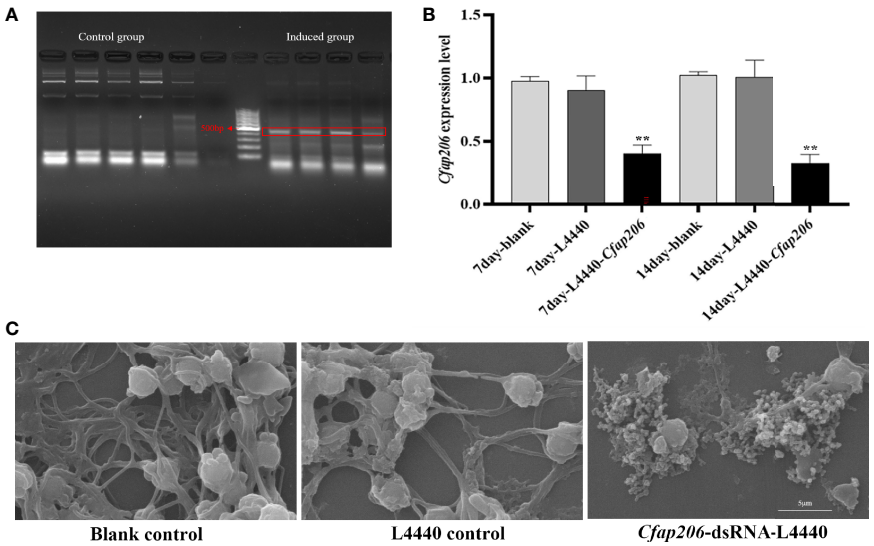

FIGURE 5 | Expression analysis of *Cfap206* and morphological observation of sperm after RNAi. **(A)** Electrophoresis results of dsRNA induced by L4440-*Cfap206*. Lanes 1–5, control group; lanes 8–11, induced group; and lane 7, 100 bp DNA ladder. **(B)** The expression of *Cfap206* on days 7 and 14. $^{**}p < 0.01$. **(C)** Sperm morphology observation using SEM.

TABLE 6 | Sperm motility after feeding *Cfap206*-dsRNA.

Sperm motility	Control	L4440	*Cfap206*-dsRNA-L4440
A	85.5%	78.4%	1%
B	11.6%	8.1%	3%
C	2.9%	10.8%	2%
D	0%	2.7%	94%

sperm flagellum in *M. lateralis*, which may facilitate a better understanding of the ciliogenesis in marine invertebrates. Crossbreeding is an effective way to improve the resistance and other production performance of bivalves in shellfish breeding. However, it is quite challenging to obtain pure gametes for hermaphroditic shellfish, making it difficult to perform crossbreeding. Gene editing technology on target genes (such as *Cfap206* in the present study) would provide a feasible scheme for producing male sterile population to improve the crossbreeding efficiency of hermaphrodite species.

DATA AVAILABILITY STATEMENT

The datasets presented in this study can be found in online repositories. The names of the repository/repositories and accession number(s) can be found in the article/**Supplementary Material**.

AUTHOR CONTRIBUTIONS

SL, SW, and ZB conceived and designed the study. YW and XZ performed the experiments. YL and NH participated in data analysis. YW, SL, and XH wrote the manuscript. All authors listed have made a substantial, direct, and intellectual contribution to the work and approved it for publication.

FUNDING

We acknowledge the grant support from the National Natural Science Foundation of China (32130107, 31871499), Major Basic Research Projects of Shandong Natural Science Foundation (ZR2018ZA0748), Project of Sanya Yazhouwan Science and Technology City Management Foundation (SKJC-KJ-2019KY01), and Taishan Scholar Project Fund of Shandong Province of China.

SUPPLEMENTARY MATERIAL

The Supplementary Material for this article can be found online at: https://www.frontiersin.org/articles/10.3389/fmars.2022.864037/full#supplementary-material

Supplementary Video 1 | Sperm motility of control group.

Supplementary Video 2 | Sperm motility of L4440-blank group.

Supplementary Video 3 | Sperm motility of *Cfap206*-dsRNA-L4440 group.

REFERENCES

Afzelius, B., and Eliasson, R. (1983). Male and Female Infertility Problems in the Immotile-Cilia Syndrome. *Eur. J. Respir. Dis.* 127, 144–147.

Alten, L., Schuster-Gossler, K., Beckers, A., Groos, S., Ulmer, B., Hegermann, J., et al. (2012). Differential Regulation of Node Formation, Nodal Ciliogenesis and Cilia Positioning by *Noto* and *Foxj1*. *Development* 139, 1276–1284. doi: 10.1242/dev.072728

Andrade, G. R., De Araujo, J. L., Nakamura Filho, A., Guanabens, A. C., Carvalho, M. D., and Cardoso, A. V. (2015). Functional Surface of the Golden Mussel's Foot: Morphology, Structures and the Role of Cilia on Underwater Adhesion. *Mater. Sci. Eng. C Mater. Biol. Appl.* 54, 32–42. doi: 10.1016/j.msec.2015.04.032

Arenas-Mena, C. (2010). Indirect Development, Transdifferentiation and the Macroregulatory Evolution of Metazoans. *Philos. Trans. R Soc. Lond. B Biol. Sci.* 365, 653–669. doi: 10.1098/rstb.2009.0253

Bangs, F., and Anderson, K. V. (2017). Primary Cilia and Mammalian Hedgehog Signaling. *Cold Spring Harb. Perspect. Biol.* 9 (5), a02817. doi: 10.1101/cshperspect.a028175

Beckers, A., Adis, C., Schuster-Gossler, K., Tveriakhina, L., Ott, T., Fuhl, F., et al. (2020). The FOXJ1 Target *Cfap206* Is Required for Sperm Motility, Mucociliary Clearance of the Airways and Brain Development. *Development* 147 (21), dev188052. doi: 10.1242/dev.188052

Calabrese, A. (1970). Reproductive Cycle of the Coot Clam, *Mulinia Lateralis* (Say), in Long Island Sound. *Veliger -Berkeley-* 12, 265–269.

Collin, R. (2013). Phylogenetic Patterns and Phenotypic Plasticity of Molluscan Sexual Systems. *Integr. Comp. Biol.* 53, 723–735. doi: 10.1093/icb/ict076

Danwei, H., Liu, A., Rakeman, A. S., Murcia, N. S., Niswander, L., and Anderson, K. V. (2003). Hedgehog Signalling in the Mouse Requires Intraflagellar Transport Proteins. *Nature* 426, 83–87. doi: 10.1038/nature02061

Dong, F. N., Amiri-Yekta, A., Martinez, G., Saut, A., Tek, J., Stouvenel, L., et al. (2018). Absence of CFAP69 Causes Male Infertility Due to Multiple Morphological Abnormalities of the Flagella in Human and Mouse. *Am. J. Hum. Genet.* 102, 636–648. doi: 10.1016/j.ajhg.2018.03.007

Dubruille, R., Laurencon, A., Vandaele, C., Shishido, E., Coulon-Bublex, M., Swoboda, P., et al. (2002). Drosophila Regulatory Factor X Is Necessary for Ciliated Sensory Neuron Differentiation. *Development* 129, 5487–5498. doi: 10.1242/dev.00148

Elliott, K. H., and Brugmann, S. A. (2019). Sending Mixed Signals: Cilia-Dependent Signaling During Development and Disease. *Dev. Biol.* 447, 28–41. doi: 10.1016/j.ydbio.2018.03.007

Feng, D., Li, Q., and Yu, H. (2019). RNA Interference by Ingested dsRNA-Expressing Bacteria to Study Shell Biosynthesis and Pigmentation in *Crassostrea gigas*. *Mar. Biotechnol. (N. Y.)* 21, 526–536. doi: 10.1007/s10126-019-09900-2

He, X., Liu, C., Yang, X., Lv, M., Ni, X., Li, Q., et al. (2020). Bi-Allelic Loss-Of-Function Variants in CFAP58 Cause Flagellar Axoneme and Mitochondrial Sheath Defects and Asthenoteratozoospermia in Humans and Mice. *Am. J. Hum. Genet.* 107, 514–526. doi: 10.1016/j.ajhg.2020.07.010

Heuser, T., Dymek, E. E., Lin, J., Smith, E. F., and Nicastro, D. (2012). The CSC Connects Three Major Axonemal Complexes Involved in Dynein Regulation. *Mol. Biol. Cell* 23, 3143–3155. doi: 10.1091/mbc.e12-05-0357

Hiruta, C., Kakui, K., Tollefsen, K. E., and Iguchi, T. (2018). Targeted Gene Disruption by Use of CRISPR/Cas9 Ribonucleoprotein Complexes in the Water Flea *Daphnia pulex*. *Genes Cells* 23, 494–502. doi: 10.1111/gtc.12589

Hou, R., Bao, Z., Wang, S., Su, H., Li, Y., Du, H., et al. (2011). Transcriptome Sequencing and *De Novo* Analysis for Yesso Scallop (*Patinopecten yessoensis*) Using 454 GS FLX. *PloS One* 6, e21560. doi: 10.1371/journal.pone.0021560

Hua, K., and Ferland, R. J. (2018). Primary Cilia Proteins: Ciliary and Extraciliary Sites and Functions. *Cell Mol. Life Sci.* 75, 1521–1540. doi: 10.1007/s00018-017-2740-5

Hu, X., Bao, Z., Hu, J., Shao, M., Zhang, L., Bi, K., et al. (2006). Cloning and Characterization of Tryptophan 2,3-Dioxygenase Gene of Zhikong Scallop *Chlamys farreri* (Jones and Preston 1904). *Aquaculture Res.* 37, 1187–1194. doi: 10.1111/j.1365-2109.2006.01546.x

Jakobsen, H. H., Everett, L. M., and Strom, S. L. (2006). Hydromechanical Signaling Between the Ciliate Mesodinium Pulex and Motile Protist Prey. *Aquat. Microb. Ecol.* 44, 197–206. doi: 10.3354/ame044197

Larkin, M. A., Blackshields, G., Brown, N. P., Chenna, R., Mcgettigan, P. A., Mcwilliam, H., et al. (2007). Clustal W and Clustal X Version 2.0. *Bioinformatics* 23, 2947–2948. doi: 10.1093/bioinformatics/btm404

Lin, J., Heuser, T., Carbajal-Gonzalez, B. I., Song, K., and Nicastro, D. (2012). The Structural Heterogeneity of Radial Spokes in Cilia and Flagella Is Conserved. *Cytoskeleton (Hoboken)* 69, 88–100. doi: 10.1002/cm.21000

Lin, C. Y., and Su, Y. H. (2016). Genome Editing in Sea Urchin Embryos by Using a CRISPR/Cas9 System. *Dev. Biol.* 409, 420–428. doi: 10.1016/j.ydbio.2015.11.018

Li, W., Wu, H., Li, F., Tian, S., Kherraf, Z. E., Zhang, J., et al. (2020). Biallelic Mutations in CFAP65 Cause Male Infertility With Multiple Morphological Abnormalities of the Sperm Flagella in Humans and Mice. *J. Med. Genet.* 57, 89–95. doi: 10.1136/jmedgenet-2019-106344

Li, H., Yu, H., Du, S., and Li, Q. (2021). CRISPR/Cas9 Mediated High Efficiency Knockout of Myosin Essential Light Chain Gene in the Pacific Oyster (*Crassostrea gigas*). *Mar. Biotechnol. (N. Y.)* 23, 215–224. doi: 10.1007/s10126-020-10016-1

Lu, J.-K., Chen, T. T., Allent, S. K., Matsubara, T., and Burns, J. C. (1996). Production of Transgenic Dwarf Surfclams, *Mulinia lateralis*, With Pantropic Retroviral Vectors. *Proc. Natl. Acad. Sci. U. S. A.* 93, 3482–3486. doi: 10.1073/pnas.93.8.3482

Lyons, R. A., Saridogan, E., and Djahanbakhch, O. (2006). The Reproductive Significance of Human Fallopian Tube Cilia. *Hum. Reprod. Update* 12, 363–372. doi: 10.1093/humupd/dml012

Nicholas, K. B. (1997). Genedoc: Analysis and Visualization of Genetic Variation, EMBNEW. *Embnew. News* 4, 14. doi: 10.11118/actaun201361041061

Orhon, I., Dupont, N., Pampliega, O., Cuervo, A. M., and Codogno, P. (2015). Autophagy and Regulation of Cilia Function and Assembly. *Cell Death Differ.* 22, 389–397. doi: 10.1038/cdd.2014.171

Paps, J., Xu, F., Zhang, G., and Holland, P. W. (2015). Reinforcing the Egg-Timer: Recruitment of Novel Lophotrochozoa Homeobox Genes to Early and Late Development in the Pacific Oyster. *Genome Biol. Evol.* 7, 677–688. doi: 10.1093/gbe/evv018

Pazour, G. J., and Rosenbaum, J. L. (2002). Intraflagellar Transport and Cilia-Dependent Diseases. *Trends Cell Biol.* 12, 551–555. doi: 10.1016/S0962-8924(02)02410-8

Pazour, G. J., and Witman, G. B. (2003). The Vertebrate Primary Cilium Is a Sensory Organelle. *Curr. Opin. Cell Biol.* 15, 105–110. doi: 10.1016/S0955-0674(02)00012-1

Ross, A. J., May-Simera, H., Eichers, E. R., Kai, M., Hill, J., Jagger, D. J., et al. (2005). Disruption of Bardet-Biedl Syndrome Ciliary Proteins Perturbs Planar Cell Polarity in Vertebrates. *Nat. Genet.* 37, 1135–1140. doi: 10.1038/ng1644

Santos, S. L., and Simon, R. J. L. (1980). Response of Soft-Bottom Benthos to Annual Catastrophic Disturbance in a South Florida Estuary. *Marine Ecol. Prog.* 3, 347–355. doi: 10.3354/meps003347

Satir, P., and Christensen, S. T. (2007). Overview of Structure and Function of Mammalian Cilia. *Annu. Rev. Physiol.* 69, 377–400. doi: 10.1146/annurev.physiol.69.040705.141236

Shen, Q., Martinez, G., Liu, H., Beurois, J., Wu, H., Amiri-Yekta, A., et al. (2021). Bi-Allelic Truncating Variants in CFAP206 Cause Male Infertility in Human and Mouse. *Hum. Genet.* 140, 1367–1377. doi: 10.1007/s00439-021-02313-z

Shimazaki, A., Sakai, A., and Ogasawara, M. (2006). Gene Expression Profiles in *Ciona intestinalis* Stigmatal Cells: Insight Into Formation of the Ascidian Branchial Fissures. *Dev. Dyn.* 235, 562–569. doi: 10.1002/dvdy.20657

Sironen, A., Shoemark, A., Patel, M., Loebinger, M. R., and Mitchison, H. M. (2020). Sperm Defects in Primary Ciliary Dyskinesia and Related Causes of Male Infertility. *Cell Mol. Life Sci.* 77, 2029–2048. doi: 10.1007/s00018-019-03389-7

Stubbs, J. L., Oishi, I., Izpisua Belmonte, J. C., and Kintner, C. (2008). The Forkhead Protein Foxj1 Specifies Node-Like Cilia in *Xenopus* and Zebrafish Embryos. *Nat. Genet.* 40, 1454–1460. doi: 10.1038/ng.267

Tang, S., Wang, X., Li, W., Yang, X., Li, Z., Liu, W., et al. (2017). Biallelic Mutations in CFAP43 and CFAP44 Cause Male Infertility With Multiple Morphological Abnormalities of the Sperm Flagella. *Am. J. Hum. Genet.* 100, 854–864. doi: 10.1016/j.ajhg.2017.04.012

Tao, F., Jiang, T., Tao, H., Cao, H., and Xiang, W. (2020). Primary Cilia: Versatile Regulator in Cartilage Development. *Cell Prolif.* 53, e12765. doi: 10.1111/cpr.12765

Thomas, J., Morle, L., Soulavie, F., Laurencon, A., Sagnol, S., and Durand, B. (2010). Transcriptional Control of Genes Involved in Ciliogenesis: A First Step in Making Cilia. *Biol. Cell* 102, 499–513. doi: 10.1042/BC20100035

Toure, A., Martinez, G., Kherraf, Z. E., Cazin, C., Beurois, J., Arnoult, C., et al. (2021). The Genetic Architecture of Morphological Abnormalities of the Sperm Tail. *Hum. Genet.* 140, 21–42. doi: 10.1007/s00439-020-02113-x

Vasudevan, K. K., Song, K., Alford, L. M., Sale, W. S., Dymek, E. E., Smith, E. F., et al. (2015). FAP206 Is a Microtubule-Docking Adapter for Ciliary Radial Spoke 2 and Dynein C. *Mol. Biol. Cell* 26, 696–710. doi: 10.1091/mbc.E14-11-1506

Verhey, K. J., Dishinger, J., and Kee, H. L. (2011). Kinesin Motors and Primary Cilia. *Biochem. Soc. Trans.* 39, 1120–1125. doi: 10.1042/BST0391120

Vij, S., Rink, J. C., Ho, H. K., Babu, D., Eitel, M., Narasimhan, V., et al. (2012). Evolutionarily Ancient Association of the Foxj1 Transcription Factor With the Motile Ciliogenic Program. *PloS Genet.* 8, e1003019. doi: 10.1371/journal.pgen.1003019

Walker, R. L., and Tenore, K. R. (1984). Growth and Production of the Dwarf Surf Clam *Mulinia lateralis* (Say 1822) in a Georgia Estuary. *Gulf Res. Rep.* 7, 357–363. doi: 10.18785/grr.0704.07

Wang, X., Liu, B., Liu, F., and Huan, P. (2015). A Calaxin Gene in the Pacific Oyster *Crassostrea gigas* and Its Potential Roles in Cilia. *Zoology. Sci.* 32, 419–426. doi: 10.2108/zs150009

Wang, J., Zhang, L., Lian, S., Qin, Z., Zhu, X., Dai, X., et al. (2020). Evolutionary Transcriptomics of Metazoan Biphasic Life Cycle Supports a Single Intercalation Origin of Metazoan Larvae. *Nat. Ecol. Evol.* 4, 725–736. doi: 10.1038/s41559-020-1138-1

Ward, J. E., Macdonald, L. B. A., and Thompson, R. J. (1993). Mechanisms of Suspension Feeding in Bivalves Resolution of Current Controversies by Means of Endoscopy. *Limnol. Oceanography* 38, 466. doi: 10.4319/lo.1993.38.2.0265

Wei, H., Li, W., Liu, T., Li, Y., Liu, L., Shu, Y., et al. (2021). Sexual Development of the Hermaphroditic Scallop *Argopecten irradians* Revealed by Morphological, Endocrine and Molecular Analysis. *Front. Cell Dev. Biol.* 9, 646754. doi: 10.3389/fcell.2021.646754

Xu, F., Domazet-Loso, T., Fan, D., Dunwell, T. L., Li, L., Fang, X., et al. (2016). High Expression of New Genes in Trochophore Enlightening the Ontogeny and Evolution of Trochozoans. *Sci. Rep.* 6, 34664. doi: 10.1038/srep34664

Conflict of Interest: The authors declare that the research was conducted in the absence of any commercial or financial relationships that could be construed as a potential conflict of interest.

Publisher's Note: All claims expressed in this article are solely those of the authors and do not necessarily represent those of their affiliated organizations, or those of the publisher, the editors and the reviewers. Any product that may be evaluated in this article, or claim that may be made by its manufacturer, is not guaranteed or endorsed by the publisher.

frontiers | Frontiers in Marine Science

ORIGINAL RESEARCH
published: 04 April 2022
doi: 10.3389/fmars.2022.863376

Designing and the Pilot Trial of Bivalve Molluscan Fishing Quotas on Maoming Coastal Waters of China, Northern South China Sea

Shaoliang Lyu[1,2], *Siman Deng*[1], *Kun Lin*[1], *Jiawei Zeng*[1,2] *and Xuefeng Wang*[1,2*]

[1] Fisheries College, Guangdong Ocean University, Zhanjiang, China, [2] Development and Research Center for Biological Marine Resources, Southern Marine Science and Engineering Guangdong Laboratory (Zhanjiang), Zhanjiang, China

In the context of the declining fishery resources, some active management measures have been taken to strive for the sustainable development of fisheries. However, these input-oriented control management measures have not realized the expectation in alleviating the depressing depletion of fishery resources. The fishing quota (FQ) system, an output-oriented control management method, has been proved to be effective in curbing overfishing and conserving fishery resources. However, it has not been formally implemented in China until now. Thus, it is urgent to start the pilot trial on the implementation of the FQ system in China. We firstly formulated a framework for the FQ system on bivalve fisheries and then conducted an empirical analysis based on the field survey of bivalve mollusks in Maoming shallow waters, Guangdong, northern South China Sea. The species composition, dominant species, and density distribution of bivalves were analyzed. The swept-area method was used to assess the total allowable catch (TAC) of bivalves. Each step of the FQ system was discussed in depth. Results showed that a total of 45 bivalve species were identified. *Meretrix planisulcata* and *Ruditapes philippinarum* were the two dominant species. The spatial distribution of density varied largely. The estimated TAC value is 4.28×10^5 kg which can be allocated to fishermen under the regulations of the FQ system. Finally, the framework for the FQ system was improved in every step of the future procedure, including target species selection, TAC determination, quota allocation, catch report, and fishing supervision. The general framework of the FQ system in this study can also be referenced to other economically important fish or other marine organisms.

Keywords: fishing quotas, total allowable catch, field surveys, bivalve mollusks, northern South China Sea

OPEN ACCESS

Edited by:
Yuehuan Zhang,
South China Sea Institute of Oceanology (CAS), China

Reviewed by:
Xizhi Huang,
Johannes Gutenberg University Mainz, Germany
Linbao Zhang,
Chinese Academy of Fishery Sciences (CAFS), China

****Correspondence:***
Xuefeng Wang
xuefeng1999@126.com

Specialty section:
This article was submitted to Marine Fisheries, Aquaculture and Living Resources, a section of the journal Frontiers in Marine Science

Received: *27 January 2022*
Accepted: *07 March 2022*
Published: *04 April 2022*

Citation:
Lyu S, Deng S, Lin K, Zeng J and Wang X (2022) Designing and the Pilot Trial of Bivalve Molluscan Fishing Quotas on Maoming Coastal Waters of China, Northern South China Sea. Front. Mar. Sci. 9:863376. doi: 10.3389/fmars.2022.863376

INTRODUCTION

Marine biodiversity loss and ecosystem degradation have been two of the most challenging ecological problems in the 21st century. Marine ecosystems could have provided valuable goods and services to humans (Sinclair et al., 2002; Worm et al., 2006). However, overfishing or destructive fishing is driving a crisis that leads to undesirable changes in marine ecosystem functioning,

especially in coastal ecosystems (Jackson et al., 2001; Lotze et al., 2006). A typical phenomenon is the declining fishery resources in coastal waters, which has posed a serious threat to the production of high-quality animal proteins and the livelihood of fishermen (Food and Agriculture Organization (FAO), 2009; FAO, 2011; O'Hara et al., 2021). To maintain the sustainable development of fisheries and conserve the coastal ecosystem, some active management measures, including the input control management (e.g., the permission of fishing, the reduction of fishing vessels, and career change of fishermen from fishing to culturing) and technical control management (e.g., gear restrictions, fishing size limits, and closed fishing zones), were given priority to fisheries management in most fisheries countries (Worm et al., 2009). Yet, these measures have not realized the desired target. Hence, fishery managers and researchers turned their attention to the output control management (catch shares or fishing quotas) (Costello et al., 2008; Essington, 2010; Gutiérrez et al., 2011). The quantifying of fishing quotas and implementing of the fishing quota (FQ) system have been a research hot spot for fisheries management (Håkanson and Gyllenhammar, 2005; Poos et al., 2010).

The FQ system, a typical output control management measure, is based on total allowable catches (TAC) that are determined by fishery resource surveys and scientific assessments (Branch, 2009). Once the fishermen reach their quota limits, they are obliged to stop fishing until they are issued to the next quotas. Internationally, the FQ system is mainly deployed by some developed countries. The international practice experience shows that the FQ system is one of the most effective fishery management measures. Following the FQ system, the Icelandic total productivity in the fishing industry increased by 73% more in 1995 than in 1973, which has been very successful in increasing efficiency in the fisheries (The Organization for Economic Cooperation and Development (OECD), 2017). The use of the FQ system covers a variety of marine organisms, including fish, crustaceans, siphonopods, and shellfish (Yu, 2009). The FQ system has been proved to be effective in curbing overfishing and conserving fishery resources, which has become a great progress in international fisheries management (Péreau et al., 2012). In China, fisheries management with most fishing vessels and most fishermen seem to be the most complex in the world (Huang and He, 2019). The administrative departments of fishery in China have carried out a series of measures to improve marine fishery resources, such as summer fishing moratorium, minimum mesh size regulation, fishing license system, the so-called "Double Control" system, fishery stock enhancement programs, establishment of artificial reefs, and placements of aquatic germplasm resource-protection areas, which belong primarily to the input and technical control management, whereas the effect is limited (Shen and Heino, 2014; Lyu et al., 2021; Zhang et al., 2021). In 2000, the government of China revised the Fishery Law of the People's Republic of China, making it clear that China will determine TAC and implement an FQ system (Gu, 2018). Due to the lack of basic conditions for the implementation of this system, the FQ system has been in the planning and designing stage for more than a decade. Until 2017, five pilot projects for FQ have successively been carried out in coastal waters from five provinces. During the study period of these projects, TAC is mainly determined on the data of historical catch yields from fishing logbooks (Zhao, 2020). However, the FQ system has not been formally implemented in China so far.

Molluscan shellfish occur in diverse habitats and are closely related to human life with great values of ecology, economy, and culture. In terms of ecological value, as filter feeders, shellfish can not only purify water but also contribute to marine carbon sink (Chauvaud et al., 2003; Tang et al., 2011; Zhao et al., 2020). The distribution of shellfish, as the main bait source of many fish (Jaworski and Ragnarsson, 2006; Thangavelu et al., 2012) and crabs (Laughlin, 1982; Bisker and Castagna, 1987), is strongly associated with the formation and variations of fishing grounds. Due to their sensibilities to the marine environmental changes (Zhao et al., 2019; He et al., 2021; Xu et al., 2022), shellfish are regarded as the biological indicator of the quality of the waterborne or sedimental environment (Latimer and Kramer, 1997; Wang et al., 2020). In terms of economic value, shellfish are a popular food in our daily diet because of their rich nutrition (Wright et al., 2018), which has driven the economic development of shellfish harvesting, breeding, processing, and other related industries. In terms of cultural value, shellfish used to be an ancient currency. Nowadays, some shellfish have become more popular as collections and jewelry (Vaughn and Hoellein, 2018). Moreover, shellfish are sedentary benthos with high fecundity; no fishing action taken will waste the catch because of their short life cycle (Dame, 2016). As a result, shellfish have become one of the main commercial fishery targets for coastal fishermen. Nevertheless, according to the data of the China Fishery Statistical Yearbook (Fishery Bureau of Ministry of Agriculture and Rural Affairs of China, 2004-2021), the yield of wild shellfish decreased from 8.06×10^8 kg in 2003 to 3.62×10^8 kg in 2020. Therefore, the sustainable development of shellfish resources is urgent for the fisheries and livelihoods of fishermen. Research on the relevant system framework has an important reference value for its implementation in the future.

The purpose of this study is to develop a sensible framework of the FQ system and conduct a pilot trial based on the field survey data. Maoming coastal waters have a long coastline of approximately 220 km and are rich in shellfish resources with a fishing yield of 1.36×10^6 kg in 2020 (Editorial committee of Guangdong Rural Statistical Yearbook, 2021). Among shellfish resources, bivalves are a class with the largest economic value (Gosling, 2003). Therefore, this study conducted an analysis based on a survey of bivalve mollusks in Maoming shallow waters, in northern South China Sea, including the identification of bivalve species and the determination of TAC. This study provides a clue for policymakers to establish the FQ system of shellfish.

MATERIALS AND METHODS

Conceptual Framework for Fishing Quotas

A conceptual framework was designed for the FQ system based on the field survey. Accordingly, the procedure of the FQ system

includes the selection of target species, determination of TAC, allocation of quotas, report of catch, and supervision of fishing (**Figure 1**).

Survey Design

The survey zone, covering nearly 3.02×10^2 km^2, is the shallow waters within 10 m of water depth in Maoming, northern South China Sea. 28 stations were set in this zone given the habitat characteristics and fishing accessibility of bivalve shellfish (**Figure 2**). In November 2020, bivalves were sampled at each station using a hydraulic clam rake (Munari et al., 2006) with a mouth width of 1.2 m and a cod-end mesh size of 20 mm. When arrived at the sampling station, the speed of the vessel was reduced to about 2 to 3 knots and the raking time was kept from 5 to 10 min. After sampling, bivalves were identified to species level (Xu and Zhang, 2008; Yang et al., 2013), weighed (total weight of species), and counted (total number of individuals).

Data Analysis

An index of relative importance (*IRI*) (Pinkas et al., 1970) was used to estimate the contribution of each bivalve species to the total catch. *IRI* was calculated using Equation 1 (Selleslagh et al., 2009):

$$IRI = (N\,\% + W\,\%) \times F\,\% \tag{1}$$

where *N*%, *W*%, and *F*% are the relative numbers, biomass, and frequency of occurrence, respectively. *IRI* >1,000 was considered as the dominant species and 100 <*IRI* <1000 was considered as the important species.

The density (ind./km^2) and biomass (kg/km^2) were estimated by the swept-area method. The raking swept area per hour (*A*, km^2/h) was calculated using Equation 2, and the density and biomass (*D*, ind./km^2 or kg/km^2) were calculated using Equation 3 (Wang et al., 2017):

$$A = M \times S \times 1.852 \times 10^{-3} \tag{2}$$

$$D = \frac{W/T}{A \times C} \tag{3}$$

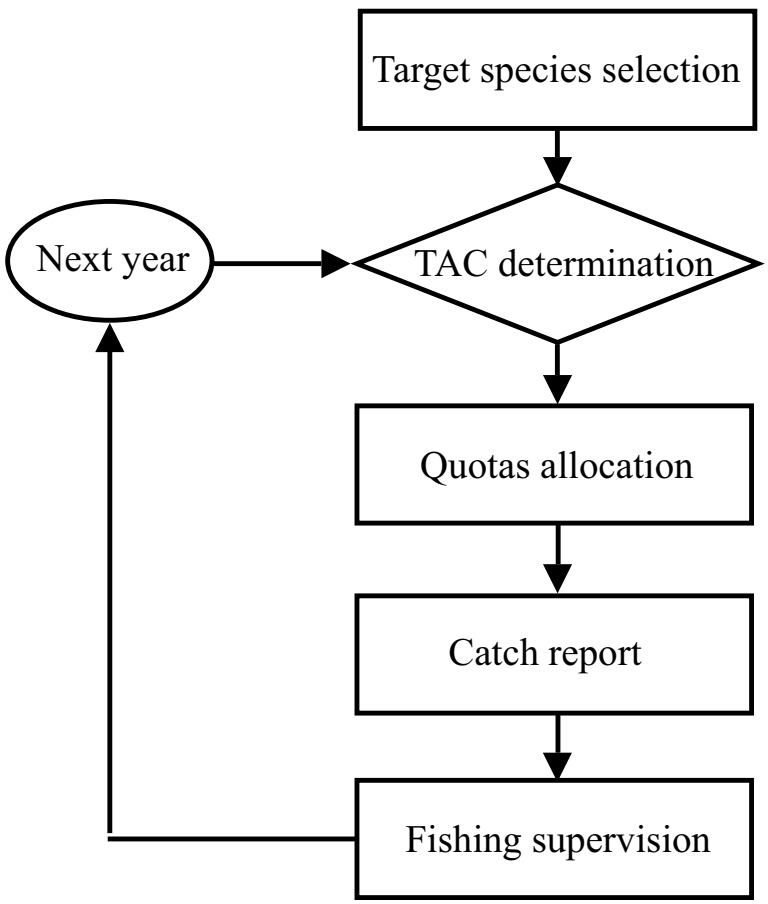

FIGURE 1 | The conceptual framework of the fishing quota system.

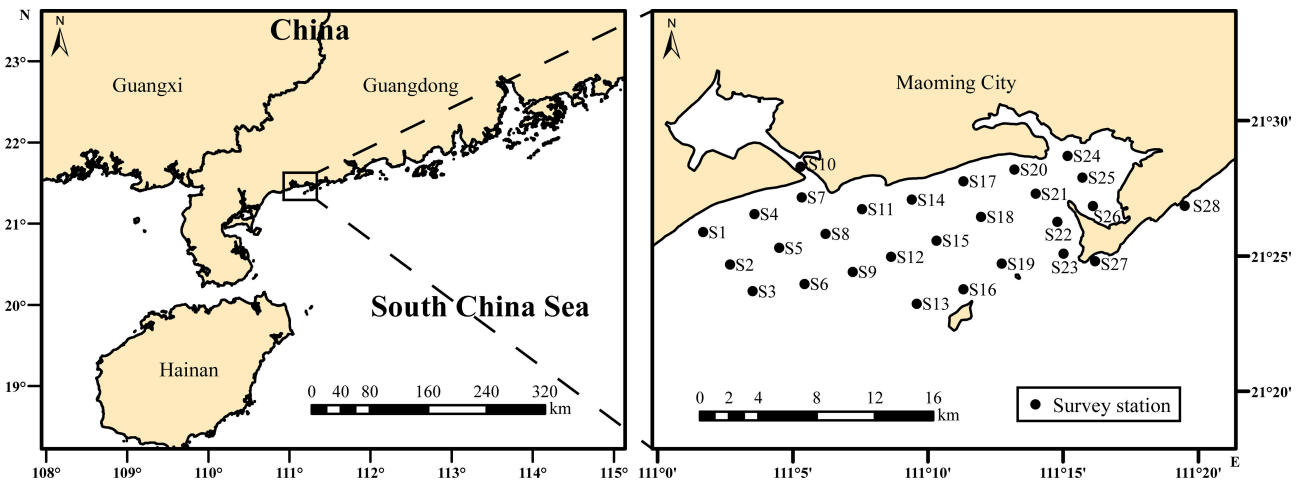

FIGURE 2 | Sampling stations of bivalves in Maoming shallow waters, northern South China Sea.

where M is the mouth width of the rake in m (here 1.2 m), S is the actual raking speed in knots at one station, 1.852 is the conversion rate of nautical miles to km, W is the catch weight of per raking at one station (kg), T is the actual raking time at one station (hours), and C is the catchability coefficient of raking, with the value of 1.0 given the weak locomotivity of bivalves.

The estimated bivalve production (P) was calculated using $P = D \times A_s$, with A_s the area of the survey zone (here 3.02×10^2 km^2). Finally, 80% of the estimated production was chosen as TAC for bivalves given the economics and sustainability.

RESULTS

Species Composition and Dominant Species of Bivalves

A total of 45 bivalve species belonging to 29 genera, ten families, and six orders were identified from the 28 stations sampled (**Table 1**). The bivalve species that occurred most frequently were from Veneroida (27 species), which accounted for 60.0% of the total number of bivalve species, followed by Arcoida (14 species), which accounted for 31.1%. The other four orders had one species for each. According to the *IRI* score, *Meretrix planisulcata* and *Ruditapes philippinarum* were the dominant bivalve species, constituting 50.1% of the total catch by biomass and 67.7% by numbers. There were eight important bivalve species, constituting 37.3% of the total catch by biomass and 21.7% by numbers.

Density Distribution and TAC of Bivalves

Both the distributions of density and biomass varied largely in the survey zone (**Figure 3**). The density value ranged from 0 ind./km^2 to 3.72×10^6 ind./km^2, with an average of 3.43×10^5 ind./km^2. The biomass values ranged from 0 kg/km^2 to 1.40×10^4 kg/km^2, with an average of 1.77×10^3 kg/km^2. Both the maximum values of density and biomass were in S7, while no bivalves were sampled in S23, S26, and S27. The estimated bivalve production was 1.03×10^8 ind. or 5.35×10^5 kg in the survey zone. To be conservative, TAC of bivalves was 8.28×10^7 ind. or 4.28×10^5 kg.

Frame Improvement and Current Completion Status of the Bivalve FQ System

The conceptual framework of the bivalve FQ system was improved (**Figure 4**). There were five steps in the FQ system frame. For step 1, the species composition of bivalves was analyzed after the field survey, and dominant species were determined by using the *IRI* index. The target species of bivalves was selected by the value of species. For step 2, the density distribution and estimated production were analyzed by the swept-area method and numbers or biomass. The TAC of bivalve was determined. For step 3, free fishing like Olympic competition (FFOC), community quotas (CQ), individual vessel quotas (IVQ), and individual transferable quotas (ITQ) can be used for quota allocation of bivalves. For step 4, the traditional and electronic fishing logbooks can be used for the catch report of bivalves. For step 5, the port inspection, maritime inspection, and punishing for illegal behavior can be used for fishing supervision of bivalves. In the end, the procedure of the bivalve FQ system can be cycled next year. To sum up, Step 1 and Step 2 were completed. Step 3, Step 4, and Step 5 were conceived, although it still needs more time before they are implemented.

DISCUSSION

Selection of Target Species

Target species selection is the beginning in the process of implementing the FQ system. In general, target species selection

TABLE 1 | Species composition and *IRI* values of bivalves from Maoming shallow waters in November 2020.

SN	Latin name	Order	Family	Genus	*IRI*
1	*Meretrix planisulcata*	Veneroida	Veneroidae	*Meretrix*	2868
2	*Ruditapes philippinarum*	Veneroida	Veneroidae	*Ruditapes*	1071
3	*Tapes belcheri*	Veneroida	Veneroidae	*Tapes*	379
4	*Scapharca inaequivalvis*	Arcoida	Arcoidae	*Scapharca*	247
5	*Meretrix meretrix*	Veneroida	Veneroidae	*Meretrix*	219
6	*Macridiscus aequilatera*	Veneroida	Veneroidae	*Macridiscus*	184
7	*Scapharca anomala*	Arcoida	Arcoidae	*Scapharca*	171
8	*Anomalodiscus squamosus*	Veneroida	Veneroidae	*Anomalodiscus*	166
9	*Meretrix lusoria*	Veneroida	Veneroidae	*Meretrix*	112
10	*Anadara kagoshimensis*	Arcoida	Arcoidae	*Anadara*	101
11	*Paratapes undulatus*	Veneroida	Veneroidae	*Paphia*	78
12	*Scapharca labiosa*	Arcoida	Arcoidae	*Scapharca*	60
13	*Scapharca satowi*	Arcoida	Arcoidae	*Scapharca*	48
14	*Scapharca indica*	Arcoida	Arcoidae	*Scapharca*	37
15	*Dosinia biscocta*	Veneroida	Veneroidae	*Dosinia*	22
16	*Lioconcha fastigiana*	Veneroida	Veneroidae	*Lioconcha*	15
17	*Meretrix lyrata*	Veneroida	Veneroidae	*Meretrix*	13
18	*Trisidos tortuosa*	Arcoida	Arcoidae	*Trisidos*	3
19	*Codakia tigerina*	Lucinida	Lucinidae	*Codakia*	3
20	*Trisidos kiyonoi*	Arcoida	Arcoidae	*Trisidos*	3
21	*Scapharca broughtonii*	Arcoida	Arcoidae	*Scapharca*	3
22	*Moerella iridescens*	Veneroida	Tellinidae	*Moerella*	2
23	*Scapharca cornea*	Arcoida	Arcoidae	*Scapharca*	2
24	*Mactra aphrodina*	Veneroida	Mactridae	*Mactra*	1
25	*Solidicorbula erythrodon*	Myoida	Corbulidae	*Solidicorbula*	1
26	*Soletellina diphos*	Veneroida	Psammobiidae	*Soletellina*	1
27	*Scapharea globosa*	Arcoida	Arcoidae	*Scapharca*	1
28	*Perna viridis*	Mytiloida	Mytilidae	*Perna*	1
29	*Dosinia japonica*	Veneroida	Veneroidae	*Dosinia*	<1
30	*Dosinia cumingii*	Veneroida	Veneroidae	*Dosinia*	<1
31	*Clausinella calophylla*	Veneroida	Veneroidae	*Clausinella*	<1
32	*Potiara pilula*	Arcoida	Arcoidae	*Potiarca*	<1
33	*Scapharca gubernaculum*	Arcoida	Arcoidae	*Scapharca*	<1
34	*Gari truncata*	Veneroida	Psammobiidae	*Gari*	<1
35	*Anadara antiquata*	Arcoida	Arcoidae	*Anadara*	<1
36	*Nitidotellina minuta*	Veneroida	Tellinidae	*Nitidotellina*	<1
37	*terocardia elliptica*	Veneroida	Veneroidae	*terocardia*	<1
38	*Crassostrea rivularis*	Pterioida	Ostreidae	*Crassostrea*	<1
39	*Angulus emarginatus*	Veneroida	Tellinidae	*Angulus*	<1
40	*Hiatula chinensis*	Veneroida	Psammobiidae	*Hiatula*	<1
41	*Vepricardium coronatum*	Veneroida	Cardiidae	*Vepricardium*	<1
42	*Dosinia troscheli*	Veneroida	Veneroidae	*Dosinia*	<1
43	*Tellinides timorensis*	Veneroida	Tellinidae	*Tellinides*	<1
44	*Apolymetis meyeri*	Veneroida	Tellinidae	*Apolymetis*	<1
45	*Pinguitellina pinguis*	Veneroida	Tellinidae	*Pinguitellina*	<1

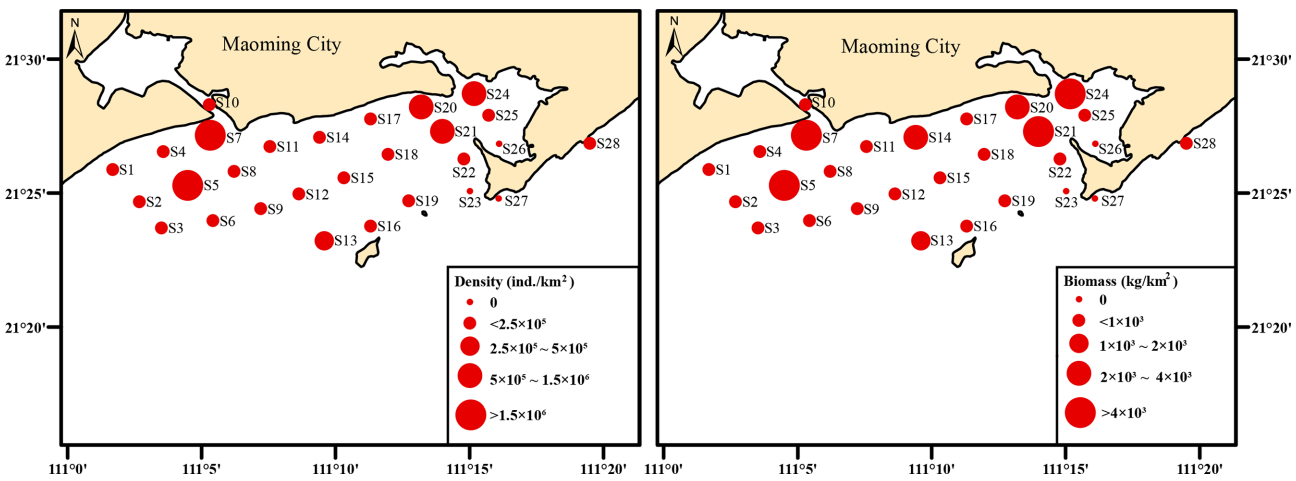

FIGURE 3 | The distribution of density and biomass of bivalves in Maoming shallow waters, northern South China Sea.

follows four principles: (1) Species has high economic value, large catch, and small bycatch. (2) Species needs to be conserved due to its severe declining resources. (3) Species needs to be adjusted due to the competition from different fishing grounds. (4) Species is used commonly by multiple countries or regions (Zhao, 2020). In the preliminary stage of the implementation of the FQ system, it follows mainly the first principle, also giving priority to the single species with fast growth, short life cycle, and small migration range (Harlyan et al., 2021). In this study, bivalve species composition and dominant species can be used as a reference to select the optimum species. There were 45 bivalve species, but most of them were of low economic value or no economic value. Further, only *M. planisulcata* (*IRI* = 2,868) and *R. philippinarum* (*IRI* = 1,071) were the dominant species. The reason why *M. planisulcata* was the first dominant species is that its number was large; however, its individual weight was smaller than that of *R. philippinarum*. To our knowledge, local fishermen tend to discard them because *M. planisulcata* belong to the bycatch. So, if a single-species FQ system

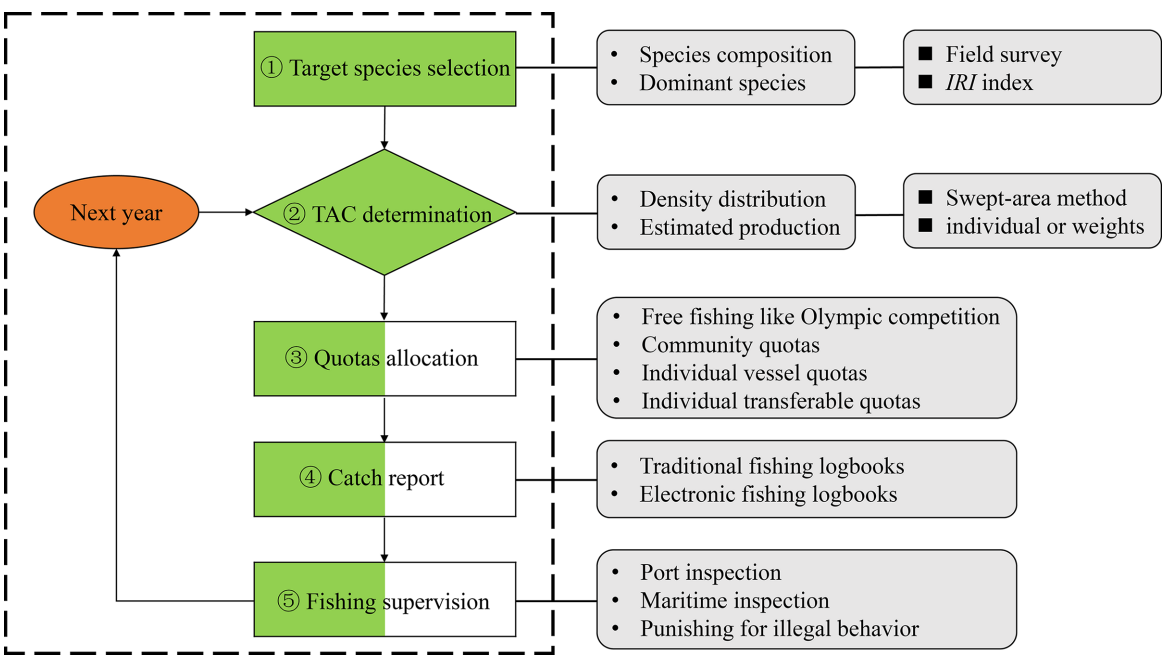

FIGURE 4 | The frame improvement of the bivalve FQ system and current perform status (the filled green color represents the degree of completion, respectively).

for bivalves needs to be implemented, the optimum species is *R. philippinarum* with higher value. The single-species FQ system is relatively easy to implement in the preliminary stage, which can accumulate more experience for the implementation of a multiple-species FQ system in the future.

Determination of TAC

TAC determination is the important precondition of the FQ system, which directly affects the implementation effect of the FQ system (Branch, 2009). If TAC is set too high, the resource depletion may be exacerbated. Whereas if it is too low, resources may be wasted. To our knowledge, TAC is determined based on the data of scientific surveys and fishing statistics. For the data of fishing statistics, previous studies used some models to assess the maximum sustainable yield (MSY) of fishing species (Brodziak and Ishimura, 2011; Martell and Froese, 2013), and in terms of the principle that the catch needs to be lower than the increase of fishery resources, TAC needs to be less than MSY to maintain sustainable development (Mace, 2001; Acheson et al., 2015). Using the models, more than 5 years of continuous fishing statistical data are required to provide a more accurate assessment of MSY. However, the long-term data of most fishery stocks have poor availability. In this study, based on the scientific survey, the swept-area method was used to estimate the bivalve production and determine the TAC value. This way is suitable for the stocks that lack the long-term fishing data. For the TAC value, TAC by weights (4.28×10^5 kg) is more suitable for use than that by individuals (8.28×10^7 ind.) due to the habitual use of weight. In addition, the density distribution of bivalves was analyzed in this study, but results showed that there were no significant geographical differences. If the density is concentrated within a certain range, it is recommended that the FQ system is mainly applied to this range to facilitate management. The survey tool in this study is a hydraulic clam rake. Munari et al. (2006) compared the effects of three raking tools (manual rake, hydraulic rake, and conveyor rake) on the benthic community, and results showed that manual raking and hydraulic raking have mild disturbances but unlikely to have persistent effects on biota. They suggested that clam fishermen should be allowed to use the hydraulic rake due to its relative efficiency. However, in China, rakes are the banned fishing facilities. Considering the problems of fishermen's livelihood, it is worth thinking about whether the hydraulic rake should be locally (and legally) used. Additionally, more selective and eco-friendly fishing tools need to be developed.

Allocation of Quotas, Report of Catch, and Supervision of Fishing

After determining TAC, fair and equitable allocation of quotas is the key to stimulating fishermen to comply with the FQ system. Well-designed quota allocation can help prevent fisheries collapse (Costello et al., 2008). In terms of whether the quotas are allocated to fishermen and whether the quotas are allowed to transfer, FQ can be divided into four types (Ding, 2019): FFOC, CQ, IVQ, and ITQ. For FFOC, fishermen can catch competitively until the TAC limit value was reached. Although this way has low management costs, it does not solve the competitive fishing mind of fishermen. Moreover, this way may make fishermen to compete for catch regardless of the risks, such as bad weather (Long, 2010). What is more, a large number of catches coming to the market at the same time will affect the prices, which leads to lower incomes for fishermen. For CQ, quotas are first allocated to different communities which are formed by fishermen, and then each community committee allocates the quotas to the members according to their own regulations. However, it is not applicable in Maoming sea areas due to the scattering of local traditional fishermen. For IVQ, quotas are allocated to the fishing vessels that meet the requirements. This is an appropriate type to allocate at present. The owner of the vessel can apply to the local department of fishery at first. The requirements are as follows: (1) Applicants must have a household register certificate in Maoming city. (2) Applicants must have a marine fisheries fishing license. (3) Applicants must have a fishing vessel with the equipment of life-saving, communication, and positioning system. After that, TAC will be allocated distributed averagely according to the number of fishing vessels who meet the requirements and granted the special fishing license of bivalve shellfish. For ITQ, the quota holders can transfer their quotas. To make the quota holders adapt to the new management system, it is recommended to forbid them to transfer the quotas at the beginning of the FQ system. Waiting until conditions mature, ITQ can be allowed. For ITQ, attention should be paid to prevent the concentration of quotas into few people, which may lead to a monopoly of the market (Eythórsson, 2000).

Fishermen must record truthfully their fishing yields in the logbooks, because this is the only approach to know if TAC is reached. Traditional logbooks are printed on paper, which is easy to lose and get damaged. In recent years, with the development of science and technology, the technology of using smart devices to record fishing information has become mature (Oviedo and Bursztyn, 2017). Fishermen can use a specialized software in mobile phones to report their fishing yields. Electronic fishing logbooks make it easy to collect and store the data of fishing and locations, so TAC can be monitored in time (Zhao, 2020). In view of the differences in age and literacy rate among fishermen, the traditional or electronic fishing logbooks should be chosen one accordingly.

On the whole, the fishing supervision includes the following aspects: (1) Port inspection. The fishing target species of FQ must be landed at the designated port. In the meantime, the port information officers collate the data of sales and logbooks every day and ensure the authenticity of data. To prevent the actual fishing yields exceeding the upper limit of quotas, the quota holders will be warned when their yields are close to the limit (Yu, 2009). (2) Maritime inspection. On the one hand, the fishery administration department can track the position of fishing vessels through the vessel monitoring system. On the other hand, it can carry out routine and surprise inspection at sea to check whether there are maritime sales. Besides, the following vessel observers should be dispatched without day to record and supervise the production status. (3) Punishing for illegal behavior. To prevent illegal production, harsh punishment

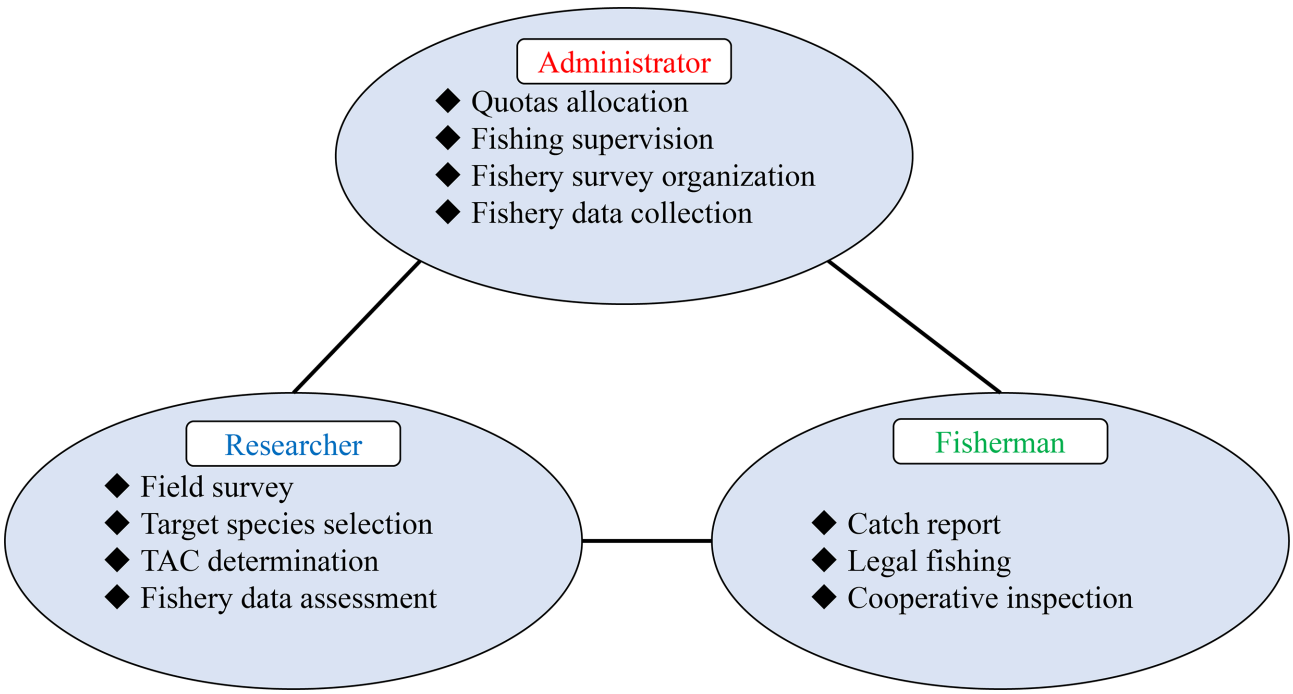

FIGURE 5 | The respective responsibilities of administrators, researchers, and fishermen under the FQ system.

with fines and special license revocation should be imposed on violators (**Figure 5**) (Zhao, 2020).

CONCLUSION

In summary, we made the practical framework for the FQ system of bivalve fisheries based on the field survey. Our findings not only contribute to the establishment of the FQ system in China but also serve as a guideline for implementing a formal FQ system for bivalve molluscan fishing quotas in the near future. Further research is needed to understand the fishermen's approbation degree of this system through questionnaires.

DATA AVAILABILITY STATEMENT

The original contributions presented in the study are included in the article/supplementary material. Further inquiries can be directed to the corresponding author.

ETHICS STATEMENT

The animal study was reviewed and approved by the Animal Experimental Ethics Committee of Guangdong Ocean University, China.

AUTHOR CONTRIBUTIONS

SL and XW conceived the study. SD, KL, and JZ conducted the field and laboratory work, assisted the identification of the species, and participated in the data analysis. SL drafted the manuscript. XW revised the manuscript. All authors contributed to the article and approved the submitted version.

FUNDING

This study was supported by the special funds for the National Key Research and Development Program (2020YFD0901103), Sino-Indonesian Technical Cooperations in Coastal Marine Ranching (12500101200021002), and Southern Marine Science and Engineering Guangdong Laboratory (Zhanjiang) Program (ZJW-2019-06).

ACKNOWLEDGMENTS

We gratefully thank our lab members Zhijie Chen, Shenzeng Zhang, Dr. Liqiang Zhao, the staff from the Maoming Fishery Administrative Department, and the local fishermen who kindly helped us to finish the whole fieldwork.

REFERENCES

Acheson, J., Apollonio, S., and Wilson, J. (2015). Individual Transferable Quotas and Conservation: A Critical Ssessment. *Ecol. Soc* 20, 7. doi: 10.5751/ES-07912-200407

Bisker, R., and Castagna, M. (1987). Predation on Single Spat Oysters *Crassostrea Virginica* (Gmelin) by Blue Crabs *Callinectes Sapidus* Rathbun and Mud Crabs *Panopeus Herbstii* Milne-Edwards. *J. Shellfish Res.* 6, 37–40.

Branch, T. A. (2009). How do Individual Transferable Quotas Affect Marine Ecosystems? *Fish.* 10, 39–57. doi: 10.1111/j.1467-2979.2008.00294.x

Brodziak, J., and Ishimura, G. (2011). Development of Bayesian Production Models for Assessing the North Pacific Swordfish Population. *Fish. Sci.* 77, 23–34. doi: 10.1007/s12562-010-0300-0

Chauvaud, L., Thompson, J. K., Cloern, J. E., and Thouzeau, G. (2003). Clams as CO_2 Generators: The *Potamocorbula Amurensis* Example in San Francisco Bay. *Limnol. Oceanogr.* 48, 2086–2092. doi: 10.4319/lo.2003.48.6.2086

Costello, C., Gaines, S. D., and Lynham, J. (2008). Can Catch Shares Prevent Fisheries Collapse? *Science* 321, 1678–1681. doi: 10.1126/science.1159478

Dame, R. F. (2016). *Ecology of Marine Bivalves: An Ecosystem Approach. 2nd ed* (Boca Raton: CRC Press).

Ding, Q. K. (2019). *Study on the Fishery Supervision Through the Implementation of Fishing Quota System in Yantai. [Dissertation]* (Qingdao: Qingdao University).

Editorial Committee of Guangdong Rural Statistical Yearbook (2021). *Guangdong Rural Statistical Yearbook* (Beijing: China Statistics Press).

Essington, T. E. (2010). Ecological Indicators Display Reduced Variation in North American Catch Share Fisheries. *P. Natl. Acad. Sci. U.S.A.* 107, 754–759. doi: 10.1073/pnas.0907252107

Eythórsson, E. (2000). A Decade of ITQ-Management in Icelandic Fisheries: Consolidation Without Consensus. *Mar. Policy* 24, 483–492. doi: 10.1016/S0308-597X(00)00021-X

Fishery Bureau of Ministry of Agriculture and Rural Affairs of China (2004-2021). *China Fishery Statistical Yearbook* (Beijing: China Agriculture Press).

Food and Agriculture Organization (FAO) (2009). *FAO Yearbook of Fishery and Aquaculture Statistics 2007* (Rome: FAO Fisheries and Aquaculture Department).

Food and Agriculture Organization (FAO) (2011). *Review of the State of World Marine Fishery Resources* (Rome: FAO Fisheries and Aquaculture Department).

Gosling, E. (2003). *Bivalve Molluscs: Biology, Ecology and Culture* (New Jersey: Blackwell Publishing).

Gu, Y. J. (2018). *Several Problems and Countermeasures on Implementing TAC Management in Zhejiang Province: A Case Study of Portunus Trituberculatus in Zhoushan Fishing Ground. [Dissertation]* (Zhoushan: Zhejiang Ocean University).

Gutiérrez, N. L., Hilborn, R., and Defeo, O. (2011). Leadership, Social Capital and Incentives Promote Successful Fisheries. *Nature.* 470, 386–389. doi: 10.1038/nature09689

Håkanson, L., and Gyllenhammar, A. (2005). Setting Fish Quotas Based on Holistic Ecosystem Modelling Including Environmental Factors and Foodweb Interactions - A New Approach. *Aquat. Ecol.* 39, 325–351. doi: 10.1007/s10452-005-3418-x

Harlyan, L. I., Matsuishi, T. F., and Md Saleh, M. F. (2021). Feasibility of a Single-Species Quota System for Management of the Malaysian Multispecies Purse-Seine Fishery. *Fisheries Manage. Ecol.* 28, 126–137. doi: 10.1111/fme.12470

He, G., Liu, X., Xu, Y., Liang, J., Deng, Y., Zhang, Y., et al. (2021). Repeated Exposure to Simulated Marine Heatwaves Enhances the Thermal Tolerance in Pearl Oysters. *Aquat. Toxicol.* 239, 105959. doi: 10.1016/j.aquatox.2021.105959

Huang, S., and He, Y. (2019). Management of China's Capture Fisheries: Review and Prospect. *Aquacult. Fish.* 4, 173–182. doi: 10.1016/j.aaf.2019.05.004

Jackson, J. B. C., Kirby, M. X., Berger, W. H., Bjorndal, K. A., Botsford, L. W., Bourque, B. J., et al. (2001). Historical Overfishing and the Recent Collapse of Coastal Ecosystems. *Science* 293, 629–637. doi: 10.1126/science.1059199

Jaworski, A., and Ragnarsson, S.Á. (2006). Feeding Habits of Demersal Fish in Icelandic Waters: A Multivariate Approach. *ICES J. Mar. Sci.* 63, 1682–1694. doi: 10.1016/j.icesjms.2006.07.003

Latimer, J. S., and Kramer, K. J. M. (1997). *Biomonitoring of Coastal Waters and Estuaries* (Boca Raton: CRC Press).

Laughlin, R. A. (1982). Feeding Habits of the Blue Crab, *Callinectes Sapidus* Rathbun, in the Apalachicola Estuary, Florida. *B. Mar. Sci.* 32, 807–822. doi: 10.1016/0198-0254(83)90286-8

Long, Z. J. (2010). *Study on ITQ Management of Marine Fishery Resource. [Dissertation]* (Zhanjiang: Guangdong Ocean University).

Lotze, H. K., Lenihan, H. S., Bourque, B. J., Bradbury, R. H., Cooke, R. G., Kay, M. C., et al. (2006). Depletion, Degradation, and Recovery Potential of Estuaries and Coastal Seas. *Science* 312, 1806–1809. doi: 10.1126/science.1128035

Lyu, S., Lin, K., Zeng, J., Liu, Y., Chen, Z., and Wang, X. (2021). Fin-Spines Attachment, a Novel External Attachment Method for the Ultrasonic Transmitters on Hard Fin-Spines Fish (Sparidae). *J. Appl. Ichthyol.* 37, 227–234. doi: 10.1111/jai.14164

Mace, P. M. (2001). A New Role for MSY in Single-Species and Ecosystem Approaches to Fisheries Stock Assessment and Management. *Fish.* 2, 2–32. doi: 10.1046/j.1467-2979.2001.00033.x

Martell, S., and Froese, R. (2013). A Simple Method for Estimating MSY From Catch and Resilience. *Fish.* 14, 504–514. doi: 10.1111/j.1467-2979.2012.00485.x

Munari, C., Balasso, E., Rossi, R., and Mistri, M. (2006). A Comparison of the Effect of Different Types of Clam Rakes on non-Target, Subtidal Benthic Fauna. *Ital. J. Zool.* 73, 75–82. doi: 10.1080/11250000500502152

O'Hara, C. C., Frazier, M., and Halpern, B. S. (2021). At-Risk Marine Biodiversity Faces Extensive, Expanding, and Intensifying Human Impacts. *Science* 372, 84–87. doi: 10.1126/science.abe6731

Oviedo, A. F. P., and Bursztyn, M. (2017). Community-Based Monitoring of Small-Scale Fisheries With Digital Devices in Brazilian Amazon. *Fisheries Manage. Ecol.* 24, 320–329. doi: 10.1111/fme.12231

Péreau, J. C., Doyen, L., Little, L. R., and Thébaud, O. (2012). The Triple Bottom Line: Meeting Ecological, Economic and Social Goals With Individual Transferable Quotas. *J. Environ. Econ.* 63, 419–434. doi: 10.1016/j.jeem.2012.01.001

Pinkas, L., Oliphant, M. S., and Iverson, I. L. K. (1970). *Fish Bulletin 152. Food Habits of Albacore, Bluefin Tuna, and Bonito in California Waters* (Berkeley: State of California, Department of Fish and Game).

Poos, J. J., Bogaards, J. A., Quirijns, F. J., Gillis, D. M., and Rijnsdorp, A. D. (2010). Individual Quotas, Fishing Effort Allocation, and Over-Quota Discarding in Mixed Fisheries. *ICES J. Mar. Sci.* 67, 323–333. doi: 10.1093/icesjms/fsp241

Selleslagh, J., Amara, R., Laffargue, P., Lesourd, S., Lepage, M., and Girardin, M. (2009). Fish Composition and Assemblage Structure in Three Eastern English Channel Macrotidal Estuaries: A Comparison With Other French Estuaries. *Estuar. Coast. Shelf S.* 81, 149–159. doi: 10.1016/j.ecss.2008.10.008

Shen, G., and Heino, M. (2014). An Overview of Marine Fisheries Management in China. *Mar. Policy* 44, 265–272. doi: 10.1016/j.marpol.2013.09.012

Sinclair, M., Arnason, R., Csirke, J., Karnicki, Z., Sigurjonsson, J., Skjoldal, H. R., et al. (2002). Responsible Fisheries in the Marine Ecosystem. *Fish. Res.* 58, 255–265. doi: 10.1016/S0165-7836(02)00168-6

Tang, Q., Zhang, J., and Fang, J. (2011). Shellfish and Seaweed Mariculture Increase Atmospheric CO_2 Absorption by Coastal Ecosystems. *Mar. Ecol. Prog. Ser.* 424, 97–104. doi: 10.3354/meps08979

Thangavelu, R., Anbarasu, M., Zala, M. S., Koya, K. M., Sreenath, K. R., Mojjada, S. K., et al. (2012). Food and Feeding Habits of Commercially Important Demersal Finfishes Off Veraval Coast. *Indian J. Fish.* 59, 77–87.

The Organization for Economic Cooperation and Development (OECD) (2017). *Sustaining Iceland's Fisheries Through Tradeable Quotas: Country Study* (Paris: OECD Publishing).

Vaughn, C. C., and Hoellein, T. J. (2018). Bivalve Impacts in Freshwater and Marine Ecosystems. *Annu. Rev. Ecol. Evol. S.* 49, 183–208. doi: 10.1146/ANNUREV-ECOLSYS-110617-062703

Wang, X., Wang, L., Chen, H., Jia, X., and Jackson, D. A. (2017). Determining a More Environmental Than Spatial Influence on Structuring Fish Communities and Ecological Boundaries of Fangcheng Coastal Waters, Northern South China Sea. *J. Coastal Res.* 80, 55–68. doi: 10.2112/SI80-009.1

Wang, L., Wang, X., Chen, H., Wang, Z., and Jia, X. (2020). Oyster Copper Levels in the Northern South China Sea From 1989 to 2015: Spatiotemporal Trend Detection and Human Health Implications. *Environ. Sci. Pollut. R.* 27, 37384–37394. doi: 10.1007/s11356-020-09106-3

Worm, B., Barbier, E. B., Beaumont, N., Duffy, J. E., Folke, C., Halpern, B. S., et al. (2006). Impacts of Biodiversity Loss on Ocean Ecosystem Services. *Science* 314, 787–790. doi: 10.1126/science.1132294

Worm, B., Hilborn, R., Baum, J. K., Branch, T. A., Collie, J. S., Costello, C., et al. (2009). Rebuilding Global Fisheries. *Science* 325, 578–585. doi: 10.1126/science.1173146

Wright, A. C., Fan, Y., and Baker, G. L. (2018). Nutritional Value and Food Safety of Bivalve Molluscan Shellfish. *J. Shellfish Res.* 37, 695–708. doi: 10.2983/035.037.0403

Xu, Y., Liang, J., He, G., Liu, X., Yang, K., Masanja, F., et al. (2022). Responses of Pearl Oysters to Marine Heatwaves as Indicated by HSP70. *Front. Mar. Sci.* 9, 847585. doi: 10.3389/fmars.2022.847585

Xu, F., and Zhang, S. (2008). *An Illustrated Bivalvia Mollusca Fauna of China Seas* (Beijing: Science Press).

Yang, W., Cai, Y., and Kuang, X. (2013). *Color Atlas of Economic Mollusca From the South China Sea* (Beijing: China Agriculture Press).

Yu, H. G. (2009). *A Study on China's Fishing Quota System. [Dissertation]* (Qingdao: Ocean University of China).

Zhang, S., Lin, L., and Wang, X. (2021). Optimization of a Marine Fish Release Strategy: A Case Study of Black Sea Bream *Acanthopagrus Schlegelii* in the Zhanjiang Estuary, Northern South China Sea. *Front. Env. Sci-Switz* 9, 779544. doi: 10.3389/fenvs.2021.779544

Zhao, L. H. (2020). *Research on the Implementation of Fishing Quota System in China's Marine Fisheries: Based on the Implementation of Five Fishing Quotas in 2017-2018. [Dissertation]* (Shanghai: Shanghai Ocean University).

Zhao, L., Liu, L., Liu, B., Liang, J., Lu, Y., and Yang, F. (2019). Antioxidant Responses to Seawater Acidification in an Invasive Fouling Mussel are Alleviated by Transgenerational Acclimation. *Aquat. Toxicol.* 217, 10533. doi: 10.1016/j.aquatox.2019.105331

Zhao, L., Shirai, K., Tanaka, K., Milano, S., Higuchi, T., Murakami-Sugihara, N., et al. (2020). A Review of Transgenerational Effects of Ocean Acidification on Marine Bivalves and Their Implications for Sclerochronology. *Estuar. Coast. Shelf. S.* 235, 106620. doi: 10.1016/j.ecss.2020.106620

Conflict of Interest: The authors declare that the research was conducted in the absence of any commercial or financial relationships that could be construed as a potential conflict of interest.

Publisher's Note: All claims expressed in this article are solely those of the authors and do not necessarily represent those of their affiliated organizations, or those of the publisher, the editors and the reviewers. Any product that may be evaluated in this article, or claim that may be made by its manufacturer, is not guaranteed or endorsed by the publisher.

frontiers | Frontiers in Marine Science

ORIGINAL RESEARCH
published: 20 April 2022
doi: 10.3389/fmars.2022.884991

Genome-Wide Identification and Expression Profiling of the *COMMD* Gene Family in Four Bivalve Molluscs

Xiaomei Chen[1,2†], *Naina Hu*[1,2†], *Shanshan Lian*[2,3*], *Luoan Li*[2], *Fengzhi Sun*[2], *Lingling Zhang*[2,3], *Shi Wang*[1,2,3], *Zhenmin Bao*[1,2,4] *and Jingjie Hu*[1,2*]

[1] Key Laboratory of Tropical Aquatic Germplasm of Hainan Province, Sanya Oceanographic Institution, Ocean University of China, Sanya, China, [2] Ministry of Education (MOE) Key Laboratory of Marine Genetics and Breeding, Ocean University of China, Qingdao, China, [3] Laboratory for Marine Biology and Biotechnology, Pilot Qingdao National Laboratory for Marine Science and Technology, Qingdao, China, [4] Laboratory for Marine Fisheries Science and Food Production Processes, Pilot Qingdao National Laboratory for Marine Science and Technology, Qingdao, China

OPEN ACCESS

Edited by:
Zhongming Huo,
Dalian Ocean University, China

Reviewed by:
Qiong Shi,
Beijing Genomics Institute (BGI), China
Lusheng Xin,
Chinese Academy of Fishery Sciences (CAFS), China
Junxia Mao,
Dalian Ocean University, China

***Correspondence:**
Shanshan Lian
lianshanshan@ouc.edu.cn
Jingjie Hu
hujingjie@ouc.edu.cn

[†]*These authors have contributed equally to this work and share first authorship*

Specialty section:
This article was submitted to Marine Fisheries, Aquaculture and Living Resources, a section of the journal Frontiers in Marine Science

Received: *27 February 2022*
Accepted: *21 March 2022*
Published: *20 April 2022*

Citation:
Chen X, Hu N, Lian S, Li L, Sun F, Zhang L, Wang S, Bao Z and Hu J (2022) Genome-Wide Identification and Expression Profiling of the COMMD Gene Family in Four Bivalve Molluscs. Front. Mar. Sci. 9:884991. doi: 10.3389/fmars.2022.884991

The *COMMD* (copper metabolism gene MuRR1 domain) gene family, highly conserved among multicellular eukaryotic organisms, plays important roles in a variety of biological processes, ranging from copper homeostasis, ionic transport, protein trafficking, NF-κB-mediated transcription, and cell proliferation. However, systematic identification, spatiotemporal expression, and stress-responsive patterns of *COMMD* genes remain obscure in molluscs. Here, we analyzed the characteristics of the *COMMD* gene family in four bivalve molluscs based on both genome and extensive transcriptomic resources. Firstly, we investigated the genomic signatures, functional domains, and phylogenetic relationships, and ten single-copy members were identified in Yesso scallop (*Patinopecten yessoensis*), Zhikong scallop (*Chlamys farreri*), Pacific oyster (*Crassostrea gigas*), and dwarf surf clam (*Mulinia lateralis*), respectively. Strong purifying selection was revealed for *COMMD4*. Higher expressions of most *COMMD*s were observed in the hepatopancreas, besides which a different tissue preference of *COMMD*s' expression was found among four bivalves. Moreover, in the dwarf surf clam, the responses of *COMMD* members under stresses were found more sensitive in the hepatopancreas than in the gill, and *MlCOMMD9* and *MlCOMMD4* might be the good candidate stress indicator genes respectively for copper ion stress and *V. Anguillarum* infection. Our study would contribute to a better understanding for the evolution of the *COMMD* gene family and provide valuable information for their innate immune roles in bivalve molluscs.

Keywords: bivalve, *COMMD*, expression profiling, phylogenetic analysis, innate immune

INTRODUCTION

The *COMMD* (copper metabolism gene MuRR1 domain) family includes ten evolutionarily conserved proteins, namely, COMMD1–10, in the extreme carboxyl terminus of which they share a unique motif known as the COMM domain (Burstein et al., 2005). The COMM domain, with 70–85 amino acids in length and being rich in tryptophan, proline, and leucine, not only defines the gene family but also provides a critical interface for protein–protein interactions with

each other (Maine et al., 2007). The hydrophobic residues located in the COMM domain could form two conserved nuclear export signals (NES1 and NES2) (Muller et al., 2009). Except COMMD6, other COMMD members possess an amino terminal region, which is divergent among the subfamilies but is highly conserved within the ortholog proteins (Burstein et al., 2005). *COMMD1* is the first identified member, which was initially termed as *Murr1* due to its proximity to the *U2af1-rs1* locus in mice, and other *COMMD* members were identified through homologous screening (Nabetani et al., 1997; van De Sluis et al., 2002). A total of ten subfamilies were found in the vast majority of vertebrates (Burstein et al., 2005), while in invertebrates, including insects, worms, and molds, only several *COMMD* members were reported, and none of the *COMMD*s were found in unicellular eukaryotic organisms or bacteria (Nabetani et al., 1997). The wide existence as well as the highly conservative characteristic of *COMMD* homologues imply their critical roles during the metazoan evolution (Riera-Romo, 2018).

As the best-characterized member, *COMMD1* may represent a prototype of the family (Burstein et al., 2005). *COMMD1* was reported to be able to participate in two distinct activities, control of copper metabolism and regulation of the transcription factor NF-κB (Riera-Romo, 2018). Researchers found that mutations of *COMMD1* are responsible for copper toxicosis in Bedlington terrier dogs, resulting in excessive copper accumulation in the liver (Tao et al., 2003). In human, biochemical findings had indicated a direct role for *COMMD1* in biliary copper transport, and *COMMD1* defect could impair the copper excretion (Tao et al., 2003; Riera-Romo, 2018). Besides *COMMD1*, various functions were found for other *COMMD* genes in vertebrates. COMMD4, as one of the protein kinase A targets, was able to interact with myomegalin and inhibit NF-κB activity (Uys et al., 2011). The COMMD3 and COMMD8 complex could selectively recruit GRK6, which induced GRK6-mediated phosphorylation of the receptor and activated the β-arrestin-mediated signaling (Nakai et al., 2019). *COMMD3* and *COMMD9*, which are endogenous regulators, regulate Na^+ transport through altering ENaC cell surface expression (Liu et al., 2013). *COMMD5* affects cell proliferation (Solban et al., 2000), and *COMMD6, 7* participates in the invasion and migration regulation of a variety of cancer (You et al., 2017; Yang et al., 2019). Research has reported that *COMMD10* is related to phagosomes in murine macrophages (Dill et al., 2015), and in myeloid cells, deficiency in *COMMD10* can cause increased NF-κB activation and then aggravate lipopolysaccharide systemic sepsis (Naugler and Karin, 2008; Mouhadeb et al., 2018). In comparison, only the functions of several *COMMD* genes were reported in invertebrates. For example, *COMMD4* is found ubiquitously expressed in amphioxus, with the highest level in gonad, and lipopolysaccharide injection could induce its expression (Jin et al., 2012). Wang et al. have cloned *COMMD1* in *Crassostrea hongkongensis*, and the transcription level of *COMMD1* was increased significantly in the gill and hemolymph after salinity stimulation (Wang et al., 2017a).

As benthic filter feeders, bivalve molluscs are well adapted to highly dynamic oceans and freshwater environments since the early Cambrian. Along with intensified human activities in recent decades, the bivalve habitats are subject to various biotic/abiotic stressors, and pathogenic microbes and heavy metals are two of the main stressors. The *COMMD* genes play critical roles in many vital functions, and exploration of whether these genes participate in heavy-metal or bacterial resistance may help gain a better understanding for the outstanding adaptability of bivalve molluscs. In the present study, a systematic identification and characterization of *COMMD* genes in four bivalves were conducted, namely, Yesso scallop, Zhikong scallop, Pacific oyster, and dwarf surf clam. Detailed genic structure comparison and spatiotemporal expression analysis provided insights into the potential function of *COMMD* genes in bivalve molluscs. Further, transcription patterns of different *COMMD* members under copper ion stress and after *Vibrio Anguillarum* infection were investigated in the gill and hepatopancreas of *M. lateralis*. This is the first comprehensive research of the *COMMD* family genes in bivalves, which notably provided helpful information regarding the classification, evolution, and function of these genes. These findings may assist a better understanding of the bivalves' adaption to adverse heavy-metal pollutions and bacterial challenge.

MATERIAL AND METHODS

Genome-Wide Identification of *COMMD* Genes

To identify *COMMD* genes, the whole genomes and transcriptomes of four bivalves (Zhang et al., 2012; Li et al., 2017; Wang et al., 2017b) were searched against the available COMMD protein sequences from representative vertebrates (*Homo sapiens*, *Mus musculus*, *Xenopus laevis*) and Cephalochordata (*Branchiostoma belcheri*). The orthologous COMMD proteins were used as query sequences for whole-genome and transcriptome-based blasts, and the threshold of the E value was 1E-5. Sequence analysis was performed by the HMM searching method (http://www.ebi.ac.uk/Tools/hmmer/search/phmmer) to ensure the integrity of *COMMD*s. BLASTN was used to confirm their genomic structure, and the ORF Finder program (https://www.ncbi.nlm.nih.gov/orffinder/) was used to predict the open reading frame. Further, to ensure the completeness of *COMMD*s, the translated sequences were submitted to the SMART tool (http://smart.embl-heidelberg.de/) and ProtParam tool (https://web.expasy.org/protparam/) to ensure the presence of the conserved COMM_domain and to predict the isoelectric point (*pI*), molecular weight, instability index, and grand average of hydropathicity (GRAVY) values, which were illustrated for all potential bivalve *COMMD*s shown in **Table 1**. Then, the drawing of the protein structure was done by IBS 1.0.3. Finally, we identified and counted *COMMD* family genes of 26 metazoan species, namely, the deuterostomes *Homo sapiens*, *Oryzias latipes*, *Danio rerio*, *Oreochromis niloticus*, *Xenopus laevis*, *Ciona intestinalis*, *Branchiostoma floridae*, and *Strongylocentrotus purpuratus*, the protostomes *Drosophila melanogaster*, *Daphnia pulex*, *Caenorhabditis elegans*, *Tribolium castaneum*, *Lingula anatina*, *Capitella teleta*,

TABLE 1 | Sequence characteristics of the *COMMD* gene family of four bivalve molluscs.

Gene	Intron number	Genomic position	Protein length	*COMM* domain position	*PI*	Molecular weight (Da)	GRAVY	Instability index
PyCOMMD1	1	2137.16:679703-680902 = 1200	135	61–134	5.91	15,765.54	-0.713	49.20
PyCOMMD2	4	5989.10:450020-460247 = 10228	199	121–189	6.09	23,379.78	-0.374	50.83
PyCOMMD3	7	10911.5:103350-117222 = 13873	196	122–194	5.01	21,617.27	-0.189	34.89
PyCOMMD4	8	9739.4:207199-226481 = 19283	200	128–200	6.10	22,355.46	-0.136	25.68
PyCOMMD5	6	2433.4:97391-108491 = 11101	220	145–212	7.72	25,079.12	-0.080	43.06
PyCOMMD6	4	11181.36:885386-891755 = 6370	80	11–80	6.53	8,894.22	-0.134	24.39
PyCOMMD7	8	4359.39:1265516-1276033 = 10518	201	132–201	5.76	22,393.30	-0.228	25.26
PyCOMMD8	4	9685.21:829055-837430 = 8376	185	116–185	4.94	21,048.57	-0.368	52.68
PyCOMMD9	5	7491.23:709119-722211 = 13093	198	120–197	5.93	22,260.12	-0.289	36.16
PyCOMMD10	7	2329.50:1883135-1896660 = 13526	198	127–198	5.72	22,886.02	-0.429	43.66
MlCOMMD1	2	12840.10:78282-82291 = 4010	186	113–184	5.00	21276.63	-0.658	56.19
MlCOMMD2	6	45.74:1970118-1985717 = 15600	240	170–237	6.06	27,717.89	-0.175	42.79
MlCOMMD3	8	12040.29:507160-516075 = 8916	198	122–193	5.05	22,323.13	-0.220	38.87
MlCOMMD4	8	12703.15:299462-305380 = 5919	201	128–200	5.45	22,428.40	-0.219	27.39
MlCOMMD5	6	11059.62:859122-866779 = 7658	220	145–212	7.72	25,072.87	-0.159	41.06
MlCOMMD6	6	10801.218:3510817-3516483 = 5667	182	113–182	5.24	20,562.56	-0.051	43.55
MlCOMMD7	6	12762.5:96783-102258 = 5476	202	133–202	4.98	22,642.41	-0.249	32.27
MlCOMMD8	4	12846.13:145184-150718 = 5535	183	113–183	5.57	20,484.17	-0.185	39.12
MlCOMMD9	5	12715.132:1758244-1793803 = 35560	197	119–196	6.73	22,066.33	-0.127	30.39
MlCOMMD10	6	12002.12:113626-123104 = 9479	197	127–197	5.00	22,767.92	-0.351	46.04
CfCOMMD1	2	22817.34787729-790581:=2853	187	113–186	5.34	21,825.27	-0.781	50.26
CfCOMMD2	2	44835.8:183117-188074 = 4958	151	73–141	6.97	17,606.36	-0.163	66.00
CfCOMMD3	7	33479.9:142988-153101 = 10114	196	122–194	4.99	21,623.27	-0.171	33.32
CfCOMMD4	2	723733.1:101-1790 = 1690	105	27–105	9.10	9,625.85	-0.379	33.73
CfCOMMD5	6	15543.1:12696-26178 = 13483	220	145–212	8.69	25,138.19	-0.095	41.58
CfCOMMD6	4	55811.12:168214-191931 = 23718	80	11–80	7.87	8,896.21	-0.193	19.53
CfCOMMD7	8	53827.18:384544-393259 = 8716	201	132–201	5.28	22,290.20	-0.201	22.97
CfCOMMD8	35	13299:134558-189797 = 55240	1339	116–180	5.62	151,426.29	-0.264	46.52
CfCOMMD9	5	64623.27:808604-820076 = 11473	198	120–197	5.62	22,258.06	-0.275	35.40
CfCOMMD10	9	63763.53:945408-1095753 = 150346	215	127–189	8.63	24,776.25	-0.368	46.48
CgCOMMD1	2	NW_011935966.1:87568-88717 = 1150	191	117–190	5.52	22,229.83	-0.741	54.41
CgCOMMD2	4	NW_011936396.1:515939-521925 = 5987	199	121–189	5.90	23,336.65	-0.347	49.02
CgCOMMD3	5	NW_011936388.1:20012-24869 = 4858	160	122–158	4.81	17,907.22	-0.193	48.20
CgCOMMD4	8	NW_011935883.1:64603-67169 = 2567	199	128–199	5.63	22,629.06	-0.255	31.13
CgCOMMD5	5	NW_011934779.1:876616-887615 = 11000	190	145–189	9.04	21,364.73	-0.109	46.65
CgCOMMD6	2	NW_011936252.1:55195-56300 = 1106	138	69–138	6.57	15,283.34	-0.469	39.87
CgCOMMD7	7	NW_011935176.1:337529-362408 = 24880	198	129–198	6.60	22,213.42	-0.013	20.75
CgCOMMD8	5	NW_011936271.1:100615-105861 = 5247	184	114–183	5.14	21,193.77	-0.478	39.28
CgCOMMD9	5	NW_011937700.1:144762-154995 = 10234	199	121–198	6.96	22,440.55	-0.340	43.82
CgCOMMD10	6	NW_011937034.1:445720-452824 = 7105	198	127–198	5.36	22,889.05	-0.418	43.62

Helobdella robusta, *Lottia gigantea*, *Elysia chlorotica*, *Biomphalaria glabrata*, *Octopus bimaculoides*, *Patinopecten yessoensis*, *Chlamys farreri*, *Crassostrea gigas*, and *Mulinia lateralis*, and the non-bilaterians *Nematostella vectensis*, *Stylophora pistillata*, and *Amphimedon queenslandica* (**Supplementary Table 1**).

Multiple Alignment and Phylogenetic Analysis

MEGA7.0 (Sudhir et al., 2016) was used to construct phylogenetic analysis to determine which *COMMD* subfamily the bivalve *COMMD* genes belong to. The whole amino acid sequences of COMMD proteins from Human (*H. sapiens*), zebrafish (*D. rerio*), medaka fish (*O. latipes*), African clawed frog (*X. laevis*), ciona (*C. intestinalis*) and Stylophora (*S. pistillata*), were downloaded from the Ensemble genome browser database. The whole amino acid sequences of COMMD proteins from Nile tilapia (*O. niloticus*), notoacmea (*L. gigantea*), Biomphalaria (*B. glabrata*), and sea snail (*E. chlorotica*) were downloaded from the Uniport database. The whole amino acid sequences of COMMD proteins from amphioxus (*B. belcheri*) and octopus (*O. bimaculoides*) were downloaded from the NCBI database. Multi-sequence alignment was performed through ClustalW (Larkin et al., 2007) and was edited by GeneDoc software (Nicholas et al., 1997), then the phylogenetic analyses based on the neighbor-joining (NJ) method and maximum likelihood (ML) method with a bootstrap of 1,000 replicates, both including all the amino acids from the COMMDs. 154 amino acids across 16 animals were involved in this analysis. The accession numbers of 154 COMMDs are listed in **Supplementary Table 2**.

Selective Pressure Analysis

COMMD gene sequences were aligned based on codons, using Muscle (codons) implemented in MEGA7.0 (Sudhir et al., 2016). MEGA7.0 was used to build the alignment result into a tree file,

and a Newick format file was formed. To explore selective pressure between *COMMD* gene sequences, after removing the gap, a strict statistical analysis was performed using the software EasyCodeML1.2 (Gao et al., 2019). Based on the Preset Site Model, the ratios of non-synonymous (dN) and synonymous (dS) substitutions for 40 *COMMD* genes among four bivalve were calculated. The LRT was used to test whether the selected model is significant ($P < 0.05$). Two likelihood ratio tests were performed to detect positively selected sites—M1a (neutral) vs. M2a (positive selection), M7 (β) vs. M8 (β and ω), and M0 (one-ratio) vs. M3 (discrete)—and the site-specific model was used for comparison. If the tests produced a significant result, then the empirical Bayes method was used to identify individual positively selected codon sites (Yang et al., 2005).

Expression Analysis

The TPM (reads per kilobase million) values were summarized from the published RNA-seq datasets of Yesso scallop (Wang et al., 2017b), Zhikong scallop (Li et al., 2017), and Pacific oyster (Zhang et al., 2012) and from our unpublished data for dwarf surf clam. During development, eleven embryo/larval developmental stages were chosen to perform expression analysis, including zygotes; multi-cells; blastula; gastrula; trochophore; D-shaped larvae; early-, mid-, and late-term umbo larvae; metamorphosis larvae; and juvenile. For adults, six tissues were chosen to perform expression analysis, namely, muscle, hepatopancreas, mantle, gill, male gonad, and female gonad. The expressional heatmaps were displayed by the heatmap package in R environment.

Copper Ion Stress and *V. anguillarum* Infection Experiment

Healthy adult dwarf surf clams were obtained from a laboratory breeding population. Dwarf surf clams were cultured in filtered and aerated seawater at 20°C–25°C. For the copper ion stress experimental group, the clams were acclimated in the sterilized seawater with a final copper ion concentration of 100 μg/l (from the anhydrous copper sulfate) (Zhang et al., 2012). For both control and experimental groups, five random clams were sampled at 0 h, 12 h, and 9 days, from which gill and hepatopancreas tissues were collected for RNA extraction. For the bacterial challenge group, gram-negative bacteria (*Vibrio Anguillarum*) were cultured in liquid 2216 E broth at 28°C to an OD600 of 0.2 and were harvested by centrifugation at 2,000 × g for 5 min. Then, the cell precipitates were suspended in filtered seawater and adjusted to 1×10^7 CFU/ml (Zhou et al., 2019) to challenge clams. For both control and experimental groups, five random clams were sampled at 0, 3, 6, 12, and 24 h, from which gill and hepatopancreas tissues were collected for RNA extraction.

RNA Isolation and Quantitative Real-Time PCR Analysis

Total mRNA was extracted from the gill and hepatopancreas of the sampled clams by using the conventional guanidinium isothiocyanate method (Chomczynski and Sacchi, 2006). The cDNA was synthesized using M-MLV Reverse Transcriptase (Promega, Madison, WI, USA). Primers of *MLCOMMD*s were designed using Primer Premier 5 software; the sequences of primers are listed in **Supplementary Table 3**. All reactions were repeated in triplicate. The transcription of target genes was standardized according to the transcription of two internal reference genes (namely, *RS23* and *NDUS4*). For the comparisons of the *COMMD* transcription changes between control experimental groups, statistical analysis of the data was performed using t-test with statistical significance at $P < 0.05$.

RESULTS

Identification and Characterization of *COMMD* Genes in Four Bivalve Molluscs

A total of 10 single-copy *COMMD* genes were identified in Yesso scallop, Zhikong scallop, Pacific oyster, and dwarf surf clam, respectively represented as *Py*COMMD*s*, *Cf*COMMD*s*, *Cg*COMMD*s*, and *Ml*COMMD*s*. The length of most bivalve COMMDs ranged from 150 to 240 aa, except four relatively short COMMDs (namely, *Py*COMMD1, 6, and *Cf*COMMD4, 6, which possess less than 135 aa) and *Cf*COMMD8 which was obviously longer (1,339 aa). The COMMD family shared the conserved COMM domain (**Figure 1**). Two highly conserved nuclear export signal regions were located at the COMM domain, namely, NES1 and NES2, which were mainly composed of the well-conserved hydrophobic amino acids L, I, V, M, and F (**Figure 2**). Besides, the COMMD1 proteins possessed an additional COMMD1_domain (PF17221) at the N-terminal, and a specific Glyco_hydro_15 domain (PF00723) was found at the C-terminal of *Cf*COMMD8 (**Figure 1**). Consistent with human COMMD6 (de Bie et al., 2006), the *Py*COMMD6 and *Cf*COMMD6 lacked a variable amino terminal, while *Cg*COMMD6 and *Ml*COMMD6 contained an extended amino terminal portion. A low-complexity region was located at the amino terminal of *Py*COMMD4, 8, *Cg*COMMD10, and *Ml*COMMD10. In comparison with *CgCOMMD*s and *MlCOMMDs*, a higher similarity of gene structure was revealed between *COMMD* orthologs from two scallops (**Table 1**). A subfamily-specific conserved intron number was found for scallop *COMMD3*, *5*, *6*, *7*, *9*, which comprised 7, 6, 4, 8, and 5 introns, respectively. Of note, the 5-intron pattern was also found in *CgCOMMD9* and *MlCOMMD9*, making *COMMD9* as the only member which showed the most conservative exon–intron structure in bivalves.

Phylogenetic and Evolutionary Analysis of the *COMMD* Family

In the present study, besides the *COMMD* family gene identification from four bivalve molluscs, we also identified *COMMD*s from 22 additional animal species, across the major representative groups in Metazoa (**Figure 3**). It revealed that five groups, namely, Deuterostomia (except Urochordata), Mollusca, Brachiopoda, Cnidaria, and Sponge, have a full set of ten *COMMD* subfamilies, while in Ecdysozoa, Annelida, and Urochordata, they usually lack several *COMMD* subfamilies (up to 9). Especially, we noted that *COMMD1, 6, 9* subfamilies were

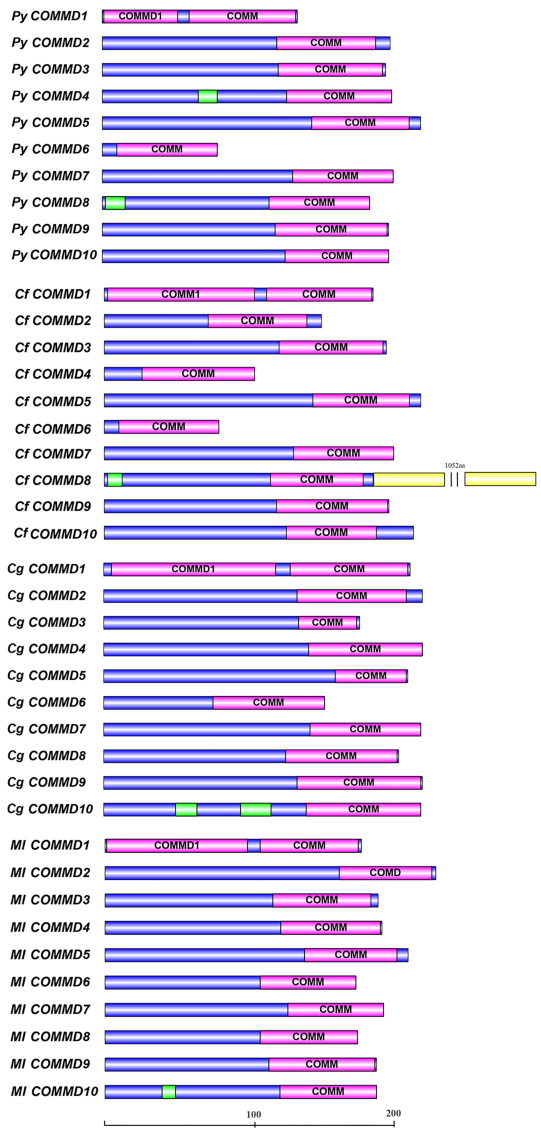

FIGURE 1 | The structure of COMMD proteins in four bivalves. The purple boxes indicate the conserved COMM domains. The green boxes indicate the low-complexity regions, and the yellow boxes indicate the Glyco_hydro_15 Pfam domain.

absent in all investigated ecdysozoans, and within Lophotrochozoa, molluscs and brachiopods have more complete *COMMD* family members than annelids. We further investigated the evolutionary relationship of bivalve *COMMD*s. Phylogenetic analysis showed that all COMMD proteins were subdivided into ten subfamilies, including COMMD1-10, and consistent topologies were revealed based on both the NJ method (**Figure 4A**) and ML method (**Figure 4B**). For each subfamily, *COMMDs* from Zhikong scallop, Yesso scallop, and Pacific oyster are always grouped together first, then clustered together with *COMMDs* from the dwarf surf clam and other bivalves, which is in line with their assured phylogenetic relationship.

Positive Selection Analysis

To explore the selective pressure of the *COMMD* genes, the CODEML program in the EasyCodeML1.2 software was further used. Results show that six subfamilies were detected with positive selection sites by the M7 vs. M8 model (**Table 2**). According to the M8 model, *COMMD4* possessed 8 positive sites, including two highly positively selected sites ($P > 0.95$), followed by *COMMD1* (5), *COMMD7* (5), and *COMMD10* (4). Only one and two positive sites were respectively detected in *COMMD3* and *COMMD6*. Overall, a total of 25 sites under potentially positive selection were identified in four bivalve *COMMDs*.

Temporal and Spatial Expression of the *COMMDs* From Four Bivalve Molluscs

The TPM (reads per kilobase million) calculated from the RNA sequence data are displayed as a heat map (**Figure 5**, **Supplementary Tables 4** and **5**). As shown in **Figure 5A**, the embryo expression profiles of *COMMDs* in four bivalves can be parted into three groups. Firstly, most of the *COMMD1, 3, 4* subfamilies were detected at the beginning of fertilization and maintained high transcriptions until the multicellular stage; a similar transcription pattern was also found in *PyCOMMD6*, *CgCOMMD2, 7*, and *MlCOMMD5, 8, 10*, suggesting their maternal origin to play protective roles. *COMMD5, 8, 9, 10* in two scallops started increasing the transcription levels during blastula, and their high transcriptions were maintained until the D-shaped veliger stage. Except the abovementioned, other members of *COMMD* genes, including *PyCOMMD2, 7*, *CfCOMMD3, 7*, *CgCOMMD1, 3, 5, 6, 8, 9, 10*, and *MlCOMMD2, 6, 7, 9*, were enhanced exponentially from the D-shaped veliger stage and sustained their high level of transcription during late larval development.

According to the spatial expression pattern of *COMMDs* in six organs/tissues (**Figure 5B**), we found that most of the *COMMD2, 3, 4, 5, 7, 8, 10* subfamilies were predominantly expressed in the hepatopancreas in four bivalves. Besides, most of the *COMMD1, 6* members were highly expressed in the female gonads, and *COMMD2, 9* of two scallops were detected with high levels in male gonads. Moreover, we noticed that *COMMDs*' transcription showed a certain tissue preference among different bivalves. For example, most *MlCOMMDs* and *CfCOMMDs* were highly expressed in the hepatopancreas and gonad, respectively, while most *CgCOMMDs* and *PyCOMMDs* were highly expressed in the hepatopancreas, mantle, and gill. Overall, organ/tissue transcription patterns of *COMMD* genes in four bivalves may imply their diverse cellular functions.

Responses of *MlCOMMD* Genes Under Copper Ion Stress and Bacterial Stress

Taking the advantages of laboratory-standardized breeding and cultivation, we investigate the potentially biological functions and defensive mechanism of *COMMD* genes in the dwarf surf clam. First, we explored the responses of *MlCOMMD* genes in the gill and hepatopancreas under copper ion stress (**Figure 6**). After the copper ion stress, *MlCOMMD1, 4, 9* showed significant responses in both tissues, with *MlCOMMD9* being remarkably upregulated, while *MlCOMMD1* and *MlCOMMD4* were

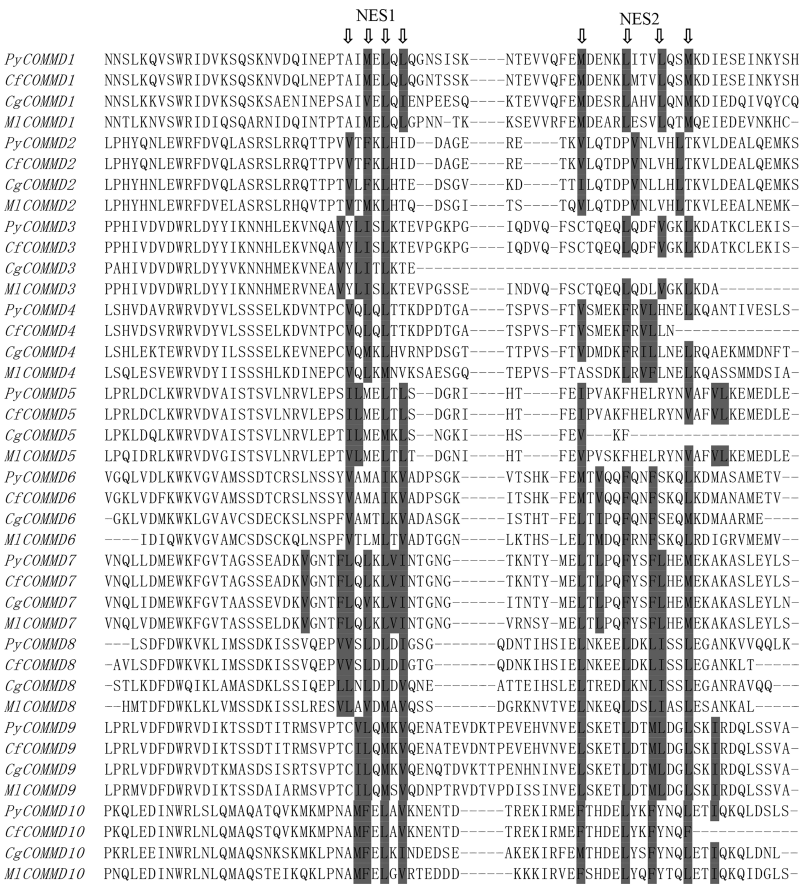

FIGURE 2 | Alignment of deduced COMM domain amino acid sequences. The two nuclear export signals (NES1 and NES2) are indicated in gray shades and by arrows pointing at conserved hydrophobic residues.

significantly suppressed. Of note, a more acute and intensive response of *MlCOMMD9* was shown in the hepatopancreas (12 h, >6-fold, $P < 0.001$) than in the gill (day 9, >2-fold, $P < 0.05$). Besides, *MlCOMMD4* and *MlCOMMD7* were found significantly upregulated on day 9 respectively in the hepatopancreas and gill. In the next scenario, the temporal responses of *MlCOMMD* genes after *V. Anguillarum* infection were as shown in **Figure 7**. In the gill, only three *COMMD* members showed significant responses after infection, with *MlCOMMD4*, *8* being found to be significantly upregulated after 12 h and *MlCOMMD7* being suppressed at 6 h. In comparison, responses of *COMMD*s in the hepatopancreas seems more ubiquitous, with six members showing significant transcription alternations. After infection, transcription of *MlCOMMD4* was significantly elevated after 6 and 12 h, and *MlCOMMD7* was significantly upregulated at 6 h. In the meantime, *MlCOMMD5* was found to be acutely suppressed after 3 h and *MlCOMMD6*, *8*, *9* showed a significantly lower transcription at 6 h. Notably, *MlCOMMD4* was the only member that showed consistent significant induction in both the gill and hepatopancreas after infection, and similar to copper ion stress, a more acute and intensive response of *MlCOMMD4* was found in the hepatopancreas (6 h, >9-fold, $P < 0.05$) than in the gill (12 h, >3-fold, $P < 0.05$). Above all, we found that responses of *COMMD* members were more sensitive in the hepatopancreas than the gill, in which *MlCOMMD9* and *MlCOMMD4* might be good candidate stress indicator genes respectively for copper ion stress and *V. Anguillarum* infection.

DISCUSSION

In this study, the *COMMD* family in four bivalve molluscs was identified and characterized based on the genomic and transcriptomic data. Similar to the human COMMD proteins, these bivalve COMMD proteins contain the conserved COMM domain in the extreme carboxyl terminus, which could mediate the interaction of COMMD-COMMD proteins and the formation of the COMMD polymer (Burstein et al., 2005). The amino terminal of COMMDs shares a low homology among members of the family but has highly conserved sequences with their ortholog proteins, which may contribute to the functional diversity of different subfamilies (Maine and Burstein, 2007). Besides four bivalve molluscs in our study, a 5-intron pattern of

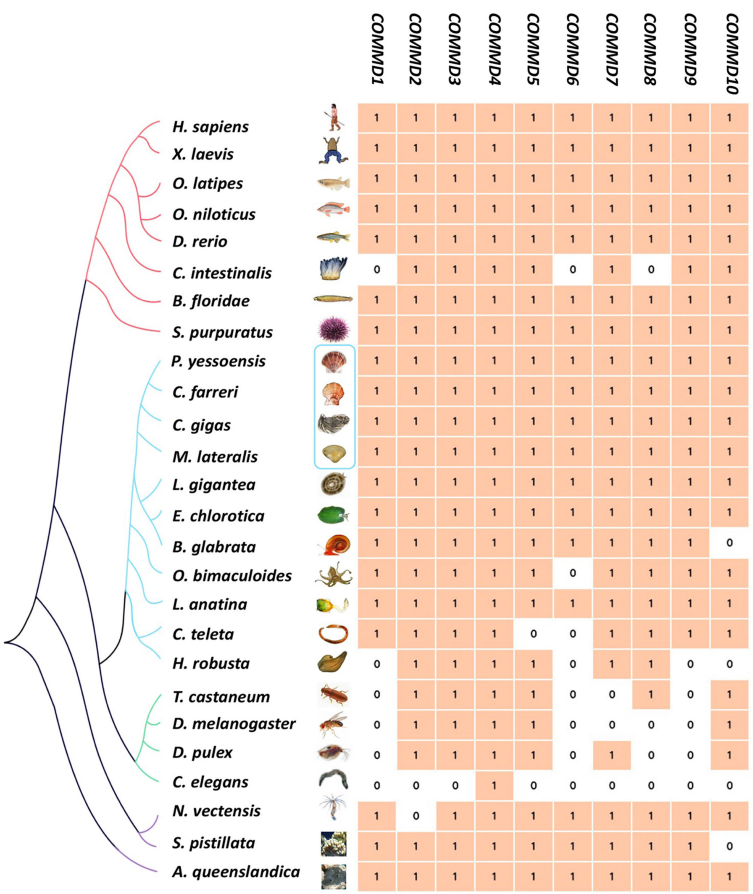

FIGURE 3 | Genome-wide identification of *COMMD* gene families of 4 bivalve molluscs (in blue box) and 22 other metazoan species. Different colors of branches represent different metazoan groups (red, Deuterostomia; blue, Lophotrochozoa; green, Ecdysozoa; purple, non-Bilateria).

COMMD9 was also discovered in human and zebrafish, which may imply that *COMMD9* has retained the ancestral exon–intron structure during the evolution. Other *COMMD* subfamilies of four bivalve molluscs have inconsistent intron patterns. Previously, researchers have found that intron insertion and loss may be associated with selective splicing, encoding the untranslated RNAs and enhancing the levels of mRNA transcription (Jin et al., 2012). The frequent occurrence of intron insertion and deletion among the *COMMD* family except for *COMMD9* may be to a certain extent related to the function of introns.

Phylogenetic analysis showed that four bivalve mollusc *COMMD* genes always clustered together in the invertebrate clades, consisting of their evolution status and conservativeness. Previous findings show that *COMMD* genes are highly conserved throughout vertebrate evolution, and *COMMD1* and *COMMD9* seem to be restricted to vertebrates (Burstein et al., 2005). In the present study, we further retrieved *COMMD* genes from 26 metazoan species (**Figure 3**). We found that both *COMMD1* and *COMMD9* could be identified in the Lophotrochozoa, Deuterostomia, Cnidaria, and Sponge groups, while they were absent in the Ecdysozoa group. Besides *COMMD1, 9*, *COMMD6, 7, 8* were also absent in most ecdysozoans and that nematodes only have the *COMMD4* subfamily, which may attribute to the fact that the Ecdysozoa genomes are rapidly evolving (Telford et al., 2008). Besides, *COMMD1, 6, 8* have been lost in ciona (Jin et al., 2018), while 10 intact single-copy *COMMD* genes were found in amphioxus as well as in most vertebrates. Species in the Mollusca, Deuterostomia (except Urochordata), Brachiopoda, Cnidaria, and Sponge groups almost have ten intact single-copy *COMMD* family genes; only several species were found to have loss of one the *COMMD* subfamily members. However, it remains unclear whether this phenomenon is due to genome assembly fragmentation or they have been lost during evolution. An across-Metazoa comparison implied that *COMMD* members diverged from each other at early stages of evolution and the integrated *COMMD* family may already exist in the metazoan last common ancestors.

Evolutionary analysis have shown that purifying selection dominated the evolution of *COMMD* genes (Jin et al., 2018). For four bivalves, a total of 25 sites under potentially positive selection were identified which may provide a support for the structural and functional diversity of the *COMMD* family members. Similarly, the selective pressure analyses of *COMMD*

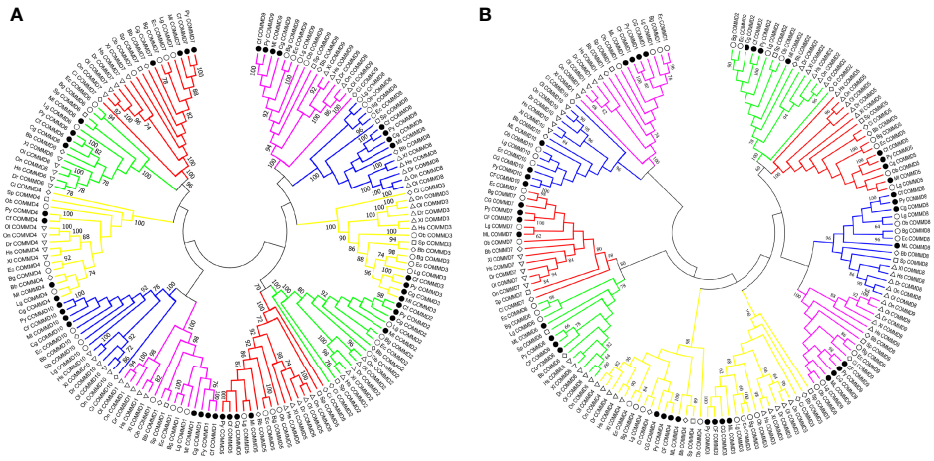

FIGURE 4 | Phylogenetic analyses of *COMMD* gene families involving 154 amino acid sequences across 16 animals were conducted based on the NJ method and ML method. **(A)** Phylogenetic analysis of COMMD proteins using the NJ method, with a bootstrap of 1,000 replicates. **(B)** Phylogenetic analysis of COMMD proteins using the ML method, with a bootstrap of 1,000 replicates. Numbers in the trees represent the confidence interval. Different symbols were used to represent different clades of animals: the circles label the molluscs, the diamonds label the chordates, the triangles label the vertebrates, and the squares label the cnidarians. Four bivalve COMMDs were specially emphasized by solid color inside the symbol. Hs, *Homo sapiens*; Xl, *Xenopus laevis*; Dr, *Danio rerio*; Ol, *Oryzias latipes*; On, *Oreochromis niloticus*; Ci, *Ciona intestinalis*; Bb, *Branchiostoma belcheri*; Sp, *Stylophora pistillata*; Py, *Patinopecten yessoensis*; Cf, *Chlamys farreri*; Cg, *Crassostrea gigas*; Ml, *Mulinia lateralis*; Ec, *Elysia chlorotica*; Ob, *Octopus bimaculoides*; Lg, *Lottia gigantean*; Bg, *Biomphalaria glabrata*.

family genes in amphioxus showed that there were 16 positive selective sites detected, although the *COMMD* family genes have undergone very strong purifying selection during evolution (Jin et al., 2018).

In previous studies, the expression profile of *COMMD* family genes has been reported in vertebrates (van De Sluis et al., 2002; Klomp et al., 2003). However, such research remains lacking in invertebrates. To better understand the characteristic and function of *COMMD* genes in molluscs, extensive transcriptome resources were used to profile the temporal and spatial expression patterns of *COMMD* genes in four bivalve molluscs (**Figure 5**). The *COMMDs* were reported to play a vital role during mouse embryonic development, and *COMMD*-knockout mice are embryonically lethal and die at different stages of embryogenesis (Semenova et al., 2003; van de Sluis et al., 2007; Bartuzi et al., 2013). Besides, researchers found that *COMMD1* has a regulatory role in the cell cycle of HEK293 cells (Jiang et al., 2019). Our results showed that bivalve *COMMD1* is highly expressed during multicellular cleavage and its transcription level declines rapidly from blastula. It may also implicate that *COMMD1* is involved in the regulation of cell proliferation. Bivalve *COMMD7*s were found to enhance their transcription exponentially from the D-shaped veliger stage and sustained a high level of transcription during late larval development. Previous studies have found that *COMMD7* promoted cell proliferation, migration, and invasion processes but suppressed cell apoptosis (Devlin et al., 2003; Zheng et al., 2018). Therefore, we speculate that *COMMD7* may be involved

TABLE 2 | Likelihood values and parameter estimates of computing position selection site by site model for the COMMD family members.

Gene name	Model (Name of parameters)	lnL	Likelihood ratio test P-value	Positively selected sites
COMMD1	M8(10)	-1,262.595448	0.000001065	1 M 0.987*, 2 W 0.979*, 3 F 0.805, 97 S 0.907, 98 I 0.598
	M7(8)	-1,276.348083		
COMMD3	M8(10)	-1,686.029432	0.013882920	44 R 0.941
	M7(8)	-1,690.306528		
COMMD4	M8(10)	-1,096.111503	0.000165421	32 A 0.671, 88 K 0.751, 89 Q 0.784, 90 A 0.572, 91 N 0.909, 95 E 0.929, 96 S 0.953*, 98 S 0.980*
	M7(8)	-1,104.818519		
COMMD6	M8(10)	-821.039991	0.002870954	7 I 0.527, 9 D 0.698
	M7(8)	-826.893102		
COMMD7	M8(10)	-1,821.686106	0.031505820	3 S 0.584, 32 R 0.638, 36 A 0.669, 61 S 0.607, 91 V 0.637
	M7(8)	-1,825.143689		
COMMD10	M8(10)	-2,032.127041	0.050129732	50 T 0.635, 186 E 0.957*, 190 K 0.904, 191 Q 0.638
	M7(8)	-2,035.120182		

For 1 M 0.987, 1 means the number of amino acid, M means abbreviations of amino acid, 0.987 means posterior possibility (P), and * means that P > 0.95 by LRT test of Bayes empirical Bayes analysis.*

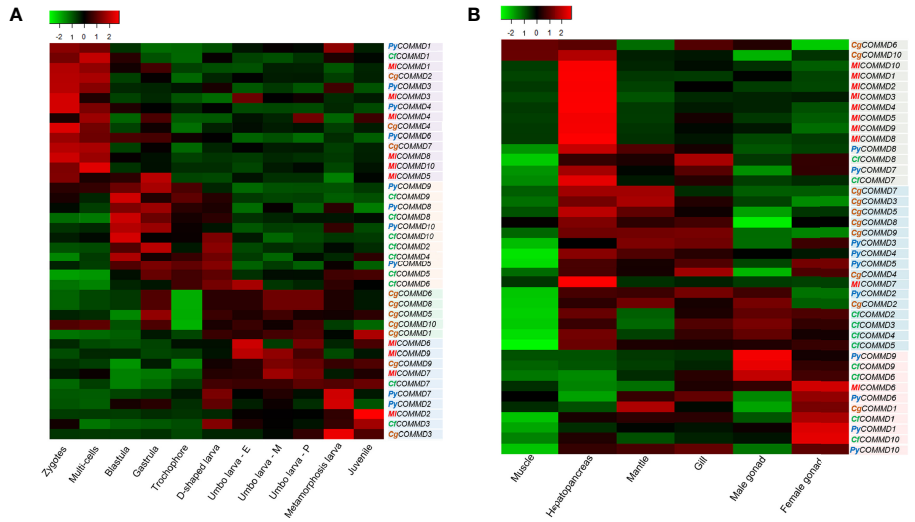

FIGURE 5 | Heatmap of *COMMD* expression profiles (TPM) in embryonic developmental stages and different tissues in four bivalves. The color varies from green to red, representing the scale of the relative expression level. **(A)** Expression of *COMMD*s during embryonic development. **(B)** Expression of *COMMD*s in adult tissues of four bivalves.

in the regulation of organogenesis during embryonic larval formation. Among different adult tissues, high transcription levels of most *COMMD*s were found in the hepatopancreas. As filter-feeding animals that mainly feed on microalgae, bivalves could accumulate hazardous substance produced through diet, and the hepatopancreas is the main organ for processing and accumulating the incoming hazardous substance (Lian et al., 2019). Therefore, the relatively higher transcription levels of *COMMD*s in the hepatopancreas may assist with toxin tolerance in bivalves. *COMMD1, 9, 10* are involved in the regulation of cell proliferation, migration, and cell-cycle progression (Yang et al., 2017; Zhan et al., 2017). We found that *COMMD1, 6, 10* from two scallops were highly expressed in the female gonads, suggesting that these three *COMMD* members may contribute to the ovarian cell homeostasis maintenance to assist with oogenesis in scallops.

The *COMMD* genes play key roles in regulating copper homeostasis and innate immune response (Bartuzi et al., 2013; Jin et al., 2018; Mouhadeb et al., 2018). To investigate the possibly biological functions of the *MlCOMMD*s, their mRNA expression levels were measured at different time points under copper ion stress and bacterial stress. *MlCOMMD1, 4, 9* transcriptions exhibited a significant alteration after copper ion stress in both assayed organs of dwarf surf clam, and

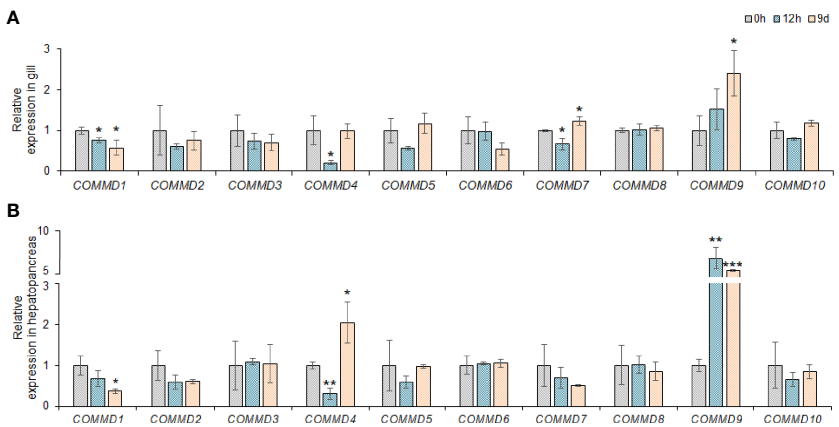

FIGURE 6 | Relative expression of COMMD genes in M. lateralis gill and hepatopancreas under copper ion stress. **(A)** Relative expression of MLCOMMDs in gill under copper ion stress. **(B)** Relative expression of MLCOMMDs in hepatopancreas under copper ion stress. The fold changes compared with the control group for each test point are shown as a bar chart (significance: ***P < 0.001; **P < 0.01; *P < 0.05). The gray, light blue and light orange boxes respectively indicate 0 h, 9h and 9d under copper ion stress.

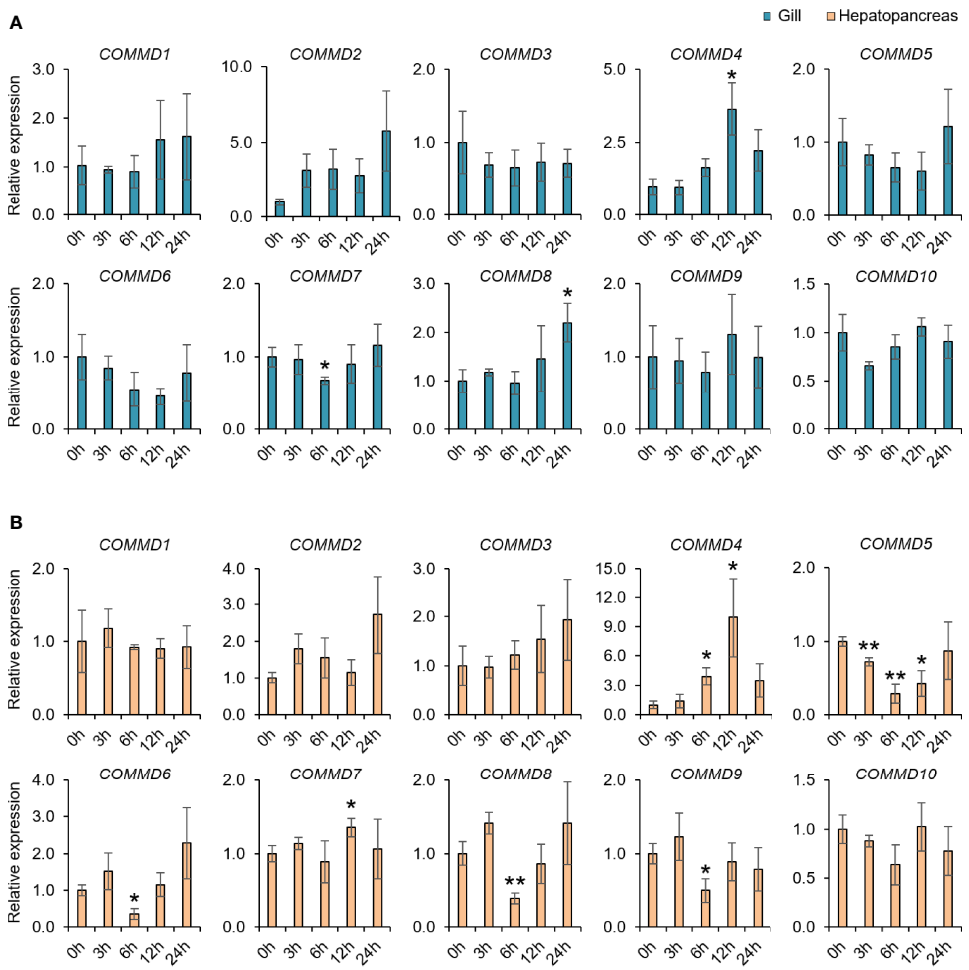

FIGURE 7 | Relative COMMD genes expression in M. lateralis gill and hepatopancreas after V. anguillarum infection. **(A)** Relative expression of MLCOMMDs in gill after V. anguillarum infection. **(B)** Relative expression of MLCOMMDs in hepatopancreas after V. anguillarum infection. The relative fold changes compared with control group for each test point are shown as a bar chart (significance: ** $p < 0.01$; * $p < 0.05$). The blue boxes indicate gill and the light orange boxes indicate hepatopancreas.

MlCOMMD9 showed the most drastic upregulation, suggesting their functional relation with cellular copper ion metabolism. It was reported that *COMMD1* regulates the endosomal sorting of the copper transporter (Phillips-Krawczak et al., 2015), and *COMMD9* may be an endogenous regulator of the epithelial sodium channel (ENaC) to regulate Na^+ transport, which could indirectly alter intracellular Cu flux (Handy et al., 2002; Liu et al., 2013). Besides, it was previously found that deficiency of *COMMD1* or *COMMD9* can result in hepatic copper accumulation under high-copper diets (Singla et al., 2021). Our *V. Anguillarum* infection experimental results revealed that *MlCOMMD4* was significantly upregulated in both the gill and hepatopancreas of dwarf surf clam. Previous studies reported that *COMMD4* has the ability to inhibit NF-κB, the key regulator of both innate and adaptive immune responses (de Bie et al., 2006; Maine and Burstein, 2007; Hayden and Ghosh, 2008; Naugler and Karin, 2008);, while whether bivalve *COMMD4* can regulate NF-κB needs further more detailed studies.

CONCLUSIONS

In this study, 10 *COMMD* genes were respectively identified from the four bivalves, namely, Yesso scallop, Zhikong scallop, Pacific oyster, and dwarf surf clam. They possessed conserved COMM domains and comprised ten subfamilies. Purifying selection of six subfamilies was revealed, with the strongest selection on *COMMD4*. The expression profiling during embryonic development and in adult organs provided valuable implications for exploring the function of the bivalve *COMMD* gene. After exposure to two different stresses, *MLCOMMD*s exhibited different regulation patterns in different tissues or organs. The responses of *COMMD* members under stresses were found more sensitive in the hepatopancreas than in the gill, and *MlCOMMD9* and *MlCOMMD4* might be the good candidate stress indicator genes respectively for copper ion stress and *V. Anguillarum* infection. This study comprehensively describes the first genome-wide characterization of the *COMMD* gene family in

bivalves, and our work will be helpful in better understanding the function and evolution of *COMMD* family bivalve molluscs.

DATA AVAILABILITY STATEMENT

The original contributions presented in the study are included in the article/**Supplementary Material**. Further inquiries can be directed to the corresponding authors.

AUTHOR CONTRIBUTIONS

SL and JH conceived and designed the study. CX and NH performed the experiments. LL and FS participated in the data analysis. XC, SL, LZ, SW, and ZB wrote the manuscript. All authors contributed to the article and approved the submitted version.

FUNDING

We acknowledge the grant support from the Project of Sanya Yazhouwan Science and Technology City Management Foundation (SKJCKJ-2019KY01), the Key R&D Project of Shandong Province (2020ZLYS10, 2021ZLGX03), and the China Agriculture Research System of MOF and MARA.

SUPPLEMENTARY MATERIAL

The Supplementary Material for this article can be found online at: https://www.frontiersin.org/articles/10.3389/fmars.2022.884991/full#supplementary-material

REFERENCES

Bartuzi, P., Hofker, M. H., and van de Sluis, B. (2013). Tuning NF-kappaB Activity: A Touch of COMMD Proteins. *Biochim. Biophys. Acta* 1832, 2315–2321. doi: 10.1016/j.bbadis.2013.09.014

Burstein, E., Hoberg, J. E., Wilkinson, A. S., Rumble, J. M., Csomos, R. A., Komarck, C. M., et al. (2005). COMMD Proteins, a Novel Family of Structural and Functional Homologs of MURR1. *J. Biol. Chem.* 280, 22222–22232. doi: 10.1074/jbc.M501928200

Chomczynski, P., and Sacchi, N. (2006). The Single-Step Method of RNA Isolation by Acid Guanidinium Thiocyanate-Phenol-Chloroform Extraction: Twenty-Something Years on. *Nat. Protoc.* 1, 581–585. doi: 10.1038/nprot.2006.83

de Bie, P., van de Sluis, B., Burstein, E., Duran, K. J., Berger, R., Duckett, C. S., et al. (2006). Characterization of COMMD Protein-Protein Interactions in NF-kappaB Signalling. *Biochem. J.* 398, 63–71. doi: 10.1042/BJ20051664

Devlin, A. M., Solban, N., Tremblay, S., Gutkowska, J., Schürch, W., Orlov, S. N., et al. (2003). HCaRG is a Novel Regulator of Renal Epithelial Cell Growth and Differentiation Causing G(2)M Arrest. *Am. J. Physiol. Renal Physiol.* 284, F753–F762. doi: 10.1152/ajprenal.00252.2002

Dill, B. D., Gierlinski, M., Hartlova, A., Arandilla, A. G., Guo, M., Clarke, R. G., et al. (2015). Quantitative Proteome Analysis of Temporally Resolved Phagosomes Following Uptake *via* Key Phagocytic Receptors. *Mol. Cell Proteom.* 14, 1334–1349. doi: 10.1074/mcp.M114.044594

Gao, F., Chen, C., Arab, D. A., Du, Z., He, Y., and Ho, S. Y. W. (2019). EasyCodeML: A Visual Tool for Analysis of Selection Using CodeML. *Ecol. Evol.* 9, 3891–3898. doi: 10.1002/ece3.5015

Handy, R., Eddy, F., and Baines, H. (2002). Sodium-Dependent Copper Uptake Across Epithelia: A Review of Rationale With Experimental Evidence From Gill and Intestine. *Biochim. Biophys. Acta* 1566, 104–115. doi: 10.1016/s0005-2736(02)00590-4

Hayden, M. S., and Ghosh, S. (2008). Shared Principles in NF-kappaB Signaling. *Cell* 132, 344–362. doi: 10.1016/j.cell.2008.01.020

Jiang, Z., Yuan, Y., Zheng, H., Cui, H., Sun, X., Zhao, W., et al. (2019). COMMD1 Regulates Cell Proliferation and Cell Cycle Progression by Modulating P21 Cip1 Levels. *Biosci. Biotechnol. Biochem.* 83, 845–850. doi: 10.1080/09168451.2019.1569497

Jin, P., Gao, Y., Chen, L., and Ma, F. (2012). Cloning and Characterization of a COMMD4 Gene From Amphioxus (Branchiostoma Belcheri): An Insight Into the Function and Evolution of COMMD4. *Immunol. Lett.* 148, 110–116. doi: 10.1016/j.imlet.2012.10.008

Jin, P., Lv, C., Peng, S., Cai, L., Zhu, J., Ma, F., et al. (2018). Genome-Wide Organization, Evolutionary Diversification of the COMMD Family Genes of Amphioxus (Branchiostoma Belcheri) With the Possible Role in Innate Immunity. *Fish. Shellf Immunol.* 77, 31–39. doi: 10.1016/j.fsi.2018.03.019

Klomp, A. E., van de Sluis, B., Klomp, L. W., and Wijmenga, C. (2003). The Ubiquitously Expressed MURR1 Protein is Absent in Canine Copper Toxicosis. *J. Hepatol.* 39, 703–709. doi: 10.1016/s0168-8278(03)00380-5

Larkin, M. A., Blackshields, G., Brown, N. P., Chenna, R., Mcgettigan, P. A., Mcwilliam, H., et al. (2007). Clustal W and Clustal X Version 2.0. *Bioinformatics* 23, 2947–2948. doi: 10.1093/bioinformatics/btm404

Lian, S., Zhao, L., Xun, X., Lou, J., Li, M., Li, X., et al. (2019). Genome-Wide Identification and Characterization of SODs in Zhikong Scallop Reveals Gene Expansion and Regulation Divergence After Toxic Dinoflagellate Exposure. *Mar. Drugs* 17, 700. doi: 10.3390/md17120700

Li, Y., Sun, X., Hu, X., Xun, X., Zhang, J., Guo, X., et al. (2017). Scallop Genome Reveals Molecular Adaptations to Semi-Sessile Life and Neurotoxins. *Nat. Commun.* 8, 1721. doi: 10.1038/s41467-017-01927-0

Liu, Y., Swart, M., Ke, Y., Ly, K., and McDonald, F. J. (2013). Functional Interaction of COMMD3 and COMMD9 With the Epithelial Sodium Channel. *Am. J. Physiol. Ren. Physiol.* 305, F80–F89. doi: 10.1152/ajprenal.00158.2013

Maine, G. N., and Burstein, E. (2007). COMMD Proteins: COMMing to the Scene. *Cell. Mol. Life Sci.* 64, 1997–2005. doi: 10.1007/s00018-007-7078-y

Maine, G. N., Mao, X., Komarck, C. M., and Burstein, E. (2007). COMMD1 Promotes the Ubiquitination of NF-κb Subunits Through a Cullin-Containing Ubiquitin Ligase. *EMBO J.* 26, 436–447. doi: 10.1038/sj.emboj.7601489

Mouhadeb, O., Ben Shlomo, S., Cohen, K., Farkash, I., Gruber, S., Maharshak, N., et al. (2018). Impaired COMMD10-Mediated Regulation of Ly6C(hi) Monocyte-Driven Inflammation Disrupts Gut Barrier Function. *Front. Immunol.* 9. doi: 10.3389/fimmu.2018.02623

Muller, P. A., van de Sluis, B., Groot, A. J., Verbeek, D., Vonk, W. I., Maine, G. N., et al. (2009). Nuclear-Cytosolic Transport of COMMD1 Regulates NF-kappaB and HIF-1 Activity. *Traffic* 10, 514–527. doi: 10.1111/j.1600-0854.2009.00892.x

Nabetani, A., Hatada, I., Morisaki, H., Oshimura, M., and Mukai, T. (1997). Mouse U2af1-Rs1 is a Neomorphic Imprinted Gene. *Mol. Cell Biol.* 17, 789–798. doi: 10.1128/MCB.17.2.789

Nakai, A., Fujimoto, J., Miyata, H., Stumm, R., Narazaki, M., Schulz, S., et al. (2019). The COMMD3/8 Complex Determines GRK6 Specificity for Chemoattractant Receptors. *J. Exp. Med.* 216, 1630–1647. doi: 10.1084/jem.20181494

Naugler, W. E., and Karin, M. (2008). NF-kappaB and Cancer-Identifying Targets and Mechanisms. *Curr. Opin. Genet. Dev.* 18, 19–26. doi: 10.1016/j.gde.2008.01.020

Nicholas, K., Nicholas, H., and Deerfield, D. (1997). GeneDoc: Analysis and Visualization of Genetic Variation. *Embnew. News* 4, 14. doi: 10.11118/actaun201361041061

Phillips-Krawczak, C. A., Singla, A., Starokadomskyy, P., Deng, Z., Osborne, D. G., Li, H., et al. (2015). COMMD1 is Linked to the WASH Complex and Regulates Endosomal Trafficking of the Copper Transporter ATP7A. *Mol. Biol. Cell.* 26, 91–103. doi: 10.1091/mbc.E14-06-1073

Riera-romo, M. (2018). COMMD1: A Multifunctional Regulatory Protein. *J. Cell Biochem.* 119, 34–51. doi: 10.1002/jcb.26151

Semenova, E., Wang, X., Jablonski, M. M., Levorse, J., and Tilghman, S. M. (2003). An Engineered 800 Kilobase Deletion of Uchl3 and Lmo7 on Mouse

Chromosome 14 Causes Defects in Viability, Postnatal Growth and Degeneration of Muscle and Retina. *Hum. Mol. Genet.* 12, 1301–1312. doi: 10.1093/hmg/ddg140

Singla, A., Chen, Q., Suzuki, K., Song, J., Fedoseienko, A., Wijers, M., et al. (2021). Regulation of Murine Copper Homeostasis by Members of the COMMD Protein Family. *Dis. Model. Mech.* 14, dmm045963. doi: 10.1242/dmm.045963

Solban, N., Jia, H. P., Richard, S., Tremblay, S., Devlin, A. M., Peng, J., et al. (2000). HCaRG, a Novel Calcium-Regulated Gene Coding for a Nuclear Protein, is Potentially Involved in the Regulation of Cell Proliferation. *J. Biol. Chem.* 275, 32234–32243. doi: 10.1074/jbc.M001352200

Sudhir, K., Glen, S., and Koichiro, T. (2016). MEGA7: Molecular Evolutionary Genetics Analysis Version 7.0 for Bigger Datasets. *Mol. Biol. Evol.* 33, 1870–1874. doi: 10.1093/molbev/msw054

Tao, T. Y., Liu, F., Klomp, L., Wijmenga, C., and Gitlin, J. D. (2003). The Copper Toxicosis Gene Product Murr1 Directly Interacts With the Wilson Disease Protein. *J. Biol. Chem.* 278, 41593–41596. doi: 10.1074/jbc.C300391200

Telford, M. J., Bourlat, S. J., Economou, A., Papillon, D., and Rota-Stabelli, O. (2008). The Evolution of the Ecdysozoa. *Philos. Trans. R. Soc. Lond. B. Biol. Sci.* 363, 1529–1537. doi: 10.1098/rstb.2007.2243

Uys, G. M., Ramburan, A., Loos, B., Kinnear, C. J., Korkie, L. J., Mouton, J., et al. (2011). Myomegalin is a Novel A-Kinase Anchoring Protein Involved in the Phosphorylation of Cardiac Myosin Binding Protein C. *BMC Cell Biol.* 12, 18. doi: 10.1186/1471-2121-12-18

van de Sluis, B., Muller, P., Duran, K., Chen, A., Groot, A. J., Klomp, L. W., et al. (2007). Increased Activity of Hypoxia-Inducible Factor 1 Is Associated With Early Embryonic Lethality in Commd1 Null Mice. *Mol. Cell Biol.* 27, 4142–4156. doi: 10.1128/MCB.01932-06

van De Sluis, B., Rothuizen, J., Pearson, P. L., van Oost, B. A., and Wijmenga, C. (2002). Identification of a New Copper Metabolism Gene by Positional Cloning in a Purebred Dog Population. *Hum. Mol. Genet.* 11, 165–173. doi: 10.1093/hmg/11.2.165

Wang, F., Xiao, S., Xiang, Z., and Yu, Z. (2017a). Molecular Cloning and Expression Analysis of Commd1 Under Salinity Stress in Crassostrea Hongkongensis. *J. Oceanogr.* 36, 48–55. doi: 10.11978/2016022

Wang, S., Zhang, J., Jiao, W., Li, J., Xun, X., Sun, Y., et al. (2017b). Scallop Genome Provides Insights Into Evolution of Bilaterian Karyotype and Development. *Nat. Ecol. Evol.* 1, 120. doi: 10.1038/s41559-017-0120

Yang, M., Huang, W., Sun, Y., Liang, H., Chen, M., Wu, X., et al. (2019). Prognosis and Modulation Mechanisms of COMMD6 in Human Tumours Based on Expression Profiling and Comprehensive Bioinformatics Analysis. *Br. J. Cancer* 121, 699–709. doi: 10.1038/s41416-019-0571-x

Yang, S., Li, X., Yang, M., Ren, X., Hu, J., Zhu, X., et al. (2017). FMNL2 Destabilises COMMD10 to Activate NF-κ B Pathway in Invasion and Metastasis of Colorectal Cancer. *Br. J. Cancer* 117, 1164–1175. doi: 10.1038/bjc.2017.260

Yang, Z., Wong, W. S. W., and Rasmus, N. (2005). Evolution, Bayes Empirical Bayes Inference of Amino Acid Sites Under Positive Selection. *Mol. Biol. Evol.* 22, 1107–1118. doi: 10.1093/molbev/msi097

You, N., Li, J., Huang, X. B., Wu, K., Tang, Y. C., Wang, L., et al. (2017). COMMD7 Promotes Hepatocellular Carcinoma Through Regulating CXCL10. *Biomed. Pharmacother.* 88, 653–657. doi: 10.1016/j.biopha.2017.01.046

Zhang, G., Fang, X., Guo, X., Li, L., Luo, R., Xu, F., et al. (2012). The Oyster Genome Reveals Stress Adaptation and Complexity of Shell Formation. *Nature* 490, 49–54. doi: 10.1038/nature11413

Zhan, W., Wang, W., Han, T., Xie, C., Zhang, T., Gan, M., et al. (2017). COMMD9 Promotes TFDP1/E2F1 Transcriptional Activity *via* Interaction With TFDP1 in non-Small Cell Lung Cancer. *Cell. Signal.* 30, 59–66. doi: 10.1016/j.cellsig.2016.11.016

Zheng, L., You, N., Huang, X., Gu, H., Wu, K., Mi, N., et al. (2018). COMMD7 Regulates NF-κb Signaling Pathway in Hepatocellular Carcinoma Stem-Like Cells. *Mol. Ther. Oncolyt.* 12, 112–113. doi: 10.1016/j.omto.2018.12.006

Zhou, L., Zhao, D., Wu, B., Sun, X., Liu, Z., Zhao, F., et al. (2019). Ark Shell Scapharca Broughtonii Hemocyte Response Against Vibrio Anguillarum Challenge. *Fish. Shellfish Immunol.* 84, 304–311. doi: 10.1016/j.fsi.2018.09.039

Conflict of Interest: The authors declare that the research was conducted in the absence of any commercial or financial relationships that could be construed as a potential conflict of interest.

Publisher's Note: All claims expressed in this article are solely those of the authors and do not necessarily represent those of their affiliated organizations, or those of the publisher, the editors and the reviewers. Any product that may be evaluated in this article, or claim that may be made by its manufacturer, is not guaranteed or endorsed by the publisher.

frontiers | Frontiers in Marine Science

ORIGINAL RESEARCH
published: 26 April 2022
doi: 10.3389/fmars.2022.865707

Interferon Regulatory Factors Functioned as Activators of the Interferon Pathway in the Scallop *Chlamys farreri*

Naina Hu[1], Shanshan Lian[1,2], Xiaomei Zhu[1], Xiaomei Chen[1], Fengzhi Sun[1], Lingling Zhang[1,3], Shi Wang[1,2,4], Zhenmin Bao[1,3,4] and Jingjie Hu[1,4]**

[1] Ministry of Education (MOE) Key Laboratory of Marine Genetics and Breeding, Ocean University of China, Qingdao, China, [2] Laboratory for Marine Biology and Biotechnology, Pilot Qingdao National Laboratory for Marine Science and Technology, Qingdao, China, [3] Laboratory for Marine Fisheries Science and Food Production Processes, Pilot Qingdao National Laboratory for Marine Science and Technology, Qingdao, China, [4] Key Laboratory of Tropical Aquatic Germplasm of Hainan Province, Sanya Oceanographic Institution, Ocean University of China, Sanya, China

OPEN ACCESS

Edited by:
Weiwei You,
Xiamen University, China

Reviewed by:
Lusheng Xin,
Chinese Academy of Fishery Sciences (CAFS), China
Yang Zhang,
South China Sea Institute of Oceanology (CAS), China

***Correspondence:**
Shanshan Lian
lianshanshan@ouc.edu.cn
Jingjie Hu
hujingjie@ouc.edu.cn

Specialty section:
This article was submitted to Marine Fisheries, Aquaculture and Living Resources, a section of the journal Frontiers in Marine Science

Received: 30 January 2022
Accepted: 29 March 2022
Published: 26 April 2022

Citation:
Hu N, Lian S, Zhu X, Chen X, Sun F, Zhang L, Wang S, Bao Z and Hu J (2022) Interferon Regulatory Factors Functioned as Activators of the Interferon Pathway in the Scallop Chlamys farreri. Front. Mar. Sci. 9:865707. doi: 10.3389/fmars.2022.865707

Interferon regulatory factors (*IRF*s) are a family of transcription factors that control many facets during innate and adaptive immune responses. Vertebrate *IRF*s play important roles in regulating the expression of interferons (IFNs) and IFN-stimulated genes, while only limited studies were conducted on invertebrate *IRF*s. In the present study, four *IRF* family genes (*CfIRF1, CfIRF1-like, CfIRF2*, and *CfIRF8*) were identified from Zhikong scallop (*Chlamys farreri*) through whole-genome scanning. *CfIRFs* contain a highly conserved N-terminal DNA-binding domain and a variable C-terminal regulatory domain. *CfIRFs* were constitutively expressed during development as well as in adult tissues, especially in hepatopancreas, hemolymph, gill, and mantle. In hemolymph, qRT-PCR analysis revealed that *CfIRF1, CfIRF1-like*, and *CfIRF2* were significantly upregulated in response to *Vibrio anguillarum* infection, and their encoding proteins could translocate into nucleus. Dual-luciferase reporter assay on *Cf*IRF1, *Cf*IRF1-like, and *Cf*IRF2 showed that these three proteins were capable to induce a strong activation of ISRE promoters. Notably, in comparison with *CfIRF1* and *CfIRF1-like*, *CfIRF2* showed the most sensitive responses in coping with *V. anguillarum*, and consistently, *Cf*IRF2 exhibited the most significant activation on ISRE. This study would provide valuable information for the innate immune roles of the *IRF* gene family in bivalve molluscs.

Keywords: *Chlamys farreri*, *IRF*, transcriptional activation, interferon-stimulated response element, immune response

1 INTRODUCTION

Interferon regulatory factors (*IRF*s) are a family of transcription factors that were first identified as regulators of IFN (Type I interferon) and IFN-inducible genes (Miyamoto et al., 1988; Harada et al., 1989), which have been extensively studied in vertebrates, showing diverse functions in regulating immune responses, stress responses, reproduction, development, and carcinogenesis (Tamura et al., 2008; Nehyba et al., 2009; Savitsky et al., 2010). So far, a total of 11 *IRF* family members (from *IRF-1*

to *IRF-11*) have been reported in vertebrates (Inkpen et al., 2019), with nine *IRFs* identified in mammals and another two members found in several avian and fish species (Nehyba et al., 2002; Huang et al., 2010). All IRF family members possess a highly conserved N-terminal helix-turn-helix DNA-binding domain (DBD). This domain consists of about 120 amino acids, binding to the core IFN-stimulated response element (ISRE) recognition sequence, GAAANNGAAAG/CT/C (Escalante et al., 1998; Marchler-Bauer et al., 2011). As for the C-terminus, most of the IRFs share an IRF-associated domain 1 (IAD1) or a similar IAD2, which mainly mediates the homomeric or heteromeric formation of IRFs as well as the interaction of IRF with non-IRF members, and the resulting protein complex acts as a transcriptional activator or repressor (Ikushima et al., 2013). It was reported that *IRF1*, *IRF3*, *IRF5*, *IRF7*, and *IRF9* are usually functioned as positive mediators of the host's IFN response, whereas *IRF4* usually acts as a repressor. Furthermore, *IRF2* and *IRF8* can participate in either activating or repressing the target gene transcription, depending on the nature of the pathogen or the signaling pathways that is involved (Taniguchi, 2006; Weiqi et al., 2008; Ikushima et al., 2013). Besides the IAD, the C-terminus is not well conserved, which may confer versatile functions to *IRF* members (Yanai et al., 2012). For example, besides IFN mediator, *IRF* activation through the TLRs or other inflammatory cytokines could interfere with NF-κB signaling, which were necessary to maintain the immunity balance (Anda et al., 2012; Cavlar et al., 2012; Xuan et al., 2020).

Previous studies have revealed that *IRF* genes are present in all principal metazoan groups, and *IRF-like* genes have been detected in genomic and expressed sequence tag (EST) databases (Davidson et al., 2006; Azumi et al., 2007; Huang et al., 2008). Based on the evolutionary molecular relationships, the IRF proteins could be classified into four subfamilies, namely, IRF-1 group (IRF1, 2, and 11), IRF-3 group (IRF3 and 7), IRF-4 group (IRF4, 8, 9, and 10), and IRF-5 group (IRF5 and 6) (Zhan et al., 2016). For the IRF-1 subfamily, IRF1 and IRF2 were first identified as transcriptional regulators of ISGs and type I IFN, which mainly play important roles in antiviral immunity (Harada et al., 1989). IRF11 has only been identified in teleost fish, and its function study is still in the infancy stage (Huang et al., 2010). For the IRF-3 family, researchers found that phosphorylated IRF7 and IRF3 could jointly regulate the rapid production of IFN initially, and ultimately induce the production of IFN in large quantities through a positive feedback regulatory loop (Marié et al., 1998; Sato et al., 1999). For the IRF-4 subfamily, they showed diverse IFN or NF-κB regulating functions depending on the nature of the binding molecules or the cellular differentiation status, and higher homology was found between IRF4 and IRF8 (Meraro et al., 2002; Lehtonen et al., 2005; Lu, 2008). As for the IRF-5 subfamily, IRF5 is mainly involved in the natural inflammatory response, while IRF6 is mainly involved in the embryonic early development (Hatada et al., 1997; Barnes et al., 2001; Barnes et al., 2004; Green et al., 2015).

Compared with the extensive knowledge of *IRFs* in vertebrates, studies on *IRFs* in invertebrates are quite limited. Previously, the interferon response has been thought to be a vertebrate innovation because the genomes of model invertebrates (i.e., *Drosophila*) do not encode interferon or its major effectors (Green et al., 2015). With the abundance and further analysis of invertebrate genome data, several key molecules in the IFN system have been identified, including IRF, interferon-like protein (IFNLP), interferon receptor (IFNR), and interferon-induced protein (Lelong et al., 2015; Zhang et al., 2015; Huang et al., 2017). More recently, studies have revealed that *IRF* genes are present in a lot of invertebrate groups, including sea sponges, placozoans, comb jellies, cnidarians, and bivalves, but are not detected in *Nematoda* and *Hexapoda* (including insects) (Nehyba et al., 2009; Huang et al., 2010). Although *IRFs* have been found in various invertebrates, they are different in number and genomic characteristics from the vertebrate *IRF* family, and there are only few preliminary functional studies on invertebrate *IRFs* through gene cloning. For example, *PfIRF-2* in pearl oyster *Pinctada fucata*; *CgIRF-1*, *-2*, and *-8* in pacific oyster *Crassostrea gigas*; and *LvIRF* in pacific white shrimp *Litopenaeus vannamei* were found to participate in the immune response against Gram-negative bacteria (Huang et al., 2013; Li et al., 2015; Huang et al., 2017; Lu et al., 2018). As invertebrates or vertebrates might have experienced a different pressure during evolution, it may in turn lead to the functional differentiation of *IRF* genes (Huang et al., 2010). Therefore, we need more research into the function of invertebrate *IRFs*, providing valuable information for the origin of the *IRF* family as well as the evolution of innate immunity.

Bivalve molluscs belong to the most speciose phylum of marine invertebrates, which could well adapt to the highly diverse and hostile environment with various stressors (bacteria, pollution, etc.). Scallops are highly prized as a food source, while in recent years, their aquaculture industry suffers huge economic loss due to the etiological diversity of pathogens that cause repeated appearance of disease outbreaks (Liu et al., 2004; Teng et al., 2012). Scallops generally lack the adaptive immune system and rely solely on innate immunity mediated by both cellular and humoral components (Loker et al., 2010). Functional studies of *IRFs* on scallops would be helpful for revealing their immune defense mechanisms and understanding the origin and evolution of bivalve innate immunity. In the present study, we take *Chlamys farreri* (Zhikong scallop), one of the most important maricultural scallop species in China, as research subject to systematically identify the *IRF* gene family. Their expression profiles during development and in different healthy adult tissues were analyzed. Meantime, their responses after *Vibrio anguillarum* challenge in hemocytes were investigated. We further explored their subcellular localization as well as the transcriptional activity using pISRE-Luc reporter plasmids in HEK293T cells, thereby providing insights into the immune function of *IRF* genes in bivalves.

2 MATERIALS AND METHODS

2.1 Database Mining, Gene Identification, and Sequence Analysis

To identify *IRF* genes, the transcriptome and whole genome sequence databases of the *C. farreri* were searched using the available IRF protein sequences from representative invertebrates and vertebrates, including *Homo sapiens, Mus*

musculus, Gallus gallus, Xenopus tropicalis, Danio rerio, C. gigas, P. fucata, Mytilus galloprovincialis, Hyriopsis cumingii, Pecten maximus, Lottia gigantea, Biomphalaria glabrata, and *Elysia chlorotica*. These IRF proteins from representative species were retrieved from NCBI (http://www.ncbi.nlm.nih.gov), Ensembl (http://useast.ensembl.org), MolluscDB (http://mgbase.qnlm.ac/), and OysterBase (http://www.oysterdb.com/) databases. TBLASTN was used to obtain the initial pool of *IRFs* transcriptome sequences from the Zhikong scallop, and then, BLASTN was performed to verify the cDNA sequences by comparing the transcriptome sequences with the whole genome sequences. The candidate *CfIRFs* sequences were submitted to the ORF Finder program (https://www.ncbi.nlm.nih.gov/orffinder/) to predict the open reading frame (ORF), and the ORFs were translated into amino acid sequences. The translated sequences were submitted to the SMART program (http://smart.embl-heidelberg.de/) for identification of the signal peptide and other conserved domains. The putative isoelectric point (*pI*) and molecular weight were computed using the Compute *pI*/Mw (http://web.expasy.org/compute_pi/). The subcellular localization and nuclear localization signals (NLSs) were predicted through the online prediction website (http://www.csbio.sjtu.edu.cn/bioinf/euk-multi-2/, https://www.genscript.com/wolf-psort.html/, https://sunflower.kuicr.kyoto-u.ac.jp/~smatsuda/slplocal.html, http://nls-mapper.iab.keio.ac.jp/cgi-bin/NLS_Mapper_form.cgi). The protein structures of all the identified IRF proteins were drawn with IBS1.0.3 software. Multiple alignment analysis of CfIRFs were performed with the ClustalW multiple alignment programs (http://www.ebi.ac.uk/clustalw/).

2.2 Phylogenetic Analysis

The IRF proteins from other vertebrates and invertebrates listed in the Section 2.1 were used for phylogenetic analysis together with the Zhikong scallop IRFs. The amino acid sequences of IRF proteins from these species were retrieved from the NCBI and Ensembl Genome Browser. Protein sequences were aligned using the ClustalW method in the MEGA-X software (Sudhir et al., 2018). Phylogenetic relationships of IRF amino acid sequences were estimated using maximum-likelihood (ML) analyses with FastTree 2.0.0. FastTree accounts for variable rates of evolution across sites by assigning each site to one of 20 categories, with the rates geometrically spaced from 0.05 to 20. FastTree sets each site to its most likely category by using a Bayesian approach with a gamma prior. Branch supports evaluated 10,000 pseudo-replicates of the ultrafast bootstrap procedure (Thi et al., 2017). Whole amino acid sequences were used in the phylogenetic analyses. This analysis involved a total of 59 amino acids across 13 species. The accession numbers of 59 IRFs are listed in **Supplementary Table 1**.

2.3 Expression Analysis

For expressional analysis, the RPKM (reads per kilo per million reads) value of each *IRF* gene was retrieved from the published RNASeq datasets of various developmental stages and adult tissues of Zhikong scallop (Li et al., 2017). To visualize the expression patterns of *IRF* genes in Zhikong scallop, the expressional heatmaps were shown *via* heatmap package under the R environment and the statistical analysis of the data was performed with edgeR package under R environment using the *F*-test. Differences were considered significant at $p < 0.05$. For examining the correlation relationship of *IRF* genes, a regression analysis was performed.

2.4 Sample Collection and Bacteria Treatment

Two-year-old healthy Zhikong scallops were collected from artificial scallop-rearing substrates installed in Xunshan Fishery Group Co., Rongcheng (Shandong Province, China). All the procedures involved in the handling and the treatment of scallops during this study were approved by the Ocean University of China Institutional Animal Care and Use Committee (OUC-IACUC) prior to the initiation of the study. The scallops were acclimated in the laboratory at ambient seawater temperature for 1 week prior to the experiments, which is within the optimum temperature range for their survival.

Gram-negative (*V. anguillarum*) bacteria were used to challenge scallops in our study (Zhi et al., 2011). *V. anguillarum* was cultured in liquid 2216E broth (5 g/L of Tryptone, 1 g/L of yeast extract, and 0.1 g/L of C6H5Fe·5H2O, pH = 7.6) at 28°C and harvested by centrifugation at 2000×*g* for 5 min, as described by Kong et al. The pellet was suspended in filtered seawater and was adjusted to 1×10^7 CFU/ml in seawater, respectively (Zhi et al., 2011; Ragab et al., 2014).

A total of 75 individuals were randomly and equally divided into five groups. At 0 h, 5 h, 24 h, 48 h, and 72 h post-infection, 5 individuals were randomly collected from each group. The 0 h group was employed as the control group, and other groups were used as experimental groups. The hemolymph samples were collected from adductor muscles using a syringe and were immediately centrifuged at 800×*g*, 4°C for 10 min to harvest the hemocytes (Gao et al., 2007). The extracted hemocyte sample was immediately frozen in liquid nitrogen and then subsequently frozen at −80°C before processing.

2.5 RNA Extraction and Quantitative Real-Time PCR Analysis

Total RNA was isolated following the method described by Hu et al. (2010), and then was digested with DNase I (TaKaRa, Shiga, Japan). A Nanovue Plus spectrophotometer (GE Healthcare, NJ, USA) was used to assess the concentration and purity of RNA; RNA integrity was determined by agarose gel electrophoresis. First-strand cDNA was synthesized using Moloney murine leukemia virus (MMLV) reverse transcriptase (Thermo, USA) following the manufacturer's protocol. All of the cDNA products were diluted to 5 ng/ml for use as the template in real-time PCR.

Real-time PCR was conducted using the SsoFast™ EvaGreen® Supermix on a Light Cycler 480 Real-time PCR System (Roche Di-agnostics, Mannheim, Germany). The running program was as follows: 50°C for 2 min, 94°C for 10 min, and 40 cycles at 94°C for 15 s and at 62°C for 1 min. Cytochrome B (CB), DEAD-βox RNA helicase (HELI), and EF1-

A gene were designated as internal reference genes for the normalization of gene expression in healthy adults and test subjects during the real-time PCR experiment, respectively (Li et al., 2010; Feng et al., 2013). All the primers used in the real-time PCR were designed using Primer Premier 5.0 and are listed in **Table 1**.

Data from the real-time PCR were analyzed using the Relative Expression Software Tool (REST) version 2009 (Pfaffl et al., 2002); gene expression is shown as the fold change. For the experimental groups, the control group (0 h) was used for normalization. The statistical analysis of the data was performed with SPSS (version 16.0) software using the independent *t*-test. Differences were considered to be significant at $p < 0.05$.

2.6 Subcellular Localizations

The full length of ORFs of three *CfIRF* genes was amplified from *C. farreri* cDNA, using primers listed in **Table 1**. For *CfIRF1* and *CfIRF2*, the PCR products were ligated and subcloned into pEGFP-N1 (Clontech, USA) by way of overlap extension PCR to construct recombinant plasmids pEGFP-*CfIRF1* and pEGFP-*CfIRF2*, while for the *CfIRF1-like*, PCR products were digested with *Kpn*I and *Sma*I, and ligated and subcloned into pEGFP-N1 vector digested by the corresponding restriction enzymes to construct recombinant plasmids pEGFP-*CfIRF1-like*. The constructed recombinant plasmids were subsequently verified by DNA sequencing.

In scallops, as well as in other marine bivalves, there are no mature cell lines. Thus, we choose HEK293T cells to perform our experiment. HEK293 cells were maintained in Modified Eagle Medium (MEM, Gibco, USA) supplemented with 10% fetal bovine serum (FBS, Invitrogen, USA) and antibiotics (100 mg/L streptomycin and 10^5 U/L penicillin, Gibco) at 37°C in a humidified incubator under 5% CO_2. For DNA transfection, cells were seeded and allowed to grow to more than 70% confluence, and then plasmids were transfected by using the Lipofectamine 3000 Reagent (Invitrogen, USA) following the manufacturer's recommendations. HEK293T cells were transiently co-transfected with 0.8 μg of expression plasmid and 1 μl of Lipofectamine 3000 in each well in a 24-well plate. All assays were performed with three independent transfections.

At 48 h post-transfection, HEK293 cells were washed with PBS twice and fixed with paraformaldehyde for 15 min. Then, the cells were washed three times with PBS and were stained with DAPI (Sigma, USA) to mark the nucleus followed by washing three times. Immunofluorescence was visualized and captured with confocal microscopy (Nikon, Japan).

2.7 Dual-Luciferase Reporter Assays

The full length of ORFs of three *CfIRF* genes was amplified from *C. farreri* cDNA, using primers listed in **Table 1**. For *CfIRF1* and *CfIRF2*, the PCR products were ligated and subcloned into

TABLE 1 | List of primers used in this study.

Name	Sequence (5'-3')
For RT-PCR	TGACGATGATGAGAGCAATG
IRF1-F	
IRF1-R	GGACGGATATTTGAAGGGATG
IRF1-like-F	CAGGTGACAATAGACCTGAAG
IRF1-like-R	ACACCACAGACACGAATATG
IRF2-F	CAGACTACCACATTGAGATCG
IRF2-R	CGACTTCTTCGTCTGTTAGG
IRF8-F	CTTATCTTACGGCCAGGAAC
IRF8-R	GGTTCTTCAGCATCGTATCA
For construction of plasmids[a]	
IRF1-GFP-F	CGTCAGATCCATGGCAATTTCCGAGATTGAAC
IRF1-GFP-R	CGGGACACACATCCCAGTCAACCATGGTGA
IRF1-GFP-N1-F	ATCCCAGTCAACCATGGTGAGCAAGGGCGAG
IRF1-GFP-N1-R	GGTTTAGTGAACCGTCAGATCCATGGCAATTT
IRF1-like-GFP-F	TCC**CCCGGG**ATGAGCAAAGTGAAGAAAAAGATGG
IRF1-like-GFP-R	GGG**ACCGGT**AACTGAATTTTTCGAATCTGGTTCG
IRF2-GFP-F	CGTCAGATCCATGGTTGTGTCAAAGAAAATGC
IRF2-GFP-R	ATACACAAGTATTTTGGGCCTGACCATGGTGA
IRF2-GFP-N1-F	TTTGGGCCTGACCATGGTGAGCAAGGGCGAG
IRF2-GFP-N1-R	GGTTTAGTGAACCGTCAGATCCATGGTTGTGT
IRF1-gene-F	ACCCAAGCTGATGGCAATTTCCGAGATTGAAC
IRF1-gene-R	GGACACACATCCCAGTCATAACCGCTGATCA
IRF1-pcDNA3.1-F	CCAGTCATAACCGCTGATCAGCCTCGACT
IRF1-pcDNA3.1-R	CTATAGGGAGACCCAAGCTGATGGCAATTT
IRF1-like-pcDNA3.1-F	ATAAGAAT**GCGGCCGC**ATGAGCAAAGTGAAGAAAAAGATGG
IRF1-like-pcDNA3.1-R	CGG**GGTACC**TCAAACTGAATTTTTCGAATCTGGTT
IRF2-gene-F	ACCCAAGCTGATGGTTGTGTCAAAGAAAATGC
IRF2-gene-R	CACAAGTATTTTGGGCCTGTAACCGCTGATCA
IRF2-pcDNA3.1-F	GGGCCTGTAACCGCTGATCAGCCTCGACT
IRF2-pcDNA3.1-R	CTATAGGGAGACCCAAGCTGATGGTTGTGT

[a]*Nucleotides in bold indicate restriction enzyme sites.*

pcDNA3.1 V5/H vector (Invitrogen, USA) by way of overlap extension PCR to construct recombinant plasmids pcDNA3.1-IRF1 and pcDNA3.1-IRF2, while for the *CfIRF1-like*, the pcDNA3.1-IRF1-like was constructed using the same method as mentioned above but digested with *Not*I and *Kpn*I. The constructed recombinant plasmids were subsequently verified by DNA sequencing. For reporter plasmids, pISRE-Luc (ClonTech, USA) was used, and pRL-TK renilla luciferase plasmid (Progema, USA) and pGL3-basic vector (Progema, USA) were used as an internal control and blank group, respectively. EndoFree Plasmid MiKit (OMEGA, USA) was used for the transfection of the plasmids according to the manufacturer's instruction.

The cell culture assays were performed according to Section 2.6. For dual-luciferase reporter assays, HEK293T cells were transiently co-transfected with 0.2 mg of expression plasmid, 0.5 mg of reporter gene plasmid, 0.01 mg of pRL-TK renilla luciferase plasmid, and 0.1 μl of Lipofectamine 3000 in each well in a 24-well plate. The luciferase reporter vector pGL3-basic was used as a blank group. All assays were performed with three independent transfections. At 48 h post-transfection, HEK293 cells were washed with PBS twice and lysed. Firefly and renilla luciferase activities were measured using the Dual-Luciferase Reporter Assay System (Promega, USA) according to the manufacturer's instruction. Cell lysate (20 μl) was transferred to a 1.5-ml EP tube and 100 μl of luciferase assay reagent II and 100 μl of Stop & Glo® Reagent were added in sequence, then firefly and renilla luciferase activities were measured, respectively.

3 RESULTS

3.1 Sequence Identification and Analysis

Four *IRF* genes, *CfIRF1, CfIRF1-like*, *CfIRF2*, and *CfIRF8*, were identified from the genome of Zhikong scallop. The basic information (total length, ORF length, number of exons, amino acids length, theoretical *pI*, and weight of protein) of these *IRF* members were summarized in **Table 2**. The ORFs of *CfIRF1, CfIRF1-like, CfIRF2*, and *CfIRF8* were respectively 1,107, 5,913, 1,053, and 1,311 bp, encoding 368, 1,970, 350, and 436 amino acids. The predicted molecular weights of these four genes ranged from 40.05 to 212.51 KD, with the predicted *pI* values from 4.97 to 6.96 (**Table 2**). The genomic structural analysis showed that the length as well as the exon–intron pattern of these four *CfIRF* genes varied greatly. The longest *CfIRF1* gene was 28,913 bp with 9 exons, and the shortest *CfIRF2* gene was 6,565 bp with 10 exons. Moreover, *CfIRF1-like* and *CfIRF8* had 9 and 8 exons, respectively (**Figure 1**).

All four *Cf*IRF proteins had a single well-conserved DBD domain (113 aa in length), which was found to be helix-turn-helix at the N-terminal (**Figure 2**). Furthermore, *Cf*IRF8 was predicted to contain an *IRF*-associated domain (IAD) at the C-terminus, and *Cf*IRF1-like possessed seven C2H2-type (classical) zinc fingers (ZnF_C2H2) at the C-terminal (**Figure 2**). Multiple sequence alignments of *Cf*IRFs showed that they share high similarity within the DBD domain (**Figure 3**). Moreover, five conserved tryptophan (W) residues were revealed, in which the W^{71} residue was found mutated as Y^{71} in *Cf*IRF1 protein.

TABLE 2 | Summary of sequence features of *CfIRF* genes.

Name	Total length (bp)	ORF length (bp)	Exon number	Protein length(aa)	*pI*	Molecular weight (Da)
IRF1	28913	1107	9	368	6.04	41469.13
IRF1-like	22192	5913	9	1970	6.96	212509.5
IRF2	6565	1053	10	350	4.97	40046.71
IRF8	10031	1311	8	436	6.21	49815.55

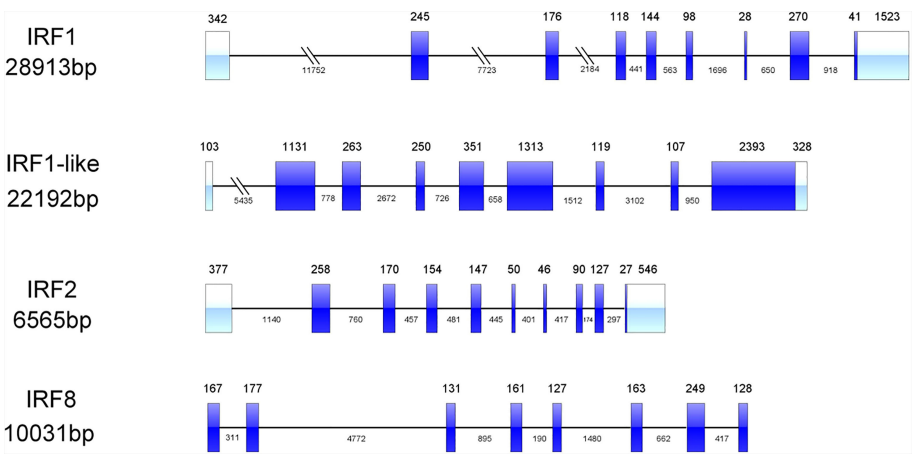

FIGURE 1 | Genetic structure of the *CfIRF* genes. The light blue boxes indicate the 3' UTRs and the 5' UTRs. The dark blue boxes indicate the exons. The horizontal line with sporadic double slash indicates the introns.

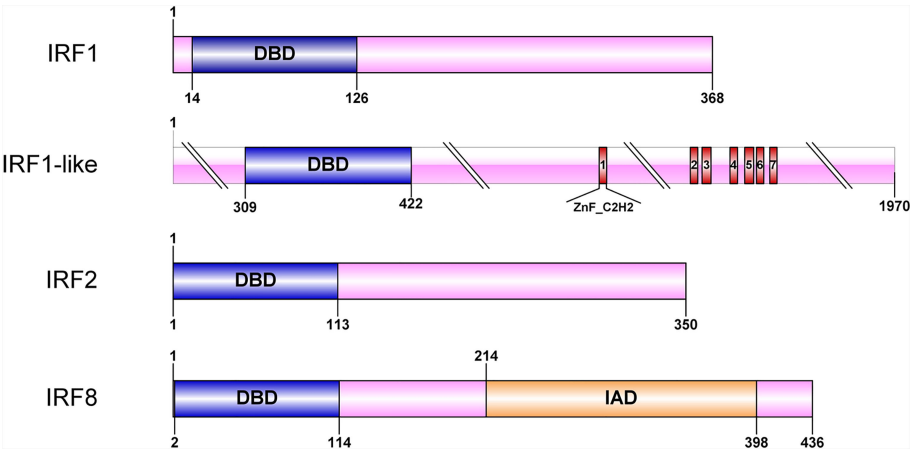

FIGURE 2 | Protein structure of the *CfIRF* genes. The blue boxes indicate the DBD domain. The orange boxes indicate the IAD domain. The red boxes indicate the ZnF_C2H2 domain.

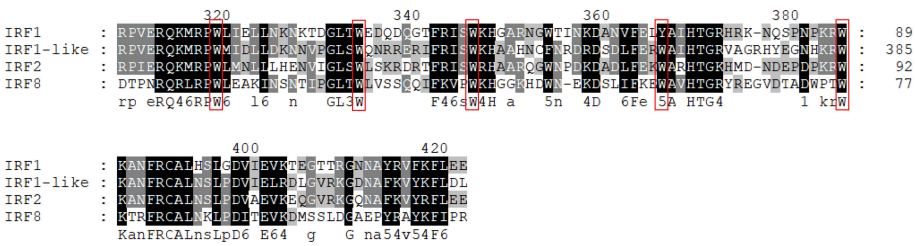

FIGURE 3 | Alignment of DBD domains of the four *Cf*IRF proteins. Alignment was performed using ClustalW2. Identical residues are indicated in black, and similar residues are in light gray. Dashes indicate gaps. Five conserved tryptophan (W) residues are marked with red boxes.

To confirm the identification of the *Cf*IRFs, a phylogenetic tree was constructed through the ML method using 59 IRF proteins across 13 species. Four IRF subfamilies (IRF-1, -3, -4, and -5) were identified (**Supplementary Figure 1**) and all *Cf*IRFs were clustered into its own clade. The result showed that *Cf*IRF1, *Cf*IRF1-like, and *Cf*IRF2 were clustered into the IRF-1 subfamily. *Cf*IRF8 was firstly grouped together with IRF8-like from *Peten maximus* and IRF8 from *C. gigas*, and they were clustered into the IRF-4 subfamily.

3.2 Spatiotemporal Expressions of *CfIRF*s

The RPKM data were used to analyze the expression patterns of four *CfIRF* genes during eleven developmental stages (**Figure 4A**, **Supplementary Figure 2A**). Their expression during early development (from zygote to trochophore larvae) was quite low (<10 RPKM). After D-shaped larvae formation, *CfIRF1-like* and *CfIRF8* remained at a low expression (<5 RPKM) while expression of *CfIRF1* and *CfIRF2* was obviously elevated. Although *CfIRF2* showed higher expression level than *CfIRF1* (>3-fold), their expression pattern was similar, both of which showing the highest expression in creeping larvae and juvenile. In adult tissues, we found that expression of *CfIRF1* and *CfIRF2* was obviously higher than *CfIRF1-like* and *CfIRF8* (**Figure 4C**, **Supplementary Figure 2B**), consistent with their expression tendency during development. In general, *CfIRF1-like* and *CfIRF8* remained low expression in all the tissues (<25 RPKM), while *CfIRF1* was dominantly expressed in hepatopancreas and hemolymph (>160 RPKM), and the highest expression of *CfIRF2* was observed in gill and hepatopancreas (>220 RPKM). To illustrate the role of *CfIRF1* and *CfIRF2* in development stages and adult tissues, we performed correlation analysis between the expression of *CfIRF1* and *CfIRF2* with E2/T ratio. According to the results, *CfIRF1* has a significantly positive correlation with *CfIRF2* expression both in different developmental stages (r = 0.86, $p < 0.001$) (**Figure 4B**) and in adult tissues (r = 0.65, $p <$ 0.05) (**Figure 4D**).

3.3 Temporal Responses of *CfIRF*s in Coping With Bacterial Infection

To examine the immune responses of *CfIRFs* to *V. anguillarum* challenge (Qiu et al., 2007; Costa et al., 2009), their expression level was investigated at four time points (5 h, 24 h, 48 h, and 72

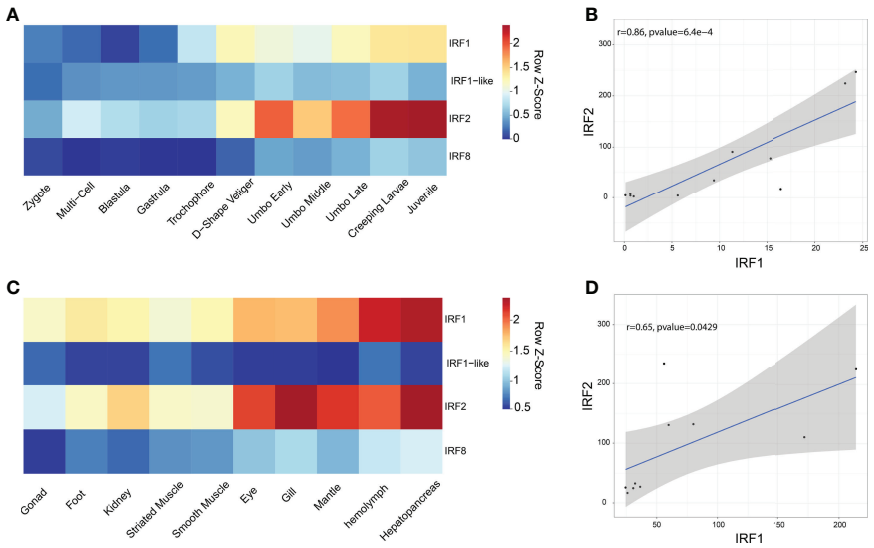

FIGURE 4 | Expression profiles of *CflRFs* in different developmental stages and adult tissues. **(A)** Heatmap of *CflRFs* expression profile in different embryonic and larval stages. **(B)** The positive correlation between *CflRF1* and *CflRF2* in different developmental stages. **(C)** Expression profiles of *CflRFs* in adult tissues. **(D)** The positive correlation between *CflRF1* and *CflRF2* in adult tissues.

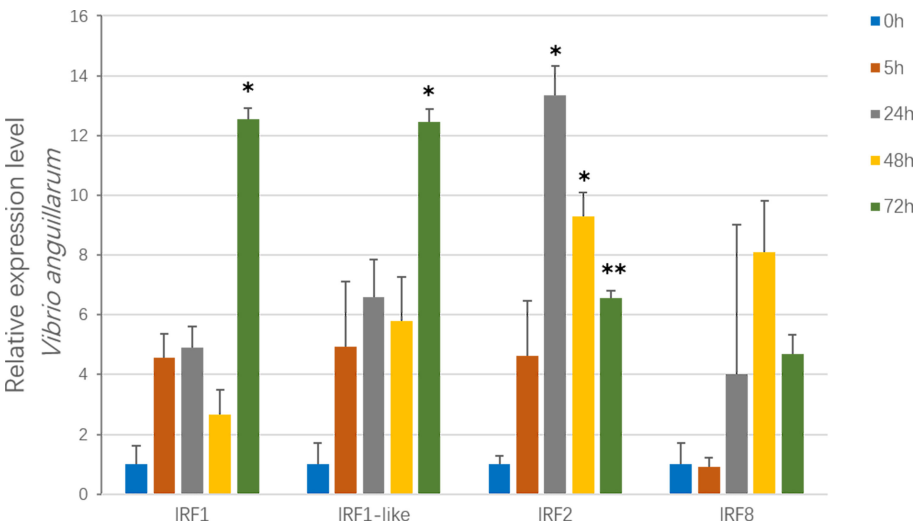

FIGURE 5 | Expression of *CflRF* genes after challenge with the *V. anguillarum*. Vertical bars represent the mean ± S.E. (*N* = 10). The asterisks indicate significant differences (*$p < 0.05$, **$p < 0.01$).

h) after infection (**Figure 5**). Overall, three *CflRFs* from the IRF-1 subfamily (*CflRF1*, *CflRF1-like*, and *CflRF2*) were significantly upregulated. Notably, *CflRF2* showed the most sensitive responses, which showed significant upregulation after 24-h infection (>13-fold, $p < 0.05$) and sustained at a significantly higher expression level till 72 h. Moreover, the expressions of *CflRF1* and *CflRF1-like* were significantly upregulated at 72 h post-infection (>12-fold, $p < 0.05$), while *CflRF8* only showed mild upregulated tendency after 24-h infection (4- to 8-fold).

3.4 Subcellular Localizations of *CflRF1*, *CflRF1-Like*, and *CflRF2*

Subcellular localization prediction showed that *Cf*IRF1, *Cf*IRF1-like, and *Cf*IRF2 all possess nucleus localization (**Table 3**). Furthermore, ^{163}RSRRRKKPCVKKE^{175} in *Cf*IRF1 was predicted as a nucleus localization signal with a high score (score: 9.5), further suggesting that *Cf*IRF1 was a nuclear-localized protein. HEK293T cells were transfected with plasmids encoding pEGFP-tagged *CflRF1*, *CflRF1-like*, or

TABLE 3 | Summary of the predicted subcellular localization of *CfIRF1, CfIRF1-like and CfIRF2*.

Name	Euk-mPLoc 2.0	WoLF PSORTⅡ	SLP-Local
IRF1	nucl. cyto.	nucl. nucl-cyto. cyto	nucl. cyto.
IRF1-like	nucl.	nucl.	nucl. cyto.
IRF2	nucl.	nucl.	nucl. cyto.

CfIRF2 to investigate their subcellular localization. The immunofluorescence image analysis showed that recombinant *Cf*IRF1-GFP protein was located in the nucleus, consisting of its subcellular localization prediction and the NLS prediction. Unlike *Cf*IRF1, the fluorescent signal of *Cf*IRF1-like and *Cf*IRF2 recombinant proteins was distributed in both nuclei and cytoplasm (**Figure 6**). Thus, the divergence of *CfIRFs* by subcellular localization tentatively suggested that these three *CfIRFs* may be involved with different cellular functions.

Dual-Luciferase Reporter Assays

To analyze the transcription activities of *Cf*IRF1, *Cf*IRF1-like, and *Cf*IRF2, dual-luciferase reporter assays were performed in HEK293T cells. As control, pcDNA3.1-IRFs were co-transfected with pGL3-basic, and it did not show any effect on the ISRE reporter. By using pISRE-Luc, after co-transfection with pcDNA3.1-IRF1, pcDNA3.1-IRF1-like, and pcDNA3.1-IRF2, the luciferase activity of the ISRE reporter was significantly upregulated (**Figure 7**), suggesting their obvious transcriptional activation on

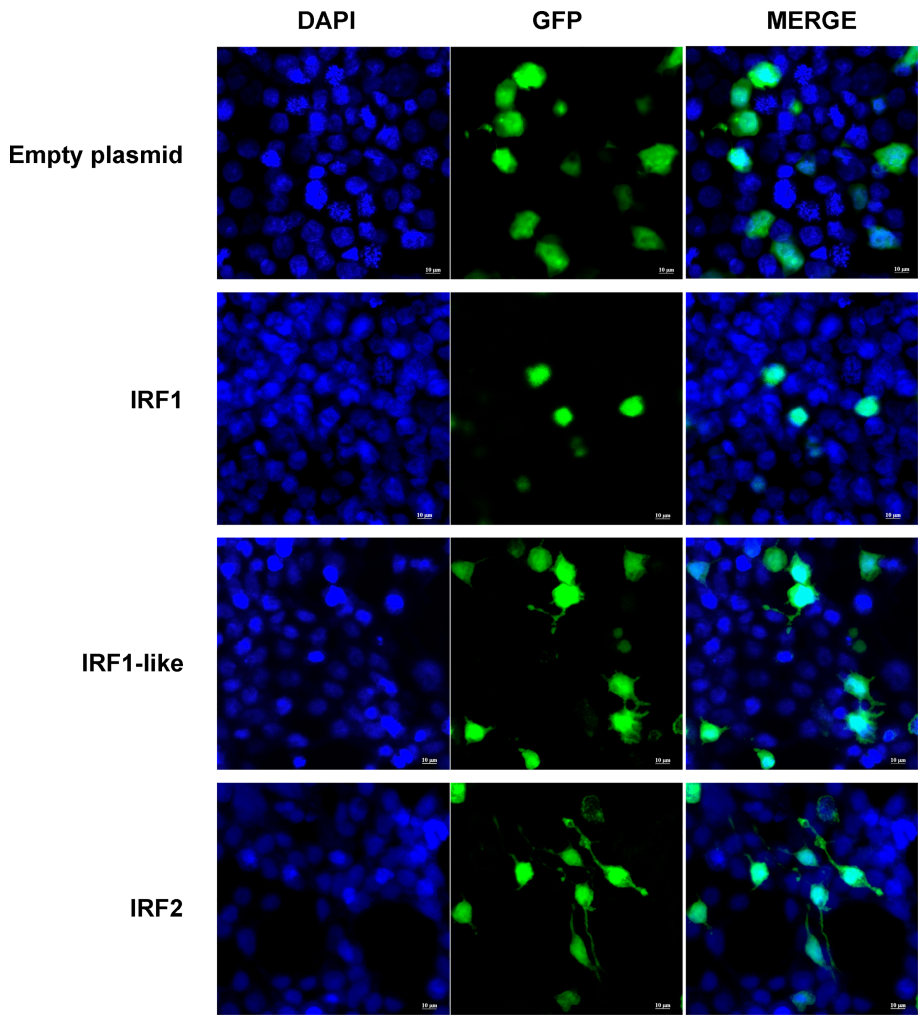

FIGURE 6 | Subcellular localization of *CfIRF* genes in HEK293T cells. Immunohistochemistry was performed to analyze the expression of *Cf*IRF in hemocytes. The left-hand panels depict DAPI staining, the middle panels depict GFP staining, and the right-hand panels depict merged DAPI/GFP staining. The upper panels depict localization of the GFP negative control, and the lower panels depict localization of the *Cf*IRF-GFP proteins.

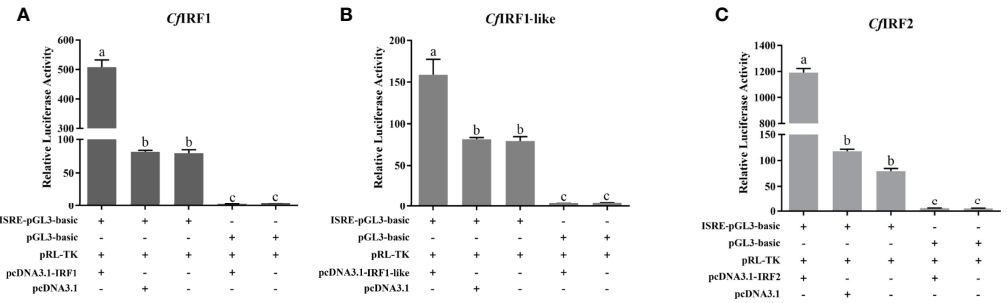

FIGURE 7 | Relative luciferase activity of expression *Cf*IRF plasmids on the luciferase reporter gene pISRE-Luc in HEK293T cells. **(A)** Relative luciferase activity of expression *Cf*IRF1 plasmids. **(B)** Relative luciferase activity of expression *Cf*IRF1-like plasmids. **(C)** Relative luciferase activity of expression *Cf*IRF2 plasmids. All of the groups were co-transfected with pRL-TK as internal reference. Vertical bars represent the mean ± S.E. ($N = 3$). p-values are calculated by one-way analysis of variance (ANOVA) in SPSS software. Different letters indicate significant differences ($p < 0.05$).

interferon-stimulated response element. These results indicated that these *CfIRFs* could activate the expression of ISRE luciferase reporter genes, suggesting that scallop *IRFs* can specifically activate interferon signaling.

4 DISCUSSION

The innate immune system is the first line of defense against the invasion of pathogens. *IRFs* are key transcription factors involved in type I IFN responses, playing a pivotal role in the regulation of interferon activity (Kimura et al., 1994). In the present study, we successfully identified four *IRF* genes in a bivalve mollusc *C. farreri*, namely, *CfIRF1*, *CfIRF1-like*, *CfIRF2*, and *CfIRF8*. All four *Cf*IRF proteins have a single well-conserved N-terminal helix-turn-helix IRF superfamily domain (also named as DBD). Through the motif of Trp repeats, the conserved DBD domain in vertebrate was proved to recognize and bind DNA sequence containing 5′-GAAA-3′ tetranucleotide as a determinant of interferon regulation (Escalante et al., 1998; Mamane et al., 1999). Consistently, we found well-conserved Trp repeats inside the DBD domain of scallop IRFs, suggesting their similar binding activities with vertebrate IRFs. Moreover, *Cf*IRF8 was predicted to contain an IRF-associated domain (IAD) at the C-terminus, which has been reported to mediate the formation of homologous dimers or the coupling with other transcription factors to form heterodimers (Honda and Taniguchi, 2006; Yanai et al., 2012). According to the phylogenetic analysis, *Cf*IRF1, *Cf*IRF1-like, and *Cf*IRF2 were clustered into the IRF-1 subfamily, and *Cf*IRF8 was clustered into the IRF-4 subfamily.

Spatiotemporal expression levels of *CfIRF1* and *CfIRF2* were found to be obviously higher than *CfIRF1-like* and *CfIRF8*, suggesting the initial requirement for them during development as well as in adult tissues. Correlation analysis showed that *CfIRF1* and *CfIRF2* have a significantly positive correlation during development as well as in adult tissues, indicating that they may be functionally synergistic. *CfIRF1* and *CfIRF2* were highly expressed after the D-shape veliger formation, especially in creeping larvae and juvenile, the key stage that multi-organs began to developed. In adult tissues, high expression of both *CfIRF1* and *CfIRF2* was detected in multiple immune-related tissues, such as hemolymph, hepatopancreas, gill, and mantle (Fan et al., 2018; Lu et al., 2018; Gan et al., 2020), indicating the crucial roles of these genes in the host immune response. Hemocytes, one of the major immune tissues in molluscs, has been reported as the main site where the recognition and elimination of bacterial pathogens occurs (Zhou et al., 2015). Hepatopancreas is the main digestive tissue; thus, it needs to cope with the pathogens incoming with the ingested algae. Furthermore, hepatopancreas was also proved as a toxin-rich tissue, acting as major "centers" for toxin accumulation in *C. farreri* (Li et al., 2017), which may also induce immune responses. The gill and mantle are constantly in contact with the external environment *via* water filtering and serve as the front line of the host defense (Lee et al., 2013). The tissue expression patterns of *IRF* genes have been widely characterized in various species, and high expression has been detected in multiple immune-related tissues. For example, high expression levels of *CgIRF-2* were detected in *C. gigas* hemocytes, hepatopancreas, and mantle, and *LcIRF* from *Larimichthys crocea* were highly expressed in hemocytes, gill, and spleen (Lu et al., 2018; Guan et al., 2020). Taken together, the high expression levels of *IRFs* in these immune-related tissues may suggest their conservative roles in scallop innate immune response.

To provide insights into the functions of *CfIRF*s during the innate immune response, one of the major bacterial pathogens, *V. anguillarum*, was employed to perform the infection experiment and the responses of *CfIRF*s in hemocytes were investigated. Only *CfIRF*s from the IRF-1 subfamily (*CfIRF1*, *CfIRF1-like*, and *CfIRF2*) were found to be increased significantly post-infection, which confirmed the involvement of these *CfIRF*s in the innate immune response against bacterial invasion. In comparison with *CfIRF1* and *CfIRF1-like*, *CfIRF2* showed the most sensitive response. Subcellular localization prediction showed that *Cf*IRF1 possessed an NLS in its DNA-binding domain, and subcellular localization analysis confirmed that it mainly translocated in the nucleus; meantime, *Cf*IRF1-like and *Cf*IRF2 were expressed in both nucleus and cytoplasm. Similarly,

IRFs have shown the divergence in subcellular localization in some other species. For example, in marine bivalves *C. gigas* and *P. fucata*, researchers found that *Cg*IRF-1 and *Cg*IRF-2 proteins were both primarily expressed in nucleus and cytoplasm (Huang et al., 2017; Lu et al., 2018), and *Pf*IRF-2 was located in the nucleus (Huang et al., 2013). Previous studies showed that most species only have one *IRF1* gene, while in *C. gigas*, there are two *IRF1* members, named *Cg*IRF1a and *Cg*IRF1b (Fan et al., 2018). They found that *Cg*IRF1a significantly activated the ISRE reporter gene, whereas *Cg*IRF1b did not. According to our data, both *CfIRF1* and *CfIRF1-like* showed significant responses against bacterial infection, and they both could activate ISRE significantly; however, they have different functional domains, spatiotemporal expression patterns, and subcellular localizations, suggesting that functional differences may exist for *CfIRF1* and *CfIRF1-like*.

Many studies have shown that *IRFs* are typical interferon-stimulated genes in mammals, birds, and fish (Andrea et al., 2002; Liu et al., 2018; Zhu et al., 2020). Among *IRF*s, *IRF1* and *IRF2* were originally characterized as transcriptional regulators of type I IFNs and IFN-stimulated genes (ISGs), which played an important role in the antiviral immune response (Miyamoto et al., 1988a; Harada et al., 1989b). Our findings from the dual-luciferase reporter gene assays showed that *Cf*IRF1, *Cf*IRF1-like, and *Cf*IRF2 could significantly activate the expression of the IRSE reporter gene, revealing obvious transcriptional activation on interferon-stimulated response element. Similar to their responses against *V. anguillarum*, in comparison with *Cf*IRF1 and *Cf*IRF1-like, *Cf*IRF2 showed the most significant activation effects, which may contribute to its most sensitive responses to bacterial infection. Similar results have been shown in other bivalves; for example, the recombinant *Cg*IRF-1 or *Pf*IRF-2 exhibited the activity to bind ISRE *in vitro*. Previous studies in vertebrates have shown that this conserved binding and activation of ISRE is mainly attributable to the DBD domain in IRFs. It was reported that the DBD in vertebrate IRFs could form a helix-turn-helix domain and bind to the core DNA sequence GAAA in the IFN-stimulated response element (ISRE, A/GNGAAANNGAAACT) (Escalante et al., 1998). For instance, IRF-1 from zebrafish (*Dr*IRF-1) could bind to ISRE/*IRF*-E motifs within the IFN promoters through the DBD helix α3 to induce its transcription (Feng et al., 2015), while compared with the extensive knowledge of *IRF*s in vertebrates, the possible mechanisms of these bivalve *IRF*s binding and activating IFN system need further investigation.

5 CONCLUSION

In conclusion, we identified four *IRF* genes in Zhikong scallop: *CfIRF1*, *CfIRF1-like CfIRF2*, and *CfIRF8*. *Cf*IRFs contained highly conserved N-terminal DNA-binding domain and variable C-terminal regulatory domain, and were constitutively expressed during development as well as in adult tissues, especially in hepatopancreas, hemolymph, gill, and mantle. Furthermore, we determined that *CfIRF1*, *CfIRF1-like*, and *CfIRF2* genes played pivotal roles in the innate immune defense against bacterial infection, and their encoding proteins could translocate into nucleus. Functionally, *Cf*IRF1, *Cf*IRF1-like, and *Cf*IRF2 had been proven to induce a strong activation of ISRE promoters. Moreover, in comparison with *CfIRF1* and *CfIRF1-like*, *CfIRF2* showed the most sensitive responses in coping with *V. anguillarum*, and consistently, *Cf*IRF2 exhibited the most significant activation on ISRE. Our data would provide valuable information for further investigations into the evolution and functional characterization of *IRFs* in bivalve molluscs.

DATA AVAILABILITY STATEMENT

The datasets presented in this study can be found in online repositories. The names of the repository/repositories and accession number(s) can be found in the article/**Supplementary Material**.

ETHICS STATEMENT

This animal study was reviewed and approved by the Ocean University of China Institutional Animal Care and Use Committee.

AUTHOR CONTRIBUTIONS

SL and JH conceived and designed the study. NH and XZ performed the experiments. FS and XC participated in data analysis. NH, SL, JH, LZ, SW, and ZB wrote the manuscript. All authors contributed to the article and approved the submitted version.

FUNDING

We acknowledge the grant support from Project of Sanya Yazhouwan Science and Technology City Management Foundation (SKJC-KJ-2019KY01), Key R&D Project of Shandong Province (2020ZLYS10, 2021ZLGX03), National Key R&D Project (2021YFD1200805) and China Agriculture Research System of MOF and MARA.

SUPPLEMENTARY MATERIALS

The Supplementary Material for this article can be found online at: https://www.frontiersin.org/articles/10.3389/fmars.2022.865707/full#supplementary-material.

Supplementary Figure 1 | The phylogenetic tree was constructed based on the protein sequences of *Cf*IRFs, in addition to those of other species. FastTree 2.0.0 was used to construct the phylogenetic tree by the maximum-likelihood (ML) analyses. Solid circle: vertebrate IRFs, Hollow circle: invertebrate IRFs, Red hollow circle: *Cf*IRFs.

Supplementary Figure 2 | The expression profiles in different developmental stages and adult tissues. **(A)**. Expression levels of *CfIRFs* in different embryonic and larval stages. **(B)**. Expression levels of *CfIRFs* in adult tissues. Vertical bars represent the mean ± S.E. (N=3). *P* values are calculated by one-way analysis of variance (ANOVA) in SPSS software. Different letters indicate significant differences ($P < 0.05$).

REFERENCES

Anda, S. D., Gómez-Martín, D., Díaz-Zamudio, M., and Alcocer-Varela, J. (2012). Interferon Regulatory Factors: Beyond the Antiviral Response and Their Link to the Development of Autoimmune Pathology. *Autoimmun. Rev.* 11, 98–103. doi: 10.1016/j.autrev.2011.08.006

Andrea, K., Mario, K., Katharina, S., Hansj, R. H., and Mueller, P. P. (2002). Activities of IRF-1. *J. Interferon Cytokine Res.* 22, 5–14. doi: 10.1089/107999002753452610

Azumi, K., Sabau, S. V., Fujie, M., Usami, T., Koyanagi, R., Kawashima, T., et al. (2007). Gene Expression Profile During the Life Cycle of the Urochordate Ciona Intestinalis. *Dev. Biol.* 308, 572–582. doi: 10.1016/j.ydbio.2007.05.022

Barnes, B. J., Moore, P. A., and Pitha, P. M. (2001). Virus-Specific Activation of a Novel Interferon Regulatory Factor *IRF-5*, Results in the Induction of Distinct Interferon α Genes. *J. Biol. Chem.* 276, 23382–23390. doi: 10.1074/jbc.M101216200

Barnes, B. J., Richards, J., Mancl, M., Hanash, S., and Pitha, P. M. (2004). Global and Distinct Targets of *IRF-5* and *IRF-7* During Innate Response to Viral Infection. *J. Biol. Chem.* 279, 45194–45207. doi: 10.1074/jbc.M400726200

Cavlar, T., Ablasser, A., and Hornung, V. (2012). Induction of Type I IFNs by Intracellular DNA-Sensing Pathways. *Immunol. Cell Biol.* 90, 474–482. doi: 10.1038/icb.2012.11

Costa, M. M., Prado-Alvarez, M., Gestal, C., Li, H., Roch, P., Novoa, B., et al. (2009). Functional and Molecular Immune Response of Mediterranean Mussel (*Mytilus Galloprovincialis*) Haemocytes Against Pathogen-Associated Molecular Patterns and Bacteria. *Fish Shellfish Immunol.* 26, 515–523. doi: 10.1016/j.fsi.2009.02.001

Davidson, E. H., and Cameron, R. A. (2006). Arguments for Sequencing the Genome of the Sea Urchin *Strongylocentrotus Purpuratus*. *Bethesda*, MD, USA: National Human Genome Research Institute. Available at: http://www.genome.gov/Pages/Research/Sequencing/SeqProposals/SeaUrchin_Genome.pdf.

Escalante, C. R., Yie, J., Thanos, D., and Aggarwal, A. K. (1998). Structure of *IRF-1* With Bound DNA Reveals Determinants of Interferon Regulation. *Nature* 391, 103. doi: 10.1038/34224

Fan, M., Yue, L., Zhou, Y., He, Z., Li, J., Yang, Z., et al. (2018). Structural and Functional Analysis of Interferon Regulatory Factors (*IRFs*) Reveals a Novel Regulatory Model in an Invertebrate, *Crassostrea Gigas*. *Dev. Comp. Immunol.* 89, 14–22. doi: 10.1016/j.dci.2018.07.027

Feng, L., Yu, Q., Xue, L., Ning, X., and Ba O, Z. (2013). Identification of Reference Genes for qRT-PCR Analysis in Yesso Scallop *Patinopecten Yessoensis*. *PloS One* 8, e75609. doi: 10.1371/journal.pone.0075609

Feng, H., Zhang, Q.-Y., Yi-Bing, G., Jian-Fang, Z., and Qi-, M. (2015). Zebrafish *IRF1* Regulates IFN Antiviral Response Through Binding to IFN Phi 1 and IFN Phi 3 Promoters Downstream of MyD88 Signaling. *J. Immunol.* 194, 1225–1238. doi: 10.4049/jimmunol.1402415

Gan, Z., Cheng, J., Hou, J., Xia, L., Lu, Y., and Nie, P. (2020). Molecular and Functional Characterization of Interferon Regulatory Factor 1 (*IRF1*) in Amphibian *Xenopus Tropicalis* - ScienceDirect. *Int. J. Biol. Macromol.* 167, 719–725. doi: 10.1016/j.ijbiomac.2020.11.217

Gao, Q., Song, L., Ni, D., Wu, L., Zhang, H., and Chang, Y. (2007). cDNA Cloning and mRNA Expression of Heat Shock Protein 90 Gene in the Haemocytes of Zhikong Scallop *Chlamys Farreri*. *Comp. Biochem. Physiol. Part B Biochem. Mol. Biol.* 147, 704–715. doi: 10.1016/j.cbpb.2007.04.010

Green, T. J., Raftos, D., Speck, P., and Montagnani, C. (2015). Antiviral Immunity in Marine Molluscs. *J. Gen. Virol.* 96, 749–759. doi: 10.1099/jgv.0.000244

Guan, Y., Chen, X., Luo, T., Ao, J., and Chen, X. (2020). Molecular Characterization of the Interferon Regulatory Factor (*IRF*) Family and Functional Analysis of *IRF11* in the Large Yellow Croaker (*Larimichthys Crocea*). *Fish Shellfish Immunol.* 107, 218–229. doi: 10.1016/j.fsi.2020.10.001

Harada, H., Fujita, T., Miyamoto, M., Kimura, Y., Maruyama, M., Furia, A., et al. (1989). Structurally Similar But Functionally Distinct Factors, *IRF-1* and *IRF-2*, Bind to the Same Regulatory Elements of IFN and IFN-Inducible Genes. *Cell* 58, 729–739. doi: 10.1016/0092-8674(89)90107-4

Hatada, S., Kinoshita, M., Takahashi, S., Nishihara, R., Sakumoto, H., Fukui, A., et al. (1997). An Interferon Regulatory Factor-Related Gene (*xIRF-6*) Is Expressed in the Posterior Mesoderm During the Early Development of *Xenopus Laevis*. *Gene* 203, 183–188. doi: 10.1016/S0378-1119(97)00512-X

Honda, K., and Taniguchi, T. (2006). *IRFs*: Master Regulators of Signalling by Toll-Like Receptors and Cytosolic Pattern-Recognition Receptors. *Nat. Rev. Immunol.* 6, 644–658. doi: 10.1038/nri1900

Huang, X. D., Liu, W. G., Wang, Q., Zhao, M., Wu, S. Z., Guan, Y. Y., et al. (2013). Molecular Characterization of Interferon Regulatory Factor 2 (*IRF-2*) Homolog in Pearl Oyster *Pinctada Fucata*. *Fish Shellfish Immunol.* 34, 1279–1286. doi: 10.1016/j.fsi.2013.02.003

Huang, S., Yuan, S., Guo, L., Yu, Y., Li, J., Wu, T., et al. (2008). Genomic Analysis of the Immune Gene Repertoire of Amphioxus Reveals Extraordinary Innate Complexity and Diversity. *Genome Res.* 18, 1112–1126. doi: 10.1101/gr.069674.107

Huang, B., Zhang, L., Du, Y., Xu, F., Li, L., and Zhang, G. (2017). Characterization of the Mollusc RIG-I/MAVS Pathway Reveals an Archaic Antiviral Signalling Framework in Invertebrates. *Sci. Rep.* 7, 8217. doi: 10.1038/s41598-017-08566-x

Huang, B., Zhi, T. Q., Zhen, X., and Nie, P. (2010). Global Characterization of Interferon Regulatory Factor (*IRF*) Genes in Vertebrates: Glimpse of the Diversification in Evolution. *BMC Immunol.* 11, 22. doi: 10.1186/1471-2172-11-22

Hu, X., Bao, Z., Hu, J., Shao, M., and Huang, X. (2010). Cloning and Characterization of Tryptophan 2,3-Dioxygenase Gene of Zhikong Scallop *Chlamys Farreri* (Jones and Preston 1904). *Aquac. Res.* 37, 1187–1194. doi: 10.1111/j.1365-2109.2006.01546.x

Ikushima, H., Negishi, H., and Taniguchi, T. (2013). The *IRF* Family Transcription Factors at the Interface of Innate and Adaptive Immune Responses. *Cold Spring Harb. Symp. Quant. Biol.* 78, 105–116. doi: 10.1101/sqb.2013.78.020321

Inkpen, S. M., Solbakken, M. H., Jentoft, S., Eslamloo, K., and Rise, M. L. (2019). Full Characterization and Transcript Expression Profiling of the Interferon Regulatory Factor (*IRF*) Gene Family in Atlantic Cod (*Gadus Morhua*). *Dev. Comp. Immunol.* 98, 166–180. doi: 10.1016/j.dci.2019.03.015

Kimura, T., Nakayama, K., Penninger, J., Kitagawa, M., and Mak, T. W. (1994). Involvement of the *IRF-1* Transcription Factor in Antiviral Responses to Interferons. *Science* 264, 1921–1924. doi: 10.1126/science.8009222

Lee, Y., Wickamarachchi, W. D. N., Whang, I., Oh, M., Umasuthan, N., De Zoysa, M., et al. (2013). Immune Response-Related Gene Expression Profile of a Novel Molluscan Iκb Protein Member From Manila Clam (*Ruditapes Philippinarum*). *Mol. Biol. Rep.* 40, 1519–1527. doi: 10.1007/s11033-012-2196-5

Lehtonen, A., Veckman, V., Nikula, T., Lahesmaa, R., Kinnunen, L., Matikainen, S., et al. (2005). Differential Expression of IFN Regulatory Factor 4 Gene in Human Monocyte-Derived Dendritic Cells and Macrophages. *J. Immunol.* 175, 6570. doi: 10.4049/jimmunol.175.10.6570

Lelong, C., Guo, X., Sourdaine, P., Yan, HE, Jouaux, A., and Mathieu, M. (2015). Transcriptome Analysis Reveals Strong and Complex Antiviral Response in a Mollusc. *Fish Shellfish Immunol.* 46 (1), 131–144.

Li, C., Li, H., Chen, Y., Chen, Y., Sheng, W., Weng, S. P., et al. (2015). Activation of Vago by Interferon Regulatory Factor (*IRF*) Suggests an Interferon System-Like Antiviral Mechanism in Shrimp. *Sci. Rep.* 5 (1), 1–13. doi: 10.1038/srep15078

Li, J., Li, L., Zhang, S., and Zhang, G. (2010). Cloning, Genomic Structure, and Expression Analysis of Peroxiredoxin V From Bay Scallop Argopecten Irradians. *Fish Shellfish Immunol.* 30, 309–316. doi: 10.1016/j.fsi.2010.11.011

Li, Y., Sun, X., Hu, X., Xun, X., Zhang, J., Guo, X., et al. (2017). Scallop Genome Reveals Molecular Adaptations to Semi-Sessile Life and Neurotoxins. *Nat. Commun.* 8, 1721. doi: 10.1038/s41467-017-01927-0

Liu, Y., Cheng, Y., Shan, W., Ma, J., Wang, H., Sun, J., et al. (2018). Chicken Interferon Regulatory Factor 1 (*IRF1*) Involved in Antiviral Innate Immunity

via Regulating IFN-β Production. *Dev. Comp. Immunol.* 88, 77–82. doi: 10.1016/j.dci.2018.07.003

Liu, S., Jiang, X., Hu, X., Gong, J., Hwang, H., and Mai, K. (2004). Effects of Temperature on non-Specific Immune Parameters in Two Scallop Species: Argopecten Irradians (Lamarck 1819) and *Chlamys Farreri* (Jones & Preston 1904). *Aquac. Res.* 35 (7), 678–682. doi: 10.1111/j.1365-2109.2004.01065.x

Loker, E. S., Adema, C. M., Zhang, S. M., and Kepler, T. B. (2010). Invertebrate Immune Systems–Not Homogeneous, Not Simple, Not Well Understood. *Immunol. Rev.* 198, 10–24. doi: 10.1111/j.0105-2896.2004.0117.x

Lu, R. (2008). Interferon Regulatory Factor 4 and 8 in B-Cell Development. *Trends Immunol.* 29, 487–492. doi: 10.1016/j.it.2008.07.006

Lu, M., Yang, C., Li, M., Yi, Q., Lu, G., Wu, Y., et al. (2018). A Conserved Interferon Regulation Factor 1 (*IRF-1*) From Pacific Oyster *Crassostrea Gigas* Functioned as an Activator of IFN Pathway. *Fish Shellfish Immunol.* 76, 68–77. doi: 10.1016/j.fsi.2018.02.024

Mamane, Y., Heylbroeck, C., Génin, P., Algarté, M., Servant, M. J., Lepage, C., et al. (1999). Interferon Regulatory Factors: The Next Generation. *Gene* 237, 1–14. doi: 10.1016/S0378-1119(99)00262-0

Marchler-Bauer, A., Lu, S., Anderson, J. B., Chitsaz, F., and Bryant, S. H. (2011). CDD: A Conserved Domain Database for the Functional Annotation of Proteins. *Nucleic Acids Res.* 39, D225–D229. doi: 10.1093/nar/gkq1189

Marié, I., Durbin, J. E., and Levy, D. E. (1998). Differential Viral Induction of Distinct Interferon-Alpha Genes by Positive Feedback Through Interferon Regulatory Factor-7. *EMBO J.* 17 (22), 6660–6669. doi: 10.1093/emboj/17.22.6660

Meraro, D., Gleit-Kielmanowicz, M., Hauser, H., and Levi, B. Z. (2002). IFN-Stimulated Gene 15 Is Synergistically Activated Through Interactions Between the Myelocyte/Lymphocyte-Specific Transcription Factors, PU.1, IFN Regulatory Factor-8/IFN Consensus Sequence Binding Protein, and IFN Regulatory Factor-4: Characterization of. *J. Immunol.* 168, 6224–6231. doi: 10.4049/jimmunol.168.12.6224

Miyamoto, M., Fujita, T., Kimura, Y., Maruyama, M., Harada, H., Sudo, Y., et al. (1988). Regulated Expression of a Gene Encoding a Nuclear Factor, *IRF-1*, That Specifically Binds to IFN-Beta Gene Regulatory Elements. *Cell* 54, 903–913. doi: 10.1016/S0092-8674(88)91307-4

Nehyba, J., Hrdlicková, R., and Bose, H. R. (2009). Dynamic Evolution of Immune System Regulators: The History of the Interferon Regulatory Factor Family. *Mol. Biol. Evol.* 26, 2539–2550. doi: 10.1093/molbev/msp167

Nehyba, J., Hrdlicková, R., Burnside, J., and Bose, H. R. (2002). A Novel Interferon Regulatory Factor (*IRF*), *IRF-10*, Has a Unique Role in Immune Defense and Is Induced by the V-Rel Oncoprotein. *Mol. Cell. Biol.* 22, 3942–3957. doi: 10.1128/MCB.22.11.3942-3957.2002

Pfaffl, M. W., Horgan, G. W., and Leo, D. (2002). Relative Expression Software Tool (REST©) for Group-Wise Comparison and Statistical Analysis of Relative Expression Results in Real-Time PCR. *Nucleic Acids Res.* 30 (9), e36-e36. doi: 10.1093/nar/30.9.e36

Qiu, L., Song, L., Xu, W., Ni, D., and Yu, Y. (2007). Molecular Cloning and Expression of a Toll Receptor Gene Homologue From Zhikong Scallop, *Chlamys Farreri*. *Fish Shellfish Immunol.* 22, 451–466. doi: 10.1016/j.fsi.2006.05.003

Ragab, A., Buechling, T., Gesellchen, V., Spirohn, K., Boettcher, A. L., and Boutros, M. (2014). *Drosophila* Ras/MAPK Signalling Regulates Innate Immune Responses in Immune and Intestinal Stem Cells. *EMBO J.* 30, 1123–1136. doi: 10.1038/emboj.2011.4

Sato, M., Hata, N., Asagiri, M., Nakaya, T., and Tanaka, N. (1999). Positive Feedback Regulation of Type I IFN Genes by the IFN-Inducible Transcription Factor *IRF-7*. *FEBS Lett.* 441, 106–110. doi: 10.1016/S0014-5793(98)01514-2

Savitsky, D., Tamura, T., Yanai, H., and Taniguchi, T. (2010). Regulation of Immunity and Oncogenesis by the *IRF* Transcription Factor Family. *Cancer Immunol. Immunother.* 59, 489–510. doi: 10.1007/s00262-009-0804-6

Sudhir, K., Glen, S., Li, M., Christina, K., and Koichiro, T. (2018). MEGA X: Molecular Evolutionary Genetics Analysis Across Computing Platforms. *Mol. Biol. Evol.* 35 (6), 1547.

Tamura, T., Yanai, H., Savitsky, D., and Taniguchi, T. (2008). The *IRF* Family Transcription Factors in Immunity and Oncogenesis. *Annu. Rev. Immunol.* 26, 535–584. doi: 10.1146/annurev.immunol.26.021607.090400

Taniguchi, T. T. (2006). Type I Inteferon Gene Induction by the Interferon Regulatory Factor Family of Transcription Factors. *Immunity* 25 (3), 349–360.

Teng, W. M., Li, W. J., Zhang, M., Yu, Z. A., and Fu, C. D. (2012). Isolation, Identification and Pathogenicity of Vibrio Chagasii From *Patinopecten Yessoensis*. *J. Fish. China* 36, 937.

Thi, H. D., Olga, C., Arndt, V. H., Quang, M. B., and Sy, V. L. (2017). UFBoot2: Improving the Ultrafast Bootstrap Approximation. *Mol. Biol. Evol.* 35 (2), 518–522.

Weiqi, H., Chunliu, Z., Hao, W., Elizabeth, H., and Elizabeth, A. (2008). The Interferon Consensus Sequence-Binding Protein (ICSBP/IRF8) RepressesPTPN13Gene Transcription in Differentiating Myeloid Cells. *J. Biol. Chem.* 283 (12), 7921–7935.

Xuan, M., Yan, X., Liu, X., and Xu, T. (2020). *IRF1* Negatively Regulates NF-κb Signaling by Targeting MyD88 for Degradation in Teleost Fish. *Dev. Comp. Immunol.* 110, 103709. doi: 10.1016/j.dci.2020.103709

Yanai, H., Negishi, H., and Taniguchi, T. (2012). The *IRF* Family of Transcription Factors: Inception, Impact and Implications in Oncogenesis. *Oncoimmunology* 1, 1376. doi: 10.4161/onci.22475

Zhang, R., Liu, R., Wang, W., Xin, L., Wang, L., Li, C., et al. (2015). Identification and Functional Analysis of a Novel IFN-Like Protein (CgIFNLP) in *Crassostrea Gigas*. *Fish Shellfish Immunol.* 44 (2), 547–554. doi: 10.1016/j.fsi.2015.03.015

Zhan, F. B., Liu, H., Lai, R. F., Jakovli, I., and Wang, W. M. (2016). Expression and Functional Characterization of Interferon Regulatory Factors (*Irf2*, *Irf7* and *Irf9*) in the Blunt Snout Bream (*Megalobrama Amblycephala*). *Dev. Comp. Immunol.* 67, 239–248. doi: 10.1016/j.dci.2016.09.014

Zhi, Z., Wang, L., Shi, X., Zhang, H., Yang, G., Wang, M., et al. (2011). The Modulation of Catecholamines to the Immune Response Against Bacteria Vibrio Anguillarum Challenge in Scallop *Chlamys Farreri*. *Fish Shellfish Immunol.* 31, 1065–1071. doi: 10.1016/j.fsi.2011.09.009

Zhou, S.-M., Liu, S., Li, M., Yang, N., and Tao, Z. (2015). First Description and Expression Analysis of Tumor Necrosis Factor Receptor-Associated Factor 6 (*TRAF6*) From the Swimming Crab, *Portunus Trituberculatus*. *Fish Shellfish Immunol.* 45 (2), 205–210. doi: 10.1016/j.fsi.2015.04.005

Zhu, K. C., Zhang, N., Liu, B. S., Guo, L., Guo, H. Y., Jiang, S. G., et al. (2020). Functional Analysis of *IRF1* Reveals Its Role in the Activation of the Type I IFN Pathway in Golden Pompano, *Trachinotus Ovatus* (Linnaeus 1758). *Int. J. Mol. Sci.* 21 (7), 2652. doi: 10.3390/ijms21072652

Conflict of Interest: The authors declare that the research was conducted in the absence of any commercial or financial relationships that could be construed as a potential conflict of interest.

Publisher's Note: All claims expressed in this article are solely those of the authors and do not necessarily represent those of their affiliated organizations, or those of the publisher, the editors and the reviewers. Any product that may be evaluated in this article, or claim that may be made by its manufacturer, is not guaranteed or endorsed by the publisher.

frontiers | Frontiers in Marine Science

ORIGINAL RESEARCH
published: 26 May 2022
doi: 10.3389/fmars.2022.912409

Electroporation-Based CRISPR/Cas9 Mosaic Mutagenesis of *β-Tubulin* in the Cultured Oyster

Jiulin Chan[1,2†], *Wei Zhang*[1,2,3†], *Yue Xu*[1,2], *Yu Xue*[1,2,3] *and Linlin Zhang*[1,2,4*]

[1] Chinese Academy of Sciences (CAS) and Shandong Province Key Laboratory of Experimental Marine Biology & Center of Deep Sea Research, Center for Ocean Mega-Science, Institute of Oceanology, Chinese Academy of Sciences, Qingdao, China, [2] Laboratory for Marine Biology and Biotechnology, Qingdao National Laboratory for Marine Science and Technology, Qingdao, China, [3] College of Life Sciences, Qingdao Agricultural University, Qingdao, China, [4] College of Marine Science, University of Chinese Academy of Sciences, Beijing, China

Genome editing using clustered regularly interspaced short palindromic repeats (CRISPR)/Cas9 is enabling genetics improvement of productive traits in aquaculture. Previous studies have proven CRISPR/Cas9 to be feasible in oyster, one of the most cultured shellfish species. Here, we applied electroporation-based CRISPR/Cas9 knockout of *β-tubulin* and built a highly efficient genome editing system in *Crassostrea gigas angulate*. We identified the *β-tubulin* gene in the oyster genome and showed its spatiotemporal expression patterns by analyzing RNA-seq data and larval *in situ* hybridization. We further designed multiple highly specific guide RNAs (sgRNAs) for its coding sequences. Long fragment deletions were detected in the mutants by agarose gel electrophoresis screening and further verified by Sanger sequencing. In addition, the expression patterns of *Cgβ-tubulin* in the trochophore peritroch and intestinal cilia cells were altered in the mutants. Scanning electron microscopy represented shortened and almost complete depleted cilia at the positions of peritroch and the posterior cilium ring in *Cgβ-tubulin* mosaic knockout trochophores. Moreover, the larval swimming behavior in the mutants was detected to be significantly decreased by motility assay. These results demonstrate that *β-tubulin* is sufficient to mediate cilia development and swimming behavior in oyster larvae. By applying *Cgβ-tubulin* as a marker gene, our study established CRISPR/Cas9-mediated mosaic mutagenesis technology based on electroporation, providing an efficient tool for gene function validation in the oyster. Moreover, our research also set up an example that can be used in genetic engineering breeding and productive traits improvement in oysters and other aquaculture species.

Keywords: mosaic mutagenesis, CRISPR/Cas9, long deletion, gene editing, gene knockout, aquaculture breeding

OPEN ACCESS

Edited by:
Yuehuan Zhang,
South China Sea Institute of Oceanology (CAS), China

Reviewed by:
Xiaotong Wang,
Ludong University, China
Yingxiang Li,
University of Michigan, United States

****Correspondence:***
Linlin Zhang
linlinzhang@qdio.ac.cn

†These authors share first authorship

Specialty section:
This article was submitted to Marine Fisheries, Aquaculture and Living Resources, a section of the journal Frontiers in Marine Science

Received: *05 April 2022*
Accepted: *27 April 2022*
Published: *26 May 2022*

Citation:
Chan J, Zhang W, Xu Y, Xue Y and Zhang L (2022) Electroporation-Based CRISPR/Cas9 Mosaic Mutagenesis of β-Tubulin in the Cultured Oyster. Front. Mar. Sci. 9:912409. doi: 10.3389/fmars.2022.912409

INTRODUCTION

Aquaculture has gradually become the main source of seafood for human diets because of the high-quality animal protein (FAO, 2020). However, compared to many terrestrial livestock and crop systems, most aquaculture species' breeding is still in the early stages (Ahmed and Thompson, 2019). Previous breeding programs such as selective, cross, and marker-assisted breeding systems

have been advancing genetic improvement of economic traits, including disease resistance, nutritional values, growth quality, and reproduction (Langdon, 2006; Dove and O'Connor, 2010; Rawson et al., 2010; Wang et al., 2012; Frank-Lawale et al., 2014; Melo et al., 2016); however, the breeding processes is significantly limited by a number of constraints, such as the low heritability of the economic traits and the long generation time of the aquaculture organisms. The oyster, *Crassostrea gigas angulata* (Li et al., 2013), is a representative bivalve mollusk, which is one of the main aquaculture shellfish worldwide. It has the complex developmental stages consisting of free-swimming trochophore, veliger larva, permanently fixated juvenile, and adult after metamorphosis, and has been widely studied in developmental biology, conservation biology, and ecology (Riviere et al., 2017; Song et al., 2017; Yue et al., 2018; Chan et al., 2021). In industry, oyster breeding is still thought to be at an early stage of domestication (Houston et al., 2020). One promising approach to solving the aquaculture challenges is to use CRISPR (clustered regularly interspaced short palindromic repeats)/Cas9 system-mediated genomic editing technology (Hollenbeck and Johnston, 2018; Abe and Kuroda, 2019).

CRISPR/Cas9 system has been developed into a revolutionary technology, which allows researchers to perform a variety of genetic experiments by inducing loss-of-function and gain-of-function mutations at a precise position (Eid and Mahfouz, 2016; Momose and Concordet, 2016; Chen et al., 2017). Due to its high efficiency, this technology has been successfully applied to at least 13 aquaculture species, including the Atlantic salmon (*Salmo salar*) (Straume et al., 2020), tilapia (*Oreochromis niloticus*) (Li et al., 2014), sea bream (*Sparus aurata*) (Ohama et al., 2020), channel catfish (*Ictalurus punctatus*) (Simora et al., 2020), southern catfish (*Silurus meridionalis*) (Li et al., 2016), common carp (*Cyprinus carpio*) (Chen et al., 2019), rohu carp (*Labeo rohita*) (Chakrapani et al., 2016), grass carp (*Ctenopharyngodon idella*) (Ma et al., 2018), northern Chinese lamprey (*Lethenteron morii*) (Zu et al., 2016), rainbow trout (*Oncorhynchus mykiss*) (Cleveland et al., 2018), Olive flounder (*Paralichthys olivaceus*) (Kim et al., 2019), ridgetail white prawn (*Exopalaemon carinicauda*) (Gui et al., 2016), and oysters (*C. gigas* and *C. gigas angulata*) (Yu et al., 2019; Li et al., 2021; Jin et al., 2021), which suggests that the CRISPR system has becoming a practical gene editing tool in molluscan studies. In the studies of two cultured molluscan species, Yu et al. knockout of the target genes *myostatin* and *Twist* by microinjection of CRISPR/Cas9 complexes and one single sgRNA, which leads to 1–24 bp small indel mutation during genotyping (Yu et al., 2019). The same group recently reported microinjection-based mutation phenotypes including defective musculature and reduced mortality in the myosin essential light chain genes knockout mutants (Li et al., 2021). With small size egg and embryo at a size <50 μm in diameter, electroporation provides a more effective method for CRISPR complex delivery in the oysters. Jin et al. reported in 2021 that a pYSY-Cas9-gRNA-GFP vector plasmid was successfully delivered into the embryos of *C. gigas angulate* by electroporation (Jin et al., 2021), suggesting that electroporation-based CRISPR genome editing is a practical, time- and labor-efficient way in molluscan. Still, the sustainable development of the oyster genome editing breeding technics calls for establishing electroporation-based CRISPR/Cas9 mutagenesis tool that generates defective phenotypes.

As one of the marine benthonic organisms, oyster has a free-swimming larval stage that facilitates dispersal and locates a suitable habitat. A large number of arranged cilia is thought to be the swimming organ driving dispersal and settlement (Nielsen, 2004; Nielsen, 2005). Besides, cilia are also considered to play important roles in predator avoidance, feeding, and intestinal motility (Davenport and Yoder, 2005; Berbari et al., 2009; Pernet, 2018). *β-Tubulin* protein has been found to be expressed in cells located in the ciliary band of the trochophore of *Patella vulgata* and polychaete *Hydroides elegans* (Damen and Dictus, 1994; Arenas-Mena et al., 2007) where they contribute to cilia microtubules. However, the cilia-related functions of this gene were not known in oysters, although our recent study based on transcriptome has demonstrated that *β-tubulin* genes were highly expressed during the trochophore stage of *C. gigas* (Zhang et al., 2012).

In this study, we used *β-tubulin* as a marker gene and performed CRISPR-mediated knockout by electroporation in *C. gigas angulate*. Through direct genotyping, long fragments deletions were detected in the target gene. By *in situ* hybridization, scanning electron microscopy, and behavioral analysis, we observed mosaic mutations including defective cilia and decreased motility in the G_0 larva. These results demonstrate that *Cgβ-tubulin* is sufficient to mediate cilia development and swimming in larval oyster. Based on convincing genotypes and phenotypes in the mutants, our study established electroporation-based CRISPR/Cas9 knockout as a practical, time- and labor-efficient method for studies of gene function in the oyster. In addition, our research also provides a robust tool for genetically engineered breeding to enhance beneficial traits in oysters and other marine bivalves for aquaculture.

MATERIALS AND METHODS

Animals

The experimental adult *C. gigas angulate* from a local oyster farm in Fujian, China, were brought back to the lab under fresh condition (~10°C). Then, the oysters were acclimated for 7 days in 1 μm of filtered seawater (FSW) at 23°C (**Figure 1**). Gamete collection and *in vitro* fertilization were performed according to the method reported in a previous study (Zhang et al., 2012). After fertilization, the fertilized eggs were transferred to a 4-mm gap cuvette for electroporation. The electroporated eggs were then cultured in 1 μm FSW at 26°C (**Figure 1**). Embryos and larvae at various developmental stages (trochophore and D-shaped larvae) were collected and fixed overnight in 4% paraformaldehyde (PFA) and 2.5% glutaraldehyde at 4°C, respectively, for the subsequent characterization of knockout phenotypes based on whole mount *in situ* hybridization (WMISH) and scanning electron microscopy (SEM) (**Figure 1**).

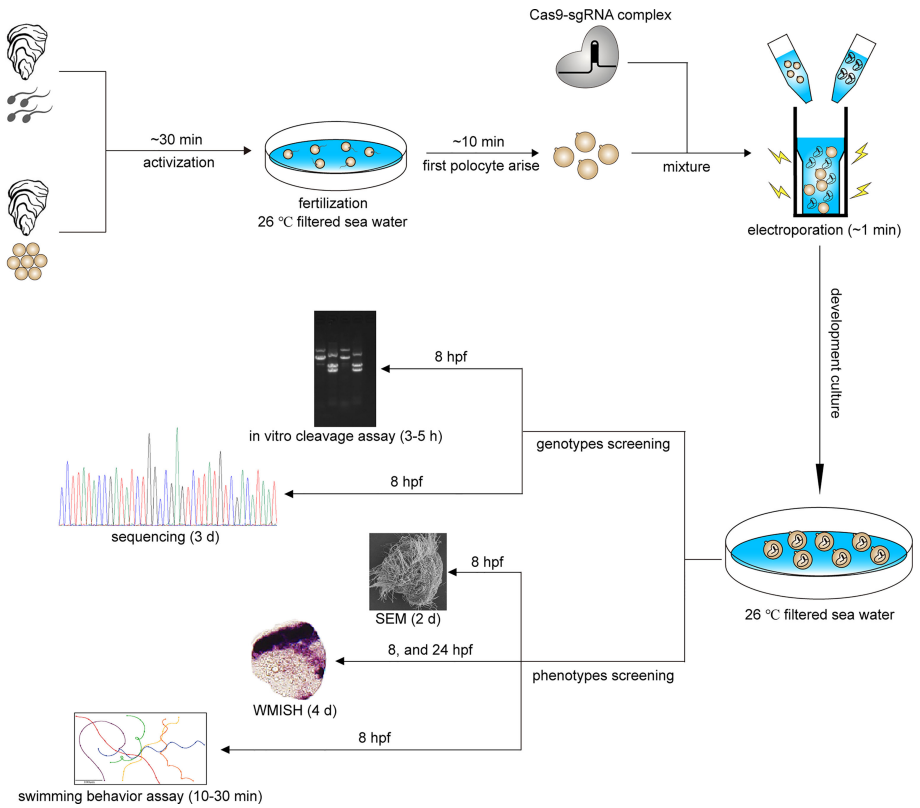

FIGURE 1 | Procedure and timeline of G_0 CRISPR/Cas9 mosaic knockout experiments in *C. gigas angulate*.

Preparation of Single-Guide RNAs and Cas9 Protein

We designed a strategy to generate two and more cut sites using multiple single-guide RNAs (sgRNAs), which induces non-homologous end joining (NHEJ) to repair the resulting gap, and finally producing long deletions flanking the target loci. We designed five sgRNAs by manually screening genome regions for GGN18NGG or N20NGG protospacer adjacent motif (PAM) sequences in the *Cgβ-tubulin* gene (**Table 1**). The DNA templates were generated by PCR with the Phusion High-Fidelity DNA Polymerase (Thermo Fisher Scientific, Waltham, USA) to synthesize *Cgβ-tubulin*-sgRNAs, using the sgRNA synthesis primers as shown in **Table 1**. Amplification was performed in a thermal cycler using a 30-s denaturation step at 95°C followed by 34 cycles of 13 s at 95°C, 15 s at 60°C, 15 s at 72°C, and a final extension at 72°C for 5 min. Then, PCR products were purified by E.Z.N.A.®Gel Extraction Kit (OMEGA). All sgRNAs were synthesized by *in vitro* transcription using the MEGAscript T7 Transcription Kit (Thermo Fisher Scientific), followed by purification using the

TABLE 1 | sgRNAs and the primers used in this study.

	Primer name	Sequence (5′–3′)
sgRNA synthesis	sgRNA1	GAAATTAATACGACTCACTATAGGGTGGTAAGTTTGAGTGTAGTTTTAGAGCTAGAAATAGC
	sgRNA2	GAAATTAATACGACTCACTATAGGCATGAAGAAGTGGAGACGGTTTTAGAGCTAGAAATAGC
	sgRNA3	GAAATTAATACGACTCACTATAGGCAGTTGTGTTTCCGACGAGTTTTAGAGCTAGAAATAGC
	sgRNA4	GAAATTAATACGACTCACTATAGGAGTAGCTGCTGTTCTTGTTCGTTTTAGAGCTAGAAATAGC
	sgRNA5	GAAATTAATACGACTCACTATAGGGTGGGATGTCACAGACGGGTTTTAGAGCTAGAAATAGC
	Rev_universal	AAAAGCACCGACTCGGTGCCACTTTTTCAAGTTGATAACGGACTAGCCTTATTTTAACTTGCTATTTCTAGCTCTAAAAC
Genotyping	GT_F0	GGAACCTATCATGGAGACTCAGACT
	GT_R0	TTCTCCCTCTTCCTCCTCAAACTC
	GT_F1	ACCCCGACAGAATCATGAACACTT
	GT_R1	CAAATCGTTCATGTTGGACTCG
Gene-specific primers	*in situs*_F	CCAGTGCGGAAACCAGATTG
	*in situs*_R	AAGAAAGCCTTACGACGGAACA

RNA clean and concentrator ™-5 Kit (ZYMO Research, California, USA; PNAbio, California, USA). Cas9 protein was purchased from PNAbio (CP01-50).

Next, the gene editing efficiencies of the five sgRNAs that we synthesized were tested by *in vitro* digestion of *Cgβ-tubulin* cDNA fragment with Cas9 protein. In brief, 250 ng of purified DNA template (*Cgβ-tubulin* PCR product) was thoroughly mixed with 250 ng each sgRNA, 500 ng Cas9 protein, 2 μl bovine serum albumin (BSA), and 2 μl restriction enzyme buffer (NEB, Ipswich, USA; TAKARA, Kusatsu, Japan) in a 20-μl reaction volume. After incubation at 37°C for 1 h, 1 μl RNaseH enzyme (TAKARA) was added to the mixture to digest the DNA template, followed by denaturation at 98°C for 5 min to terminate the reaction. Finally, the gene editing efficiency of each sgRNA was analyzed by electrophoresis on a 2% agarose gel.

Electroporation

For electroporation, one-cell stage *C. gigas angulate* embryos were collected and diluted to an appropriate concentration of about 5×10^4 cells/ml. Then, the five sgRNA mixtures (with a final concentration of 30 ng/μl), the tracing dye Lucifer Yellow (Invitrogen, cat. no. D7156) and Cas9 protein (with a final concentration of 30 ng/μl) were added to the CRISPR/Cas9 system; then, the mixture was incubated for 10 min at room temperature (20–24°C). The mixture and the fertilized eggs were then transferred into an electroporation cuvette (1 mm, BTX, Cat. No. 45-0140). Electroporation was conducted in an ECM 830 Square Wave Electroporation system (BTX) using a square wave pulse (40 V, 50 ms, 1 pulse). After electroporation, the fertilized eggs were washed in 1 μm FSW and further developed at 26°C.

Mutation Genotyping

Genomic DNA of the trochophores were extracted by proteinase K digestion method. Briefly, 20 μl of DNA extraction buffer [50 mM KCl, 10 mM Tris–HCl pH 8, 10 mM ethylene diamine tetraacetic acid (EDTA), 0.03% Nonidet P 40 (NP-40), 0.3% Tween-20, 0.5 mg/ml proteinase K] was added for digestion. Then, each individual specimen was incubated for 2 h at 55°C, followed by denaturation at 98°C for 5 min and cooling to 4°C. The DNA fragments covering the target sites and their flanking sequences were generated by PCR using the Premix ExTaq Mix (TAKARA) according to the *Cgβ-tubulin* gene-specific primers (**Table 1**). To define the genetic mutations, the amplified DNA were then cloned into pMD18-T vector (TAKARA) and sequenced on an ABI 3730 sequencer.

Evaluation of Larval Survival Rate and Motility

To calculate the survival rate, 4% PFA was used to fix the living embryos that were collected 24 h post-fertilization (hpf). We calculated the survival rate by dividing the number of normal D-shaped larvae by the total number of embryos (including normal D-shaped larvae and undeveloped and malformed larvae). To evaluate the larval motility, the trochophore of *C. gigas angulate* at 8 hpf were collected to record their swimming status under a microscope (Olympus BX53). Larval motility was then assessed by analyzing the microscopically recorded trajectory of the larvae described above. Briefly, the position of each larva was recorded in 1-s intervals during a time window of 10–11 s. Then, Adobe Illustrator software (Wood, 2016) was used to track the position of the larva, and the trajectory of the larva was simulated.

Scanning Electron Microscopy

For SEM, the trochophore individuals were collected at 8 hpf and fixed overnight in 2.5% glutaraldehyde at 4°C and then dehydrated in 100% ethanol. After drying and coating, the observations of specimens were performed under a scanning electron microscope.

Whole Mount *In Situ* Hybridization

The cDNA fragment of the *Cgβ-tubulin* gene was generated by using the gene-specific primers (**Table 1**) and used to clone into the pMD18-T vector that contains the T7 promoter. The recombinant plasmid was linearized and used as templates when *in vitro* transcription was subsequently used to synthesize the digoxigenin-labeled probes. WMISH was performed as previously described (Wang et al., 2015) with minor modifications. Briefly, the rehydrated specimens were perforated at room temperature for 5 min with 10 μg/ml of proteinase K, followed by post-fixation with 4% PFA. The specimens were then incubated for 2 h at 65°C in the hybridization solution containing 50% formamide, 5× Denhart's, 5× SSC, 100 μg/ml yeast tRNA, 50 μg/ml heparin, 0.1% Tween-20, followed by 16 h at 65°C in the above hybridization solution containing 1 μg/ml of denatured RNA probe. Then, the specimens were incubated at room temperature in 1× blocking buffer (Roche, Basel, Switzerland) for 2 h, followed by overnight incubation in an alkaline-phosphate-conjugated rabbit anti-digoxigenin antibody (Roche) at 4°C. The specimens were then extensively washed with PBST and incubated in Nitro blue tetrazolium/5-Bromo-4-chloro-3-indolyl phosphate (NBT/BCIP) solution (Roche). Finally, the hybridization signals were visualized by using an Olympus BX53 microscope. In the negative control, the anti-sense probe with a final concentration of 1 μg/ml was replaced with sense probe of the *Cgβ-tubulin* gene.

Statistical Analyses

All results were obtained from at least three independent experiments and expressed as the mean ± standard deviation (SD). The main statistical test was the unpaired Student's t-test. For experiments involving multiple comparisons, we used one-way analysis of variance (ANOVA) tests or *post-hoc* comparisons (Tukey's) tests. All the statistical analyses were performed using PRISM software (version 8.0.2.263). p values <0.05 were considered to be statistically significant.

RESULTS

Expression of *β-tubulin* in Oyster-Ciliated Cells

To test the approach of CRISPR/Cas9 in G_0 deletion mosaic mutants, we targeted the cilia-relevant gene *Cgβ-tubulin*, given

that the potential ciliated defect phenotypes should allow for easy visualization. Genomic DNA covering the complete coding region of *Cgβ-tubulin* was amplified and revealed to consist of seven exons and six introns. *Cgβ-tubulin* was characterized with conserved domain architecture with *β-tubulin* from other species, composed of Tubulin and Tubulin_C domains (**Figure 2A**). We next analyzed the expression patterns of *Cgβ-tubulin* during larval development and found that *Cgβ-tubulin* was significantly upregulated at gastrula and later larval stages (**Figure 2B**). *In situ* hybridization indicated that the *β-tubulin* gene was specifically expressed in cells localized to the prototroch of *C. gigas angulate* trochophore (**Figures 2C, D**). In summary, developmental and tissue expression patterns of *Cgβ-tubulin* are closely associated with the ciliated cells (**Figures 2C–F**).

Testing Electroporation Efficiency

We used a standard laboratory electroporation setup to knock out *Cgβ-tubulin* with Lucifer yellow dye as report carrier to test the electroporation efficiency. Oyster embryos observed with green fluorescence indicated that exogenous dye had been successfully electroporated into the fertilized embryos (**Figures 3A, B**). We calculated the electroporation efficiency by dividing the number of embryos with fluorescence by the number of embryos. Considering that the setting of electroporation parameter has a significant impact on the survival rate and efficiency for gene delivery in the manipulated embryos, we generated multivariate experiments to determine electroporation parameters by evaluating penetrance efficiency and embryo survival rate. By comparing the results of multivariate experiments, the most balanced electroporation parameter with low voltage (40 V), long pulse duration (50 ms), and single pulse time was obtained, which not only ensured the gene delivery efficiency but also improved the survival rate of the larval. As shown in **Figure 3C**, compared with 98.0% in the control group without electroporation, the larval survival rates after electroporation with and without Cas9-sgRNA complex were close to 77.2% and 76.3%, respectively, which were far higher than that (0.6% and 1%) in a previous study (Jin et al., 2021). Finally, we achieved an electroporation efficiency of approximately 10% in the present study based on counting the number of embryos with green fluorescence. In brief, 100–110 embryos with green fluorescence were detected out of 1,000 embryos included in the statistics after electroporation with Lucifer yellow dye (**Figure 3D** and **Table 2**). These results suggest that the optimized parameters in this study can effectively avoid the serious impact of electroporation on larval development, and significantly improve the survival rates of oyster larvae.

CRISPR/Cas9-Mediated Genome Editing of *Cgβ-Tubulin*

Our loss-of-function experiment aimed to produce long deletion genotypes and mosaic phenotypes in G_0 generation. We designed five sgRNAs directed against *Cgβ-tubulin*, one targets the fourth exon, one targets the fifth exon, and the other three target the sixth exon (**Figure 4B**). We further assessed the efficiency of different sgRNAs by *in vitro* digestion of isolated *Cgβ-tubulin* DNA with Cas9. We found that all the five sgRNAs were effective in guiding Cas9-induced mutagenesis (**Supplementary Figure S1**). Among them, sgRNA1 and sgRNA2 showed high efficiency of introducing mutation, resulting in almost complete digestion of wild-type PCR bands.

We further generated *Cgβ-tubulin* mutants by mixing five sgRNAs with Cas9 protein and electroporating them into one-cell embryos. We aimed to identify long deletions produced by

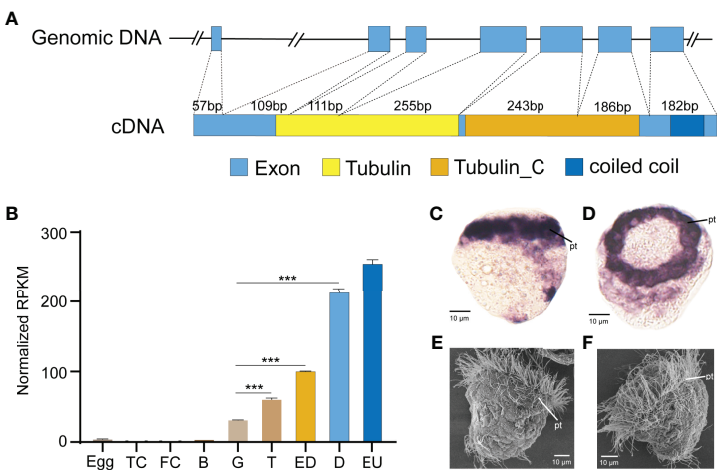

FIGURE 2 | Expression and gene structure of *Cgβ-tubulin*. **(A)** Structures of the genomic DNA and cDNA of *Cgβ-tubulin*. Seven exons and six introns in total. cDNA was predicted to encode two tubulin domains, one coiled-coil domain. **(B)** Expression profile of *β-tubulin* gene in *C. gigas angulate* at different developmental stages, TC, two cells; FC, four cells; B, blastula; G, gastrula; T, trochophore; D, D-shape larvae; EU, early umbo larva. Error bars represent means ± SD of three independent repeats. One-way ANOVA were used for significance analysis (three asterisks represent $p < 0.001$). **(C, D)** *In situ* hybridizations shows *C. gigas angulate* larvae at 8 hpf, which high-level expression of *Cgβ-tubulin* is detected in ciliated cells. **(E, F)** SEM shows a comparable developmental stage of *C.gigas angulate* larvae. pt, peritroch.

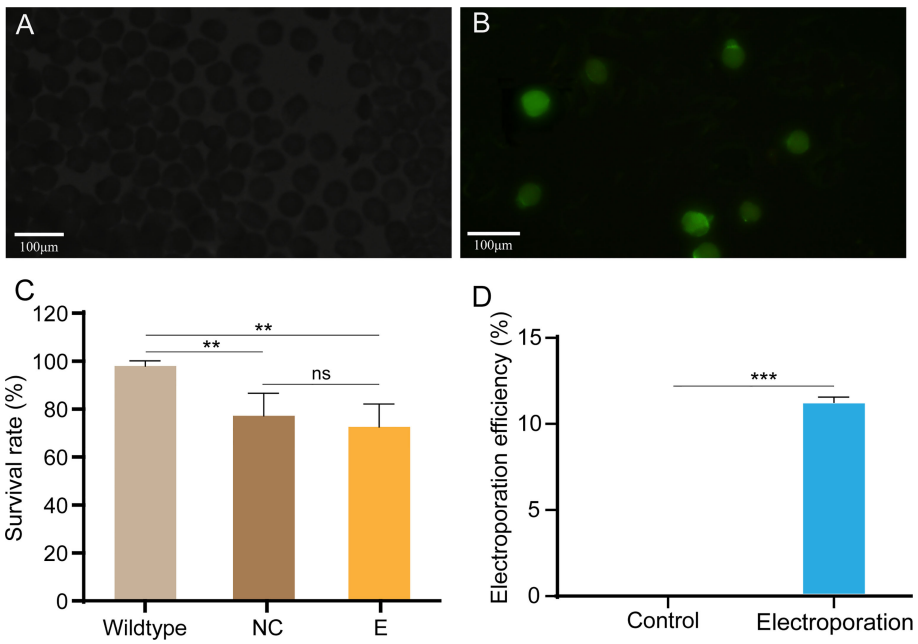

FIGURE 3 | Electroporation efficiency and survival rate of *C. gigas angulate* larvae after electroporation. **(A, B)** Early embryos electroporated with Cas9-sgRNA complex **(A)** or not **(B)**. Green fluorescence was only seen in the fertilized eggs after by electroporation (caused by the fluorescent dye in the electroporation solution). **(C)** Survival rate of *C. gigas angulate* larvae after electroporation. Wild type, wild-type control; NC, wild type by electroporation without sgRNA/Cas9 complex; E, electroporation group with sgRNA/Cas9 complex. One-way ANOVA were used for significance analysis ($p < 0.01$, two asterisks; ns, non-significant). **(D)** Electroporation efficiency statistics based on fluorescent dyes. Control, electroporation without dye Lucifer Yellow; electroporation, electroporation with dye Lucifer Yellow. *t*-Test confirmed the significantly increased number of embryos with green fluorescence in the electroporation group ($p < 0.001$, three asterisks). Error bars represent means ± SD of three independent repeats.

TABLE 2 | Summary of electroporation efficiency and survival rate.

Cas9 protein concentration (ng/μl)	sgRNAs concentration (ng/μl)	Lucifer yellow concentration (1:1000)	Voltage/pulse duration (V/ms)	Electroporation efficiency	Survival
–	–	√	–	–	490/500 (98.0%)
–	–	√	40/50	55/500 (11%)	386/500 (77.2%)
30	30	√	40/50	50/500 (10%)	363/500 (72.6%)

NHEJ following double-strand breaks (DSBs) because it facilitates rapid screening. Genome editing events analysis was performed in individual *C. gigas angulate* larvae by PCR screening of genomic DNA, analyzing fragment sizes by agarose gel electrophoresis, and cloned sequencing (**Figure 4**). We observed ~360 bp long deletion in the gel with the genotyping primers (**Figure 4A**). Sanger sequencing of TA clones (red arrow in **Figure 4A**) showed that mutations were frameshift mutations or in-frame mutations with long deletion, suggesting altered protein translation and disrupted gene function of *Cgβ-tubulin*. Further analysis demonstrated that no mutation was detected in the unelectroporated group, while the 16 truncated sequences (10%, from 160 sequences of the electroporated larvae) were all composed of long deletion mutations (100%, 363 bp deletion) (**Figure 4B**). These results suggested that electroporation mediated high-throughput delivery of the Cas9/sgRNA complex indeed caused mutations in the target gene *Cgβ-tubulin*.

Knockout of *Cgβ-Tubulin* Induced Defective Cilia Phenotypes

To test whether *Cgβ-tubulin* knockout could affect the cilia phenotypes of *C. gigas angulate* larvae, we performed *in situ* hybridization in the *Cgβ-tubulin* mosaic knockout larva. Multiple distinct expression patterns for *Cgβ-tubulin* were affected resulting from Cas9/sgRNA mosaic knockout in the trochophore and D-shaped stages of oyster larva (**Figure 5**). We observed that the multiple mosaic ciliary defects in the *Cgβ-*

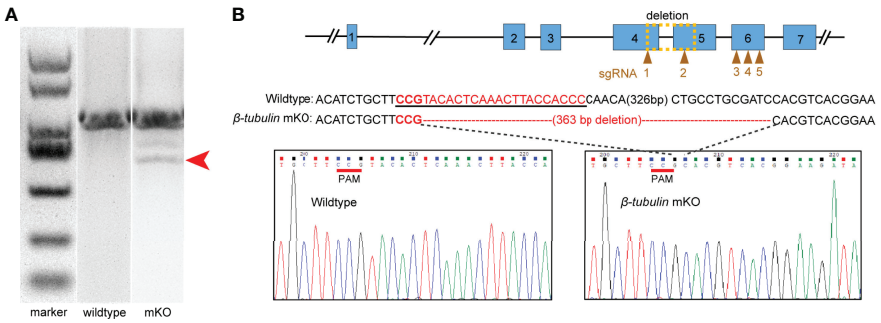

FIGURE 4 | Characterization of deleted mutations in the electroporated embryos. Embryos electroporated with Cas9-sgRNA complex were sacrificed for PCR and sequencing. **(A)** Fragment sizes analysis by agarose gel electrophoresis. Mutant PCR bands were detected (red arrow). **(B)** DNA sequence analysis showed the presence of 363 bp deletion around the *Cgβ-tubulin*-sgRNA-1 and *Cgβ-tubulin*-sgRNA-2 (yellow dotted box); sgRNA sequences are shown in the black underline, PAM sequences are shown in red underline, and the deleted nucleotides are shown in short straight lines.

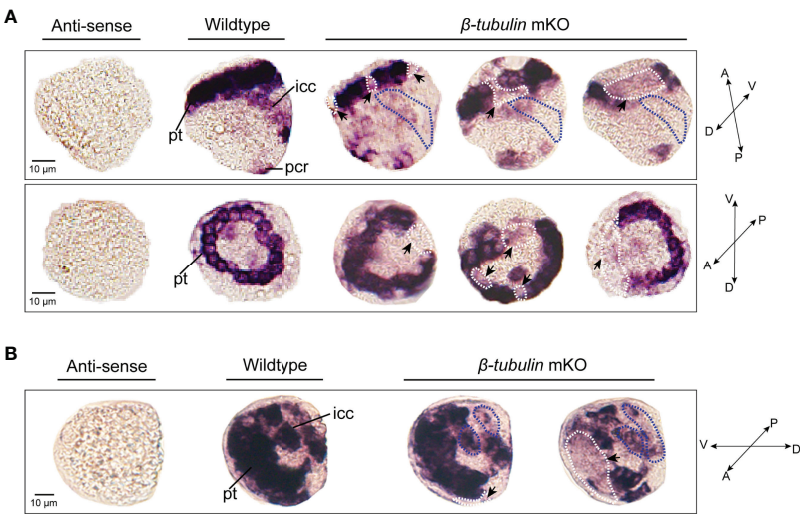

FIGURE 5 | Effects of *β-tubulin* somatic mutagenesis in *C. gigas angulate* larvae based on WMISH. The mosaic expression patterns of *β-tubulin* at the positions of peritroch (white dotted boxes) and intestinal cilia (blue dotted boxes) in *C. gigas angulate* trochophore **(A)** and D-shaped larvae **(B)** after *Cgβ-tubulin* knock out. pt, peritroch; icc, intestinal cilia cluster; pcr, posterior cilium ring; A, anterior; P, posterior; D, dorsal; V, ventral.

tubulin mosaic knockout larva (**Figure 5**). In details, *β-tubulin* knockout caused the mosaic expression patterns of *Cgβ-tubulin* at the positions of peritroch (**Figures 5A, B**, white dotted boxes and black arrows), intestinal cilia cluster (**Figures 5A, B**, blue dotted boxes) in the trochophore (**Figure 5A**) and D-shaped larvae (**Figure 5B**), including bilateral mosaics, which ranged in severity. Moreover, scanning electron microscopy revealed mosaic ciliary defects in the manipulated larvae including shortened (white arrows) and almost complete depleted cilia (white dotted boxes) at the positions of peritroch and the posterior cilium ring of *C. gigas angulate* trochophore (**Figures 6B–D'**). In addition, no abnormal development in other tissues of the manipulated *C. gigas angulate* individual was observed except for cilia shortening/depletion under ordinary light microscopy (**Figure 6A**).

Knockout of *Cgβ-Tubulin* Induced Defective Swimming Behavior

To determine whether swimming behavior was also affected in the *β-tubulin* knockout larvae, the trochophore of *C. gigas angulate* at 8 hpf were collected to perform the motility assay. The results showed that *Cgβ-tubulin* knockout resulted in a significant decrease in motility of *C. gigas angulate* larvae, especially in swimming direction and speed, compared with

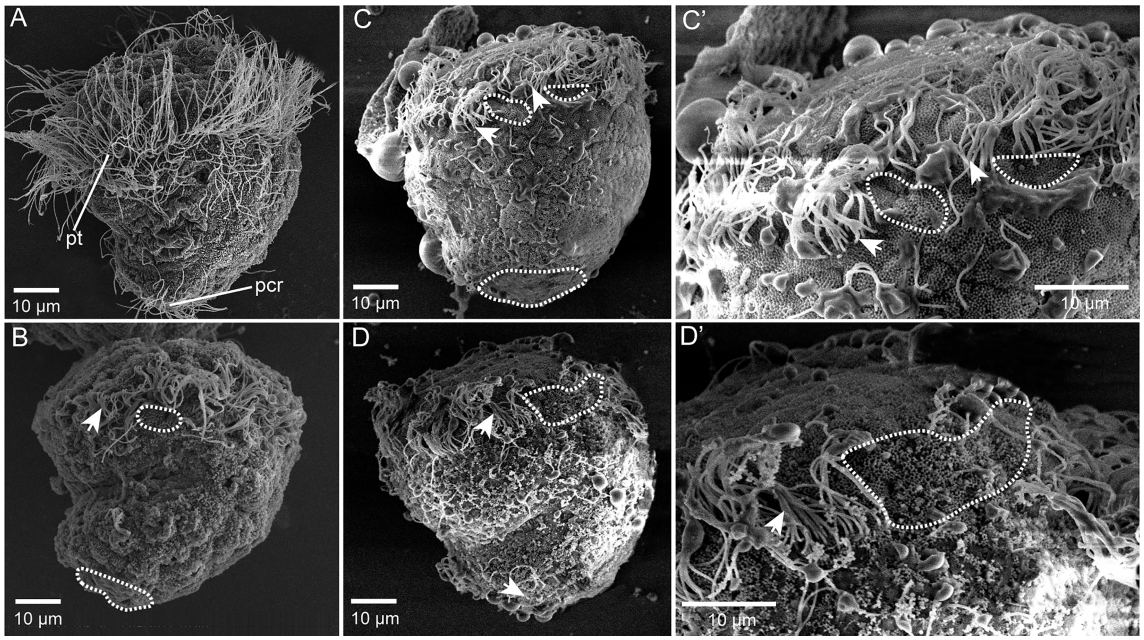

FIGURE 6 | Mosaic ciliary defects in the *β-tubulin* knockout larvae based on SEM. **(A)** Wild-type control, normally developing larvae under ordinary light microscopy. pt, peritroch. **(B–D')** Mosaic ciliary defects in the manipulated larvae based on the SEM data, including shortened (white arrows) and almost complete depleted cilia (white dotted boxes) at the positions of peritroch **(B, C, C', D, D')** and the posterior cilium ring **(B–D)** of *C. gigas angulate* trochophore.

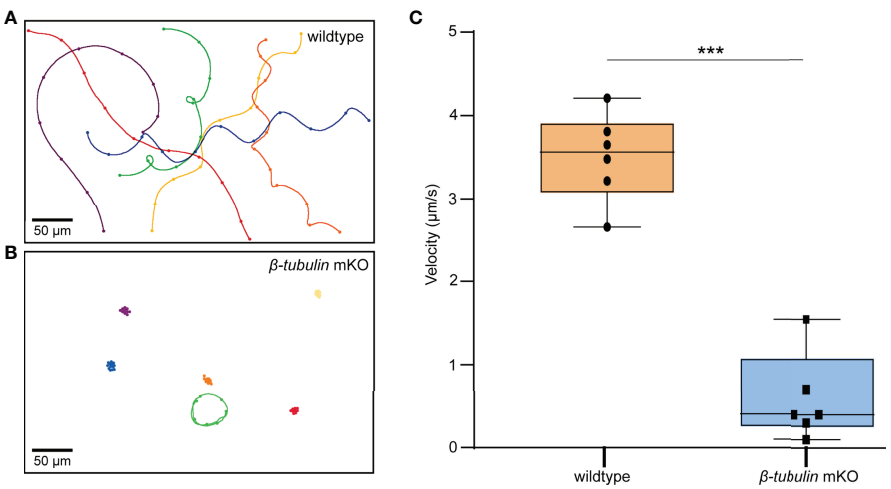

FIGURE 7 | Motility assay in *C. gigas angulate* G_0 larvae. Swimming trajectories of larvae (8 hpf) by electroporation with sgRNA/Cas9 complex **(B)** or not **(A)**. Original microscopy videos are provided in **Supplementary Video 2** (electroporation with sgRNA/Cas9 complex) and **Supplementary Video 1** (electroporation without sgRNA/Cas9 complex). **(C)** *t*-test shows the significantly reduced larvae swimming velocity in the electroporation group with sgRNAs/Cas9 complex ($p < 0.001$, three asterisks).

the wild-type larvae (**Figures 7A–C**, and **Supplementary Videos 1** and **2**). These results demonstrated that the *β-tubulin* gene was vital to cilia motility in *C. gigas angulate* larvae.

In conclusion, with the use of ciliated marker gene, we demonstrate that electroporation-based CRISPR/Cas9 system can be used to generate mosaic oyster larvae with targeted deletions. This ability to generate long fragments deletion and somatic mosaics is a powerful tool in the mollusks experimental system, as it allows the rapid evaluation of candidate gene function *in vivo* that would be embryonically lethal in pure mutant lines.

DISCUSSION

Since the first reported application of CRISPR/Cas9 in mollusks (Perry and Henry, 2015), the applications of this technology in mollusks (including gastropods and bivalves) have been described in an increasing number of studies in recent years (Yu et al., 2019; Huan et al., 2021; Jin et al., 2021; Li et al., 2021). With small size egg and embryo at a size <50 μm in diameter, electroporation was considered to be a practical, time- and labor-efficient way in molluscan CRISPR genome editing, providing a more effective method for CRISPR complex delivery in the oysters than microinjection (Yu et al., 2019; Jin et al., 2021; Li et al., 2021). Still, the sustainable development of the oyster genome editing breeding system calls for establishing efficient CRISPR/Cas9 mutagenesis tool that generates significant defective phenotypes. In this report, we performed the CRISPR-mediated *β-tubulin* gene knockout by electroporation and described the long fragments deletions and mosaic mutations including defective cilia and decreased motility in the G_0 larva of *C. gigas angulate*.

CRISPR/Cas9 Mediated *β-Tubulin* Knockout in Oyster *C. gigas angulate* by Electroporation

Cilium is a tubulin-based cytoplasmic extension and is thought to have functions of interrogating the extracellular environment in many biological contexts (Davenport and Yoder, 2005; Berbari et al., 2009). A large number of arranged cilia is thought to be the swimming organ of many zooplankton and larvae of aquatic protostomes, including mollusks (Nielsen, 2004; Nielsen, 2005). The tubulin subunits (*β-tubulin*) was considered to be required for the formation of the tubulin heterodimers, the main compounds that polymerized into microtubules and constitute the major compound of cilia in the mollusks *P. vulgata* (Damen and Dictus, 1994), *Crepidula fornicata* (Hejnol et al., 2007), and *Ilyanassa obsoleta* (Gharbiah et al., 2013), and in the annelid *Polygordius lacteus* (Woltereck, 1904) and polychaete *H. elegans* (Arenas-Mena et al., 2007). In our present study, a *β-tubulin* gene was identified in *C. gigas angulate* and found to be highly expressed in ciliated cells based on *in situ* hybridization. In present study, we used *β-tubulin* as a marker gene and performed CRISPR-mediated knockout by electroporation in *C. gigas angulate*. Through direct genotyping, long fragments deletions (363 bp) were detected in the target gene. By *in situ* hybridization, scanning electron microscopy, and behavioral analysis, we observed mosaic mutations including defective cilia and decreased motility in the G_0 larva. This result demonstrates that *Cgβ-tubulin* is sufficient to mediate cilia development and swimming in larval oyster. In conclusion, with the use of ciliated marker gene, we demonstrate that electroporation-based CRISPR/Cas9 mutagenesis can be used to generate mosaic oyster larvae with targeted deletions and for studies of gene function in the oyster.

We optimized the parameters to improve the survival rate of oyster larvae under the premise of ensuring good perforation efficiency. Compared with the electroporation parameters (100 V, with 15 ms pulse duration and four pulses separated by 100-ms pulse interval) set by Jin et al. (2021), we reduced the voltage of electroporation to 40 V, the pulse times to 1, while the pulse time was increased to 50 ms. After optimization, the larval survival rate after electroporation with and without Cas9-sgRNA complex was close to 77.2% and 76.3% in the present study, respectively, which was far higher than that (0.6% and 1%) of Jin et al. (2021). Moreover, based on our previous experience, the higher final concentrations of Cas9-sgRNA complex tend to give larger effects and is suitable for less potentially lethal loci. In the present study, by adjusting the concentrations of Cas9-sgRNA complex, we have been able to induce mosaic mutants using as low as 30 ng/μl Cas9 and 30 ng/μl of each sgRNA in oyster larvae. Although the efficiency of successful gene editing is still low (10%, 16/160), we can still obtain a certain number of successfully edited larvae because of the large number of oyster eggs. In addition, it is worth noting that only the long fragment deletions were used to evaluate the gene editing efficiency, while the small indels mutations were ignored, which may result in a serious underestimate of editing efficiency in the present study.

CRISPR/Cas9-Mediated Long Deletion Knockout in the Oyster Larvae

Loss-of-function deletion mutations can be produced by NHEJ following DSBs. In previous studies, long deletion knockout strategies generated by two and more cut sites using multiple single-guide RNAs (co-injection of more than two sgRNAs) have been applied in a variety of species including *Danio rerio* (Höijer et al., 2022), *Bombyx mori* (Wang et al., 2013), *Helicoverpa armigera* (Khan et al., 2017), *Vanessa cardui* (Zhang and Reed, 2016), and *Bicyclus anynana* (Zhang et al., 2017), but not in mollusks, such as *L. goshimai* (Huan et al., 2021), *C. gigas* (Yu et al., 2019; Li et al., 2021), and *C. gigas angulate* (Jin et al., 2021). In the present study, five sgRNAs were simultaneously used to generate long fragment deletions, as it allowed us to perform rapid screening and genotyping of mutants using PCR and conventional agarose gel electrophoresis. According to genotyping, we detected a long fragment deletion of 363 bp in the target gene, which was the longest known deletion in mollusks, and much longer than the studies in *L. goshimai* (<25 bp deletion), *C. gigas* (<30 bp deletion), and *C. gigas angulate* (single base substitution). This strategy of co-injecting more than two sgRNAs is a significant improvement over the difficult detection of small indels generated by single cleavage using normal agarose gels, which significantly simplifies the genome editing workflow. Moreover, the small indels often inevitably produce truncated proteins function more similar to the original protein (theoretically, in-frame mutations occurred in 33.3% of cases). The long fragment deletion at the first functional Tubulin domain of *Cgβ-tubulin* gene in our study could significantly increase the probability of generating truncated proteins with deletion of the remaining functional domains and cause convincing knockout phenotypes.

Mosaic Ciliary Defects in the Oyster Larvae

Genetic mosaicism is the presence of more than one genotype in one individual. Mosaicism can be produced by a variety of natural mechanisms including chromosome non-disjunction, anaphase hysteresis, endoreplication, and mutations arising during development (Taylor et al., 2014), and by manipulative mechanisms such as genome editing. In essence, target genes at different stages of embryonic development can be continuously targeted and cleaved by the CRISPR/Cas9 system, resulting in mosaic mutant individuals (Mizuno et al., 2014; Oliver et al., 2015; Xin et al., 2016). Typically, mosaicism generated by the CRISPR/Cas9 system in animal models is considered an undesirable outcome. In some cases, however, this phenomenon can be valuable. Due to the embryonic lethality of many target genes and the difficulties of maintenance and genotyping, most of our attention has been focused on analysis of mosaic G_0 phenotypes. The advantages of focusing on somatic mosaicism are that data can be collected over a generation, and the phenotypic effects of lesions are limited to the subset of cell lineages with deletions, thereby reducing the harmful effects of many deletions (Zhong et al., 2015; Mehravar et al., 2019). *β-Tubulin* knockout mediated the mosaic expression patterns of *Cgβ-tubulin*, and mosaic ciliary defects were commonly found at the positions of peritroch, intestinal cilia, and the posterior cilium ring in *C. gigas angulate* trochophore and D-shaped larvae. Overall, we suggest that CRISPR/Cas9 can be applied to generate oyster larvae with phenotypic mosaic defects for targeted deletions. In the future, this ability to produce somatic deletion mosaics could be a powerful tool for studying oyster gene function in the mollusks experimental systems.

CONCLUSION

The application of CRISPR-mediated gene editing in marine mollusks is still facing great challenges, both in functional studies after gene knockout and in genetic engineering breeding. Here, we found that *β-tubulin* knockout could induce mosaic phenotypes in G_0 larvae of *C. gigas angulate* by using electroporation, characterized by shortened/depleted cilia and decreased larval motility. Since the *β-tubulin* knockout phenotypes are easy to detect at very early developmental stages, it may serve as the optimal preliminary candidate gene for establishing CRISPR-based gene editing technology. In addition, our study reveals the strategy of generating long fragments deletion, and somatic mosaics are a powerful tool in the mollusks experimental system. Together, our report can provide useful reference for a widespread application of CRISPR/Cas9-based gene editing technology in mollusks in the future.

DATA AVAILABILITY STATEMENT

The original contributions presented in the study are included in the article/**Supplementary Material**. Further inquiries can be directed to the corresponding author.

AUTHOR CONTRIBUTIONS

Conceived and designed the experiments: LZ. Performed the experiments: JC, WZ, YueX, and YuX. Data analysis: JC, WZ, and YueX. Contributed reagents/materials/computer resources: LZ. Wrote the paper: JC and LZ. All authors contributed to the article and approved the submitted version.

FUNDING

This research was supported by the National Natural Science Foundation of China (41976088) to LZ, Strategic Priority Research Program of the Chinese Academy of Sciences (XDB42000000) to LZ, Key Development Project of Centre for Ocean Mega-Research of Science, Chinese Academy of Science (COMS2019R01) to LZ.

ACKNOWLEDGMENTS

We thank the high-performance computing center of Institute of Oceanology, CAS. We also would like to thank Fucun Wu for oyster culture support and Yuanyuan Sun for SEM help.

SUPPLEMENTARY MATERIAL

The Supplementary Material for this article can be found online at: https://www.frontiersin.org/articles/10.3389/fmars.2022.912409/full#supplementary-material

Supplementary Figure 1 | *In vitro* cleavage assay for testing the sgRNAs guided DNA cleavage by Cas9. WT represented the mixture of sgRNA and *Cgβ-tubulin* cleavage templates. SgRNA1-sgRNA5 shown the *in vitro* cleavage band types by Cgβ-tubulin-sgRNA1-5, respectively.

Supplementary Video 1 | Original microscopy video of larval trajectories in the wildtype group.

Supplementary Video 2 | Original microscopy video of larval trajectories in the electroporation group with sgRNAs/Cas9 complex.

REFERENCES

Abe, M., and Kuroda, R. (2019). The Development of CRISPR for a Mollusc Establishes the Formin Lsdia1 as the Long-Sought Gene for Snail Dextral/Sinistral Coiling. *Development* 146, dev175976–dev175976. doi: 10.1242/dev.175976

Ahmed, N., and Thompson, S. (2019). The Blue Dimensions of Aquaculture: A Global Synthesis. *Sci. Total Environ.* 652, 851–861. doi: 10.1016/j.scitotenv.2018.10.163

Arenas-Mena, C., Wong, S. Y., and Arandi-Forosani, N. (2007). Ciliary Band Gene Expression Patterns in the Embryo and Trochophore Larva of an Indirectly

Developing Polychaete. *Gene Expr. Patterns* 7, 544–549. doi: 10.1016/j.modgep.2007.01.007

Berbari, N. F., Connor, A. K., Haycraft, C. J., and Yoder, B. K. (2009). The Primary Cilium as a Complex Signaling Center. *Curr. Biol.* 19, 526–535. doi: 10.1016/j.cub.2009.05.025

Chakrapani, V., Patra, S. K., Panda, R. P., Rasal, K. D., Jayasankar, P., and Barman, H. K. (2016). Establishing Targeted Carp TLR22 Gene Disruption *via* Homologous Recombination Using CRISPR/Cas9. *Dev. Comp. Immunol.* 641, 242–247. doi: 10.1016/j.dci.2016.04.009

Chan, J. L., Wang, L., Li, L., Mu, K., Bushek, D., Xu, Y., et al. (2021). Transcriptomic Response to *Perkinsus Marinus* in Two Crassostrea Oysters Reveals Evolutionary Dynamics of Host-Parasite Interactions. *Front. Genet.* 12, 795706. doi: 10.3389/fgene.2021.795706

Chen, H. L., Wang, J., Du, J. X., Si, Z. X., Yang, H., Xu, X. D., et al. (2019). *ASIP* Disruption *via* Crispr/Cas9 System Induces Black Patches Dispersion in Oujiang Color Common Carp. *Aquaculture* 498, 230–235. doi: 10.1016/j.aquaculture.2018.08.057

Chen, Y., Wang, Z., Ni, H., Yong, X., Chen, Q., and Jiang, L. (2017). CRISPR/Cas9-Mediated Base-Editing System Efficiently Generates Gain-of-Function Mutations in Arabidopsis. *Sci. China Life Sci.* 60, 520–523. doi: 10.1007/s11427-017-9021-5

Cleveland, B. M., Yamaguchi, G., Radler, L. M., and Shimizu, M. (2018). Editing the Duplicated Insulin-Like Growth Factor Binding Protein-2b Gene in Rainbow Trout (*Oncorhynchus Mykiss*). *Sci. Rep.* 8, 16054. doi: 10.1038/s41598-018-34326-6

Damen, P., and Dictus, W. (1994). Cell Lineage of the Prototroch of *Patella Vulgata* (Gastropoda, Mollusca). *Dev. Biol.* 162, 364–383. doi: 10.1006/dbio.1994.1094

Davenport, J. R., and Yoder, B. K. (2005). An Incredible Decade for the Primary Cilium: A Look at a Once-Forgotten Organelle. *Am.J. Physiol. Renal Physiol.* 289, 1159–1169. doi: 10.1152/ajprenal.00118.2005

Dove, M. C., and O'Connor, W. A. (2010). Commercial Assessment of Growth and Mortality of Fifth-Generation Sydney Rock Oysters *Saccostrea Glomerata* (Gould 1850) Selectively Bred for Faster Growth. *Aquaculture Res.* 40, 1439–1450. doi: 10.1111/j.1365-2109.2009.02243.x

Eid, A., and Mahfouz, M. M. (2016). Genome Editing: The Road of CRISPR/Cas9 From Bench to Clinic. *Exp. Mol. Med.* 48, e265. doi: 10.1038/emm.2016.111

FAO. (2020). *The State of World Fisheries and Aquaculture 2020-Sustainability in Action* (Rome: FAO). doi: 10.4060/ca9229en

Frank-Lawale, A., Allen, S. K., and Dégremont, L. (2014). Breeding and Domestication of Eastern Oyster (*Crassostrea Virginica*) Lines for Culture in the Mid-Atlantic, Usa: Line Development and Mass Selection for Disease Resistance. *J. Shellfish Res.* 33, 153–165. doi: 10.2983/035.033.0115

Gharbiah, M., Nakamoto, A., and Nagy, L. M. (2013). Analysis of Ciliary Band Formation in the Mollusc *Ilyanassa Obsoleta*. *Dev. Genes Evol.* 223, 225–235. doi: 10.1007/s00427-013-0440-1

Gui, T., Zhang, J., Song, F., Sun, Y., Xie, S., Yu, K., et al. (2016). CRISPR/Cas9-Mediated Genome Editing and Mutagenesis of EcChi4 in *Exopalaemon Carinicauda*. *G3-Genes Genomes Genet.* 6, 3757–3764. doi: 10.1534/g3.116.034082

Hejnol, A., Martindale, M. Q., and Henry, J. Q. (2007). High-Resolution Fate Map of the Snail *Crepidula Fornicata*: The Origins of Ciliary Bands, Nervous System, and Muscular Elements. *Dev. Biol.* 305, 63–76. doi: 10.1016/j.ydbio.2007.01.044

Höijer, I., Emmanouilidou, A., Östlund, R., van Schendel, R., Bozorgpana, S., Tijsterman, M., et al. (2022). CRISPR-Cas9 Induces Large Structural Variants at on-Target and Off-Target Sites *In Vivo* That Segregate Across Generations. *Nat. Commun.* 13, 627. doi: 10.1038/s41467-022-28244-5

Hollenbeck, C. M., and Johnston, I. A. (2018). Genomic Tools and Selective Breeding in Molluscs. *Front. Genet.* 9. doi: 10.3389/fgene.2018.00253

Houston, R. D., Bean, T. P., Macqueen, D. J., Gundappa, M. K., and Robledo, D. (2020). Harnessing Genomics to Fast-Track Genetic Improvement in Aquaculture. *Nat. Rev. Genet.* 21, 389–409. doi: 10.1038/s41576-020-0227-y

Huan, P., Cui, M. L., Wang, Q., and Liu, B. Z. (2021). CRISPR/Cas9-Mediated Mutagenesis Reveals the Roles of Calaxin in Gastropod Larval Cilia. *Gene* 787, 145640. doi: 10.1016/j.gene.2021.145640

Jin, K., Zhang, B., Jin, Q., Cai, Z., Wei, L., Wang, X., et al. (2021). CRISPR/Cas9 System-Mediated Gene Editing in the Fujian Oysters (*Crassostrea Angulate*) by Electroporation. *Front. Marine Sci.* 8, 763470. doi: 10.3389/fmars.2021.763470

Khan, S. A., Reichelt, M., and Heckel, D. G. (2017). Functional Analysis of the ABCs of Eye Color in *Helicoverpa Armigera* With CRISPR/Cas9-Induced Mutations. *Sci. Rep.* 7, 40025. doi: 10.1038/srep40025

Kim, J., Cho, J. Y., Kim, J. W., Kim, H. C., Noh, J. K., Kim, Y. O., et al. (2019). CRISPR/Cas9-Mediated Myostatin Disruption Enhances Muscle Mass in the Olive Flounder *Paralichthys Olivaceus*. *Aquaculture* 512, 734336. doi: 10.1016/j.aquaculture.2019.734336

Langdon, E. C. (2006). Effects of Genotype × Environment Interactions on the Selection of Broadly Adapted Pacific Oysters (*Crassostrea Gigas*). *Aquaculture* 261, 522–534. doi: 10.1016/j.aquaculture.2006.07.022

Li, M., Feng, R., Ma, H., Dong, R., Liu, Z., Jiang, W., et al. (2016). Retinoic Acid Triggers Meiosis Initiation *via* Stra8-Dependent Pathway in Southern Catfish, *Silurus Meridionalis*. *Gen. Comp. Endocrinol.* 232, 191–198. doi: 10.1016/j.ygcen.2016.01.003

Li, C., Wang, H. Y., Liu, C. F., Li, Y. W., and Guo, X. M. (2013). Classification and Distribution of Oysters Off Coastal Guangxi, China. *Oceanologia Limnologia Sin.* 5, 1318–13240.

Li, M., Yang, H., Zhao, J., Fang, L., Shi, H., Li, M., et al. (2014). Efficient and Heritable Gene Targeting in Tilapia by CRISPR/Cas9. *Genetics* 197, 591–599. doi: 10.1534/genetics.114.163667

Li, H., Yu, H., Du, S., and Li, Q. (2021). CRISPR/Cas9 Mediated High Efficiency Knockout of Myosin Essential Light Chain Gene in the Pacific Oyster (*Crassostrea Gigas*). *Marine Biotechnol.* 23, 215–224. doi: 10.1007/s10126-020-10016-1

Ma, J., Fan, Y., Zhou, Y., Liu, W., Jiang, N., Zhang, J., et al. (2018). Efficient Resistance to Grass Carp Reovirus Infection in JAM-A Knockout Cells Using CRISPR/Cas9. *Fish Shellfish Immunol.* 76, 206–215. doi: 10.1016/j.fsi.2018.02.039

Mehravar, M., Shirazia, A., Nazaric, M., and Banan, M. (2019). Mosaicism in CRISPR/Cas9-Mediated Genome Editing. *Dev. Biol.* 445, 156–162. doi: 10.1016/j.ydbio.2018.10.008

Melo, C. M. R., Durland, E., and Langdon, C. (2016). Improvements in Desirable Traits of the Pacific Oyster, *Crassostrea Gigas*, as a Result of Five Generations of Selection on the West Coast, USA. *Aquaculture* 460, 105–115. doi: 10.1016/j.aquaculture.2016.04.017

Mizuno, S., Dinh, T. T. H., Kato, K., Mizuno-Iijima, S., Tanimoto, Y., Daitoku, Y., et al. (2014). Simple Generation of Albino C57BL/6J Mice With G291T Mutation in the Tyrosinase Gene by the CRISPR/Cas9 System. *Mamm. Genome* 25, 327–334. doi: 10.1007/s00335-014-9524-0

Momose, T., and Concordet, J. P. (2016). Diving Into Marine Genomics With CRISPR/Cas9 Systems. *Mar. Geonomics* 30, 55–65. doi: 10.1016/j.margen.2016.10.003

Nielsen, C. (2004). Trochophora Larvae: Cell-Lineages, Ciliary Bands, and Body Regions. 1. Annelida and Mollusca. *J. Exp. Zoology Part B Mol. Dev. Evol.* 302, 35–68. doi: 10.1002/jez.b.20001

Nielsen, C. (2005). Trochophora Larvae: Cell-Lineages, Ciliary Bands and Body Regions. 2. Other Groups and General Discussion. *J. Exp. Zoology Part B Mol. Dev. Evol.* 304, 401–447. doi: 10.1002/jez.b.21050

Ohama, M., Washio, Y., Kishimoto, K., Kinoshita, M., and Kato, K. (2020). Growth Performance of Myostatin Knockout Red Sea Bream Pagrus Major Juveniles Produced by Genome Editing With CRISPR/Cas9. *Aquaculture* 529, 735672. doi: 10.1016/j.aquaculture.2020

Oliver, D., Yuan, S., McSwiggin, H., and Yan, W. (2015). Pervasive Genotypic Mosaicism in Founder Mice Derived From Genome Editing Through Pronuclear Injection. *PloS One* 10, e0129457. doi: 10.1371/journal.pone.0129457

Pernet, B. (2018). "Larval Feeding: Mechanisms, Rates, and Performance in Nature," in *Evolutionary Ecology of Marine Invertebrate Larvae*. Eds. T. J. Carrier, A. M. Reitzel and A. Heyland (Oxford: Oxford University Press), Pp. 87–102.

Perry, K. J., and Henry, J. Q. (2015). CRISPR/Cas9-Mediated Genome Modification in the Mollusc, *Crepidula Fornicata*. *Genesis* 53, 237–244. doi: 10.1002/dvg.22843

Rawson, P., Lindell, S., Guo, X., and Sunila, I. (2010). Cross-Breeding for Improved Growth and Disease Resistance in the Eastern Oyster. NRAC Publication No. 206-2010. Available at: https://www.researchgate.net/publication/247778319.

Riviere, G., He, Y., Tecchio, S., Crowell, E., Gras, M., Sourdaine, P., et al. (2017). Dynamics of DNA Methylomes Underlie Oyster Development. *PloS Genet.* 13, e1006807. doi: 10.1371/journal.pgen.1006807

Simora, R., Xing, D., Bangs, M. R., Wang, W., and Dunham, R. A. (2020). CRISPR/Cas9-Mediated Knock-in of Alligator Cathelicidin Gene in a Non-Coding Region of Channel Catfish Genome. *Sci. Rep.* 1, 22271. doi: 10.1038/s41598-020-79409-5

Song, K., Li, Y., Huang, B., Li, L., and Zhang, G. (2017). Genetic and Evolutionary Patterns of Innate Immune Genes in the Pacific Oyster *Crassostrea Gigas.* Dev. *Comp. Immunol.* 77, 17–22. doi: 10.1016/j.dci.2017.07.012

Straume, A. H., Kjærner-Semb, E., Kai, O. S., Güralp, H., and Edvardsen, R. B. (2020). Indel Locations are Determined by Template Polarity in Highly Efficient *In Vivo* CRISPR/Cas9-Mediated HDR in Atlantic Salmon. *Sci. Rep.* 10, 409. doi: 10.1038/s41598-019-57295-w

Taylor, T. H., Gitlin, S. A., Patrick, J. L., Crain, J. L., Wilson, J. M., and Griffin, D. K. (2014). The Origin, Mechanisms, Incidence and Clinical Consequences of Chromosomal Mosaicism in Humans. *Hum. Reprod. Update* 20, 571–581. doi: 10.1093/humupd/dmu016

Wang, Q., Li, Q., Kong, L., and Yu, R. (2012). Response to Selection for Fast Growth in the Second Generation of Pacific Oyster (*Crassostrea Gigas*). *J. Ocean Univ. China* 2012, 413–418. doi: 10.1007/sl1802-012-1909-7

Wang, X., Liu, B., Liu, F., and Huan, P. (2015). A Calaxin Gene in the Pacific Oyster *Crassostrea Gigas* and its Potential Roles in Cilia. *Zoological Sci.* 32, 419–426. doi: 10.2108/zs150009

Wang, Y., Li, Z., Xu, J., Zeng, B., Ling, L., You, L., et al. (2013). The CRISPR/Cas System Mediates Efficient Genome Engineering in *Bombyx Mori*. *Cell Res.* 23, 1414–1416. doi: 10.1038/cr.2013.146

Woltereck, R. (1904). Beiträge Zur Praktischen Analyse Der PolygordiusEntwicklung Nachdem "Nordsee-" Und Dem "Mittelmeer-Typus". *Dev. Genes Evol.* 18, 377–403. doi: 10.1007/BF02162440

Wood, B. (2016). *Adobe Illustrator CC 2017 Release* California, USA: Adobe Press.

Xin, L., Min, L., and Bing, S. (2016). Application of the Genome Editing Tool CRISPR/Cas9 in Non-Human Primates. *Zool. Res.* 37, 241. doi: 10.13918/j.issn.2095-8137.2016.4.214

Yue, C., Li, Q., and Yu, H. (2018). Gonad Transcriptome Analysis of the Pacific Oyster *Crassostrea Gigas* Identifies Potential Genes Regulating the Sex Determination and Differentiation Process. *Mar. Biotechnol.* 20, 206–219. doi: 10.1007/s10126-018-9798-4

Yu, H., Li, H., Li, Q., Xu, R., Yue, C., and Du, S. (2019). Targeted Gene Disruption in Pacific Oyster Based on CRISPR/Cas9 Ribonucleoprotein Complexes. *Mar. Biotechnol.* 21, 301–309. doi: 10.1007/s10126-019-09885-y

Zhang, G., Fang, X., Guo, X., Li, L., Luo, R., Xu, F., et al. (2012). The Oyster Genome Reveals Stress Adaptation and Complexity of Shell Formation. *Nature* 490, 49–54. doi: 10.1038/nature11413

Zhang, L., Martin, A., Perry, M. W., Van, D., Matsuoka, Y., Monteiro, A., et al. (2017). Genetic basis of melanin pigmentation in butterfly wings. *Genetics* 205, 1537–1550. doi: 10.1534/genetics.116.196451

Zhang, L., and Reed, R. D. (2016). Genome Editing in Butterflies Reveals That *Spalt* Promotes and Distal-Less Represses Eyespot Colour Patterns. *Nat. Commun.* 7, 11769. doi: 10.1038/ncomms11769

Zhong, H., Chen, Y., Li, Y., Chen, R., and Mardon, G. (2015). CRISPR-Engineered Mosaicism Rapidly Reveals That Loss of Kcnj13 Function in Mice Mimics Human Disease Phenotypes. *Sci. Rep.* 5, 8366. doi: 10.1038/srep08366

Zu, Y., Zhang, X., Ren, J., Dong, X., Zhu, Z., Jia, L., et al. (2016). Biallelic Editing of a Lamprey Genome Using the CRISPR/Cas9 System. *Sci. Rep.* 6, 23496. doi: 10.1038/srep23496

Conflict of Interest: The authors declare that the research was conducted in the absence of any commercial or financial relationships that could be construed as a potential conflict of interest.

Publisher's Note: All claims expressed in this article are solely those of the authors and do not necessarily represent those of their affiliated organizations, or those of the publisher, the editors and the reviewers. Any product that may be evaluated in this article, or claim that may be made by its manufacturer, is not guaranteed or endorsed by the publisher.

Advantages of publishing in Frontiers

OPEN ACCESS
Articles are free to read for greatest visibility and readership

FAST PUBLICATION
Around 90 days from submission to decision

HIGH QUALITY PEER-REVIEW
Rigorous, collaborative, and constructive peer-review

TRANSPARENT PEER-REVIEW
Editors and reviewers acknowledged by name on published articles

Frontiers
Avenue du Tribunal-Fédéral 34
1005 Lausanne | Switzerland

Visit us: www.frontiersin.org
Contact us: frontiersin.org/about/contact

REPRODUCIBILITY OF RESEARCH
Support open data and methods to enhance research reproducibility

DIGITAL PUBLISHING
Articles designed for optimal readership across devices

FOLLOW US
@frontiersin

IMPACT METRICS
Advanced article metrics track visibility across digital media

EXTENSIVE PROMOTION
Marketing and promotion of impactful research

LOOP RESEARCH NETWORK
Our network increases your article's readership